U.S. Department of Energy • Office of Fossil Energy
National Energy Technology Laboratory

2006
Office of Fossil Energy
Fuel Cell Program Annual Report

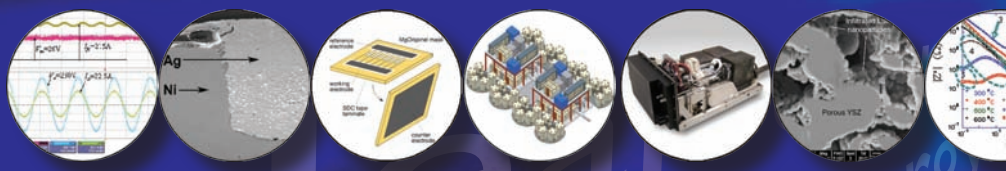

2006
OFFICE OF FOSSIL ENERGY
FUEL CELL PROGRAM ANNUAL REPORT

September 2006

Table of Contents

III. SECA RESEARCH & DEVELOPMENT (CONTINUED)

VI. ADVANCED RESEARCH (CONTINUED)

I. INTRODUCTION

I. INTRODUCTION

Competitive Innovation: Accelerating Technology Development

The Administration's Office of Management and Budget recently cited the Solid State Energy Conversion Alliance (SECA) program as leading the way in Government-industry partnerships.

"The SECA program leverages private-sector ingenuity by providing Government funding to Industry Teams developing fuel cells, as long as the Teams continue to exceed a series of stringent technical performance hurdles. This novel incentive structure has generated a high level of competition between the Teams and an impressive array of technical approaches. The SECA program also develops certain core technologies that can be used by all the Industry Teams to avoid duplication of effort. The program exceeded its 2005 performance targets, and it is on track to meet its goal for an economically competitive technology by 2010."

The U.S. Department of Energy (DOE) Office of Fossil Energy, through the National Energy Technology Laboratory (NETL) and in collaboration with the Pacific Northwest National Laboratory, is forging government/industry partnerships under SECA to reduce the cost of fuel cells and to develop fuel cell coal-based systems for clean and efficient central power generation. These goals equate to removing environmental and climate change concerns associated with fossil fuel use while simultaneously establishing a foundation for a hydrogen-based economy and a secure energy future in the United States. With the successful completion of the first cost reduction phase in fiscal year (FY) 2006, SECA is one step closer to realizing its vision of cost-effective, near-zero-emission fuel cell technology for commercial applications.

Launched in 2000, SECA is an inventive collaboration between government, the private sector and the scientific community to accelerate the development of modular, low-cost, fuel-flexible solid oxide fuel cell (SOFC) systems that can operate on coal gas, natural gas, bio-fuels, diesel fuel and hydrogen. This approach will facilitate deployment into the marketplace by making SOFCs fuel flexible and an affordable option for energy generation. SECA's DOE mission is to have its fuel cell systems ready for FutureGen, soon to be the world's cleanest coal-fueled power plant.

The SECA cost reduction goal is to develop and design SOFCs capable of manufacture at $400 per kilowatt (kW) by 2010. Concurrently, SECA coal-based systems will scale and integrate SECA SOFC technology for delivery to FutureGen in 2011. Development of large (greater than 100 megawatts) SOFC power blocks will enable affordable, efficient, and environmentally-friendly electrical power from coal. Key system capabilities to be proven by 2015 include 50 percent or greater integrated gasification combined cycle (IGCC) plant efficiency in converting the energy contained in coal (higher heating value, HHV) to grid electrical power; the capture of 90 percent or more of the carbon contained in the coal fuel (as CO_2); elimination of NOx to well below levels of environmental concern; and a cost of $400/kW for the fuel cell power block, exclusive of the coal gasification unit and CO_2 separation subsystems.

The alliance is comprised of three groups: Industry Teams, Core Technology program participants, and federal government management. The Industry Teams design the fuel cells and handle most hardware and market penetration issues. The Core Technology program is made up of universities, national laboratories, small businesses, and other R&D organizations and addresses applied technological issues common to all Industry Teams. Findings and inventions under the Core Technology program are made available to all Industry Teams under unique intellectual property provisions that serve to accelerate development. The federal government management facilitates interaction between Industry Teams and the Core Technology program, as well as establishes technical priorities and approaches.

Across the United States, SECA Core Technology participants are working on dozens of fuel cell projects, led by the brightest minds from leading universities, national laboratories and businesses. These competitively selected projects work together to provide vital R&D and testing in support to the Industry Teams.

In the same spirit of healthy competition, the Industry Teams leverage the collective ingenuity of the Core Technology participants to independently pursue innovations in fuel cell design that can be mass-produced at lower cost. Focusing on Cost Reduction and Coal-Based Systems, the Industry Teams are working to solve the challenges of fuel cell technology,

SECA CORE TECHNOLOGY & ADVANCED RESEARCH PARTICIPANTS

each using different design and manufacturing approaches. As a result, the SECA program is rich in innovation, allowing it to reach its goals much faster.

Annual Report Sections

The Office of Fossil Energy and NETL are pleased to present this FY 2006 Office of Fossil Energy Fuel Cell Program Annual Report, a compilation of abstracts from the fuel cell projects managed through these offices. These abstracts are divided into sections as detailed below.

SECA Cost Reduction: To achieve cost targets, Industry Teams are engaged in refining and validating advanced technology in 3-10 kW SOFC modules that can be mass produced, aggregated, and scaled to meet a broad range of applications. This development activity is blending established manufacturing processes with state-of-the-art fuel cell technology advancements in order to leverage the advantages of economies of high-volume production. It also requires reaching a full spectrum of large markets, such as auxiliary power units (APUs) for trucks and recreational vehicles. SOFC-based APUs provide on-board power while the vehicle engine is off, addressing the challenges of anti-idling legislation enacted in many states while at the same time establishing production capacity to reduce cost and enable delivery of large SECA systems to FutureGen and the new breed of coal plants that follow. Additional markets include residential-commercial-industrial power, a wide range of distributed power generation, and specialized applications for the military. Producing a common module for these vast markets will create the opportunity for the high-volume production required to reduce cost to the necessary level.

SIEMENS

GE Power Systems

DELPHI Driving Tomorrow's Technology

FuelCell Energy

Cummins Power Generation

Acumentrics Advanced Power & Energy Technologies

SECA R&D: The Core Technology program provides comprehensive applied research support in five focus areas. This structure and the provisions in place reduce cost by leveraging resources so that all Industry Teams do not engage in separate applied research programs paying multiple times for the same research done once in the Core program. This approach also ensures that only major issues are addressed. SECA R&D's goal is to raise the technology bar in large strides rather than small steps. Core program areas are also funded by special topics under Science Initiatives, Small

Business Innovative Research, Basic Energy Sciences, University Coal Research, and Historically Black Colleges and Universities. The Core Technology focus areas include the following:

- Materials and Manufacturing – Research focuses on improved reliability, improved performance, ability to tolerate any fuel or air contaminants, and reducing cost;
- Fuel Processing – Develop fuel processing technologies that will meet application requirements such as zero water addition, space and volume constraints, and transient capability;
- Power Electronics – Optimizes fuel cell power system efficiency and cost in conversion of fuel cell output to usable DC (direct current) and AC (alternating current) power;
- Modeling and Simulation – Creates design models to determine a reliable operating space and guide manufacturing; and
- Balance of Plant – Focuses on high temperature heat exchangers and blowers to enable achieving high efficiency, low cost, and a simple system.

SECA Fuel Cell Coal-Based Systems: To address the issue of scalability and incorporation into IGCC plants, DOE integrated the SECA Cost Reduction activities with the SECA Coal-Based Systems program. The goal of this program element is to develop and demonstrate the fuel cell technology required for central power stations and provide a power block to FutureGen. It leverages the advances made in SOFC cost reduction and technology under the SECA program by extending that technology to large central power generation. Three Industry Teams will transition their SECA cost reduction projects into SECA coal-based systems projects and develop systems for fuel cell incorporation into an IGCC plant. All SECA Industry Teams will continue SECA cost reduction activities through 2010 with the best fuel cell stacks available for delivery to FutureGen. It is anticipated that the best technology from any Industry Team will be available for incorporation into one or more of the SECA coal-based systems projects in preparation for operation at FutureGen.

Fuel Cell Systems: The Hybrids program has provided research advances in fuel cell systems by linking technologies in a common system to generate electricity from coal syngas at high efficiencies. Power systems that contain a combination of high-temperature fuel cells and integrated heat recovery devices (e.g., gas turbines, steam generators, and Stirling engines) have the potential for ultrahigh efficiency in converting fossil fuels to electricity. The total efficiency of a hybrid system can in principle be raised to greater than 70 percent (55% demonstrated in small size), while NOx emissions are essentially eliminated. Carbon dioxide reduction is also facilitated through increased efficiency and capture. The inherent ability to keep the fuel and air streams of the fuel cell separated while producing power makes carbon capture a particularly simple process.

Advanced Research: The High Temperature Electrochemistry Center (HiTEC) was formed in 2004 to provide crosscutting, multidisciplinary research that leads to advanced electrochemical technologies minimizing the environmental consequences of using fossil fuels in energy generation. HiTEC supports future advances in the SECA and Office of Fossil Energy Coal and Power programs by developing novel electrochemical energy-conversion and integrated technologies that advance the efficiency, reliability, and cost goals of fuel cell systems beyond what can be accomplished in the next five to ten years.

FY 2006 Key Program Accomplishments

SECA Cost Reduction: The Power of a Goal

The SECA program's Industry Teams are hard at work on the design and manufacture of a variety of low-cost fuel cell prototypes. Recent testing of these prototypes has demonstrated giant leaps made toward fuel cell commercialization. Manufactured with a scalable mass-production technique, these SOFC prototypes have exceeded all of SECA's Phase I targets for availability, efficiency, endurance, and cost. Representative data include an availability of 90 percent, over and above the SECA Phase I target of 80 percent, and an efficiency of 41 percent in a 5.4 kW system, surpassing the first SECA target of 35 percent. The demonstrated superior efficiency in this small size confirms the ability to achieve much higher efficiencies in larger systems. And most significant of all, the $746/kW system cost is well on its way to $400/kW by 2010.

2006 Annual SECA Workshop and Peer Review Held in Philadelphia, Pennsylvania

The SECA program held its annual workshop, including a peer review, during September 12-14, 2006, in Philadelphia, Pennsylvania. Principal Investigators of 26 projects provided presentations/oral briefings. A panel of independent technical experts covering all aspects of fuel cell technologies conducted peer reviews of all the presented projects. The findings and recommendations of the peer reviewers will be used by the project managers to guide their future work and by the Technology Development Manager at DOE to make programmatic and funding decisions for the upcoming fiscal years. The workshop proceedings and the peer review report will be found on the program's website at http://www.netl.doe.gov/seca/.

Summary

SECA has surpassed its first set of cost reduction targets providing strong confidence in the 2010 $400/kW goal. By developing fuel cells to operate cost-effectively on coal gas as well as natural gas, bio-fuels, diesel, and hydrogen, it is building a bridge to the hydrogen economy while solving today's environmental, climate change, and fuel availability issues. The once distant vision of using clean, low-cost fuel cell technology for everyday applications is now within reach.

As these progress reports show, the SECA program is on track to meet its goals of producing efficient, affordable, low-emission, and robust fuel cells that are able to operate using the current fuel production and distribution infrastructure. The combination of basic R&D and application of the new technologies developed by the Industry Teams is proving to be highly effective. The fuel cell technology being developed by SECA has application to residential and commercial power, industrial combined heat and power, transportation APUs, and the primary goal of mega-watt scale units for advanced power plants using coal with high efficiency, carbon capture, and very low emissions. These advances will permit the production of power from coal in any state in the U.S. without environmental concern, ensuring a secure and economical energy future.

II. SECA COST REDUCTION

II.1 Development of a Low Cost 10 kW Tubular SOFC Power System

Objectives

- Design of a common low cost generator to meet all chosen markets.
- Development of an anode supported micro-tubular cell capable of twice the power density presently achieved.
- Design, build, and test an inverter with 94% efficiency for conversion of DC to AC electricity.
- Prototype testing of a natural gas fueled unit meeting and exceeding SECA Phase I goals.

Accomplishments

- **Successful Fabrication and Testing of a Closed End Isopressed Anode Tube:** Anode tubes, presently fabricated by extrusion, have been manufactured through isostatic pressing containing an integral closed end. Successful completion of this development allows the reduction in the number of steps required to make an anode tube from four to one significantly decreasing cost. This process also decreases the total manufacturing operation by removing the need for a metallic braze cap presently used to form a closed end.
- **Exceed 250 mW/cm^2 on Multiple Interconnection Cells:** A number of multiple interconnection cells have been manufactured achieving >250 mW/cm^2. This increases the average value from 120 mW/cm^2 thereby cutting the required number of cells in half for the same power level as well as cutting cost in half.
- **Demonstrate a Tubular SOFC Achieving >60 W/tube:** Further advancements in larger diameter tube technology and multiple take-off connections have been integrated into a single cell design. Previous advancements in isopressing technology have also been incorporated. These advancements take the single cell power from 5 W/tube at the start of the SECA program to >60 W/tube.
- **Cell Testing Exceeds 13,000 hours of Operation:** Cells that have been on test for 12,253 hours (59 thermal cycles) and 13,429 hours (70 thermal cycles) have been taken off test for analysis. These cells operated at or above 75% fuel utilization for the entirety of the test achieving high efficiency. The results of this post-test analysis will be used to enhance further generations of anode supported SOFCs.
- **Ceramic Interconnection Stack Test Exceeds 2,400 hours of Operation:** The first small stack test incorporating ceramic interconnections has exceeded 2,400 hours of operation and completed thirteen thermal cycles. To date, there has been no noticeable power degradation.
- **Prototype Assembly:** A prototype system has been partially fabricated to complete SECA Phase I testing. This system incorporates the latest cell technology advancements as well as generator and balance of plant (BOP) enhancements. The unit will be tested in the next few months according to the outlined SECA test plan.

Norman Bessette
Acumentrics Corporation
20 Southwest Park
Westwood, MA 02090
Phone: (781) 461-8251; Fax: (781) 461-8033
E-mail: nbessette@acumentrics.com

DOE Project Manager: Heather Quedenfeld
Phone: (412) 386-5781
E-mail: Heather.Quedenfeld@netl.doe.gov

Introduction

The Acumentrics SECA project has focused on the design and manufacture of micro-tubular SOFC power systems approaching twice the power density now achieved from state-of-the-art anode supported tubular designs. Based upon DOE funding and a focused research effort, these cells are now very near to achieving this goal. These units will be capable of entry into the telecommunication, remote residential, and military markets. Operation on fuels including natural gas and propane will be developed for the telecommunication and remote residential markets. Operation on liquid fuels, including diesel and JP-8, will be developed for the military markets.

Working with Acumentrics to define market segments and market requirements are a number of key investors that are strategic players in their respective markets. They include:

- Chevron Texaco for remote markets and liquid fuels.
- General Dynamics for liquid fuels as well as military operations.
- Northeast Utilities and NiSource for integration in the natural gas and electricity infrastructure.
- Sumitomo Corporation of Japan for introduction and product definition into the Japanese market.

Approach

To achieve the final SECA goal of a manufactured unit cost of less than $400/kW, work can focus on increasing cell power thereby decreasing the number of cells per kilowatt or decreasing the cost of each component. With such an aggressive goal, work must focus on both paths. To increase cell power, work is centered on improved materials as well as enhancements in geometry. Cells with increased anode conductivities to decrease electrical bus losses are being investigated. Improved conductivity of cathodes is also being investigated to decrease the potential loss associated with the electrochemical reaction on the air side. Increases in cell tube diameter as well as multiple contact points along the length are also being studied.

For subsystem cost reductions, the machine is divided into four major sub-systems: the SOFC generator, the control system, the power conditioning system, and the fuel and airflow system. In the SOFC generator, advanced materials and manufacturing techniques are being investigated including metal injection molding (MIM) as well as metal stampings. Vacuum cast insulation to near net shape is also being considered. For the control system, a controller area network bus (CANBUS) architecture is being developed as well as integration of control of all valves and power electronics. For the power electronics sub-system, the focus is on improving the overall DC/AC conversion efficiency to avoid excessive losses which compromise overall system efficiency and require more cells and therefore more cost. In the air and fuel sub-system, removal of redundant components as well as qualification of equivalent components at lower cost is the path chosen.

Results

Single Cell Power

In the past fiscal year, substantial advancements have been made in increasing individual cell power. To achieve the Phase III SECA goal of <$400/kW, continual strides must be made in cell power to reduce the number of cells as well as overall size of the machine. By decreasing size and weight, there is a direct relationship with overall cost at high volumes. Figure 1 shows the progress in increasing the power/tube from the Acumentrics anode supported cell. The lower curves, achieved in the 2002 to 2003 timeframe, show a cell with a peak power of 7-15 W/tube. In the late 2005 timeframe, power was enhanced to >60 W/tube representing a 4-8x increase in power from a single tube. What is also worth noting is that the same number of manufacturing steps is required for the 7 W tube as those needed for a 60 W tube.

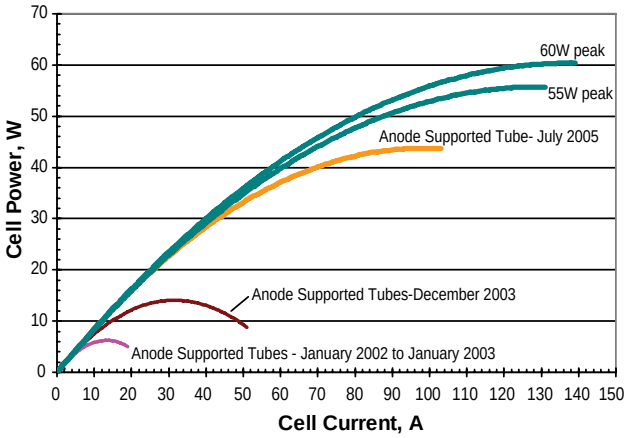

FIGURE 1. Single Cell Power Evolution

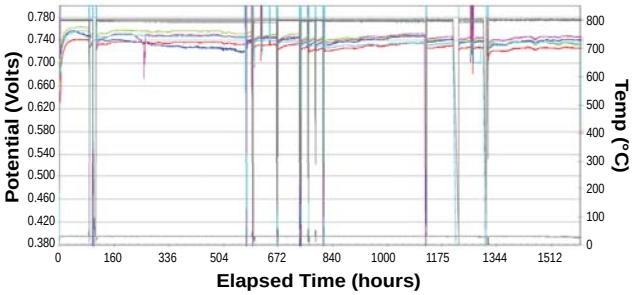

FIGURE 2. Single Cell Performance Stability

Performance stability of these latest high power cells has also been improved from those of the 2002 pre-SECA stage. Figure 2 shows a voltage versus time plot for a group of five cells from the latest generation of multiple interconnection cells. The plot shows that for operating times exceeding 1,500 hours, the degradation of these cells is well below the SECA Phase I and II goals of <2% and <1%/500 hours and approaching that of <0.1%/500 hours for Phase III. What should be noted is that these operating times are nearing the requirements for stand-by or peaking generators which would be needed for 100 kW+ machines to offset high demand loads. Cells of this vintage have now been tested for >4,000 hours with very stable performance and will continue to validate the requirements of 40,000 hours for continuous duty machines.

Stack Performance

In addition to substantial strides in cell performance, significant progress has been made in stack performance. To complete the SECA Phase I machine testing, the unit must complete >1,500 hours of operation with >80% availability, >35% efficiency, and <4%/1,000 hours degradation. To validate the

Acumentrics design, a 24-cell stack was tested under the Phase I test conditions to assure that these conditions could be met. Figure 3 shows the performance timeline for this stack for a greater than 2,000-hour run. As can be seen in the figure, the unit ran for greater than 1,900 hours and achieved an availability of >88%. A peak efficiency of 35.2% was achieved and a degradation of 1.2%/1,000 hours was achieved. Based upon these results, Acumentrics is confident in their ability to pass the SECA Phase I performance goals.

Generator Design

Work has continued in cost reduction of the generator design with the goal of a simple system to site and operate requiring a minimal amount of site services. Figure 4 shows the existing system capable of achieving >5 kW electrical output. This system is mounted in a NEMA 3R cabinet for outdoor installation with two separate cabinet spaces: one for the fuel cell generator and gaseous balance of plant components and the other for the electrical and control devices. Progress has been made in advancing both metallic and ceramic recuperators for thermal recovery on the SOFC stack side as well as cost and power reduction on the valve and blower components. All of these improvements reduce the parasitic load thereby increasing the overall net electrical output. On the electrical side, the integration of a >98% efficient DC/DC converter as well as a >94% DC/AC inverter has been progressing. This unit will be packaged and integrated into the existing machine in the next fiscal year.

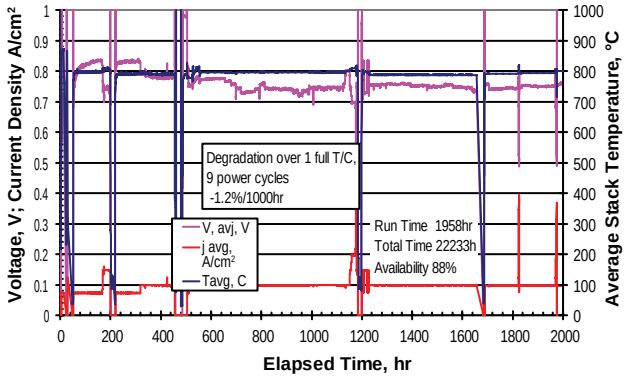

FIGURE 3. SOFC Stack Performance Stability

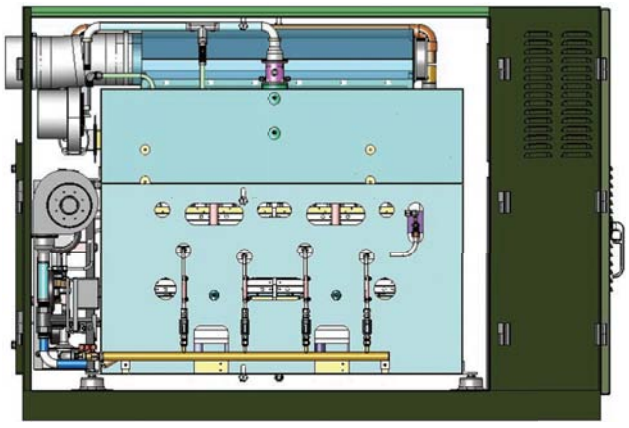

FIGURE 4. Generator Configuration

Conclusions and Future Directions

Continual advancements have been made toward the SECA cost and performance targets in the Acumentrics' SOFC project. These advancements can be summed as:

- Cell power densities exceeding 250 mW/cm^2 or 2x greater than previous technology.
- Individual cell power exceeding 60 W/tube or 4-8x previous limits.
- Stack stabilities with slightly over 1%/1,000 hour degradation or only 30% of the SECA allowable target.
- Generator design with significant size and weight reductions over pre-SECA designs well suited for mass production.

The following activities are planned to futher advance progress toward the SECA targets:

- **Complete SECA Phase I Generator Performance Testing:** The SECA Phase I generator is nearing completion of manufacture. The test plan is near final review between Acumentrics and the DOE project manager. The unit will then be tested according to this plan.
- **Complete 95% Efficient Inverter Development:** By demonstrating the integration of an inverter capable of over 95% efficiency versus the market standard of 82-90%, overall system efficiencies can rise by nearly 5 percentage points. This improvement in overall efficiency can be taken as fuel savings to reduce the overall cost of electricity (COE). Another option is to operate the fuel cell stack at a lower cell voltage point thereby increasing the individual cell power requiring fewer fuel cells and less overall capital cost.
- **Complete Preliminary Testing on Liquid Fuels and Integration with an SOFC Stack:** Preliminary tests on liquid fuel delivery to single SOFC tubes has been completed in the past with good success. To further evolve to a complete machine, existing reformer technology for liquid fuels will be integrated with an SOFC stack to determine issues such as thermal balance, flow distribution,

and potential carbon formation. These results will be used to successfully design a complete system capable of operation on commercially available liquid fuels.

FY 2006 Publications/Presentations

1. "Status of the Acumentrics SOFC Program", N.F. Bessette, Presented at the 2005 Fuel Cell Seminar, Palm Springs, CA, November 16, 2005.

II.2 10 kW Solid Oxide Fuel Cell Power System Commercialization

Objectives

- Demonstrate SOFC stacks that achieve target performance, stability, and cost.
- Develop a waterless catalytic partial oxidation (CPOX) or zero net water autothermal reforming process that efficiently and cost effectively converts ultra-low sulfur diesel fuel (ULSD) into a hydrogen-rich synthesis gas for mobile applications.
- Develop a SOFC hot box (an insulated enclosure containing SOFC stacks, manifolds, heat exchangers, start-up burner, and reformer) design that is compact and can be mass-produced at a cost meeting the SECA Phase 1 cost target.
- Design and develop a SOFC system balance of plant (BOP), including air and fuel supply systems, that meets the cost and reliability targets.
- Demonstrate a control system to manage the SOFC power system, including regulation of fuel and air flows, management of electrical power generation, and load sharing. The control system must operate in conjunction with an energy storage system through start-up, steady-state and transient loads, and shut-down including emergency shut-down without damage to the SOFC stack.
- Demonstrate an efficient electrical power conditioning system to convert DC voltages and invert to produce useable AC output.

Accomplishments

- Redox tolerance of a cell has been improved as compared to a standard cell through the use of modified materials and thermal processing. This reduces redox degradation by more than 50%.
- A sulfur-tolerant anode was proposed, constructed and tested with target levels of H_2S addition with promising results. Further investigation will be conducted to confirm the mechanism and validate the results.
- A baseline compressive seal has been reformulated to improve compliance in stack assembly. These improved seals achieved compression targets as the design intended, and have been tested with single cell, short and tall stacks with positive results.
- Control hardware and software have been developed to provide steady-state and transient control of a SOFC system.
- The Phase 1 deliverable prototype BOP, including air and fuel supply systems, is nearing completion and scheduled to begin testing in August.
- Significant progress in identifying, characterizing, and applying cost-effective BOP utilizing high volume, low cost, mass production components from industrial and automotive sources.

Daniel Norrick
Cummins Power Generation
1400 73rd Avenue NE
Minneapolis, MN 55432
Phone: (763) 574-5301; Fax: (763) 528-7229
E-mail: Daniel.a.norrick@cummins.com

DOE Project Manager: Heather Quedenfeld
Phone: (412) 386-5781
E-mail: Heather.Quedenfeld@netl.doe.gov

Subcontractors:
Versa Power Systems, Inc., Denver, CO

Introduction

Solid oxide fuel cell power systems offer the potential to generate electrical power from hydrogen or hydrocarbon fuels cleanly, quietly, and efficiently. The objective of the Cummins Power Generation (CPG)-Versa Power Systems (VPS) project is to design and develop a 3-10 kW SOFC-based power system that can be competitive with existing small diesel generating systems in terms of cost and package size, but offer significant benefits in efficiency, emissions, and lower noise and vibration. Achieving these objectives requires advancement in five major areas:

1. Cell, interconnect, and SOFC stack performance and robustness.
2. Optimized manufacturing processes for production of cells, interconnects, and stack assemblies.
3. System design, thermal integration, and packaging of the hot components and sub-systems including stacks, fuel reformer, heat exchangers, and insulation system.
4. Control system for regulating air and fuel flows to the stacks in proportion to electrical load and operating temperatures, and for managing electrical load distribution between the fuel cell and batteries during steady-state and transient loading.
5. Electrical power conditioning, including DC voltage boosts (converters) and DC to AC power (inverter).

The team has made significant progress in all five areas during 2006 and is on plan to meet the Phase 1 objectives of the SECA program.

Approach

The CPG-VPS approach coordinates development in a number of major areas, including the development of planar solid oxide fuel cells, metallic interconnects, and stacks as well as parallel development in planar SOFC manufacturing and scale-up for economic manufacturing. Parallel work will focus on development of a diesel fuel reforming system compatible with application requirements, fuel cell BOP, fuel cell and power electronics system controls, and electronic power conditioning.

Specifically, the CPG-VPS team is conducting work to develop and evaluate advanced solid oxide fuel cells that provide the required performance and durability using ULSD reformate. Part of that development requires conducting a progressive sequence of SOFC stack tests to validate development of materials and assembly methods for useable stacks that can achieve high fuel utilization and low degradation rates. In order to support the proposed application, we will develop a diesel reforming process and scale-up the reformer to system sized units, design and develop a hot box subsystem which can be integrated into complete SOFC power systems, and develop control hardware and software required to regulate system operation. Finally, we will integrate the BOP components, hot box subsystem, and controls into a working deliverable prototype, initiate prototype operation with stack simulators to shakedown the system, install fully operable SOFC stacks and conduct operation of the full prototype through the SECA Phase 1 test sequence.

Results

Development work has continued to improve cell performance, primarily through the development of sulfur tolerant electrodes and cells with good performance at reduced methane levels.

CPG demonstrated a high-efficiency inductor-based DC-DC boost system which will be used to control current flow and voltage supply to the inverter section from the fuel cell stacks. The efficiency characteristics of the boost as configured for the Phase 1 deliverable unit are shown in Figure 1. A second transformer-based DC-DC bi-directional boost is developed to provide and regulate a mix of energy flows from the fuel cell and the system's battery pack.

Redox tolerance of a cell has been improved as compared to a standard cell through the use of modified materials and thermal processing. Redox induced degradation has been reduced more than 50% as compared to a standard cell.

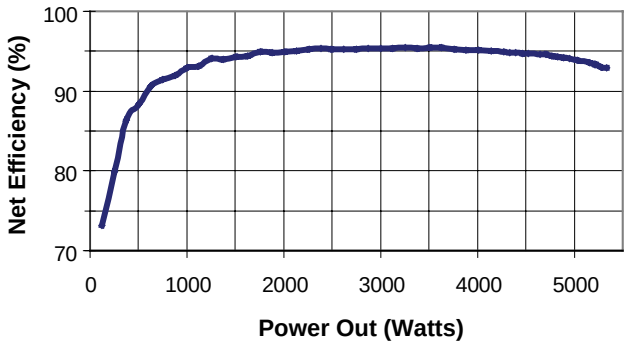

FIGURE 1. Fuel Cell Boost

A sulfur-tolerant anode was proposed, constructed and tested at 1 ppm and 5 ppm by volume H_2S concentration with promising results. Further investigation will be conducted to confirm the mechanism and validate the results.

A baseline production compressive seal has been reformulated to improve compliance in the stack assembly. These improved seals achieved compression targets as the design intended and have been tested in single cells, short and tall stacks with positive results.

Conclusions and Future Directions

Conclusions drawn from work to date include revised cells that exhibit improved tolerance to sulfur. A fully integrated SOFC prototype system is on schedule to demonstrate SECA Phase 1 metrics by the end of 2006. A fully controllable DC-DC boost can be provided at high efficiency consistent with cost targets, and a preliminary commercialization requirements document for SOFC APUs in recreational vehicle and truck applications has been written.

Future directions include work to define and test a solution to allow system start-up, shutdown and operation without purge gas and without stack damage. Work to define and test a solution to allow stacks to run reliably and with low degradation on diesel reformate with up to 5 ppm by volume hydrogen sulfide equivalent in the fuel stream will be conducted, and seals and assembly methods, including cost-effective methods of manufacture, will be developed. Part of that work will involve development of a robust and self-contained stack clamping solution demonstrating progress consistent with mobile applications. Instrumented short stacks and ongoing optimization of materials and stack design will be used to assemble stacks that demonstrate target performance and power degradation rates at design conditions for reformate supply and power.

The team will complete the final tailoring and development of the DC boosts for the fuel cell and battery system, and complete the development and integration of the control system with the fuel cell, BOP, and power electronics.

Culmination of 2006 work will be the SECA Phase 1 evaluation test including steady-state and transient evaluations and reporting results to NETL before making the unit available to NETL, Morgantown for evaluation.

FY 2006 Publications/Presentations

1. Cummins Power Generation SECA Program Phase 1 Results and Experience, Presentation given at the Fuel Cell Seminar 2005, Palm Springs, CA.

II.3 Solid State Energy Conversion Alliance

Objectives

- Develop a 3-5 kW SOFC power system for a range of fuels and applications.
- Develop and demonstrate technology transfer efforts on a 3-10 kW stationary distributed power generation system that incorporates endothermic reforming of methane, and then natural gas.
- Initiate development of a 3-5 kW system for future mass-market transportation auxiliary power unit applications, incorporating endothermic reforming of diesel and gasoline.

Accomplishments

- Peak Power Performance-Delphi's SECA demonstration system produced peak power of 4.24 kW on methane, achieving the SECA Phase I goal of 3-10 kW.
- Peak Efficiency-Delphi's system demonstrated a peak efficiency of 37 percent, exceeding the SECA Phase 1 goal of 35 percent.
- Power Degradation-Delphi's demonstration system matched the SECA Phase I durability goal with power degradation of just 7 percent over 1,500 hours of operation.
- Factory Cost-Delphi met the SECA Phase I goal of $800.00 per kW by achieving an estimated $770 per kW.
- Successful fabrication, integration and testing of 30-cell stacks in the SECA Phase I demonstration system.
- Development of a capable reformer was substantially accomplished as the SECA demonstration system reformer design underwent significant systems level durability testing with minimal degradation.
- Delphi's BOP component hardware was fabricated and tested for SECA Phase I. With the commencement of system durability testing, BOP design efforts focused on supporting system hardware builds and maintaining hardware currently on system test. Supplier sourcing activity during this period included identifying future prototype and production suppliers for process air manifolds, and cast integrated component manifolds.

Steven Shaffer
Delphi Automotive Systems
5725 Delphi Drive
Troy, MI 48098-2815
Phone: (585) 359-6615; Fax: (585) 359-6061
Website: www.delphi.com

DOE Project Manager: Heather Quedenfeld
Phone: (412) 386-5781
E-mail: Heather.Quedenfeld@netl.doe.gov

Subcontractors:
Battelle/Pacific Northwest National Laboratory, Richland, WA
Electricore, Inc., Valencia, CA

Introduction

Delphi has been developing SOFC systems since 1999. After demonstrating its first generation SOFC power system in 2001, Delphi teamed with Battelle under the SECA program to improve the basic cell and stack technology, while Delphi developed the system integration, system packaging and assembly, heat exchanger, fuel reformer, and power conditioning and control electronics, along with other component technologies. Compared to its first-generation system in 2001, the Delphi-led team has reduced system volume and mass by 75 percent. By January 2005, the Delphi team was able to demonstrate test cells to DOE with power density more than required to meet the SECA 2011 goals.

In addition to its compactness, another key advantage of the SOFC is its high system fuel-efficiency, particularly when its high temperature co-product heat can be used in combination with its high electrical output. For example, SOFCs can be teamed with gas turbines driven by the SOFC's co-product heat to potentially generate power at 55 percent to 80 percent thermal efficiency (depending on scale and fuel used). This is significantly more efficient than today's typical coal-fueled power plant thermal efficiency of 35 percent to 40 percent. By co-generating power on-site at industrial facilities, commercial businesses, or even residences, the SOFC's high-grade co-product heat will enable up to 90 percent efficiency in distributed, combined heat and electrical power (CHP) generation. Similarly, heavy-duty trucks will be able to utilize SOFC auxiliary power systems for both heat and electrical power when parked, to save 85 percent of the fuel that today they consume when idling their main engine, and likewise reduce idling emissions.

While size and efficiency advantages are important for many potential applications, the SOFC's most significant advantage overall is its very broad applicability due to its inherent fuel-flexibility. With relatively small changes, SOFC systems can potentially operate on a full range of conventional and alternative fuels.

Approach

Delphi utilized a staged approach to develop a modular solid oxide fuel cell (SOFC) system for a range of fuels and applications including:

- Develop and test major subsystems and individual components as building blocks for applications in targeted markets.
- Integrate major subsystems and individual components into a "close-coupled" architecture for integrated bench testing.
- Integrate major subsystems and individual components into a stationary power unit (SPU) for the stationary market.
- Integrate major subsystems and individual components into an auxiliary power unit (APU) for the transportation market.

Results

To achieve the objectives of DOE/SECA Phase I, the Delphi effort focused on the performance testing and final system development to support Delphi's SECA Phase I demonstration tests. The SECA Phase I demonstration system was able to produce 4.2 kW net electric power output at greater than 35% fuel-to-electric system efficiency. The system met the 1,500 hour durability target including one full-thermal cycle at better than 99% operational availability. Delphi was also able to meet the cost target for Phase I of $800 per kW by achieving an estimated $770 per kW. All of these deliverables were achieved with a highly integrated system design weighing in at 85 kg (39 kg/kW), and with a package volume of 65 liters (30 liters/kW). Achieving these Phase I deliverables was the result of system design and integration efforts performed during Phase I, most notably:

- Delphi demonstrated cell power density in a 30-cell stack assembly of 700 mW/cm^2 at greater than 0.7 V/cell at operating conditions of 750°C nominal stack temperature, and simulated natural gas reformate fuel with greater than 60% utilization resulting in total power of 2.2 kW for the 30-cell stack. The complete stack assembly has a mass of 9 kg and volume of 2.5 liters for a mass specific power density of less than 4 kg/kW and volumetric power density of more than 0.9 kW/l.
- High efficiency fuel reforming strategy encompassing both internal reforming of methane gas in the SOFC stack and anode tail-gas recycle. This provided efficient thermal management of the SOFC stack, as well as effective fuel processing efficiencies which resulted in high system efficiencies.
- High reliability fuel reformer, SOFC stack, process air blower, electronic controller and electronic subsystems, sensors and actuators were developed. Delphi's dedication to integration and leverage of reliable automotive technology allowed for excellent durability performance.
- MATLAB/Simulink-based control software with rapid auto-code generation capability was utilized to enable a rapid software development process and the opportunity for many design iterations allowed for deployment and optimization of new technology in an efficient manner.

The SOFC system development effort during Phase I benefited from the experience and lessons-learned from several design generations of hardware. The current design is shown in Figures 1-3.

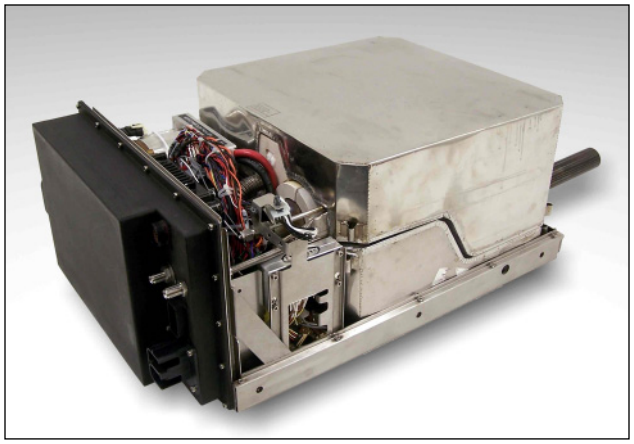

FIGURE 1. Delphi SOFC Uncovered with Insulation

FIGURE 2. Delphi SOFC Covered Complete

One of the key achievements in stack development has been the successful fabrication and testing of 30-cell stack modules for integration into the system. The 30-cell stacks have produced power greater than 2 kW each. Figure 4 shows the Delphi 30-cell stack.

With the commencement of system durability testing, BOP engineering efforts focused on supporting system hardware builds and maintaining hardware currently on test. Supplier sourcing activity during this period included identifying future prototype and production suppliers for process air manifolds, cast integrated component manifolds, composite insulation shells, and a new generation mass air flow sensor. Coating tests for cathode heat exchangers were completed and resulted in the optimization of the Vapor Phase Aluminizing process at Delphi's coating supplier.

A multi-point fuel delivery system for gaseous fuels was refined and produced in small quantities in order to execute system level testing. Further development of the endothermic reformer was carried out resulting in initial recycle-based reforming performance that met system requirements.

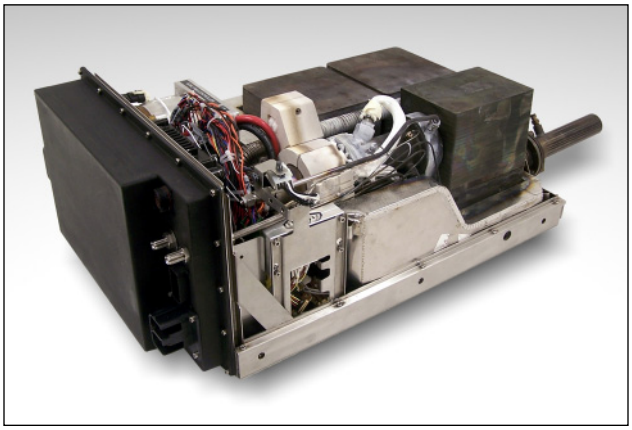

FIGURE 3. Delphi SOFC Uncovered with Application Interface Module

FIGURE 4. Delphi 30 Cell Stack

Conclusions and Future Directions

- Phase I SECA objectives have been met for power rating, efficiency, durability and cost.
- Improvements to reformer substrate and washcoat thermal stability permitted rigorous durability tests to surpass 2,500 hours of operation.
- Develop capability to operate using pipeline natural gas with fuel desulfurizer.
- Work on Phase II SECA requirements has begun.
- Continue materials development for improving cells, interconnects and seals.
- Continue work on increasing durability and capability to withstand more thermal cycles.
- Ultimately, the SECA Phase III goals are to deliver an SOFC power system capable of 40 percent or greater efficiency at a factory cost of $400 per kilowatt.

Special Recognitions & Awards/Patents Issued

1. Patents issued: The US Patent Office Grant Numbers: 7008709, 7025903, 6984466, 6974646, 7001682, 1376725, 6967064, 7008715, 6989211, 1387427, 7001685, 7008716

FY 2006 Publications/Presentations

1. November 2005: 2005 Fuel Cell Seminar in Palm Springs, CA., SOFC Stack and System Development: Latest Results, Steven Shaffer, Dr. Subhasish Mukerjee, Sean Kelly, Delphi Corporation.

II.4 SECA Solid Oxide Fuel Cell Power Plant System Cost Reduction

Objectives

Specific cost-related objectives for this project include:

- Scale up existing SOFC cell area and stack size (number of cells) within a building block unit and stack tower to minimize cost.
- Scale up existing manufacturing infrastructure and capabilities for SOFC cell and stack production on a cost-effective basis.
- Increase SOFC cell and stack performance to maximize power and efficiency for reduced cost on a per kilowatt basis.
- Power block unit system cost goal is to be <$400/kW.

Approach

The project is organized in three phases according to schedule, technical and cost objectives. Following is a short description of the approach as it relates to cost:

- Phase I of the DOE-managed SECA program will focus on cell and stack development activities. This will include scale up of existing SOFC cell area and stack size (number of cells) and performance improvements. The Phase I deliverable for the 3-10 kW development project will be test demonstration of a 3 kW power block system that meets all DOE performance and cost metrics. This includes demonstration of system peak power performance that will be used as the basis for cost. The DOE specified metric for the Phase I 10 kW system factory cost must be less than $800/kWe. The Phase I deliverable for the Coal-Based, large-scale SOFC project will be a test demonstration of a representative SOFC stack building block unit on simulated coal syngas. The system cost, exclusive of the coal gasification and CO_2 separation subsystems, must be $600/kWe or less at the end of the Phase I project.
- Phase II of the Coal-Based project will focus on modularization of the Phase I stack building block units into MW-size modules. Detailed design engineering and analysis for multi-MW power plant systems will be conducted. The Phase II deliverable will be a test demonstration of a MW-size representative SOFC stack module on simulated coal syngas. Phase II system cost, exclusive of the coal gasification and CO_2 separation subsystems, must be $400/kWe or less at the end of Phase II, and is applicable to both the baseline (>100 MWe) system and the proposed Phase III proof-of-concept system. The cost estimate must establish and fully justify a reasonable estimate of the number of systems and their respective size that must be manufactured per year to support this cost goal. An independent audit of the Phase II cost report will be required.
- Phase III of the Coal-Based project will focus on design and fabrication of a proof-of-concept multi-MW power plant including turbine for high efficiency and CO_2 separation for low emissions. Phase III system cost objectives are the same as in Phase II. The Phase III deliverable will be long-term testing of a multi-MW size power plant at a site selected for FutureGen.

Jody Doyon
Vice President, Government Programs Administration
Fuel Cell Energy, Inc.
3 Great Pasture Road
Danbury, CT 06813
Website: www.fce.com
Phone: (203) 825-6125
E-mail: jdoyon@fce.com

DOE Project Manager: Travis Shultz
Phone: (304) 285-1370
E-mail: Travis.Shultz@netl.doe.gov

Subcontractor:
Versa Power Systems Inc.
900 18th Street, Suite 130
Golden, CO 80401-1887
Website: www.versa-power.com

Accomplishments

- Increased SOFC cell area and number of cells per stack building block unit resulting in ~5-fold increase in stack volumetric power output from early generation stacks units.
- Completed SECA Phase I 3 kW SOFC stack and system test demonstration validating performance of the scaled-up components. This test validation included successful demonstration at the peak power performance used to calculate system cost.
- Developed preliminary factory cost bill-of-materials (BOM) for stack and 3 kW system for DOE third party audit validation. Estimated stack and system costs for the 3 kW unit meets DOE metric for the Phase I project.

Introduction

Fuel Cell Energy, Inc. (FCE) has been engaged in a Department of Energy (DOE)-managed SECA Phase I project to develop a 3-10 kW SOFC power plant system since April, 2003. FCE has recently been selected by DOE to participate in a multi-phase project for development of very efficient coal to electricity, large scale (multi-MW) power plants with near zero-emissions. This new project's technical objectives will be merged with the existing 3-10 kW project's Phase I technical objectives based on similarities for cell and stack development. The primary objectives of these projects are to develop affordable, SOFC based power plant systems with high efficiency that are cost competitive with other power generating technologies of similar capacity without incentive funding support. In order to be cost competitive with other power generating technologies of similar capacity without the need for incentive funding programs, significant SOFC stack and system cost reduction must occur from the current low volume development level to high volume, mass production prices. The achievement of the program cost targets is a key facet of the SECA projects. FCE is ideally suited for these projects based on experience with cost reduction successes for their commercial fuel cell power plants now being installed worldwide. FCE will use the cell and stack design of their SOFC technology partner, Versa Power Systems, Inc (VPS) as the basis for these projects. VPS has been actively engaged in cost effective SOFC manufacturing process research and development since 1998 and has well establish processes, quality procedures and equipment for the manufacture of small to intermediate size cells and stacks as depicted in Figure 1. The DOE-specified metric for the final program system cost determined to be competitive with other power generating technologies of similar capacity without incentive funding is <$400/kW for a multi-MW power plant, exclusive of coal gasification and CO_2 separation subsystem costs.

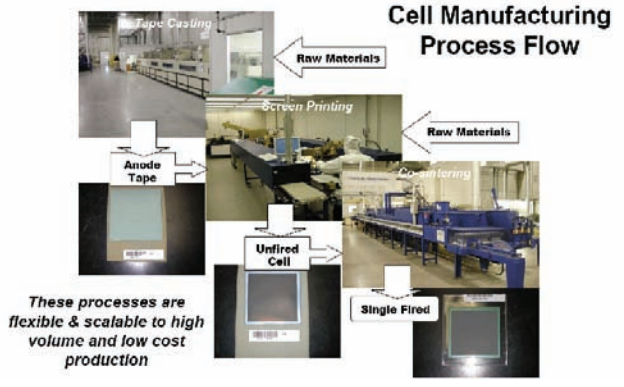

FIGURE 1. Versa Power Systems SOFC Manufacturing

Approach

The path forward for development of cost competitive SOFC power block systems includes a multi-faceted approach for both SOFC stack module design as well as system balance-of-plant (BOP) development. The technical approach consists of an innovative fuel cell stack configuration, fabrication of scaled-up cells, newly developed fuel cell seals, novel implementation of a fuel cell clustering concept and integration of SOFC clusters with a gas turbine. The future development plans include investigation of both fabrication and operational issues related to scale-up of the fuel cell active area. For the Coal-Based project, an innovative and patented power cycle will be utilized to achieve very high efficiencies by integration of the fuel cell with an indirectly heated gas turbine. The power plant design is projected to have a factory cost of $400/kW, based on a production capacity of about 1.4 GW/year or twelve 120 MW power plants per year. This cost is very competitive with today's cost of combined cycle technologies.

The project is organized in three phases according to schedule, technical and cost objectives. Details for the three phases are as follows:

- Phase I (2-3 years):
  - Scale up SOFC cell area and stack height (number of cells) and improve performance.
  - Design a baseline system that meets the project technical objectives.
  - Ensure stack and power plant designs are consistent with a projected cost of $800/kW for the 10 kW development project, and $600/kW for the large scale Coal-Based project.
  - Fabricate and validation test representative stack building block units under simulated commercial operational conditions.
- Phase II (2 years):
  - Develop a detailed design and cost analysis for the proposed power plant system that meets project objectives.
  - Ensure stack and power plant design are consistent with a projected cost of $400/kW for a multi-MW system (exclusive of coal gasification and CO_2 separation subsystem costs) for the Coal-Based project.
  - Fabricate and validation test a representative fuel cell module building block unit for the multi-MW power plant on simulated coal syngas.
- Phase II (5 years):
  - Complete detailed design for multi-MW power plant system that meets project performance and cost objectives. Cost objectives are the same as in Phase II.

- Procure and fabricate SOFC stack and system components and assemble proof-of-concept multi-MW power plant system including gas turbine (>1 MW).
- Locate coal gasifier site and integrate multi-MW power plant.
- Conduct long-term (~25,000 hours) test demonstration of multi-MW power plant system on coal based syngas meeting project technical objectives for performance (power, efficiency), durability (load transients and thermal cycles), degradation and cost.

Results

FCE has been engaged in a DOE-managed SECA Phase I project to develop a 3-10 kW SOFC power plant system since April, 2003. Much progress has been made in the SECA Phase I project on cell and stack scale-up, increased performance and cost reduction. A detail factory cost estimate analysis and report for a 3-10 kW stack and system was submitted and audited by DOE selected auditors. Results indicate the total 3-10 kW system cost estimated to be $773/kW based upon an annual production rate of 50,000 units and a peak power rating of 5.37 kW. This is less than the SECA Phase I metric of $800/kW using the same assumptions. As shown in Figure 2, the stack accounts for ~16% of the total system cost, while the BOP components account for ~73% of the cost. The remainder of the system cost (~11%) is associated with building, commissioning and testing (BC&T) of the power block unit. The low cost associated with the stack reflects the many years of process development and cost reduction activities at VPS. The current cell manufacturing process has three major fabrication operations for anode-supported planar cells: tape casting, screen-printing and co-firing (TSC) as shown in Figure 1. The TSC process is a fully integrated cell manufacturing process. Major process improvements have resulted in reduced process steps (number of sinter firings) with an associated reduction in costs. Figure 3 shows that such process improvements have resulted in ~65% cost reduction while overall yields have improved by ~40%. All major manufacturing and process steps have been demonstrated to be cost-effective by the semiconductor packaging and multi-layer capacitor industries. The TSC process can be further engineered into repeatable mass manufacturing modules for additional product cost savings. Economies of scale and automation will provide the greatest effect on cell equipment cost. Scale-up of SOFC cell area and number of cells per building block unit was continued in the SECA Phase I project, culminating in an approximate 5-fold increase in stack volumetric power density as shown in Figure 4. Technology developments that result in decreased material usage have also contributed significantly to reduced cell component cost. Figure 5 shows a 51% cost savings attributed to decreasing the thickness of the SOFC active cell component. While the majority of the system cost is associated with the BOP,

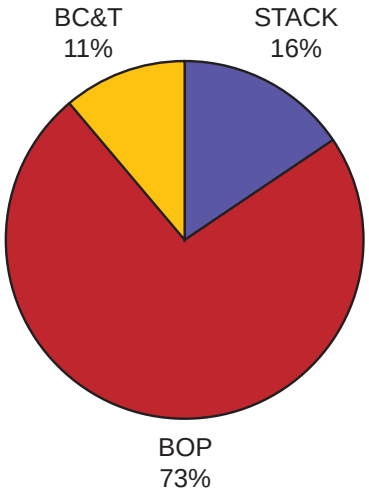

FIGURE 2. SECA Phase I 3-10 kW SOFC System Costs Breakdown

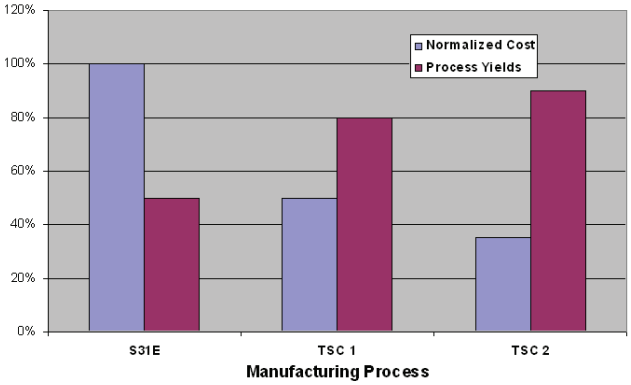

FIGURE 3. SOFC Cell Manufacturing Process Improvements

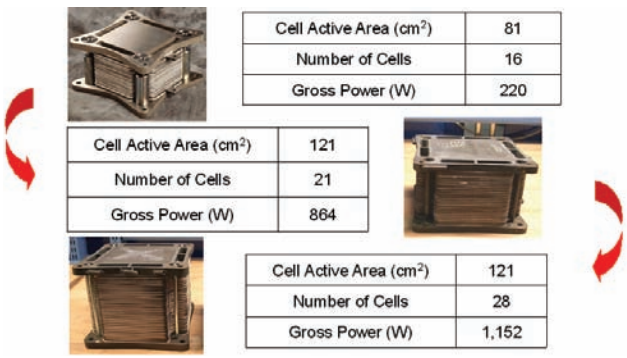

FIGURE 4. SOFC Scale-Up SECA Phase I Program Accomplishments

this is the area that presents the greatest opportunity for further cost reduction. Greater than 75% of the BOP costs are procured components. Once a design configuration is stabilized to enable volume pricing, multiple vendor sourcing is established and value-engineering programs are in play, it is anticipated that significant cost savings (>50%) will be realized. As the power plant size becomes larger, the BOP and associated costs will also diminish proportionally on a cost-per-kilowatt basis. This provides the greatest cost reduction opportunity for the Coal-Based, multi-MW sized power plants to be developed in the new program. Finally, technology improvements focused on enhanced cell power output will be a major driver in reducing power plant system costs. Figure 6 presents improvements in cell power density output on a normalized basis developed by VPS over the years and continued in the SECA Phase I project. As can be seen, ~2-fold increase in power density is expected over the current state-of-the-art technology for the pre-commercial power block units. This peak power performance operation was demonstrated with the SECA phase I, 3 kW system test. The high power density operation was executed at the end of the 3-1 system test period, with stacks that had operated for greater than 2,000 hours including multiple load transients and thermal cycles providing confidence in achieving this milestone performance goal.

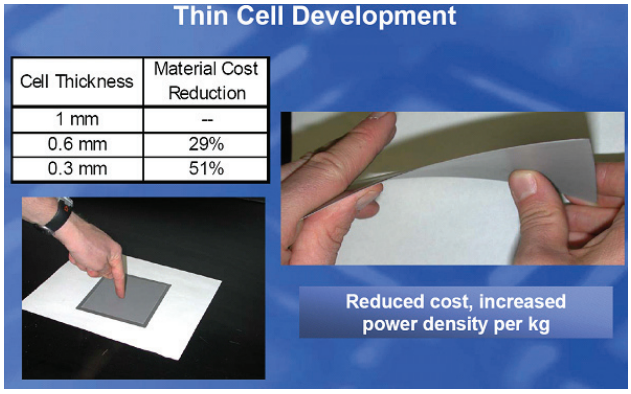

FIGURE 5. SOFC Cell Thickness and Material Reduction

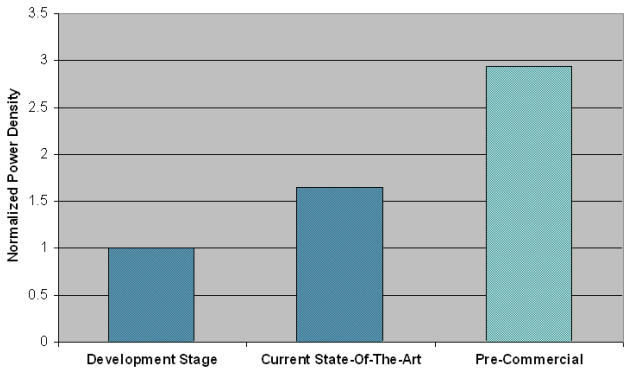

FIGURE 6. SECA 3kW SOFC Cell Performance Improvement

Summary

- FCE has been engaged in a DOE-managed SECA Phase I project to develop a 3-10 kW SOFC power plant system since April, 2003. FCE has recently been selected by DOE to participate in a multi-phase project for development of very efficient, large scale (multi-MW) coal to electricity power plants with near zero-emissions with similar SOFC cell and stack development and cost objectives.
- The primary objectives of these projects are to develop affordable, SOFC-based power plant systems with high efficiency that are cost-competitive with other power generating technologies of similar capacity without incentive funding support.
- FCE is ideally suited for these projects based on their cost reduction experience with commercial fuel cell power plants now being installed worldwide and the successes of their SOFC technology partner, VPS, with SOFC cell and stack manufacturing development and operational performance.
- Accomplishments in FCE's SECA 3-10 kW development Phase I project include expanded manufacturing process capabilities, scale-up of SOFC cell area and stack height and improved performance resulting in ~5-fold increase in volumetric power density.
- Completed SECA Phase I 3 kW SOFC test demonstration of a system that contained scaled-up cell and stack units as final validation of the scale-up process and components. Peak power performance was demonstrated that will be used for the cost of electricity basis.
- The FCE team developed a preliminary factory cost bill-of-materials (BOM) for stack and 3 kW system to be audited by DOE third party expert. Stack and system costs are below SECA Phase I program requirements.

FY 2006 Publications/Presentations

1. "Coal Based Large SOFC/T Systems", H. Ghezel-Ayagh, J. Doyon, Fuel Cell Energy Inc. Paper presented at the 2006 Fuel Cell Seminar on November 13-17, 2006, Honolulu, Hawaii.

2. "Development of Solid Oxide Fuel Cells at Versa Power Systems", B. Borglum, E. Tang, M. Pastula, J. Kelsall, R. Petri, Versa Power Systems. Paper and presentation at the 2006 Fuel Cell Seminar on November 13-17, 2006, Honolulu, Hawaii.

3. "SOFC Development Status at Versa Power Systems, Inc.", B. Borglum, Versa Power Systems. Presentation at the 2006 Lucerne Fuel Cell Forum, July 4, 2006.

II.5 Solid State Energy Conversion Alliance (SECA) Solid Oxide Fuel Cell Program

Objectives

- Develop a fuel-flexible and modular solid oxide fuel cell (SOFC) system (3 to 10 kW) that can serve as the basis for configuring and creating low-cost, highly efficient, and environmentally benign power plants tailored to specific markets.
- Demonstrate a prototype system of the baseline design with desired cost projections and required operating characteristics (Phase I); assemble and test a packaged system for a selected specified application (Phase II); field test a packaged system for extended periods (Phase III).

Approach

Phase I

- Establish a baseline system concept and analyze its performance characteristics.
- Perform a cost study to estimate system costs.
- Develop a robust, reliable high-performance SOFC stack technology amenable to low-cost manufacturing.
- Develop a fuel processor as a pre-reformer for processing a variety of fuels.
- Evaluate system thermal management to establish a suitable recuperation scheme for the system.
- Develop and implement a flexible control structure incorporating required sensors.
- Identify a flexible low-cost power management subsystem.
- Evaluate component integration.
- Design, assemble and test a prototype system to demonstrate performance meeting the program requirements.

Nguyen Minh (Primary Contact),
Tony Campbell
GE Energy, Hybrid Power Generation Systems
19310 Pacific Gateway Drive
Torrance, CA 90502-1031
Phone: (310) 538-7250; Fax: (310) 538-7204
E-mail: nguyen.minh@ge.com

DOE Project Manager: Travis Shultz
Phone: (304) 285-1370
E-mail: Travis.Shultz@netl.doe.gov

Phase II

- Deliver and test Phase I prototype at NETL.
- Conduct a market study to identify and define a specified application for Phase II.
- Perform system design and analysis to define system configuration and packaging for the selected application.
- Design, manufacture, test, and validate system components and component integration.
- Conduct cost estimate and Design-to-Cost to establish a system cost that meets the Phase II cost goal.
- Assemble and operate a packaged system under required conditions and demonstrate operational characteristics meeting the Phase II requirements.
- Continue technology, engineering, and manufacturing developments for SOFC stacks and balance of plant (BOP) to improve system cost, performance, life, and reliability.

Accomplishments

The major accomplishment is the successful completion of the Phase I prototype testing with the demonstrated performance meeting or exceeding the key Phase I requirements.

- An extensive system build and integration process was conducted to verify/validate/assess the various components and integrated prototype system before the final demonstration testing.
- Demonstration testing was carried out for the prototype. The system demonstrated the performance that met/exceeded the key Phase I minimum requirements. The prototype achieved an efficiency of 41% (vs. 35% requirement) and a degradation rate of 1.8% per 500 hours (vs. <2% per 500 hours requirement). The system operated for 1,720 hours (vs. 1,500 hours requirement) with three thermal cycles (vs. one thermal cycle requirement) and 15 power cycles (vs. nine power cycle requirement). A projected high-volume cost for the system is $724/kW (vs. $800/kW target).
- Phase II of the project has been initiated. Detailed plans and key activities have been developed for Phase II work.

Future Directions

Continue activities defined in the Phase II project plan.

- Deliver a Phase I unit to DOE/NETL.
- Conduct various technology improvement/ advancement activities on the SOFC and the BOP to improve system cost, performance, life, and reliability.
- Design, assemble and test a packaged system under required conditions and demonstrate performance meeting the Phase II requirements.

Introduction

This project focuses on developing a low-cost, high-performance solid oxide fuel cell (SOFC) system suitable for a broad spectrum of power generation applications. The overall objective of the project is to demonstrate a fuel-flexible, modular 3-10 kW system that can be configured to create highly efficient, cost-competitive, and reliable power plants tailored to specific markets. The key features of the SOFC system include a fuel-flexible pre-reformer, a low-cost, high-power-density SOFC stack, integrated thermal management, and suitable control and power management subsystems. When fully developed, the system is expected to meet the projected cost of $400/kW.

Approach

The SOFC system is a stationary power module (3-10 kW) capable of operating on different fuels. The system consists of all the required components for a self-contained unit, including fuel cell stack, fuel processing subsystem, fuel and oxidant delivery subsystem, thermal management subsystem, and various control and regulating devices.

- The SOFC is a compact of anode-supported cells (fabricated by the GE HPGS tape-calendering process) and metallic interconnects. The stack design is based on an advanced concept that maximizes cell active area and minimizes sealing. The fuel cell can operate directly on light hydrocarbon fuels and incorporates materials for high performance at reduced temperatures (<800°C). These characteristics provide a low-cost, fuel-flexible fuel cell suitable for operating under various conditions. The tape calendering process for manufacturing thin-electrolyte, anode-supported cells is a potentially low-cost, mass-customization technique suitable for high-volume production and automation using available commercial equipment.
- The fuel processor is a catalytic reactor that functions as a pre-reformer. The system employs an integrated thermal management approach to utilize byproduct heat and reduce heat losses, and, consequently, increase the overall system efficiency. The system also has a flexible control structure that can be modified or optimized for different applications.

The project consists of three phases. Phase I of the project focuses on developing system components having the required operating characteristics, resolving critical technological issues, and demonstrating a prototype system. The Phase I work concentrates on system design and analysis, cost study, stack technology development, fuel processing development, controls and sensors, power electronics, and system prototype assembly and testing. Phase II will demonstrate a packaged system selected for a specified application and further improve technology and assess system cost. Phase III will extend the Phase II effort to field test a packaged system for extended periods to verify all the required performance, cost, reliability, and lifetime for commercial uses.

Results

A prototype system was constructed to demonstrate system performance as required in the Phase I project objectives. This prototype system intended to be flexible and robust to accommodate design changes throughout the entire system integration process. The assembly process began with specifications for various components flowing down from the systems and controls designs via scorecards so that components could be sourced. A computer model and drawing package of the system geometry was also used to guide construction. Although many items were standard components, a number were developed, modified or designed specifically for the program.

The prototype system that was tested can be seen Figure 1. There was an extensive system build and integration process leading to the final testing of the unit which was comprised of the following major steps:

- Component tests to verify basic operation of components in stand-alone testing, develop component performance maps, and support component selection process.
- Cold tests (operation of system with only nitrogen/ air and without fuel cell stacks) to validate basic operation of components integrated in system and verify plumbing and electrical wiring.
- Hot tests (operation of system on methane without fuel cell stacks) to verify and tune control system hardware and software, combustor operation and temperature controls, integrated operation of fuel

FIGURE 1. SECA Phase I Prototype System

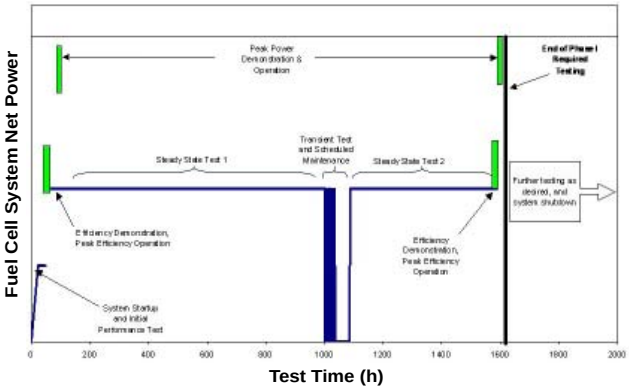

FIGURE 2. Prototype System Test Sequence

processor, and thermal mapping of system and improved insulation.

- Gen 1 System Test (operation of integrated system without power electronics due to half-sized stacks) to verify system operation including stack operation, integrated operation of stacks with fuel processor, thermal self sustaining operation and thermal management, and startup and shutdown strategies.
- Gen 2 System Test (operation of integrated system with power electronics) to demonstrate system operation with performance meeting the Phase I requirements.

The Gen 2 System Test is the final prototype system demonstration test for Phase I. The timeline test sequence for this test is shown graphically in Figure 2. Figure 3 shows the average cell voltage, gross DC

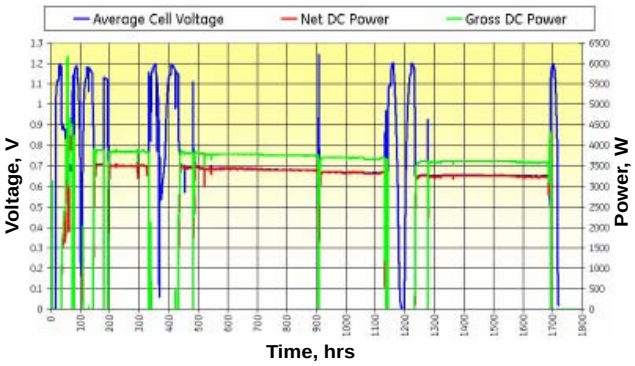

FIGURE 3. Average Cell Voltage, Gross DC Power, and Net DC Power of Prototype System (Average Operating Temperature 800°C)

power, and net DC power of the prototype system over the entire test period (note that the peaks in the figure are those relating to various transient events during the test). The prototype system achieved a peak efficiency of 41%, a peak power of 5.4 kW, and a degradation rate of 1.8% per 500 hours. The system met/exceeded all of the key Phase I minimum. A summary of the Phase I results versus the requirements are given in Table 1.

TABLE 1. Summary of Prototype System Demonstration Test Results

Performance Parameter	Requirements	Results
DC Efficiency	35%	41%
Estimated Cost	<$800/kW	$724/kW
DC Peak Power	3-10 kW	5.4 kW
Steady State Degradation	<2% per 500 hrs	1.8% per 500 hrs
Thermal Cycle	1	3
Power Cycle	9	15
Cycle Degradation	<1%	1.8%
Availability	80%	90%
Test Time	1,500 hrs	1,720 hrs

Conclusions and Future Directions

SECA Phase I was successfully completed. During Phase I, major advances in SOFC technology were made in the areas of performance, degradation/life, stack design, manufacturing, and scaleup. Supporting technology such as fuel processing, controls, power electronics, and thermal management were also developed/matured for integration in an SOFC power system. Phase I culminated in the system test that tied all of these advances in technology together in a prototype system that was able to meet or exceed the key SECA minimum requirements. The system achieved a peak efficiency of 41% (vs. 35% requirement) and a degradation rate of 1.8% per 500 hours (vs. <2% per

500 hours requirement). The system operated for 1,720 hours (vs. 1,500 hours requirement) with three thermal cycles (vs. one thermal cycle requirement) and 15 power cycles (vs. nine power cycle requirement). A projected high-volume cost for the system is $724/kW (vs. $800/kW target).

Phase II of the project has been initiated. Phase II focuses on delivering a Phase I prototype to DOE/NETL, advancing SOFC and BOP technologies to improve system cost, performance, life, and reliability, and demonstrating a packaged system for a selected application.

FY 2006 Publications/Presentations

1. N. Q. Minh, "Solid Oxide Fuel Cell Based Power System Development" 2005 Fuel Cell Seminar Extended Abstracts, Courtesy Associates, Washington, DC, 2005.

2. N. Q. Minh, "Solid Oxide Fuel Cell Technology: Status and Future Direction" Plenary Presentation at the Third International Symposium on Solid Oxide Fuel Cells Materials and Technology" Cocoa Beach, FL, January 20-26, 2006.

II.6 Small-Scale Low-Cost Solid Oxide Fuel Cell Power Systems

Objective

- To develop a commercially viable 5-10 kWe solid oxide fuel cell power generation system that achieves a factory cost goal of $400 per kWe.

Accomplishments

- Demonstrated 90% higher power density (W/cm^2) and more than 2.5 times more power per cell for Delta9 cells compared to tubular cells.
- Demonstrated over 3,000 hours voltage stability for Delta9 cells at 1,000°C and 80% fuel utilization.
- Developed an alternate cathode composition with 10% lower cost and 50% higher conductivity (at 900°C) than present cathode composition.
- Completed assembly of a prototype system.

Introduction

The objective of this project is to develop a standard high-performance, low-cost SOFC system that can be manufactured in high volume for application in a number of different end uses, including residential and as auxiliary power units in commercial and military transportation applications. The proposed project is a 10-year, three-phase project with prototype SOFC systems being tested at the end of every phase, the first of which will be completed this year. Performance and cost improvements made during each phase will be incorporated in each prototype, and products based on each prototype will be made ready for market entry as they become available.

Shailesh D. Vora
Siemens Power Generation
1310 Beulah Road
Pittsburgh, PA 15235
Phone: (412) 256-1682; Fax: (412) 256-1233
E-mail: Shailesh.Vora@siemens.com

DOE Project Manager: Don Collins
Phone: (304) 285-4156
E-mail: Donald.Collins@netl.doe.gov

Subcontractors:
Blasch Precision Ceramics, Albany, NY

Approach

We have identified key technical issues that must be resolved to achieve low-cost commercial SOFC systems. We will focus on cost reductions and performance improvements to transform today's SOFC technology into one suitable for low-cost mass production of small systems for multi-market applications. The key advances identified are:

- Improved cell performance through design and materials innovations to more than double the power and thus reduce cost/kWe
- On-cell reformation of natural gas fuel to eliminate high-cost internal reformer components
- Use of low-cost insulation and containment vessels by lowering the system operating temperature
- Use of net shape cast components to reduce machining costs
- Simplification of stack and balance of plant (BOP) designs to lower parts count
- High efficiency (95%) power conditioning systems to improve overall system electrical efficiency

In addition to the key advances noted above, adoption of more automated, mass production techniques for cell, module and BOP manufacturing will ensure overall SOFC system cost effectiveness.

Results

Prior to the start of the project, it was recognized that Siemens' seal-less tubular cell design would not be able to meet the cost and performance targets of the project. A need to develop a cell with higher power density and compact design was identified.
A new design that combined the seal-less feature and a flattened cathode with integral ribs was chosen. This new design, referred to as a high power density (HPD) cell, has a closed end similar to the tubular design. The ribs reduce the current path length by acting as bridges for current flow. The ribs also form air channels that eliminate the need for air feed tubes. This cell design, due to its shorter current path, has lower cell resistance and hence higher power output than tubular cells.
A variation of the HPD design, Delta9, has a corrugated surface which significantly increases the active area of the cell, yielding higher power per cell. Figure 1 shows the tubular and Delta9 cells.

During FY 2006, Delta9 cells produced 90% higher power density and more than 2.5 times more power per cell than tubular cells at 0.65 V, 900ºC operating

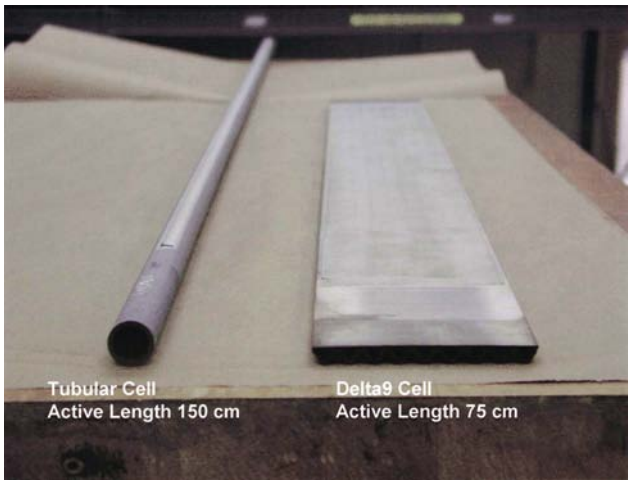

FIGURE 1. Tubular and Delta9 Cells

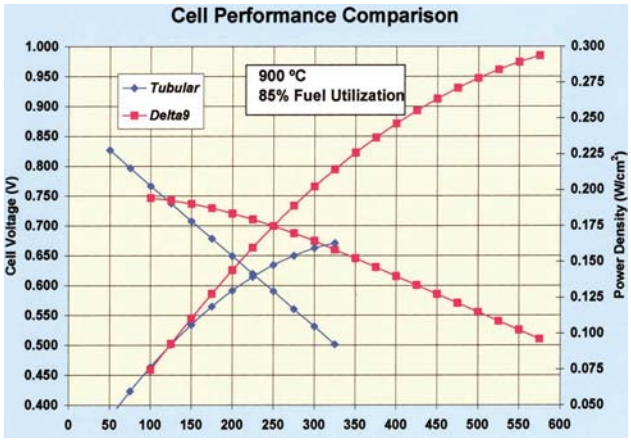

FIGURE 2. Voltage versus Current Density Comparison for Tubular and Delta9 Cell

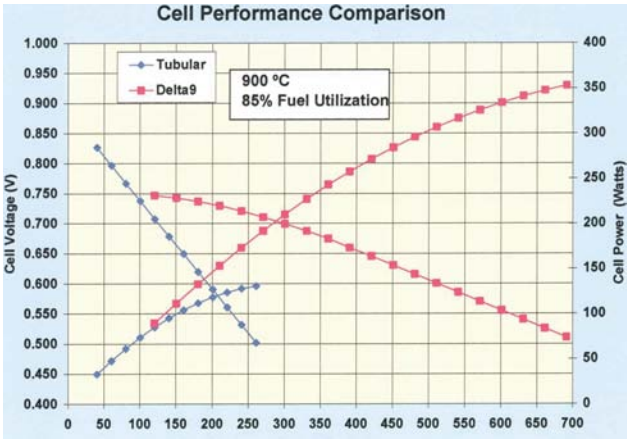

FIGURE 3. Voltage versus Current Comparison for Tubular and Delta9 Cell

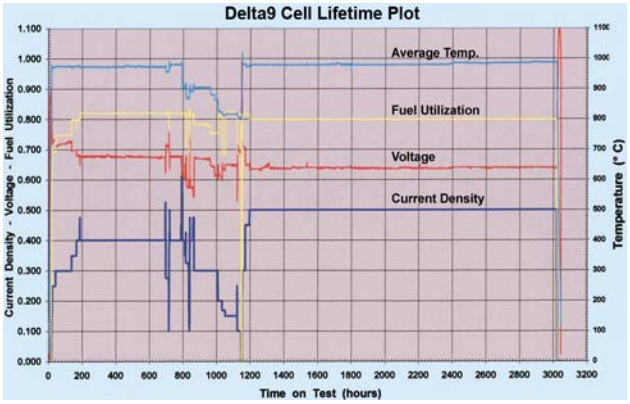

FIGURE 4. Voltage versus Time Plot for Delta9 Cell

temperature and 85% fuel utilization. Figure 2 shows the voltage versus current density comparison for tubular and Delta9 cells. Figure 3 shows the voltage versus current for tubular and Delta9 cells.

Delta9 cells were fabricated and tested for voltage stability. Figure 4 shows voltage stability of a Delta9 cell over approximately 3,000 hours of operation at 1,000°C and 80% fuel utilization. There was no noticeable voltage degradation for the Delta9 cell when tested at conditions described above. This exceeds SECA program goals for voltage stability.

Computational modeling of thermal and electrical fields initiated in FY 2005 to optimize the cell and stack design for maximum power and mechanical stability from thermal stresses during stack operation continued during FY 2006. Efforts were also directed towards the development of cell-to-cell connections to bundle cells.

An alternative cathode composition was developed and evaluated through cell testing. Initial results show acceptable cell properties and performance, with material costs approximately 10% lower than that of present compositions. This is very significant because over 95% of the cell material is the cathode.

Assembly of a prototype system for residential applications was completed. Figure 5 shows the flow schematics of this system. The primary objective of the system is to demonstrate operation of HPD cells in a generator environment. The system will run on natural gas; fuel reformation will be internal to the cell stack.

Conclusions and Future Directions

- Fabrication processes for Delta9 cells were established, and electrical testing showed significant improvement in power density over tubular cells.
- Developed a new low-cost cathode composition.
- Constructed prototype system to run on internally reformed natural gas.
- We will optimize cell and stack design for maximum power and reliability.

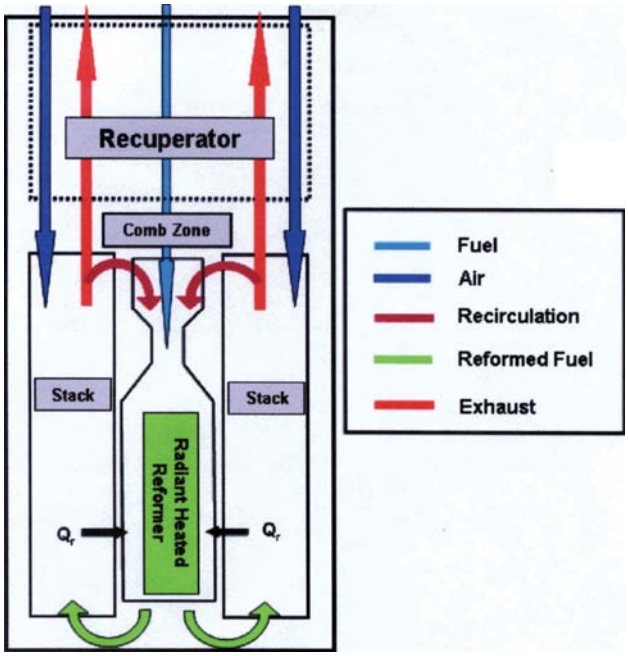

FIGURE 5. Flow Schematics of Prototype Residential System

- We will evaluate and develop automated mass production processes for cell, module and BOP components.

FY 2006 Publications/Presentations

1. S. D. Vora, "Development of High Power Density Seal-less SOFCs", Presented at the 2005 Fuel Cell Seminar, November 14-18, 2005, Palm Springs, CA.

2. G. Zhang, "New Cathode and Interlayer Materials Development at Siemens Power Generation", Presented at 209th Electrochemical Society Meeting, May 7-12, 2006, Denver, CO.

3. A. Iyengar, G. DiGiuseppe, N.A. Desai, S. D. Vora and L. A. Shockling, "Computational Modeling of Thermal and Electrical Fields of a High Power Density Solid Oxide Fuel Cell", Presented at the ASME Fuel Cell Conference 2006, June 19-21, Irvine, CA.

4. K. Huang, "Cell Power Enhancement via Materials Selection", Proceedings of the 7th European Fuel Cell Forum, July 4-7, 2006, Lucerne, Switzerland.

III. SECA RESEARCH & DEVELOPMENT

A. Materials and Manufacturing

III.A.1 Evaluation of a Functional Interconnect System for SOFCs

Objectives

Evaluate complex interconnect structures based on metallic substrates, including, but not limited to, clad and coated systems and SOFC sub-cell structures.

- Demonstrate the production of complex interconnect structures and systems.
- Evaluate the interactions of simple and complex interconnect systems with simulated local SOFC environmental conditions, including atmospheres and materials of construction expected to be in contact with interconnects.
- Quantify performance of simple and complex interconnect systems, particularly in the areas of electrical properties (ALC/Pitt) and layer adhesion (CMU/WVU).

Accomplishments

ATI Allegheny Ludlum / University of Pittsburgh

- Successfully produced multi-layered clad interconnect structures and tested in simulated anode gas and dual atmosphere exposures, with initial results showing promise.
- Applied novel processing to common ferritic stainless steels, resulting in the production of desired structures.
- Melted and processed novel stainless steel compositions.
- Exposed E-BRITE alloy (Fe-26Cr-1Mo) and model alloy RV 2103 (Fe-22Cr) specimens in simulated cathode gas environments for indentation spallation studies at Carnegie Mellon University. The exposures were designed to simulate actual exposures of up to 40,000 hrs at 800°C.
- Provided Type 430 substrates to Arcomac Surface Engineering for application of their coating systems.

Carnegie Mellon University

- Performed macro-scale indentation spallation tests on E-BRITE alloy (Fe-26Cr-1Mo) and model alloy RV 2103 (Fe-22Cr) specimens exposed by Allegheny Technologies, Inc. (ATI) in simulated cathode gas. Tracked spallation densities as a function of exposure time.
- Initiated macro-scale indentation tests on coated Type 430 specimens from Arcomac Surface Engineering (with substrates from ATI).
- Performed proof-of-concept nanoindentation tests on exposed E-BRITE alloy specimens from ATI. Identified cracking geometries needed for nanoindent modeling work.
- Initiated nanoindentation modeling to relate crack size measurements from tests to stress intensity factors and energy release rates.

West Virginia University

- Identified and tested several silver cermets as contact paste materials for SOFCs.
- Completed the study of evaporation characteristics and microstructure changes of sterling silver and pure silver under high-temperature exposure conditions.

James M. Rakowski
Allegheny Technologies, Inc. (ATI Wah Chang)
ATI Allegheny Ludlum (ALC)
Technical and Commercial Center
1300 Pacific Avenue
Natrona Heights, PA 15065
Phone: (724) 226-6483; Fax: (724) 226-6452
E-mail: jrakowski@alleghenyludlum.com

DOE Project Manager:
Ayyakkannu Manivannan
Phone: (304) 285-2078
E-mail: Ayyakkannu.Manivannan@netl.doe.gov

Subcontractors:

Professor Jack Beuth
Carnegie Mellon University (CMU), Pittsburgh, Pennsylvania

Professor Bruce Kang
West Virginia University (WVU), Morgantown, West Virginia

Professor Gerald Meier
University of Pittsburgh (Pitt), Pittsburgh, Pennsylvania

Introduction

The interconnect is a critical part of planar solid oxide fuel cells (SOFCs). The interconnect serves to separate the fuel and oxidant gas streams and also collects the electrical output of the SOFC. A shift from relatively inert ceramic interconnects to metallic structures has been driven primarily by cost considerations. Interconnect alloy selection has been identified as one of two primary issues impeding the

commercialization of SOFCs [1]. High-temperature degradation due to surface oxidation is the primary form of attack. Oxides in general have poor electrical conductivity, leading to increased contact resistance as they form and get thicker. This degrades the output of the fuel cell over time and should be minimized.

In addition, oxides can spall due to high compressive residual stresses at room temperature, increases in oxide thickness, and/or changes in scale adhesion to the substrate. Chromia scales, which have higher conductivities than other oxides, can also experience evaporation at high temperature, with evaporated chromium degrading cathode performance. Successful low-temperature SOFC interconnect systems will have to address these concerns while minimizing cost.

Approach

The approach in this project is to address the evaluation of new ferritic stainless steel-based SOFC interconnect systems in an integrated way, using expertise from each of our four project participants. Allegheny Ludlum is studying new interconnect alloys and surface treatments to achieve optimal combinations of reduced chromia scale growth, spallation resistance and reduced chromia scale evaporation, while minimizing cost. This includes the development of novel clad systems and interactions with DOE laboratories and industrial collaborators developing interconnect coating systems. The University of Pittsburgh is performing dual atmosphere tests on clad systems from ALC and providing support for microstructural studies. Carnegie Mellon is testing interconnects for chromia scale spallation resistance using macro-scale and nano-scale indentation tests. The goal of these tests is to accelerate the evaluation of new interconnect systems and to understand mechanisms leading to premature interconnect failure by spallation. Tests include bare alloys from ALC and coated systems from DOE laboratories and industrial partners, using ATI alloy substrates. West Virginia University is studying silver cermet pastes to enhance the contact between interconnects and cathode materials. Fundamental studies of the performance of different paste compositions will be followed up by studies of paste/alloy combinations using alloys from ALC.

Results

ATI Allegheny Ludlum / University of Pittsburgh

Clad panels were produced using a variety of alloys which are expected to be inert in the anode environment, notably nickel 201 (UNS N02201), oxygen-free copper (UNS C10100), and a commercially produced Ni-32Cu alloy (UNS N04400). Some panels were also clad on the cathode side with oxidation-resistant nickel-base superalloys. Examples of two as-processed clad panels are shown in Figure 1. A test plan was formulated to determine the resistance to oxidation in simulated anode gas (SAG) and dual atmospheres, along with the effects of thermal cycling.

- Testing in SAG resulted in a significant reduction in weight gain as compared to a Type 430 stainless steel control sample, attributable to the cladding side exhibiting little to no oxidation. This can be seen visibly in Figure 2 for a nickel-clad stainless steel sample. Some accelerations in the rate of weight gain were noted, which is due to mixed oxide nodule formation on exposed Type 430 surfaces.
- Initial dual atmosphere results indicated that T430 stainless steel clad with copper or nickel resulted in no oxidation on the anode side. There was evidence of hydrogen migration to the air side, resulting in the formation of mixed oxide nodules and oxide blade-type features (Figure 3). The samples clad with the Ni-32Cu alloy formed a thin, adherent manganese oxide layer on the SAG side. Evidence of hydrogen migration on the air side is much reduced to a few scattered blade-like oxide grains (Figure 4). It is hypothesized that the MnO scale is helping to block transport of hydrogen across the interconnect.
- The thermal cycling tests indicated that differential thermal expansion between the clad outer layers

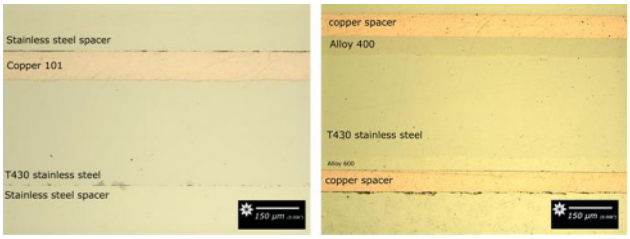

FIGURE 1. As-processed Clad Panels (light optical micrographs of polished metallurgical cross-sections): Bi-Layer Type 430 Stainless Steel Clad with Copper 101 Alloy on the Anode Side (left), Tri-Layer Type 430 Stainless Steel Clad with Ni-32Cu Alloy on the Anode Side and Ni-Base Superalloy 600 on the Cathode Side (right)

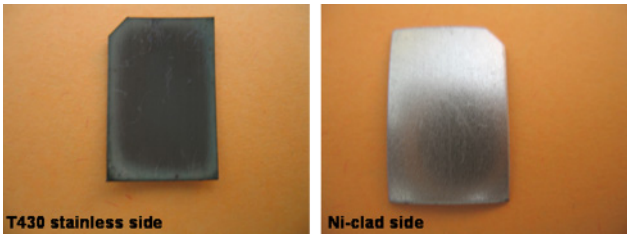

FIGURE 2. Example of a Clad Sample Exposed for 1,371 Hours at 800°C in SAG (Ar-4%H_2-3%H_2O): Type 430 Stainless Steel Substrate (left) and Nickel Cladding (right)

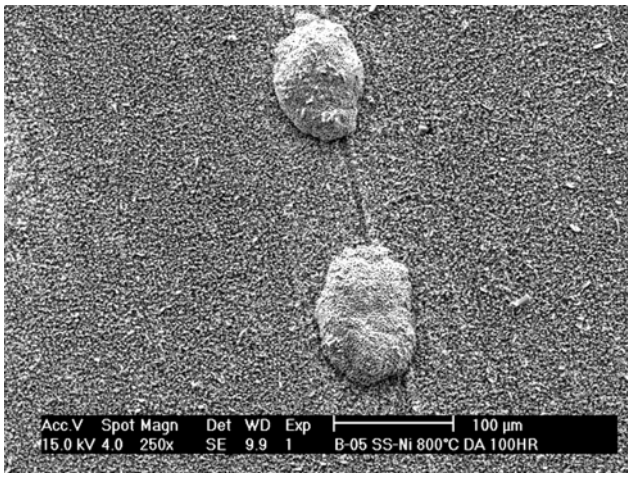

FIGURE 3. Oxide Scale as Formed on the Air Side of a Type 430 Stainless Steel Sample Clad with Nickel during a 100 Hour Dual Atmosphere Exposure at 800°C (surface SEM micrographs; stainless steel side exposed to air, nickel-clad side exposed to Ar-4%H_2-10%H_2O)

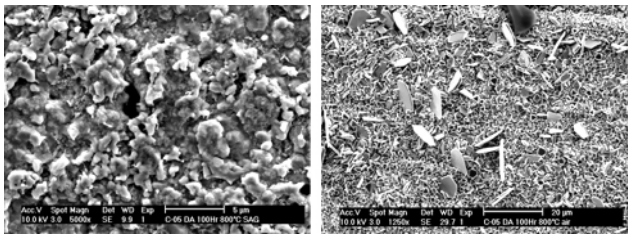

FIGURE 4. Oxide Scale as Formed on a Type 430 Stainless Steel Sample Clad with Ni-32Cu Alloy during a 100 Hour Dual Atmosphere Exposure at 800°C (surface SEM micrographs): Ni-32Cu Cladding (left, as exposed to Ar-4%H_2-10%H_2O), Type 430 Stainless Steel (right, as exposed to air)

and the inner core is not negligible. Some of the samples, notably the two-layer ones clad with Ni-32Cu, exhibited some curling.

Post-process treatments are being investigated in an attempt to improve the performance of typical ferritic stainless steels in the SOFC environment by mitigating the formation of electrically resistive oxides of aluminum and silicon at the scale/alloy interface.

- Samples of AL453 alloy, a Fe-22Cr-0.5Al alloy, were treated in an attempt to sequester aluminum in the form of stable particles. The initial results were successful. Measurements and calculations indicate that nominally all of the aluminum initially present in the substrate has been sequestered with a beneficial effect on ASR (Figure 5).
- Samples of Type 430 stainless steel (Fe-16.5Cr-0.3Si) were treated in an attempt to remove silicon from the surface without removing other elements,

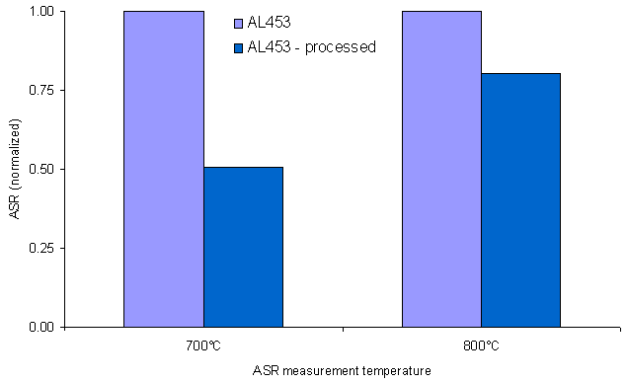

FIGURE 5. Effect of Surface Treatment on Relative ASR of AL453 Alloy

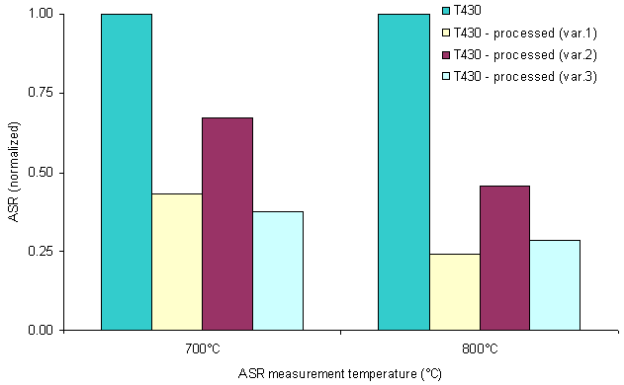

FIGURE 6. Effect of Surface Treatment (Three Variants) on Relative ASR of T450 Stainless Steel

notably chromium. The intent is to leave behind silicon-depleted metal. The initial results were successful, with scanning Auger microprobe analysis (SAM) indicating that silicon was depleted at the surface by a nominal factor of 40. Calculations indicate that the treatment as-applied is capable of removing approximately 40% of the total silicon in a 0.5 mm thick substrate. The effect is likely to be magnified near the surface due to the presence of a silicon depletion gradient. The effect on ASR was beneficial (Figure 6).

Base alloy development is progressing at ALC. Several heats have been melted, cast, and processed to flat rolled plates. Some surface issues were encountered and were bypassed by machining the plates after rolling. Testing is ongoing, with results expected by the end of September 2006 for monolithic samples and samples coated with oxidation-resistant layers and/or cathode contact paste. Two primary alloy compositions are being investigated:

- A superferritic stainless steel based on a modified E-BRITE composition. The goal is to produce

an alloy with the beneficial qualities of E-BRITE alloy, while improving the resistance to oxide scale evaporation and sigma formation.

- A Fe-Cr-Al alloy family containing a high level of rare earth metals.

Carnegie Mellon University

ATI is providing CMU with interconnect alloy specimens that have undergone exposures simulating 800°C for times up to 40,000 hours. Most exposures are being performed in lab air at 900°C. Specimens tested thus far are E-BRITE, having composition Fe-26Cr-1Mo-0.2Si, and RV 2103, a 21.8Cr-0.033Mn alloy with Ti, C, N, Ce, La, Al and Si in percentages of 0.02 or less. Specimens of RV 2103 were provided to yield a comparison between 26Cr and 22Cr alloys. Specimens were in the as-rolled condition, with ground finish rolls used for the final rolling operation. This yields a surface Ra of approximately 8 μin.

A macro-scale indentation test has been developed by the principle investigator J. Beuth and his students (under DOE and National Science Foundation support) for measuring the fracture toughness of interfaces between oxide scales and metallic substrates [2-4]. The test consists of indenting a coated or uncoated oxide/alloy system with a Brale type conical indenter. The indenter penetrates the brittle coatings (if present) and oxide layer and plastically deforms the metallic substrate below. This plastic deformation induces compressive radial strains in the substrate. Because these strains are transferred to the oxide, they can act to drive its debonding. As illustrated in Figure 7 (as viewed from above), indentation induces a radial distribution of flaking-type spalls of the chromia scale. Systems with poor adhesion between the chromia and interconnect alloy exhibit a higher density of debonds and a larger radial extent of debonding. Image analysis allows the percentage of indentation-induced debonding to be quantified as a function of radial distance from the indent.

Each of the specimens sent to CMU has been subjected to macro-scale indentation testing. Results of debond density vs. radial distance from the indent center are still being analyzed. However, some initial observations and trends in the results are worth noting. First, E-BRITE specimens with short exposure times showed no debonding at all. In contrast, RV 2103 specimens subjected to the same exposures showed clear debonding, with the density of debonding increasing with exposure. It is clear that the E-BRITE alloy is much more resistant to spallation at early exposure times than the RV2103 alloy. Indentation tests on E-BRITE specimens exposed for extended exposure times have shown progressive increases in debond density with exposure time. Further analysis of these tests is underway.

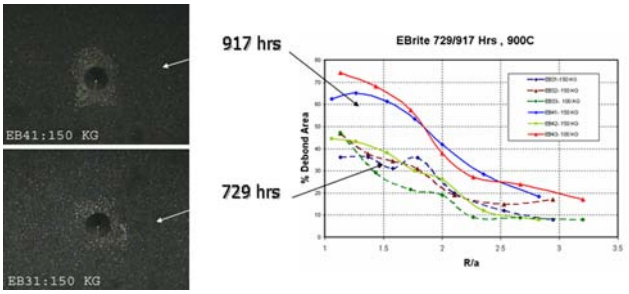

FIGURE 7. Indentation of E-BRITE specimens, as viewed from above. White areas indicate spalls induced by indentation strains. Image analysis yields a plot of debond percentage vs. normalized radius.

Macro-scale indent tests have also been performed on coated specimens from Arcomac Surface Engineering. These tests in the as-processed state will be followed up by exposures at ATI and indentation tests at CMU. A nano-scale indentation test is under development for use in combination with the macro-scale test, to probe toughnesses of chromia scales and chromia/alloy interfaces on a local scale. The test involves nanoindentation of the scale region of cross-sectioned samples. Nanoindents induce cracks in the scale or at the interface, and the length of the cracks can be related to the scale or interface toughness. This test is a means of measuring toughness directly, independent of scale residual stress and thickness which have a strong influence on toughness measurements on the macro scale.

West Virginia University

The experimental procedure for this research involved creating an environment similar to what the material would be exposed to in a real functioning fuel cell. This was accomplished using a simple tube furnace setup, illustrated in Figure 8. The tube furnace was maintained at 800°C, and air flow rate was controlled at approximately 3 l/min. The samples for this experiment were small sterling silver and pure silver plates. The main property of concern is the thickness reduction of the sample during exposure. Each week the samples were weighed, and the mass of the samples was taken as the average of several measurements. Samples were also evaluated using scanning electron microscopy (SEM) to evaluate microstructure changes taking place on the surface of the samples.

The evaporation characteristic of the sterling silver samples during high-temperature exposure was a relatively constant loss of mass over a duration of 27 weeks. Both types of pure silver samples (50 and 700 micron thickness) exhibited similar evaporation characteristics, with the rate of evaporation decreasing over time until a relatively constant rate was reached. A plot of the rates for the exposed samples is shown in Figure 9.

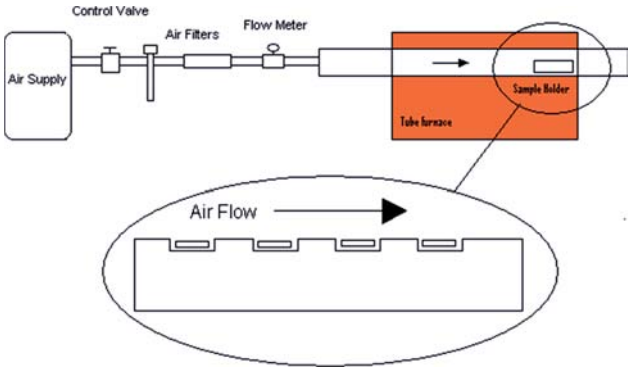

FIGURE 8. Experimental Setup for Exposure of Samples

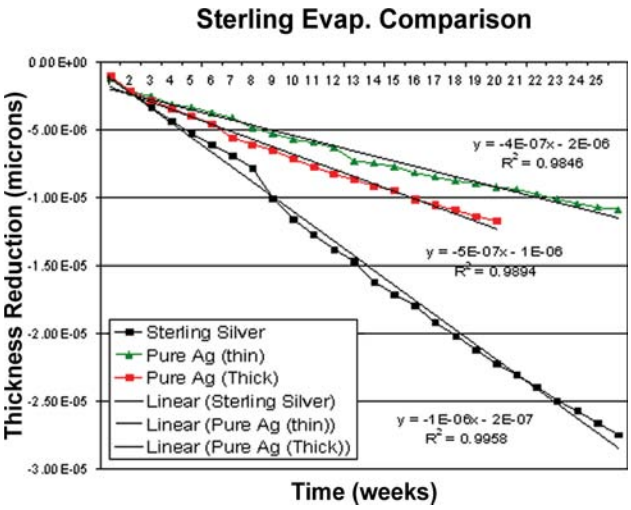

FIGURE 9. Comparison of Evaporation Rate for Various Samples

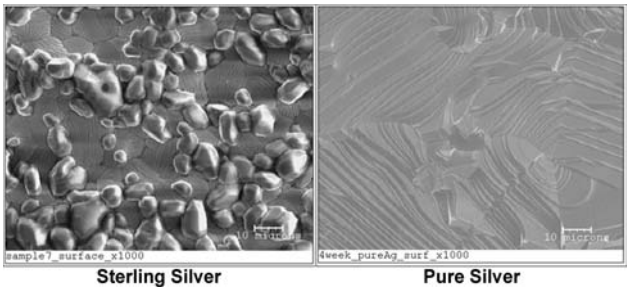

FIGURE 10. Comparison of Faceting of Sterling Silver and Pure Silver after High-Temperature Exposure

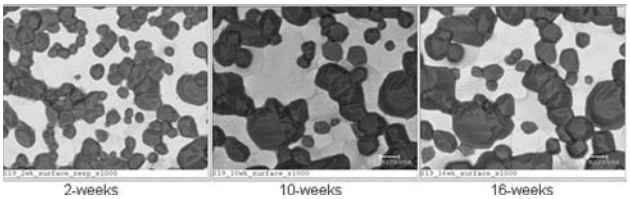

FIGURE 11. Time-Series SEM Backscatter Images of a Sterling Silver Sample

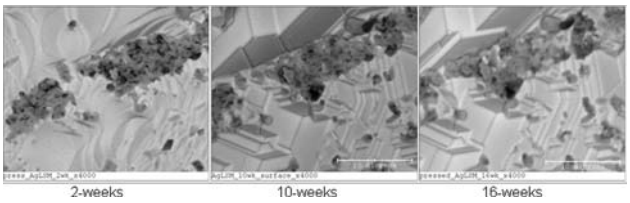

FIGURE 12. Time-Series SEM Backscatter Images of a Ag/LSM Sample

It can be seen in Figure 9 that the sterling sample evaporates the fastest, roughly 1 micron per week, while the pure samples evaporate much slower, roughly 0.4–0.5 microns per week. SEM analysis of the samples showed dramatic differences in the faceting behavior of the silver in the samples. Figure 10 illustrates the differing surface microstructures of the pure silver and sterling silver samples.

The faceting of the silver in the pure silver samples is much more dramatic than that of the sterling silver samples. It appears that through high-temperature exposure, the surfaces of the samples change until the surface eventually reaches an orientation that is not favorable to evaporation. It appears that the copper oxide in the sterling silver samples may inhibit the surface silver's ability to reach the desired orientation, whereas this is not the case in pure silver samples. Therefore, the sterling silver samples continue to lose mass at a higher rate, while the pure silver sample's rate of evaporation is able to further decrease.

The evaporation test results and the follow-up SEM analyses indicated that copper oxide may be volatile when used as a protective oxide due to migration and agglomeration of the oxide particles. Figure 11 illustrates the behavior of the copper-oxide particles during long-term high-temperature exposure. Experiments were also carried out utilizing silver cermet with lanthanum strontium manganese oxide (LSM) to examine the volatility of LSM during high-temperature exposure. Figure 12 shows the SEM results for the samples. The LSM appears much more stable over long-term high-temperature exposure than copper oxide. For this reason as well as the evaporation characteristics of sterling silver, the focus of our future research will be on samples fabricated utilizing silver/LSM or silver/CeO.

Conclusions and Future Directions

ATI Allegheny Ludlum / University of Pittsburgh

- Cladding appears to be a viable means of mitigating anode-side oxidation. Certain alloys may also be beneficial in reducing hydrogen migration.
- Novel post-processing appears to be capable of removing aluminum and silicon from finished stainless steel.
- Future laboratory evaluation will focus on electrical characterization of clad and post-processed materials, novel compositions, and complex sub-cell systems.

Carnegie Mellon University

- Macro-scale indent results are sensitive enough to show a clear difference in spallation behavior between 22Cr and 26Cr alloys at very short exposure times. This suggests that the test could be used for quick screening of new alloy systems for spallation resistance.
- Macro-scale indent tests performed on E-BRITE have shown a progressive increase in spallation density with exposure. The tests appear to be able to track progressive loss of debond resistance with exposure, for exposure times that would not yield any spontaneous spallation in standard thermogravimetric analysis tests.
- Macro-scale tests also appear well-suited for tracking debond resistance in coated specimens.
- Nano-scale indent tests have shown the ability to induce cracks in grown chromia scales, allowing the direct quantification of scale or interface toughness. These tests are under development.
- Fracture analyses of macro-scale tests will be performed to link test results to fracture toughnesses, for predicting times to spallation in alloy specimens.
- Coated specimens will be exposed and tested using the macro-scale test.
- Nano-scale testing will proceed on specimens subjected to a wide range of exposures to determine directly if scale or interface toughness is changing with exposure.

West Virginia University

- Surface orientation of silver appears to play an important role in the evaporation rate of any potential silver cermet materials.
- Due to migration and agglomeration of copper oxide particles at high temperature, silver cermet containing copper oxide particles is volatile when used as a contact paste material in a SOFC environment.

FY 2006 Publications/Presentations

1. Quarterly Report for 3rd calendar quarter 2005, including content from subcontractors CMU and WVU, 12/19/05.

2. Quarterly Report for 4th calendar quarter 2005, including content from subcontractors CMU and WVU, 01/25/06.

3. Project Fact Sheet , including content from subcontractors CMU and WVU, 02/22/06.

4. Quarterly Report for 1st calendar quarter 2006, including content from subcontractors CMU and WVU, 04/26/06.

5. "Evaluation of a Functional Interconnect System for SOFC's", Status Presentation at NETL Morgantown to Program Management. Meeting included presentations on the project from subcontractors CMU and WVU. 06/02/06.

6. *J. L. Beuth, and N. Dhanaraj,* Carnegie Mellon University, *J. E. Hammer, S. J. Laney, F. S. Pettit, and G. H. Meier,* University of Pittsburgh, "Interfacial Fracture Testing to Evaluate the Durability of SOFC Interconnect Alloys", ASM International/TMS, "Materials Solutions", Pittsburgh, PA, September 2005.

7. *N. Dhanaraj, J. L. Beuth, G. H. Meier, F. S. Pettit, J. Hammer, and S. J. Laney*, "Interfacial Fracture Testing to Evaluate the Durability of SOFC Interconnect Alloys", Materials for the Hydrogen Economy (J. J. Petrovic, I. E. Anderson, T. M. Adams, G. Sandrock, C. F. Legzdins, J. W. Stevenson, and Z. G. Yang, eds.), Proc. Materials Science and Technology 2005, Pittsburgh, PA, September 2005, pp 165-175.

8. "Elevated Temperature Environmental Degradation of Complex Interconnect Systems for Solid Oxide Fuel Cells", accepted for publication in the Fuel Cells and Energy Storage Systems Symposium at the MS&T 2006 Conference, Cincinnati, OH, October 15-19, 2006.

References

1. Surdoval, W., "SECA Program Overview" presented at SECA Workshop and Peer Review, Boston, MA, May 11, 2004.

2. Vasinonta, A. and Beuth, J.L., "Measurement of Interfacial Toughness in Thermal Barrier Coating Systems by Indentation," *Engineering Fracture Mechanics*, Vol. 68, 2001, p. 843.

3. Handoko, R.A., Beuth, J.L., Meier, G.H., Pettit, F.S. and Stiger, M.J., "Mechanisms for Interfacial Toughness Loss in Thermal Barrier Coating Systems," *Durable Surfaces* (D.R. Mumm, M.E. Walter, O. Popoola and W.O. Soboyejo, eds.), Proceedings of the Materials Division Symposium on Durable Surfaces, 2000 ASME International Mechanical Engineering Congress and Exposition, Orlando, November 2000, Trans Tech Publications, Switzerland, 2001, p. 165.

4. Ma, Q., "Indentation Methods for Adhesion Measurement in Thermal Barrier Coating Systems," Ph.D. Thesis, Carnegie Mellon University, 2004.

III.A.2 Oxidation Resistant, Cr Retaining, Electrically Conductive Coatings on Metallic Alloys for SOFC Interconnects

Objectives

- Enable the use of inexpensive metallic alloys as planar SOFC interconnects (ICs) via protective coatings.
- Develop and demonstrate novel, cost-effective deposition processes to establish dense and uniform protective and functional coatings on metallic substrates.
- Evaluate protective coatings during exposures relevant to SOFC ICs.
- Optimize deposition process parameters to maximize SOFC metallic IC performance and ultimately reduce cost.

Accomplishments

- Developed and tested new, hybrid surface engineering technologies combining large area filtered arc deposition (LAFAD), electron beam physical vapor deposition (EBPVD), unbalanced magnetron (UBM) and thermal evaporation to deposit dense and defect-free protective coatings in an economically favorable manner.
- Reduced metallic alloy oxidation rate by an order of magnitude. Rutherford backscattering spectroscopy (RBS) results indicate stainless steel samples with nanolayered CrN/AlN coatings exhibit an order of magnitude increase in oxidation resistance compared to uncoated counterparts. Further improvement of diffusion/oxidation barrier properties is achieved by newly developed nanolayered and/or nanocomposite MCrAlYO oxicermet coating were M=Co, Ti, Mn, or Ni.
- Developed two-segment coating architecture with bottom oxidation barrier MeCrAlO nanocomposite oxicermet segment, deposited by the LAFAD process, followed by a $(Mn,Co)_3O_4$ spinel, Cr retaining, cathode compatible segment, deposited by the hybrid filtered arc deposition (FAD)-EBPVD process.
- Significantly reduced Cr volatility. Coated samples of commercially-available 430 stainless steel exhibited over a thirty-fold decrease in Cr volatility compared with their uncoated counterparts. Effectively complete blocking of Cr volatility is expected, as uncoated portions of these samples were exposed during this testing.
- Demonstrated over 1,000 hours of low (<10 $m\Omega \cdot cm^2$) and stable area specific resistance (ASR) values with coated stainless steel samples. Negligible chemical or physical changes were observed in sample post-mortem analyses.
- Developed thermochemical modeling of multielemental high temperature oxicermet coatings.

Dr. Vladimir Gorokhovsky
Arcomac Surface Engineering, LLC
151 Evergreen, Suite D
Bozeman, MT 59715
Phone: (406) 522-7620; Fax: (406) 522-7617
E-mail: vgorokhovsky@arcomac.com

DOE Project Manager:
Ayyakkannu Manivannan
Phone: (304) 285-2078
E-mail: Ayyakkannu.Manivannan@netl.doe.gov

Introduction

The Arcomac Surface Engineering, LLC (ASE) SECA project has focused on the development of protective and functional coatings to enable the use of inexpensive metallic alloys as SOFC ICs. Currently, the IC components of planar SOFC systems account for a dominant portion of the overall SOFC stack cost. Inexpensive ferritic stainless steels are under consideration for these components. However, when exposed to the typical SOFC operation environment, metallic alloys form blanketing oxide scales, which dramatically degrade SOFC performance and limit device lifetime. To date, deleterious issues with Cr volatility, electrical resistance, and thermal-mechanical and chemical incompatibilities have restricted the use of metallic alloys as ICs in planar SOFC systems. ASE has developed advanced coating deposition technologies, which show promise for resolving these issues in an economically-viable manner.

Approach

To achieve the SECA cost and performance goals, the use of inexpensive ferritic stainless steels as IC components is under investigation. ASE is developing advanced, hybrid vapor plasma deposition technologies to establish protective coatings on commercially available alloys of interest as SOFC ICs. These coatings are aimed at inhibiting thermally grown oxide scale formation and outward Cr diffusion while retaining low area electrical resistivity at 750ºC

in air during long-term exposures. Desired coating compositions and architectures are determined through thermodynamic and transport modeling in addition to prior art. Appropriate deposition materials are acquired and deposition processes are designed and executed using ASE equipment. Coated samples are evaluated under exposures simulating SOFC IC operation, and sample coupon performance is analyzed. Results are employed to assist in developing new coating deposition process formulations. Promising coating systems from preliminary testing are then subjected to more prototypical SOFC IC conditions for further assessments. Concurrently, economic evaluations of coating process and interconnect component fabrication are ongoing.

Results

The patented filtered arc plasma source ion deposition (FAPSID) system developed by ASE utilizes two dual filtered cathodic arc LAFAD sources in conjunction with two UBM sputtering sources, two EBPVD evaporators and a thermal resistance evaporation source in one, universal vacuum chamber layout as illustrated in Figure 1 [1,2]. This system has demonstrated the capability to deposit nanocomposite, nanolayered coatings with a wide variety of compositions and architectures.

The present ASE two-segment hybrid coating approach is shown schematically in Figure 2. Filtered arc deposited, nanostructured coatings from the MCrAlYO system (where M = Co, Ti, Mn or Ni), are being investigated to comprise a lower, oxidation-resistant, adhesion-promoting bond coating segment. This layer is designed to function as an effective barrier, blocking both inward and outward diffusion of oxidizing species, while acting as an adhesion system to the upper coating segment. The transition metal dopants are selected to increase high temperature electronic conductivity by forming nanolaminated and/or nanocomposite thermistor-like oxicermets. Thermochemical modeling, using newly developed "TERRA" thermodynamic equilibrium calculation code is developed to estimate phase composition of multielemental oxicermet coatings and its interaction with SOFC IC operating environments. A matrix of these lower segment coatings have been successfully deposited with excellent adhesion to metallic substrates under consideration for SOFC interconnects. A $(Mn,Co)_3O_4$ spinel coating deposited by the hybrid FAD-EBPVD process comprises an electrically conductive, Cr-retentive and SOFC cathode-compatible upper coating segment. Other hybrid deposition methods, employing filtered arc assisted thermal resistance evaporation are also being explored to deposit the upper segment coating. A matrix of upper segment coatings has been successfully deposited in combination with and apart from the matrix of lower segment coating compositions.

SOFC IC-related behavior of coated and uncoated samples, i.e. high temperature oxidation, ASR, and

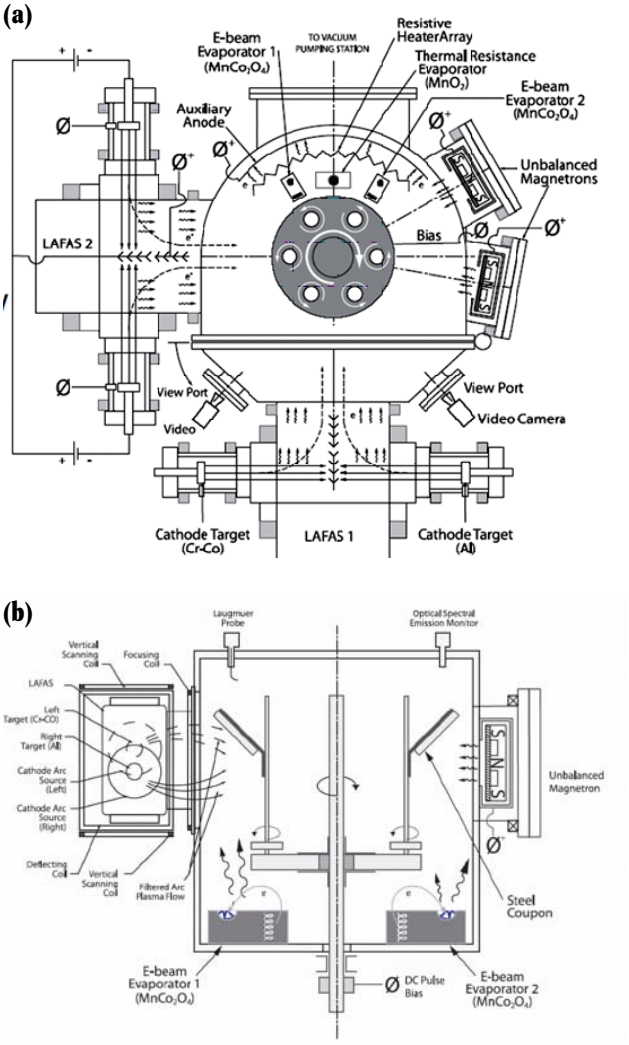

FIGURE 1. Schematic Illustration of the FAPSID Surface Engineering System, Showing (a) Top View and (b) Side View

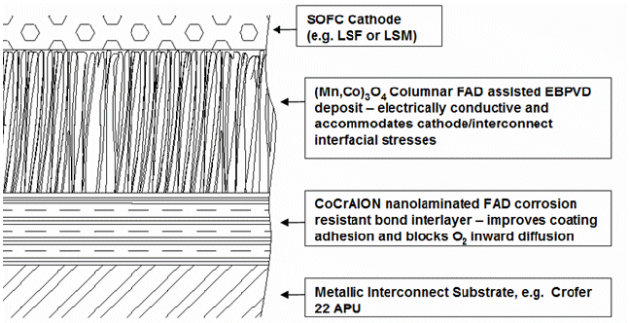

FIGURE 2. ASE's Two-Segment, Hybrid Coating Concept

Cr volatility have been investigated in collaboration with researchers at Montana State University, Pacific Northwest National Laboratory, Lawrence Berkeley National Laboratory and NASA-Glenn Research Center. Cross-section scanning electron microscopy (SEM) images in Figure 3 illustrate the thermal stability of the coating system. Figures 3a and 3b are of a two-segment coating on 430 stainless steel before and after 300 hours exposure to 800°C air (throughout several thermal cycles), respectively. Figure 4 displays a summary of the ASR and Cr volatility results. Low ASR values, excellent adhesion, oxidation stability and promising Cr volatility data suggest the efficacy of the ASE two-segment coating approach.

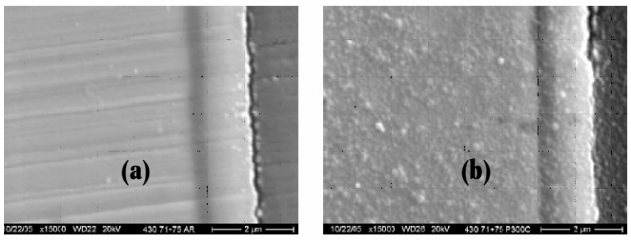

FIGURE 3. Cross Sectional SEM Images of Two-Segment Coating: FAD CrCoAlYO Nanostructured Bottom Segment Coating with Filtered Arc-Assisted EBPVD $(Co,Mn)_3O_4$ Upper Segment Coating on 430 Stainless Steel: (a) As-Deposited and (b) Subsequent to 300 Hours Exposure to 800°C Air

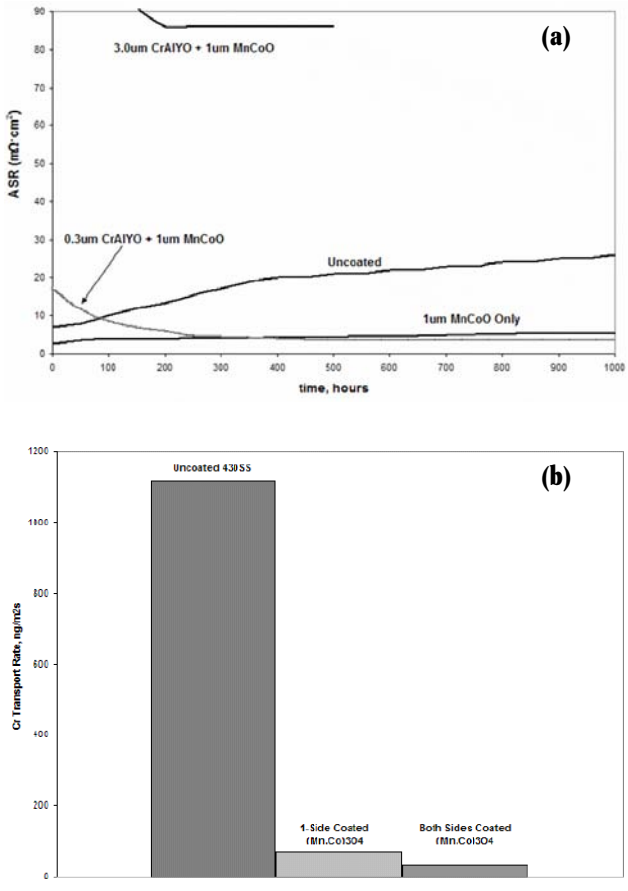

FIGURE 4. (a) Summary of ASR Results on Coated and Uncoated Crofer 22 APU; (b) Cr Volatility Results from Coated and Uncoated 430 Stainless Steel

Conclusions and Future Directions

ASE has developed advanced coating deposition processes, which may enable the use of inexpensive metallic alloys as interconnect components in planar SOFC systems. Multilayered nanostructured oxicermet coatings, deposited by hybrid filtered arc assisted techniques are being investigated to meet SECA SOFC IC performance and cost requirements. A large-scale FAPSID surface engineering process, offering favorable economics through high yield and advanced hybrid design, is under investigation for deposition of protective coatings on SOFC ICs. Future work is dedicated to optimizing the composition and architecture of nanocomposite oxicermet coatings on prototype-size SOFC ICs made of ferritic stainless steels to further improve its thermal-chemical and mechanical stability, barrier properties and reduced ASR during long-term SOFC IC operation.

FY 2006 Publications/Presentations

1. V.I. Gorokhovsky, "Filtered arc plasma assisted PVD coatings for SOFC metallic interconnects", Presented at the SECA Core Technology Review Meeting, Lakewood, CO, October 2005.

2. V.I. Gorokhovsky, P.E. Gannon, M.C. Deibert, R.J. Smith, A. Kayani, M. Kopczyk, D. VanVorous, Z. Gary Yang, J.W. Stevenson, S. Visco, C. Jacobson, H. Kurokawa, S.W. Sofie, "High temperature oxidation, Cr volatility and surface electrical conductivity of ferritic steel with filtered arc and hybrid filtered arc-assisted EBPVD coatings", Accepted for publication in the *Journal of the Electrochemical Society.*

3. P.E. Gannon, V.I. Gorokhovsky, M.C. Deibert, R.J. Smith, A. Kayani, P.T. White; Z. Gary Yang, J.W. Stevenson, S. Visco, C. Jacobson, H. Kurokawa, S.W. Sofie, "Enabling inexpensive metallic alloys as SOFC interconnects: an investigation into hybrid coating technologies to deposit nanocomposite functional coatings on ferritic stainless steels", Presented at the 135th annual TMS meeting and submitted for publication in the *International Journal of Hydrogen Energy.*

4. C. Collins, J. Lucas, T.L. Buchanan, M. Kopczyk, A. Kayani, P.E. Gannon, M.C. Deibert, R.J. Smith, D.S. Choi, V.I. Gorokhovsky, "Chromium volatility of coated and uncoated steel interconnects for SOFCs", Submitted to the 2006 International Conference on Metallurgical Coatings and Thin Films to be published in *Surface and Coatings Technology.*

5. A. Kayani, T.L. Buchanan, M. Kopczyk, C. Collins, J. Lucas, K. Lund, R. Hutchinson, P.E. Gannon, M.C. Deibert, R.J. Smith, D.S. Choi, V.I. Gorokhovsky, "Oxidation resistance at 800°C for magnetron-sputtered CrAlN coatings on 430 steel", Submitted to the 2006 International Conference on Metallurgical Coatings and Thin Films to be published in *Surface and Coatings Technology.*

6. V.I. Gorokhovsky, P.E. Gannon, M.C. Deibert, R.J. Smith, A. Kayani, S. Sofie, Z. Gary Yang, J.W. Stevenson, "Investigating hybrid filtered arc plasma source ion deposition technologies to deposit nanostructured functional coatings on ferritic stainless steels. *Part I: Deposition process parameters and basic coating characteristics*", Presented at the 2006 International Conference on Metallurgical Coatings and Thin Films.

7. P.E. Gannon, V.I. Gorokhovsky, M.C. Deibert, R.J. Smith, A. Kayani, S. Sofie, Z. Gary Yang, J.W. Stevenson, S. Visco, C. Jacobson, H. Kurokawa, "Investigating hybrid filtered arc plasma source ion deposition technologies to deposit nanostructured functional coatings on ferritic stainless steels. *Part II: Simulated solid oxide fuel cell interconnect performance*", Presented at the 2006 International Conference on Metallurgical Coatings and Thin Films.

References

1. V. Gorokhovsky, US Patent No. 6,663,7552.

2. V.I. Gorokhovsky, "Filtered arc plasma assisted PVD coatings for SOFC metallic interconnects", Presented at the SECA Core Technology Review Meeting, Lakewood, CO, October 2005.

III.A.3 SOFC Research and Development in Support of SECA

Objectives

- Explore the effects and mechanisms of chromium migration in SOFCs.

Approach

- Operate cells with E-Brite current collectors and determine voltage degradation rates.
- Identify chromium deposits in cathodes.

Accomplishments

- It was shown that direct contact of a metallic interconnect with the cathode paste/cathode leads to more rapid voltage degradation than expected from the oxyhydroxide mechanism.
- In such cells, a manganese chromium spinel was found near the metal interface, and chromium oxide near the electrolyte.
- It appears that a volatile chromate species, perhaps potassium dichromate, contributes to the degradation.

Future Directions

- The second volatile species will need to be unambiguously identified.
- Methods for diminishing the chromium migration will be explored.

Introduction

Chromium contamination of SOFC cathodes has been observed by several groups of researchers developing cells with metallic bipolar plates. Hilpert et al. have attributed the chromium transport to the formation of a volatile oxyhydroxide species that forms when chromium-containing steels are exposed to oxygen and water at elevated temperatures [1,2]. The volatile oxyhydroxide $CrO_2(OH)_2$ can form either by reaction of the surface oxide with oxygen and water, or by direct reaction of metallic chromium [3]. It has also been shown that $CrO_2(OH)_2$ is the dominant species in the gas phase when water is present [4], and that the cathode acts as a nucleation site for the deposition of chromium [5]. Quadakkers et al. provide an overview of this and other issues related to metallic-based interconnects [6]. There is also work that indicates that both the cathode and electrolyte composition can play a role in chromium poisoning [7,8].

Michael Krumpelt (Primary Contact), Terry A. Cruse, Di-Jia Liu
Argonne National Laboratory
Argonne, IL 60439
Phone: (630) 252-8520; Fax: (630) 252-4176
E-mail: krumpelt@cmt.anl.gov

DOE Project Manager: Lane Wilson
Phone: (304) 285-1336
E-mail: Lane.Wilson@netl.doe.gov

As discussed by Hilpert and others [9,10], the chromium oxyhydroxide is presumed to be reduced to chromium trioxide at the triple phase boundaries in the cathode as shown:

$$2CrO_2(OH)_2 + 6e^- + 3V.. = Cr_2O_3 + 2H_2O + 3O^{2-}$$

The oxide deposits block the access of oxygen to the electrochemically active sites and cause the performance decay of the cell. However, the magnitude of the effect varies greatly between cells and stacks from various organization. To better define the quantitative relations, DOE set up a task force between General Electric, the Pacific Northwest National Laboratory, and Argonne. Our role was to experimentally determine the cell degradation rates in cells with current collectors made of E-Brite, an alloy made by Allegheny Ludlum.

Approach

A new experimental apparatus was jointly developed by the three parties that would simulate the flow field geometry of a typical planar stack. As shown in Figure 1, the fuel cell housing is a two-piece circular structure made of a machinable ceramic (MACOR) that contains a 2.5-cm^2 metal current collector with five flow channels. Under the channels is a fuel cell consisting of a lanthanum manganite cathode, a zirconia electrolyte and a nickel/zirconia anode. These cells were purchased from InDec.

All the team members used identical fixtures and cells and operated them at 250 mA/cm^2 and air flow rates of 70 standard cubic centimeters per minute. Argonne ran three types of experiments. In the first, a current collector made of E-Brite was used. In the second the current collector was gold, and in the third, the current collector was E-Brite with the ribs covered with a gold foil. In the first set, chromium oxyhydroxide was expected to form on the channel surfaces and under the ribs. In the second, no oxyhydroxide was expected

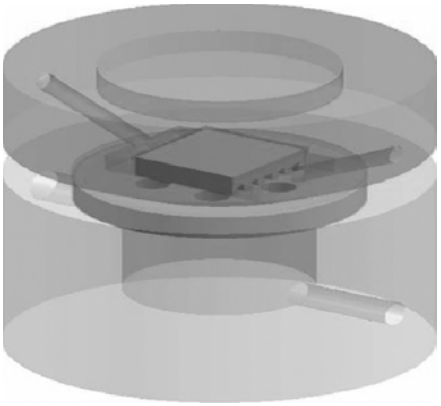

FIGURE 1. Schematic of the Cell Test Stand

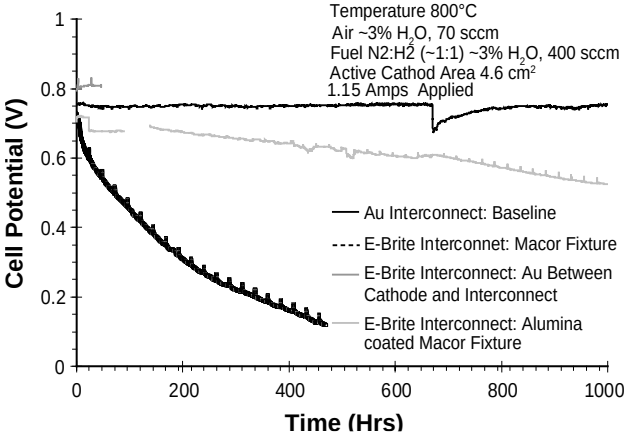

FIGURE 2. Cell Performance Under Various Conditions

to form, and in the third, oxyhydroxide formation was expected only in the channels, where direct contact between E-Brite and cathode is avoided.

Post-test analyses were conducted on the cathodes by scanning electron microscopy and wide-angle X-ray beam spectroscopy using the Advanced Photon Source at Argonne National Laboratory.

Results

Cell Tests

A summary of various electrochemical cell tests is shown in Figure 2. The dark line represents a 1000-hour run with the gold current collector, showing virtually constant performance. In contrast, the cell potential declined rapidly when an E-Brite current collector was used. In that test, a small amount of a yellow deposit was noticed in the exit tube and on the cell after shutdown and disassembly. This yellow deposit was identified as $K_2Cr_2O_7$.

As discussed below, the potassium seems to have come from the MACOR fixture, and to prevent this interference, the MACOR housing was coated with alumina. The lighter trace shows a more stable performance of a cell with an E-Brite current collector in the alumina-coated housing. Finally, a short light trace represents a cell with an E-Brite current collector that had the ribs covered by a gold foil.

Post-test Analyses

Figure 3 shows the distribution of chromium in the cathode. Note that the cathodes consisted of two distinct regions. The layer closest to the electrolyte, labeled as "lower cathode" in the figure contained zirconia to enhance the electrochemical performance, while the "upper cathode" was single-phase strontium-

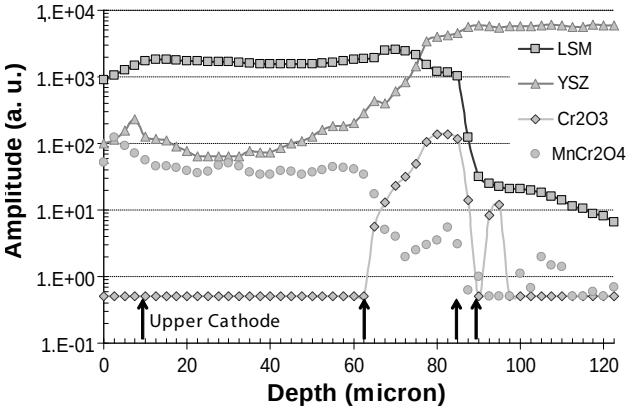

FIGURE 3. Distributions of Cr_2O_3 and $MnCr_2O_4$

doped lanthanum manganite. The figure reveals unambiguously identified Cr_2O_3 deposits (by two distinct X-ray peaks) that are found mostly near the electrolyte but also distributed to some extent in the zirconia-containing part of the cathode. The manganese chromium spinel $MnCr_2O_4$, that has been observed by others, is found primarily near the interconnect interface, and to a lesser extent, throughout the upper cathode. A small rise is noticeable near the electrolyte, as will be discussed further.

Discussion

Our chromium profiles across the cathode clearly show chromium oxide deposits at the electrolyte interface, which is consistent with the mechanism proposed by Hilpert, where the chromium oxyhydroxide is electrochemically reduced to chromium oxide and affects the cell performance. Our profile also confirms that a manganese-chromium spinel forms at the interface of the cathode and the metal. This spinel is the result

of a chemical reaction between the chromium oxide covering the metal and the cathode:

$$7.5\ Cr_2O_3 + 5\ La_{.8}Sr_{.2}MnO_3 = 4\ LaCrO_4 + 5\ MnCr_2O_4 + SrCrO_4 + 1.5\ O_2$$

The spinel is confined to the structural part of the cathode and would not seem to affect the electrochemistry. One should note the small amount of spinel near the electrolyte, which, in our view, is formed by the chromium oxide deposits at the electrolyte reacting with the cathode as shown above.

We did not find the spinel phase in cells where the interconnect ribs had been covered with gold foil.

The amount of chromium oxide near the electrolyte was 3-4% in cells that were run in the MACOR fixture and that were rapidly deteriorating. A mass balance calculation that is beyond the scope of this report reveals that the oxyhydroxide mechanism cannot account for the amount of chromium oxide that was detected in the MACOR cells. Since we found potassium dichromate in the exit tube of these cells, we suspect that the latter did contribute to the chromium transport.

We believe it is important to note this finding because potassium oxide is present in many cements, sealants, and glass/ceramic components. If the potassium dichromate can contribute to the chromium migration it could explain the wide range of cell degradation rates reported in the literature.

Conclusions and Future Directions

It appears that the oxyhydroxide mechanism is valid but may have only an insignificant effect on long-term cell performance. Other volatile species such as potassium and/or strontium dichromates seem to contribute to the chromium transport. Future experiments will focus on these compounds.

References

1. Hilpert, K., D. Das, M. Miller, D. H. Peck, and R. Wei, *J. Electrochem. Soc*., **143**, 3642, (1996).

2. Gindorf, C., L. Singheiser, and K. Hilpert, *Steel Research*, **72,** 528 (2001).

3. Fryburg, G., F. Kohl, and C. Stearns, *J. Electrochem. Soc*., **121,** 952 (1974).

4. Ebbinghaus, B. B., *Combustion and Flame*, **93**, 119 (1993).

5. Jiang, S. P., et al., *J. European Ceramic Society*, **22**, 361 (2002).

6. Quadakkers, W. J., J. Piron-Abellan, V. Shemet, and L. Singheiser, *Materials at High Temperatures*, **20**,115 (2003).

7. Matsuzaki, Y., and I. Yasuda, *J. Electrochem. Soc*., **148**, A126 (2001).

8. Kaun, T. D., T. A. Cruse, and M. Krumpelt, *Ceramic Engineering and Science Proceedings*, **25** (2004).

9. Jiang, S. P., *J. Power Sources,* **124**, 390 (2003).

10. Matsuzaki,Y. and I. Yasuda, *J. Electrochem. Soc.,* **148**, A126 (2001).

Publications/Presentations

1. M. Krumpelt and T. A. Cruse, "Chromium Volatility and Transport in Solid Oxide Fuel Cells," Ceramic Society, Cocoa Beach, FL, January 25–28, 2006.

III.A.4 Intermediate Temperature Solid Oxide Fuel Cell Development

Objectives

- Fabricate and test a thin, supported lanthanum gallate electrolyte based solid oxide fuel cell stack.
- Determine operating characteristics of the stack in the intermediate temperature range.

Approach

- Develop fabrication process for thin, supported lanthanum gallate electrolyte.
- Verify performance of thin cells in button cell configuration.
- Evaluate low temperature cathode materials using symmetric cells.
- Test the new cathode material in short stacks.

Accomplishments

- Button cells were fabricated using the tape lamination technique.
- Preliminary cathode half-cell evaluation was conducted using new cathode compositions.

Future Directions

- Conduct round robin evaluation of cathode half-cells.
- Select promising cathode compositions and develop cathode application process.
- Fabricate and test short stacks.

S. (Elango) Elangovan (Primary Contact), Brian Heck, Mark Timper
Ceramatec, Inc.
2425 South 900 West
Salt Lake City, UT 84119-1517
Phone: (801) 978-2162; Fax: (801) 972-1925
E-mail: Elango@ceramatec.com
Website: www.ceramatec.com

DOE Project Manager: Lane Wilson
Phone: (304) 285-1336
E-mail: LaneWilson@netl.doe.gov

Subcontractors:
Caltech, Pasadena, CA; Dr. Sossina Haile
Northwestern University, Evanston, IL; Dr. Scott Barnett

Introduction

Reducing the operating temperature of solid oxide fuel cells (SOFCs) offers several benefits: improvement in long-term stability by slowing physical and chemical changes in the cell materials, lower cost systems by the use of less expensive balance-of-plant components, compatibility with hydrocarbon reformation process allowing partial internal reformation which in turn reduces the heat exchanger duty, and finally, the potential to improve thermal cycle capability. In addition, the use of stainless steel interconnects is also facilitated by the lower operating temperature. A temperature range of 600°C to 700°C is ideally suited to derive the performance stability, system integration and cost benefits.

In order to derive the advantages of the lower operating temperature, two factors that limit the cell performance, namely the electrolyte resistance and electrode polarization must be addressed. Lanthanum gallate compositions have shown high oxygen ion conductivity when doped with Sr and Mg. Unlike other oxygen ion conductors, such as ceria and bismuth oxide, that are potential candidates for lowering cell operating temperature, the Sr and Mg doped lanthanum gallate (LSGM) compositions are stable over the oxygen partial pressure range of interest. The combination of stability in a fuel gas environment and the high oxygen ion conductivity makes the LSGM material a potential choice for intermediate temperature SOFCs. However, challenges in the development of electrode materials and thin cell fabrication processes need to be overcome to make use of the potential of the LSGM electrolyte.

Approach

Tape cast process development was performed to cast LSGM tape of various thicknesses to provide sintered electrolyte thicknesses ranging from 50 to 200 microns. The process variables included: powder surface area, organic content in the tape slip, and sintering temperature. The primary objectives of the activity were to achieve sintered electrolyte density and flatness required for stacking. Single cells and symmetric cells with 2.5 cm^2 active area were tested for performance characteristics.

While lanthanum cobaltite cathode has good intermediate temperature catalytic activity, the primary issues related to the use of cobaltite cathode are excessive diffusion of Co into LSGM causing phase

destabilization of the electrolyte, and the high coefficient of thermal expansion of cobaltite compositions. Two alternative cathode compositions were evaluated in half-cell tests at the two universities.

Results

Thin electrolyte single cells were fabricated using the tape lamination technique. Both anode and cathode structures were evaluated as the support for the electrolyte. The performance of a cathode-supported cell is shown in Figure 1. The thin, 75 micron LSGM electrolyte cells showed an area specific resistance of 0.5 ohm-cm^2 at an operating temperature of 700°C. The long-term performance of selected cells is shown in Figure 2. Similar performance and stability results were also obtained using cells with the anode-support configurations. Thus, the performance benefits of using high conductivity LSGM electrolyte and the stability improvement by using the modified anode were established in single cell tests.

Sintering process development for fabricating 10 x 10 cm electrolytes was conducted. Initial trials with thick electrolyte defined the sintering process to achieve flat, dense electrolyte. Fabrication development of thin cell structures has been initiated.

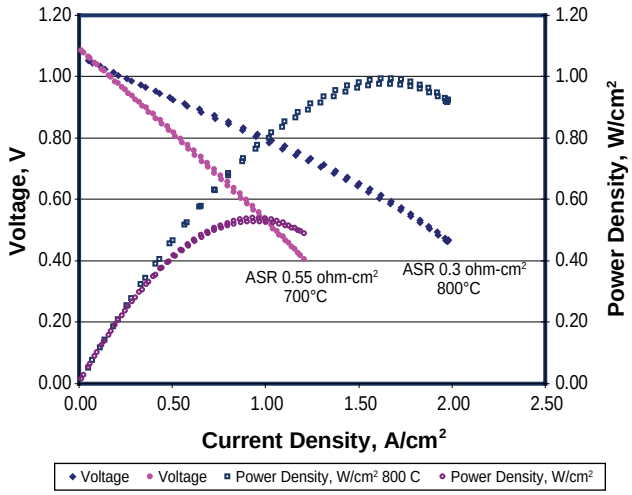

FIGURE 1. Performance of a Cathode Supported LSGM Cell; Electrolyte Thickness of 75 Microns Was Used

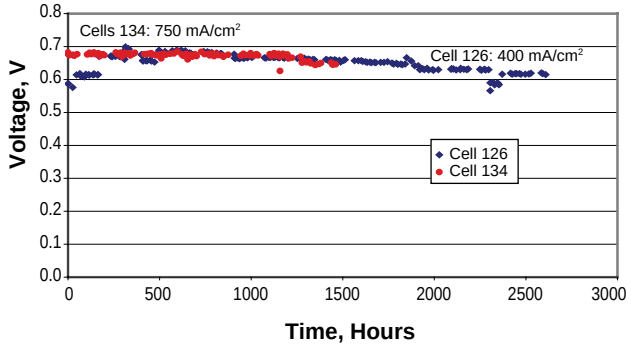

FIGURE 2. Long-Term Stability of Cathode Supported Cells at an Operating Temperature of 700°C

Conclusions

- Thin, supported cells meet the performance target of 0.5 ohm-cm^2 resistance at 700°C.
- Long-term tests of single cells show stable performance.
- Alternative cathode materials show low cathode polarization at temperatures < 700°C.

III.A.5 Metal Interconnect for Solid Oxide Fuel Cell Power Systems

Objectives

- Select a surface treatment process for commercial ferritic stainless steel to reduce oxide scale growth rate.
- Optimize treatment process condition to provide a stable, conductive scale.
- Measure the scale properties in SOFC relevant conditions.
- Evaluate treated metal interconnects under SOFC stack conditions.

Approach

- Select a heat treatment process to achieve a thin, dense scale of a conductive oxide composition.
- Measure scale conductivity in air at target operating temperature.
- Measure air-side scale conductivity when the opposite side is exposed to fuel conditions (dual atmosphere test condition).
- Evaluate scale morphology under fuel cell operating conditions.
- Evaluate the effect of surface treatment on chromium volatility.
- Measure interconnect repeat unit resistance under stack operating conditions.

Accomplishments

- The surface treatment was found to reduce the scale growth rate as determined by thermogravimetry at 750°C. The treated metal coupons showed a parabolic rate constant of 5 x 10^{-9} $gm^2/cm^4/hr$ compared to 7 x 10^{-8} $gm^2/cm^4/hr$ of uncoated coupons. The low oxidation rate of treated interconnects will enable achieving the target fuel cell operating life of 40,000 hours.
- Scale resistance was 10 millohm-cm^2 in air at 750°C and less than one milliohm-cm^2 in humidified hydrogen.
- Scale morphology was characterized as a function of treatment process and test conditions relevant to fuel cell operation.
- Stable, low air-side resistance was demonstrated under dual atmosphere test conditions.
- Significant reduction in chromium evaporation was observed with treated metal coupons.
- No detectable reactivity of treated metal and potential cell joining perovskite compositions.

Future Directions

- Verification of performance improvement in fuel cell stack tests.

S. (Elango) Elangovan (Primary Contact),
J. Hartvigsen, S. Balagopal, I. Bay, M. Timper
Ceramatec, Inc.
2425 South 900 West
Salt Lake City, UT 84119-1517
Phone: (801) 978-2162; Fax: (801) 972-1925
E-mail: Elango@ceramatec.com

DOE Project Manager:
Ayyakkannu Manivannan
Phone: (304) 285-2078
E-mail: Ayyakkannu.Manivannan@netl.doe.gov

Introduction

Interconnects perform essential functions in a fuel cell stack, namely, electrical connection between adjacent cells and separation of air and fuel. In many cases they also provide structural support for the stack. The use of commercial alloy offers the potential for low-cost interconnect components. This allows for achieving the DOE target of low cost, modular fuel cell stacks.

The SOFC interconnect must simultaneously satisfy several functional requirements. These functions require materials with high electronic conductivity for the series connection of individual single cells, gas impermeability to separate fuel and oxidant gases, and chemical stability and conductivity over a large oxygen concentration range in order to maintain integrity in both the fuel and air atmospheres. Thermal expansion match with the rest of the cell elements is desired. Metal interconnects are very desirable from the viewpoints of manufacturing cost in addition to other functional requirements, provided that the high conductivity can be maintained at the operating conditions. It also lends itself to ease of fabrication of gas channels and greater control over dimensions to help improve the conformity as well as uniform reactant distribution to ensure uniform current density, high fuel utilization and high fuel efficiency. The use of thin metallic sheets will also reduce overall weight in the fuel cell system. High thermal conductivity of metal interconnects will help distribute the heat generated during the operation of the cell, thereby reducing the cooling air requirement as well as eliminating thermal stress failure of ceramic components caused by sharp thermal gradients.

The principal requirements of metal interconnects can be summarized as follows: 1) thermal expansion match with other cell components, 2) oxidation resistance in air and fuel at the operating temperature, 3) conductive interface (scale) in air and fuel atmospheres, 4) prevention of reactivity with electrode materials to form insulating compounds, 5) low volatility of major or minor constituents that poison electrode activity, 6) compatibility with anode and cathode environments, 7) uniformity in contact with the cells, 8) thermal cycle capability, and 9) cost. The present work focuses on the development and evaluation of conductive oxide scale on commercial ferritic stainless alloys.

Approach

A commercial stainless steel alloy was selected. The surface oxide scale was modified using an appropriate coating and heat treatment process to provide a dense conductive oxide scale. A second treatment layer was applied to provide a low chromium activity in the surface. Process development to achieve both treatments in a single step was completed. The growth rate, resistivity, and morphology of the scale were determined as a function of time for the various surface treatment conditions. The evaluations were made both in single atmosphere (air or fuel) or dual atmosphere (air and fuel on the opposite sides) conditions. Comparison of chromium evaporation characteristics of treated and untreated metal coupons was made using alumina powder as the chromium getter.

Results

Thermogravimetry of a 400-series commercial stainless steel was performed. Both untreated and treated coupons were evaluated. Two types of treatments were done. The first one was to heat treat the coupon to grow a controlled, dense oxide scale layer (treatment 50C940). In a second variation, an additional treatment was done to provide a stable chromium oxide composition as the outer layer (treatment MI2). The comparison of the oxide scale growth, via weight gain, is shown in Figure 1. The pre-grown oxide layer was found to reduce the scale growth significantly while the second treatment provided an additional reduction in scale growth rate.

The resistances of the coupons were measured after they were surface treated. Two coupons were sandwiched using a conductive perovskite (e.g., Sr-doped lanthanum cobaltite) as the contact paste. The change in measured resistance values of the coupon couples at 750°C in air is shown in Figure 2. The coupons were subjected to several thermal cycles. Similar measurements were also made in humidified hydrogen using nickel paste as the contact layer,

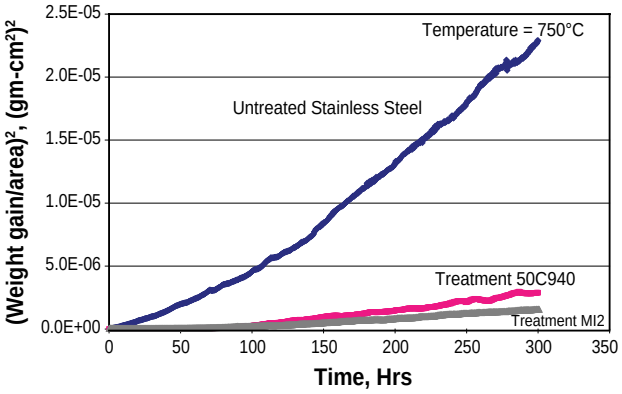

FIGURE 1. Thermogravimetry of Ferritic Stainless Steel Coupons

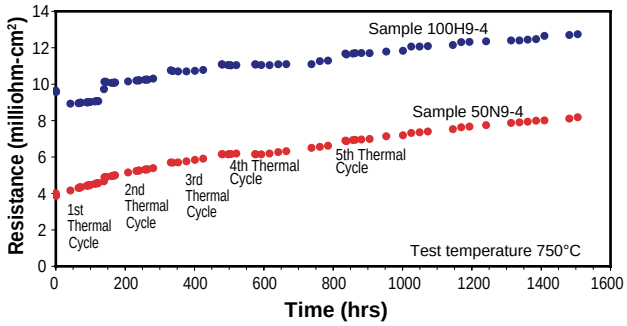

FIGURE 2. Resistance of Coupon Couples in Air at 750°C

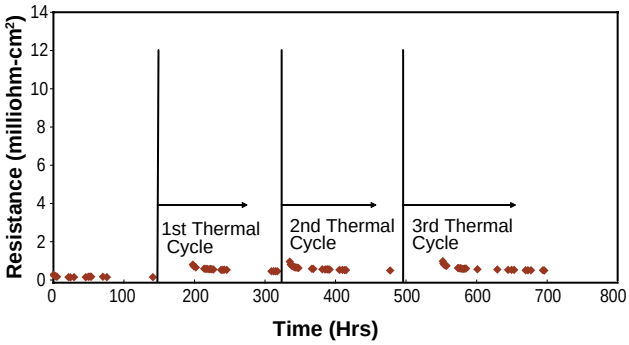

FIGURE 3. Resistance of Coupon Couples in Humidified Hydrogen at 750°C

shown in Figure 3. In both atmospheres, the resistance values were below 10 milliohm-cm^2, meeting the target interconnect resistance.

Earlier work showed that the oxide scale on the air-side is disrupted when the opposite side is exposed to hydrogen at the target cell operating temperature. In order to evaluate the effect of dual atmosphere exposure, resistance of coupon couples were measured when one coupon is exposed to dual atmosphere. The test arrangement and the results of a test using the graded scale composition are shown in Figures 4a and

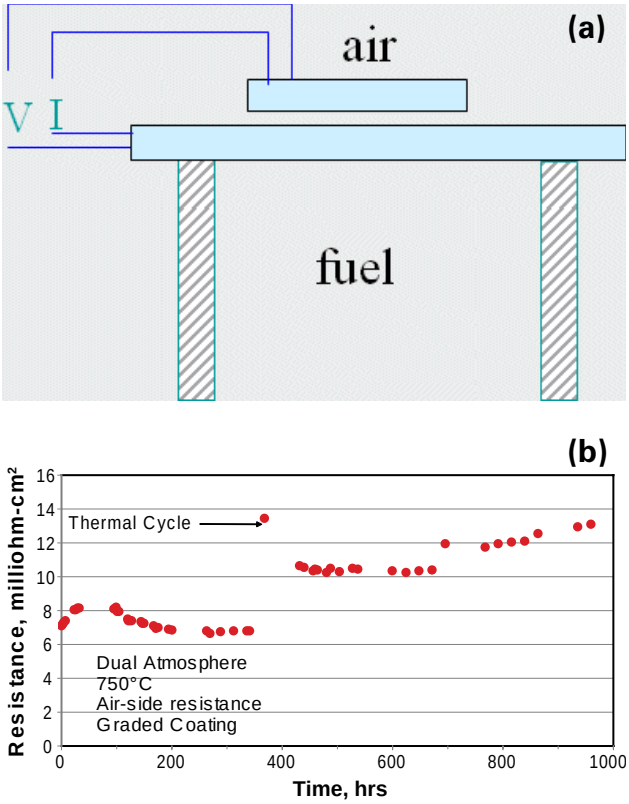

FIGURE 4. Test Configuration (a) and Resistance (b) of Coupon Couples in Dual Atmosphere at 750°C

4b, respectively. The low resistance measured under realistic exposure conditions is encouraging. The scale microstructure after the 1,000-hour test is shown in Figure 5. Both the sandwich area with the current flow in and away from the sandwich area show thin (~3 micron) oxide scale, thus confirming the effectiveness of the treatment under a dual atmosphere exposure.

Chromium evaporation characteristics of the untreated and treated metal coupons were evaluated using an alumina getter. A schematic of the test arrangement is shown in Figure 6. Various coupons were exposed to the getter material at 750°C for 300 hours. A significant reduction in chromium content was noted for the treated coupons as shown in Table 1.

Mixtures of treated and untreated stainless steel powder and perovskite powder were heat treated to evaluate the reactivity. The treated metal powder did not show any evidence of new phases based on x-ray diffraction analysis.

A resistance stack consisting of a series of interconnects with different treatments was tested to simulate the dual atmosphere stack conditions. Initial results showed low resistance for some segments. Additional tests are required to obtain statistical information on the performance variations.

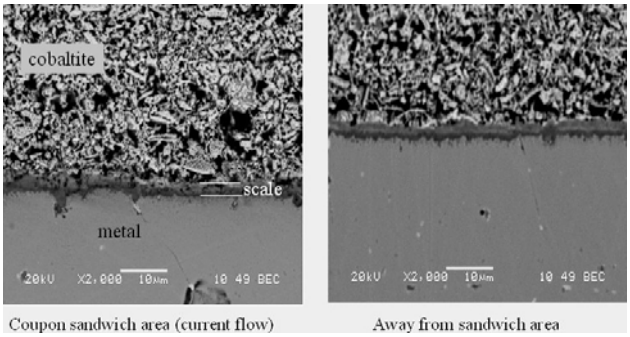

FIGURE 5. Scale Microstructure after the 1,000-Hour Test

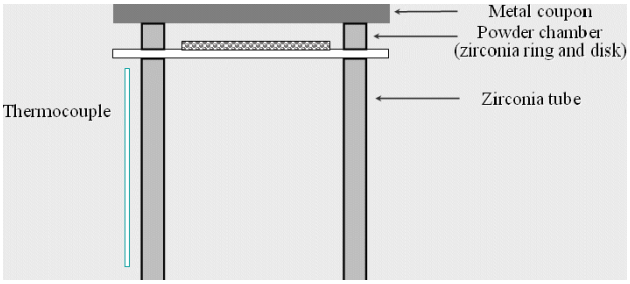

FIGURE 6. Test Configuration for Chromium Evaporation Assessment

TABLE 1. ICP Analysis of Al_2O_3 Powder (ppm by weight)

	Cr
Baseline powder	< 0.5
Powder exposed to untreated coupon	250
Powder exposed to treated coupon	140
Powder exposed to treated and LSCo thermal sprayed coupon	4.1

Conclusions

- Surface treatment to commercial ferritic stainless steel is shown to reduce the oxidation rate in air at SOFC operating temperatures.
- The resistance values of the stainless interconnect meet the target.
- The surface treatment provides improved stability to the scale under dual atmosphere exposure conditions.
- A significant reduction in chromium evaporation rate demonstrated.
- The treatment also suppresses reactivity of metal with cell joining perovskite materials.

FY 2006 Publications/Presentations

1. "Selection and Surface Treatment of Alloys in Solid Oxide Fuel Cell Systems," S. Elangovan, S. Balagopal, J. Hartvigsen, I. Bay, D. Larsen, M. Timper, and J. Pendleton, Journal of Materials Engineering and Performance, August 2006, in press.

III.A.6 Novel Cathodes Prepared by Impregnation Procedures

Objectives

- Examine the feasibility of using different precursor species to impregnate lanthanum strontium manganite (LSM) into porous yttria-stabilized zirconia (YSZ) using fewer steps.
- Determine whether the addition of Co species could be used to enhance performance of LSM-based cathodes.
- Assess the stability of impregnated lanthanum strontium ferrite (LSF)-YSZ cathodes.
- Compare the fabrication cost of impregnated cathodes to one made by screen printing.

Accomplishments

- We showed that similar results were obtained when using various LSM precursors to produce LSM-YSZ cathodes.
- We showed that enhanced performance could be achieved by adding LSCo to LSM-YSZ cathodes.
- We have preliminary results showing that there is a slow deactivation with LSF-YSZ cathodes.

Introduction

While the performance of conventional Sr-doped $LaMnO_3$ (LSM)-YSZ cathodes is adequate at high temperatures, LSM-YSZ composites exhibit only modest performance at 700ºC and poor performance at lower temperatures. Since there is a move towards operation at lower temperatures, cathodes with properties superior to LSM-YSZ are clearly needed. In fact, cathode performance can be improved dramatically by replacing LSM with other perovskites, such as Sr-doped $LaFeO_3$ (LSF) or $LaCoO_3$ (LSCo) [1,2]. Unfortunately, it is not a simple matter to substitute these alternative perovskites for LSM. The conventional fabrication of LSM-YSZ composites involves a high-temperature calcination of LSM-YSZ mixtures to the electrolyte in order to establish good connectivity between the electrode and electrolyte. With LSM, calcination can be performed at 1,250ºC, a temperature that is sufficiently high to sinter the YSZ in the electrode to the YSZ in the electrolyte, thus forming a good three-phase boundary. Unfortunately, it is not possible to calcine LSF-YSZ and LSCo-YSZ mixtures at high temperatures due to the fact that these oxides will undergo solid-state reactions.

An alternative approach to preparing composite cathodes involves eliminating high-temperature sintering of LSF (or LSCo) with YSZ. It has been pointed out that the driving force for reaction between the perovskites and YSZ disappears below 900˚C. This implies that the problem of interfacial reactions may be primarily associated with processing the composite electrode, rather than fuel-cell operation, although interfacial reaction could also occur because of the reducing conditions associated with the electrode-electrolyte interface.

Eduardo Paz (Primary Contact), Naiffer Romero, Shung Ik Lee
Franklin Fuel Cells, Inc.
83 Great Valley Parkway
Malvern, PA 19355
Phone: (610) 640-7545; Fax: (610) 640-2352
Website: www.franklinfuelcells.com

DOE Project Manager: Lane Wilson
Phone: (304) 285-1336
E-mail: Lane.Wilson@netl.doe.gov

Subcontractors:
Raymond Gorte and John Vohs
University of Pennsylvania, Philadelphia, PA

Approach

One way to form an oxide composite that is well connected to the electrolyte, while avoiding the high-temperature co-firing of YSZ and perovskite, involves adding the perovskite to a porous matrix of the YSZ that has already been sintered to high temperatures. The porous YSZ matrix can be produced by simple methods, such as tape casting or tape calendaring with pore formers. The tapes with pore formers can be laminated onto electrolyte tapes in the green state and co-fired together with the green anode. Finally, the perovskite is incorporated into the porous YSZ by infiltration.

Results

A. SOFC Cathodes Prepared by Infiltration with Various LSM Precursors

The cathode properties of LSM-YSZ composites formed by infiltration of porous YSZ with aqueous salt solutions, with LSM nano-particles, and with molten salts are essentially identical. The relatively high mobility of LSM on YSZ, associated with surface interactions between LSM and YSZ, causes the final composite structures to be essentially the same, independent of how the LSM is added. Figure 1 shows

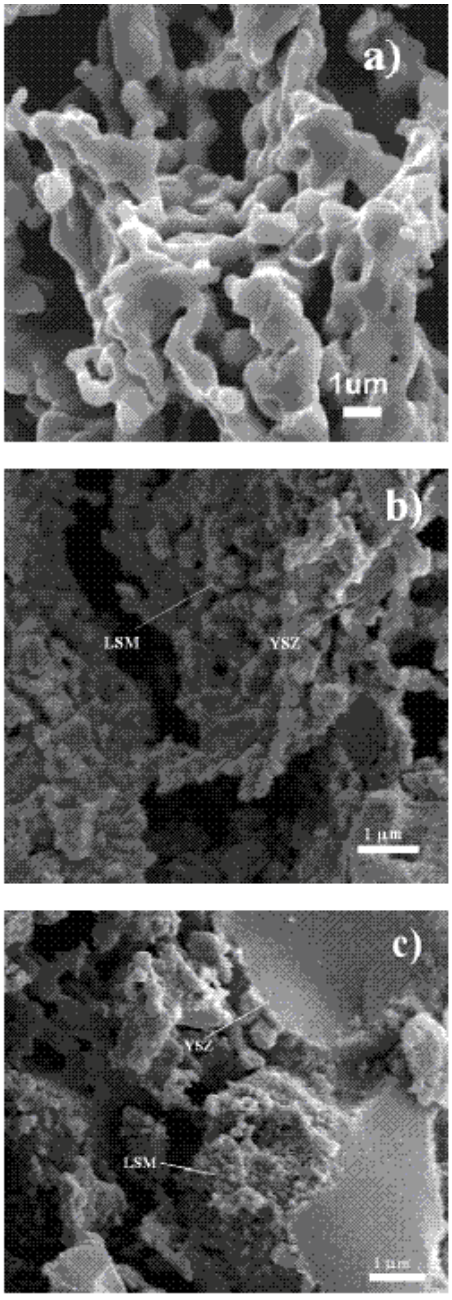

FIGURE 1. SEM images of a) the initial porous YSZ matrix; b) the LSM-YSZ composite prepared by infiltration of the LSM nano-particle suspension; c) the LSM-YSZ composite prepared by impregnation of LSM molten salts.

SEM images of a) the porous YSZ before impregnation, b) LSM-YSZ composite made by impregnation of LSM nano-particle suspension, and c) LSM-YSZ composite prepared by impregnation of the LSM molten salt. Figure 2 shows fuel cell performance data for impregnated LSM cathode cells made by impregnation of a) aqueous salt solutions, LSM-YSZ (aq), b) molten salt, LSM-YSZ (molten), and c) nano-particle suspension, LSM-YSZ (nano). Based on

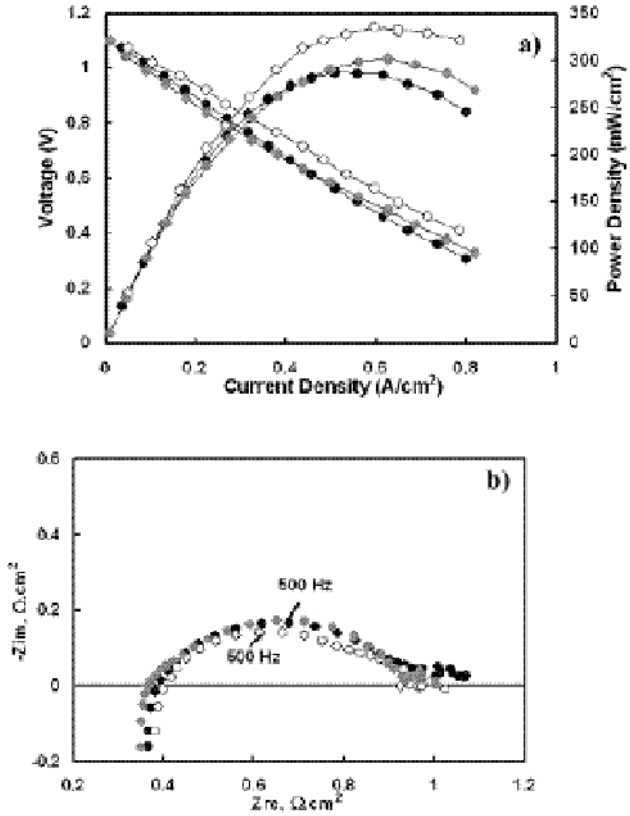

FIGURE 2. Fuel-cell data for cells operating in humidified H_2 (3% H_2O) at 973 K with LSM-YSZ cathodes prepared using different impregnation methods, followed by calcination at 1,323 K: a) V-I Polarization curves; b) Cole-Cole plots of impedance data measured in humidified H_2 (3%H_2O) at 973 K at 300 mA/cm^2. (●) LSM-YSZ (aq); (●) LSM-YSZ (nano); (○) LSM-YSZ (molten).

previous work, we have estimated that the Co-ceria-YSZ anode in these cells contributes an impedance of approximately 0.2 Ω.cm^2, independent of current density. The resistance associated with the electrolytes in each of the cells is predicted to be above 0.3 Ω.cm^2, in reasonable agreement with the observed high-frequency impedance between 0.35 and 0.40 Ω.cm^2 observed in Figure 2b. Therefore, it is straightforward to extract the performance of the cathodes from these data, namely in the range of 0.4 to 0.5 Ω.cm^2.

B. Stability Studies of LSF-YSZ Electrodes

This work is still ongoing but recent data obtained with a "symmetric" cell appears to be the most reliable information we have on the stability of the LSF-YSZ electrodes. This data is shown in Figure 3. The data shows that the ohmic resistance of the cell does not appear to be changing over a period of 1,300 h. That is very encouraging, since any solid-state reactions at the interface between the electrolyte and the electrode would be expected to form insulating layers that would

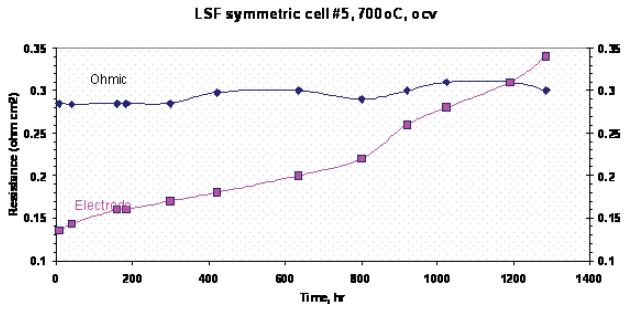

FIGURE 3. Results from a "symmetric" cell, using one of the LSF-YSZ electrodes as a support. One of the LSF-YSZ electrodes is 300 microns thick, while the other is 50 microns. The electrolyte is approximately 70 microns thick. The data in the figure shows the total ohmic and polarization resistances, divided by two to account for the two electrodes.

result in an increased ohmic resistance. However, significant increases have occurred in the polarization losses. While it is possible that these could be due to diffusion through the Ag contact paste, we suggest that something else is causing the increase. We are still attempting to identify the mechanism for this deactivation.

Conclusions and Future Directions

- The cathode properties of LSM-YSZ composites formed by infiltration of porous YSZ with aqueous salt solutions, with LSM nano-particles, and with molten salts are essentially identical. The relatively high mobility of LSM on YSZ, associated with surface interactions between LSM and YSZ, causes the final composite structures to be essentially the same, independent of how the LSM is added. Infiltration of the molten salt allows for the fewest number of infiltration steps, as few as two steps, while infiltration with nano-particles required as many as 40 steps.
- We have preliminary results on the deactivation of LSF-YSZ electrodes at 973 K. Ohmic losses appear to be stable after 1,300 h. However, we are observing an increase in the polarization losses after this period of time. We are presently working to identify the deactivation mechanism.

Special Recognitions & Awards/Patents Issued

1. US Patent # 6,958,196, "Porous Electrode, Solid Oxide Fuel Cell, and Method of Producing the Same", issued October 25, 2005.

FY 2006 Publications/Presentations

1. "An Examination of LSM-LSCo Mixtures for Use in SOFC Cathodes", Y. Huang, J. M. Vohs, and R. J. Gorte, Journal of the Electrochemical Society, Journal of the Electrochemical Society, 153 (2006) A951-55.

2. "SOFC Cathodes Prepared by Infiltration with Various LSM Precursors", Y. Huang, J. M. Vohs, and R. J. Gorte, Electrochemical & Solid-State Letters, 9 (2006) A237-240.

References

1. A. Mineshige, M. Kobune, S. Fujii, Z. Ogumi, M. Inaba, T. Yao, and K. Kikuchi, J. of Solid State Chem., 142, 374 (1999).

2. H. Uchida , S. Arisaka, and M. Watanabe, Solid State Ionics, 135, 347 (2000).

III.A.7 Characterization of Atomic and Electronic Structure of Electrochemically Active SOFC Cathode Surfaces

Objectives

- Investigate the atomic/electronic structures of various cathode materials using quantum chemical calculations.
- Predict the oxygen reduction mechanism on the surfaces of these cathode materials in a solid oxide fuel cell (SOFC).

Accomplishments

- The geometrical and electronic structures of the possible O_2 adsorption on the modeled surfaces of silver and CeO_2-supported silver have been predicted using density function theory (DFT) calculations. Results indicate that the adsorption of peroxide O_2^{2-} is more stable than that of superoxide O_2^- on silver surfaces.
- The mechanisms of O_2 reduction and oxygen ion transport on the modeled surfaces of silver and CeO_2-supported silver have been predicted from the computed potential energy surface (PES). Results suggest that oxygen reduction is more energetically favorable on the CeO_2-supported silver surface than on unsupported silver surfaces.
- The effective charges of the intermediate oxygen species on different silver surfaces have also been estimated from DFT calculations.

Introduction

The interaction of oxygen molecules with oxide-supported metal surfaces is considered as one of the modern classics of heterogeneous reactions for fuel cell and catalytic applications [1,2]. The reduction processes of oxygen molecules on the metal/oxide interface, which correspond to the electrode/electrolyte system, are the key reactions in the cathode region of SOFCs. The oxygen reduction process may occur via three parallel reaction routes, depending on the ionic and electronic transport properties of the cathode and electrolyte materials [3,4]. In the first route, oxygen molecules are adsorbed on the triple-phase boundary (TPB), where the electrolyte, electrode, and oxygen gas meet, and the reduced oxygen ions can directly combine with oxygen vacancies in the electrolyte. In the second route, oxygen molecules are adsorbed and dissociated on the cathode surface, which is a two-phase boundary (2PB), followed by the transport of the dissociated oxygen ions through the cathode to the electrolyte or along the surfaces of the cathode to the TPB. In the third route, oxygen molecules are adsorbed and/or dissociated on the electrolyte 2PB surface, followed by the transport of the adsorbed/dissociated oxygen ions along the surfaces of the electrolyte to the TPB, where they are reduced and incorporated into the electrolyte. For SOFCs with metallic electrodes, it is generally believed that oxygen reduction occurs predominantly at the TPB since metal electrodes are electronic conductors rather than ionic conductors. Nevertheless, the detailed mechanism of oxygen-metal/oxide interaction is still not well understood, and many fundamental concepts at the microscopic level remain unclear.

Meilin Liu (Primary Contact), Jeng-Han Wang
Georgia Institute of Technology
771 Frest Drive
Atlanta, GA 30332
Phone: (404) 894-6114; Fax: (404) 894-9140
E-mail: meilin.liu@mse.gatech.edu
Website: http://www.prism.gatech.edu/~ml44/liu.htm

DOE Project Manager: Lane Wilson
Phone: (304) 285-1336
E-mail: Lane.Wilson@netl.doe.gov

Approach

The electronic calculation to identify the intermediate and transition states in the oxygen reduction process on the 2PB and TPB is optimized by the spin-polarized DFT with the projector-augmented wave method (PAW) [5,6]. The exchange-correlation function is treated with the generalized gradient approximation (GGA) of PW91 formulation [7] for the total energy calculations. The Brillouin zone is sampled by the Monkhorst-Pack scheme [8].

The 2PB is modeled by Ag(111) and Ag(110) surfaces, which are constructed by 6-layer (111) and (110) slabs. Both the (111) and (110) slabs have 2×2 surface cells with 4 Ag atoms. The Monkhorst-Pack k-points, applied for the super cells of Ag(111) and Ag(110) surfaces, are set as 8×8×1 along $(11\bar{2})$ x $(1\bar{1}0)$ x (111) and 8×4×1 along $(1\bar{1}0)$ x (001) x (110) directions, respectively. The cutoff energy and vacuum space are kept at 400 eV and 10 Å, respectively. The top three layers are relaxed and the bottom three layers are fixed at the computed lattice constant during the structure optimization. The TPB is modeled by one Ag

monolayer covered on Ce- or O-terminated CeO_2(111) surfaces. The CeO_2(111) surface is constructed by a p(2x2) 9-layer slab with 12 [CeO_2] units. The top three layers are relaxed, the Monkhorst-Pack k-points are set as 3×3×1 along (211) x (011) x (111) directions, and a 10-Å vacuum space is presented along the (111) direction during the calculation.

Results

O_2 Adsorption: Calculations of adsorption energy suggest that the adsorptions on atop sites are less stable than those on 3-fold hollow sites, which can be rationalized from their bonding structures. Each adsorbed O_2 at the atop position forms one chemical bond with a single Ag atom; in contrast, the adsorbed O_2 at the 3-fold hollow site forms more bonds with nearby Ag atoms. The calculations also suggest that the side-on adsorbed O_2^{2-}(a) is more stable than the end-on adsorbed O_2^{-}(a). In the end-on adsorption of superoxide, only one O atom bonds with the surface, while in side-on adsorption of peroxide, both O atoms bond with the surface Ag atoms. The trends are consistent with the results of previous experimental observations [9,10].

The analysis of the bond lengths indicates that, first, all adsorbed O_2(a) has longer bond lengths than that in the gas phase, 1.236 Å; second, the adsorbed O_2(a) with longer bond lengths has higher adsorption energies because the adsorbate can donate more electrons and form stronger Ag–O bonds to stabilize the whole system. Therefore, the overall stability can be attributed to the energy produced by forming strong Ag–O bonds, which is more than the energy consumed by partially breaking the O–O bond.

The vibration frequencies of the most stable superoxide and peroxide on the modeled TPB, atomic Ag covered on Ce- and O-terminated CeO_2(111) surface, were computed. The adsorptions of superoxide forms with shorter O–O bonds have higher vibration frequencies (1003–1079 cm^{-1}) than those of peroxide forms (750–916 cm^{-1}). The O–O vibrations on the modeled TPB are closer to the experimental observations of O_2(a) on the pure CeO_2(111) surface, O_2^{-}(a): 1127–1135 cm^{-1} and O_2^{2-}(a): 831–877 cm^{-1} (11), than to those of O_2(a) on metal surfaces, O_2^{-}(a): 870–1020 cm^{-1} and O_2^{2-}(a): 610–660 cm^{-1} [12]. This implies that the Ag-covered CeO_2 surfaces still retain the surface properties of CeO_2(111) rather than those of silver surfaces.

O_2 Reduction: The reduction process is related to the O-O dissociation process from the most stable O_2(a) adsorption. On the modeled TPB of Ag-covered O-terminated CeO_2(111) surface, the transition state of the O_2 reduction process has a 0.43-eV reaction barrier when the O-O bond is extended to ~2 Å. The resulting product of the two dissociated O(a) prefers being adsorbed on the two nearest 3-fold hollow sites with an exothermicity of -0.44 eV. On the other modeled TPB of Ag-covered Ce-terminated CeO_2(111) surface, the O_2 reduction process has a 0.28-eV reaction barrier. The dissociated O atoms prefer bonding with subsurface Ce compared to surface Ag atoms with a much higher exothermicity of 4.70 eV because the adsorption energies on atop sites of O–Ce (5.55 eV) are much higher than that of O–Ag (1.99 eV). The potential energy surface (PES) with Bader charge [13] analysis of this process is shown in Figure 1. As a result, the reduction processes on the two modeled TPBs have low reaction barriers and are highly exothermic.

On the other hand, the reduction processes on the modeled 2PB of Ag(111) and Ag(110) surfaces have 0.85-eV and 0.60-eV reaction barriers, respectively. The PES of the O_2 dissociation process on the Ag(111) surface with Bader charge analysis, for example, is shown in Figure 2. Unlike the TPB cases, the reduction

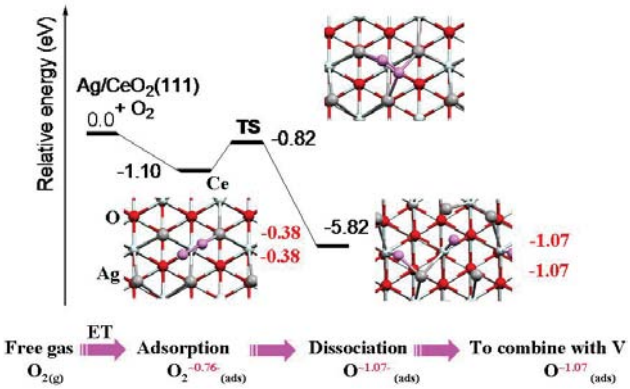

FIGURE 1. PES and geometrical structures of O_2(a) → 2O(a) dissociation processes on a Ag-covered, Ce-terminated, CeO_2(111) surface. The black numbers are the relative energies referenced to O_2(g)/surfaces (= 0). The red numbers are the Bader charges of the adsorbed O.

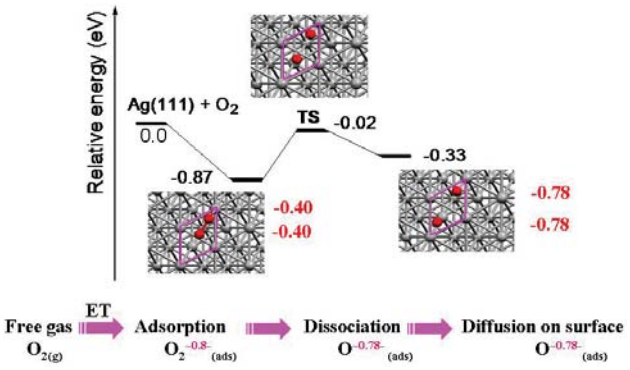

FIGURE 2. PES and geometrical structures of O_2(a) → 2O(a) dissociation processes on a Ag(111) surface. The black numbers are the relative energies referenced to O_2(g)/surfaces (= 0). The red numbers are the Bader charges of the adsorbed O.

processes on the modeled 2PB are endothermic, 0.54 eV on Ag(111) and 0.25 eV on Ag(110) surfaces. Therefore, from the mechanism calculations, the O_2 reduction process is energetically more favorable to occur on the TPB than on the 2PB since the process has a lower reaction barrier and higher exothermicity on the TPB.

Oxygen Ion Transport: The O ion transport refers to the motion of the dissociated O(a) from one stable site to another on the surface. Compared with surface morphology, the separation between the stable sites on the TPB is larger than that on the 2PB. Compared with the electronic structure, the subsurface atoms of the TPB have stronger interaction with surface O(a) than those of the 2PB. Therefore, the transport process near the TPB of Ag supported by the O-terminated CeO_2(111) surface has a higher energy barrier (~0.59 eV) than on the 2PB of silver: the Ag(111) surface has a barrier of 0.37 eV and the Ag(110) surface has a barrier of 0.17 eV. On the other modeled TPB of Ag supported by Ce-terminated CeO_2(111) surface, the O ions transport from the surface Ag layer directly to the subsurface Ce without any barrier and with a high exothermicity of -3.56 eV. This result suggests that any dissociated O at the TPB will be dragged into the unsaturated Ce^{3+} in the electrolyte quickly.

These calculations predict that the TPB of Ag supported by the Ce-terminated CeO_2(111) surface has the lowest energy barrier for O_2 reduction, and the dissociated O ions can directly transport to the CeO_2 bulk without any energy barrier, implying that the TPBs are the most active sites for oxygen reduction. This result agrees well with the experimental observation that cell performance can be enhanced by increasing the TPB area [14,15].

Conclusions and Future Directions

Oxygen-reduction mechanisms on silver-based cathodes have been examined by spin-polarized DFT calculation with the PAW method. The stepwise reactions occurring on a silver-based SOFC cathode can be described as

$$O_2(g)\ (+\ e) \rightarrow O_2^-\ (+\ e) \rightarrow O_2^{2-} \rightarrow 2O^{2-}\ (+V_o^{\bullet\bullet}) \rightarrow O_o^x$$

where $V_o^{\bullet\bullet}$ represents an oxygen vacancy in the electrolyte and O_o^x corresponds to an oxygen ion at a regular oxygen site in the electrolyte.

The computed energies of these reactions, as summarized in Figure 3, show that the cathodic reactions in an SOFC, the O_2 adsorption, dissociation, and reduction as well as the combination of the dissociated O ions with oxygen vacancies in the electrolyte are energetically more favorable to take place in the TPB region where subsurface Ce atoms are present (together with oxygen vacancies). This prediction is consistent with the experimental

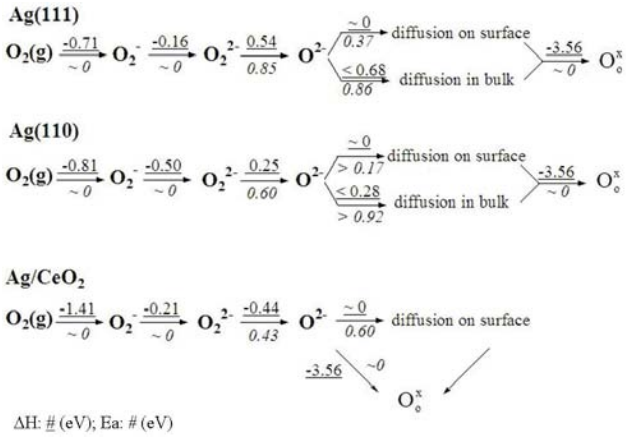

FIGURE 3. The stepwise reaction mechanisms of oxygen reduction processes on Ag(111) and Ag(110) surfaces and at a TPB, silver-covered, Ce-terminated CeO_2(111) surface. The underlined numbers represent the heat of reaction, ΔH, in eV whereas the italic numbers represent the reaction barrier, Ea, in eV.

observations that the efficiency of a SOFC can be enhanced by increasing the TPB areas.

Future studies are briefly outlined as follows:

- Predict O_2 reduction mechanisms on different cathode materials using similar approaches.
- Take into consideration the effect of temperature and pressure in the calculations to predict the catalytic activity of different cathode materials under various conditions.
- Take into consideration the effect of an applied direct current polarization in the calculations to simulate practical SOFC operating conditions.

FY 2006 Publications/Presentations

1. J. H. Wang, M. Liu, M. C. Lin, Oxygen reduction reactions in the SOFC cathode of Ag/CeO_2; *Solid State Ionics.* **177**, 939 (2006).

2. J. H. Wang, M. Liu, Catalytic ability in Ag electrode and Ag/CeO_2 triple phase boundary, to be submitted.

3. J. H. Wang, M. Liu, Mechanism of Oxygen Reduction on a Ag/CeO_2 Based SOFC Cathode; Strategic Energy Initiative (SEI) Energy Research Exposition, Atlanta, GA, February 28th, 2006.

References

1. M.S. Chen, D.W. Goodman, Science 306 (2004) 232.

2. C.T. Campbell, Science 306 (2004) 234.

3. M. Liu and J. Winnick, "Fundamental Issues in Modeling of Porous Electrodes of Mixed Ionic-Electronic Conductors", *Solid State Ionics*, Vol. **118** (1999) 11-21.

4. J. Fleig, Annual Review of Materials Research 33 (2003) 361.

5. P.E. Blöchl, Physical Review B 50 (1994) 17953.

6. G. Kresse, D. Joubert, Physical Review B 59 (1999) 1758.

7. J.P. Perdew, J.A. Chevary, S.H. Vosko, K.A. Jackson, M.R. Pederson, D.J. Singh, C. Fiolhais, Physical Review B 46 (1992) 6671.

8. H.J. Monkhorst, J.D. Pack, Physical Review B 13 (1976) 5188.

9. M.R. Salazar, C. Saravanan, J.D. Kress, A. Redondo, Surface Science 449 (2000) 75.

10. H. Nakatsuji, H. Nakai, Chemical Physics Letters 197 (1992) 339.

11. V.V. Pushkarev, V.I. Kovalchuk, J.L. d'Itri, Journal of Physical Chemistry B 108 (2004) 5341.

12. R.D. Jones, D.A. Summerville, F. Basolo, Chemical Reviews 79 (1979) 13.

13. R.F.W. Bader, Atoms in Molecules - A Quantum Theory, Oxford, Oxford University Press, 1990.

14. T. Horita, K. Yamajia, N. Sakaia, Y. Xionga, T. Katoa, H. Yokokawa, T. Kawada, Journal of Power Sources 106 (2002) 224.

15. R. Radhakrishnan, A.V. Virkar, S.C. Singhalb, Journal of The Electrochemical Society 152 (2005) A927.

III.A.8 Functionally Graded Cathodes for Solid-Oxide Fuel Cells

Objectives

- Elucidate the mechanism of the oxygen-reduction reaction using *in situ* vibrational spectroscopy and *ab initio* analysis.
- Develop micro-impedance spectroscopy system to discern the reaction mechanisms for oxygen reduction and to elucidate the effect of electrode geometry on overall performance of SOFCs.
- Complete the construction of an ultra high vacuum (UHV) system for temperature programmed desorption (TPD) and sticking probability measurements relevant to O_2-cathode interactions.
- Analyze the kinetics of oxygen-reduction reactions occurring at charged mixed ionic-electronic conductors (MIECs) using two-dimensional finite volume models with *ab initio* calculations.
- Determine oxygen permeation rate through dense silver membranes to estimate the oxygen transport rate under SOFC operating conditions.

Accomplishments

- Two distinct oxygen bands appeared at 825 and 1131 cm^{-1}, corresponding to peroxo- and superoxo-like species, respectively, when partially reduced CeO_2 was exposed to 10% O_2. Periodic density functional theory (DFT) calculations aided the interpretation of spectroscopic observations.
- A lanthanum strontium manganese (LSM) microelectrode (ME) generated from a patterned LSM electrode was used to examine the electrode-geometry effect using micro-impedance spectroscopy.
- A UHV system has been built for fundamental study of cathode materials under well-controlled conditions.
- A numerical finite volume scheme was devised to solve a nonlinear DC polarization problem for mixed conductor thin films in two dimensions, including the effect of sheet resistance.
- Oxygen permeation through dense silver membranes was determined to follow an Arrhenius relation with an activation energy of 0.94 eV (21.7 kcal mol^{-1}). The effective leaking current density was calculated to be 0.0146 mA cm^{-2} at 750°C.

Meilin Liu (Primary Contact), Harry Abernathy, SongHo Choi, Y. M. Choi, Charles Compson, Jian Dong, Erik Koep, David Mebane, Robert Williams, Jr.

Georgia Institute of Technology
School of Materials Science and Engineering
771 Ferst Drive, Atlanta, GA 30332-0245
Phone: (404) 894-6114; Fax: (404) 894-9140
E-mail: meilin.liu@mse.gatech.edu

DOE Project Manager: Lane Wilson
Phone: (304) 285-1336;
E-mail: Lane.Wilson@netl.doe.gov

Introduction

This project has centered on elucidating the reaction mechanism of oxygen reduction on SOFC cathode materials using experimental measurements in conjunction with advanced theoretical tools (i.e., quantum-chemical calculations and continuum modeling). Accelerating the oxygen-reduction rate is imperative to reduce the cathode/electrolyte interfacial polarization resistance, which can be achieved by understanding the elementary steps of the oxygen-reduction reaction. The elementary steps of oxygen reduction on cathode materials generally include: (1) molecular and dissociative adsorption of oxygen species, (2) dissociation of adsorbed oxygen species along with charge transfer, (3) diffusion of adsorbed molecular or dissociated oxygen species to the cathode/electrolyte interface, and (4) incorporation of partially charged oxygen ions into the electrolyte lattice.

Approach

Experimental methods along with theoretical analyses have been carried out to guide the design of functionally graded cathode materials in SOFCs. *In situ* vibrational spectroscopy in conjunction with advanced *ab initio* surface modeling was applied to measure surface oxygen species at various metal-oxide surfaces. Micro-impedance spectroscopy has been utilized to elucidate the reaction mechanism of oxygen reduction and to better discern the effect of electrode geometry on the cathode materials. A TPD system has been set-up to study adsorbed oxygen species on cathode materials while concurrently running *in situ* vibrational spectroscopy. To examine the surface mechanism of LSM thin films, we have produced a model of direct current (DC) response in thin films. The inert properties of silver over a wide temperature range could prove it a strong candidate for intermediate-temperature SOFC interconnect applications. Therefore, the oxygen permeation rate through dense silver was measured in

order to determine the effective leaking current density under SOFC operating conditions.

Results

Interactions between O_2 and CeO_2 were examined experimentally by *in situ* Raman spectroscopy and theoretically by density functional slab model calculations. The ceria studies were carried out as a way to test our quantum-chemical calculation methods since the structure of ceria is simpler than the mixed conducting oxide perovskites used for SOFC cathodes. As illustrated in Figure 1(a), when partially reduced CeO_2 was exposed to 10% O_2, two distinct oxygen bands appeared at 825 and 1131 cm^{-1}, corresponding to peroxo- and superoxo-like species, respectively. In order to verify the peaks were indeed an oxygen-containing species, another Raman spectrum was recorded by exposing the sample to 10% $^{18}O_2$ and observing any shift in peak position. Periodic DFT calculations based on the surface mode shown in Figure 1(b) aided the interpretation of spectroscopic observations and provided energetics and geometrical information for the dioxygen species adsorbed on CeO_2. The O_2 adsorption energies on unreduced CeO_2 surfaces are endothermic ($0.91 < \Delta E_{ads} < 0.98$ eV), while those on reduced surfaces are exothermic ($-4.0 < \Delta E_{ads} < -0.9$ eV), depending on other relevant surface processes such as chemisorption and diffusion into the bulk. Partial reduction of surface Ce^{4+} to Ce^{3+} (together with the formation of oxygen vacancies) can alter geometrical parameters and, accordingly, lead to a shift in the vibrational frequencies of adsorbed oxygen species compared to those on unreduced CeO_2. Moreover, the location of oxygen vacancies affects the formation and subsequent dissociation of oxygen species on the surfaces. DFT predictions of the adsorption energetics support the experimental observation that oxygen adsorption and reduction is energetically more favorable on reduced ceria surfaces than on unreduced surfaces.

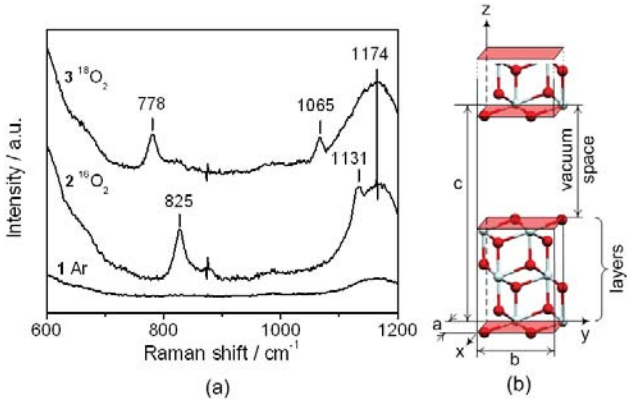

FIGURE 1. (a) A representative surface model with nine layers for the O_2-CeO_2(111) interactions. (b) Typical Raman spectra of CeO_2 sample treated by 5% H_2 at 673 K before 298 K exposure to (1) Ar, (2) 10% $^{16}O_2$, and (3) 10% $^{18}O_2$ atmospheres (all mixtures are diluted with Ar).

To examine adsorbed oxygen species on cathode materials, nanoparticles of the desired mixed oxides (LSM, lanthanum strontinum cobalt [LSC], and samarium strontium cobalt [SSC]) were deposited on a yttria-stabilized zirconia (YSZ) substrate using combustion CVD (CCVD). To generate a surface enhanced Raman signal (SERS) effect, silver nanoparticles were deposited simultaneously with the cathode material. Besides having a greater intensity, the SERS spectrum also has more distinct peaks. The key to observing adsorbed oxygen peaks in the Raman spectra – besides having a high exposed surface area – is having a surface sufficiently clear of surface hydroxyl groups and other unwanted adsorbants before exposing the sample to oxygen. We are currently testing various evacuation regiments at different temperatures to find a method that cleans the cathode surface sufficiently enough to generate a detectable adsorbed oxygen species signal.

Shown in Figures 2(a) and 2(b) are typical SEM images of a tungsten carbide (WC) tip used for current collection and an LSM microelectrode generated from a patterned LSM electrode using an electrochemically etched tungsten-carbide tip, respectively. The height and width of the LSM patterned electrode and the space between two adjacent LSM electrodes are 0.8, 11.5, and 20 μm, respectively. The rest of the patterned LSM electrodes were used as the counter electrode (CE). By controlling the position of the LSM ME, we can separate the ME and CE by a single YSZ grain boundary, or put the ME and CE onto a single YSZ grain. Shown in Figure 2(c) is the effect of the LSM ME perimeter on LSM-YSZ interfacial impedance at 650°C. It was found that the Ohmic portion of the impedance decreased as the perimeter of the LSM ME was increased. In addition, we found that the product of the ME perimeter and the Ohmic portion of the impedance also decreased with an increase of the ME perimeter. The product should remain constant if triple-phase boundaries (TPBs) are single lines around the ME. It seems that the small ME has a larger perimeter specific resistance as compared to the larger perimeter MEs. A possible explanation is that some unobservable delamination caused by the scratching process has occurred. The smaller the ME, the higher the relative percentage of delaminated area and thus, the larger the Ohmic portion of the impedance resistance. The proposed delamination issue could be resolved by scratching the patterned ME before the annealing process. Specifically, after the patterned electrode was fabricated by the sputtering process, the ME would be scratched, and then annealed at higher temperature. Another observation was an

increase in the impedance with increased DC bias, suggesting the electrode reaction is mass transfer limited. Application of DC bias should not change the shape of the impedance spectrum, as the DC bias should only influence the non-ohmic component. After applying DC voltage, the impedance was collected without DC bias again. No significant change was found indicating that application of DC bias did not damage or alter the ME. More detailed studies to interpret the experimental observations with an electrochemical modeling are in progress.

We have developed a model to predict the electrochemical response of thin-film and patterned electrodes, which we then used to account for sheet resistance in 60 nm thick LSM thin films with current collectors 50 μm apart. We found that electrical potential increases along the length of the film between current collectors due to sheet resistance. Shown in Figure 3 is a simulated, normalized cathodic current density-voltage curve for the film. Note the Tafelian behavior in Figure 3. The semi-log scale in the left-hand plot of the figure reflects the shape of a co-limited process. In this case, the limiting factors are ionic transport at low overpotentials, and sheet resistance at high overpotentials. The reason for the switch is that the vacancy transfer at the interface is potential-dependent, with an exponential response to potential changes (hence the Tafelian profile), while bulk electronic transport is only linearly responsive to potential. A greater concentration of vacancies in the bulk leads to higher ionic conductivity, in turn leading to greater sheet resistance losses. The problem is a difficult one to solve, since consideration of sheet resistance obviates the common assumption of ambipolar diffusion in MIECs, which simplifies the mathematics considerably but will not always be true for thin films. In addition, the problem is in two dimensions and is nonlinear. A numerical finite volume scheme was devised to solve the problem. The scheme used is time-dependent (even though the model results prior to steady-state are not reliable), which enables the use of a linear solver. This scheme works quite well at low overpotentials, however at cathodic overpotentials above 500 mV, the method slows down and ultimately becomes unstable. However, the instability in the numerical solver we have found so far is limited to high potential regions in which the material itself would not be chemically stable in reality.

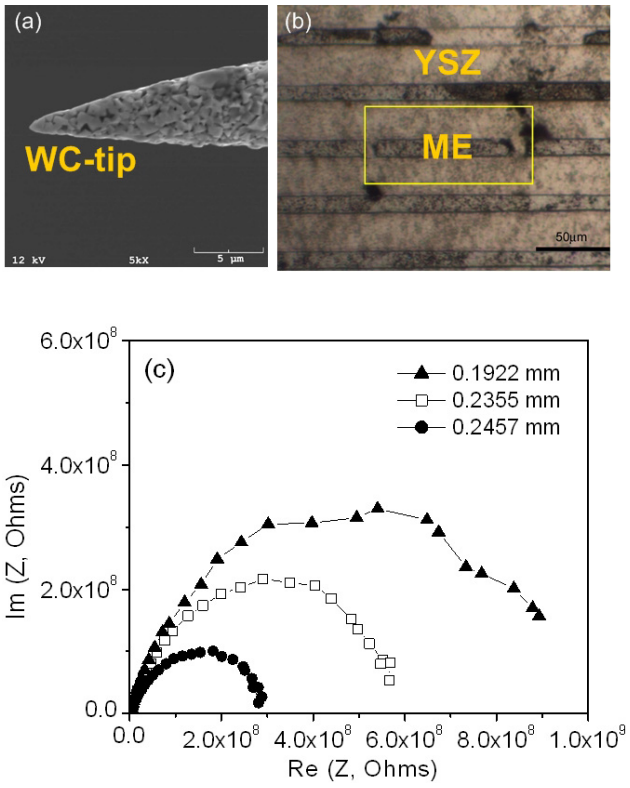

FIGURE 2. (a) An SEM image of a WC tip used for current collection of ME. (b) An LSM microelectrode generated from a patterned LSM electrode fabricated onto YSZ with large grains. (c) Impedance plots of the LSM microelectrode on YSZ at 650°C. The different plots correspond to the different ME perimeters listed in the plot. Note the decrease in overall impedance with increased the ME perimeter.

As illustrated in Figure 4, oxygen permeation through dense silver membranes was determined to follow an Arrhenius relation with an activation energy of 0.94 eV (21.7 kcal mol^{-1}), which is comparable to literature values. The quantitative oxygen permeation and flux were also in agreement with reported values from the literature. Though oxygen permeation rates increased with temperature, the effective leaking current density generated at high temperatures (0.0146 mA cm^{-2} at 750°C) is still minimal enough to allow silver to meet the gas separation requirements for SOFC materials.

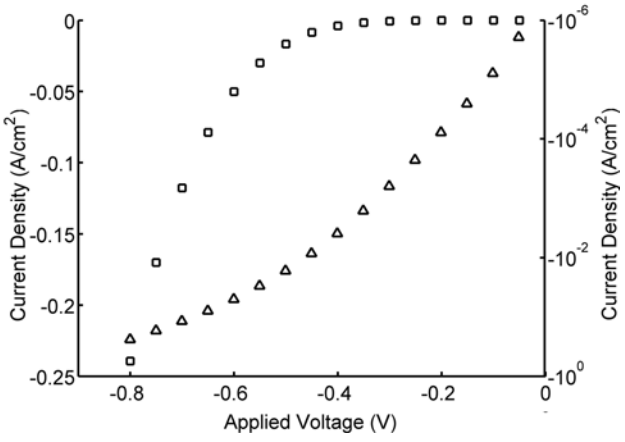

FIGURE 3. Current density-voltage curve for a 60 nm thick LSM film with current collectors 50 μm apart. Both linear (□) and semilog (Δ) plots are shown.

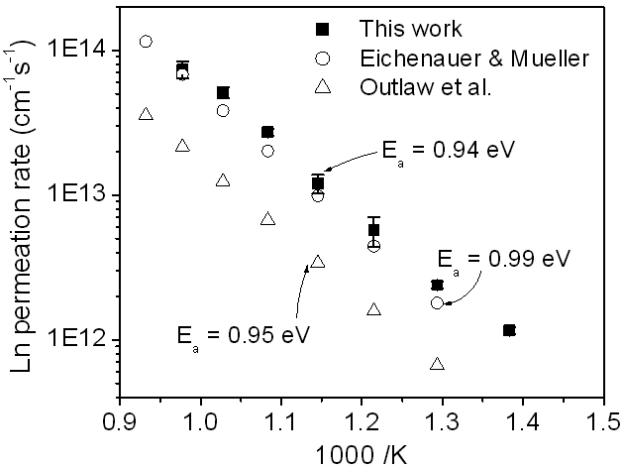

FIGURE 4. Arrhenius plot of measured oxygen permeation rate through dense silver versus inverse temperature (solid symbols) compared to literature values (open symbols).

Similar to what has been found in previous literature, degradation of the silver surface was observed to occur at the grain boundaries after only a few hours. A silver layer of about 12 µm (deposited by DC sputtering) was sufficient to prevent a quantifiable oxidation front within the Ni-YSZ anode after 8-hour exposure to SOFC operating conditions, nevertheless significant surface porosity was still observed. As silver theoretically makes a viable SOFC interconnect material for intermediate- and low-temperature SOFCs, the study on the grain boundary degradation will be examined in more detail for successful application.

Conclusions and Future Directions

In the past year, we made important progress in elucidation of the reaction mechanism of oxygen reduction on cathode materials for SOFCs by means of experimental and computational approaches. The combination of *in situ* Raman microscopy with *ab initio* calculations has provided detailed molecular-level information about surface adsorbed oxygen species. A model for electrochemical response was established to account for the effect of sheet resistance in LSM thin films using a numeric finite volume scheme. Silver was evaluated as a potential intermediate-temperature SOFC interconnect by measuring the oxygen permeation rate through dense silver membranes, which were determined to follow an Arrhenius relation with an activation energy of 0.94 eV (21.7 kcal mol^{-1}). Future studies are briefly outlined as follows.

- Suitable methods for application of noble metal nano-particles onto cathode materials, which result in acceptable surface enhanced Raman signals, need to be developed. Once a method has been found that can generate a strong surface signal, we will use the mapping feature of our Raman spectrometer to explore the presence of this signal near and around the TPBs of our micropatterned electrode samples. In addition, advanced *ab initio* modeling will be carried out to interpret the surface adsorbed species detected by SERS.
- TPD and sticking probabilities for O_2-MIEC interactions will be conducted to identify surface adsorbed oxygen species and their desorption rates including the kinetics of adsorption and desorption.
- We plan to devise a steady-state scheme (not time-dependent) to model the DC response of MIEC thin films, which will require a nonlinear solver but should be much faster at high overpotentials. After combing the model with DFT calculations, it will be compared with experiments.

FY 2006 Publications/Presentations

Publications

1. H. Chen, Y. Chen, A. Aleksandrov, J. Dong, M. Liu, and T. M. Orlando, "Charging Effects on Electron-Stimulated Desorption of Cations from Gadolinia-doped Ceria Surfaces", *Applied Surface Science*, 243(1-4), 166-177, 2005.

2. H. Chen, A. Aleksandrov, Y. Chen, S. Zha, M. Liu, and T. M. Orlando, "Probing Water Interactions and Vacancy Production of Gadolinia-doped Ceria Surfaces Using Electron Stimulated Desorption", *Journal of Physical Chemistry B* 109 (22), 11257-11262, 2005.

3. Y. Liu, E. Koep, and M. Liu, "A Highly Sensitive and Fast Responding SnO_2 Sensor Fabricated by Combustion Chemical Vapor Deposition (CVD)", *Chem. Mater.*, 17, 3997-4000, 2005.

4. Y. Liu, M. Liu, "Creation of Porous Ceria by Sublimation of Tin Dioxide during Sintering", *Advanced Eng. Materials*, 8, 89-93, 2006.

5. H. Chen, A. Aleksandrov, S. Zha, M. Liu, and T. M. Orlando, "Highly Efficient Electron Stimulated Desorption of O+ from Gadolinia-Doped Ceria Surfaces", *Journal of Physical Chemistry,* 110(22), 10779-10784, 2006.

6. Y. Liu, M. Liu, "Porous SOFC Anodes Prepared by Sublimation of an Immiscible Metal Oxide during Sintering", Electrochemical and Solid-State Letters, 9(5), B25-B27, 2006.

7. J. H. Wang, M. Liu and M.C. Lin, "Oxygen Reduction Mechanism on Ag/CeO_2 Cathodes of SOFCs", Solid State Ionics, 177(9-10), 939-947, 2006.

8. D. Mebane and M. Liu, "Classical, phenomenological analysis of the kinetics of reactions at the gas-exposed surface of mixed ionic electronic conductors", *J. Solid State Electrochemistry,* 10(8), 575-580, 2006.

9. E. Koep, D. Mebane, R. Das, C. Compson, and M. Liu, "The Characteristic Thickness for a Dense LSM Electrode" *Electrochemical and Solid State Letters*, in press.

10. E. Koep, M. Liu, "Fabrication and Characterization of Thin-Film Mixed-Conducting Electrodes for Fundamental Studies", *Journal of Power Sources*, accepted.

11. R. Das, D. Mebane, E. Koep, and M. Liu, "Modeling of Patterned Mixed-Conducting Electrodes and the importance of sheet resistance at small feature sizes," *Solid State Ionics*, submitted.

12. H. T. Chen, Y. M. Choi, M. Liu, and M. C. Lin, "A Mechanistic Study of the Reduction of Ceria (111), (110) and (100) Surfaces by H_2", *J. Phys. Chem. B*, submitted.

13. Y. M. Choi, A. Harry, H. T. Chen, M. C. Lin, and M. Liu, "Characterization of O_2-CeO_2 interactions using in-situ Raman spectroscopy and first-principles calculations," *ChemPhysChem*, accepted.

14. H. Chen, A. Aleksandrov, Y. Chen, S. Zha, M. Liu, and T. M. Orlando, "Defect Structure of Gadolinia-doped Ceria Surfaces Using Electron Stimulated Desorption", *Journal of Physical Chemistry*, submitted.

15. D. Mebane and M. Liu, "Modeling of MIEC Cathodes: Effect of Sheet Resistance", *Ceramic Transitions*, in press.

16. Y. M. Choi, D. Mebane, M. C. Lin, and M. Liu, "Characterization of Oxygen Reduction on Electrochemically Active Cathode Surfaces in Solid Oxide Fuel Cells," *J. Alloys. Comp.*, to be submitted.

Presentations

1. D. Mebane and M. Liu, "Modeling of MIEC Cathodes: Effect of Sheet Resistance", 30th International Conference & Exposition on Advanced Ceramics and Composites, Cocoa Beach, FL. (2006).

2. H. Abernathy, Y. M. Choi, M. C. Lin, and M. Liu, "Characterization of Oxygen Reduction in Solid Oxide Fuel Cells", Symposium for the Georgia Tech Strategic Energy Initiative, Atlanta, GA (2006).

3. J. H. Wang and M. Liu, "Mechanism of Oxygen Reduction on a Ag/CeO_2 Based SOFC Cathode", Symposium for the Georgia Tech Strategic Energy Initiative, Atlanta, GA (2006).

4. R. Das and M. Liu, "Modeling of Micro-Impedance Measurements of Mixed-Conducting Electrodes for SOFCs", Symposium for the Georgia Tech Strategic Energy Initiative, Atlanta, GA (2006).

5. J. Dong, R. Williams Jr., H. Abernathy, and M. Liu, "Characterization of Chromium Poisoning of SOFC's Cathodes", Symposium for the Georgia Tech Strategic Energy Initiative, Atlanta, GA (2006).

6. H. T. Chen, Y. M. Choi, M. Liu, and M. C. Lin, "A Theoretical Study of the Reduction of Ceria (111), (110) and (100) Surfaces by H_2", Vietnam-Taiwan Quantum Chemistry Conference, Taiwan (2005).

7. H. T Chen, Y. M. Choi, M. Liu, and M. C. Lin, "A Computational Study of the Reduction of Ceria (111), (110) and (100) Surfaces by H_2", Chemical and Physical Processes in Combustion, FL (2005).

8. Y. M. Choi, M. C. Li, and M. Liu, "A Computational Study of Gas-Solid Interactions in Solid Oxide Fuel Cells", Georgia Local Section of the Electrochemical Society, Atlanta, GA (2005).

9. J. Dong, R. Williams Jr., and M. Liu, "Investigation of Reaction Mechanism of Ag/Gd Doped Ceria (GDC) Using Micro-Impedance Spectroscopy", Georgia Local Section of the Electrochemical Society, Atlanta, GA (2005).

10. D. Mebane and M. Liu, "Phenomenological Kinetics of Gas-Surface Reactions at Mixed Conducting Electrodes", Georgia Local Section of the Electrochemical Society, Atlanta, GA (2005).

References

1. S. Pizzini, Fast Ion Transport in Solids. (1973).

2. B. C. H. Steele, Solid State Ionics 86-88, 1223 (1996).

3. E. I. Tiffee and A. V. Virkar, High Temperature Solid Oxide Fuel Cells: Fundamentals, Design and Applications (Elsevier, New York, 2003).

4. R. Radhakrishnan, A. V. Virkar, and S. C. Singhal, J. Electrochem. Soc. 152 (5), A927 (2005).

5. Y. M. Choi, H. Abernathy, H. T. Chen, M. C. Lin, and M. Liu, ChemPhysChem, accepted (2006).

III.A.9 Novel Sulfur-Tolerant Anodes for Solid Oxide Fuel Cells

Objectives

- Characterize the effect of sulfur poisoning on solid oxide fuel cell (SOFC) performance and its recovery process under various operating conditions.
- Investigate the detailed mechanisms for sulfur poisoning of nickel-based anodes in SOFCs.
- Establish scientific principles for rational design of sulfur tolerant anodes.
- Explore new sulfur tolerant anode materials to meet SECA program objectives.

Accomplishments

- Revealed the effects of cell operating conditions [including temperature, hydrogen sulfide (H_2S) concentration, cell voltage/current density, etc.] on sulfur poisoning and recovery of nickel-based anode in SOFCs.
- Demonstrated experimentally that sulfur poisoning of nickel-yttria stabilized zirconia (Ni-YSZ) anodes is not due to formation of conventional nickel sulfides.
- Characterized in real time the nickel sulfide formation process on the surface of a Ni-YSZ electrode and the corresponding morphology change as the sample was cooled in H_2S-containing fuel.
- Predicted sulfur tolerance and catalytic activity towards hydrogen oxidation for various transition metals/alloys.
- Fabricated new anode materials that exhibit excellent tolerance to H_2S and promising cell performance.

Meilin Liu (Primary Contact), Shaowu Zha, Zhe Cheng, Songho Choi, Y. M. Choi
School of Materials Science and Engineering,
Georgia Institute of Technology
771 Ferst Drive NW
Atlanta, GA 30332-0245
Phone: (404) 894-6114; Fax: (404) 894-9140
E-mail: meilin.liu@mse.gatech.edu

DOE Project Manager: Lane Wilson
Phone: (304) 285-1336
E-mail: Lane.Wilson@netl.doe.gov

Introduction

One of the unique advantages of SOFCs over other types of fuel cells is the possibility of direct internal reforming of commercial hydrocarbon fuels, thereby eliminating the need for a separate fuel processing subsystem. However, all fossil fuels contain some sulfur compounds, which are converted to gaseous H_2S in the reforming process. Current SOFC anodes have very limited tolerance to H_2S. As a result, the H_2S concentration in the feed fuel must be reduced to less than 1 ppm (by volume) for optimum performance, which increases the complexity of the system and the cost of operation. Although considerable efforts have been devoted to the development of sulfur-tolerant anode materials, a detailed understanding of the sulfur poisoning process and its mechanism is still lacking, and there is no anode material that is both sulfur-tolerant and compatible with current cell materials/fabrication techniques. The design of new materials largely proceeds via trial-and-error, without much theoretical guidance.

In view of these deficiencies, this project focuses on (i) investigating the poisoning process of Ni-based anodes by H_2S in SOFCs and understanding the poisoning mechanism, (ii) developing new anode materials that have better sulfur tolerance and comparable performance with current Ni-based anodes, and (iii) establishing scientific principles that may guide the selection of candidate sulfur resistant anode materials for SOFCs.

Approach

The cell current at a constant voltage was monitored continuously when H_2S gas (at the ppm level) was introduced and removed from the fuel flow under different conditions (temperature, H_2S concentration and cell current density/voltage, etc.). The impedance responses of the cell under open-circuit conditions were also measured in fuels with and without H_2S to determine the contributions from the electrolyte and different interfaces. The sulfur–anode interaction was investigated by characterizing the chemical and structural changes on the surface of dense Ni-YSZ composites. This includes *in situ* Raman spectroscopy, in which the Raman signal and structure at elevated temperatures were obtained on a real-time basis when H_2S was introduced and removed from the Raman cell. The results from *in situ* Raman spectroscopy were

also correlated with other ex-situ techniques such as scanning electron microscopy (SEM), energy dispersive x-ray (EDX), and x-ray diffraction (XRD), etc. to study the sulfur-anode interaction.

Meanwhile, quantum-chemical calculations were used to predict the adsorption energy and bond length for sulfur and hydrogen atoms on various metal surfaces. The results were used to predict sulfur tolerance and anode activity toward electrochemical oxidation of H_2 fuel for those different materials. An impregnation method was used to introduce the precursors for sulfur-resistant anodes into a porous YSZ layer bonded onto a dense YSZ electrolyte. The anode was reduced in-situ and tested in fuels with H_2S under various conditions.

Results

Sulfur poisoning of the Ni-YSZ cermet anode for SOFCs consists of two stages. The first is a rapid degradation within a few minutes that causes the majority of the decrease in performance, followed by a gradual degradation that occurs over several hours or even days. The extent of degradation is influenced by cell voltage (or, alternatively, the cell current density). The higher the cell current density (or the lower the cell operating voltage), the lower the extent of sulfur poisoning. The recovery of the poisoned anode can be realized by continuous flowing of sulfur-free fuel, and the recovery is faster when the cell current density is higher [Figure 1(a)]. Impedance studies show that the degradation in cell performance was caused by a large increase in anode interfacial resistance while there is no significant change in bulk resistance [Figure 1(b)]. The anode interfacial resistance increases as H_2S concentration increases [Figure 1(c)]. Correspondingly, at certain temperature and cell voltage, the extent of sulfur poisoning increases with increasing H_2S concentration until saturation is reached. With the same concentration of H_2S, the extent of sulfur poisoning increases dramatically with decreasing temperature. The lowest tolerable H_2S level also decreases dramatically with decreasing temperature [Figure 1(d)].

In situ Raman spectroscopy experiments show no sign of conventional nickel sulfide formation on the surface of the Ni-YSZ composite and there is also no significant change in surface morphology when the sample is exposed to fuels containing 50 ppm H_2S at high temperatures (>~500°C). However, when the Ni-YSZ composite sample was cooled down in H_2S-containing fuels, conventional nickel sulfide (e.g., Ni_3S_2) gradually forms on the Ni surface, accompanied by dramatic change in surface morphology [Figures 2(a) and 2(b)]. When the sample is cooled down completely, the surface of Ni particles is full of ball-

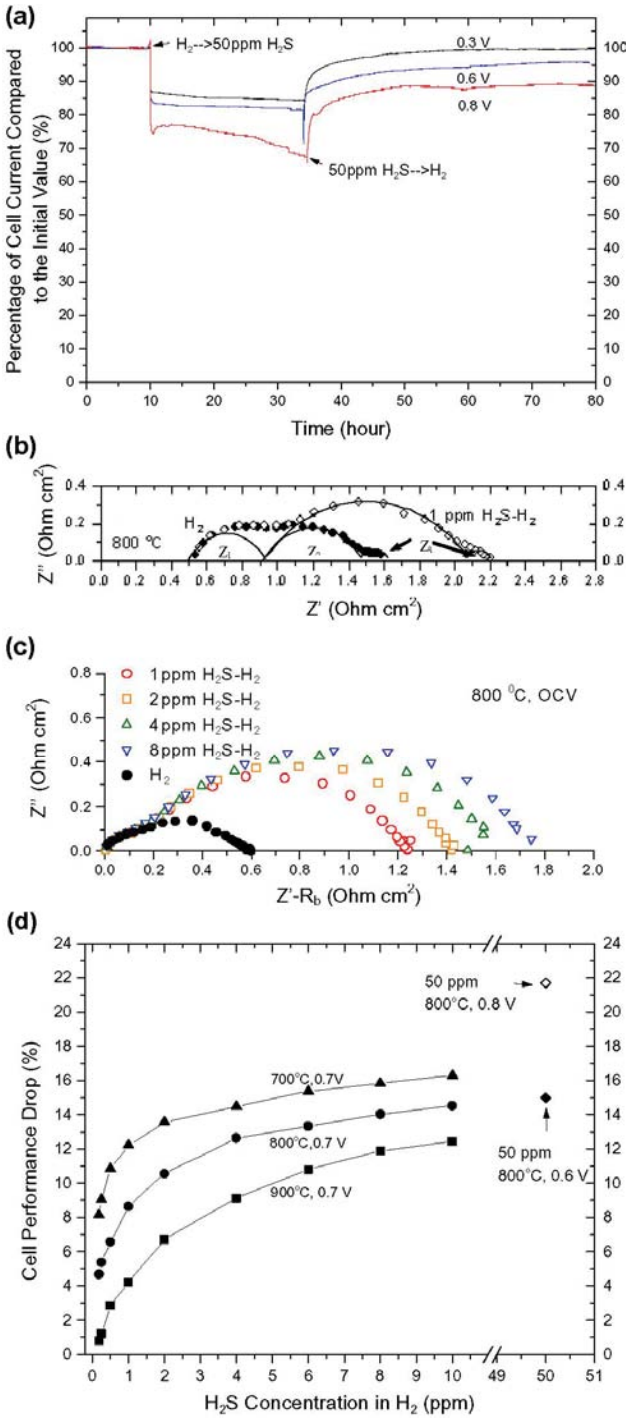

FIGURE 1. (a) Influence of cell voltage on sulfur poisoning and regeneration for Ni-YSZ cermet anode at 800°C; (b) change in impedance spectrum for a cell measured at OCVs using 2-electrode configuration in fuels with and without 1 ppm H_2S; (c) change in impedance spectrum for the anode/electrolyte interface measured at OCV using 3-electrode configuration in fuels with different concentration of H_2S; (d) influence of H_2S concentration on the extent of sulfur poisoning for Ni-YSZ anode at different temperatures. R_b represents the ohmic resistance of the cell and Z'-R_b the anode polarization resistance of the cell.

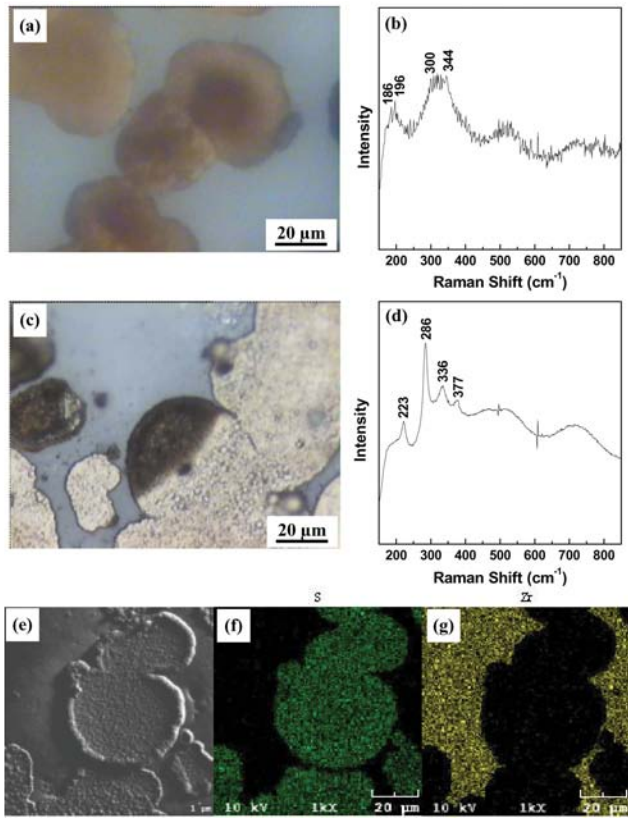

FIGURE 2. Optical microscopy image (a) and corresponding Raman spectrum from the Ni region (b) for the Ni-YSZ composite in *in situ* Raman experiment at 216°C in a fuel with 50 ppm H_2S; optical microscopy image (c), corresponding Raman spectrum taken from the Ni region (d), SEM image (e), S elemental map (f) and Zr element map (g) for the Ni-YSZ composite heated treated at 600°C in 50 ppm H_2S/50% H_2/1.5% H_2O/48.5% N_2 for 20 h.

like and/or edge-like structures as shown in Figures 2(c) and 2(e). The Raman spectra give sharp peaks corresponding to Ni_xS_y. The distribution of sulfur on the Ni-YSZ composite is confined to the Ni region [Figures 2(e) – 2(f)]. This preliminary study indicates that the fundamental reasoning for sulfur poisoning is most likely sulfur adsorption on the anode. Cooling of the anode in H_2S-containing fuel (even in the ppm range) should be avoided since it causes formation of bulk nickel sulfides and irreversible morphology changes.

Quantum-chemical calculations have been used to estimate the adsorption energy of sulfur species and hydrogen on different transition metal surfaces. Figure 3 shows the normalized adsorption energy for H_2S and H_2 on various transition metals surfaces obtained from quantum-chemical calculations. According to the study, the adsorption of sulfur on metals such as Ag, Cu, V, Cr and Mo is significantly weaker compared with Ni, suggesting possible sulfur tolerance for these materials. New sulfur-resistant anodes have been prepared using impregnation methods. They demonstrate acceptable

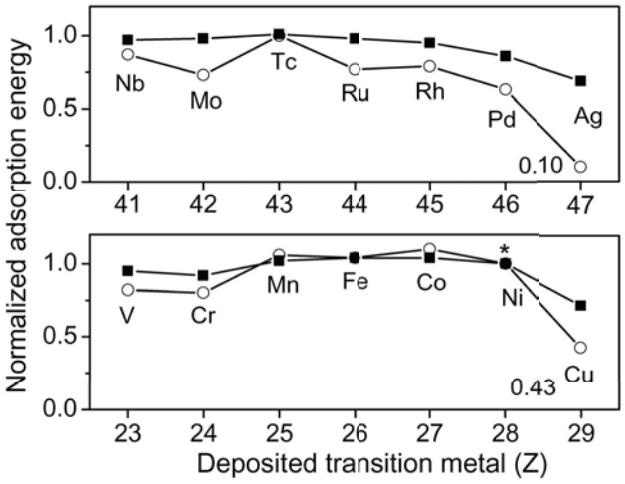

FIGURE 3. Comparison of Predicted Molecular Adsorption Energies for H_2S (open circle) and Dissociative Adsorption Energies for H_2 (closed square) on Modified Ni Surfaces

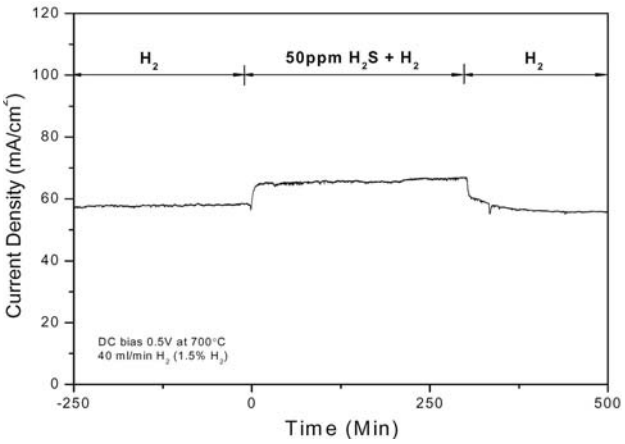

FIGURE 4. Change of Current Density versus Time for Cells with New Anode When 50 ppm H_2S Was Introduced into and Removed from the Fuel

cell performance and excellent sulfur tolerance or even sulfur enhancement behavior in fuels with H_2S concentration up to 50 ppm, as shown in Figure 4.

Conclusions and Future Directions

The sulfur poisoning and recovery for SOFC Ni-YSZ anodes is strongly influenced by operating parameters such as temperature, H_2S concentration, and cell current density/voltage. Generally, sulfur poisoning is more severe at lower temperature, higher H_2S concentration or lower cell current density (higher cell voltage). The *in situ* Raman spectroscopy experiment suggests that sulfur poisoning is not likely to be caused by formation of conventional sulfide. However, bulk sulfides do form at lower temperature (<400°C) in fuels with H_2S in the

ppm range, also causing dramatic morphology changes at the Ni surface. Quantum-chemical calculations suggest that some metals such as Ag, Cu and Mo have lower sulfur adsorption energy and are potential candidate materials for sulfur resistant anodes for SOFCs. Based on the theoretical calculations, new anodes have been prepared using impregnation methods. Initial testing indicates that the new anode materials display reasonable activity and excellent sulfur tolerance (or even sulfur enhancement) in fuels containing up to 50 ppm of H_2S.

Future work is briefly outlined as follows:

- Improve the sensitivity of detecting specific adsorbed sulfur species on Ni anodes using *in situ* Raman spectroscopy. Characterize the depth profile of sulfur in the anode surface layer after exposure to H_2S for different periods of time.
- Determine the time evolution of surface reactive sites, surface species, and anode microstructure during long-term (>10^3 hours) exposure to H_2S contaminated fuel.
- Use the experimentally observed correlations and deduced mechanisms of sulfur-anode interactions to predict the long term stability of Ni/YSZ anodes when exposed to low level H_2S contamination (<10 ppm).
- Establish an effective operational window (in terms of temperature, H_2S concentration, cell voltage, etc.) for SOFCs fed with sulfur-containing fuels.
- Suggest possible modifications to the baseline Ni-YSZ anode materials set that might increase the performance stability and lifetime tolerance to sulfur contaminated fuels.
- Develop new sulfur-resistant anode materials with better sulfur tolerance and long-term stability.

FY2006 Publications/Presentations

1. Z. Cheng, S. Zha, L. Aguilar, and M. Liu, "Chemical, electrical, and thermal properties of strontium doped lanthanum vanadate," *Solid State Ionics*, **176**, 1921-1928 (2005).

2. Z. Cheng, S. Zha, L. Aguilar, D. Wang, J. Winnick, and M. Liu, "A Solid Oxide Fuel Cell Running on H_2S/CH_4 Fuel Mixtures," *Electrochemical and Solid State Letters*, **9**, A31-A33 (2006).

3. Z. Cheng, S. Zha, and M. Liu, "Stability of Materials as Candidates for Suflur-Resistant Anodes of Solid Oxide Fuel Cells," *Journal of The Electrochemical Society*, **153**, A1302-A1309 (2006).

4. Y. M. Choi, C. Compson, Charles, M. C. Lin, M. Liu, "A mechanistic study of H_2S decomposition on Ni- and Cu-based anode surfaces in a solid oxide fuel cell," *Chemical Physics Letters*, **421**, 179-183 (2006).

5. Y. M. Choi, C. Compson, M.C. Lin, and M. Liu, "Ab initio analysis of sulfur tolerance of Ni, Cu, and Ni–Cu alloys for solid oxide fuel cells," *Journal of Alloys and Compounds*, in press.

6. J. Dong, Z. Cheng, S. Zha, and M. Liu, "Identification of Nickel Sulfides on Ni-YSZ Cermet Exposed to H_2 Fuel Containing H_2S Using Raman Spectroscopy," *Journal of Power Sources*, **156**, 461-465 (2006).

7. J. Dong, S. Zha, and M. Liu, "Study of Sulfur-Ni Interactions using Raman Spectroscopy", *in: Proceedings of 207th ECS* Meeting, 2005.

8. S. Zha, P. Tsang, Z. Cheng, and M. Liu, "Electrical properties and sulfur tolerance of $La_{0.75}Sr_{0.25}Cr_{1-x}Mn_xO_3$ under anodic conditions," *Journal of Solid State Chemistry*, **178**, 1844-1850 (2005).

9. S. Zha, Z. Cheng, and M. Liu, "A Sulfur-Tolerant Anode for SOFCs $Gd_2Ti_{1.4}Mo_{0.6}O_7$," *Electrochemical and Solid State Letters*, **8**, A406-A408 (2005).

10. S. Zha, Z. Cheng, and M. Liu, "Sulfur Poisoning and Regeneration of Ni-based Anodes in Solid Oxide Fuel Cells", *Journal of The Electrochemical Society*, submitted.

III.A.10 Quantitative Characterization of Chromium Poisoning of Cathode Activity

Objectives

- Develop *in-situ* chemical mapping techniques to measure the accumulation of chromium (Cr) chemical species at the cathode of an operating solid oxide fuel cell (SOFC).
- Prepare SOFC cathode samples with controllable amounts of electrode and electrolyte surfaces as well as cathode-electrolyte interfaces that are easily accessible to *in-situ* electrochemical and optical (Raman) characterization techniques.
- Correlate Cr contamination delivered by vapor phase Cr-containing molecules and the electrochemical charge transfer resistance of the cathode.
- Deduce the mechanism for Cr poisoning of the SOFC cathode.

Accomplishments

- Measured the Raman detection limit of Cr_2O_3 thin films on the surface of a lanthanum strontium manganese (LSM) cathode. Without additional enhancement methods, accumulations as thin as 10 nm can be detected.
- Created LSM/gadolinia-doped ceria (GDC) composite electrode samples with quantifiable cathode/electrolyte interfaces suitable for our *in situ* Raman measurements. Also fabricated samples with micron-scaled patterned LSM electrodes (with precise geometries) deposited on yttria-stabilized zirconia (YSZ) substrates.
- Generated a surface enhanced Raman signal (SERS) effect on LSM and Cr_2O_3 films by co-depositing silver nanoparticles within the film using combustion chemical vapor deposition (CCVD). Signal enhancement factors between 5 and 1000 were obtained.
- Fabricated silver-coated atomic force microscopy (AFM) tips with diameters as small as 30 nm to be used for generating tip enhanced Raman signal (TERS) effects to obtain sub-micron resolution of surface Raman mapping.

Meilin Liu (Primary Contact), Harry Abernathy, Xiaoyuan Lou, Jian Dong, Songho Choi
Georgia Institute of Technology
Center for Innovative Fuel Cell and Battery Technologies
School of Materials Science and Engineering
771 Ferst Drive NW, Room 288
Atlanta, GA 30332-0245
Phone: (404) 894-6114; Fax: (404) 894-9140
E-mail: meilin.liu@mse.gatech.edu

DOE Project Manager: Lane Wilson
Phone: (304) 285-1336
E-mail: Lane.Wilson@netl.doe.gov

Introduction

One primary suspected cause of long-term performance degradation of SOFCs is the accumulation of Cr species at or near the cathode/electrolyte interface due to reactive Cr molecules originating from Cr-containing components (such as the interconnect) in fuel cell stacks. To date, considerable efforts have been devoted to the characterization of cathodes exposed to Cr sources; however, little progress has been made because a detailed understanding of the chemistry and electrochemistry relevant to the Cr-poisoning processes is still lacking. This project applies multiple characterization methods – including various Raman spectroscopic techniques and various electrochemical performance measurement techniques – to elucidate and quantify the effect of Cr-related electrochemical degradation at the cathode/electrolyte interface. Our chosen methods and unique experimental setup allow for direct spectroscopic observation of the Cr poisoning process while simultaneously monitoring performance degradation of an operating cell. The study will establish the scientific basis for achieving rational design of Cr-tolerant cathode materials and structures for low-temperature SOFCs with Cr-based interconnect materials.

Approach

This project centers around coupling standard electrochemical performance measurements with our unique *in situ* Raman spectroscopy experimental setup to map the concentration of Cr-containing species on the electrode surface as a function of cell operating conditions. Raman spectroscopy identifies the various chemical species in the system by measuring the way in which the sample scatters an incident laser light signal. By using a microscope and motorized stage to direct the laser light, we can map the chemical environment on and around the cathode/electrolyte interface. To more easily probe this interface, composite cathode surfaces (primarily GDC/LSM) are constructed with dense,

well-defined surface structures, and the boundary length vs. surface area are quantified with scanning electron microscopy (SEM). The performance of the cathode under different operating conditions is measured using electrochemical impedance spectroscopy (EIS) while simultaneously monitoring the distribution of Cr species deposited on the cathode surface using Raman mapping. The kinetics of Cr mass transport and deposited surface structures will be determined relative to its effect on electrochemical performance at various temperatures, polarizations, and atmospheres.

In order to detect extremely small amounts of Cr species on the surface, the Raman signal can be enhanced through either deposition of metal nanoparticles on the cathode surface (surface enhanced Raman signal, or SERS) or by bringing a nano-sized metal scanning tip near the cathode surface (tip enhanced Raman signal, or TERS). The increased sensitivity through SERS or TERS methods will allow for earlier detection of deposited Cr species on the sample. The *in situ* Raman data will be verified using various *ex situ* characterization methods including scanning Auger mapping (SAM), X-ray photoelectron spectroscopy (XPS), and further Raman measurements.

Results

The first round of Raman measurements involved demonstrating the utility of normal Raman spectroscopy (measurements without signal enhancements) with respect to Cr contamination of an LSM cathode. As shown in Figure 1, the Raman signals from possible chromium containing contaminants are different from that of the LSM cathode, meaning Raman spectroscopy can indeed distinguish between the multiple species present. For example, the sharp peaks at 350 cm^{-1} and 550 cm^{-1} in the spectrum of Cr_2O_3 can be used as a marker in contrast with the relatively flat spectrum of the LSM. For each desired species, an algorithm has been created to quantify the intensity of the Raman signal from the specific species so that Raman maps can be created from our samples that plot the Raman signal from the species as a function of position. Figure 2 shows an example of a Raman map of Cr_2O_3 from a sample containing a mixture of Cr_2O_3 and LSM. The spatial resolution of the map is on the order of 2 μm^2.

The sensitivity of the Raman microscope to the presence of Cr_2O_3 was then determined by sputtering thin Cr_2O_3 films of varying thicknesses onto LSM samples and measuring the Raman signal. Films as thin as 10 nm could be detected, even without signal enhancements. Further, a calibration curve was obtained to correlate the Raman signal from the Cr_2O_3 film to its thickness. To detect extremely thin layers of Cr_2O_3 (< 10 nm), we have attempted incorporation of Ag or Au nanoparticles into the cathode, which has been shown to increase the Raman signal from the volume around the nanoparticles through a phenomenon known as the SERS effect. The nanoparticles have been introduced so far through two different methods: (1) the evaporation of Ag or Au colloids placed on the cathode surface, leaving behind the nanoparticles within the colloid, and (2) the co-deposition of Ag nanoparticles with the cathode upon an electrolyte substrate using CCVD. Both of these methods have produced varying degrees of success, increasing the Raman signal from LSM or Cr_2O_3 by a factor between 5 and 1000, depending on the technique and the material. Specific peaks within a given Raman spectrum are enhanced by different amounts, and previously undetected peaks have also appeared with the addition of the metal nanoparticles. Figure 3 shows the SERS effect generated from a Cr_2O_3 film that was prepared by CCVD with and

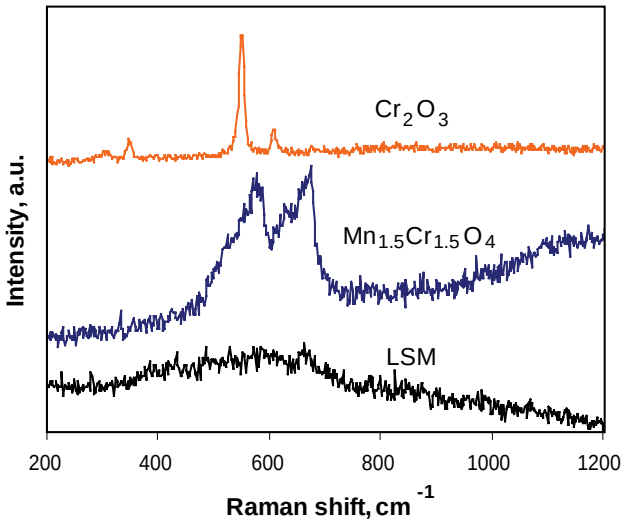

FIGURE 1. Raman spectrum of LSM cathode compared to those of Cr_2O_3 and $Mn_{1.5}Cr_{1.5}O_4$ powders.

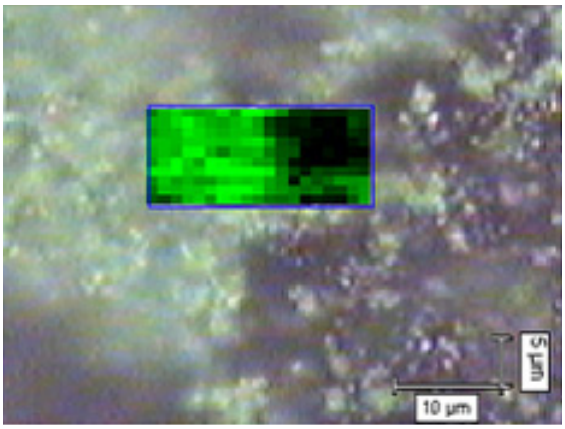

FIGURE 2. Raman map (overlaid on top of an optical micrograph) showing the presence of Cr_2O_3 on the surface of a dense LSM cathode. A brighter shade of green indicates a stronger Cr_2O_3 signal.

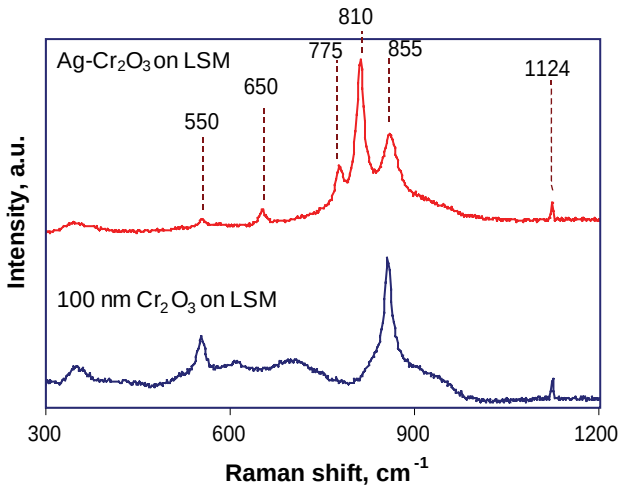

FIGURE 3. Raman spectra from Cr_2O_3 films deposited by CCVD with and without Ag nanoparticles onto an LSM substrate.

without the presence of Ag nanoparticles. Ongoing experiments and theoretical calculations are being undertaken to standardize the methods used to generate the SERS effects and to account for the presence of new peaks in the spectra.

Work has also been completed towards increasing Raman sensitivity through the TERS effect. Instead of placing metal nanoparticles directly on the cathode surface, a silver-coated AFM tip is brought within a few nanometers of the cathode surface, close enough to obtain a signal enhancement effect. To this end, we finalized a process for manufacturing silver-coated tungsten tips with diameters ranging from 30 to 300 nm. We are currently integrating the AFM control apparatus with our Raman experimental chamber so that we can measure the ability of these tips for creating a significant TERS effect.

To perform Raman mapping around the cathode/electrolyte interface, we created samples consisting of GDC/LSM composites with dense samples surfaces consisting of regions of LSM and GDC large enough to be able to effectively distinguish between the two phases within the spatial resolution of our Raman microscope. The triple phase boundary (TPB) per unit area between the LSM, GDC, and air has been quantified statistically using SEM micrographs. Figure 4 shows a typical composite sample surface. These composite samples are currently being used in our ongoing *in situ* Raman mapping experiments. The samples are subjected to normal SOFC operating conditions and exposed to Cr-containing vapor while simultaneously monitoring the performance of the sample and collecting Raman spectra from the surface.

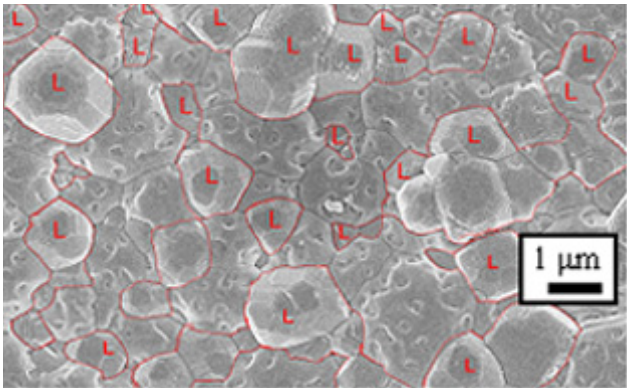

FIGURE 4. SEM micrograph of LSM/GDC composite surface. The red lines indicate the TPB between the GDC, LSM, and air. Grains labeled with an 'L' are LSM.

Conclusions

- Even without signal enhancement, Raman mapping of Cr-containing species can be performed on SOFC cathodes for deposits thicker than 10 nm.
- A SERS effect from LSM and Cr_2O_3 can be generated by depositing silver nanoparticles on the sample surface.
- Raman spectroscopy (including SERS and TERS) has the potential for *in situ* probing and mapping of Cr species deposited on cathode surfaces in a functional SOFC under practical operating conditions.

Future Directions

- Continue *in situ* Raman mapping experiments to measure deposition of Cr species around the cathode/electrolyte interface.
- Incorporate TERS measurements into *in situ* and *ex situ* characterization of Cr-contaminated cathode surfaces to increase the sensitivity of our Raman measurements.
- Correlate the distribution of Cr species (as determined by Raman mapping) with the electrochemical performance (as determined by impedance spectroscopy) of cathodes in operating SOFCs to understand the mechanism of Cr poisoning.
- Design and fabricate cathodes of improved tolerance to Cr contamination.

FY 2006 Publications/Presentations

1. H. Abernathy, Y. Choi, S. Zha, Z. Cheng, J. Wang, R. Das, E. Koep, R. Williams, J. Dong, M. Liu, "Recent Progress in Understanding Interfacial Reactions in SOFCs", Presented to The 30th International Conference on Advanced Ceramics and Composites (American Ceramic Society), Cocoa Beach, FL, January 2006.

2. H. Abernathy, J. Dong, S. Choi, and M. Liu, "In Situ Probing and Mapping of Cr_2O_3 Deposition on LSM-Based Cathodes in SOFCs", in preparation.

3. J. Dong, R. Williams Jr., H. Abernathy, and M. Liu, "Characterization of Chromium Poisoning of SOFC's Cathodes", Symposium for the Georgia Tech Strategic Energy Initiative, Atlanta, GA (2006).

III.A.11 Development of Inexpensive Metal Alloy Electrodes for Cost-Competitive Solid Oxide Fuel Cells

Objectives

- Improve low temperature performance of the air electrode using catalyst infiltration technology developed at Lawrence Berkeley National Laboratory (LBNL). Three approaches are being evaluated for eventual transfer to industrial teams:
  - Dispersed catalyst infiltration on functional air electrodes (i.e. yttria-stablized zirconia/ lanthanum strontium manganate [YSZ/LSM]).
  - Continuous islands of nano-particle electrode coated on functional air electrodes.
  - Electronically connected nano-particle assembly coated onto porous ionically conductive network.
- Determine degradation rate of commercial air electrode structures with and without catalyst infiltration.
- Engineer performance of interconnect alloys through control of oxide scale growth and conductivity.
- Minimize Cr vaporization from stainless steel alloys.
- Transfer technology to industrial teams where appropriate.

Approach

- Develop low-cost metal salt infiltration technology to boost the performance of the air electrode, particularly at temperatures below 700°C. The three approaches involve the use of simple catalyst impregnation to yield dispersed nano-particles, or a viscous catalyst precursor is vacuum impregnated into porous structures to yield a connected catalyst network. Vacuum impregnation can be accomplished with a porous electrolyte structure or an electrode/electrolyte (LSM/YSZ) network.

Steven J. Visco (Primary Contact),
Craig Jacobson, and Lutgard De Jonghe
Lawrence Berkeley National Laboratory
Materials Science Division
Berkeley, CA 94720
Phone: (510) 486-5821; Fax: (510) 486-4881
E-mail: sjvisco@lbl.gov

DOE Project Manager: Lane Wilson
Phone: (304) 285-1336
E-mail: Lane.Wilson@netl.doe.gov

- Measure the baseline performance and long-term stability of commercially produced air electrodes with and without infiltrated catalyst.
- Determine oxidation rates and Cr vaporization rates of commercial and specialty alloys under consideration for interconnect plates.
- Determine Cr vaporization coated alloys to determine quality of coating for minimization of Cr loss.
- Analyze Cr vaporization data to understand fundamental limits of coatings.

Accomplishments

- **Refinement of infiltration technology**: The LBNL infiltration technology has undergone continual refinement over the past 12 months, and we are now able to infiltrate a variety of complex microstructures including conventional air electrodes and porous electrolyte networks. In one approach the LBNL team infiltrates a dispersed catalyst using simple nitrate precursors. We are now collecting data on commercial air electrodes with and without infiltration to see the effect of instantaneous performance and long-term degradation. In another approach we impregnate a wide variety of microstructures with electrode catalysts using vacuum infiltration.
- **Successful determination of Cr vaporization rates for a number of coated and uncoated stainless steel alloys in humidified air**: The LBNL group has been very successful in determination of Cr vaporization from coated and uncoated stainless steel samples in humidified air, including coated samples provided from industrial developers such as Arcomac. The LBNL team has shown that although the Cr vaporization rate from uncoated ferritic steel is unacceptably high, the addition of a relatively simple coating as developed at LBNL can minimize this problem while simultaneously improving resistance to high temperature oxidation.
- **Demonstration of long-term suppression of Cr vaporization from coated ferritic steel**: The LBNL group developed simple, cost-effective coatings for ferritic steel that greatly improve stability towards high temperature oxidation, significantly decrease the Cr vaporization rate in humidified air, and maintain negligible Cr vaporization for at least 1,000 hours.

Future Directions

- **Determine long-term stability of infiltrated electrodes**: The LBNL group is presently conducting a study of baseline degradation of symmetrical LSM/YSZ/LSM and LSCF-CeO_2/YSZ/CeO_2-LSCF cells supplied to us by InDec/H.C. Starck. The LBNL group will determine the performance and degradation rate of the cells in air at 650°C for 1,000 hour tests, after which the electrodes will be infiltrated with appropriate catalysts and the test will be repeated. In this way the long-term stability of infiltrated electrodes can be separated from the long-term stability of the standard electrodes. The LBNL team will run tests on both electrode types, and with multiple infiltration species, and will do post-mortem studies on the electrode morphology.
- **Optimize infiltration technology**: The LBNL team is continually refining the technology for catalyst infiltration to accommodate a wide range of air electrode compositions and microstructures. This capability allows industrial teams to adapt the LBNL approach to their specific need. We will also use the results from the long-term stability studies to refine the composition and process of infiltration to ensure long-term performance improvement at reduced SOFC operating temperatures.
- **Use of analytical focused ion beam (FIB) and transmission electron microscopy (TEM) at the National Center for Electron Microscopy (NCEM)**: The LBNL team continues to develop infiltration technologies to assist the industrial teams in improving the low-temperature performance of the SOFC air electrode. A key aspect of this work is determination of the long-term benefit of this technology and elucidation of the mechanism(s) of degradation of the air electrode over time. Limited studies with NCEM are quite promising, and we hope to expand this effort with the ultimate goal of working with industrial teams on problems specific to their SOFC stacks.
- **Technology transfer**: The LBNL development of coating technology for ferritic steel interconnects is effectively complete and is ready for technology transfer. We anticipate that the LBNL infiltration technology will be ready for transfer to the industrial teams at the end of this 12-month period.

Introduction

Among the most challenging hurdles to the commercialization of SOFC technology is the need to manage cost such that SOFCs are competitive with entrenched power generation technologies. The LBNL group has long maintained that the key to a cost-effective SOFC solution is to develop systems operating in the 650 to 700°C range. A number of SECA industrial teams are now pursuing that goal as well. In order to achieve the 40,000-hour life needed for distributed generation, it is clear that stainless steel interconnects will have to be maintained at temperatures below 800°C. Since electrode kinetics (and electrolyte conductivity) are thermally activated, it is not a trivial task to maintain SOFC performance as the operating temperature is lowered. The LBNL group has developed several infiltration techniques whereby standard LSM electrodes can be modified to perform well at temperatures as low as 650°C. Electrode modification can be as simple as infiltrating a metal nitrate such as $Co(NO_3)_2$, involve a mixture of precursors to form a known electrocatalyst such as $Sm_{0.6}Sr_{0.4}CoO_{3-\delta}$ (SSC), or use the newly developed LBNL technique of vacuum impregnation of porous structures with connected nano-particle architectures. The LBNL group has also performed extensive investigations into high temperature corrosion of stainless steel alloys for interconnects, determined the Cr vaporization rates for steels in humidified air, and developed low-cost coating technologies that reduce Cr vaporization to negligible levels while simultaneously improving oxidation behavior. The LBNL team has initiated measurement of degradation rates of infiltrated and non-infiltrated air electrodes produced in-house and by commercial suppliers. We are also conducting FIB and TEM studies to aid in the elucidation of fundamental mechanisms for air electrode degradation and failure.

Approach

In order to achieve SECA commercialization targets, a number of SOFC developers are targeting reduced operating temperatures as a means of controlling cost. The LBNL effort is aligned with that goal through the use of electrode infiltration technology to boost the performance of the air electrode. The LBNL team has now expanded its infiltration technology to cover 3 basic types of infiltration: ***(1)*** *infiltration of simple metal nitrates to form dispersed nano-particle catalyst on the surface of functional air electrodes in order to boost low-temperature performance,* ***(2)*** *single-step infiltration into porous electrolyte networks to form a continuous nano-structured electrode surface, and* ***(3)*** *single-step infiltration of nano-particulate electrodes onto functional air electrodes such as YSZ-LSM*. The 1st infiltration technique is the simplest to implement and would not require significant change of SOFC processing by the industrial teams. It is clear that this technique results in a fairly dramatic boost in low-temperature air electrode performance. The LBNL group is now investigating the effects of infiltration on long-term performance and air electrode degradation. If the performance enhancement persists for several

thousand hours, it may be possible to re-infiltrate the air electrode later in SOFC stack life by injection of metal nitrates into the air inlet. We are now conducting 1,000-hour tests on symmetric LSM-YSZ/YSZ/LSM-YSZ air electrodes provided to us by InDec, both infiltrated and non-infiltrated. The results of this testing will be used to make recommendations to the SECA vertical teams. The 2nd infiltration technique is quite different in concept from traditional SOFC design in that a porous electrolyte structure is co-fired with a dense electrolyte film at temperatures sufficient to fully densify the electrolyte. This technique allows the SOFC developer to use air electrode materials that are too reactive for conventional co-firing methodology. It also enables the use of porous metal supports and/or co-firing of electrolyte structures onto metal interconnects in reducing atmospheres; then the air electrode is infiltrated in a single-step and fired at low temperature in air. Such single-step infiltrated air electrodes have shown good performance and excellent stability for at least 500 hours at 700°C. The 3rd infiltration technique developed by the LBNL team represents a modification to the 2nd technique in that the single-step infiltration has been altered to allow infiltration of a highly connected nano-structure onto an existing air electrode network. For example, a nano-structured LSM feature can be added to the surface of a conventional LSM-YSZ air electrode. We initiated this work with in-house prepared LSM-YSZ air electrodes but will soon shift to commercial suppliers. This technique is more complex that the 1st infiltration technique but can also be adapted by the industrial teams, and may offer a higher performing and more stable structure.

Our work on high-temperature oxidation and Cr vaporization from coated and uncoated stainless steel is nearing completion. This has been a highly successful effort as we have shown that although Cr vaporization from stainless steel samples exposed to humidified air is unacceptably high, it can be reduced to negligible levels through the use of simple and inexpensive coating developed by the LBNL group. In the past 12 months we have also determined the Cr vaporization rate from coated and uncoated steel samples over a period of several weeks to ensure that the beneficial properties of the coatings are long lasting.

Results

The LBNL group fabricated a transpiration apparatus (Figure 1) and has used this equipment to successfully determine the Cr vaporization rate from a variety of Cr containing samples. As can be seen from the data illustrated in Figure 2, the rate of Cr loss is unacceptably high for uncoated ferritic steel, but is reduced by 2 orders of magnitude through the simple and inexpensive technique of aerosol spray-coating the steel surface with perovskites such as $La_{0.65}Sr_{0.3}MnO_{3-\gamma}$ (LSM),

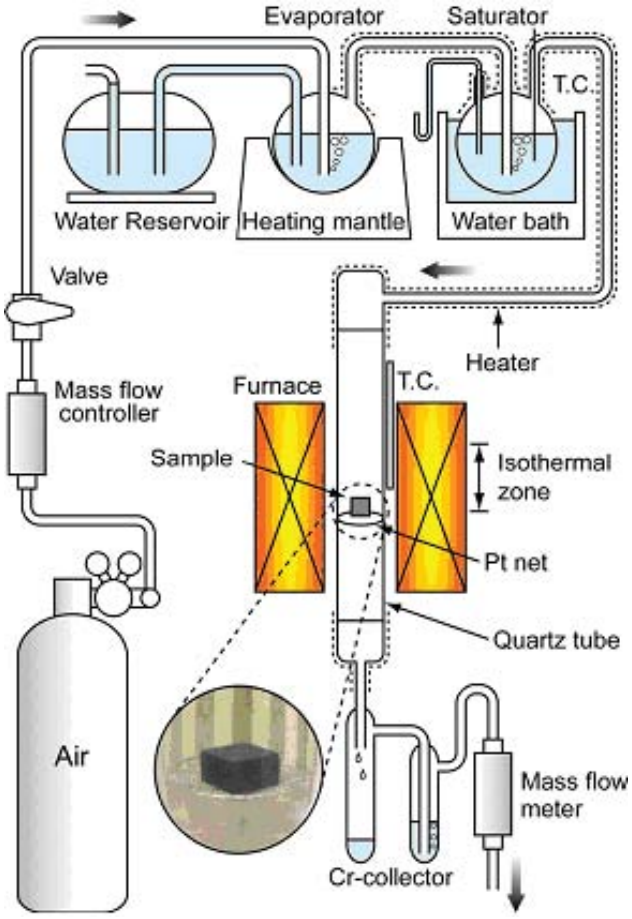

FIGURE 1. Chromium Transpiration Apparatus

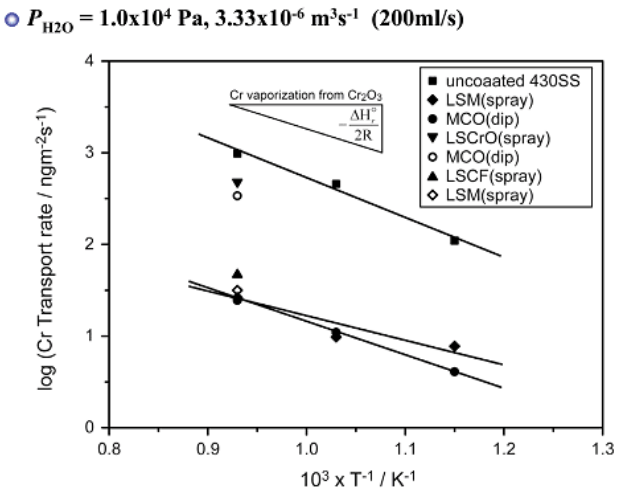

FIGURE 2. Cr transport Rate for Coated and Uncoated Steel Samples

$La_{0.6}Sr_{0.3}Co_{0.8}Fe_{0.2}O_3MnO_{3-\gamma}$ (LSCF), and $MnCo_2O_4$ (MCO). Another remarkable benefit of such simple coating technology is a factor of 10 decrease in oxidation rate leading to a lower area specific resistance (ASR) for

the interconnect. The benefits of simple aerosol coating are therefore:

- Decrease oxidation rate >10x
- Decrease Cr vaporization by 10-100x
- Decreases spallation (thermal cycling)
- Decreases contact resistance

The LBNL team decided to examine the long-term effect of coatings on the Cr vaporization rates and the results of this study are shown in Figure 3. It is clear that coating the steel surface with a simple perovskite such as LSM lowers the Cr transpiration rate significantly and this benefit persists over time. This is certainly good news for SOFC developers, and the use of a LSM coating as an effective barrier for Cr transport provides an additional incentive for its use as a contact paste.

As described above, the LBNL group has developed several unique approaches to catalyst infiltration for high performance air electrodes. In Figure 4, LBNL researchers use an FIB to etch a trench into the infiltrated SOFC exposing a cross-section of the cell. Given that the infiltration technique produces a nano-particulate covering on the porous YSZ framework, a logical study would be the long-term stability of such a high surface area material at the cell operating temperature. As can be seen in Figure 5 the infiltrated structure exhibits excellent microstructural stability, at least for a period of 500 hours at the cell operating temperature. The LBNL team is also investigating the suitability of silver as an air electrode material and contact paste. The high mobility of Ag at operating temperatures above 600°C is a concern, but work at LBNL has shown that co-infiltration of LSM with Ag actually improves the performance of both materials as an air electrode and leads to good long-term stability (Figure 6). The LBNL group is also developing a technique for single-step infiltration of connected nano-structure on an existing air electrode such as conventional LSM-YSZ. The result of such an infiltration is shown in Figure 7; we have not yet tested the performance of such a structure. In the next performance period we will refine this technology to infiltrate connected nano-structures into commercially supplied air electrodes from InDec, and test their short-term and long-term performance.

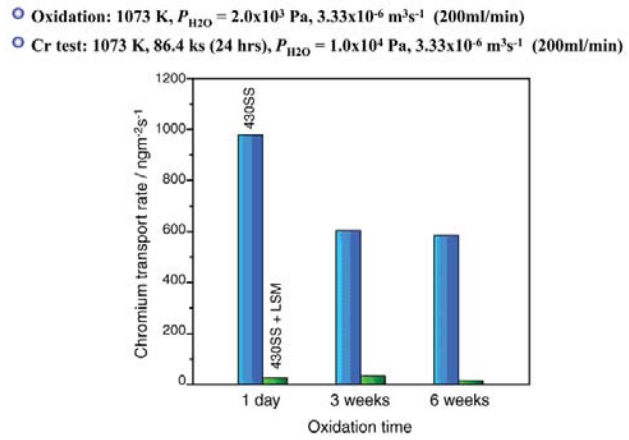

FIGURE 3. Chromium Transport Rate over Time for Coated and Uncoated Stainless Steel

FIGURE 4. FIB Trench Showing Cross-Section of Single-Step LSM Infiltrated Thin-Film SOFC

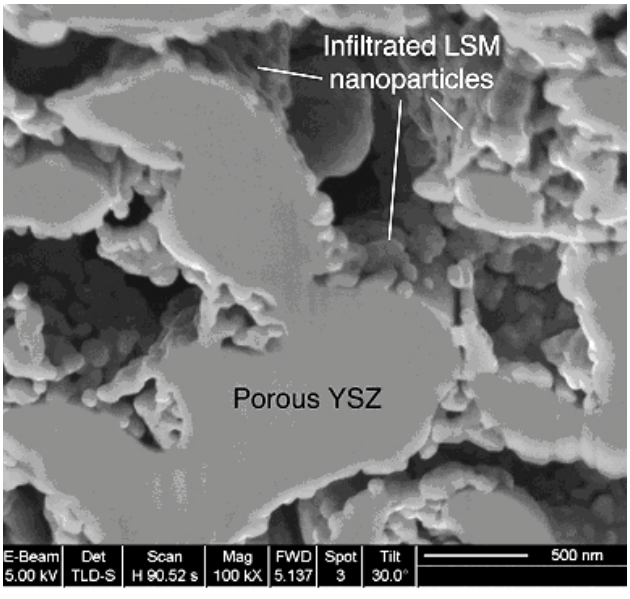

FIGURE 5. FIB Cross-Section Showing Intact Nano-Particle Superstructure on Porous YSZ Network after 500 hours Continuous Operation at 650°C

The LBNL group is monitoring the long-term stability of infiltrated electrodes by running 1,000-hour tests on commercially produced symmetric air electrode cells (i.e. LSM-YSZ/YSZ/LSM-YSZ) with and without infiltration of dispersed catalyst (type 1) and single-step connected nano-structures (type 3). In addition to determination of the voltage profile over time at constant current, we are doing pre- and post-mortem studies of the air electrode microstructure as well as analytical studies of the interfaces by FIB and TEM techniques. The LBNL team has initiated work with the user facilities of the National Center for Electron Microscopy (NCEM). Using the high resolution TEM we been able to observe changes in electrode structure after testing at the interface between the infiltrated catalyst and electrolyte. We will continue to expand the relationship between NCEM and the LBNL SOFC group with the aim of providing industrial teams with the ability to analyze their cell microstructures. We believe that the analysis of cells before and after testing will allow us to study regions with high probability of failure and aid us in providing solutions for the improvement of these regions. In Figure 8, a TEM image is shown of an LSM single-step infiltrated cathode. In Figure 9 an EDX spectroscopy line scan is highlighted which was taken between the backbone electrolyte particle and the catalytic LSM particle of an infiltrated cell that was operated continuously for 500 hours. A deficiency of oxygen that was not seen before testing was found at this boundary, suggesting that this is the "active" region of the electrode (see Figure 10). We are currently probing the "active" regions of infiltrated cells and have found some initial signs of a correlation between the surface energy between electrode components and electrode stability; we are optimistic that these studies will provide mechanistic information to further improve conventional

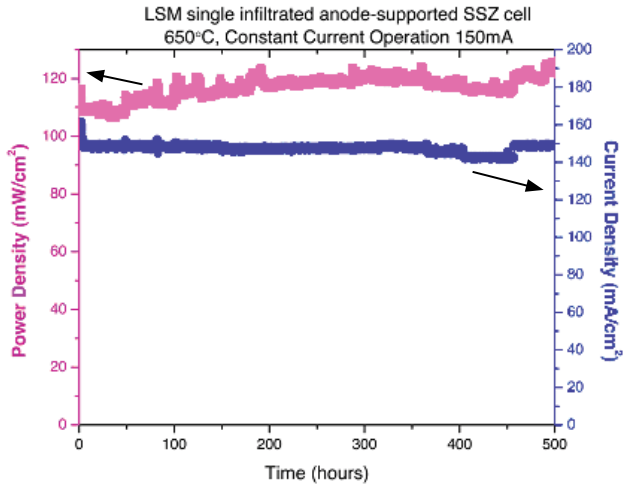

FIGURE 6. Performance and Long-Term Stability of SOFC Having Single-Step Infiltrated LSM Air Electrode

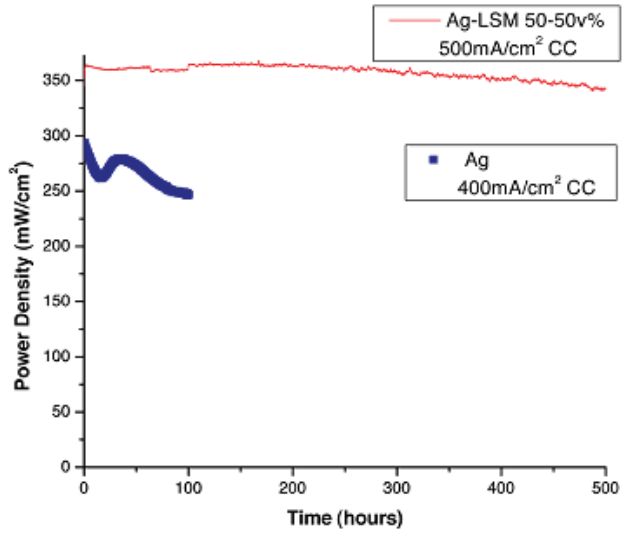

FIGURE 7. Improvement of Ag Electrode Performance through Co-Infiltration of Ag and LSM

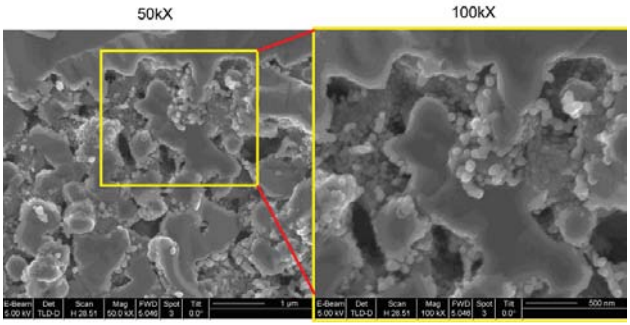

FIGURE 8. Single-Step Infiltration of LSM Nano-Particles into Conventional LSM-YSZ (1:1 wt%) Electrode; Sintered at 1300°C for 4 Hours

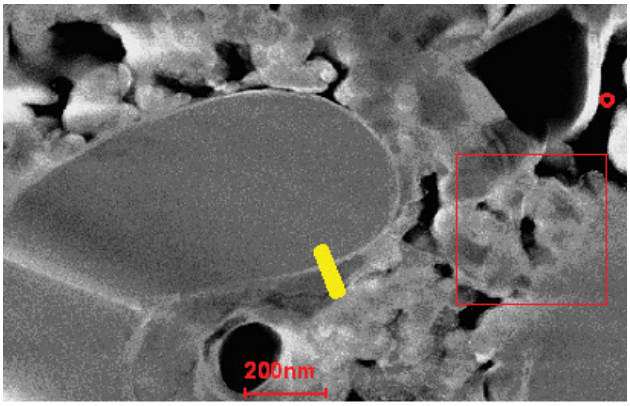

FIGURE 9. TEM of an LSM Single-Step Infiltrated Cathode (EDX line scan taken between backbone electrolyte particle and the catalytic LSM particle of an infiltrated cell that was operated continuously for 500 hours)

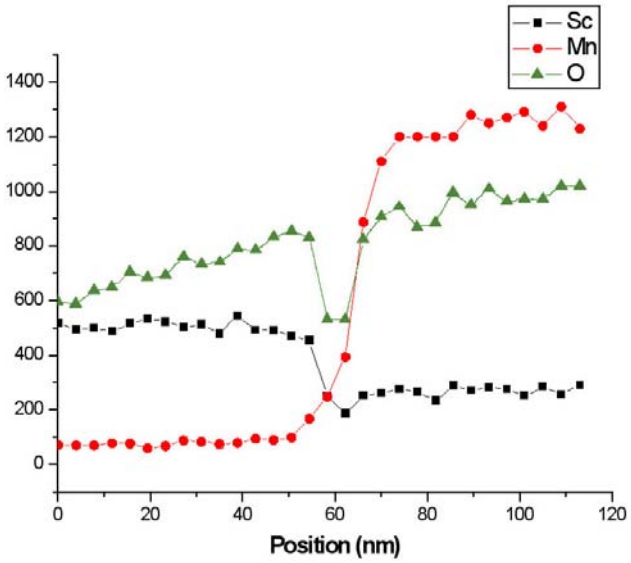

FIGURE 10. EDX Line Scan (indicated in Figure 9) Showing Oxygen Deficiency at the SSZ-LSM Boundary

and single-step infiltrated electrodes for long-term SOFC operation.

Conclusions

The use of simple and inexpensive coating technology developed at LBNL affords excellent protection of stainless steel components used in SOFC stacks against high temperature corrosion, spallation, and chromium vaporization in humidified air; such coating improve oxidation resistance by an order of magnitude and Cr vaporization rates are decreased by almost 2 orders of magnitude. The LBNL group has completed long-term testing of the coated steel samples and concluded that the beneficial effect of coatings in minimization of Cr vaporization is maintained, for at least 1,000 hours. The LBNL project has succeeded in refining its infiltration technology to allow infiltration of dispersed catalysts into conventional air electrodes to boost low temperature performance, or introduce an interconnected nano-particulate superstructure on the surface of conventional air electrodes. In all cases tested so far, the introduction of a dispersed catalyst improves air electrode performance at temperatures below 800°C; we are nearing completion of 1,000-hour tests and will report on the long-term stability shortly. Although single-step infiltrations of perovskite electrodes into porous YSZ have demonstrated excellent performance and stability (up to 500 hours of testing), we have not yet tested conventional electrodes with single-step infiltrated catalysts. The LBNL group has also initiated FIB and TEM analytical studies of air electrodes prior to and after long-term testing in an effort to elucidate the mechanism(s) for performance degradation over time; initial results are promising in that anomalies in oxygen concentration have been detected at the interface between the LSM electrode and YSZ electrolyte after 500 hours of SOFC operation.

FY 2006 Publications/Presentations

Papers

1. Michael C. Tucker, Hideto Kurokawa, Craig P. Jacobson, Lutgard C. De Jonghe and Steven J. Visco, "A Fundamental Study of Chromium Deposition on Solid Oxide Fuel Cell Cathode Materials" *Journal of Power Sources*; in press, corrected proof available online 10 March 2006.

2. Michael C. Tucker, Craig P. Jacobson, Lutgard C. De Jonghe and Steven J. Visco, "A Braze System for Sealing Metal-Supported Solid Oxide Fuel Cells," *Journal of Power Sources*, in press, corrected proof available online 31 March 2006.

Presentations

1. "Enhanced Low Temperature Electrode Performance by Infiltration," Craig Jacobson, Xuan Chen, Tal Sholklapper, Steve Visco, Lutgard De Jonghe American Ceramic Society 30th International Conference and Exposition on Advanced Ceramics and Composites, Cocoa Beach, FL, January 23-27, 2006.

2. "Metal-Supported Thin Film Zirconia and Ceria SOFCs," Mike Tucker Craig Jacobson, Jason Nicholas, Steve Visco, Lutgard De Jonghe; American Cermaic Society 30th International Conference and Exposition on Advanced Ceramics and Composites, Cocoa Beach, FL, January 23-27, 2006.

3. "Interconnect Performance in SOFC Environments," Craig Jacobson, Hideto Kurokawa, Mike Tucker, Peggy Hou, Steve Visco, Lutgard De Jonghe 2006 TMS Annual Meeting, March 14th 2006, San Antonio, Texas.

Special Recognitions & Awards/Patents Issued

1. U.S. Patent No. 6,979,511; Steven J Visco; Craig Jacobson; Lutgard C. DeJonghe, *"Structures and fabrication techniques for solid state electrochemical devices"* issued December 27, 2005.

2. U.S. Patent No. 6,921,557; Craig Jacobson, Steven J Visco, Lutgard C. DeJonghe; *"Process for making dense thin films"* issued July 26, 2005.

III.A.12 Continuous Process for Low-Cost, High-Quality YSZ Powder

Objectives

- Develop a robust process for producing yttrium-stabilized zirconia (YSZ) powder that can be tailored to meet the SECA industry team needs.
- Produce YSZ powder in 5-10 kg batches, and demonstrate reproducibility of the process.
- Demonstrate the advantages of tailoring YSZ powder characteristics to specific requirements of fabrication processes used in SOFC manufacture.
- Demonstrate the process provides YSZ powder at low manufacturing cost.

Approach

- Use of chemical precipitation methods to produce hydroxide precursors that can be converted into crystalline YSZ via thermal treatments.
- Use of ball milling and attrition milling methods to reduce particle size of YSZ powders to below one micron.
- Use of uniaxial and isostatic pressing methods followed by sintering to fabricate ceramic samples for density and ionic conductivity measurements.

Accomplishments

- Established a homogeneous precipitation process for preparing an yttrium-zirconium hydrous oxide precursor, which can be converted to crystalline YSZ via calcination.
- Established calcination and milling methods to prepare YSZ powders with controlled surface area and particle size distribution.
- Demonstrated that YSZ powder produced by the process can be sintered to densities greater than 98 percent theoretical at temperatures less than 1,400ºC.
- Demonstrated sintered YSZ ceramics with high ionic conductivity (>0.04 S/cm at 800ºC), equivalent to the best values reported in the literature.
- Demonstrated a high surface area and fine particle size grade of YSZ powder that can be sintered at low temperatures (1,200°C to 1,250°C).
- Provided samples of low-temperature sintering grade YSZ electrolyte powder to one of SECA's industry team leaders.
- Demonstrated that the manufactured cost of YSZ powder produced using the process will be less than $27 per kilogram at large production volumes.

Scott L. Swartz, Ph.D. (Primary Contact), Michael Beachy, and Matthew Seabaugh
NexTech Materials, Ltd.
404 Enterprise Drive
Lewis Center, OH 43035
Phone: (614) 842-6606; Fax: (614) 842-6607
E-mail: swartz@nextechmaterials.com

DOE Project Manager: Lane Wilson
Phone: (304) 285-1336
E-mail: Lane.Wilson@netl.doe.gov

Introduction

One of the current barriers to reducing the manufacturing cost of SOFCs is the high cost of some of the critical raw materials. The availability of a low-cost, highly reliable and reproducible supply of engineered raw materials is needed to assure successful commercialization of SOFC technology. The yttrium-stabilized zirconia (YSZ) electrolyte material is a primary ingredient for two of the three layers comprising an SOFC element: the dense electrolyte layer and the porous nickel-based cermet (Ni/YSZ) anode layer. In addition, YSZ often is used as a performance-enhancing additive to lanthanum strontium manganite (LSM) based cathode layers. In practice, the same YSZ raw material is used for each of the component layers, even though different fabrication processes are used for each layer. Significant opportunities for performance optimization and cost reduction would be possible if the YSZ raw material is tailored for each component layer. This project focuses on the development of YSZ powder synthesis technology that is "tailored" to the process-specific needs of different SOFC designs being developed under DOE's Solid-State Energy Conversion Alliance (SECA) program.

Approach

NexTech's approach to developing a low-cost YSZ electrolyte powder production process is based on the following principles: (1) the process must be scaleable to low-cost, high-volume production; (2) the process must be sufficiently versatile so that powder characteristics can be tailored to a specific customer's requirements; (3) the process must be reliable, providing consistent batch-to-batch quality; and (4) the process must provide a relatively pure YSZ powder that meets performance criteria relative to particle size, surface

area, sintering activity, and ionic conductivity. With the homogeneous precipitation process that was developed in this project (see Figure 1), the pH and solids content remain constant throughout the process, which is the key to achieving uniformity and reproducibility of the finished product. Another attribute of the homogeneous precipitation process is that it can be made continuous with constant replenishment of the feed solutions. This provides considerable cost and reliability advantages, relative to current chemical synthesis processes.

In the project, synthesis studies are being conducted to identify optimum precipitation conditions for producing hydrous oxide precursors. These precursors then are processed into YSZ powders by washing and drying of the precipitates, calcination of the dried precursor to form a crystalline YSZ powder with targeted surface area (~10 m^2/gram), and milling of the calcined YSZ powder to sub-micron particle size. The YSZ powders are subjected to a comprehensive characterization protocol, involving x-ray diffraction, chemical analyses, particle size distribution, surface area measurements, and sintering studies. Performance of sintered YSZ ceramics are being assessed by density measurements, ionic conductivity measurements, mechanical property measurements, and scanning electron microscopy.

Results

In this project, NexTech has demonstrated a laboratory-scale continuous (homogeneous) precipitation process for YSZ electrolyte powder with equivalent, and in some ways superior performance to YSZ powder that is commercially available from non-domestic suppliers. Key results of the project are discussed below:

- The initial precipitation conditions were shown to have a profound effect on the performance of fully processed (calcined and milled) YSZ powders. After optimization of precipitation conditions, YSZ powders produced by NexTech's baseline process sinter to high densities (>98 percent theoretical) at temperatures of 1,300ºC and higher. The NexTech powder also exhibits improved low-temperature sinterability, compared to commercial powder (Tosoh, TZ-8Y) with similar surface area (see Figure 2).
- NexTech demonstrated reproducibility of its synthesis process by producing three separate batches of YSZ powder, and characterizing these powders through all stages of processing. Particle size distribution measurements (see Figure 3) indicated average particle sizes of 0.30, 0.27 and 0.31 microns, and surface areas of the three powders ranged from 13.9 to 14.5 m^2/gram. Sintering performance (see Figure 4) and ionic conductivity (see Figure 5) were identical for the three batches (within experimental error of the measurements).
- NexTech demonstrated improved densification through doping with alumina (Al_2O_3), nickel oxide (NiO), manganese oxide (Mn_2O_3) and cobalt oxide (CoO) dopants, especially at low sintering temperatures (less than 1,300ºC). NiO and Mn_2O_3 dopants resulted in significant depression of ionic conductivity, whereas this effect was less pronounced with Al_2O_3 and CoO dopants (depending on the dopant amount and method of incorporation). Results obtained with CoO dopants are presented in Figures 6 and 7. With a 0.1 wt% addition of CoO, the sintering temperature was reduced by about 50°C, with little change in ionic conductivity at 800°C. With increased cobalt doping (1 wt%), the sintering performance is further improved, but with a significant loss of ionic conductivity.
- NexTech's synthesis process also was demonstrated for scandium-stabilized zirconia (ScSZ) electrolyte compositions, both partially stabilized ScSZ-6 and fully-stabilized ScSZ-10 compositions. The

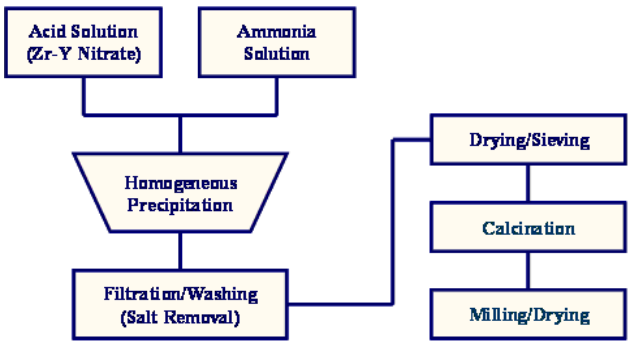

FIGURE 1. Homogenous Precipitation Process for YSZ Powder

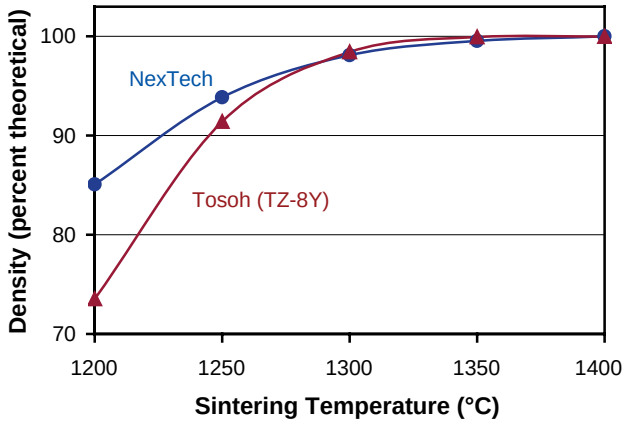

FIGURE 2. Sintering Performance of NexTech's YSZ Powder (baseline process), Compared to Commercially Available YSZ Powder (Tosoh, TZ-8Y)

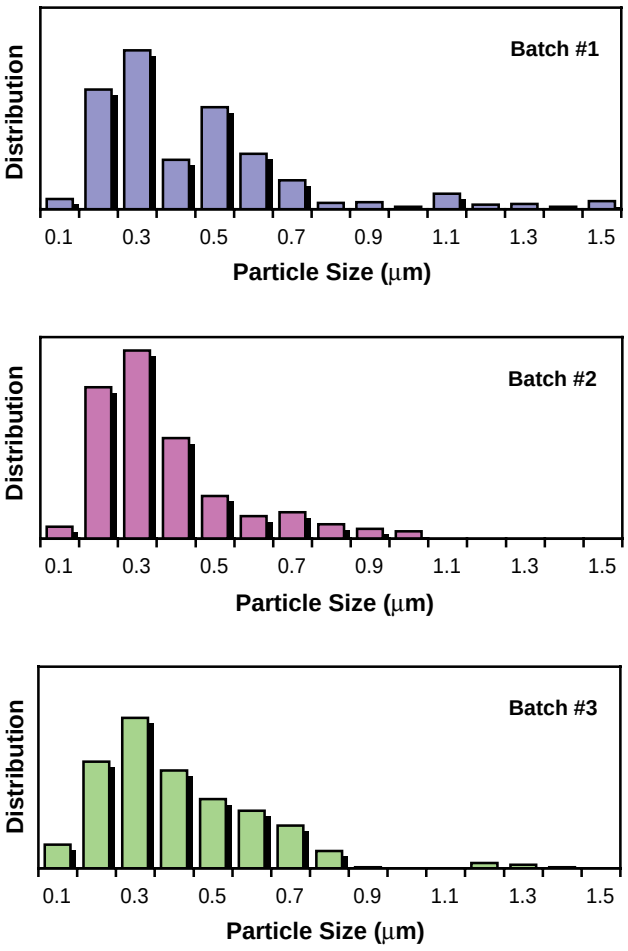

FIGURE 3. Particle Size Distributions of YSZ Powder from Three Separate Batches

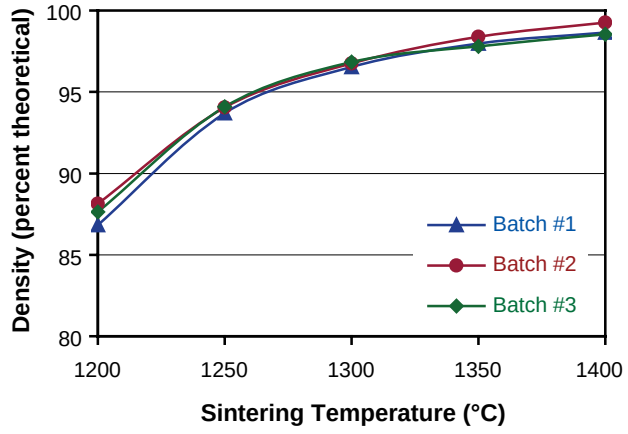

FIGURE 4. Sintering Performance Data for YSZ Powders from Three Separate Batches

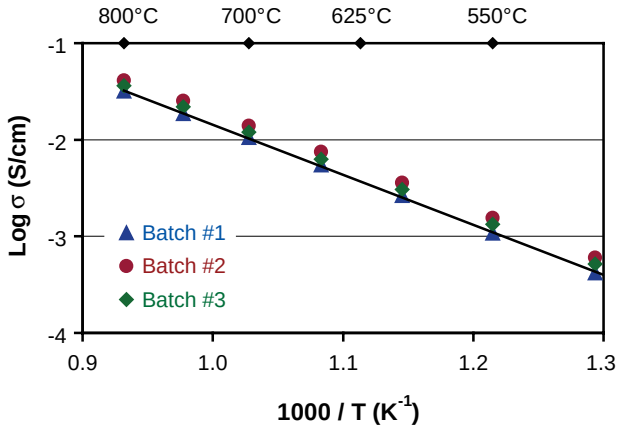

FIGURE 5. Ionic Conductivity Data for YSZ Ceramics Prepared from Three Separate Batches

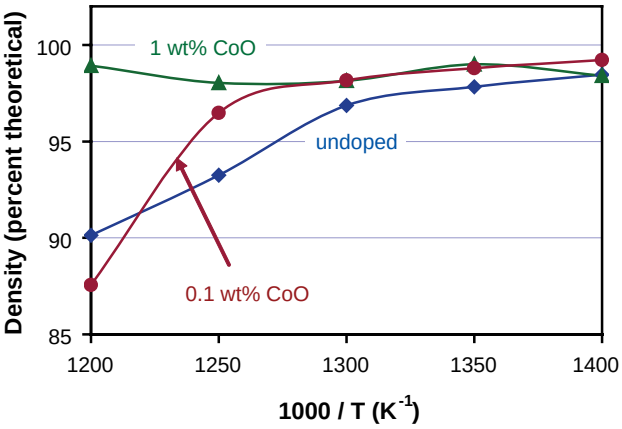

FIGURE 6. Effect of Cobalt Doping on Sintering Performance of YSZ Powder

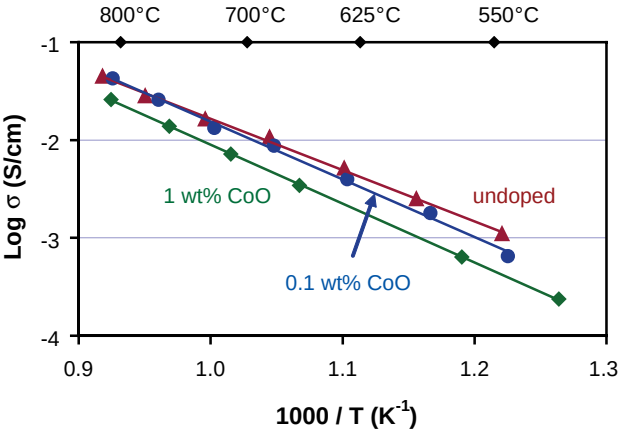

FIGURE 7. Effect of Cobalt Doping on Ionic Conductivity of Sintered YSZ Ceramics

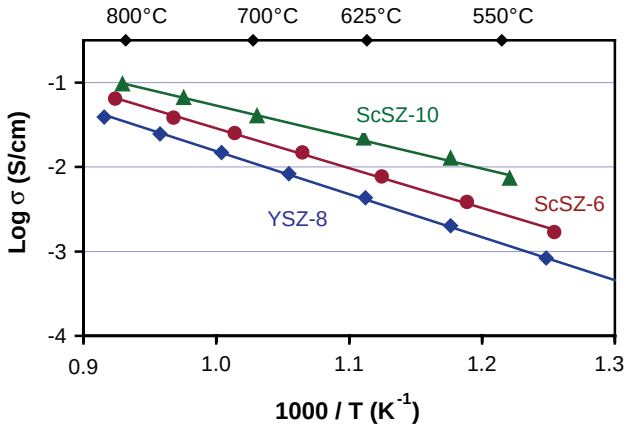

FIGURE 8. Ionic Conductivity of Yttrium Stabilized and Scandium Stabilized Zirconia Ceramics

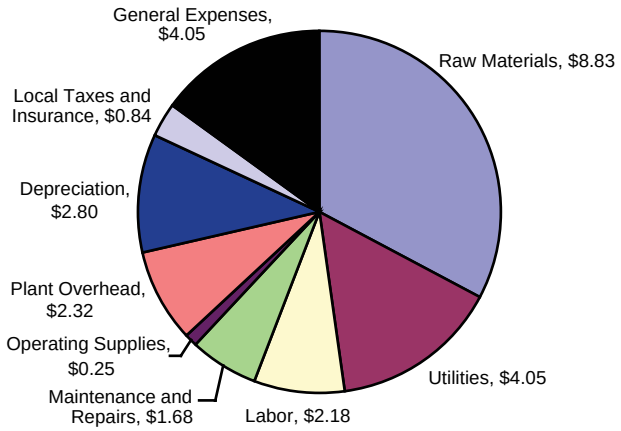

FIGURE 9. Results of Manufacturing Cost Analysis

increased conductivity of ScSZ electrolytes was confirmed (see Figure 8).

- A manufacturing cost analysis confirmed that YSZ powder prepared by NexTech's homogeneous precipitation process could be manufactured for a cost of $27 per kilogram (see Figure 9). This analysis was based on a production volume of 500 metric tons per year, which is a fraction of the volume necessary when SOFC are in full-scale production.

Conclusions

In this project, NexTech Materials developed a low-cost and flexible homogeneous precipitation process for production of high quality YSZ electrolyte powders required for the manufacture of solid oxide fuel cells. Work on the project involved development, refinement and scale-up of the powder synthesis process, along with comprehensive characterization by particle size distribution measurements, surface area analyses, sintering performance evaluations, and ionic conductivity measurements. The two primary advantages of the YSZ powder produced by the process, compared to commercially available YSZ electrolyte powders, included tailorability of particle size and surface area and low temperature sintering capability. Specific conclusions from the work on this project are provided below:

- The homogeneous precipitation process developed on this project provides a hydrous oxide precursor that can be processed into high quality YSZ electrolyte powder. The process involved simultaneous pumping of an acidic solution containing yttrium and zirconium salts and a basic solution containing ammonium hydroxide to form a slurry of yttrium-zirconium hydroxides (or hydrous oxides). The precipitation process is controlled so that the pH and solids content of the hydrous oxidize precursor is maintained at a constant level throughout the precipitation process. Specific variables of the precipitation process that are important to achieving high performance of the resulting YSZ powder include precipitation pH, dilution levels of the starting acid and base solutions, and the pump flow rates of the starting acidic and basic solutions.
- Processing of the hydrous oxide precursor into YSZ electrolyte powder involves the steps of washing of the precipitated slurry (to remove residual salts), modification of the slurry, either by addition of surfactants or solvent exchange with isopropyl alcohol, to minimize unwanted agglomeration during drying, drying of the hydrous oxide precursor into an amorphous powder, calcination of the precipitate to form a crystalline YSZ powder, and milling of the YSZ powder to a targeted surface area (10-15 m^2/gram) and particle size (<0.5 µm). It was found that all of these processing steps had an impact on the sintering performance of the YSZ powder.
- The milling step in the process was found to be critically important for producing high performance YSZ electrolyte powder. In particular, high energy milling processes were required to achieve optimized particle size distributions and enhanced sintering performance. The elimination of particles greater than one micron in size led to significant improvements in sintering performance, especially at temperatures of less than 1,300°C. The use of milling aids was found to help the milling process, and two especially suitable milling additives were identified.
- Calcination and milling methods were established for controlling surface area and particle size of YSZ powders within the targeted surface area

and particle size ranges (10-15 m^2/gram and 0.3 to 0.4 microns, respectively). The synthesis and processing methods were further refined to produce YSZ powders with improved low-temperature sinterability and equivalent ionic conductivity compared to commercially available YSZ powder. The process provides a YSZ powder that can be sintered to high density (>95 percent theoretical) at temperatures as low as 1,250ºC.

- A number of oxide additives were evaluated and found to improve sintering performance of YSZ electrolyte powders produced by the process. Nickel, manganese, and aluminum oxide dopants (at levels of 0.1 to 1.0 wt%) all were found to be effective for increasing sintered densities and reducing sintering temperatures. However, these dopants led to significant reductions in ionic conductivity, even at low dopant levels. Cobalt oxide dopants, on the other hand, were found to improve sintering performance without negative impacts on ionic conductivity when added in sufficiently low levels (~0.1 wt%).
- All of the unit operations associated with the synthesis and processing of YSZ powders by the homogeneous precipitation process were scaled up at NexTech to allow YSZ powder production at 10-20 kilogram batch sizes. A number of processing studies were performed to characterize each step of the process to aid identification and specification of manufacturing scale equipment for full-scale production. A manufacturing cost analysis was performed, which confirmed that YSZ powder produced by the continuous precipitation process would have an estimated production cost of about $27/kg for a 500-ton per year production rate. Opportunities for further cost reduction were identified.

FY 2006 Publications/Presentations

1. S.L. Swartz, et al., *Continuous Process for Low-Cost, High-Quality YSZ Powder*, DOE Contract Number: DE-FC26-02NT41575, Final Report (March 31, 2006).

III.A.13 Highly Textured Glass Composite Seals for Intermediate-Temperature SOFCs

Objectives

- Fabricate a compliant seal that is hermatic at solid oxide fuel cell (SOFC) operating conditions.
- Achieve target leak rates with minimum compressive loading.
- Identify a glass composition that is chemically compatible with a metal interconnect and does not support chromium migration or silicon degradation.

Accomplishments

- Identified powder characteristics for glass and zirconia powders to formulate dense and low shrinkage composite at 850°C.
- Fabricated glass-ceramic composite seal that demonstrates a leak rate below 0.094 sccm/cm with seal area pressurized to 13.8 kPa with helium. Seal was measured from 650-850°C at 0.55 MPa compressive load.
- Demonstrated stable seal performance for over 50 hours with multiple pressurization cycles.

Introduction

Many planar SOFC designs have been proposed using a number of sealing materials, with mixed degrees of success. The simplest methods have been single composition glass seals, which have been compositionally designed to melt at relatively low temperature and yet maintain sufficient viscosity at the operating temperature to provide a robust seal [1,2]. More complex approaches have attempted to use multiple glass phases in layers or to add a minority fraction of ceramic particles to the mixture to fulfill the seal requirements [3,4].

These experiments focus on the development of a composite sealing system for intermediate-temperature solid oxide fuel cells (600-800°C). These two-phase glass/ceramic mixture structures are targeted to provide high durability, low cost and scalability for manufacturing. The proposed seals combine a crystalline ceramic phase that will provide a skeletal structure to the seal, and a glass matrix that will improve wetting at the seal interfaces and allow the seal to densify at lower operating temperatures. The composite structure is also anticipated to provide a degree of compliance to the stack at the operation temperature.

Matthew M. Seabaugh (Primary Contact), Kathy Sabolsky, Gene B. Arkenberg, Jerry L Jayjohn
NexTech Materials, Ltd.
404 Enterprise Drive
Lewis Center, OH 43035
Phone: (614) 842-6606; Fax: (614) 842-6607
Website: www.nextechmaterials.com

DOE Project Manager:
Ayyakkannu Manivannan
Phone: (304) 285-2078
E-mail: Ayyakkannu.Manivannan@netl.doe.gov

Consultant: Dr. Dick Brow
University of Missouri – Rolla, Rolla, MO
Phone: (573) 341-6812
E-mail: brow@umr.edu

Subcontractors: Dr. John Lannutti
The Ohio State University, Columbus, OH

Approach

Two approaches have been evaluated–the development of isotropic seal materials, in which equiaxed ceramic powders have been added to a glass matrix, and the development of textured seal materials, in which anisotropic ceramic particles have been oriented in a glass matrix. Examples of the resultant structures are shown in Figures 1 and 2. In both cases, it is expected that the majority crystalline phase will dominate the thermal expansion behavior and present a tortuous path for gas species with the possible added benefit of the textured seals in improved fracture toughness and creep resistance.

A range of particulate materials and glass compositions have been evaluated to determine those best suited for SOFC sealing applications. This paper documents the development of isotropic seal materials and their validation testing.

Results

Figure 1 shows the results of the sintering study for the composite mixtures of the selected seal material and zirconia powder at 850°C. The surface area of the seal material and zirconia powder was 4 m^2/g and 1.5 m^2/g, respectively. The two powders were mixed in varying ratios by ball milling mixtures of the glass and zirconia powder. The study showed that the composites with seal material content of less than 50% saw little

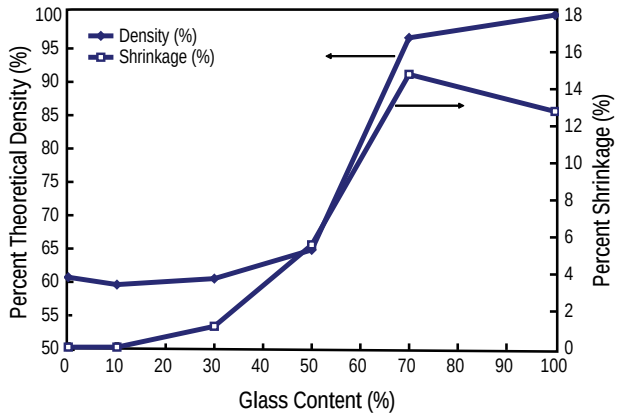

FIGURE 1. Impact of Glass Content on Composite Densification and Shrinkage

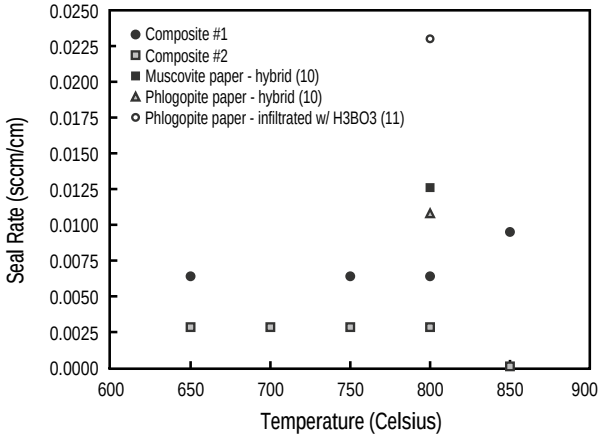

FIGURE 2. Screening Tests

to no improvement in density over the pure zirconia samples. The composites with seal material content greater than 70% achieved over 95% density with shrinkage over 14%. The pure glass material sample achieved 100% density at 850°C with approximately 13% shrinkage. Based on this assessment, for this mixture of powders, a high glass content was selected. Alternative formulations (particularly those using higher surface area glasses) use higher concentrations of the crystalline component.

Figures 2 and 3 provide composite seal performance data obtained using the 70% glass formulations identified in Figure 1. In Figure 2, a screening test of short term performance, the calculated leak rate for two composites utilizing similar compositions to that described in Figure 1 but with varying glass formulations is compared. Both seals perform well below the targeted leak rate of 0.094 sccm/cm at all temperatures and below reported values for seals tested under similar conditions [5,6].

The seal test target leak rate was calculated based upon the metric of 1% fuel loss. A fuel flow rate of 376 sccm was calculated based upon a fuel cell with the following specifications: area of 81 cm^2, current density of 0.5 A/cm^2, and 75% fuel utilization. The amount of fuel loss was then determined to be 3.76 sccm. The seal length (40 cm) is the perimeter of a 10 cm square seal. Finally, the target seal leak rate of 0.094 sccm/cm is obtained by dividing the fuel loss by the seal length.

Figure 3 shows pressure decay curves for a promising seal material, demonstrating stable seal performance over 50 hours with multiple pressurization cycles. The pressure decay data has been analyzed to determine the leak rate over several hours, before the pressure was again raised to the starting value on a periodic basis. Based on the pressure decay data, it is

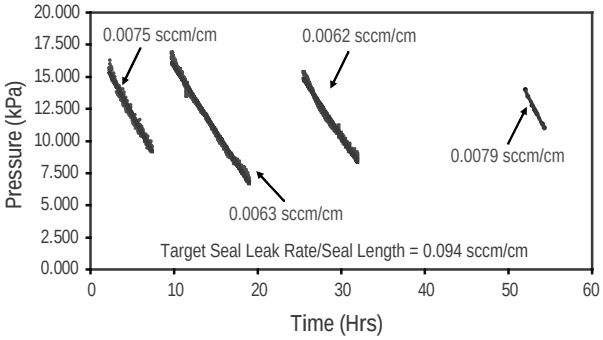

FIGURE 3. Long Term Seal Test

clear that the seals retain their hermeticity over the 50-hour test. Ongoing evaluations are being performed to determine the applicability of the reported seals during fuel cell operation.

Conclusions and Future Directions

Using a combination of glass formulations and crystalline materials, a range of seal materials have been developed. Using *in situ* measurements of seal performance, materials offering good hermeticity have been identified. Continuing evaluations of performance under fuel cell operation are underway.

Special Recognitions & Awards/Patents Issued

1. Best Commercial Presentation, "Composite Seals for Intermediate Temperature SOFCs," ASM International Conference on Joining of Advance and Specialty Materials VII, October 18-20, 2004, Columbus, OH.

FY 2006 Publications/Presentations

1. "Composite Seal Development and Evaluation." Presentation at 30st International Conference and Exposition on Advanced Ceramics and Composites, January 22-27, 2006, Cocoa Beach, FL.

2. "Composite Seal Development and Evaluation." Manuscript for Proceeding of 30st International Conference and Exposition on Advanced Ceramics and Composites, January 22-27, 2006, Cocoa Beach, FL.

References

1. A. Bieberle, et al., "Glass Seals," Oxygen Ion and Mixed Conductors and Their Technological Applications, Tuller, et al., ed. Kluwer, Boston MA (2000).

2. I.D. Bloom and K.L. Ley, U.S. Patent No. 5,453,331.

3. Y. Harufuji, Japanese Patent JP04-47,672.

4. L.A. Xue, US Patent No. 6,271,158.

5. Y.S. Chou et al., J. of Power Sources 112 (2002) 130-136.

6. Y.S. Chou et al., J. of Power Sources 135 (2004) 72-78.

III.A.14 Reliability and Durability of Materials and Components for Solid Oxide Fuel Cells

Objectives

- To support the SECA industrial teams towards the development of reliable and durable SOFCs.
- To support SECA Core Technology Program (CTP) modeling efforts by establishing material property databases.
- To establish failure criteria for SOFC materials and components associated with thermal fatigue and other degradation mechanisms.
- To determine the fracture behavior of SOFC materials and their interfaces.

Approach

- Standardized test methods were employed to determine the thermal and mechanical properties of SOFC materials.
- Scanning electron microscopy and spectroscopic techniques were used to characterize the evolution of the microstructure and the composition of SOFC materials when subjected to thermal cycling and thermal aging.
- The fracture behavior of SOFC materials and their interfaces was investigated by the load relaxation in double-torsion and by the four-point bending of bi-material notched test specimens with symmetrical interfacial cracks.
- Focused ion beam micromachining techniques were used to prepare test specimens to determine the fracture toughness of interfaces in SOFC material.

Accomplishments

- Developed methodologies and experimental facilities to assess the resistance of SOFC materials to thermal cycling and thermal aging.
- Determined the thermal properties of Ni-YSZ as a function of temperature and porosity.
- Characterized the microstructure of Ni-YSZ materials after thermal cycling and thermal aging.
- Developed microfabrication techniques to prepare bimaterial notched four-point bending test specimens with symmetrical interfacial cracks for the determination of interfacial toughness.

Edgar Lara-Curzio (Primary Contact), Miladin Radovic, Rosa Trejo, and Christopher Cofer
Oak Ridge National Laboratory
1 Bethel Valley Road
Oak Ridge, TN 37831-6069
Phone: (865) 574-1749; Fax: (865) 574-6098
E-mail: laracurzioe@ornl.gov

DOE Project Manager: Travis Shultz
Phone: (304) 285-1370
E-mail: Travis.Shultz@netl.doe.gov

Introduction

The durability and reliability of SOFCs are not only defined in terms of their electrochemical performance, but also by the ability of their components to withstand mechanical stresses that arise during processing and service. Specifically, the mechanical reliability and durability of the SOFC is determined by the stress distribution to which its components are subjected and by their distribution of strengths. The stress distribution is a complex function of several parameters that include the geometry of the SOFC, the properties of its components, the temperature distribution and external mechanical loads. The determination of the stress distribution in SOFC materials and components requires the use of computational tools (e.g., computational fluid dynamics and finite-element stress analyses), which in turn require knowledge of their physical and mechanical properties. The stochastic distribution of strengths of SOFC materials is primarily determined by the type and distribution of strength-limiting flaws, which are intrinsic to the material or that are introduced during processing and/or manufacturing.

During normal operation SOFC materials and components will experience large-amplitude low-frequency thermal cycles as a result of start-ups and shutdowns, and small-amplitude high-frequency thermal cycles during transients that are intrinsic to the operation and control processes of the SOFC. Under such operational conditions, the long-term reliability (durability) of SOFCs will be dictated in great measure by the resistance of the SOFC materials and components to degradation mechanisms that become activated during thermal cycling and thermal aging. These degradation mechanisms, which include creep deformation, thermal fatigue and slow-crack growth will not only affect the distribution of strengths of the material with time, but they will also affect the distribution of stresses to which these are subjected, including residual stresses.

Therefore, the development of reliable and durable SOFCs requires that the mechanisms responsible for the degradation of their materials and components be identified and characterized.

Approach

The Ni-based materials used in this investigation were prepared from a powder mixture of 75 mol% NiO and ZrO_2 stabilized with 8 mol% Y_2O_3 (YSZ). Different amounts of organic pore former (0, 15 or 30 vol% rice starch) were added to the powder mixture to obtain test specimens with different levels of porosity. Green test specimens were prepared by tape casting four 250-μm thick layers, which were subsequently laminated. A 15-μm thick layer of YSZ was screen-printed over some of the NiO-YSZ test specimens to obtain bi-layers. Mono- and bi-layer discs were sintered at 1,400°C in air for 2 hours and subsequently reduced in a 4%H_2+96%Ar gas mixture at 1,000°C. The weight of the test specimens was determined before and after reduction to confirm that NiO had been completely reduced to metallic Ni. The porosity of all test specimens was determined by alcohol immersion. A technique was developed to metallographically prepare thin bi-layer test specimens without having to embed them in a medium (e.g., epoxy). This became necessary to allow for the periodic microstructural examination of test specimens after they had been subjected to a predetermined number of thermal cycles or thermal aging time. The microstructure of bi-layer test specimens was characterized using scanning electro microscopy while energy dispersive x-ray spectroscopy (EDXS) was used to perform chemical analyses and to obtain elemental map distributions. Quantitative image analysis was used to assess microstructural changes in SOFC materials.

The fracture toughness, K_{IC}, and slow-crack growth behavior of SOFC materials were determined using the double torsion test method. Double torsion test specimens consisted of rectangular plates (20 mm in width, 40 mm in length) with notches 1 mm in width and 12.5 mm in length that were cut into one side of the test specimen using a circular diamond blade. The notch tip was machined such that the thickness of the test specimen at the notch tip tapered from very thin to the full thickness. The fracture tests were performed using a fixture fabricated out of alumina. Prior to testing, all notched test specimens were pre-cracked by loading the test specimen at a rate of 0.01 mm/min in a double torsion fixture. The reduction in the thickness at the notch tip facilitated the formation of a sharp pre-crack at relatively low loads, well below that required to cause fast fracture of the test specimen.

The slow crack growth behavior of SOFC materials was determined using the load relaxation version of the double torsion test configuration. According to this test procedure, a pre-cracked double-torsion test specimen is fast loaded at a constant displacement rate of 2 mm/min up to a load equivalent to 95% of the load associated with the fracture toughness of the material at particular temperature. At that point, the crosshead displacement of the mechanical testing machine is arrested and the load is monitored and recorded as a function of time. Under those conditions, cracks propagate in a stable manner, resulting in the relaxation of the load.

Focused ion beam and laser micromachining techniques were used to prepare notches in test specimens for the determination of the fracture toughness of Ni-YSZ/YSZ and YSZ/LSM interfaces according to a test method in which bi-material notched test specimens with symmetrical interfacial cracks are subjected to four-point bending.

Results

During FY 2005 work was carried out to quantify the effect of thermal cycling on the properties of Ni-YSZ and YSZ/Ni-YSZ bi-layers. These test specimens were subjected to thermal cycles between 100°C and 800°C under a constant flow rate (100 cc/min) of a gas mixture of 4%H_2 and 96%Ar. To distinguish between the effects of thermal exposure at 800°C from those that could result from thermal cycling on the physical and mechanical properties of these materials, thermal aging tests were carried-out at 800°C. Changes in the curvature of test specimens suggested that the residual stresses in bi-layer test specimens relax rapidly after a few cycles, or short periods of aging time, and that subsequently these stresses remain more or less constant. It had also been found that while the porosity and elastic modulus of YSZ/Ni-YSZ bi-layers do not change significantly with the number of thermal cycles or thermal aging time, their characteristic strength decreased by as much as 20%.

During FY 2006, these studies were continued and efforts were focused to identify relationships among the observed changes in the state of residual stress and mechanical properties of YSZ/Ni-YSZ bi-layers and any microstructural changes that might have occurred in these materials as a result of thermal cycling or thermal aging. The microstructure of these materials was characterized by scanning electron microscopy. To determine if any changes had occurred in the microstructure of these materials, a fixed region of the test specimen was analyzed periodically after a predetermined number of thermal cycles or thermal aging time. To facilitate monitoring potential changes at different scales, a collage of high-magnification images was obtained in each case. Figure 1 shows a scanning electron micrograph of a Ni-YSZ/YSZ bi-layer test specimen in which a 30% volume fraction of pore former had been used. The region of the test specimen that was used to monitor the occurrence of potential microstructural changes has been identified. Also shown

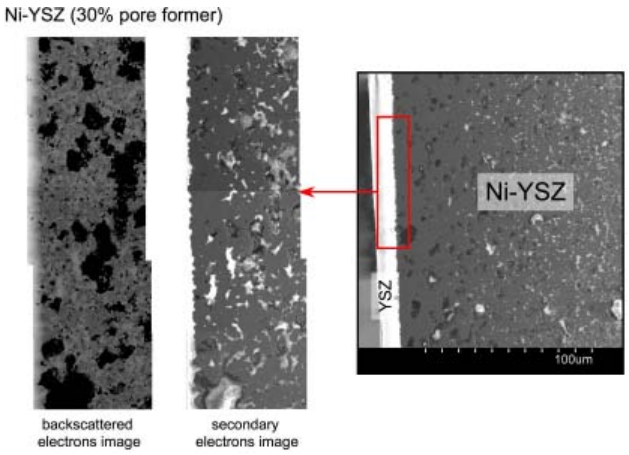

FIGURE 1. Scanning electron micrograph of Ni-YSZ/YSZ bi-layer test specimen (30% pore former). The red frame identifies the region that was characterized to track microstructural changes. Also shown is the backscattered electron image.

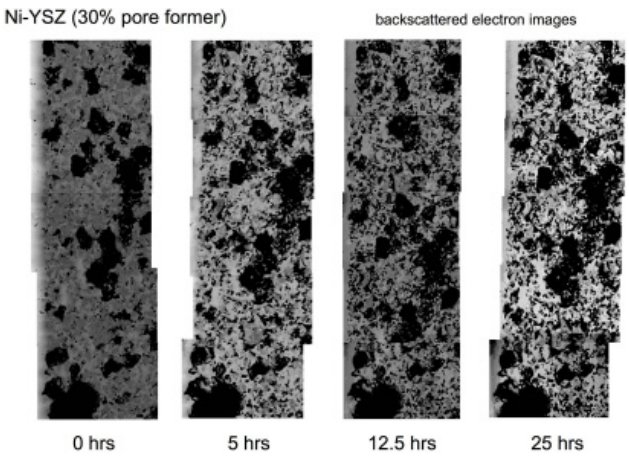

FIGURE 2. Backscattered Electron Images of Ni-YSZ/YSZ Bi-Layer Test Specimen (30% pore former) after Various Periods of Aging Time at 800°C

in Figure 1 is the backscattered electron image (BSE) of this region.

Figure 2 shows a collection of BSE images obtained for this test specimen after 0, 5, 12.5 and 25 hours at 800°C. Although the brightness in BSE images is directly proportional to the atomic number of the material being analyzed, the use of EDXS elemental maps became necessary to complement information provided by the BSE images, which in some cases can't be used to distinguish among the various phases in these materials. In each case elemental maps for nickel, oxygen and zirconium were obtained using EDXS. The images associated with the distribution of these elements for a Ni-YSZ/YSZ bi-layer test specimen in which a 30% volume fraction of pore former had been used, after 25 hours at 800°C are shown in Figure 3. To provide a uniform criterion to assess microstructural changes, a quantitative analysis of these images was performed using a commercial computer program as illustrated in Figure 4. In this analysis, each particle, grain or pore is identified and its dimensions are recorded and monitored as a function of aging time. Similar analyses have been performed for test specimens that have been subjected to thermal cycling. At the time of the preparation of this report, this work was in progress.

Slow crack growth is a phenomenon in which cracks grow in a material assisted by stress and the environment. It is known that hydrogen and water vapor, which are environments that are present in SOFCs, can induce slow-crack growth in materials that are being used to manufacture SOFCs. Therefore, the determination of the propensity of SOFC materials to embrittlement by hydrogen or water vapor is necessary to develop durable SOFCs.

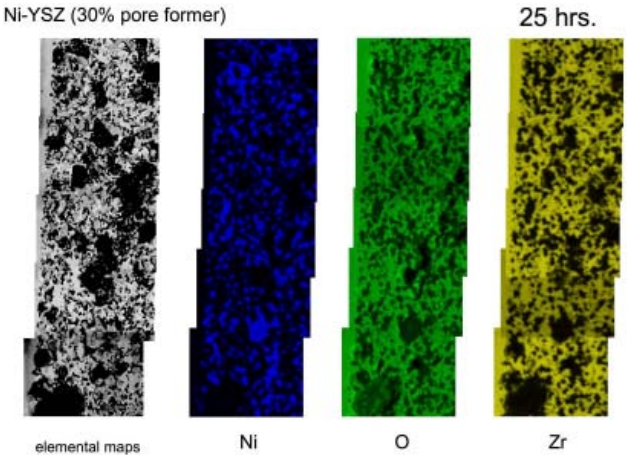

FIGURE 3. Elemental Maps for Nickel, Oxygen and Zirconium for a Ni-YSZ/YSZ Bi-Layer Test Specimen (30% pore former) after 25 Hours Aging at 800°C

The fracture toughness and slow-crack growth resistance of Ni-YSZ in a gas mixture of 4% H_2 and 96% Ar were found to decrease significantly with temperature. Figure 5 presents data for the fracture toughness of Ni-YSZ test specimens (30% volume concentration of pore former). Analysis of the fracture surfaces of these test specimens revealed the existence of Ni ligaments bridging the wake of the main crack (Figure 6). The plastic deformation of Ni grains at the crack tip is probably responsible for the tougher behavior of Ni-YSZ compared to NiO-YSZ. However, the concentration of plastically deformed Ni ligaments decreased with test temperature. To assess the sensitivity of these materials to hydrogen embrittlement, the fracture toughness Ni-YSZ test specimens was evaluated

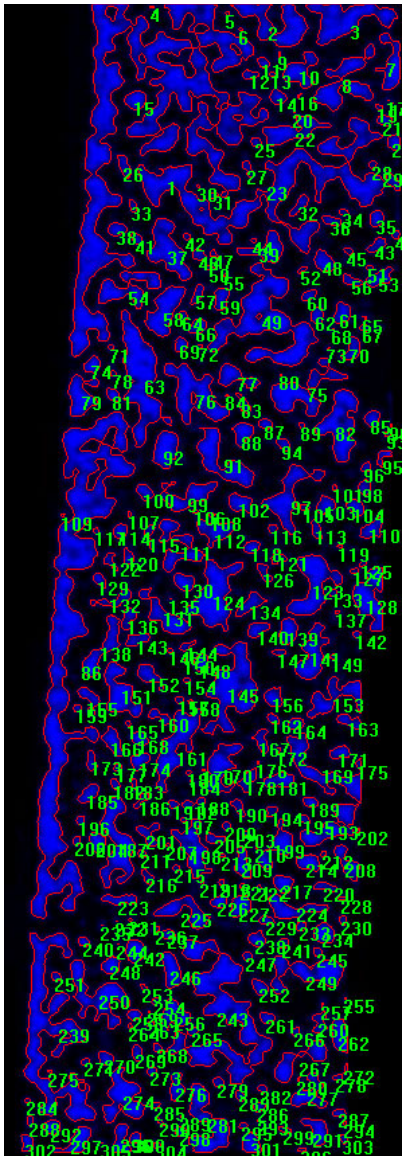

FIGURE 4. Quantitative Analysis of Elemental Map for a Ni-YSZ/YSZ Bi-Layer Test Specimen (30% pore former) after 25 Hours Aging at 800°C

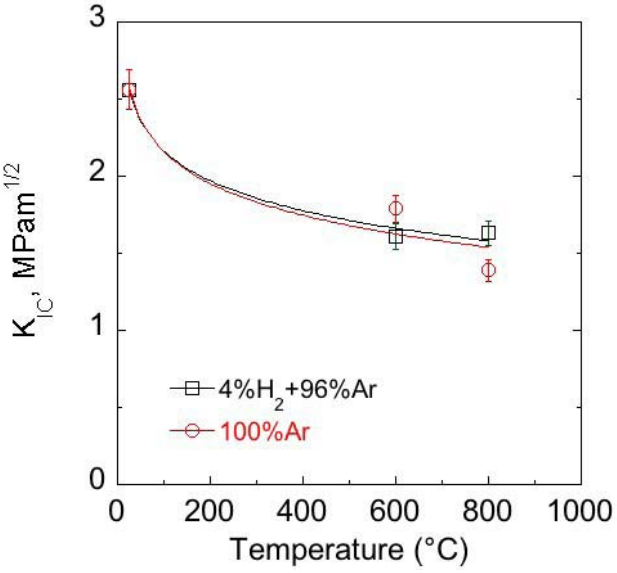

FIGURE 5. Fracture toughness of Ni-YSZ as a function of temperature. Data are presented from tests performed in a gas mixture of 4%H_2+96% Ar or in 100% Ar.

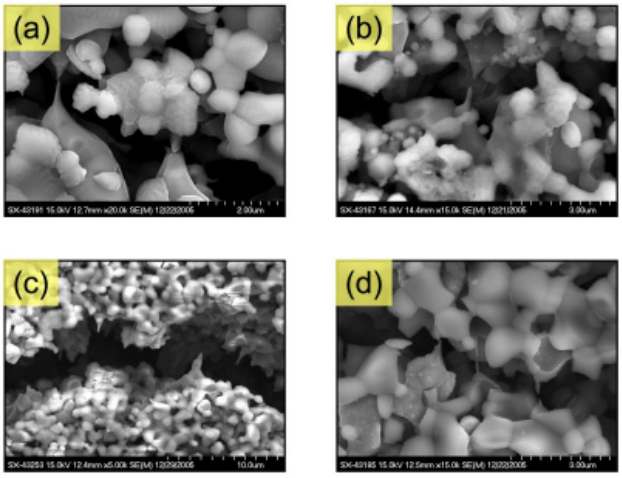

FIGURE 6. Scanning Electron Micrographs Illustrating Ni Ligaments in the Wake of a Crack after Fracture Toughness Tests for (a) and (b) Ni-YSZ (0% pore former) at Room Temperature, (c) Ni-YSZ (30% pore former) at 600°C and (d) Ni-YSZ (30% pore former) at Room Temperature

at 600 and 800°C in pure argon and it was found that a reducing environment with up to 4% hydrogen does not affect the fracture behavior of Ni-YSZ at these temperatures (Figure 5). It was also found that the threshold stress intensity factor for the onset of slow-crack growth decreases with temperature and with the porosity of the material and while the slow-crack growth exponent decreases with increasing temperature it decreases with porosity.

Delamination between the different layers in a SOFC has been identified as a potential damage mechanism that could affect the electrochemical performance of cells. During FY 2006, work was initiated to identify and implement test methods to determine the fracture toughness of these interfaces. Subsequently, the occurrence of changes in interfacial fracture toughness as a result of thermal cycling and thermal aging will be investigated. A bi-material notched four-point bending specimen with symmetrical interfacial cracks was selected to determine the fracture toughness of SOFC interfaces. Although this test method has been used successfully to evaluate the interfacial properties of several engineering systems, its applicability of test specimens that are a few

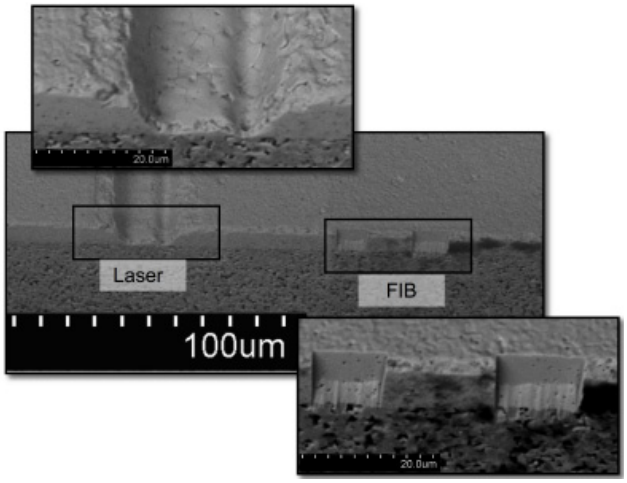

FIGURE 7. Scanning Electron Micrographs Illustrating Notches Made with Laser and Focused Ion Beam to Prepare Test Specimens for the Determination of Interfacial Fracture Toughness

micrometers in thickness, such as those being analyzed here, poses significant challenges. Both focused ion beam and laser micromachining techniques have been used to prepare these specimens as shown in Figure 7 in order to meet the requirements of a sharp notch that would initiate an interfacial crack. At the time this report was prepared, this work was in progress.

Summary

The development of models to predict the reliability and durability of SOFCs requires knowledge of the physical, electrochemical and mechanical properties of the SOFC materials and components and how these properties change with time under the influence of factors such as stress, temperature and environment. During FY 2006, work continued towards the goal of supporting the development of models to predict the reliability and durability of SOFCs. For example, it was found that while the fracture toughness of Ni-YSZ decreases both with temperature and with the porosity of the material, it was not affected by the presence of H_2 (up to 4% concentration) in the environment. During normal operation SOFC materials and components will experience large-amplitude low-frequency thermal cycles as a result of start-ups and shutdowns, and small-amplitude high-frequency thermal cycles during transients that are intrinsic to the operation and control processes of the SOFC. The effect of thermal cycling and thermal aging on the physical and mechanical properties of SOFC materials was investigated and work is in progress to establish relations between potential changes in the microstructure of these materials and the changes that have been observed in their properties. Work will continue to support the activities of the SECA Core Technology Program and the SECA industrial teams towards the design and demonstration of reliable and durable SOFCs.

FY 2006 Publications/Presentations

1. E. Lara-Curzio, M. Radovic, R. M. Trejo, K. L. More, T. R. Watkins, "Effect of Thermal Cycling and Thermal Aging on the Mechanical Properties of, and Residual Stresses in, Ni-Ysz/Ysz Bi-Layers," *Ceramic Engineering and Science Proceedings*, **27**, Issue 2 (2006).

2. J. Salem, M. Radovic and E. Lara-Curzio, "Using the Double-Torsion Test Method to Determine the Fracture Toughness of Thin Ceramic Plates," *Ceramic Engineering and Science Proceedings*, **27**, Issue 2 (2006).

3. M. Radovic and E. Lara-Curzio, "Fracture Toughness and Slow-Crack Growth Behavior of Ni-YSZ and YSZ as a Function of Porosity and Temperature," *Ceramic Engineering and Science Proceedings*, **27**, Issue 2 (2006).

4. M. Radovic, E. Lara-Curzio, R. Trejo, H. Wang and W. D. Porter, "Thermo-Physical Properties of Ni-YSZ as a Function of Temperature and Porosity," *Ceramic Engineering and Science Proceedings*, **27**, Issue 2 (2006).

5. E. Lara-Curzio, M. Radovic, R. M. Trejo, K. L. More, T. R. Watkins, "Effect of Thermal Cycling and Thermal Aging on the Mechanical Properties of, and Residual Stresses in, Ni-Ysz/Ysz Bi-Layers," Presented at the *30th International Conference & Exposition on Advanced Ceramics and Composites*, Cocoa Beach, FL, January 22-27 (2006).

6. J. Salem, M. Radovic and E. Lara-Curzio, "Using the Double-Torsion Test Method to Determine the Fracture Toughness of Thin Ceramic Plates," Presented at the *30th International Conference & Exposition on Advanced Ceramics and Composites*, Cocoa Beach, FL, January 22-27 (2006).

7. M. Radovic and E. Lara-Curzio, "Fracture Toughness and Slow-Crack Growth Behavior of Ni-YSZ and YSZ as a Function of Porosity and Temperature," Presented at the *30th International Conference & Exposition on Advanced Ceramics and Composites*, Cocoa Beach, FL, January 22-27 (2006).

8. M. Radovic, E. Lara-Curzio, R. Trejo, H. Wang and W. D. Porter, "Thermo-Physical Properties of Ni-YSZ as a Function of Temperature and Porosity," Presented at the *30th International Conference & Exposition on Advanced Ceramics and Composites*, Cocoa Beach, FL, January 22-27 (2006).

III.A.15 Combined Theoretical and Experimental Investigation and Design of H_2S Tolerant Anode for Solid Oxide Fuel Cells

Objectives

- Investigate the mechanism for deterioration of solid oxide fuel cell (SOFC) anodes operating at the H_2: H_2S: CO ratios found in coal syngas.
- Molecular modeling of the anode materials interacting with chemical species.
- Validate the theoretical model with experimental data.

Accomplishments

- Established the detrimental influence of H_2S on H_2 oxidation at anode material from quantum chemistry calculations; binding energy for H_2 was reduced from -80.1 kcal/mol to -21.6 kcal/mol in the presence of H_2S gas molecules.
- Molecular dynamics calculations confirm that H_2S gas molecules slow the diffusion of H_2 molecules towards anode material.
- Analyzed the impact of CO on the mixture of H_2 and H_2S; CO decreased the diffusion coefficient of H_2S.

Introduction

Coal syngas is the gas produced from the burning of coal and has a good amount of hydrogen along with other chemical species as such as CO and CO_2. However, coal syngas also contains H_2S at high concentrations between 0.5-5% depending on where the coal is mined [1]. Of the different types of fuel cell, the solid oxide fuel cell (SOFC) is the most viable option to use coal syngas as its fuel supply because it operates at 850-1000°C. It is also known that SOFCs can handle CO and CO_2 as contaminants in the H_2 supply because of its high operating temperature. But the presence of H_2S in the fuel stream will deteriorate the anode material. Most of the research has been focused on developing new anode materials for SOFCs rather than studying the cause of the anode deterioration due to H_2S. In this project, we propose to use a systematic approach to understanding the effect of H_2S from syngas on the anode materials (Ni-YSZ, Ni-CeO_2-YSZ) with molecular modeling computations, and to perform experiments to validate the models.

Gerardine Botte (Primary Contact), Madhivanan Muthuvel, Andres Marquez
Department of Chemical and Biomolecular Engineering, Ohio University
183 Stocker Center
Athens, OH 45701
Phone: (740) 593-9670; Fax: (740) 593-0873
E-mail: botte@ohio.edu

DOE Project Manager: Lane Wilson
Phone: (304) 285-1336
E-mail: Lane.Wilson@netl.doe.gov

Approach

In this study, molecular modeling is used to understand the interaction of H_2S with anode materials (Ni-YSZ, Ni-CeO_2-YSZ). Molecular modeling consists of first principle quantum chemistry (QC) calculations using Gaussian 03 software to optimize the structure of each compound and the systems consisting of anode and different chemical species. Physical properties, such as diffusion coefficient of the chemical species and their interactions with anode material, are calculated using molecular dynamics (MD) simulations with Cerius2 (v 4.8) software. Finally, an experimental set-up will be constructed to perform SOFC experiments with different anode materials and validate the mathematical models.

Results

Molecular modeling of different SOFC anode material chemical species was studied. First, the electrolyte of SOFC, yttria-stabilized zirconia (YSZ), was optimized by QC calculations using Gaussian 03 software. NiO was added to the optimized YSZ structure to form Ni-YSZ, the anode material. All the possible systems consisting of Ni-YSZ (anode), H_2, H_2S and CO were constructed and quantum calculations were performed. The binding energies for each system are shown in Table 1. The binding energy for each system has a negative value which means the oxidation of the components on the Ni-YSZ surface is thermodynamically feasible. In case of single molecules, oxidation of H_2 is favored more than oxidation of H_2S and CO because the binding energy for H_2 (-80.1 kcal/mol) is lower than H_2S (-21.4 kcal/mol) and CO (-23.9 kcal/mol).

The binding energy for the system where H_2S is combined with H_2 (-21.6 kcal/mol) is higher than the system with only H_2, which means H_2 oxidation on the Ni-YSZ surface is obstructed by the presence of H_2S molecules. But when CO is mixed with H_2, the binding

TABLE 1. Binding Energies for Various Combinations of Gas Components

Systems	Binding Energy (kcal/mol)
H_2	-80.1
H_2S	-21.4
CO	-23.9
$H_2 + H_2S$	-21.6
H_2 + CO	-155.5
H_2S + CO	-134.6

energy (-155.5 kcal/mol) is far less than the binding energy for the CO+H_2S system (-134.6 kcal/mol), which suggests that oxidation of both CO and H_2 on the surface of Ni-YSZ anode is more favored than the CO+H_2S system.

The computational chemistry model was extended and MD calculations were performed to understand the interactions between the atoms in the anode and the chemical species (H_2, H_2S and CO) in its environment. The radial distribution function (RDF) was used to determine the packing and orientation of the chemical species and anode material. The RDF plot gives the interaction of each chemical species with different atoms in the anode as a function of distance from the surface of the anode.

One of the RDF plots for the H_2 system at 25°C showed that H_2 has a higher affinity for the Ni atom in the anode than other atoms (Y, Zr and O), which means H_2 oxidizes at Ni sites in the Ni-YSZ anode. Figure 1 shows the RDF plot for the Ni-H_2 pair at 850°C in the presence of H_2S and CO molecules. The pure H_2 system has the highest peak value, which decreases with the addition of H_2S and CO to the mixture. This proves again that oxidation of H_2 at Ni sites are slowed down by the presence of H_2S and CO molecules. In addition, one can observe the position of the Ni-S pair from the H_2/H_2S system, which is farther away from the anode surface as compared to the Ni-H_2 pair. This confirms that H_2 is more likely to get oxidized at Ni sites than the H_2S molecule. Interaction of H_2S with different atoms in the anode and H_2 molecules at 850°C is shown in Figure 2. The RDF plot shows that S forms a pair with Ni and H_2 rather than with any other atoms. The Ni-S pair is slightly farther away from the anode than the Ni-H_2 pair.

Other than the RDF plot, MD calculations can be used to find the diffusion coefficient of each gas molecule. In Table 2 the diffusion coefficients for H_2, H_2S and CO in various systems are listed. Diffusivity for pure H_2 was found to be 1.35 x 10^{-4} cm^2/s, but when H_2S

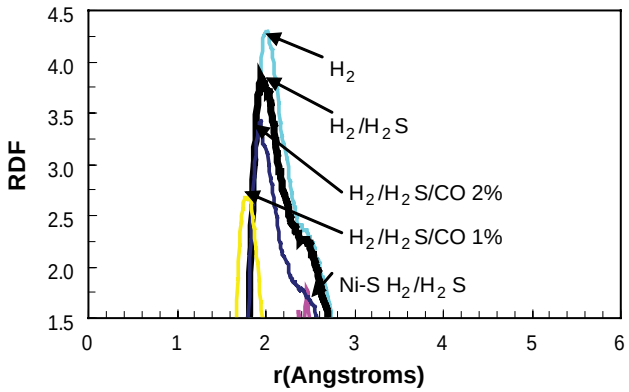

FIGURE 1. RDF Plot for Ni-H_2 Pair at 850°C with the Presence of H_2S and CO

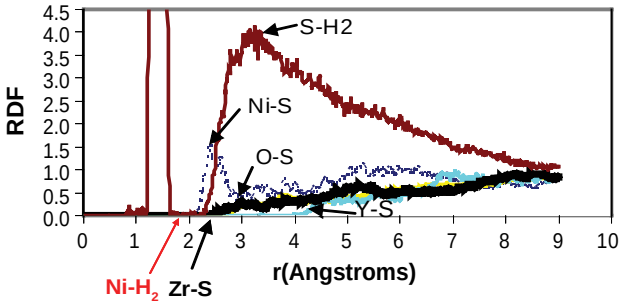

FIGURE 2. Interaction of H_2S Molecule with Ni, Y, O, Zr Atoms and H_2 Molecule at 850°

gas was mixed with H_2, the diffusion coefficient of H_2 was lowered by 20% to 1 x 10^{-4} cm^2/s. This observation agrees with QC calculations that in a H_2+H_2S mixture, oxidation of H_2 takes place at a slower pace due to transport limitations. Now with the addition of CO to H_2 gas, the H_2 diffusivity has been dropped to 5 x 10^{-6} cm^2/s, which is 96% lower than the pure H_2 system. In the case of a H_2+H_2S(2%)+CO(2%) mixture, CO slows down both the diffusion of H_2 (9 x 10^{-6} cm^2/s) and also H_2S (2 x 10^{-9} cm^2/s).

TABLE 2. Diffusivities of the Gas Components at 850° C for Different Systems

Systems	H_2 Diffusivity (cm^2/s)	H_2S Diffusivity (cm^2/s)	CO Diffusivity (cm^2/s)
H_2	1.35 x 10^{-4}	–	–
$H_2 + H_2S$ (2%)	1 x 10^{-4}	1 x 10^{-5}	–
H_2 + CO (2%)	5 x 10^{-6}	–	3 x 10^{-7}
$H_2 + H_2S$ (1%) + CO (1%)	2 x 10^{-5}	8 x 10^{-9}	6 x 10^{-9}
$H_2 + H_2S$ (2%) + CO (2%)	9 x 10^{-6}	2 x 10^{-9}	6 x 10^{-9}

Conclusions and Future Directions

- Quantum chemistry calculation proves oxidation of pure H_2 is more thermodynamically favored on the Ni-YSZ surface than pure H_2S and CO.
- RDF plots for H_2 indicate that H_2 has a greater affinity for the Ni atom than any other atoms in the anode material.
- Diffusion of H_2 was slowed down in the presence of H_2S and CO, but when all the three gases are mixed, CO reduces the diffusion coefficient of H_2S.
- In the future, we would like to include N_2 and H_2O (moisture) atoms to the anode environment and perform QC and MD calculations.
- Perform molecular modeling with another anode material – Ni-CeO_2-YSZ.
- Design and construct a SOFC experimental set-up to verify the theoretical model.

FY 2006 Publications/Presentations

1. "Theoretical Investigation of NiYSZ in the Presence of H_2S" Marquez, A., De Abreu, Y., and Botte, G. G., *Electrochemical and Solid-State Letters*, 9 (**3**) A163-A166 (2006).

2. "Theoretical Investigations of Solid Oxide Fuel Cell Anode Materials" AIChE 2005 Annual Meeting, October 30th – November 4th, 2005, Cincinnati, OH.

3. "Theoretical Investigations of Solid Oxide Fuel Cell Anode Materials in the Presence of $H_2/H_2S/CO$" The 31st International Technical Conference on Coal Utilization & Fuel Systems, The Clearwater Coal Conference, May 21-25, 2006, Clearwater, FL.

References

1. G. Y. Lai, *High Temperature Corrosion of Engineering Alloys*, ASM International, Materials Park, OH (1990) p. 117.

III.A.16 SOFC Glass-Ceramic Seal Development at PNNL

Objectives

- Develop cost effective seals for SOFC stacks that offer low leak rates and desired reliability during long-term isothermal and thermal cyclic operation.
- Develop a scientific understanding of the degradation processes affecting performance and integrity of seals, including intrinsic materials degradation in SOFC environment and interactions with adjacent SOFC components.

Accomplishments

- Synthesized and characterized new "refractory" sealing glass compositions.
- Fabricated sealed joints for leak testing (anode-supported electrolyte/glass/ferritic stainless steel).
- Performed leak tests on joined coupons followed by microstructural characterization.
- Identified promising glass seal compositions with improved coefficient of thermal expansion (CTE) match and reduced interfacial reactivity for further evaluation and testing.

Introduction

Planar SOFC stacks require adequate seals between the interconnect and cells in order to prevent mixing of the oxidant and fuel gases, and to prevent leaking of gases from the stack. In addition, the seals must also allow the stack to be thermally cycled repeatedly (between ambient conditions and the operating temperature). Several different approaches to sealing SOFC stacks are available, including rigid, bonded seals (e.g., glass-ceramics), compliant seals (e.g., viscous glass), and compressive seals (e.g., mica-based composites). Rigid seals typically soften and flow slightly during stack fabrication (at a temperature above the operating temperature) but then become rigid (to avoid excessive flow or creep) when cooled to the operating temperature. The thermal expansion of rigid seals must be closely matched to the other stack components in order to avoid damaging the stack during thermal cycling. Compliant seals attempt to simultaneously perform the sealing function and prevent thermal stress generation between adjacent components. Compressive seals typically utilize materials such as sheet-structure silicates that do not bond adjacent SOFC components; instead, the sealing material acts as a gasket and gas-tightness is achieved by applying a compressive force to the stack.

Yeong-Shyung "Matt" Chou (Primary Contact), Jeff Stevenson
Pacific Northwest National Laboratory (PNNL)
P.O. Box 999, MS K2-44
Richland, WA 99352
Phone: (509) 375-2527; Fax: (509) 375-2186
E-mail: Yeong-Shyung.Chou@pnl.gov

DOE Project Manager: Travis Shultz
Phone: (304) 285-1370
E-mail: Travis.Shultz@netl.doe.gov

Approach

Candidate glass-ceramic sealing compositions were prepared by melting and casting of appropriate oxide constituents. Structural, thermal, and mechanical properties were evaluated utilizing x-ray diffraction, scanning electron microscopy (SEM), energy dispersive x-ray spectroscopy, dilatometry, and optical microscopy. Seal quality of joined interconnect/anode-supported electrolyte coupons was evaluated through room temperature leak testing following isothermal and/or thermal cycling heat treatment.

Results

The main emphasis of glass seal development work at PNNL is to identify, synthesize, characterize, and validate sealing glass formulations (glass-ceramics) with desired thermal, mechanical, electrical, and chemical properties for long-term SOFC applications. The current approach is based on a "refractory" sealing glass-ceramic concept. The refractory sealing glasses are designed to have a higher sealing temperature (e.g., 900-1,050°C), compared to a state-of-the-art glass (e.g., G18, a Ba-Ca-Al-B silicate glass) which typically seals at ≤850°C for operation at ~750°C. The potential advantages of refractory sealing glasses are long-term thermal stability (particularly coefficient of thermal expansion, CTE), minimal interfacial reaction with metallic interconnects, and stronger bonding at cell/interconnect interfaces due to a higher stack fabrication temperature. The glass system under investigation is similar to G18 but contains a different primary glass modifier, i.e., Sr instead of Ba. Three glass systems were evaluated:

1. YS series: Sr-Ca-Al-Y-B-Si
2. YSO series: Sr-Ca-Y-B-Si
3. YSP series: Sr-M-Y-B-Si (M=Mg, Ca, Sr, Ba)

The first glass series investigated was the YS series based on Sr-Ca-Al-Y-B-Si. In order to increase the

sealing temperature, the glass composition was tailored by varying the B_2O_3 content from 9.5 to 3.5 mole% in seven glasses, and the lower bound of B_2O_3 content for forming a homogeneous glass was established. These glasses did appear to be more refractory, as evidenced by their higher softening points (for example, see the dilatometric plots for glass G18 (Figure 1) and for glass YS-1 (Figure 2) after short-term crystallization). Hermetic sealing was obtained for anode-supported electrolyte/ferritic stainless steel joins in the as-sealed condition and was maintained after 10 thermal cycles in air, or 10 thermal cycles in a reducing environment. However, the YS glasses had a lower CTE than G18, and also, like G18, exhibited a trend of decreasing CTE after aging for 1,000 h and 2,000 h. The decrease in CTE was likely due to the formation of a low CTE celsian phase similar to the $BaAl_2Si_2O_8$ formed in G18 glass.

The second glass series (YSO series) was developed by removing Al_2O_3 from the YS series; eight glasses were batched with varying SrO (42.5% to 47.5%), varying B_2O_3 (7.5% to 9.5%), varying Y_2O_3 (6% to 10%) content, and/or La_2O_3 (6%). Adding La_2O_3 to 6% or Y_2O_3 to 10% resulted in poor glass-forming behavior, i.e, bulk crystallization during the glass making process. The other glasses typically had a softening point >720°C and the CTE appeared stable over 1,000 h or 2,000 h aging with values ~$11.5x10^{-6}$/°C. Glass YSO-1 was selected for further investigation of sealing properties and interfacial microstructure development. Results from SEM analysis showed undesirable $SrCrO_4$ formation along the glass/metal interface for samples sealed at lower temperatures (900-950°C, see Figure 3). At higher sealing temperatures (1,000-1,050°C), however, no chromates were found, as shown in Figure 4. Thermodynamic calculations indicated that formation of chromates is favorable for Ba- or Sr-containing glasses if oxygen is available, but such reaction was apparently avoided when oxygen was excluded from the interfacial region by rapid densification of the glass at the higher sealing temperatures. The CTEs of both chromates phases were also experimentally determined and were found to be undesirably high (~21-22 $x10^{-6}$/°C), indicating that a protective layer may be required to minimize the formation of these interfacial phases. Both in-house developed $(Mn,Co)_3O_4$ spinel coatings and commercial Al_2O_3 coatings are under investigation. Concerning electrolyte/glass interfaces, the refractory sealing glasses exhibited improved chemical compatibility compared to G18, as no interfacial reaction phases were observed.

The final glass series (YSP) involved partial substitution of Sr with Mg, Ca, and Ba; several glasses

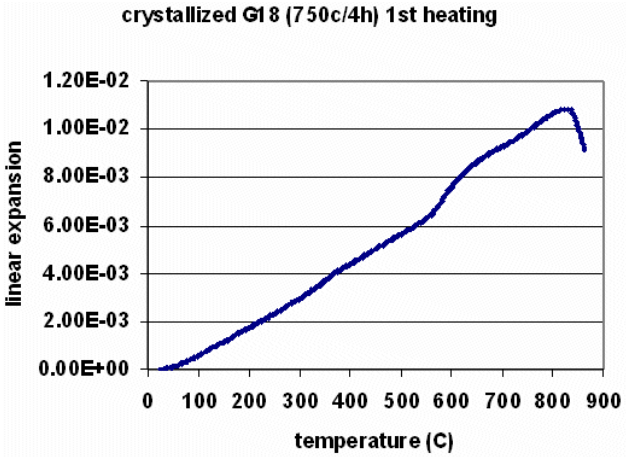

FIGURE 1. Linear Thermal Expansion of G18 Sealing Glass after Short-Term Crystallization in Air (850°C for 1 hour followed by 750°C for 4 hours)

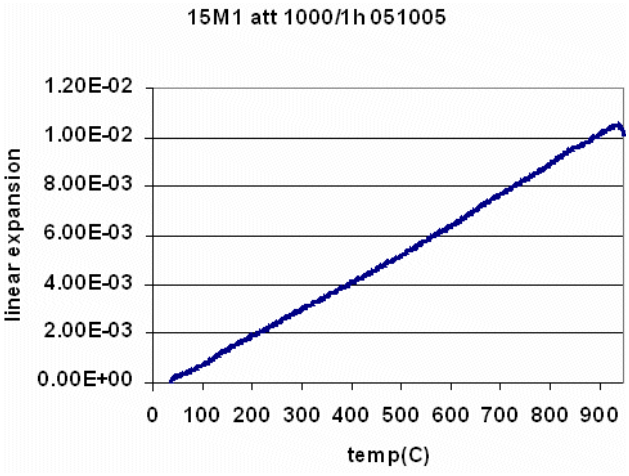

FIGURE 2. Linear Thermal Expansion of YS-1 Sealing Glass after Short-Term Crystallization in Air (850°C for 1 hour followed by 750°C for 4 hours)

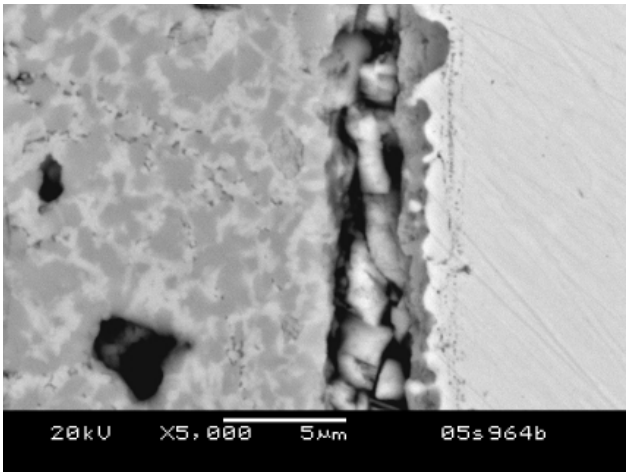

FIGURE 3. Interfacial microstructure of glass (YSO-1) at the glass/metal (Crofer22APU) interface. Sealed at 950°C/2 h in air. Note undesirable formation of $SrCrO_4$ near the interface (arrow).

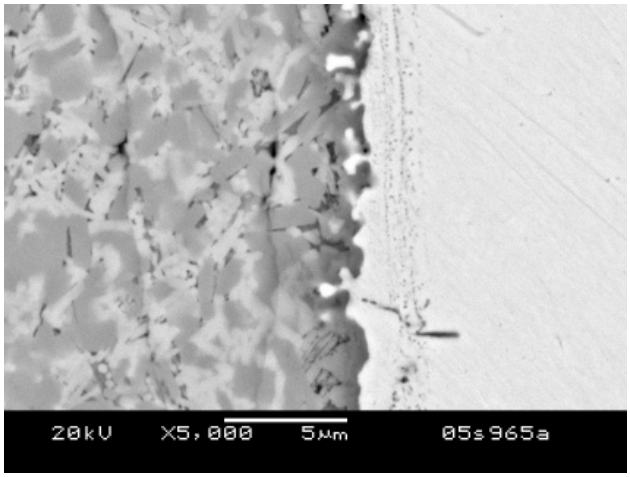

FIGURE 4. Interfacial microstructure of glass (YSO-1) at the glass/metal (Crofer22APU) interface. Sealed at 1,000°C/2 h in air. No chromate formation was observed for the higher sealing temperature, likely due to exclusion of oxygen from the interface.

were identified with CTE in the ~12.3x10^{-6}/°C range. However, again it was apparent that the issue of chromate formation must be addressed. Candidate sealing glasses were also tested in dual environments; some YSO series glasses survived four deep thermal cycles and aging up to 1,000 h at 850°C.

Conclusions and Future Directions

- Refractory glass seals have been developed, which offer excellent, stable CTE matching to other SOFC stack components. Hermetic seals have been obtained which survived isothermal and thermal cycle heat treatments. These compositions also exhibit improved interfacial stability compared to other SOFC sealing glasses, although further interfacial optimization (such as interconnect coatings) may be required to mitigate formation of undesirable, high CTE phases.
- Future work will focus on continued optimization of refractory glass seal compositions as well as larger scale testing (e.g., 4.5 inch x 4.5 inch), including isothermal and thermal cycle tests in dual environments (e.g., air/70% H_2-30% H_2O).

FY 2006 Publications/Presentations

Publications

1. Y.S. Chou, J.W. Stevenson, and P. Singh, "Thermal Cycle Stability of a Novel Glass-Mica Composite Seal for Solid Oxide Fuel Cells: Effect of Glass Volume Fraction and Stresses," J. Power Sources, 152, 168 (2005).

2. Y.-S. Chou, J.W. Stevenson, and P. Singh, "Glass Mica Composite Seals for Solid Oxide Fuel Cells," 29th International Conference on Advanced Ceramics and Composites - Advances in Solid Oxide Fuel Cells (Ceramic Engineering and Science Proceedings, Volume 26, Issue 4), p. 257 (2005).

3. Y.-S. Chou, J.W. Stevenson, and P. Singh, "Combined Ageing and Thermal Cycling of Compressive Mica Seals for Solid Oxide Fuel Cells," in Proc. 29th International Conference on Advanced Ceramics and Composites - Advances in Solid Oxide Fuel Cells (Ceramic Engineering and Science Proceedings, Volume 26, Issue 4), p. 265 (2005).

Presentations

1. "Effect of Sealing Temperature on the Interfacial Reactions of a SOFC Sealing Glass with a Metallic Interconnect Material," Y. Chou, J.W. Stevenson, and P. Singh, 30th International Conference & Exposition on Advanced Ceramics and Composites, Cocoa Beach, FL, January 22-27, 2006.

2. "Effect of Ageing on the Thermal Properties of a Novel SOFC Sealing Glass," Y. Chou, J.W. Stevenson, and P. Singh, 30th International Conference & Exposition on Advanced Ceramics and Composites, Cocoa Beach, FL, January 22-27, 2006.

3. "SOFC Interconnect and Compressive Seal Development at PNNL," Y.S. Chou, Z. Yang, G. Maupin, S. Simner, P. Singh, J.W. Stevenson, and G. Xia, 2005 Fuel Cell Seminar, Palm Springs, CA, November 14-18, 2005.

III.A.17 SOFC Cathode Materials Development at PNNL

Objectives

- Develop and optimize SOFC cathode electrode materials and microstructures offering low polarization losses and long-term stability at intermediate SOFC operating temperatures (650-800ºC).
- Improve understanding of mechanisms affecting cathode performance, including both intrinsic (e.g., composition, microstructure) and extrinsic factors (e.g., Cr poisoning).

Accomplishments

- Electrically tested and characterized lanthanum strontium cobalt ferrite (LSCF) cathodes and developed underlying degradation mechanisms.
- Developed LSCF/Ag composite cathode material and architecture intended for SOFCs operating at ~650ºC.
- Participated in a joint study with General Electric and Argonne National Laboratory (ANL) investigating Cr-related degradation in LSM cathodes.

Introduction

Minimization of cathodic polarization losses represents one of the greatest challenges to be overcome in obtaining high, stable power densities from SOFCs. Cathodic polarization typically exhibits high activation energy relative to other internal power losses, so the need to improve cathode performance becomes increasingly important as the targeted SOFC operating temperature is reduced. The severe environmental conditions experienced by the cathode during operation limit the number of likely candidate materials. In particular, the cathode material must be stable at the SOFC operating temperature in air; and it must have high electronic conductivity, high catalytic activity for the oxygen reduction reaction, and a thermal expansion compatible with the SOFC electrolyte. Chemical interactions with the electrolyte and interconnect materials must be minimal. In addition, the cathode material must have a stable, porous microstructure so that gaseous oxygen can readily diffuse through the cathode to the cathode/electrolyte interface.

For high-temperature SOFCs operating at around 1,000ºC, the preferred cathode material is A and B site doped lanthanum manganite, which offers adequate electrical conductivity and electrocatalytic activity, reasonable thermal expansion, and stability in the SOFC cathode operating environment. For SOFCs operating at substantially lower temperatures, such as 650-800ºC, alternative cathode materials may be required. Alternative perovskite compositions - typically containing La on the A site, and transition metals such as Co, Fe, and/or Ni on the B site - have received attention. In general, they offer higher oxygen ion diffusion rates and exhibit faster oxygen reduction kinetics at the electrode/electrolyte interface than lanthanum manganite, but are subject to degradation of performance over time.

Steve Simner (Primary Contact),
Mike Anderson, Jeff Stevenson
Pacific Northwest National Laboratory (PNNL)
P.O. Box 999, MS K2-44
Richland, WA 99352
Phone: (509) 375-4577; Fax: (509) 375-2186
E-mail: steven.simner@pnl.gov

DOE Project Manager: Travis Shultz
Phone: (304) 285-1370
E-mail: Travis.Shultz@netl.doe.gov

Approach

Selected candidate cathode materials were evaluated using a number of techniques including x-ray diffraction (XRD), scanning electron microscopy (SEM), energy dispersive spectroscopy (EDS), transmission electron microscopy (TEM), and x-ray photoelectron spectroscopy (XPS). The electrochemical performance was measured by sintering the cathode material onto anode-supported YSZ membranes with a samarium-doped ceria (SDC) interlayer. After attachment of current collectors, the resulting cells were placed into test fixtures and their current-voltage characteristics were evaluated using dc and impedance spectroscopy measurements. Cells were tested in air vs. moist (~3% H_2O) hydrogen at low fuel utilizations. After cell tests were completed, the cells were analyzed by SEM/EDS, and other techniques as appropriate.

Results

LSCF Cathode Degradation

While LSCF-6428 cathodes typically provide significantly higher power densities compared to LSM-based cathodes (particularly in the 600-800ºC temperature range), LSCF is subject to long-term

instability (see Figure 1). Analysis of pre- and post-tested samples indicated that segregation of Sr at the LSCF cathode interfaces may be at least partially responsible for the observed degradation of LSCF. For example, XPS data from the cathode/current collector interface, before and after testing, is presented in Table 1. It indicates significant Sr enrichment after testing. Though the Sr-rich phase may not be pure SrO, it is interesting to note that the conductivity of SrO at 750°C is very low: ~5 x 10^{-5} S/cm [1]. Hence, thin films of SrO formed at cathode/current collector and cathode/electrolyte interfaces could result in significant increases in ohmic resistance, and might also increase non-ohmic polarization by de-activating TPB reaction sites.

LSCF/Ag Composite Cathodes

Recently, PNNL developed a novel oxide-Ag composite cathode morphology consisting of silver spherical cores up to ~50 μm in diameter coated with a ~1 micron layer of LSCF-6428 powder. The primary purpose for applying the oxide coating (via a dry coating technique known as "mechanofusion") was the reduction of silver diffusivity and/or volatility. Figure 2 shows cross-sections of processed LSCF-coated Ag spheres; it should be noted that significantly smaller particles can be equally well coated using this technique.

Figure 3 shows >2,000 hours of data for a cell conditioned at 750 hours for 50 hours and then operated at 700°C. The cell exhibited additional conditioning up to 650-700 hours, and then relatively stable performance. However, degradation was observed for this cell, and a drop of ~4.9% in power density (at 0.7 V) was measured between 660 and 2,270 hours (~3% power drop per 1,000 hours). Phenomena responsible for the conditioning and degradation characteristics of these materials have not been conclusively established, though it appears that increased contact of the coated spheres

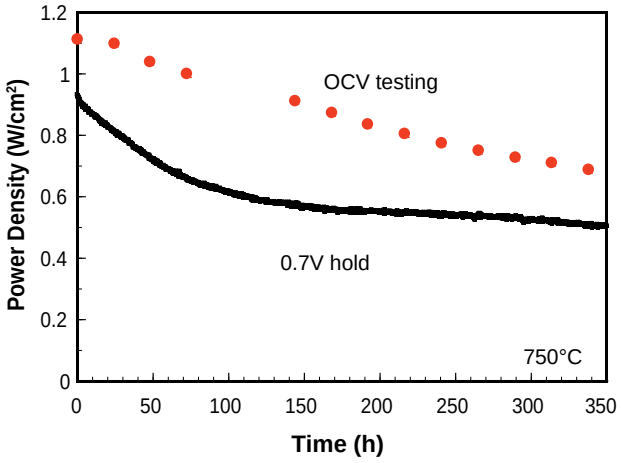

FIGURE 1. Power Density of Anode-Supported Cells Held at Constant 0.7 V, or Held at OCV Except for Brief Intermittent Testing at 0.7 V (for 5 minutes every 24 hours)

TABLE 1. XPS results for LSCF cathode surface at cathode/current collector interface. Note that Sr enrichment is greater and deeper in tested cell compared to untested or thermally annealed (but undischarged) cell.

	Surface	5 nm below surface (Ar+ ion sputtering)
Pre-Tested	29% La, 32% Sr, 35% Fe, 4% Co	45% La, 16% Sr, 36% Fe, 3% Co
Annealed (750°C/500h)	30% La, 30% Sr, 36% Fe, 4% Co	45% La, 17% Sr, 35% Fe, 3% Co
Tested (750°C/0.7V/500 h)	11% La, 68% Sr, 21% Fe	19% La, 52% Sr, 29% Fe

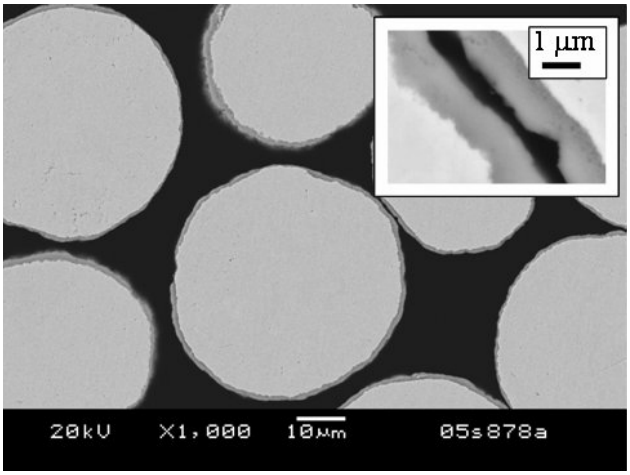

FIGURE 2. Cross-Sectional Micrograph of Silver Spheres Coated with LSCF-6428 Predominantly Indicating Excellent Coating Adhesion

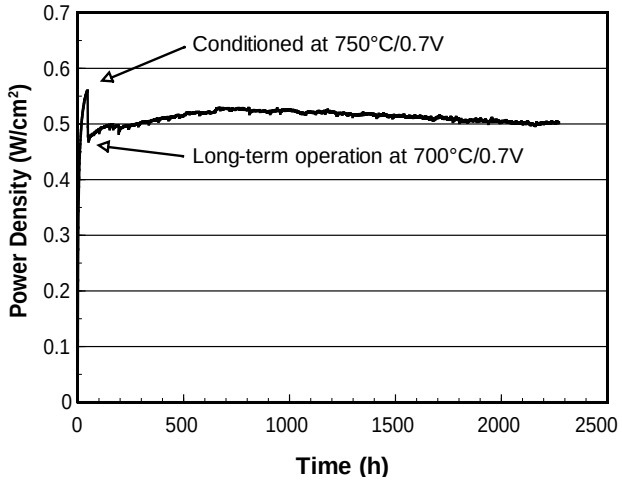

FIGURE 3. Performance Data for an Anode-Supported YSZ Cell Utilizing the Ag-LSCF Composite Cathode at 700°C and 0.7 V

along the electrolyte surface due to diffusion may play a role by increasing the cathode-electrolyte contact area. It is anticipated that optimization of the oxide composition and composite morphology may lead to improved stability. One final factor worth consideration is cost. Preliminary estimates indicate that the cost of the coated Ag-spheres is approximately 2x the cost of a typical perovskite cathode material. However, it should be noted that the use of these materials has the potential of removing two high temperature-sintering steps. First, it may be possible to sinter the cathode in situ during stack fabrication/sealing, thereby eliminating a separate sintering step at temperatures >1,000ºC. In addition, preliminary results indicate that an SDC interfacial layer (and its separate sintering step) may not be required if detrimental zirconate formation is avoided at the low cathode sintering temperature (~800ºC). For example, cells without the protective SDC-20 interlayer exhibited maximum power densities of ~650 and 500 mW/cm^2, at 750 and 700ºC, respectively (tested at 0.7 V). These results are promising in that they suggest that a protective ceria layer may not be required.

Chromium Degradation Experiments

A joint study to assess Cr-related poisoning effects on standard LSM-YSZ anode-supported SOFCs was performed by a task force consisting of three organizations: PNNL, GE, and ANL. Three main types of experiments (cell performance tests with Cr vapor dosing only (Au interconnect), steel interconnect with ribs covered, and bare steel interconnect) were conducted by the task force using identical test vehicles and components. The results showed stable cell performance without chromium dosing and ~3%/1,000 hours with Cr vapor species dosing at 800ºC. Much higher cell performance degradation rates were observed when the cells were in direct contact with stainless steel interconnects. Species such as $(Cr,Mn)_3O_4$, Cr_2O_3, and $MnCr_2O_4$ were identified in the cathode and near cathode/electrolyte interfaces.

Conclusions and Future Directions

- Degradation of SOFC with LSCF cathodes may be related to Sr segregation at cathode interfaces.
- LSCF/Ag composite cathodes show promising behavior at relatively low SOFC operating temperatures (e.g., 650-700ºC).
- Cr vapor species in cathode air streams can have adverse effects on cell performance.
- Future work in the short term will focus on continued optimization of LSCF/Ag composite cathodes and the investigation of degradation mechanisms in alkaline earth-doped perovskite cathodes.

FY 2006 Publications/Presentations

Publications

1. S.P. Simner, M.D. Anderson, G.-G. Xia, Z. Yang, and J.W. Stevenson, "Long-Term SOFC Stability with Coated Ferritic Stainless Steel Interconnect," in Proc. 29th International Conference on Advanced Ceramics and Composites - Advances in Solid Oxide Fuel Cells (Ceramic Engineering and Science Proceedings, Volume 26, Issue 4), p. 83 (2005).

Presentations

1. "SECA Core Technology Program: Materials Development at PNNL," J.W. Stevenson, Y.S. Chou, O.A. Marina, S.P. Simner, K.S. Weil, Z. Yang, and P. Singh, SECA Core Technology Program Review Meeting, Lakewood, CO, October 25-26, 2005.

2. "State of the Art of SOFC Cathodes," J.W. Stevenson, S.P. Simner, M.D. Anderson, and P. Singh, U.S. Department of Energy Workshop: Fundamental Mechanisms of SOFC Cathode Reactions, Cocoa Beach, FL, January 22-27, 2006.

3. "Long-Term Behavior of La(Sr)Fe(Co)O_3 SOFC Cathodes," S. Simner, M. Anderson, and J.W. Stevenson, 30th International Conference & Exposition on Advanced Ceramics and Composites, Cocoa Beach, FL, January 22-27, 2006.

References

1. W.D. Copeland, *J. Phys. Chem. Solids,* 29, 313 (1968).

III.A.18 SECA Core Technology Program Activities - PNNL

Objectives

- Prioritize technology development needs and develop R&D plan.
- Coordinate SECA Core Technology Program (CTP) activities.
- Develop materials, designs and systems-based solutions to meet SECA cost and performance targets.
- Execute experimental plan, summarize technical findings and develop topical reports, and disseminate technical information and technology transfer to SECA industrial teams.
- Participate and organize technical and topical meetings and workshops.
- Publish and present technical papers and reports.

Approach

- Hold technical meetings to identify key technology gaps and barriers, and review technology background and present technical findings.
- Organize topical area workshops and exchange technical information.
- Transfer technologies to industries.
- Provide quarterly, annual and topical technical reports.
- Meet with industrial participants on regular basis.
- Lead and organize technical society meetings.

Accomplishments

- Held SECA CTP workshop in Golden, Colorado.
- Held workshops on SOFC interconnection stability and Cr evaporation.
- Provided coating and glass seal materials to SECA industrial teams for evaluation and developed an integrated "on-anode" reforming and cell stack temperature simulation task for optimized thermal management.
- Published quarterly progress reports and topical reports.
- Presented invited lectures at technical societies, universities, and industries.
- Organized MST 06, AcerSoc Cocoa-Beach meetings on SOFC technology.

Future Directions

- Continue technology prioritization in consultation with SECA participants.
- Provide technical and CTP progress reports to SECA participants.
- Organize technical society meetings to exchange technical information.
- Hold SECA CTP meetings and topical workshops.

Prabhakar Singh
Pacific Northwest National Laboratory (PNNL)
P.O. Box 999, MS K2-44
Richland, WA 99354
Phone: (509) 375-5945; Fax: (509) 375-2186
E-mail: Prabhakar.Singh@pnl.gov

DOE Project Manager: Travis Shultz
Phone: (304) 285-1370
E-mail: Travis.Shultz@netl.doe.gov

Introduction

The overall objectives of the Solid-State Energy Conversion Alliance Core Technology Program (SECA CTP) at PNNL are to:

a. Coordinate technology development activities at universities, national laboratories, and other research organizations.
b. Identify technology gaps, and prioritize technology development needs for meeting the cost and performance targets of the SECA SOFC power generation systems.
c. Develop, test and implement component- and system-based technology solutions.
d. Promote technology transfer and dissemination of technical information to SECA industrial teams.

PNNL works closely with SECA participants in identifying and prioritizing the technology gaps in areas related to the long-term stability, reliability, and cost reduction of modular SOFC power generation systems. Technical findings in areas related to materials, design and balance-of-plant are integrated to develop scientific and engineering solutions for operational and systems related issues. Technology activities at PNNL include advanced cell and stack component materials development and testing with a focus on improving performance stability, development of computational tools and techniques for electrical performance optimization and improved reliability, and hydrocarbon fuel processing technologies for achieving multi-fuel capability in SOFC systems. Technical findings and results, generated under the core program, are provided

to industrial teams in a timely manner. PNNL provides topical and technology development status reports to SECA participants.

Approach

Our approach and methodology for meeting the overall SECA cost and performance targets not only include the timely development and optimization of the cell and stack component technologies but also the development and implementation of systems-based solutions. The core technology focuses on coordinating the development activities at universities, national laboratories and industries as well as leveraging technologies being developed by other government agencies and related organizations. Technical findings are rigorously analyzed and presented at workshops and technical meetings. Topical reports are published for the timely dissemination of information. Approaches include:

- Discuss and present results and technical findings to SECA participants. Summarize the technical status and provide topical reports.
- Publish program required quarterly and annual progress reports describing the progress.
- Provide topical reports after completion of the task.
- Organize SECA annual and SECA CTP meetings.
- Present technical work at national/international meetings and workshops.
- Organize and participate in topical workshops, assess development status and provide future direction.
- Participate and lead technical forums related to SOFCs.
- Coordinate the program activities with the National Energy Technology Laboratory.

Results

The SECA Core Technology Program at PNNL identifies and prioritizes the technology development needs and conducts research to develop integrated science- and engineering-based solutions to meet the cost and performance targets of SECA. The program focuses on the development of advanced component materials, modeling and design tools, and fuel processing techniques, as well as coordinates technology development activities at universities, national laboratories, and industries. CTP management disseminates technical information gained through workshops and meetings to SECA participants on a frequent basis through topical and technical reports. Workshops are held to ensure and update the progress, exchange technical information, as well as identify and prioritize technical needs. Technology transfer and implementation of cost reduction schemes are highlighted. Related technical work at other government agencies is examined and technical experts are invited for information exchange.

In FY 2006, the SECA CTP held a workshop in Golden, CO to review the status of materials technology, modeling and simulation, fuel processing and balance-of-plant. PNNL held a topical workshop (in collaboration with General Electric and Argonne National Laboratory) on chromia transport. Findings based on computational simulation of integrated “on-anode” reforming, tailoring of the hydrocarbon reformation rate, and thermal management, in both small and large stacks, were discussed with SECA industrial teams.

Technology development activities at PNNL, in concert with the overall SECA program priorities remain focused on the selection, optimization, testing and characterization of cell-to-cell interconnection bulk materials and surface coatings, novel gas sealing concepts and seal materials, and high performance cathode electrodes and electrode poisoning [1]. Topical reports covering the findings and results have been prepared and published. Computational design and simulation activity is targeted towards the development of multi-physics-based tools for structural, thermal, and electrical analysis of single cells and multi-cell stacks. Current activity focuses on the optimization of gas flow, partial hydrocarbon utilization, and cell footprint for thermal management and electrical performance optimization. Our efforts are also targeted towards the identification of cell failure mechanisms in conventional and larger cell footprints. Fuel processing activity evaluates both external and “on-anode” reforming with emphasis on the later for efficient thermal management.

Conclusions and Future Directions

PNNL has identified and prioritized technology development needs and has developed advanced materials, cell and stack designs for improved reliability and performance stability, as well as integration of fuel processing with thermal management. Technical findings have been presented at meetings and SECA workshops, along with publications of topical reports and technical papers. Highlights include:

- Development of advanced cell anodes for tailoring reformation rate to manage localized cell temperature and cell-to-cell temperature distribution.
- Development of cell and stack thermal, structural, and electrical performance model, highlighting the role of “on-anode” reformation on temperature distribution.
- Development of a suite of computational tools for cell and stack design analysis and reliability prediction.

- Testing and validation of interconnection coatings for improved corrosion resistance and Cr transport barriers; development of modified glass formulations and surface coatings for high temperature rigid seals, and prevention of interface reaction and Cr dissolution; and development of composite cathode electrodes for improved electrical performance and performance stability.
- Participation in technical society meetings (ASM International, AcerSoc, TMS, Gordon Research Conference).
- Dissemination of technical information through topical reports, technical publications, and program-required documents.
- Transfer of technology to SECA industrial teams.

FY 2006 Publications/Presentations

1. "Corrosion in Fuel Cells", Singh, P., Yang, Z., ASM Handbook, Vol. 13C.

2. "Application of Vacuum Deposition Methods to Solid Oxide Fuel Cells", Pederson, L., Singh, P., Zhou, X.D., Review paper, Vacuum (Accepted for publication).

3. "SOFC Technology Status Review", Surdoval, W., Singh, P., 30th International Conference on Advanced Ceramics and Composites, American Ceramic Society, January 2006.

4. "SOFC Power Generation Systems: Technology Status and R&D Needs", Singh, P., presented at University of Cincinnati, 2006.

5. "Overview of SOFC Power Generation Systems", Singh, P., Sprenkle, V., presented at IBM, Fishkill, 2006.

References

1. SECA CTP meeting, Wayne Surdoval, Golden, CO.

III.A.19 SOFC Interconnect Materials Development at PNNL

Objectives

- Develop and optimize cost-effective materials for intermediate temperature SOFC interconnect and interconnect/electrode interface contact applications.
- Develop, characterize, and validate materials degradation processes in SOFC operating environments.
- Utilize the basic understanding in the development of advanced alloys and surface coatings with adequate bulk and interface corrosion tolerance.

Accomplishments

- Compiled structural, electrical, and chemical properties of $(Mn,Co)_3O_4$ spinels.
- Synthesized, tested, and characterized spinel coatings on ferritic stainless steel (FSS) substrates.
- Completed the evaluation of Mn-modified Ni-base alloys under SOFC operating conditions.
- Initiated dual atmosphere oxidation tests on selected FSS alloys using simulated reformate fuel.

Introduction

With the reduction in SOFC operating temperatures, low-cost high-temperature oxidation alloys have become promising candidates to replace lanthanum chromite, a ceramic that can withstand operating temperatures in the 1000°C range. To improve the understanding of the advantages and limitations of alloy interconnects, PNNL has been engaged in systematic evaluation and development of candidate materials. Challenges to be overcome include chromia scale evaporation, scale electrical resistivity, oxidation/corrosion under interconnect dual exposure conditions and scale adherence, and compatibility with adjacent components, such as seals, electrodes and/or electrical contact materials.

Zhenguo "Gary" Yang (Primary Contact), Guanguang Xia, Jeff Stevenson, and Prabhakar Singh

Pacific Northwest National Laboratory (PNNL)
P.O. Box 999, MS K2-44
Richland, WA 99352
Phone: (509) 375-3756; Fax: (509) 375-2186
E-mail: zgary.yang@pnl.gov

DOE Project Manager: Travis Shultz
Phone: (304) 285-1370
E-mail: Travis.Shultz@netl.doe.gov

Approach

Oxidation behavior of candidate alloys is being investigated under dual atmospheres (simultaneous exposure to an oxidizing and reducing environment) conditions typical of SOFC interconnect operation conditions. Studies are being performed in both air/hydrogen/steam and air/simulated-reformate environments in the 600-800°C temperature range. Bulk modifications, as well as surface coatings, are being investigated to provide long-term oxidation resistance, mitigate Cr evaporation and facilitate electronically conducting interface formation.

Results

$(Mn,Co)_3O_4$ spinel coatings have been successfully fabricated onto Crofer22APU FSS substrates. Recently, spinel coatings were successfully applied to two other ferritic stainless steels, E-brite and 430, by slurry coating followed by heat treatment in a reducing environment and then oxidation in air. Figure 1 shows a scanning electron microscope (SEM) micrograph of a coated 430 sample after the initial heat treatment (reduction in $Ar/3\%H_2O/2.75\%H_2$ at 800°C). At this stage, the spinel phase was reduced into a porous mixture of Co and MnO. During subsequent oxidation in air at 800°C, the MnO and Co reacted with oxygen to re-form the spinel phases, as confirmed by x-ray diffraction (XRD) analysis. A cross-section SEM image (Figure 2) after the oxidizing heat-treatment shows that the spinel layer was well bonded to the 430 substrate via an ~1.5 μm thick scale. Some residual porosity is present in the spinel layer. The partial densification of the spinel layer from the highly porous layer of MnO and Co is attributed to a sintering process that is enhanced by the spinel formation reactions occurring during the oxidizing heat treatment. As no obvious boundary was discernible between the scale and the spinel coating, it appears that the Mn-Co spinel and the native oxide scale grown on 430 are mutually compatible. Also, energy dispersive spectroscopy (EDS) analysis on the cross-section indicated that no detectable chromium penetration into the spinel layer had occurred after 100 hours at 800°C. The same approach was also successfully used for coating of E-brite samples. As in the case for 430, the protection layer acted as an effective Cr barrier during the 100 hours of heat treatment.

$Mn_{1.5}Co_{1.5}O_4$ spinel coating has been found to substantially improve the electrical behavior of simulated interconnect/cathode interfaces. In recent tests, enhanced electrical performance was also observed for the other FSS substrates when spinel coatings were applied. Figure 3 shows the contact area-specific resistance (ASR) for coated 430 and E-brite, measured as a function of time during tests in air at 800°C. The contact ASR between the coated E-brite and cathode was as low as 7 mohm-cm^2 in the early stages of the test and increased only slightly with time during the 400 hours measurement. Thus, E-brite behaved similarly to Crofer22APU. In comparison, the coated 430 exhibited a higher ASR, which substantially increased over time.

After the ASR measurements, SEM analysis on the cross-sections of the tested samples indicated that the spinel coatings were well-bonded to the ferritic substrate and free of spallation or cracks. In the case of the coated E-brite, a scale about 1.0 μm thick grew between the metal substrate and the $Mn_{1.5}Co_{1.5}O_4$ coating. EDS analysis did not find evidence of Cr penetration through the spinel coating into either the contact paste or the cathode. Figure 4 shows an SEM cross-section of the coated 430. After ~400 hours at 800°C in air, a scale about 2.0~2.5 μm thick grew between the ferritic substrate and the coating. Both point and line EDS analyses indicated no penetration of Cr through the coating into the contact paste or the cathode. The EDS line scan did, however, find segregation of Si, likely in form of silica, at the interface between the

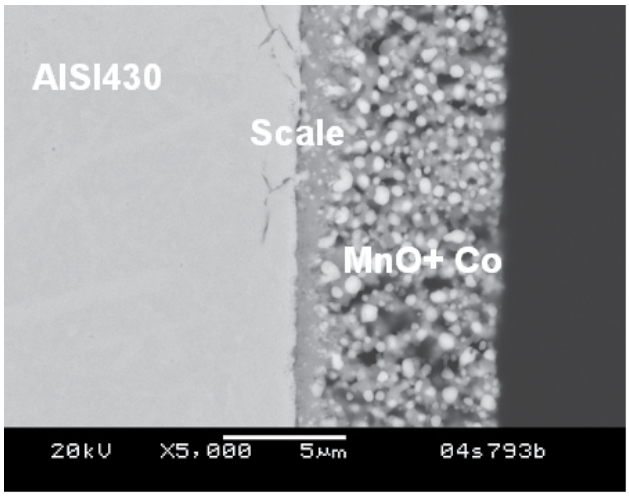

FIGURE 1. SEM Image of Cross-Section of Protection Layer on 430 Stainless Steel after Heat Treatment at 800°C in 2.75%H_2/bal. Ar

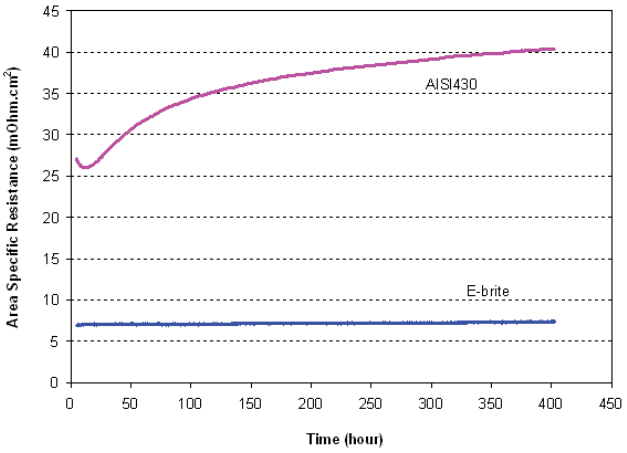

FIGURE 3. Contact ASR between LSF Cathode and a 430 or E-brite Current Collector with $Mn_{1.5}Co_{1.5}O_4$ Spinel Protection Layer

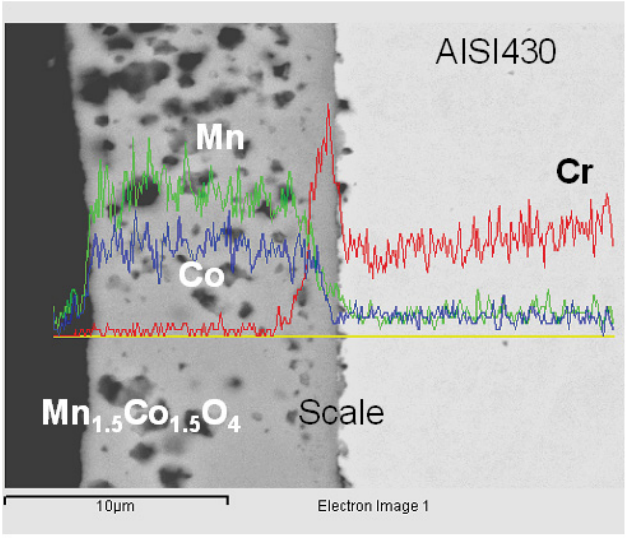

FIGURE 2. SEM Image of Cross-Section of Protection Layer on 430 Stainless Steel after Re-Oxidation at 800°C in Air

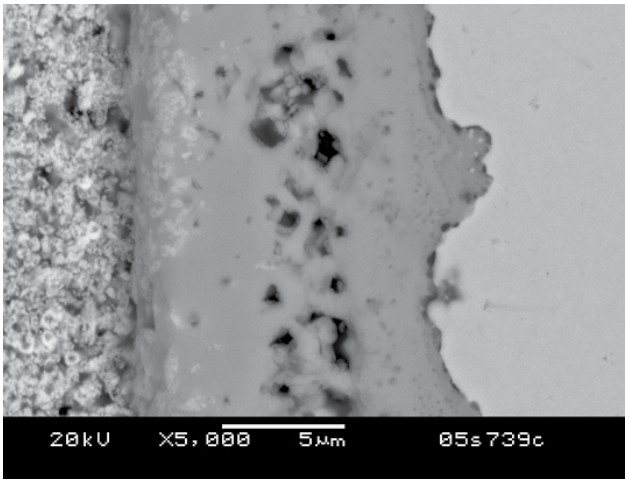

FIGURE 4. SEM Image of Cross-Section of 430 with $Mn_{1.5}Co_{1.5}O_4$ Protection Layer after Contact ASR Measurement at 800°C in Air for ~400 Hours

scale and the metal substrate, due to residual Si in the 430 substrate. This silica layer is the likely cause of the relatively high ASR observed for the coated 430 test. Additionally, the higher growth rate of the scale beneath the spinel coating would be another contributor to the high ASR. Fe was also observed in the scale and the spinel coating, indicating Fe outward migration from the metal substrate. It is known that, with ~17% Cr, 430 forms a scale that contains Fe during high temperature exposure in air and grows faster than the scale grown on ferritic substrates with a higher Cr concentration. For example, Crofer22APU and E-brite, containing 23% and 27% Cr, respectively, exhibit a lower scale growth rate, i.e. a higher oxidation resistance, than 430. The scales grown on Crofer22APU and E-brite in air are comprised of $(Mn,Cr)_3O_4$ + Cr_2O_3 and Cr_2O_3, respectively, with negligible Fe.

Conclusions and Future Directions

- $Mn_{1.5}Co_{1.5}O_4$ spinel composition demonstrates excellent electrical conductivity, thermal and structural stability, and thermal expansion match to selected ferritic stainless steel interconnects.
- Thermally grown surface coatings of $Mn_{1.5}Co_{1.5}O_4$ not only decreases the interconnect/cathode contact resistance, but also acts as (a) an anionic transport barrier to inhibit scale growth on the stainless steel and (b) barrier for the penetration of Cr through the coating.
- Future work on the development and optimization of protective coatings will focus on tailoring the spinel coating composition as well as the development of cost-effective fabrication techniques for near net shape application. Additional activities will include oxidation and corrosion tests of alloys and coatings in air/simulated reformate dual atmospheres and development of optimized contact materials for cathode/interconnect interfaces.

FY 2006 Publications/Presentations

Publications

1. Z. Yang, G.G. Xia, P. Singh, and J.W. Stevenson, "Electrical Contacts between Cathodes and Metallic Interconnects in Solid Oxide Fuel Cells," J. Power Sources, 155, 246 (2006).

2. Z. Yang, G. Xia, S.P. Simner, and J.W. Stevenson, "Thermal Growth and Performance of Manganese Cobaltite Spinel Protection Layers on Ferritic Stainless Steels SOFC Interconnects," J. Electrochem. Soc, 152, A1896 (2005).

3. Z. Yang, G.-G. Xia, S.P. Simner, and J.W. Stevenson, "Ferritic Stainless Steel SOFC Interconnects with Thermally Grown $(Mn,Co)_3O_4$ Spinel Protection Layers," in Proc. 29th International Conference on Advanced Ceramics and Composites - Advances in Solid Oxide Fuel Cells (Ceramic Engineering and Science Proceedings, Volume 26, Issue 4), p. 201 (2005).

4. Z. Yang, G.-G. Xia, and J.W. Stevenson, "Electrical Contacts between Cathodes and Metallic Interconnects in Solid Oxide Fuel Cells," in Proc. 29th International Conference on Advanced Ceramics and Composites - Advances in Solid Oxide Fuel Cells (Ceramic Engineering and Science Proceedings, Volume 26, Issue 4), p. 217 (2005).

Presentations

1. "Conductive Protection Layers on Ferritic Stainless Steels for SOFC Interconnect Applications," Z.G. Yang, S.H. Li, G.D. Maupin, S.P. Simner, and G.G. Xia, International Conference on Metallurgical Coatings and Thin Films, San Diego, CA, May 1-5, 2006.

2. "Development of $(Mn,Co)_3O_4$ Protection Layers on Ferritic Stainless Steels for SOFC Interconnect Applications," Z.G. Yang, G.G. Xia, G.D. Maupin, X. Li, P. Singh, J.W. Stevenson, 135th Annual TMS Meeting, San Antonio, TX, March 12-16, 2006.

3. "High Temperature Corrosion Behavior of Metals and Alloys under Influence of a Hydrogen Gradient," Z.G. Yang, G. Coffey, D.M. Paxton, P. Singh, J.W. Stevenson, and G.G. Xia, 135th Annual TMS Meeting, San Antonio, TX, March 12-16, 2006.

4. "High Temperature Corrosion Behavior of Oxidation Resistant Alloys under SOFC Interconnect Exposure Conditions," Z. Yang, G. Coffey, P. Singh, J.W. Stevenson, and G. Xia, 30th International Conference & Exposition on Advanced Ceramics and Composites, Cocoa Beach, FL, January 22-27, 2006.

5. "Properties of $(Mn,Co)_3O_4$ Spinel Protection Layers for SOFC Interconnects," Z. Yang, S. Li, G. D. Maupin, P. Singh, S.P. Simner, J.W. Stevenson, and G. Xia, 30th International Conference & Exposition on Advanced Ceramics and Composites, Cocoa Beach, FL, January 22-27, 2006.

6. "Manganese-Cobalt Mixed Spinel Oxides as Surface Modifiers for Stainless Steel Interconnects of SOFCs," G. Xia, Z. Yang, G.D. Maupin, S.P. Simner and J.W. Stevenson, 208th Meeting of The Electrochemical Society, Los Angeles, CA, October 16-21, 2005.

III.A.20 Reliable Seals for Solid Oxide Fuel Cells

Objectives

- Develop reliable, cost-effective sealing techniques for solid oxide fuel cells (SOFCs).
- Determine performance-limiting features of sealing methods.
- Optimize seal properties.
- Determine seal degradation mechanisms and predict useful seal lifetimes.

Approach

- We are making glass matrix composite seals with a wide range of chemical and mechanical properties.
- The composite approach allows glass and filler properties to be optimized independently.
- Seal thermal and mechanical strains are reduced by selecting glass compositions with glass transition temperatures (Tg) below the SOFC operating temperature.
- Viscosity, coefficient of thermal expansion (CTE), and other seal characteristics can be tailored by adding unreactive powder.
- The volume fraction of the glass phase can be reduced to a minimum for the seal, which reduces reactivity with fuel cell materials.

Accomplishments

- We have made over 30 different glass compositions with potential for the composite seal approach and measured their physical properties.
- We have modified our glass compositions to provide better control over flow and thermal expansion properties.
- A new high temperature optical-mechanical measuring instrument (TOMMI) allowing in-situ video recording of specimens at elevated temperatures (to 1,700°C) has been purchased and set up and is being used to measure glass viscosities and to determine the effect of additive powder composition, size, and aspect ratio on composite seal flow and adhesion.
- A series of 2,000-hour tests at 750°C in air of two glass-ceramic compositions on two ferritic SS alloys (Ebrite and Crofer), on YSZ, and on anode material have been completed.
- One of our glass compositions (Glass 14A: 40% B_2O_3, 10% Al_2O_3, 10% BaO, 20% MgO, 20% CaO) was studied for reactivity with SS alloys (Crofer and 410 SS).

Future Directions

- Conduct additional 2,000-hour tests to demonstrate long-term stability of the glass ceramic seals.
- The 2,000-hour test protocol will be expanded to include effects of water vapor on seal performance at 750°C.
- Develop screening test for adhesion of different seal compositions and processes.
- Conduct thermal cycling tests of anode-interconnect seals to improve long-term stability.
- Refine reaction studies of sealants with SOFC components.
- Perform more fundamental mechanical tests on composite seal materials at operating temperatures; e.g., flexural strength and fracture toughness.

Ronald E. Loehman (Primary Contact), Bryan Gauntt, Alicia Ayala, Erica Corral, Raja Shah
Sandia National Laboratories, MS 1349
Albuquerque, NM 87185-1349
Phone: (505) 272-7601; Fax: (505) 272-7304
E-mail: loehman@sandia.gov

DOE Project Manager:
Ayyakkannu Manivannan
Phone: (304) 285-2078
E-mail: Ayyakkannu.Manivannan@netl.doe.gov

Introduction

Developing reliable methods for sealing solid oxide fuel cell stacks presents the most challenging set of performance criteria in the entire field of ceramic joining. For SOFC applications, the requirements on the sealing method include:

- Adhesion of the sealing material to fuel cell components from room temperature to as high as 1,000°C.
- Ability to provide a leak-tight seal at the SOFC operating temperature.
- Ability to maintain a seal while accommodating strains from SOFC components with different coefficients of thermal expansion (CTEs).
- Lack of adverse reaction between the sealing material(s) and the fuel cell components.
- Chemical and physical stability of the sealant at temperatures up to 1,000°C in oxidizing and reducing atmospheres.

- Thermal shock tolerance
- Electrically insulating for some SOFC designs

All of the above properties must be maintained for SOFC operating lifetimes of up to 40,000 hours. The list is written in approximate order of decreasing stringency. That is, no matter what the SOFC design, the seal must be adherent and leak-tight. On the other hand, some stack designs may require joining only similar materials and, thus, a matched CTE seal may be sufficient. Note also that the requirements may be contradictory. For example, being leak-tight and adherent at high temperatures suggests a refractory, stiff sealant, which may work against the requirement for thermal strain accommodation. Such situations are common, and seal developers know that seal design is specific to a particular component geometry and usually requires compromises among competing requirements.

Approach

Under DOE sponsorship, this project is developing an approach to sealing SOFCs that can be tailored to the specific requirements of the vertical teams in the DOE/SECA (Solid State Energy Conversion Alliance) program. The technique combines extensive capabilities in ceramic joining and composites that have been developed at Sandia over the past 20 years. In our judgment, relief of thermal expansion mismatch stresses will require SOFC seals to incorporate either a ductile metal or a high-viscosity glass that can relieve stresses through viscous creep. Other design and operational constraints on SOFCs, which as discussed above frequently are in opposition, severely restrict the options for seal materials. Based on our prior experience in ceramic joining and on results obtained so far on this project, we believe we have greatest design flexibility using ceramic-filled glasses and metal-filled glass composites. We have demonstrated that we can control properties such as glass transition temperature and thermal expansion coefficient by varying the compositions, amounts, and microstructures of the different phases. The choices are guided by thermochemical and composite microstructural models that allow us to target specific seal properties for a given design. Several seal systems are showing promise in functional tests.

Results

We have made over 30 different glass compositions with potential for the composite seal approach and measured their physical properties. Our glasses exhibit a range of glass transition temperatures (Tg), coefficients of thermal expansion (CTE) and viscosities, potentially applicable to a wide range of properties that may be appropriate for different SOFC component materials.

Our approach to SOFC sealing techniques consists of engineering ceramic-filled glass composites, metal-filled glass composites, and/or ceramic-filled metal composites that can meet SOFC requirements.

Glass composite seal materials were made using both zirconia (ZrO_2) and silver particles suspended in a glass composition previously found not to react with solid SOFC components including the YSZ electrolyte, the Ni-YSZ anode, and several potential stainless steel interconnect materials. The effects of the particle phases on the viscosity of the resulting composites were determined using a new high temperature optical-mechanical measuring facility (TOMMI) that allows in-situ video recording of specimens at elevated temperatures (up to 1,700°C). A parallel plate viscometer setup (Figure 1) was used to determine the

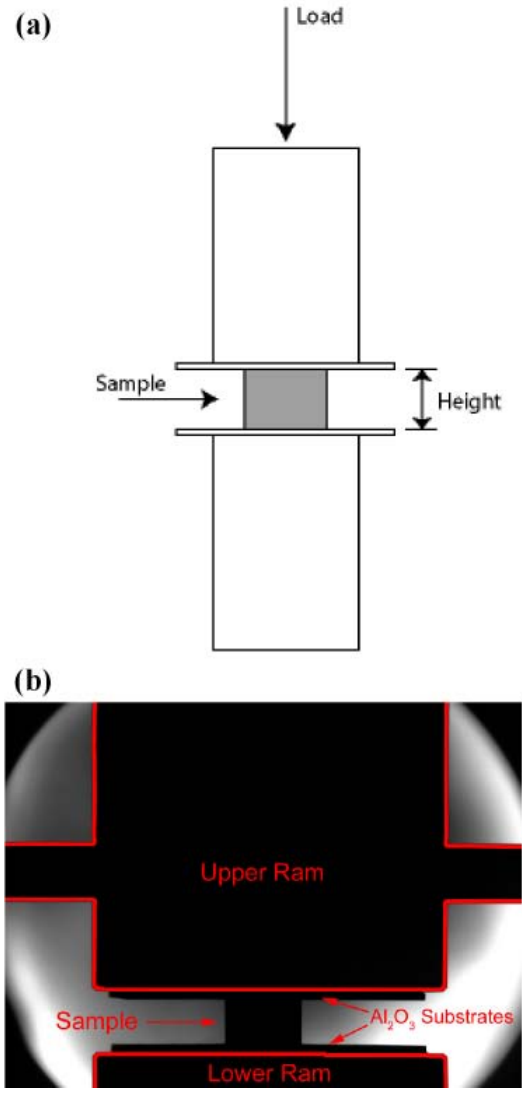

FIGURE 1. Parallel Plate Viscometer Setup Used for Viscosity Measurements; (a) Parallel Plate Viscometer; (b) Furnace Setup

effect of additive powder composition, size, and aspect ratio on composite seal flow and adhesion.

Composite viscosity was found to increase with an increased volume fraction of either metal or ceramic particles. The added particles increased the available surface area for wetting by the glass and helped retain the glass in the composite seal material. The effect of the YSZ filler was compared to that of Ni additions to the glass. We have shown that YSZ fillers have a greater effect on viscosity than added Ni because the YSZ nucleates glass crystallization (Figure 2).

The addition of ceramic particles also altered the glass crystallization behavior. The crystallization kinetics of the pure glass and the metal and ceramic composites were studied using differential thermal analysis. It was found that the ceramic particles had a much greater effect on the crystallization of the glass than the metal additives. The crystallization of the glass resulted in an increased volume fraction of refractory particles in the glass seal and a corresponding increase in the seal viscosity beginning at the onset of the crystallization.

The viscosity results were fit using classical suspension rheology models. The viscosity data, coupled with the suspension rheology models, gave us an increased understanding of the effects of added particles on the viscosity of the composite seal materials. A wide range of temperature-viscosity behaviors can be attained using the glass composite approach, and the constraints imposed by a pure glass seal approach can be overcome with the selective addition of a solid particle phase.

Having gained an understanding of how to engineer glass-ceramic viscosity, the reactivity and long-term stability of the composites was addressed. A series of 2,000-hour tests at 750°C in air of two glass-ceramic compositions (Glass 14a and Glass 14a +10% YSZ) on two ferritic SS alloys (Ebrite and Crofer) and on anode material have been completed. A detailed microprobe analysis of the samples was performed to determine the long-term stability of the composite seal and the substrates (Figure 3). Complex borate, Ca/Al, and Mg phases were identified in both glass compositions on the three different substrates. Ni diffusion was not observed along the interface in any case. The absence of appreciable reactions and Ni diffusion indicate long-term stability of the glasses at 750°C.

One of our glass compositions (Glass 14A: 40% B_2O_3, 10% Al_2O_3, 10% BaO, 20% MgO, 20% CaO) was studied for reactivity with SS alloys (Crofer and 410 SS). Testing conditions were (1) 850°C for 5 hours and (2) 850°C for 5 minutes and 750°C for 24 hours. Microprobe analysis shows the formation of a Cr_2O_3 layer along the glass/metal interface, the occurrence of complex boron phases in the bulk glass,

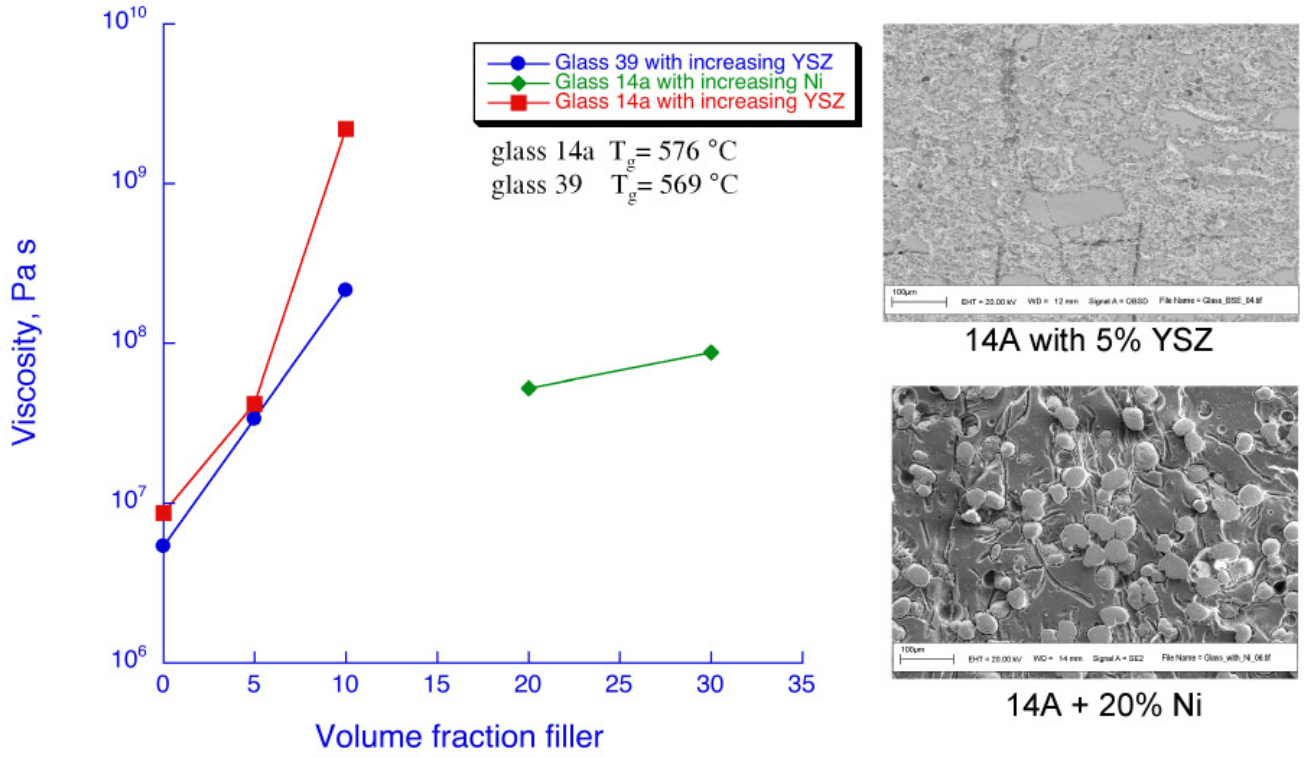

FIGURE 2. Glass-ceramic composite viscosity increases with increasing volume fraction of fillers. YSZ fillers have a greater effect on viscosity than added Ni because YSZ nucleates glass crystallization.

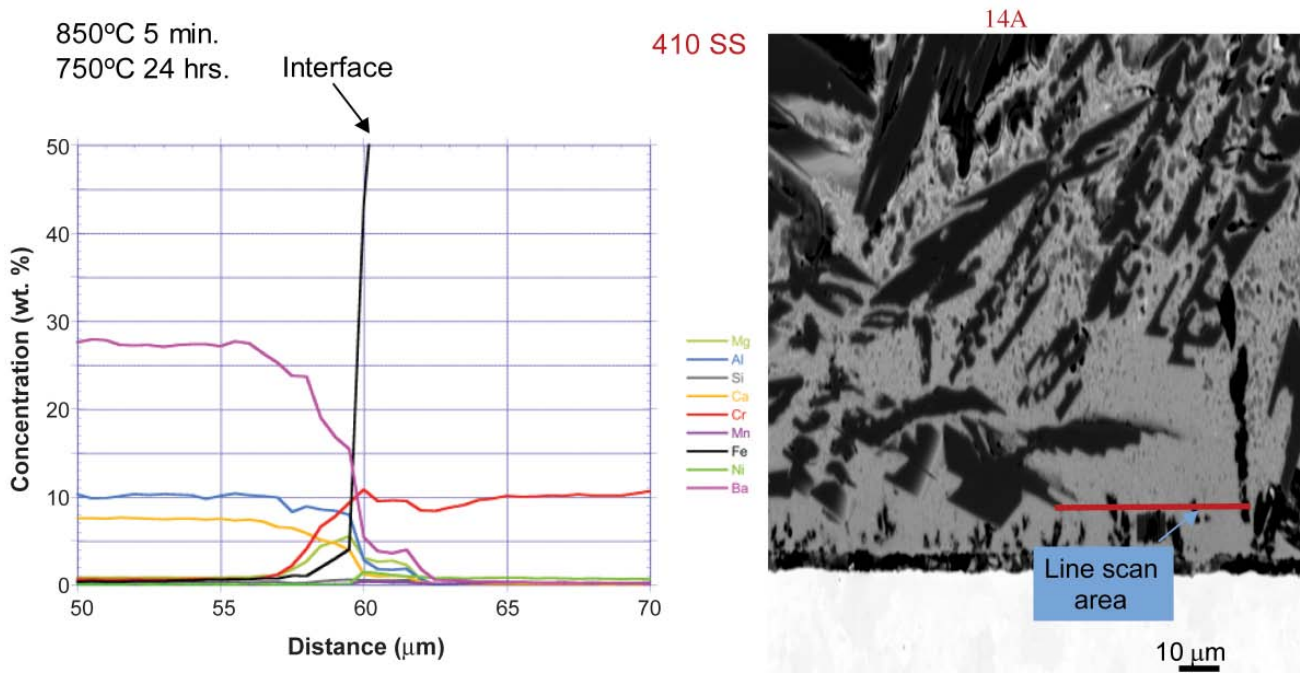

FIGURE 3. Electron microprobe analysis shows that glass 14A in contact with 410 SS forms Cr_2O_3 layer at interface and complex boron oxide phases in the bulk glass.

and Fe migration into the glass. This suggests that the glass-ceramic/SS combination is not stable for longer exposure time at higher temperatures.

Conclusions and Future Directions

Our work has demonstrated that glass composites are a favorable method for joining solid oxide fuel cell components. We have shown that seal properties can be varied to satisfy design criteria and materials constraints in SOFCs by varying the compositions, volume fractions, and microstructures of the different phases. Properties can be targeted using models that incorporate thermophysical data that are being obtained as part of the project. Long-term tests under representative SOFC operating conditions that are presently underway are providing compatibility data that will be used to decide whether seal compositions need to be tweaked to improve high temperature stability. Future work will be directed to detecting possible reactions, elucidating degradation mechanisms, and optimizing the seal system to ameliorate them. We also plan to test additional glasses and powder additives to qualify composite combinations with an even wider range of seal properties.

FY 2006 Publications/Presentations

1. R.E. Loehman, B. Gauntt, A. Ayala, and E. Corral, "Development of Glass-Ceramic Composites for Sealing Solid Oxide Fuel Cells", Invited speaker, 30th Meeting of the American Ceramic Society (Cocoa Beach), January 25, 2006.

2. R.E. Loehman, A. Ayala, M. Brochu, and B. Gauntt, "Sealing Solid Oxide Fuel Cells with Glass-Matrix Composites," 3rd International Brazing & Soldering Conference (IBSC) (ASM International), April 23-26, 2006, San Antonio, TX.

III.A.21 Dense Membranes for Anode Supported All-Perovskite IT-SOFCs

Objectives

- Synthesize fine, homogeneous, phase pure perovskites in the form of bulk (powders) and thin films to be used as components for developing zero-emission SOFCs capable of operating at reduced temperatures (≈800°C).
- Study of the effect of composition on the microstructure (grain size, grain boundaries, surface texture), magnitude of oxygen permeation, O_2 exchange rates and long term stability.
- Measure the impedance at higher temperatures and investigate the effect of electrical conductivity on the electronic structure using x-ray absorption near edge spectroscopy (XANES) and extended absorption fine structure spectroscopy (EXAFS).
- Assemble an all-perovskite-based SOFC made from a dense ceramic electrolyte membranes ($La_{0.8}Sr_{0.2}Ga_{0.875}Mg_{0.125}O_{3-x}$) sandwiched between porous electrodes (based on Ni as anode and electronically conducting $LaNi_{0.6}Fe_{0.4}O_3$ and/or $La_{0.8}Sr_{0.23}CoO_3$ ceramic cathode).
- Evaluate cost, performance, power generation capabilities, and emissions, while optimizing the reduced dimensionality structures needed to demonstrate a zero-emission demonstrator unit by the end of the three-year period.
- Create interest among undergraduate and graduate African American students to develop theses related to the development of all-perovskite-based anode-supported intermediate temperature solid oxide fuel cells (IT-SOFCs).

Rambabu Bobba

Department of Physics
Southern University and A&M College
Baton Rouge, LA 70813
Phone: (225) 771-2493; (225) 771-4130 (V); E-mail: rambabu@grant.phys.subr.edu or Rambabu@cox.net

DOE Project Manger: Lane Wilson

Phone: (304) 285-1336
E-mail: Lane.Wilson@netl.doe.gov

Project Staff:

Jonathon Dooley, Kourtney Jackson (Undergraduate Students)
Carahma Quiett, Yunfeng Li, and Vinaybabu V. Sivsareddy (Graduate Students)
Samrat Ghosh, Hrudananda Jena, Wiechang Zhao (Senior Research Associates)

Approach

To make solid oxide fuel cells (SOFCs) commercially viable for environment-friendly energy generation, it is of considerable interest to develop new synthetic techniques for large-scale, cost-effective preparation of perovskite-based multicomponent materials for applications as cathodes, anodes and electrolyte. We are developing inexpensive oxygen-permeable, dense and high surface area membranes in the form of bulk and highly oriented thin films using soft solution chemical routes and pulsed laser deposition techniques for fabricating natural gas fueled, anode-supported all-perovskite planar intermediate temperature SOFCs. Figure 1 shows the schematic of an all-perovskite anode-supported planar SOFC system, under progress at the Solid State Ionics Laboratory of Southern University.

We are investigating the influence of preparation techniques on the microstructure, grain-size and consequently on the electrical transport properties of the ABO_3 structured materials used as electrodes and electrolytes in all-perovskite IT-SOFCs. Wet chemical methods like metal-carboxylate gel decomposition, hydroxide co-precipitation, sonochemical and the regenerative sol-gel process followed by microwave sintering of the powders, have been used. Microwave sintering parameters were optimized by varying sintering time, and temperature to achieve higher density of pellets. Nano-crystalline perovskites with multi-element substitutions at A- and B-sites achieve physico-chemical compatibility for fabricating zero-emission all-perovskite IT-SOFCs.

During this year 2005-2006, we have been investigating the following systems:

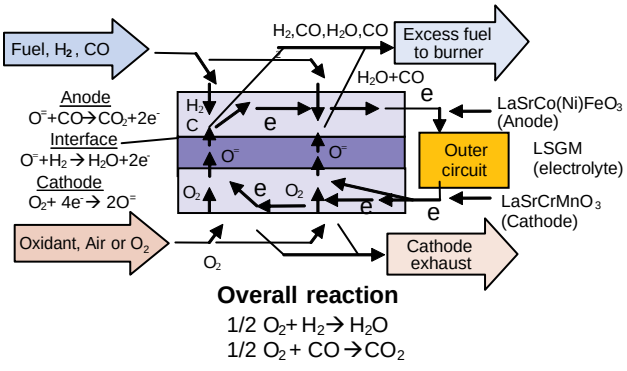

FIGURE 1. All-Perovskite SOFC

1. Hydroxy apatites. $Ca_{10}(PO_4)_6(OH)_2$, stoichiometry and off-stoichiometry compositions prepared by (i) urea combustion, (ii) ball-milling, (iii) hydrothermal, and (iv) Sonochemical reaction. Mg and Sr substitution at the Ca site has also been carried out. Structural and phase behavior investigations are in progress.
2. $Gd_{1-x}Ca_xCoO_3$ systems as novel electrodes for SOFCs and optimization of substitution to find its phase stability and solid solubility of aliovalent and isovalent ions in these matrixes. The glycine nitrate method is used to prepare these compositions.
3. $LaCr_{1-x}M_xO_3$, M = Mn, Mg, Co, Fe, x = 0.1 as interconnect materials and catalytic applications. Phase stability and structural transformation due to substitution on the Cr site. The glycine nitrate method is used to prepare these materials.
4. $LaNi_{1-x}Fe_xO_3$, x = 0.1 –0.9, cathode materials and sensor applications. The glycine nitrate method is used to prepare these materials.
5. $SrCe_{1-x}M_xO_3$ M = Dy, Er, Eu, Tb, x = 0.1 as proton conducting perovskites and its phase stability with respect to the rare earth substitution.

Results

To date, the following electrocerceramic materials were prepared in the form of bulk and thin films using innovative wet chemical processing methods and pulsed laser deposition techniques: 1) nanocrystalline $(La,Sr)(Ga,Mg)O_3$ (LSGM) electrolyte, 2) $La_{0.9}Sr_{0.1}Co_{0.9}M_{0.1}O_3$ (M = Fe, Ni, Mn) cathode, 3) Ni-based perovskite cermet or $(La,Sr)(Ga,Mn)O_3$ (LSGMn) anode, 4) $LaCrO_3$ interconnect, and 5) ceria-based anodic catalyst materials. The exceptional structural and chemical compatibility of LSGM with $La_{0.9}Sr_{0.1}Co_{0.9}M_{0.1}O_3$ (M = Fe, Ni, Mn) as a perovskite-based cathode, and anode, makes it a unique electrolyte for all-perovskite-based IT-SOFCs. To produce submicron LSGM powders for high-quality membrane fabrication, the combustion technique via aqueous solutions is usually preferred to the conventional solid-state mixed-oxide method. The solution route provides many advantages, for example, molecular homogeneous precursors, reduced sintering temperature for obtaining dense ceramics, and controllability of uniform superfine grain size. One major disadvantage of LSGM is the high cost of the gallium containing precursors. Once LSGM materials are used as electrolytes commercially, regeneration of LSGM will be a cost-effective effort. Based on this concern, we have explored the possibility of regenerating the LSGM ceramics to be aqueous solution precursor. Although the solid Ga_2O_3 remains insoluble, our experiments have shown the LSGM ceramics are completely soluble in an acidic solution. In addition, the regenerative route is also cost-effective and time-saving for in-lab researchers who usually prepare large amounts of LSGM samples, for example, to tailor effects of composition or synthesis conditions on the properties of LSGM.

The sintering behavior of the materials prepared from the various routes was examined by scanning electron microscopy (SEM) shown in Figure 2. The pellets prepared by the regenerative sol-gel technique produces nano-crystalline powders which have better sintering properties as indicated in Figure 2a-b and Figure 2c-d.

Recently, the synthesis of and electrical property measurements on nano-crystalline ceria and Gd-doped ceria have been done in our lab. The X-ray diffraction (XRD) and transmission electron microscopy (TEM) results are given in Figure 3 (top and bottom), respectively.

Simultaneously, we have also investigated dense proton conducting (PC) perovskite membranes such as $SrCeO_3$, and $SrCe_{1-x}M_xO_3$ that were synthesized by sonochemical treatment followed by the hydrothermal method and sintering done by microwave heating. Figure 4 shows the electrical conductivity measurements of $SrCeO_3$.

Also, an investigative study was performed for developing materials to fabricate a natural gas fueled SOFC hybridized to a gas turbine (SOFC-GT) to enhance power production and maximum utilization of resources in Trinidad.

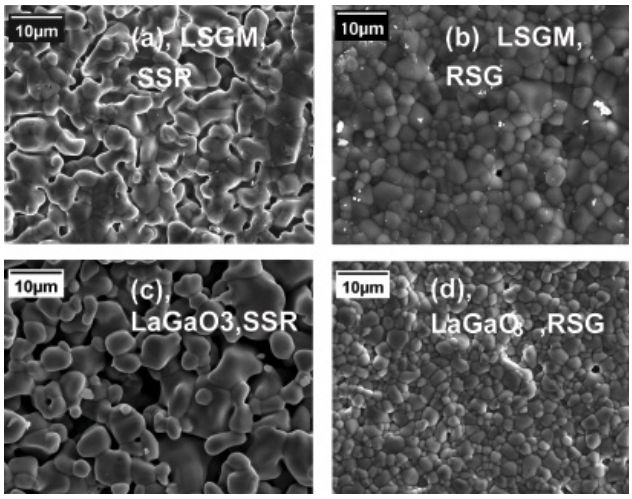

FIGURE 2. SEM Micrographs of $La_{0.8}Sr_{0.2}Ga_{0.85}Mg_{0.15}O_{2.825}$ (LSGM-2015) and $LaGaO_3$ Heated at 1,400°C/8h; (a) Solid-State Route (SSR) Pellet of LSGM-2015; (b) RSG Pellet of LSGM-2015; (c) SSR Pellet of $LaGaO_3$; and (d) RSG Pellet of $LaGaO_3$

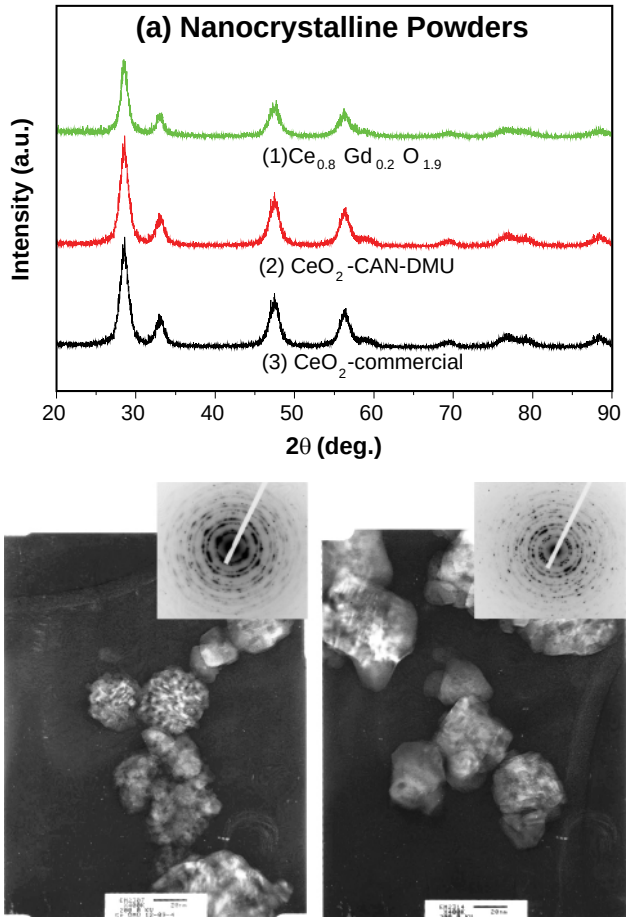

FIGURE 3. XRD Measurements (top) and TEM Photographs (bottom) of Nano-Crystalline Ceria and Gd-doped Ceria

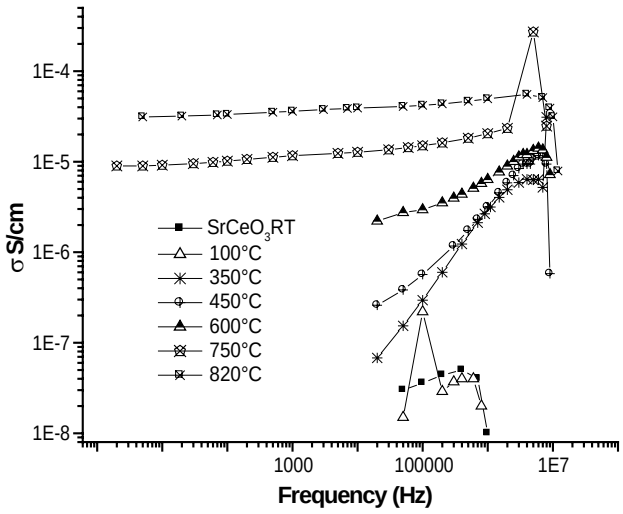

FIGURE 4. Electrical Conductivity Measurements of $SrCeO_3$

FY 2006 Publications

1. Novel wet-chemical synthesis and characterization of nanocrystalline CeO_2 and $Ce_{0.8}Gd_{0.2}O_{1.9}$ as solid electrolyte for intermediate temperature solid oxide fuel cell (IT-SOFC) applications, B.Rambabu, Samrat Ghosh and Hrudananda Jena, J. Mater. Sci. (in press, 2006).

2. An exploratory study on solution assisted synthetic routes to prepare nano-crystalline $La_{1-x}MxGa_{1-y}NyO_3$ (M=Sr, N=Mn,Mg) for IT-SOFC applications. Hrudananda Jena and B. Rambabu, Mater. Chem. Phys. (in Press, 2006).

3. Innovative processing of dense LSGM electrolytes for IT-SOFC's, B. Rambabu, Samrat Ghosh, Weichang Zhao and Hrudananda Jena, J. Power Sources (Accepted), 2006.

4. Effect of sonochemical, regenerative sol gel, and microwave assisted synthesis techniques on the formation of dense electrolytes and porous electrodes for all perovskite IT-SOFCs, Hrudananda Jena, and B. Rambabu, Journal of Fuel Cell Science and Technology, 2006.

5. Proton Transport in Nanocrystalline Hydroxy apatite $(Ca_{10}(PO_4)_6(OH)_2$, Hrudenanada Jena, and B. Rambabu, Accepted for publication in the Journal of Materials Science, (in press 2006).

III.A.22 Novel Composite Materials for SOFC Cathode-Interconnect Contact

Objectives

- Elucidation of the mechanism of Ag evaporation at elevated temperatures.
- Alloy design of new Ag-based alloys with significantly reduced Ag evaporation/migration.
- Optimization of the processing and the microstructures of Ag alloy/perovskite composites.
- Demonstration/assessment of performance of the new contact materials.

Accomplishments

- Elucidated the Ag evaporation mechanism based on the experimental evaluation of various factors affecting the evaporation rate of pure Ag.
- Identified the optimal conditions for evaluating the Ag evaporation of Ag-based alloys as contact material: exposure environment – flowing air; air flow rate – 1.5 $cm.s^{-1}$; exposure temperature – 850°C; exposure time – 40 hours.
- Synthesized a well-distributed Ag+$La_{0.8}Sr_{0.2}CoO_3$ composite with an average particle size of less than 1 µm via a glycine nitrate combustion process.

Introduction

To reduce the electrode/interconnect interfacial resistance in SOFC stacks, electrical contact layers are often applied between the interconnect and electrodes during construction of an SOFC stack by compensating for the corrugations present on their respective surfaces. Three major criteria for SOFC contact materials are (1) sufficient high electrical conductivity over the SOFC lifetime; (2) chemical stability under high current condition and compatibility with other cell components, especially negligible effects on the formation of protective oxides on interconnect alloy; and (3) reasonable match in coefficient of thermal expansion (CTE) with other cell components. Because of the stringent criteria, finding a suitable material for the interconnect-cathode contact is very challenging, particularly in the intermediate temperature (600-800°C) SOFCs where high-temperature oxidation-resistant alloys are used as interconnect material.

The materials currently under consideration for cathode/interconnect contact application include low melting-point ceramics (such as doped $LaCoO_3$), noble metals (e.g. Ag or Pt), and their composites [1-3]. Pt, Au, and Pd are not desirable for this application because of their high raw material cost. However, Ag is an exception due to its relatively low price. Ag-ceramic composite is one of the very promising candidates for SOFC contact due to the inherent properties of Ag, such as high chemical stability, high electrical conductivity, high ductility, and relatively low melting point. The perovskite component in the composite is expected to provide a more desirable CTE match and act as a Cr absorbent and/or a barrier for Cr migration to the cathode. One major drawback of Ag as SOFC interconnect/cathode contact material is its tendency to evaporate at the SOFC operating temperatures and subsequent migration to other cell components, potentially causing the cell performance degradation. To date, the evaporation behavior of Ag under SOFC operating conditions has not been systematically investigated, even though numerous studies have been carried out on thermal etching of Ag at elevated temperatures [4-6].

Approach

Ag would be a wonderful contact material if its evaporation/migration can be reduced. Alloying with other elements such as noble metals, surface-active elements, or certain transition metals might reduce the evaporation/migration of Ag. What is desired of the alloying elements is to effectively reduce Ag evaporation/migration without significantly altering the overall properties of Ag. To provide guidelines for the selection of alloying additions, fundamental studies on the evaporation mechanism of Ag at elevated temperatures are being conducted. Based on the mechanistic understanding, alloy design and physical metallurgy principles will be employed for developing a series of new Ag-base alloys with significantly reduced Ag evaporation rates. These alloys will be evaluated under realistic SOFC operating conditions; furthermore,

J.H. Zhu (Primary Contact), Z.G. Lu, Y.Q. Qian, and D.A. Ballard
Department of Mechanical Engineering
Tennessee Technological University
115 W. 10th St., Box 5014
Cookeville, TN 38505
Phone: (931) 372-3186; Fax: (931) 372-6340
E-mail: jzhu@tntech.edu

DOE Project Manager:
Ayyakkannu Manivannan
Phone: (304) 285-2078
E-mail: Ayyakkannu.Manivannan@netl.doe.gov

Ag alloy/perovskite composites will be synthesized and the performance of the composite materials as interconnect/cathode contacts will be assessed.

Results

The effects of a number of exposure parameters such as time, temperature, and air flow rate on Ag evaporation were investigated. For all evaporation experiments, a linear relationship was observed between the weight loss of Ag and the duration of thermal exposure. As illustrated in Figure 1, the weight loss of pure Ag after 50-hour exposure at both 900°C and 850°C initially increased linearly with air flow rate and then reached a plateau at a flow rate of about 1.0 $cm.s^{-1}$; further increase in air flow rate had no effect on the Ag evaporation, i.e. a plateau was observed. The loss of weight at the flow rate above 1.0 $cm.s^{-1}$ was about 2.6 times of that in stagnant air for both exposures at 900°C and 850°C. It is concluded that when Ag vapor pressure is below a critical point, the evaporation rate of Ag is controlled by both evaporation from the surface of solid Ag and back-condensation of Ag vapor. Therefore, the net evaporation rate is the difference of these two processes. If the vapor pressure of Ag drops below that critical value, the evaporation of Ag is essentially controlled by the evaporation process alone.

To determine the effect of temperature on Ag evaporation rate, a relatively high air flow rate of 1.5 $cm.s^{-1}$ was selected as a standard flow rate and the test temperature was varied from 750ºC to 925ºC. It was found that the evaporation rate of pure Ag increased significantly with exposure temperature. An exponential relation was obtained between the weight loss of Ag and the reciprocal of temperature, as shown in Figure 2. The heat of Ag evaporation, calculated from the slope of the figure, was equal to 280 $KJ.mol^{-1}$. The heat of evaporation was very close to the heat of atomization for pure Ag, which is 284.09 $KJ.mol^{-1}$. This implies that the evaporation of Ag under these conditions is essentially controlled by breaking of the bond between Ag atoms in the solid state. Several evaporation experiments were carried out in the presence of various vapor phase constituents, such as air, air+3%H_2O, Ar+5%H_2, or Ar+5%H_2+3%H_2O. The results indicate that none of the exposing atmospheres had a measurable influence on the evaporation rate of Ag, i.e. the Ag evaporation rate is essentially the same in both reducing and oxidizing atmospheres.

The surface morphological features of pure Ag after thermal exposure were also observed with a scanning electron microscope (SEM). As is clear from Figures 3(a)-(c), the samples exposed to air developed a striation structure (parallel ledges) after thermal exposure at temperatures from 750°C to 900°C. The space between the ledges increased with the increase in exposure temperature. However, very smooth surfaces only with some grain boundary grooves were observed after thermal exposure in both Ar+5%H_2 and Ar+5%H_2+3%H_2O (Figure 3(d)).

This study indicates that with typical SOFC operating conditions, such as an air flow rate of 1.1 $cm.s^{-1}$ at 800°C in air, the evaporation rate of Ag is $4x10^{-10}$ $g.cm^{-2}.s^{-1}$. This value is very high considering the targeted SOFC operation time of 40,000 hours. Therefore, pure Ag is not suitable for this application due to its excessive evaporation during service. However, since the evaporation of Ag is determined by breaking of the bond between Ag atoms in the solids, alloying with other elements that increase the bonding energy might

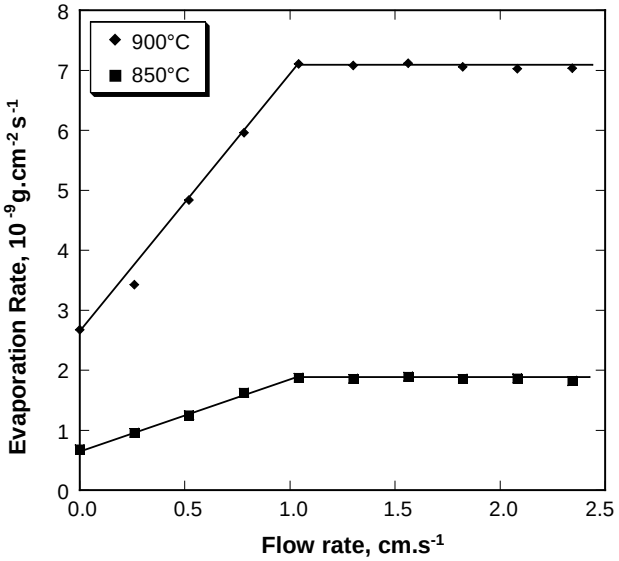

FIGURE 1. The Evaporation Rate of Pure Ag as a Function of Air Flow Rate at Both 900°C and 850°C

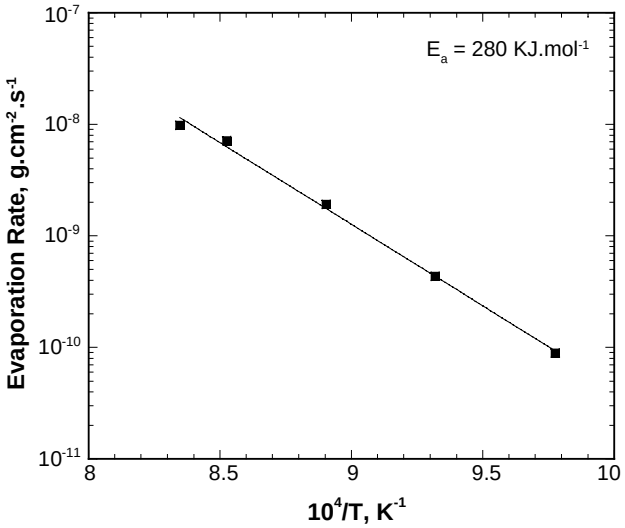

FIGURE 2. The Evaporation Rate of Pure Ag as a Function of Exposure Temperature in a Flowing Air of 1.5 $cm.s^{-1}$

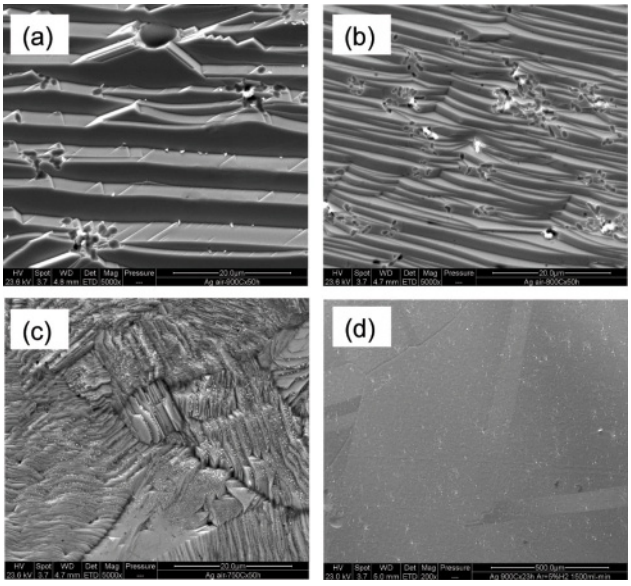

FIGURE 3. Surface morphological features of polycrystalline Ag developed after thermal exposure with a gas flow rate of 1.5 cm.s-1: (a) 900°C, air, 50 hours; (b) 800°C, air, 50 hours; (c) 750°C, air, 50 hours; and (d) 900°C, Ar+5%H2, 20 hours.

decrease the evaporation of Ag. The effects of various alloying elements, such as other noble metals which can form solid solution and surface-active elements which segregate to the alloy surface, on reducing the evaporation rate of Ag is under investigation in the PI's lab. The fundamental study on the evaporation of pure Ag has also helped define the optimal exposure conditions for evaluating the effect of alloying additions on Ag evaporation. The parameters for the exposure experiments in evaluating the Ag evaporation of Ag-based alloys as contact materials have been identified as follows: exposure environment – flowing air; air flow rate – 1.5 cm/s; exposure temperature – 850°C; exposure time – 40 hours. These parameters are being used in the systematic study of the effects of alloying additions on the Ag evaporation.

Conclusions and Future Directions

The following conclusions can be drawn based on this study:

- The evaporation of Ag initially increased linearly with air flow rate and then reached a plateau at a flow rate of about 1.0 $cm.s^{-1}$; further increase in air flow rate had no effect on the Ag evaporation.
- The exposing atmosphere has no noticeable influence on the Ag evaporation rate, although different surface morphologies developed after thermal exposure.
- The heats of evaporation were very close to the heat of atomization for pure Ag.
- Alloying Ag with other elements, which can increase the bonding energy, might decrease the evaporation of Ag.

The future directions for this project are listed below:

- A number of binary and ternary Ag alloys will be prepared and the evaporation rate of these alloys with various alloying additions will be measured and potential alloying elements which can significantly reduce the Ag evaporation will be identified.
- A series of Ag+ perovskite composites with different particle sizes and different volume ratios of Ag/perovskite will be synthesized and the sintering behavior of these composites will be studied.
- The performance of the contact materials will be evaluated including their interaction with interconnect and cathode materials and their effectiveness on blocking Cr migration from the interconnect alloy to the cathode.

FY 2006 Publications/Presentations

1. "Evaporation and Thermal Etching of Pure Ag at Elevated Temperatures", Z.G. Lu and J.H. Zhu (manuscript to be submitted to J. Electrochem. Soc.).

References

1. K. Murata and M. Shimotsu, J. Ceram. Soc., Jpn., 111, 222 (2003).

2. S. Koch, and P.V. Hendriksen, Solid State Ionics, 168, 1 (2004).

3. Z. Yang, G. Xia, P. Singh, J.W. Stevenson, J. Power Sources, 155, 246 (2006).

4. B. D. Cuming and A. J. W. Moore, J. Aust. Inst. Met., 3, 124 (1958).

5. R. Shuttleworth, Metallurgia 38, 125 (1948).

6. T. Wei and J. Phillips, Adv. Catal., 41, 359 (1996).

III.A.23 Developing Low-Cr Fe-Ni-Based Alloys for Intermediate Temperature SOFC Interconnect Application

Objectives

- Develop a series of new Fe-Ni based alloys without Cr or with low Cr for intermediate temperature solid oxide fuel cell (SOFC) interconnect application.
- Demonstrate suitable oxidation resistance, oxide scale area specific resistance (ASR), and coefficient of thermal expansion (CTE) for these new alloys.
- Achieve low Cr evaporation rates for these alloys without surface coatings.

Accomplishments

- Over 200 alloys have been made by arc melting and drop casting, with various alloying elements added to narrow down some promising compositional ranges for further alloy development. Several strategies have been identified to improve oxidation resistance of low-Cr Fe-Ni-based alloys.
- A new low-Cr Fe-Ni-based alloy system has been identified. The oxidation resistance of the new low-Cr Fe-Ni-based alloy is much better than that of Fe-60Ni and comparable to that of Crofer22 APU. Furthermore, the new alloy also exhibits excellent resistance to cyclic oxidation.
- A low oxide scale ASR has been demonstrated for the new developmental low-Cr Fe-Ni-based alloy.
- The Cr evaporation rate of the new developmental alloy is much lower than that of Crofer22 APU under similar exposure conditions.

Jiahong Zhu (Primary Contact), Shujiang Geng, David Ballard, Xiaochuan Lu, Zigui Lu
Department of Mechanical Engineering
Tennessee Technological University
115 W. 10th St., Box 5014
Cookeville, TN 38505
Phone: (931) 372-3186; Fax: (931) 372-6340
E-mail: jzhu@tntech.edu

DOE Project Manager:
Ayyakkannu Manivannan
Phone: (304) 285-2078
E-mail: Ayyakkannu.Manivannan@netl.doe.gov

Subcontractors:
Oak Ridge National Laboratory, Oak Ridge, TN
University of Missouri - Rolla, Rolla, MI

Introduction

Solid oxide fuel cells (SOFCs) have attracted significant attention due to their benefits of environmentally benign power generation with fuel flexibility. However, the main hurdle thwarting the SOFC commercial introduction is lack of appropriate interconnect materials, which is of key importance for SOFC development. There has been recent interest in Cr_2O_3-forming alloys for SOFC interconnect applications because of the reduction in SOFC operating temperature. However, volatile Cr species generated from Cr_2O_3 in oxidizing atmospheres (on the cathode side) can cause severe degradation of the long-term performance of SOFCs because of cathode poisoning [1,2]. This SECA project has focused on the development of new low-Cr Fe-Ni-based interconnect alloys with low CTE and scale ASR, suitable oxidation resistance, and reduced Cr evaporation, which is expected to resolve the Cr poisoning issue for SOFC stacks.

Approach

Using alloy-design principles, we have developed a series of new low-Cr Fe-Ni-based alloys. These low-Cr Fe-Ni-based alloys with 6 wt.% Cr maximum are expected to develop a double-layer oxide scale consisting of a Cr-free, electrically-conductive $(Fe,Ni)_3O_4$ spinel outer layer to act as a surface seal for blocking Cr evaporation from the alloy surface atop a protective, electrically-conductive Cr_2O_3 inner layer. This project is being carried out as an interdisciplinary and collaborative endeavor with the involvement of two universities and one national laboratory.

So far, we have demonstrated the feasibility of thermally growing the double-layer oxide structure on the low-Cr Fe-Ni-based alloys. We have also characterized the isothermal and cyclic oxidation resistance, oxide scale ASR, and Cr evaporation rate of these low-Cr Fe-Ni-based alloys.

Results

Through a systematic alloy design effort, a low-Cr Fe-Ni-based alloy with drastically improved oxidation resistance has been developed. A preliminary evaluation of this alloy is summarized here. It should be noted that further alloy composition modifications are being pursued to optimize its overall performance.

Long-term isothermal oxidation testing at 800°C in air indicates that the oxidation resistance of the new low Cr Fe-Ni-based alloy was much higher than that of Fe-60Ni, and comparable to that of Crofer22 APU. As shown in Figure 1, after the first week, the weight gain of this low-Cr alloy increased slightly with time and its oxidation rate was similar to that of Crofer22 APU. The initially larger weight gain during the first week exposure for this alloy over Crofer22 APU is actually desirable, as it is due to the formation of a surface spinel outer layer. Compared to the binary Fe-60Ni alloy, an order of magnitude reduction in weight gain was achieved. The improved oxidation resistance of this new alloy resulted from the formation of a continuous, dense Cr_2O_3 inner layer between the Cr-free spinel layer and the substrate alloy as shown in Figure 2, which is the a cross-sectional view of this alloy after oxidation for 12 weeks at 800°C in air. The Cr_2O_3 inner layer acts as a barrier against the oxidation process. From Figure 2, some internal oxidation was apparent and we are currently continuing our alloy design efforts to reduce/eliminate the internal oxidation problem.

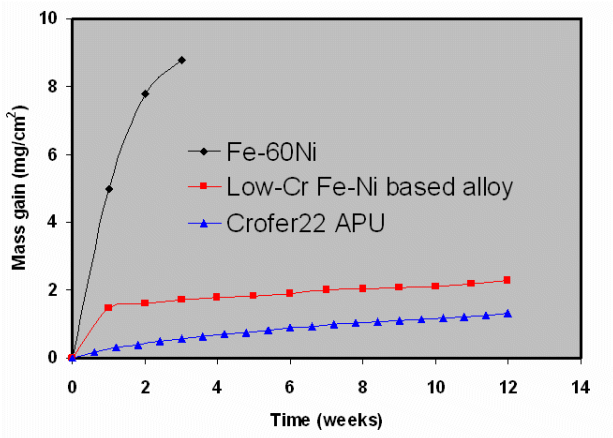

FIGURE 1. Isothermal Oxidation Kinetics of the Low-Cr Fe-Ni-Based Alloy in Air at 800°C

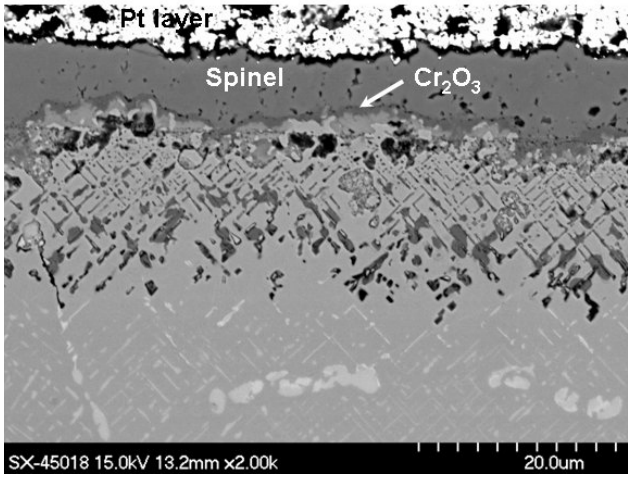

FIGURE 2. Cross-Section of the Low-Cr Fe-Ni-Based Alloy after 12-Week Oxidation in Air at 800°C

The ASR of the oxide scale formed on this alloy after oxidation for 12 weeks is shown in Figure 3. The oxide scale ASR of this alloy was lower than that of Crofer22 APU after similar exposure. The low ASR of the oxide scale thermally grown on this alloy should be attributed to the high electrical conductivity of the spinel outer layer.

Cyclic oxidation tests were conducted to determine the adherence of the oxide scales formed on the new low-Cr Fe-Co-Ni-based alloy. Each cycle consisted of holding at 800°C in air for 25 hours followed by cooling to room temperature in air. No spallation was observed after 80 cycles with a cumulative exposure time of 2,000 hours, indicating good adhesion between the oxide scales and the alloy substrate. The mass gain of the low-Cr Fe-Ni-based alloy was significantly lower than that of the Fe-50Ni alloy, as shown in Figure 4. The adequate resistance to spallation resulted from the CTE match between the oxide scale and the substrate alloy.

Initial work was conducted by PNNL to evaluate the Cr volatility of the new low-Cr Fe-Co-Ni base alloy in moist air at 800°C for 500 hours with an air velocity of 1.1 $cm \cdot s^{-1}$. The Cr transport rate was 5.7×10^{-12} $kg \cdot m^{-2} \cdot s^{-1}$ for this new alloy. For purpose of comparison, under identical conditions a value of 3.3×10^{-11} $kg \cdot m^{2} \cdot s^{-1}$ for Crofer22 APU was obtained. Therefore, the Cr volatility for the new low-Cr alloy was about a factor of almost six lower than that of Crofer22 APU. This is mainly due to the formation of the Cr-free spinel outer layer that blocks the Cr evaporation from the chromia inner layer.

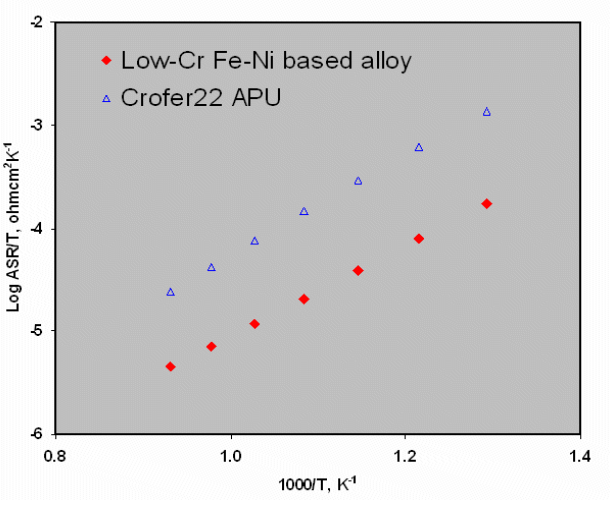

FIGURE 3. Comparison in Scale ASR of the Low-Cr Fe-Ni-Based Alloy with Crofer22 APU after 12-Week Oxidation in Air at 800°C

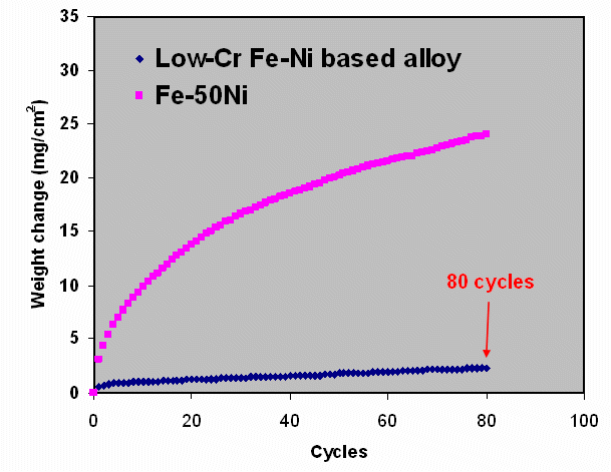

FIGURE 4. Cyclic Oxidation Kinetics of the Low-Cr Fe-Ni-Based Alloy and the Fe-50Ni Alloy in Air at 800°C

Conclusions and Future Directions

The formation of an electrically conductive, Cr-free spinel outer layer atop a protective, electrically conductive oxide inner layer on the metallic interconnects is highly desirable to mitigate the Cr poisoning problem in the SOFC stack. Our preliminary results indicate that a double-layer oxide structure with an electrically conductive, Cr-free spinel outer layer and a protective Cr_2O_3 inner layer could be thermally grown on a new low-Cr Fe-Ni-based alloy with drastically improved oxidation resistance, low scale ASR, and CTE match with other cell components. While additional alloy design and production scale-up is clearly needed, this study has demonstrated that it is feasible to develop a low-Cr Fe-Ni alloy with balanced properties for SOFC interconnect application. This alloy system contains significantly less Ni than Ni-based superalloys and much less Cr than ferritic steels, while their manufacturability is similar to ferritic steels. Therefore, the cost-effective new alloy interconnects will be very attractive for reducing the overall cost and improving the durability of SOFC stacks.

Future directions for this project are listed below:

- **Further optimization of the composition range of the new Fe-Ni base alloys.** The composition range of these alloys will be further narrowed down with special attention paid to reduce/eliminate the internal oxidation zone between the Cr_2O_3 inner layer and the alloy substrate after thermal exposure in air.
- **Characterization of oxidation/corrosion behavior in both single and dual-atmosphere condition.** The oxidation behavior of the low-Cr Fe-Ni-based alloys will be studied at 700-900ºC in both air (cathode environment) and Ar+4%H_2+3%H_2O which corresponds to the anode environment. In addition, selected alloy coupons will also be exposed to dual atmospheres (one side air and the other side H_2+3%H_2O) at 800°C. The oxide scale features formed after the dual-atmosphere exposure will be compared to those formed in single atmosphere alone.
- **Compatibility and in-cell performance evaluation.** The interaction and compatibility of the new interconnect alloys with the contact and cathode materials will be conducted using screen-printed interconnect/contact/cathode couples. After thermal exposure of the couple, ASR measurement will be conducted to get the overall resistance of the couple and possible formation of insulating phase(s) at the interface and Cr migration into the cathode will be identified. The effect of the new interconnect alloys on the cell performance will be conducted with a SOFC test stand. The cell performance with different interconnect alloys will be compared and the Cr volatility of the new Fe-Ni alloys will be assessed.

Special Recognitions & Awards/Patents Issued

1. An invention disclosure on the new low-Cr Fe-Ni alloys has been completed.

FY 2006 Publications/Presentations

1. "Oxidation Behavior and Electrical Properties of NiO- and Cr_2O_3- Forming Alloys for Solid Oxide Fuel Cell Interconnects", *Oxidation of Metal,* in press, 2006.

2. "Evaluation of Several Low Thermal Expansion Fe-Co-Ni Alloys as Interconnect for Reduced-Temperature Solid Oxide Fuel Cell", *International Journal of Hydrogen Energy*, submitted, 2006.

3. "Evaluation of Several Fe-Ni Alloys for SOFC Interconnect Application", Poster Presentation, Gordon Research Conference on High-Temperature Corrosion, New London, NH, July 24-27, 2005.

4. "Tailoring Fe-Ni Based Alloys for Intermediate Temperature SOFC Interconnect Application", Presentation, SECA Core Technology Program Peer Review Meeting, Denver, CO, October 25-26, 2005.

5. "Evaluation of Fe-Ni Alloys for Reduced-Temperature SOFC Interconnect Application", Invited Presentation, Symposium on Materials in Clean Power Systems: Applications, Corrosion, and Protection, TMS Annual Meeting & Exhibition, San Antonio, TX, 12-16 March 2006.

References

1. Gindorf, C., Singheiser, L & Hilpert, K. Chromium Vaporization from Fe,Cr Base Alloys Used as Interconnect in Fuel Cells. Steel Research 72 (11-12), 528-533 (2001).

2. Matsuzaki, Y. & Yasuda, I. Electrochemical Properties of a SOFC Cathode in Contact with a Chromium-Containing Alloy Separator. Solid State Ionics 132, 271-278 (2000).

III.A.24 Innovative Seals for Solid Oxide Fuel Cells (SOFCs)

Objectives

- Select self-healing glasses for functionality as seals for SOFCs.
- Demonstrate functionality of the self-healing seals by leak tests.
- Measure stability of the self-healing glass in SOFC environments.
- Develop approaches to toughening self-healing glasses as seals for SOFCs.
- Survey commercial glasses suitable for making seals for SOFCs.

Approach

- Select glasses suitable for self-healing and expansion matching, measure thermophysical properties, prepare seals with SOFC components, and test seals over a range of temperatures including thermal cycles.
- Determine thermal stability of the glasses in SOFC environments, measure thermal properties after annealing, and fabricate seals for leak testing at cell operating conditions.
- Develop approaches for toughening sealing glasses through the reinforcing phase, select a reinforcing fiber, fabricate reinforced glasses, and incorporate toughened glasses into seals and seal tests.
- Perform literature search on glasses suitable for seals in SOFC.

Accomplishments

- Demonstrated ability of a self-healing glass in sealing SOFC components through leak tests over a range of temperatures between 25-800°C.
- Achieved ~300 thermal cycle between 25-800°C without leak of a self-healing glass and accumulated ~3,000 hours of hermetic cell performance at 800°C.

Professor Raj N. Singh
University of Cincinnati
Department of Chemical and Materials Engineering
Cincinnati, OH 45221-0012
Phone: (513) 556-5172; Fax: (513) 556-3773
E-mail: Raj.Singh@uc.edu

DOE Project Manager:
Ayyakkannu Manivannan
Phone: (304) 285-2078
E-mail: Ayyakkannu.Manivannan@netl.doe.gov

- These results provide great promise towards meeting SECA goals of seals for SOFCs.

Introduction

A functioning SOFC requires seals that prevent electrode leakage and internal gas manifold leakage if internal gas manifolds are utilized. The seals must prevent the mixing of fuel and oxidant streams as well as prevent reactant escape to the surrounding environment. The seal material must be electrically isolating and be mechanically and chemically stable in contact with interfacing cell components in humid dual reducing and oxidizing conditions. Particular importance is the ability to seal between metallic and ceramic components with differing coefficients of thermal expansion (CTE), and do so while exposed to temperature transients over a range from room temperature up to SOFC operating temperature (≈800ºC). This project is developing innovative sealing concepts for both short- and long-term functionality of SOFCs, addressing the aforementioned issues.

Approach

A novel concept of in situ crack healing by glasses is pursued in Phase I of the project. The fundamental idea underlying this concept is based on the fact that a glass with suitable low viscosity can heal cracks created by thermal expansion mismatch between materials that are being joined by a glass seal in a SOFC. The functionality of this innovative sealing approach based on in situ crack healing by a glass is demonstrated and quantified. Toughening and strengthening of the glass by fibers/particulates is pursued to minimize or eliminate bulk cracking of the seals. These concepts are pursued further in Phase I to address sealing capabilities and durability issues related to a functioning seal for a SOFC.

Results

Self-healing glasses were selected, fabricated, and used for making seals. A test fixture was constructed for leak testing and leak tests under appropriate SOFC test conditions were performed. The assembled system was successful in meeting the project goals of testing seals at both room and high temperatures. The results demonstrated self-healing behavior of seals with a significant capability for thermal cycles between 25 and 800°C. These results are very promising for meeting some of the goals of the SECA program for SOFCs. The details on these activities are given in the following.

In order to develop seals suitable for joining electrolyte (yttria-stabilized zirconia [YSZ]) to a metal using a glass that can show self-healing behavior requires selection of glasses with appropriate thermophysical properties and expansion match with YSZ and metals. A number of glasses were considered and synthesized. Samples of glass powders were used for x-ray diffraction studies to insure that the starting materials are indeed amorphous in crystal structure. The glass and YSZ powders were processed to fabricate samples for measurements of properties and testing. Expansion behaviors of all the samples, glasses, metals, and YSZ were measured between 25-1,000°C in a high-temperature dilatometer. The stability of glasses against crystallization was measured using an x-ray diffractometer after annealing samples in air and SOFC testing environments over extended time periods. Figure 1 shows the expansion behavior of a glass used in self-healing study and effect on annealing for 500 hours indicating insignificant change in the expansion behavior. The x-ray diffraction from annealed samples of glass indicated no crystallization, which is consistent with the expansion behavior.

The diffusion processes at high temperatures can heal cracks in ceramics and glasses. Crystalline ceramics require higher temperatures for healing than some of the glasses because of the thermally activated nature of the diffusion process responsible for healing. The self healing behavior was studied by heating the glass to desired temperatures between 25-1,000°C and observing the surface of the glass sample with cracks by a video camera (in a unique facility) for detecting the temperature-time history of the self-healing process to begin and end. These data were used for selecting the processing temperatures for making the seals and appropriate conditions required for demonstration of the self-healing behavior.

The leak test fixture developed was used for leak tests at room temperature and high temperatures. A seal was made using Crofer metal, Glass 4, and YSZ. The YSZ was sealed to Crofer by this glass and then the Crofer metal was welded to 304 SS housing. The inside of the SS 304 housing was connected to high-pressure side of the seal and the outside of the SS 304 housing was maintained at the atmospheric pressure. During the test the seal assembly was heated to the desired temperature inside a furnace and the seal was pressurized from inside for leak testing via monitoring the pressure as a function of time. The leak tests were performed at room temperature and at various temperatures during heating as well as during cooling. In addition, during the course of the leak testing the seal developed a small leak but the leak was repaired in situ in each case by keeping the seal at the test temperature. The seal has been tested further for its durability against thermal cycles and the results in Figure 2 show that the seal remained hermetic even after 271 thermal cycles and 2,900 hours of seal test at 800°C. The seal test was terminated after ~3,000 hours and 300 thermal cycles of testing and the post-test data showed that the glass remained amorphous even after such a long test indicating the potential of the glass for making self healing seals.

These results on thermal-cycle-ability of SOFC seals are quite promising for developing seals to meet the SECA goals for SOFCs.

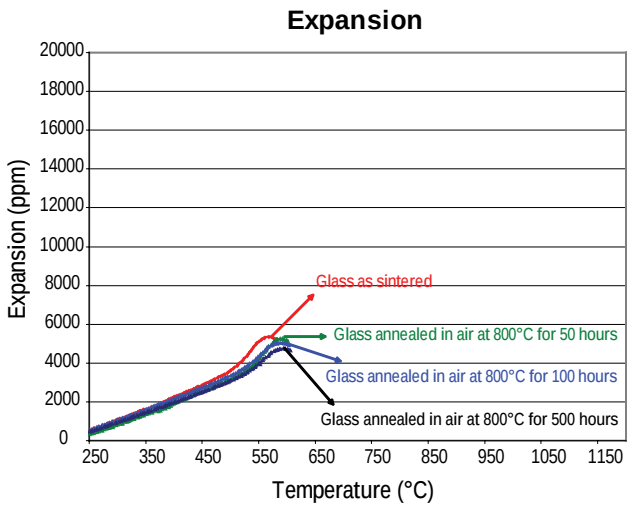

FIGURE 1. Effect of thermal annealing time at 800°C on the expansion behavior of a glass. Note an insignificant change in the expansion behavior.

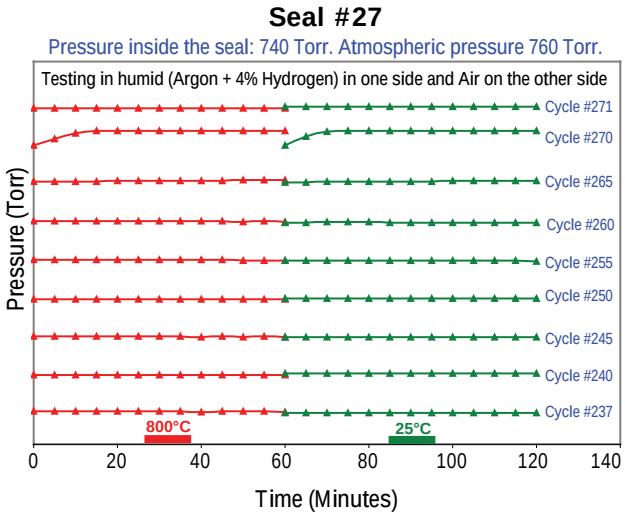

FIGURE 2. Pressure-time plots up to 271 thermal cycles of the leak tests at 800°C and 25°C of the seal made using Crofer-Glass-YSZ. This seal showed hermetic and self-healing behaviors even after 271 thermal cycles between 25-800°C. The data for each cycle shows pressure on the Y-axis vs time. A horizontal line for each cycle indicates hermetic response.

Conclusions and Future Directions

- Glasses were selected for demonstration of self-healing behavior and potential for making seals that display self-healing response. The thermal properties, densification behavior, and wetting behavior of glasses with YSZ electrolyte, Crofer, SS 430, and Nickel metals were determined for suitability of making seals.
- A new methodology based on video imaging of cracks was applied to characterize self-healing behavior of all the selected glasses and glass-ceramics as a function of temperature and time. Generally, glass-ceramics showed slower self-healing kinetics than the glassy state but the exact kinetics were dependent on the specific glass or glass-ceramics.
- Reinforced glasses were fabricated using alumina fibers. The effect of fiber addition to glass properties was characterized by dilatometer. Strengthening of the reinforced glass was demonstrated.
- Seals incorporating self-healing glasses were fabricated. Effect of up to ~300 thermal cycles between 25 and 800°C and ~3,000 hours at 800°C on hermeticity of the seals was demonstrated. Self-healing behaviors of the leaking seals were also demonstrated. These results are important for achieving the SECA goals of SOFC sealing systems.
- Plans are to pursue (in Phase II of the project) long-term stability of the self-healing glasses, reinforced glasses, and seals made thereof to further demonstrate long-term performance, stability, and applicability of the self-healing glass seals to SOFCs.

FY 2006 Publications/Presentations

1. Project Monthly Reports between October (2005)-March (2006).

2. Phase-I Program Report (December, 2005).

3. S. Parihar and R.N. Singh, "Self-Healing Glass Seals for Solid Oxide Fuel Cells", Proc. of Am. Ceram Soc. Annual Meeting (2005), in press.

4. R.N. Singh and S.S. Parihar, "Performance of Self-Healing Seals for Solid Oxide Fuel Cells," Ceram Eng. Sci. Proc. (2006), in press.

III.A.25 Low-Cost Integrated Composite Seal for SOFC: Materials and Design Methodologies

Objectives

- Investigate the effects of the ceramic layer on the chemical stability of the composite seal
- Investigate the mechanical failure and strength of the composite seal

Accomplishments

- Proved that the ceramic layer in the composite seal effectively isolates the chemical interaction of certain reactive filler glass and stainless steel substrates
- Observed the failure modes and quantified the strength of the composite seal

Introduction

Previous work [1] reported by the author has demonstrated an integrated composite seal concept for SOFCs. The composite seal samples were fabricated and tested for leak performance at steady state and thermo-cycling conditions. The composite seal sample with one combination of constituents has demonstrated a leak rate of 0.017 sccm/cm (2 psig helium) and survived over 60 thermo-cycles from 150ºC to 650ºC at 5ºC/min.

If placed in direct contact, glass and glass-ceramic materials may chemically interact with Fe-Cr-based stainless steel at high temperature. For example, barium-calcium-aluminosilicate (BCAS) based sealing glasses seem to be susceptible to this form of interactions, especially when used in combination with high-chromium-content stainless steels. Under prolonged exposure to high temperature, the chromium in the steel combines with Barium in the glass to form $BaCrO_4$ at the edges where air is available to supply oxygen [1,2]. In the sample interior, chromium dissolves into the glass to form solid solutions and produce porosity at the interface. Such interactions compromise the hermetic sealing and bonding strength of the seal. In the composite seal concept, an inert ceramic layer is disposed in between the filler (e.g. glass) and the substrate [1]. By eliminating direct contact between the glass and the Fe-Cr alloy, the ceramic layer in the composite seal was expected to help reduce adverse chemical interactions between the glass fillers and the metal substrates, thus improving long-term stability and/or mechanical bonding strength of the seal. And it was the purpose of this work to prove such advantages of the composite seal structure.

Xinyu Huang
Connecticut Global Fuel Cell Center
University of Connecticut
44 Weaver Rd., Unit 5233
Storrs, CT 06269
Phone: (860) 486-5284; Fax: (860) 486-8378
E-mail: xinyu@engr.uconn.edu

DOE Project Manager:
Ayyakkannu Manivannan
Phone: (304) 285-2078
E-mail: Ayyakkannu.Manivannan@netl.doe.gov

Subcontractors:
Inframat Corp., Farmington, CT
Physical Acoustics, Princeton Junction, NJ

Approach

Experimental studies were carried out to compare seal samples made with and without the ceramic layer. The stability study utilized metal-glass-metal and metal-ceramic-glass-ceramic-metal sandwich specimens made from Fe-Cr stainless steel with and without a ceramic interlayer. Alloy strips without the ceramic layer were cut into 10 mm x 10 mm squares, then ground and polished using 600-grit SiC paper. The samples were then ultrasonically cleaned in ethanol for 10 minutes and rinsed using acetone to eliminate contamination. A thin layer of G18 sealing glass was applied in the form of green tape. The samples were then transferred to a high temperature oven for curing under a small dead load pressure, approximately 7 kPa. The cured samples were subjected to a constant temperature of 800°C for a week (168 hours) and then cooled down at 1°C/min. After aging, the specimens were mounted in epoxy, sectioned and polished to a surface finish of 1 micron for SEM and electron micro probe analysis. Standard tensile adhesion tests (ASTM C633-01) were conducted on plasma sprayed ceramic coatings to evaluate mechanical pull-out strength of the coating itself and then sandwich samples with a glass interlayer were made and tested in the same pull out setup to gauge bond strength. Samples were bonded with FM1000 epoxy adhesive from Cytec Engineered Materials, Inc. to the pull-out bars, which were connected through two universal joints to an Instron servo hydraulic loading frame. The samples were pulled apart with a cross head speed of 0.015 mm/sec. A minimum of five samples was tested for each material combination.

Results

For the sample without an atmospheric plasma spray (APS) ceramic buffer layer, the interaction between the Fe-Cr substrate and the G18 glass is apparent. A back scattered electron (BSE) image and electron probe micro analysis (EPMA) elemental mappings after aging are shown in Figure 1. Notably, Cr and Ba inter-diffused and probably formed a reaction layer.

A BSE electron image and EPMA elemental mappings for samples with APS coating after aging are shown in Figure 2. For samples with an APS buffer layer, no trace of chemical interaction between the glass and the Fe-Cr substrate was identified. However, Fe-Ni inter-diffusion occurred between the bond coat of the APS coating and the Fe-Cr substrate.

Tensile adhesion test results, shown in Table 1, show that the APS ceramic layer has significant contribution to the adhesion strength of the glass seal. The average failure stress of the Fe-Cr/G18 increased from 2 MPa to about 17 MPa. This is likely due to the elimination of the weak reaction layer between G18 and the Fe-Cr substrates and better chemical compatibility of the G18 glass and the APS ceramic layer (Al_2O_3 and YSZ).

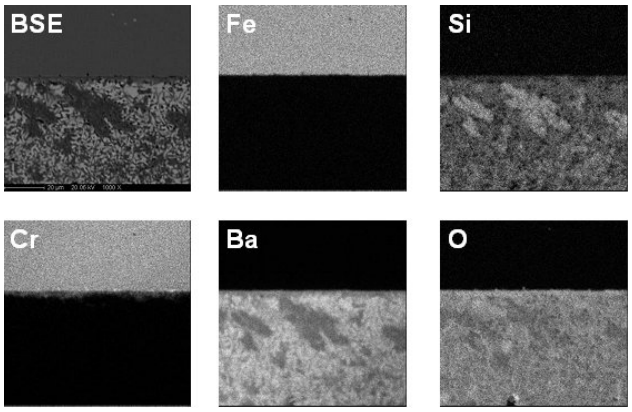

FIGURE 1. Scanning Electron Microscopy (SEM) Images of the Cross-Section of Fe-Cr/G18 Sample after High Temperature Aging; BSE Electron Image; Elemental Maps Shown Are Obtained by EPMA

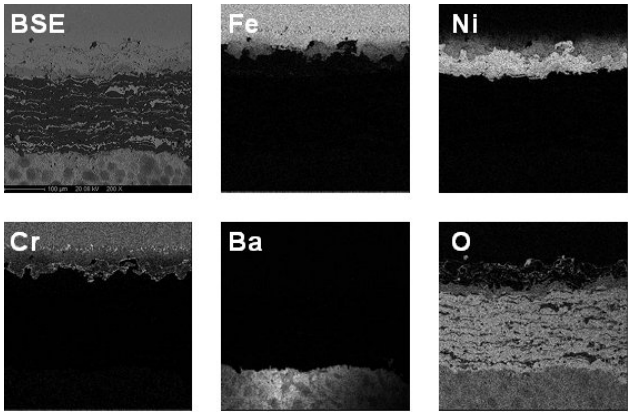

FIGURE 2. SEM Images of the Cross-Section of Fe-Cr/APS/G18 Interface after High Temperature Aging; BSE Electron Image; Elemental Maps Shown Are Obtained by EPMA

TABLE 1. Tensile Adhesion Test Results

	APS Coat Only	APS Coat with Glass	No Coat with Glass
Failure Stress (MPa)	41.52	11.27	0.35
	21.88	23.50	3.26
	30.19	25.90	*N/A
	34.07	12.96	2.35
	27.19	11.27	*N/A
Mean	30.97	16.98	1.99
Standard Deviation	7.39	7.13	1.49

* Sample failed during handling

Conclusions and Future Directions

The work clearly showed the advantages of the composite seal in (1) avoiding adverse chemical interaction between reactive glass and the Fe-Cr stainless substrate and (2) improving the bonding strength due to the ceramic interlayer.

FY 2006 Publications/Presentations

1. Srivatsan Narasimhan, Xinyu Huang, Serg Timin, Lindsay Wright, Kris Ridgeway, Leon Shaw, Ken Reifsnider, "Effect of Ceramic Coating on Chemical Stability of a Composite Seal for Solid Oxide Fuel Cells," 2006 TMS Annual Meeting & Exhibition, Session: Interconnection and Sealing in Fuel Cells I, Session Chair(s): Frederick S. Pettit; Lorenz Singheiser; Mach 12~16, San Antonio, TX.

2. Xinyu Huang, Xinqing Ma, Kristoffer Ridgeway, Srivatsan Narasimhan, and Ken Reifsnider, "Application of Plasma Sprayed Coatings in a Novel Integrated Composite Seal for SOFCs" (ID #11683) International Thermal Spray Conference (ITSC) & Exposition May 15-18, 2006 Seattle, WA.

References

1. X. Huang, "Low-cost integrated composite seal for SOFC: Materials and design methodologies," Section III.A.18, Office of Fossil Energy Fuel Cell Program, FY 2005 Annual Report.

2. Z. Yang, J.W. Stevenson, K.D. Meinhardt, "Chemical interactions of barium-calcium-aluminosilicate-based sealing glasses with oxidation resistant alloys," Solid State Ionics 160 (2003) 213.

3. V.A.C. Haanappel,V. Shemet, I.C. Vinke, S.M. Gross, T.H. Koppitz, N.H. Menzler, M. Zahid, W.J. Quadakkers, "Evaluation of the suitability of various glass sealant-alloy combinations under SOFC stack conditions," Journal of Materials Science 40 (2005) 1583.

III.A.26 Electrocatalytically Active High Surface Area Cathodes for Low Temperature SOFCs

Objectives

- Develop a fundamental understanding of heterogeneous electrocatalytic phenomena at the surface of ion conducting ceramics.
- Fabricate high surface area SOFC cathodes with controlled microstructure and porosity.
- Develop cathodes for low to intermediate temperature SOFCs.

Accomplishments

- Optimized high performance Ag-erbia-stabilized bismuth oxide (ESB) cathode with low area specific resistance (ASR).
- Demonstrated stability issues of Ag-ESB composite cathodes.
- Improved stability of Ag-ESB composite cathodes by addition of 10-15 vol% nano-scale yttria-stabilized zirconia (YSZ) powder.
- Synthesized nano-sized bismuth ruthenate ($Bi_2Ru_2O_7$), lead ruthenate ($Pb_2Ru_2O_7$) and praseodymium-doped yttrium ruthenate ($Y_{2-x}Pr_xRu_2O_7$) powders via co-precipitation method and a novel wet chemical route.
- Developed higher conductivity $Y_{2-x}Pr_xRu_2O_7$ resulting in lower ASR cathodes.
- Determined the effects of microstructure and thickness on ASR of $Bi_2Ru_2O_7$-ESB composite cathodes.
- Developed high performance $Bi_2Ru_2O_7$-ESB composite cathodes with an ASR of 0.03 Ωcm^2 at 700°C.

Eric D. Wachsman
Department of Materials Science and Engineering
University of Florida
Gainesville, FL 32611-6400
Phone: (352) 846-2991; Fax: (352) 846-0326
E-mail: ewach@mse.ufl.edu

DOE Project Manager: Lane Wilson
Phone: (304) 285-1370
E-mail: Lane.Wilson@netl.doe.gov

Introduction

For extensive deployment of SOFCs into industrial and consumer markets to become a reality, further performance optimization is necessary. Currently cathode overpotential is the most significant drag on total SOFC *electrochemical* performance. A significant increase in cathode performance would enable higher power densities at lower temperature, which would mean lower cost and therefore greater commercial viability. Towards that end, we are in the process of developing high performance cathodes for use in conventional and intermediate to low temperature SOFCs.

Approach

We have focused our cathode research on pyrochlore ruthenates because of two reasons. First, the pyrochlore structure has proven to have very tunable conductivity. Depending on the characteristics of the A- and B-site cations, pyrochlores can be designed to be insulating, ionically conducting, semi-conducting or even metallic conducting (~10^3 S/cm). Second, ruthenium oxide is known to be catalytic active towards oxygen reduction so it can be expected that these ruthenates will have low activation polarization when used as SOFC cathodes.

To develop pyrochlore ruthenates for SOFC cathodes two approaches were used: (1) compositional optimization to maximize electrical conductivity and (2) microstructural optimization to minimize the ASR. The results of these efforts are described below.

Results

1. Compositional Development and Processing of Pyrochlore Ruthenates.

Lead ruthenate, $Pb_2Ru_2O_{6.5}$ (PRO), has been studied and reported in the literature as a potential high performance cathode material [1]. Our studies of PRO have been focused on making nano-sized powders for use in composite electrodes. Through novel processing we have been able to achieve our goals and were able to produce nano-sized lead ruthenate crystallites. This was discussed in greater detail in our previous report.

Yttrium ruthenate, $Y_2Ru_2O_7$ (YRO) has been evaluated as a candidate IT-SOFC cathode because of its stability in a wide range of temperature and its lack of reactivity in contact with yttria-stabilized zirconia and gadolinia-doped ceria [2]. We prepared, nanocrystalline powders of YRO by a co-precipitation method. Phase and morphology were studied by x-ray diffraction (XRD) and field emission scanning electron microscope (FE-SEM), showing a particle size of about 100 nm. The nanocrystalline particle size makes the powder amenable for the triple phase boundary tailoring in order to minimize ASR.

The electronic behavior of ruthenium pyrochlores is explained in terms of the Mott–Hubbard mechanism of electron localization, which shows high electrical (metallic) conductivity when their structure allows a Ru–O–Ru bond angle larger than 133˚ [3]. Moreover, since the Ru–O–Ru angle increases with increasing size of the A cation, Pr was chosen as an A-site dopant in order to increase the electrical conductivity of yttrium ruthenate.

X-ray diffraction studies confirmed that the doped powders were single pyrochlore phase, and SEM-EDS measurements confirmed the presence of the dopant in the pyrochlore structure. The electrical conductivity was measured at several temperatures by the d.c. 4-probe method, for a range of 5-25% dopant concentration, in a range of 473-1,073 K. Our results, Figure 1, show that doping with Pr significantly increases the conductivity of yttrium ruthenate.

Figure 1 shows a comparison of the total electrical conductivity of bismuth ruthenate, lead ruthenate, and Pr-doped yttrium ruthenate as a function of reciprocal temperature. In general, it shows that bismuth ruthenate and lead ruthenate are significantly more conductive than the yttrium ruthenates. Moreover, bismuth ruthenate and lead ruthenate display metallic-type conductivity while the yttrium ruthenates are semiconducting.

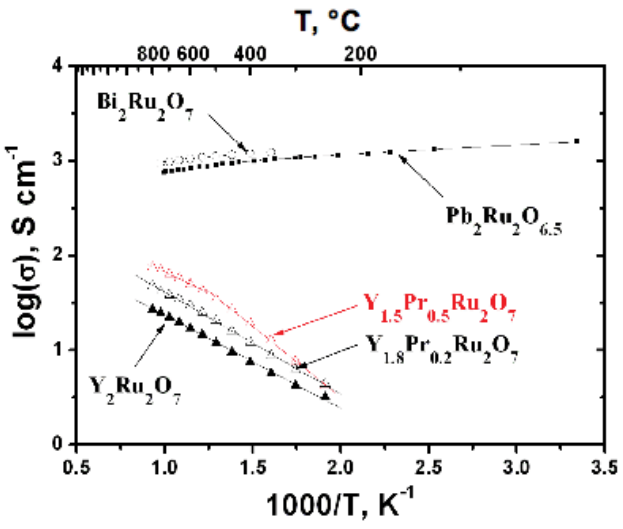

FIGURE 1. Comparison of Temperature-Dependent Conductivity of Ruthenate Pyrochlores

Figure 1 also shows the effect of doping yttrium ruthenate with Pr. As the Pr content increases so does the overall conductivity. Our studies on the conductivity dependence of praseodymium-doped yttrium ruthenate on oxygen partial pressure (P_{O_2}) showed insensitivity to P_{O_2} changes. This suggests the observed increase in conductivity over undoped yttrium ruthenate is due mainly to the size effect of Pr increasing electronic the conductivity through the aforementioned Mott–Hubbard mechanism of electron localization. More tests will be conducted to confirm this inference. Nevertheless, Pr-doped yttrium ruthenate shows potential for use as a high performance SOFC cathode on YSZ.

2. Microstructural Optimization of Bismuth Ruthenate

Phase-pure $Bi_2Ru_2O_{7.0}$ (BRO) and $Er_{0.4}Bi_{1.6}O_3$ (ESB) were obtained by conventional solid-state synthesis. Leaching with HNO_3 was required to remove the Bi-rich sillenite phase from the BRO powders. Powders were then crushed and sieved. A portion of these powders were then vibratory milled to reduce particle size. Particle size distributions were narrowed using sedimentation. Powders containing large-size particles–those which have been sieved but not vibratory milled–are designated with a subscript "S". Powders containing small-size particles–those which have been vibratory milled–are designated with a subscript "VM".

Electrode ink slurries were prepared by combining a 50-50 wt% mixture of BRO and ESB powders with appropriate organic vehicles. Four different inks were prepared, using the different particle size combinations–BRO_S-ESB_S, BRO_S-ESB_{VM}, BRO_{VM}-ESB_S, and BRO_{VM}-ESB_{VM}. The inks were applied to both sides of dense ESB pellets, dried, and fired at 800˚C for 2 h. The symmetrical cells were then electrochemically tested using impedance spectroscopy.

An Arrhenius plot of the electrode ASR for the four different microstructures is shown in Figure 2. Both composites containing coarse BRO particles have the highest ASRs while both composites containing fine BRO particles have the lowest ASRs. The composite composed of fine particles of both phases has the lowest ASR (0.074 Ωcm^2 at 650°C and 0.048 Ωcm^2 at 700˚C).

For comparison, the two lowest-ASR cathode systems prepared without sedimentation are also plotted in the figure (BRO_{VM}-ESB_{VM} and BRO_{VM}-ESB_S). These two systems exhibit the lowest ASR after sedimentation, but the order is reversed, and the values are significantly lower (50-85% reduction in ASR). The reduced particle size distribution translates into a larger number fraction

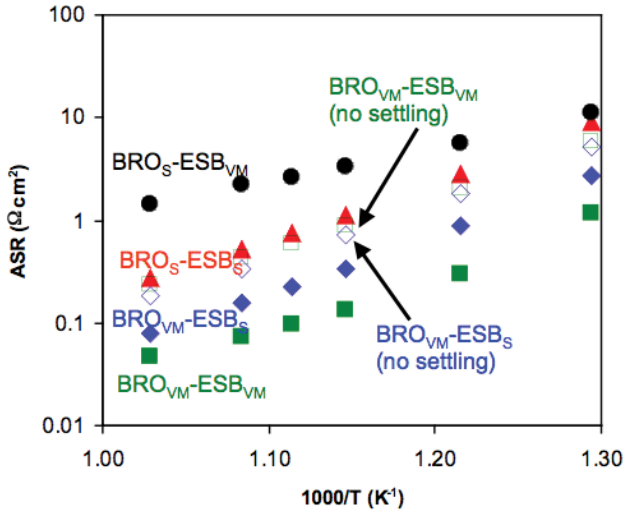

FIGURE 2. Ahhrenius Plot of Nominally-Similar BRO-ESB Cathodes Containing Different Microstructures for Powders with Sedimentation (closed symbols) and without Sedimentation (open symbols)

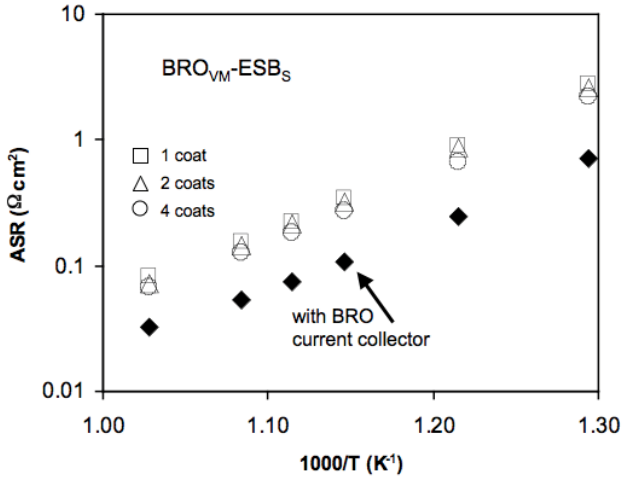

FIGURE 3. Ahhrenius plot of ASR for the BRO_{VM}-ESB_S system at various thicknesses with no current collector (open symbols). Also shown is the same system with two coats of the electrode ink and a pure BRO_S current collector (closed symbols).

of sub-micron sized particles in the vibratory milled phase. This in turn translates into longer three-phase boundary (TPB) lines between the oxidant (air), the ion-conducting phase (ESB) and the electron conducting pages (BRO). The fact that the BRO_{VM}-ESB_{VM} system (where both phases are composed of vibratory-milled powder) exhibits the most dramatic reduction in ASR after sedimentation gives credence to this argument.

In order to improve the connectivity of the two phases in the composite and reduce lateral resistance, the thickness of the electrodes was increased. Additional layers were added after drying of the previous layers. For each microstructurally distinct electrode system, cells having one, two, and four coats of electrode material were tested. Additionally, for each of the four systems, a pure BRO_S current collector was added to a pellet coated twice with the electrode ink. Just before testing the samples, a multimeter was used to ensure the lateral resistance of each was at or below 1 Ω.

The results of these studies are shown in Figure 3. For the composite system shown (and for all other systems), ASR decreased with number of coatings. The addition of a pure BRO_S current collector to these cathode systems results in a more dramatic reduction in ASR than changes in thickness alone. A minimum ASR was achieved for the BRO_{VM}-ESB_S system, with a value of 0.054 Ωcm^2 at 650°C and 0.034 Ωcm^2 at 700°C. Further improvement is expected with the BRO_{VM}-ESB_{VM} system.

This particular system exhibits the lowest ASR produced to date by our research group, and is compared against a literature survey as well as some of our group's earlier results in Figure 4. Shown is a comparison between the ASR vs. 1/T profiles for

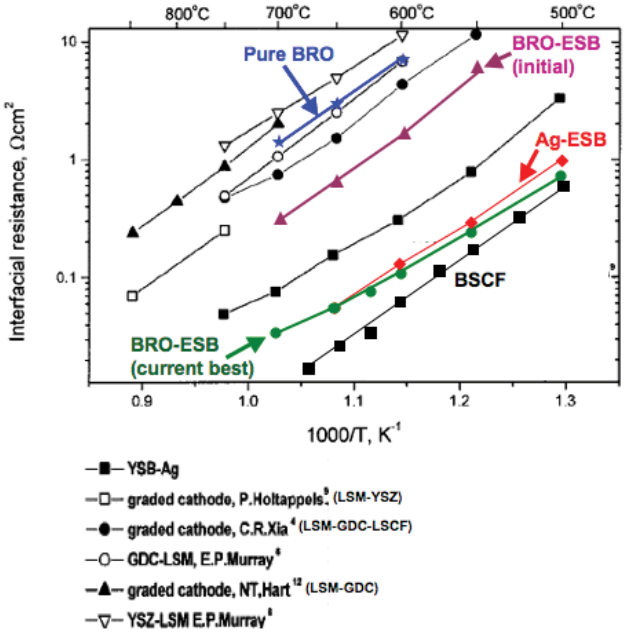

FIGURE 4. Ahhrenius plot of ASR for the current optimized cathode system with some previous results. Also shown is the BSCF system, overlaid on a recent literature survey of composite cathode systems.

(i) an optimized Ag-ESB system, (ii) pure BRO (no ESB phase), (iii) a compositionally-optimized BRO-ESB system without any microstructural considerations (initial), the lowest ASR BRO-ESB system obtained to date (current best) and a composite literature survey from C. Xia, et. al [4], as well as the results from Z. Shao and S.M. Haile [5] for $Ba_{0.5}Sr_{0.5}Co_{0.8}Fe_{0.2}O_{3-\delta}$ (BSCF) cathodes which exhibit the lowest ASR reported to date in the literature.

The current microstructurally optimized BRO-ESB composite is approaching those values reported for barium strontium cobalt ferrite (BSCF). Additionally, the lower activation energy of BRO-ESB (~1.04 eV) compared to that of BSCF (~1.20 eV) should translate to better performance at lower temperatures. Initial long-term stability studies on the BRO-ESB cathode system under fuel cell operating conditions show it to be very stable, with a rise in cathode polarization of only a few percent over 500 h at 625°C. We have not been able to achieve similar stability with the BSCF system.

Conclusions and Future Directions

- Synthesized nano-sized $Bi_2Ru_2O_7$, $Pb_2Ru_2O_7$ and doped $Y_2Ru_2O_7$ powders via co-precipitation and a novel wet chemical route.
- Increased $Y_2Ru_2O_7$ conductivity by 20% by doping with 15 mol% Pr.
- Developed stable, low ASR $Bi_2Ru_2O_7$-ESB composite cathodes.
- Optimized the microstructure of $Bi_2Ru_2O_7$-ESB composite cathodes with an ASR of 0.03 Ωcm^2 at 700°C.

FY 2006 Publications/Presentations

1. "Novel Bismuth Ruthenate based Cathodes for IT-SOFCs; Part I: Doped Bismuth Ruthenates," A. Jaiswall and E.D. Wachsman, *Solid State Ionics*, submitted.

2. "Applicability of $Bi_2Ru_2O_7$ Pyrochlore Electrodes for ESB and BiMEVOX Electrolytes," V. Esposito, E. Traversa, and E.D. Wachsman, *Journal of the Electrochemical Society*, accepted.

3. "Synthesis and Characterization of $Y_2Ru_2O_7$ and $Y_{2-x}Pr_xRu_2O_7$ for the Cathode Application in Intermediate Temperature Solid Oxide Fuel Cells," C. Abate, K. Duncan, V. Esposito, E. Traversa, and E. D. Wachsman, *Solid State Ionic Devices IV, ECS Transactions*, E.D. Wachsman, F.H. Garzon, E. Traversa, R. Mukundan, and V. Birss, Ed., **1-7**, 255-262 (2006).

4. "$Bi_2Ru_2O_7$ Pyrochlore Electrodes for Bi_2O_3 Based Electrolyte for IT-SOFC Applications," V. Esposito, B. H. Luong, E. Di Bartolomeo, E. D. Wachsman, and E. Traversa, *Solid State Ionic Devices IV*, *ECS Transactions*, E.D. Wachsman, F.H. Garzon, E. Traversa, R. Mukundan, and V. Birss, Ed., **1-7**, 263-278 (2006).

5. "Ag-$Bi_{1.6}Er_{0.4}O_3$ as a Potential Cathode Material for IT-SOFCs," M. Camaratta and E. D. Wachsman, *Solid State Ionic Devices IV*, *ECS Transactions*, E.D. Wachsman, F.H. Garzon, E. Traversa, R. Mukundan, and V. Birss, Ed., **1-7,** 279-292 (2006).

6. "Direct Current Bias Studies on $(Bi_2O_3)_{0.8}(Er_2O_3)_{0.2}$ Electrolyte and Ag-$(Bi_2O_3)_{0.8}(Er_2O_3)_{0.2}$ Cermet Electrode," A. Jaiswall and E.D. Wachsman, *Solid State Ionics*, **177** (7-8), 677-685 (2006).

7. "$Pb_2Ru_2O_{6.5}$ as a Low-Temperature Cathode for Bismuth Oxide Electrolytes," V. Esposito, E. Traversa, and E.D. Wachsman, *Journal of the Electrochemical Society*, **152** (12), A2300-2306 (2005).

References

1. J. Prakash, D. Tryk, and E. B. Yeager, *J. Electrochem. Soc*., **146** (1999) 4145.

2. A. Bencan, M. Hrovat, J. Holc, and M. Kosec, *Materials Research Bulletin* **35**, (2000) 2415.

3. K. S. Lee, *J. Solid State Chem*. **131** (1997), 405.

4. C.R. Xia, Y. Zhang, M.L. Liu, *Applied Physics Letters*, **82** (2003) 901.

5. Z. Shao, S. M. Haile, *Nature*, **431** (2004) 170.

III.A.27 New Cathode Materials for Intermediate Temperature Solid Oxide Fuel Cells

Objectives

- Evaluate $La_xPr_{2-x}NiO_{4+\delta}$ (x = 0-2) compositions as cathodes for intermediate temperature (500-800°C) SOFCs.
- Investigate other perovskite phases, for example, $LnBaCo_2O_{5.5+\delta}$ (Ln = rare earth element), as cathodes for intermediate temperature SOFCs.
- Develop model systems based on oxide thin films to investigate surfaces, interfaces and triple phase boundaries using isotope exchange and depth profiling.
- Deposit patterned combinatorial oxide layers on single crystal and ceramic substrates to investigate the role of composition on the activation and transport of oxygen.

Accomplishments

- Completed the evaluation of the performance of $La_2NiO_{4+\delta}$ and $Pr_2NiO_{4+\delta}$ as cathode materials: the resistance of these electrodes was measured in half cells and compared with previous results for symmetric cells using ceria electrolytes.
- Studied impedance of dense polycrystalline thin films of $La_2NiO_{4+\delta}$: measured and analyzed impedance data for symmetric cells with single crystal yttria stabilized zirconia (YSZ) as the electrolyte and dense $La_2NiO_{4+\delta}$ electrodes.
- Prepared thin films of $PrBaCo_2O_{5.5+\sigma}$ on different substrates by pulsed laser deposition: developed synthesis conditions for deposition of oriented and epitaxial films on YSZ, strontium titanate (STO), and lanthanum aluminate (LAO) single crystal substrates.
- Measured the surface exchange rate on thin films by isotope exchange and depth profiling (IEDP) and electrical conductivity relaxation (ECR). The surface exchange and the interface transfer rate on YSZ and gadolinium doped ceria (CGO)/YSZ were measured by IEDP.
- Measured oxygen transport in bulk $PrBaCo_2O_{5.5+\delta}$ cathodes by IEDP and ECR.
- Demonstrated low area specific resistance (ASR) (0.15 ohms-cm^2) for $PrBaCo_2O_{5.5+\delta}$ cathodes in symmetric cells.

Allan J. Jacobson (Primary Contact), Shuangyan Wang, Guntae Kim
University of Houston
4800 Calhoun Rd.
Houston, TX 77204
Phone: (713) 743-2785; Fax: (713) 743-2787
E-mail: ajjacob@uh.edu

DOE Project Manager: Lane Wilson
Phone: (304) 285-1336
E-mail: Lane.Wilson@netl.doe.gov

Subcontractors:
Charles A. Mims, University of Toronto, Toronto, Ontario, Canada
Peter Rieke, Pacific Northwest National Laboratory, Richland, Washington

Introduction

The objectives of the project are to discover new oxide cathode materials that meet a performance target of 1.0 W/cm^2 at 0.7 V in combination with YSZ at 700°C and with CGO electrolytes at 600°C. The target area-specific resistance of the cathode is 0.15 Ωcm^2. An ancillary objective of the project is to increase fundamental understanding of the intrinsic transport properties of mixed electronic ionic conducting oxides and oxide-oxide interfaces that can be used to accelerate further progress in the development of cost effective high performance solid oxide fuel cells.

Approach

The rates of oxygen activation and transport are key factors in determining cathode performance. The rates are described by the oxygen surface exchange coefficient, k_{ex} (also denoted as k_O), and the oxygen bulk diffusion coefficient, D_O. We use the ECR technique combined with composition data from thermo-gravimetric analysis and IEDP to obtain these two coefficients. The research strategy is to investigate both established classes of materials and new candidates as cathodes and to use model systems based on thin films to investigate surfaces, interfaces and triple phase boundaries. The fundamental performance parameters such as bulk diffusion, surface reactivity and interfacial transfer, are coupled to performance in single cell tests. The real performance data is then used to design new systems that meet the overall performance targets.

Results

Evaluation of the Performance of $La_2NiO_{4+\delta}$ (LNO) and $Pr_2NiO_{4+\delta}$ (PNO) as Cathode Materials

Sintering studies were carried out at Pacific Northwest National Laboratory (PNNL) to determine the optimum temperatures for electrode preparation on CGO. LNO and PNO electrodes were prepared for 2 h at 1,200°C and 1,150°C, respectively. A reference electrode was inserted from the anode side to within less than 1 mm of the other surface. The samples were tested at 850, 750, 650 and 600°C in flowing air and oxygen. The electrochemical response was determined by cyclic voltammetry at 1 mV/sec scan rate and with potential limits that kept the current under about 1.5 Amps. Current interrupt with a 27 μs time delay was used to remove the series resistance usually associated with the electrolyte resistance. AC impedance spectra were also obtained using a 10 mV input stimulus at zero potential bias. The results in general are consistent with the ASR measurements on symmetric cells though for LNO the cyclic voltammetry and the impedance gave values at 600°C (5 and 3.5 ohm-cm^2) that are somewhat higher than previously measured on symmetric cells (1 ohms-cm^2). For PNO at 750°C and above, all the results are in good agreement and indicate a very low electrode resistance (< 0.1 ohm-cm^2). At lower temperature, the ASR increases very rapidly for reasons that are not yet understood. A higher activation energy for PNO compared with LNO is observed in the ASR results but the increase is much smaller than observed in half cell measurements. In conclusion, PNO shows low reactivity with ceria electrodes and low electrode resistances at 750°C. Further work to understand the lower temperature behavior is warranted.

Isotope Exchange and Depth Profiling of Thin Films of $PrBaCo_2O_{5+x}$ (PBCO)

In a continuation of the thin film studies of $PrBaCo_2O_{5+x}$ the surface exchange rate and interface transfer rates were determined for a PBCO/CGO/YSZ film sample by isotope exchange and depth profiling. The sample was prepared by pulsed laser deposition on a single crystal of YSZ. Initially half the sample was masked and CGO deposited and then PBCO deposited over the whole sample to give the structure shown schematically in Figure 1. The sample was exposed to ^{18}O at 0.2 atm at 700°C for 120 s and then rapidly quenched. The ^{18}O profile in both regions of the sample was then analyzed by time-of-flight secondary ion mass spectroscopy (ToFSIMS) using an ION-TOF IV with Ga gun. The sample was sputtered with Cs^+ at 20 keV in "burst" mode (multiple primary ion pulses) to avoid saturation in the ^{16}O signal. The surface exchange coefficient was determined from the oxygen concentration. The ion signals from the PBCO layer

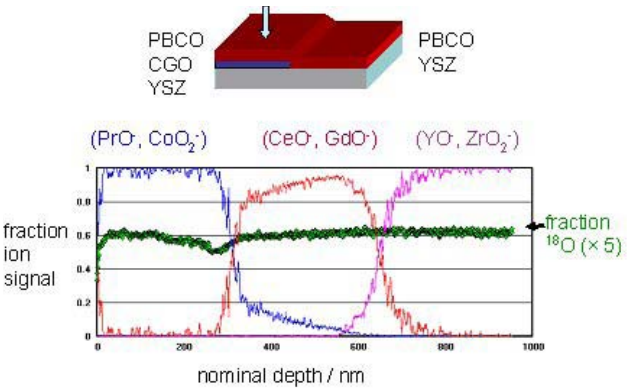

FIGURE 1. Depth Profile of a Thin Film PBCO/CGO/YSZ Structure

(PrO^- and CoO_2^-), the CGO (CeO^- and GdO^-), and from YSZ (YO^- and ZrO_2^-) are shown in Figure 1 and indicate sharp interfaces. The fraction of ^{18}O is uniform across the film and the PBCO/CGO and CGO/YSZ interfaces. The fall off into the YSZ itself is not apparent on this length scale. Under these conditions, no resistance to oxygen transfer is observed. The surface exchange coefficient determined from these measurements and the earlier results on STO and the ECR thin film measurements are all in good agreement.

Oxygen Transport in Bulk $PrBaCo_2O_{5.5+\delta}$ Cathodes by IEDP and ECR

The total conductivity (see Figure 2) was measured on a rectangular bar of $PrBaCo_2O_{5+x}$ (1.3×0.19×0.15 cm). Near ambient temperature, the conductivities reaches 2,000 Scm^{-1} and as the temperature is increased, the conductivity begins to decrease at ~150°C due to the loss of oxygen atoms from the lattice and reduction of Co(IV) to Co(III). The values of the oxygen transport parameters D_O derived from the ECR data using the measured values of the thermodynamic factor for oxygen ions (Γ_O) are shown in Figure 3. A value of D obtained directly from the IEDP measurements is also shown in Figure 3. The D_O values from the two techniques are in good agreement. By contrast, the k_O values from IEDP and ECR differ substantially. The surface activation rates can depend critically on subtle variations in sample preparation and pretreatment which, in turn, affect such important parameters as surface roughness and the surface density of defect sites and sample-to-sample variability in k_O is a common feature of similar studies on both ceramic and thin-film materials. The central role of surface defects in the oxygen activation rate has been clearly shown on high quality thin films of cobaltite perovskite materials [1]. The role of surface defects is further illustrated by the much higher values of k_O measured on these ceramic samples than those measured on high-quality $PrBaCo_2O_{5.5+x}$ thin films [2].

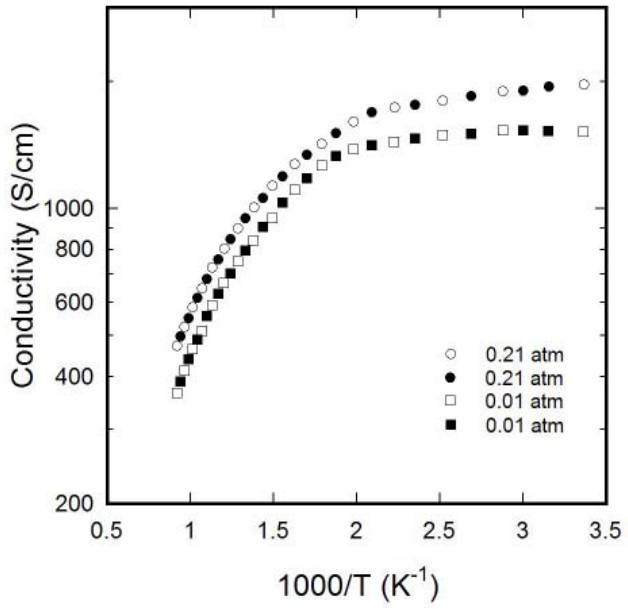

FIGURE 2. Total Conductivity of $PrBaCo_2O_{5.5+x}$ at 0.01 (■) and 0.21 (●) atm; Open and Closed Symbols Correspond to Measurements on Cooling and Heating

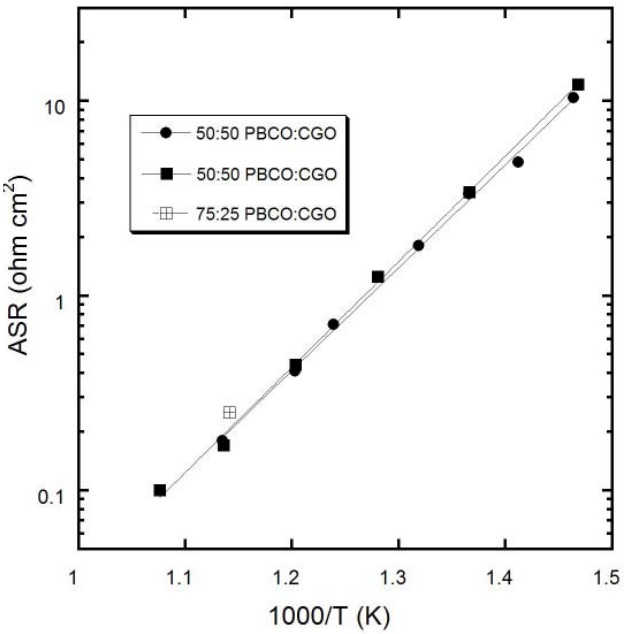

FIGURE 4. Area Specific Resistances for Three Symmetric Cells PBCO/CGO/PBCO

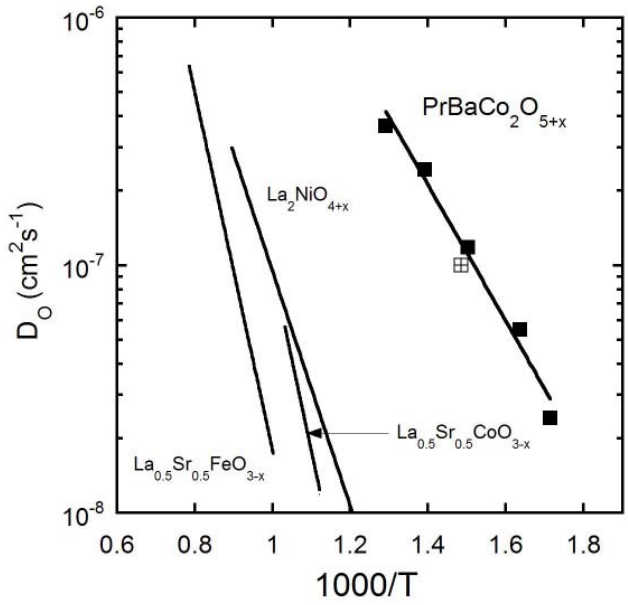

FIGURE 3. Comparison of the Values of D_0 Measured by ECR for Ceramic Samples [5-8]; The Open Square Is the IEDP Result

Impedance Measurements of $PrBaCo_2O_{5.5+x}$ Electrodes in Symmetric Cells

CGO powder containing 10% gadolinia was purchased from Rhodia. The CGO-powder was cold isostatically pressed into pellets at 40,000 psi and sintered in air at 1,350°C for 10 h. The pellet density was greater than 96% of the theoretical value. Films with the compositions 50 to 50 and 75 to 25 (PBCO to CGO) were made by tape-casting (Transionics Company) and used to fabricate symmetrical PBCO+CGO/CGO/PBCO+CGO cells with 1 cm^2 active area. The electrodes were sintered at 1,100°C in air for 2 h. Instead of using Pt, which is known to catalyze the oxygen reduction reaction, gold gauze was used as the current collector on both electrodes. The symmetrical PBCO+CGO/CGO/PBCO+CGO cell and the Au gauzes were pressed together physically with spring loading. Electrochemical impedance spectra were obtained using a Solatron 1260 frequency response analyzer. The applied frequency ranges from 2 MHz to 0.01 Hz and operating temperature ranges are 400 $\leq$ T $\leq$ 650ºC. An electrical perturbation (30 mV amplitude) was used throughout the impedance measurements. The results for the area specific resistance as a function of temperature are shown in Figure 4. At 600ºC the lowest area specific resistance observed was 0.15 ohm-cm^2.

Conclusions and Future Directions

The oxygen transport kinetics of the oxygen deficient double perovskite $PrBaCo_2O_{5.5+x}$ were studied with the electrical conductivity relaxation (ECR) technique and by isotope exchange and depth profiling. Despite some uncertainties in the surface exchange rate, it is clear that these double perovskite materials exhibit unusually high activity for oxygen activation and mobility. The solid lines in Figure 3 represent the average values of several measurements by different groups on La_2NiO_4 [5-8] and ECR measurements on

$La_{0.5}Sr_{0.5}MO_{3-x}$ (M= Fe, Co) [3,4]. Initial tests of the performance of PBCO as a cathode material were carried out in symmetric cells. Composite electrodes of PBCO/CGO were used and gave ASR values as low as 0.15 ohm-cm^2 at 600°C. Further electrode studies are in progress to verify the performance of PBCO as a cathode under fuel cell operating conditions.

Special Recognitions & Awards/Patents Issued

1. A provisional patent application on A site ordered perovskites was converted in 8/06 to a PCT application.

FY 2006 Publications/Presentations

1. N. Bayani, C. A. Mims, A. J. Jacobson, and P. A. W. van der Heide, "Modes of surface exchange in $La_{0.2}Sr_{0.8}Cr_{0.2}Fe_{0.8}O_{3-d}$" Solid State Ionics (2005) 176(3-4) 319-323.

2. Huang, D. X.; Chen, C. L.; Jacobson, A. J. "Interface Structures and periodic film distortions induced by substrate surface steps in Gd-doped ceria thin film growth," Journal of Applied Physics (2005), 97(4), 043506/1-043506/5.

3. Kim, G.; Wang, S.; Jacobson, A. J.; Yuan, Z.; Donner, W.; Chen, C. L.; Reimus, L.; Brodersen, P.; Mims, C. A. "Oxygen exchange kinetics of epitaxial $PrBaCo_2O_{5+\delta}$ thin films," Applied Physics Letters 88, 024103 (2006).

4. Kim, G.; Wang, S.; Jacobson A. J.; Chen, C. L. "Measurement of Oxygen Transport Kinetics in Epitaxial $La_2NiO_{4+\delta}$ Thin Films by Electrical Conductivity Relaxation," Solid State Ionics in press.

5. The Oxygen Non-stoichiometry and Electrical Conductivity of $La_{0.7}Sr_{0.3}Cu_{0.2}Fe_{0.8}O_{3-\delta}$ Park, C. Y.; Azzarello, F.; Jacobson, A. J., J. Mat. Chem. in press.

6. "Some Insights from Studies of Thin Film Cathode Materials for Solid Oxide Fuel Cells," Allan J. Jacobson, C. A. Mims, DOE Workshop Cocoa Beach, Florida, January 26, 2006.

7. "Oxygen Non-stoichiometry and Transport Properties of Mixed Conducting Oxides," New Directions in Materials Chemistry, Allan J. Jacobson, University of Liverpool, June 7, 2006.

8. "Fast Oxygen Ion Diffusion and Surface Exchange Kinetics in the Oxides $LnBaCo_2O_{5+x}$ (Ln = Pr, Nd) with Perovskite Related Structures and Ordered A Cations," G. Kim, S. Wang, A. J. Jacobson, L. Reimus, P. Brodersen, C. A. Mims, Electrochem. Soc. Meeting, Los Angeles, October 16, 2005.

9. "Oxygen Exchange Kinetics of $PrBaCo_2O_{5.5+\delta}$ Thin Films Prepared by Pulsed-Laser Deposition," G. Kim, S. Wang, A. J. Jacobson, Z. Yuan, W. Donner, C. L. Chen, L. Reimus, P. Brodersen, and C. A. Mims, Electrochem. Soc. Meeting, Los Angeles, October 16, 2005.

References

1. X. Chen, S. Wang, Y. L. Yang, L. Smith, N. J. Wu, B.-I. Kim, S. S. Perry, A. J Jacobson, A. Ignatiev, Solid State Ionics 146/3-4, 405 (2002).

2. G. Kim, S. Wang, A. J. Jacobson, W. Donner, C. L. Chen, L. Reimus, P. Brodersen, C. A. Mims. Appl Phys. Lett. 88, 2006, 024103.

3. S. Wang, A. Verma, Y.L. Yang, A.J. Jacobson, Ben Abeles, Solid State Ionics 140 (2001) 125-133.

4. J. Yoo, A. Verma, S. Wang, A. J. Jacobson, J. Electrochem. Soc. 152, 2005, A497.

5. J. A. Kilner and C. K. M. Shaw, Solid State Ionics 154-155, 2002, 523.

6. F. Mauvy, J. M. Bassat, E. Bohem, P. Dordor, J. P. Loup, Solid State Ionics 158, 2003, 395.

7. E. Boehm, J.-M. Bassat, M. C. Steil, P. Dordor, F. Mauvy, J.-C. Grenier, Solid State Sciences 5, 2003, 973.

8. J. M. Bassat, P. Odier, A. Villesuzanne, C. Marin, M. Pouchard, Solid State Ionics 167, 2004, 341.

III.A.28 Resilient Sealing Materials for Solid Oxide Fuel Cells

Objectives

- Develop silicate-based glasses with requisite properties to be used for hermetic seals for solid oxide fuel cells (SOFCs).
- Characterize the properties of composite sealing materials prepared by adding fillers to base sealing glasses.
- Demonstrate hermeticity and materials compatibility for seals under SOFC operational conditions.

Accomplishments

- Formulated new alkaline earth silicate glass–ceramic compositions with requisite thermal properties, including sealing temperatures at or below 900ºC and coefficients of thermal expansion (CTE) in the range 10-12x10^{-6}/ºC.
- Developed processing procedures for preparing composite SOFC sealing materials (tapes and pastes), with and without ceramic and metallic filler materials to modify CTE behavior.
- Developed new differential thermal analytical (DTA) techniques to characterize the effects of filler materials on glass crystallization kinetics.
- Produced seals between SOFC components using new materials that remain hermetic after ten thermal cycles between 800ºC and room temperature.

Introduction

Reliable hermetic sealing technologies must be developed in order to achieve the high power densities possible for solid oxide fuel cells (SOFC) stacks. For the past decade, considerable effort has gone into the development of glasses and glass-ceramics for these seals (see Fergus, [1], for a recent review). Compositions with the requisite thermal properties for seals have been developed, but questions about long-term property stability, deleterious interfacial reactivity, and component volatility make the development of new, reliable sealing materials a priority.

One concern with the use of 'rigid' glass or glass-ceramic hermetic SOFC seals is the brittle nature of the materials and the consequences of their mechanical failure. Lacking the 'resiliency' of polymers or metals, rigid glasses must be engineered with tight CTE tolerances to avoid the development of catastrophic thermal stresses during thermal cycling. The use of composite materials could enhance the fracture toughness of the seals, and the development of compositions with a stable glassy (viscous) phase with a glass transformation temperature (T_g) below the operational temperature could provide a means (i.e., viscous flow) for 'healing' cracks that form in the seal as a result of thermal stresses. These approaches are presently under study by various groups supported by the DOE (e.g., University of Cincinnati/Raj Singh, NexTech/Matt Seabaugh) and similar ideas were also explored in the present project.

Richard K. Brow (Primary Contact),
Signo T. Reis, Teng Zhang, Mary Reidmeyer
University of Missouri-Rolla
Department of Materials Science & Engineering
222 McNutt Hall
Rolla, MO 65409-0330
Phone: (573) 341-4401; Fax: (573) 341-6934
E-mail: brow@umr.edu

DOE Project Manager:
Ayyakkannu Manivannan
Phone: (304) 285-2078
E-mail: Ayyakkannu.Manivannan@netl.doe.gov

Approach

The glasses developed at the University of Missouri-Rolla (UMR) have relatively low silica contents (<45 mole%) with molecular-level structures that are much less connected than conventional silicate glasses, allowing the melts to readily flow at relatively low temperatures before crystallizing to form glass-ceramic phases with the desired thermal properties. Some compositions were designed to fully-crystallize to form rigid glass-ceramic seals, and others were designed to retain a significant fraction of a glassy phase after crystallization to allow viscous relaxation of thermal stresses. Base glasses were mixed with filler materials (metal and ceramic powders) to tailor CTE and to modify the mechanical behavior of the sealing material.

Results

Over fifty glass compositions have been prepared and evaluated. Many of the compositions have the requisite thermal properties required for SOFC seals (e.g., CTE match to SOFC components and sealing temperatures at or below 900ºC) and have received closer examination for their suitability as potential sealing materials. Figure 1 shows how one compositional variation affects the CTE of crystallized sealing glasses. In this case, increasing the relative

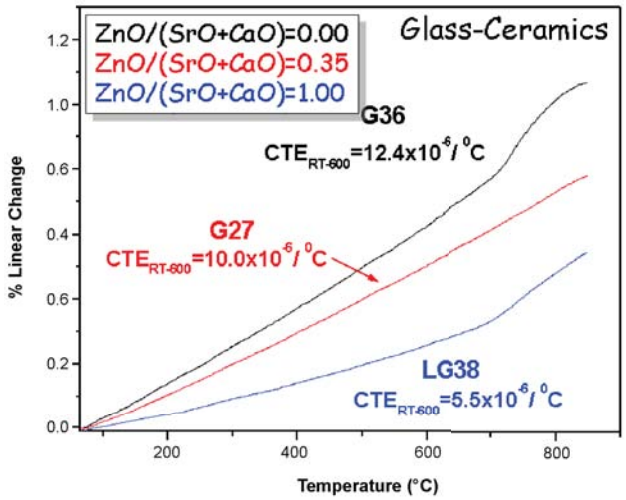

FIGURE 1. Coefficient of Thermal Expansion (CTE) Curves for Several UMR Sealing Glass-Ceramics as a Function of Relative ZnO-Contents

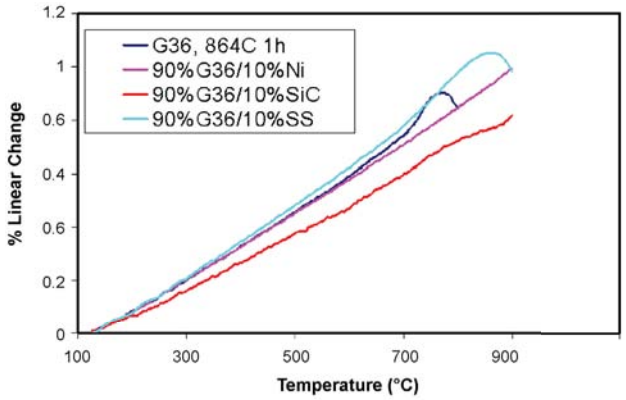

FIGURE 2. CTE Curves for Glass 36 Composites Made with 10 vol% of Ni, SiC, and 304 Stainless Steel Powders, Compared with the CTE Curve of Glass 36 Sintered at 864ºC for One Hour

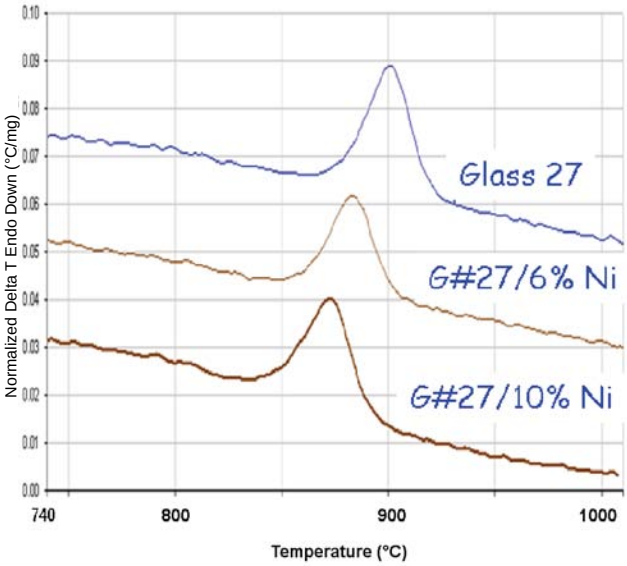

FIGURE 3. DTA Traces from Glass 27 with up to 10 vol% Ni Powder Added

ZnO content of the base glass decreases the CTE of the crystallized material, through the formation of lower expansion Zn-silicate phases, including Zn_2SiO_4. Glass 27 is fully crystallized after several hours at 850ºC, whereas a significant residual glassy phase remains in glass 36, as indicated by the break in CTE near 700ºC (the glass transition temperature, T_g, of the residual glass) and the dilatometric softening behavior near 800ºC. Evidence for residual glass remains in monolithic samples of glass 36 after four weeks at 750ºC.

The presence of an apparently stable residual viscous phase makes glass 36 an interesting candidate as a base composition for composite seal formulations. A variety of different filler materials with different expansion coefficients and elastic moduli were added (10 vol%) to the base glass by a ball-milling/mixing technique and these mixtures were sintered to form dense samples that were then evaluated. Figure 2 shows the CTE curves for composites made with Ni, SiC and 304 stainless steel powders. The 'bulk' CTE of the composite material can be tailored over a range of values with the use of different filler materials.

The effects of filler materials on the crystallization behavior of composite sealing materials were studied by a differential thermal analysis technique developed at UMR [2]. By considering changes in the areas of crystallization exothermic peaks from DTA analyses of glass samples following isothermal heat treatments, the fraction of glass crystallized can be measured. Figure 3 shows the DTA responses of glass 27 with and without 6 or 10 vol% Ni. Increasing Ni-contents cause the crystallization exotherm to shift to lower temperatures, an indication for enhanced crystallization kinetics. This is confirmed by a quantitative DTA crystallization study, the results of which are summarized in Figure 4. This figure shows, for example, that at 800ºC, glass 27 with 10 vol% Ni is completely crystallized after two hours, whereas 'pure' glass 27 is only about half-crystallized after 12 hours in the absence of this filler phase.

Rapid crystallization of composite sealing materials occurred for all glasses studied. For example, the CTE data for glass 36 in Figure 2 shows that the T_g and dilatometric softening points for the composite materials are much less evident (or nonexistent) compared with the pure glass after similar sintering treatments. These results indicate that the long-term stability of a residual viscous-phase in a composite seal will be difficult to achieve, at least in the glass-forming systems under investigation. As a result, the UMR program has concentrated on the development of optimized 'rigid' glass-ceramic sealing materials.

One promising sealing composition is glass 50. This ZnO- and BaO-free glass crystallizes to form $Sr_2Al_2SiO_7$ and $CaSrSiO_4$ major phases in a material with a CTE of $11.5x10^{-7}$/ºC that does not change after 100 days at 800ºC. A series of simple seals have been fabricated using glass 50 and their hermeticity has been tested at room temperature using helium gas. The seals were fabricated using glass tapes (PVB binder, 10 μm glass particles) fired in air to 850-900ºC, between 430SS as the interconnect material and either YSZ (electrolyte) or Ni-YSZ (anode) substrates. These test samples were heated to 800ºC at 2ºC/minute in different atmospheres, held for 24 hours, then cooled to room temperature (-2ºC/minute) where they were tested for hermeticity using helium gas at 2 psig. Samples that did not leak (hold 2 psig for four hours) were reheated for another 800ºC/24 hour heat treatment, and cycled back to room temperature for another hermeticity measurement. Table 1 summarizes the results of some of these tests. Glasses fabricated both at UMR and by a commercial vendor have been evaluated.

TABLE 1. Summary of thermal cycling/hermeticity tests on sealed components. All tests were done using helium at room temperature, following the thermal treatment indicated.

Sealing materials	Test conditions	Number of cycles	Notes
430SS/ glass 50/YSZ	800ºC, 24 hours, wet forming gas	10	Still on test; glass prepared at UMR
430SS/ glass 50/Ni-YSZ	800ºC, 24 hours, wet forming gas	4	Still on test; glass prepared at UMR
430SS/ glass 50/Ni-YSZ	800ºC, 24 hours, air	10	Still on test; glass prepared at UMR
430SS/ glass 50/YSZ	800ºC, 24 hours, air	9	Failed after ninth cycle; glass prepared by commercial vendor
430SS/ glass 50/Ni-YSZ	800ºC, 24 hours, wet forming gas	4	Failed after fourth cycle; glass prepared by commercial vendor

Conclusions and Future Directions

- Promising sealing glass compositions have been developed and evaluated.
- Hermetic seals have been fabricated and tested at room temperature after thermal treatments at operational temperatures.
- Glass crystallization kinetics have been evaluated using new DTA techniques.
- Optimize glass compositions for commercial suppliers and commercial processing techniques.

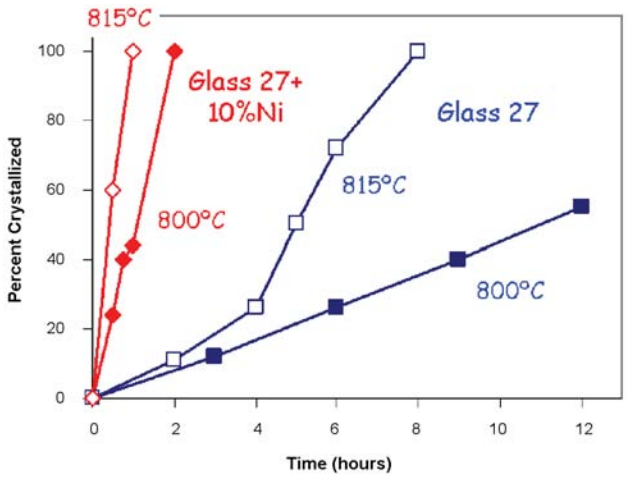

FIGURE 4. Crystallization Kinetic Isotherms for Glass 27 with and without 10 vol% Ni Added

- Characterize viscosity and creep properties of sealing glasses.
- Complete characterization of long-term, high temperature interfacial reactions between glasses and SOFC components.
- Produce and characterize 'at temperature' hermetic seals between SOFC component materials using new glasses.

Special Recognitions & Awards/Patents Issued

1. R.K. Brow, S. T. Reis, G. M. Benson, "Glass and glass-ceramics for solid oxide fuel cell hermetic seals," US Patent Application, UM Disclosure No. 04UMR023 entitled "Glass and Glass-Ceramic Sealant Compositions," filed January 2005.

FY 2006 Publications/Presentations

1. S.T. Reis, R.K. Brow, "Designing Sealing Glasses for Solid Oxide Fuel Cells," Journal of Materials Engineering and Performance, 15[4], XXX-XXX, (2006)- (Proceedings of the ASM Materials Solution Conference, Fuel Cells: Materials, Processing and Manufacturing Technologies, Columbus, OH Oct. 18-20, 2004).

2. T. Zhang*, S. T. Reis, R. K. Brow, and C.S. Ray, "Crystallization Studies of SOFC Sealing Glasses," 3rd International Symposium on Solid Oxide Fuel Cell: Materials and Technology, 30th International Conference & Exposition on Advanced Ceramics & Composites, Cocoa Beach, FL, Jan. 22-27, 2006.

3. S.T. Reis*, R.K. Brow, and T. Zhang, "Glass-Ceramic Seals for Solid Oxide Fuel Cells: Thermo-Phase Stability," 3rd International Symposium on Solid Oxide Fuel Cell: Materials and Technology, 30th International Conference &

Exposition on Advanced Ceramics & Composites, Cocoa Beach, FL, Jan. 22-27, 2006.

4. S.T. Reis, R.K. Brow. P. Jasinski, and T. Zhang, "Properties of Glass-Ceramic Seals for Solid Oxide Fuel Cells," proceedings of the 3rd International Symposium on Solid Oxide Fuel Cells, 30th International Conference & Exposition on Advanced Ceramics & Composites, Cocoa Beach, FL, Jan. 22-27, 2006.; accepted for publication by the American Ceramic Society, 3/14/06.

5. T. Zhang, C.S. Ray, S.T.Reis, and R.K. Brow, "Isothermal Crystallization of Solid Oxide Fuel Cell Sealing glass by Differential Thermal Analysis," J. Amer. Ceram. Soc. (in preparation).

References

1. J.W. Fergus, *J. Power Sources*, 147 46-57 (2005).

2. C. S. Ray, T. Zhang, S. T. Reis and R. K. Brow, "Determining Kinetic Parameters for Isothermal Crystallization of Glasses," *Nucleation and Crystal Growth in Glasses and Liquids*, (submitted).

III.A.29 Thermochemically Stable Sealing Materials for Solid Oxide Fuel Cells

Objectives

- Develop 'invert' glasses with requisite properties and chemical stability for hermetic seals for solid oxide fuel cells (SOFCs).
- Develop processing techniques to fabricate hermetic seals for SOFC components.
- Demonstrate hermeticity and materials compatibility for seals under SOFC operational conditions.

Accomplishments

- Developed alkaline earth/zinc silicate glasses that form glass-ceramics with requisite thermal properties, including sealing temperatures at or below 900ºC and coefficients of thermal expansion (CTE) in the range of 10-12x10^{-6}/ºC.
- Demonstrated stability of promising sealing materials under SOFC operational conditions; e.g., stable CTE and low material volatility at temperatures up to 800ºC, for up to 100 days, in air and in wet forming gas.
- Produced hermetic seals between interconnect alloys and SOFC components, including Y-stabilized zirconia (YSZ) electrolytes and Ni-YSZ anodes, that pass He-leak tests after at least ten thermal cycles between 800ºC and room temperature.

Richard K. Brow (Primary Contact), Signo T. Reis, Teng Zhang
University of Missouri-Rolla
Department of Materials Science & Engineering
222 McNutt Hall
Rolla, MO 65409-0330
Phone: (573) 341-4401; Fax: (573) 341-6934
E-mail: brow@umr.edu

DOE Project Manager:
Ayyakkannu Manivannan
Phone: (304) 285-2078
E-mail: Ayyakkannu.Manivannan@netl.doe.gov

Technical Advisor: Dr. Ronald E. Loehman
Sandia National Laboratories
Phone: (505) 272-7601; E-mail: loehman@sandia.gov

Introduction

Solid oxide fuel cells (SOFCs) are multi-layered structures formed primarily from high-purity metal oxide components, including an ionic conducting electrolyte, which generate electricity from the electrochemical oxidation of a fuel source. Within the SOFC stack, an effective seal must have a thermal expansion match to the fuel cell components, must be electrically insulating and must be thermochemically stable under the operational conditions of the stack. The seal should exhibit no deleterious interfacial reactions with other cell components, should be stable under both the high temperature oxidizing and reducing operational conditions, should be created at a low enough temperature to avoid damaging other cell components (under 900ºC for some materials), and should not migrate or flow from the designated sealing region during sealing or cell operation. In addition, the sealing system should be able to withstand thermal cycling between the operational temperature and room temperature. That is, thermal stresses that develop because of mismatches in the thermal contraction characteristics of the different SOFC materials must either be reduced to well below the failure strengths of the materials or must be relieved in some fashion. Finally, the sealing material should not adversely react with other SOFC components, to avoid producing deleterious interfacial reaction products or to volatilize and contaminate components elsewhere in the cell.

There have been many attempts to develop seals for planar SOFCs using a wide variety of glass and glass-ceramic compositions; see the review by Fergus [1] for many compositional examples. Most materials have drawbacks, including thermal expansion mismatches, excessive sealing temperatures, and long-term interfacial reactivity with other fuel cell materials. Thus, the seal has become a critical need for meeting the long-term operational milestones of the DOE fuel cell programs. The materials developed in the present project have unusual structural characteristics that contribute to a desirable set of thermal and chemical properties required for SOFC seals.

Approach

The glasses developed at the University of Missouri-Rolla (UMR) have relatively low silica contents (<45 mole%) and so possess molecular-level structures that are much less connected than conventional silicate

glasses. These depolymerized structures contribute to desirably low viscosities at the sealing temperatures (900ºC), and lead to the formation of crystalline phases that possess relatively high CTEs and good thermal stabilities when the seals are crystallized to form glass-ceramics. The glass compositions are designed to avoid the formation of deleterious interfacial reaction products, like the Ba-chromates that form when BaO-containing glasses are sealed to ferritic interconnect alloys [2].

Results

Over fifty glass compositions have been prepared and evaluated. Many of the compositions have the requisite thermal properties required for SOFC seals (e.g., CTE match to SOFC components and sealing temperatures at or below 900ºC) and have been included in long-term materials stability experiments. The properties of two representative compositions are summarized in Table 1. Glass 27 has a CTE match to YSZ and glass 50 has a CTE that is intermediate to Cr-containing ferritic steel interconnect alloys and YSZ. Both glasses can be sealed and crystallized at or below 900ºC.

Of particular concern for SOFC seals is the long term stability of the properties of the sealing glasses. Figure 1 shows that the average CTE (over the temperature range from room temperature to 600ºC) of glass 27 and of glass 50 does not change with time at 800ºC for up to several months. X-ray diffraction studies (not shown) of the materials reveal that the dominant crystalline phases present in these glass-ceramics (Table 1) do not change with time at temperature. This phase stability is necessary if these glasses are to fulfill the fuel cell program requirements for functional SOFC lifetimes in excess of 10,000 hours at operational temperatures (700-800ºC).

TABLE 1. Characteristics of UMR Sealing Glass-Ceramics

	Major crystalline phases	Sealing conditions	CTE after sealing
Glass 27	$CaSrAl_2SiO_7$, $Ca_2ZnSi_2O_7$	850ºC/2 hours	$10.0x10^{-6}$/ºC
Glass 50	$Sr_2Al_2SiO_7$, $CaSrSiO_4$	900ºC/5 min, then 800°C/2 hrs	$11.5x10^{-6}$/ºC

Seals between YSZ and ferritic interconnect alloys have been prepared with the glasses developed in this project. Sealing materials include tapes and pastes prepared using materials and techniques based on commercial processes. Figure 2 shows a scanning electron micrograph of the interface between a glass 27 tape and a Cr-ferritic steel substrate after the seal was held at 750ºC for 100 hours. The crystalline microstructure of the glass-ceramic is evident in the micrograph, and there are no obvious heterogeneities at the glass/metal interface that indicate deleterious interfacial reactions. Ron Loehman (Sandia National Labs, Albuquerque, NM) has performed detailed analytical electron microscopic studies of interfaces between glass 27 and different SOFC component materials, including YSZ electrolytes, Ni-YSZ anodes, and several different Cr-containing ferritic interconnect alloys, and reports good wetting and good chemical compatibility of the glass with these different materials. For example, little Ni or Cr diffuses from the anode or the interconnect alloy, respectively, into the sealing glass after several days at elevated temperatures.

A series of simple seals have been fabricated and their hermeticity has been tested at room temperature using helium gas (2 psig). Figure 3 shows a photograph of one of these samples; this sample is about 25 mm

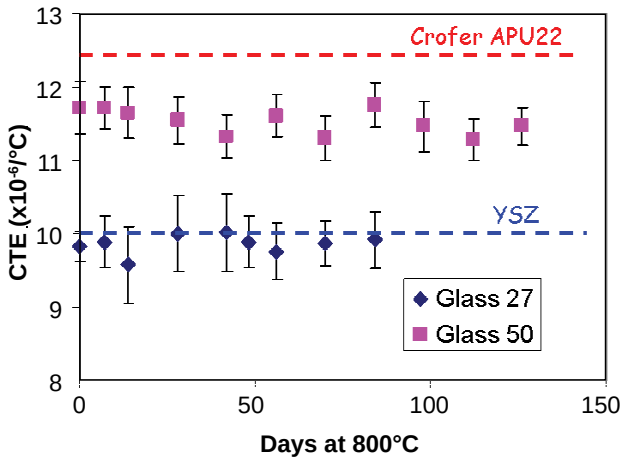

FIGURE 1. CTE for UMR Sealing Glass-Ceramics as a Function of Time in Air at 800ºC

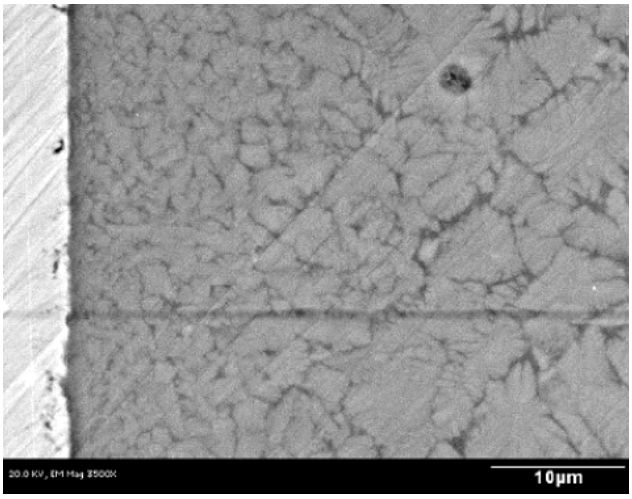

FIGURE 2. Scanning Electron Micrograph of the Interface of a Glass 27 (right)/Crofer APU 22 Seal after 100 Hours at 750ºC

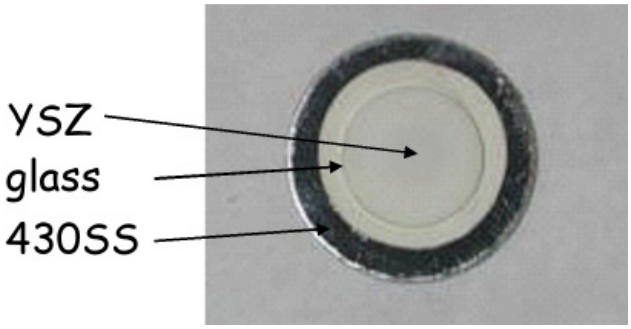

FIGURE 3. Optical Image of a Seal Couple Used for Helium Hermeticity Tests

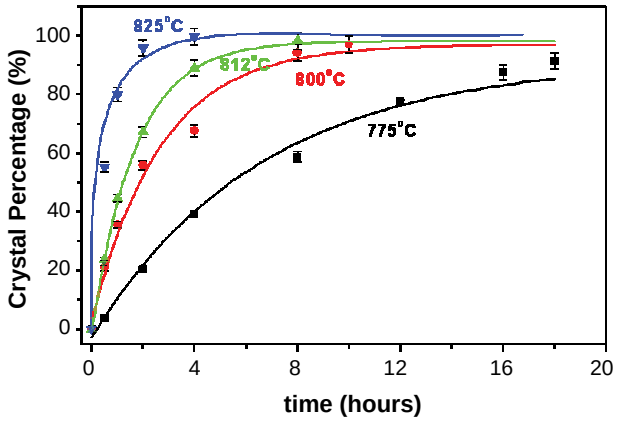

FIGURE 4. Crystallization Kinetics Curves for Glass 27 Obtained by Isothermal DTA Analyses

in diameter. The seals were fabricated using glass tapes (PVB binder, 10 μm glass particles) fired in air to 850-900ºC, between 430SS as the interconnect material and either YSZ (electrolyte) or Ni-YSZ (anode) substrates. These test samples were heated to 800ºC, at 2ºC/minute, in different atmospheres, held for 24 hours, then cooled to room temperature (-2ºC/minute) where they were tested for hermeticity using helium gas at 2 psig. Samples that did not leak (hold 2 psig for four hours) were reheated for another 800ºC/24 hour heat treatment, and cycled back to room temperature for another hermeticity test. Table 2 summarizes the results of some of these tests. Glasses fabricated both by UMR and by a commercial vendor have been evaluated.

TABLE 2. Summary of thermal cycling/hermeticity tests on sealed components. All tests were done using helium at room temperature, following the thermal treatment indicated.

Sealing materials	Test conditions	Number of cycles	Notes
430SS/glass 50/YSZ	800ºC, 24 hours, wet forming gas	10	Still on test; glass prepared at UMR
430SS/glass 50/Ni-YSZ	800ºC, 24 hours, wet forming gas	4	Still on test; glass prepared at UMR
430SS/glass 50/Ni-YSZ	800ºC, 24 hours, air	10	Still on test; glass prepared at UMR
430SS/glass 50/YSZ	800ºC, 24 hours, air	9	Failed after ninth cycle; glass prepared by commercial vendor
430SS/glass 50/Ni-YSZ	800ºC, 24 hours, wet forming gas	4	Failed after fourth cycle; glass prepared by commercial vendor

Quantitative studies of SOFC glass crystallization behavior have been performed using differential thermal analysis (DTA) techniques developed at UMR [3]. By considering changes in the areas of crystallization exothermic peaks from DTA analyses of glass samples following isothermal heat treatments, the fraction of glass crystallized can be determined. An example of these analyses is shown in Figure 4 for glass 27 particles about 100 μm in diameter. These experiments have provided useful processing related information used to optimize sealing times and temperatures. In addition, these experiments have shown the effects of glass particle size on crystallization kinetics, and have shown how the addition of a second phase, intended to modify CTE, also affects crystallization kinetics.

Conclusions and Future Directions

- Promising 'invert' sealing glass compositions have been developed and evaluated.
- Hermetic seals have been fabricated and tested at room temperature after thermal treatments at operational temperatures.
- Glass crystallization kinetics have been evaluated using new DTA techniques.
- 'Invert' glass compositions for commercial suppliers and commercial processing techniques will be optimized.
- Viscosity and creep properties of sealing glasses will be characterized.
- We will complete characterization of long-term, high temperature interfacial reactions between glasses and SOFC components.
- We will produce and characterize 'at temperature' hermetic seals between SOFC component materials using new 'invert' glasses.

Special Recognitions & Awards/Patents Issued

1. R.K. Brow, S. T. Reis, G. M. Benson, "Glass and glass-ceramics for solid oxide fuel cell hermetic seals," US Patent Application, UM Disclosure No. 04UMR023 entitled "Glass

and Glass-Ceramic Sealant Compositions," filed January 2005.

FY 2006 Publications/Presentations

1. S.T. Reis, R.K. Brow, "Designing Sealing Glasses for Solid Oxide Fuel Cells," Journal of Materials Engineering and Performance, 15[4], XXX-XXX, (2006)- (Proceedings of the ASM Materials Solution Conference, Fuel Cells: Materials, Processing and Manufacturing Technologies, Columbus, OH Oct. 18-20, 2004).

2. T. Zhang*, S. T. Reis, R. K. Brow, and C.S. Ray, "Crystallization Studies of SOFC Sealing Glasses," 3rd International Symposium on Solid Oxide Fuel Cell: Materials and Technology, 30th International Conference & Exposition on Advanced Ceramics & Composites, Cocoa Beach, FL, Jan. 22-27, 2006.

3. S.T. Reis, R.K. Brow, and T. Zhang, "Glass-Ceramic Seals for Solid Oxide Fuel Cells: Thermo-Phase Stability," 3rd International Symposium on Solid Oxide Fuel Cell: Materials and Technology, 30th International Conference & Exposition on Advanced Ceramics & Composites, Cocoa Beach, FL, Jan. 22-27, 2006.

4. S.T. Reis, R.K. Brow. P. Jasinski, and T. Zhang, "Properties of Glass-Ceramic Seals for Solid Oxide Fuel Cells," proceedings of the 3rd International Symposium on Solid Oxide Fuel Cells, 30th International Conference & Exposition on Advanced Ceramics & Composites, Cocoa Beach, FL, Jan. 22-27, 2006.; accepted for publication by the American Ceramic Society, 3/14/06.

5. T. Zhang, C.S. Ray, S.T.Reis, and R.K. Brow, "Isothermal Crystallization of Solid Oxide Fuel Cell Sealing glass by Differential Thermal Analysis," J. Amer. Ceram. Soc. (in preparation).

References

1. J.W. Fergus, *J. Power Sources*, 147 46-57 (2005).

2. C. S. Ray, T. Zhang, S. T. Reis and R. K. Brow, "Determining Kinetic Parameters for Isothermal Crystallization of Glasses," *Nucleation and Crystal Growth in Glasses and Liquids*, (submitted).

3. Z. Yang , J. W. Stevenson, and K. D. Meinhardt, *Solid State Ionics*, 160 213-222, (2003).

III.A.30 Fundamental Studies of the Durability of Materials for Interconnects in Solid Oxide Fuel Cells

Objectives

- Develop mechanism-based evaluation procedures for the stability of SOFC interconnect materials and use these procedures to study and modify a group of alloys, which have already been identified as candidate interconnect materials, i.e., ferritic stainless steels.
- Study fundamental aspects underlying the thermomechanical behavior of interconnect materials and develop accelerated testing protocols. (CMU Subcontract)
- Investigate the potential for the use of "new" metals as interconnect materials.
- Develop a durable, conductive ceramic/metal (cermet) material, suitable for long-term use as a contacting material in the cathode chamber of a SOFC. (WVU Subcontract)

Accomplishments

- Determined that even very small concentrations of Al or Si in ferritic alloys (on the order of tenths of a percent) result in the formation of internal films with high electrical resistivity.
- Discovered that exposure under some fuel cell operating conditions (e.g., water vapor) accelerates sigma phase formation in some ferritic stainless steels. Alloy purity is also important for retarding sigma phase formation.
- Discovered that it is possible to modify a ferritic stainless steel to form an overlayer of TiO_2 which suppresses the evaporation from the underlying chromia scale.
- Determined that the growth rate of chromia on ferritic alloys can be greatly suppressed by surface doping with CeO_2.
- Found that the growth rate of NiO can be slowed significantly by surface doping with SrO or CeO_2.
- Found that, unlike ferrous alloys, the oxidation of Ni is not altered significantly under dual atmosphere conditions.
- Showed that Ni interconnects containing Ag conduction paths are feasible.
- Developed an image analysis technique for analyzing indentation-induced chromia scale flaking failures for interconnects exposed in wet air [simulated cathode gas (SCG)].
- Exposed 26 Cr Ferritic alloy specimens to a range of short-term SCG exposures at 900°C, performed indentation tests, and tracked the evolution of flaking-type spallation failures with exposure.
- Completed three M.S. theses and six Senior Projects.

Gerald H. Meier (Primary Contact),
Frederick S. Pettit
Department of Materials Science and Engineering
848 Benedum Hall
University of Pittsburgh
Pittsburgh, PA 15261
Phone: (412) 624-9720; Fax: (412) 624-8069
E-mail: ghmeier@engr.pitt.edu, pettit@engr.pitt.edu

DOE Project Manager:
Ayyakkannu Manivannan
Phone: (304) 285-2078; Fax: (304) 285-4403
E-mail: Ayyakkannu.Manivannan@netl.doe.gov

Subcontractors:

1. Jack L. Beuth, Carnegie Mellon University (CMU)
Phone: (412) 268-3873; Fax: (412) 268-3348
E-mail: beuth@andrew.cmu.edu

2. James R. Rakowski, ATI Allegheny Ludlum
Phone: (724) 226-6383; Fax: (724) 226-5067
E-mail: JRakowski@AlleghenyLudlum.com

3. Bruce Kang, West Virginia University (WVU)
Phone: (304) 293-3111 x2316; Fax: (304) 293-6689
E-mail: bruce.kang@mail.wvu.edu

Introduction

Solid oxide fuel cells provide a potential way to generate electricity with high efficiency and low pollution. The operating principles of fuel cells have been known for over 100 years, and low-temperature fuel cells provided the electric power on all the Gemini and Apollo spacecraft. However, fuel cells have not achieved widespread commercial use for a number of economic and technical reasons.

One of the most important technical challenges for solid oxide fuel cells, which operate in the temperature range 700°-900°C, is the design of interconnects (current collectors). These components, in addition to electrically connecting individual cells in a stack, must separate the anode compartment of one cell from the cathode compartment of the adjacent cell. This means that one side of an interconnect is exposed to the fuel, typically hydrogen or hydrocarbons in which the oxygen partial pressure is low, and the other side is exposed to the oxidant, which is typically air with some amount

of water vapor. Metallic alloys have many attractive features as potential interconnect materials.

Oxidation resistant alloys are designed to form one of three protective oxides: alumina, silica, or chromia. Of these, the electrical resistivities of alumina and silica are much too high for interconnect applications. For metallic interconnects, interconnect system resistance can be greatly increased by oxide layer thickening and spallation. For chromia formers, evaporation of the chromia scale can severely degrade cathode performance. Thus, chromia scale growth, scale spallation and scale evaporation are the three principal "failure mechanisms" for interconnects forming chromia scales on their surfaces. Because the mechanisms are coupled, alloy changes to address one failure mechanism can affect one or more of the other failure mechanisms, making alloy design a complex task.

Approach

The project consists of four major tasks aligned with its four objectives.

Task 1. Mechanism-based Evaluation Procedures

A variety of chromia-forming interconnect alloys are being subjected to thermal cycling in air, in simulated anode gas (Ar-H_2-H_2O) and with simultaneous exposure to air on one side and simulated anode gas on the other. Combined exposures have been shown at Pacific Northwest National Laboratory to often yield different behavior than exposures with the same gas on both sides of the specimen. Exposure temperatures range from 700°C to 900°C. Oxidation kinetics is being tracked by mass change measurements, and corresponding changes in oxide scale resistances are being measured. Exposed specimens are being examined in cross-section by scanning electron microscopy (SEM) to document changes in structure with exposure.

Methods are being studied to slow the growth of chromia scales on Cr and Ferritic alloys with exposure, to decrease the contribution of the scale to interconnect resistance. The effect of alloying additions (e.g., Mn, Ti) to ferritic steels to reduce harmful CrO_3 and $CrO_2(OH)_2$ evaporation by forming a sealing outer layer over the chromia scale is being evaluated. The ability of chromite coatings to reduce evaporation from chromia-forming interconnect alloys is also being investigated.

Task 2. Fundamental Aspects of Thermomechanical Behavior (CMU)

Understanding the resistance of growing chromia scales to spallation requires a fundamental understanding of the mechanics of chromia adhesion. From a fracture mechanics standpoint, the adherence of protective oxide scales to alloy substrates is governed by 1) the stored elastic energy in the scale, which drives delamination, and 2) the fracture toughness of the alloy/oxide interface, which quantifies the resistance to fracture.

The stored elastic energy in the scale is increased by increases in the scale thickness (which can be measured by cross-section SEM) and increases in the residual stress in the scale. In this task, x-ray diffraction (XRD) is being used to measure stresses in chromia films formed on pure chromium and chromia-forming alloys after the exposures described for Task 1.

An indentation test is also being used to quantify the fracture toughness of chromia/alloy interfaces for the same exposures. In the test, the chromia scale is penetrated by the indenter, and the plastic deformation of the underlying substrate induces compressive radial strains in the substrate. These strains are transferred to the scale, and the associated scale stress drives scale spallation. Scales can spall as intact coatings, with an interface crack propagating radially outward, or spallation can occur as the debonding of small flakes, with the density of flaking decreasing with distance from the indent. The interfacial toughness can be estimated from the results of a mechanics analysis of the indentation problem and a measurement of the extent of the delamination failures.

Task 3. Alternative Material Choices

Metallic materials other than chromia-formers are being considered for use as low-temperature SOFC interconnects. Experiments similar to those described for Task 1 are being performed on pure Ni. Its only oxide, NiO, has no vapor species with high partial pressures and has a higher electrical conductivity than chromia. Also, NiO should not even form in the anode gas. The doping of the NiO scale with SrO or CeO_2 is being investigated as a way to slow the growth rate. Finally, the use of Ag conducting paths through Ni interconnects is being studied.

Task 4. Development of Durable Contacting Material (WVU)

At present, candidate cermets have been developed by ball-milling of various oxide powders with silver or silver-oxide powders, followed by dry-pressing and sintering in a high-temperature furnace. The cermets are evaluated by SEM to determine the compatibility of silver with the candidate oxide materials, as well as the dispersion of silver throughout the cermet. The cermets are also tested for hardness/ductility using Vickers hardness testing. At this time, conductivity is evaluated using a simple multimeter test to evaluate the resistance of the cermet. A thermomechanical analyzer is also used to evaluate the coefficient of thermal expansion of the materials to verify compatibility with

other SOFC components. Lastly, cermets are placed in a high-temperature furnace to be exposed to the SOFC operating temperature (~800˚C), while a high-volume air flow is introduced to simulate the cathode environment of the SOFC.

All measurements–conductivity, hardness, and mass–are taken before and after exposure to the simulated cathode environment in order to make a determination of the effects on the cermet material.

Results

Task 1. Mechanism-based Evaluation Procedures

In attempts to reduce the growth rate of chromia and, therefore, the electrical resistance, E-Brite samples have been doped with CeO_2 using pulsed laser deposition. Oxidation experiments for 100 hours at 800°C in air show that the doping drastically reduced the thickness of the chromia scale.

Sigma phase was observed to form at 700°C in the alloys with higher chromium concentrations, e.g., 26 Cr Ferritic and E-BRITE. Sigma phase is promoted in these alloys by the presence of Mo. (Additions of W would have a similar effect.) It was also found that impurity elements, such as Si, accelerated the formation of the sigma phase, e.g., 26 Cr Ferritic developed this phase more rapidly than did E-BRITE. A previously unknown result was that sigma phase formation was dramatically accelerated in atmospheres containing water vapor. Sigma phase must be avoided since it is very brittle and tends to crack.

It was found that even small amounts of Al or Si (less than 0.5 wt %) in ferritic steels result in the formation of continuous alumina or silica films, which greatly increases the area specific resistance. Therefore, future alloy development should hold these elements to the minimum values possible.

A major problem with chromia-forming alloys is oxide volatility as CrO_3, particularly in the cathode gas, since the CrO_3 partial pressure increases with oxygen partial pressure. The volatile species are reduced at electrochemically active sites on the cathode during SOFC operation, which inhibits the required oxygen reduction. Analysis of the Cr vapor species indicates that water contents above about 0.1% in air result in partial pressures of $CrO_2(OH)_2$ which exceed the partial pressure of CrO_3 and result in cathode poisoning. There are three potential solutions to this problem:

1. Develop cathode materials that are not affected by Cr contamination.
2. Suppress the evaporation of Cr species from ferritic alloys.
3. Develop Cr-free materials with suitable interconnect properties.

The latter two approaches are being pursued in this research. Approach 3 is described in Task 3 below.

An ideal approach to suppressing Cr volatility would be to develop an alloy which forms a Cr-free oxide overlayer. Experiments on Ni-base superalloys indicated that Ti additions might provide such a layer. Four heats of novel Fe-Cr-Ti alloys with Ti contents varying between 1 and 4 wt% and one Ti-free control heat were produced in a vacuum induction melting furnace in the form of fifty-pound ingots at ATI Allegheny Ludlum. Isothermal and cyclic oxidation experiments indicate that indeed these alloys can form a continuous TiO_2 overlayer, and this layer is very effective in reducing chromia evaporation. A patent disclosure has been filed, and this alloy system is being vigorously pursued.

Task 2. Fundamental Aspects of Thermomechanical Behavior (CMU)

Previous reports have described the indentation fracture testing of ferritic stainless steel alloys exposed to simulated anode gas (SAG) $Ar/H_2/H_2O$ environments. Indented chromia scales formed in SAG debond as an intact coating, and the radial extent of the debonding observed in short-term exposures has been used to estimate the long-term exposure time when spallation can occur. Previous reports also presented indentation results for ferritic stainless steels exposed in air with 0.1 atm H_2O, representing a moist SCG environment. When indented, those specimens exhibited a flaking type of debonding with a decreasing density of flaking with radial distance from the indent. Results for both types of tests are summarized in the paper by Dhanaraj et al. [1].

In this past year, an image analysis technique has been developed to analyze the failures seen in SCG-exposed interconnects. In these specimens, bonded areas are black or dark grey, which is the shade of the chromia scale. Areas of spallation appear white or very light grey due to the exposed metal substrate. The imaging technique involves quantifying the distribution of white/grey/black pixels in a single image in regions far from the indentation. The distributions of greys in 5-7 rings around the indentation are also determined. The percentage of debonding in a ring is determined by subtracting the distributions of grey from that ring from the far-field image distribution. The result from the analysis of multiple rings is a plot of the percentage of debonding scale vs. radial distance from the debond. Results from images taken after different exposures allow the tracking of debonding vs. radius as a function of exposure.

Figure 1 gives an example of results from this type of analysis. In the figure, images from indentation of a 26 Cr Ferritic alloy exposed in SCG from 10 to 200 hours have been analyzed. Images at 10 and 200 hours are included in the figure, as is a plot of the percentage of debonding vs. R/a for different exposures. R is the

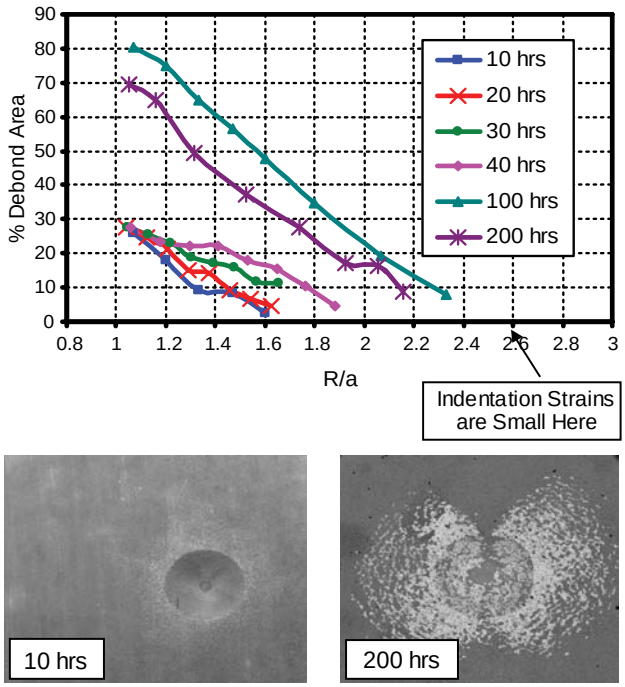

FIGURE 1. Percentage of Debonding vs. Radial Distance for a 26 Cr Ferritic Alloy Exposed in Wet Air (Simulated Cathode Gas) at 900°C for 10 – 200 Hours

radial distance from the indentation and a is the radius of the indentation. The images taken in these tests show a fairly consistent decrease in debonding density with radius and an increase in debonding density with exposure. Plots of debond percentage vs. R/a from the image analyses are consistent with these qualitative observations. As exposures are increased, the curves of percentage debonding rise, but the increases in debonding stop at 100-200 hours of exposure. At this point, some amount of debonding is observed even at radial distances where the strains due to indentation are almost zero.

The conclusion from these results is that after 100-200 hours of exposure in SCG at 900°C, spontaneous spallation (spallation that can occur without the use of indentation) has begun to occur. At this point, spontaneous spalls (and perhaps some scale evaporation) act to keep the average thickness of the chromia scale more or less constant, so that plots of debond percentage vs. R/a reach a steady-state. This is consistent with weight gain measurements performed as part of Task 1 of this project. Weight gains in these specimens stop after 100 hrs of exposure, and specimen weight remains constant from that point on.

Task 3. Alternative Material Choices

Experiments are being carried out on pure Ni as a possible alternative interconnect material since the oxygen partial pressure in the anode gas is too low to oxidize Ni. The primary challenge in making Ni perform satisfactorily as an interconnect is to reduce the electrical resistance of the thermally grown oxide that forms on the cathode side during fuel cell operation.

Efforts to decrease the electrical resistance of the interconnect oxide are twofold. First, we are trying to reduce the scale thickness by the use of surface dopants. Pulsed laser deposition is used to deposit thin films of SrO and CeO_2 onto the surface of nickel. Our tests have shown that CeO_2 decreases the thickness of NiO by a factor of 4 (Figure 2) and SrO doping decreases it by a factor of 2. Area specific resistance is proportional to scale thickness, and the resistance decreases accordingly. These dopants can be deposited by inexpensive techniques once the optimum dopants are identified.

Finally, the resistance introduced by the thermally grown oxide is being by-passed by the use of high-conductivity pathways. Silver is not considered as a possible interconnect material due to the high permeability of hydrogen and oxygen in silver, which causes water nucleation and mechanical instability. However, silver may be able to provide a high-conductivity pathway through another material. Systems in which silver wires are passed through nickel and silver powder is melted into holes drilled in nickel are being examined. Figure 3 shows the cross-section of a Ni specimen where Ag has been melted in a hole drilled in the Ni. After exposure there is some porosity in the silver, and it appears the grain boundaries are delineated with pores far into the silver. Importantly, despite the porosity, the specimen had resistance values typical of a metal when measured at room temperature following exposure. In this configuration, the Ni provides the physical integrity of the interconnect and the silver only provides the conduction path through the scale.

Task 4. Development of Durable Contacting Material (WVU)

Samples have been fabricated using various compositions of silver and differing oxides such as lanthanum strontium manganese oxide (LSM) and copper oxide. The samples were fabricated by dry

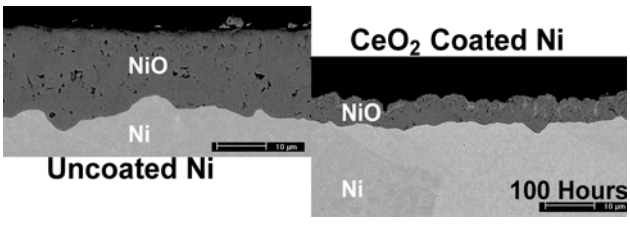

FIGURE 2. Effect of CeO_2 Deposited by Pulsed Laser Deposition on the Growth Rate of NiO at 800°C in Dry Air

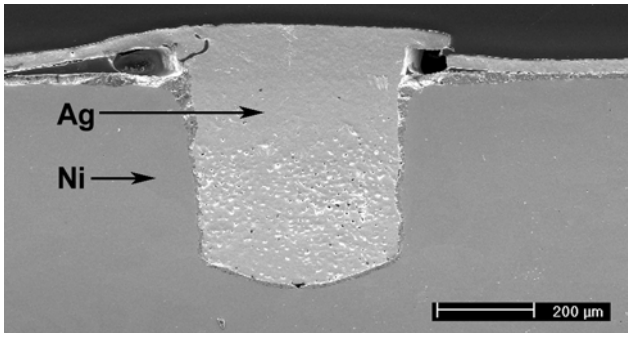

FIGURE 3. Silver Via, 800°C, 100 hours, exposed under dual atmospheric conditions. The upper surface was exposed to dry air while the lower surface was exposed to simulated anode gas of Ar-10%H_2O-4%H_2.

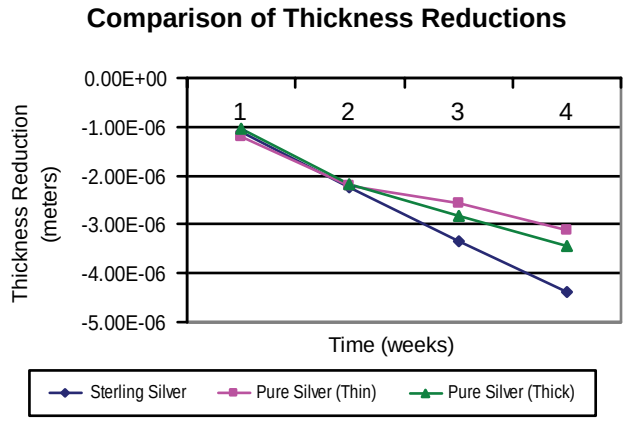

FIGURE 4. Comparison of Thickness Reductions for Various Silver Samples

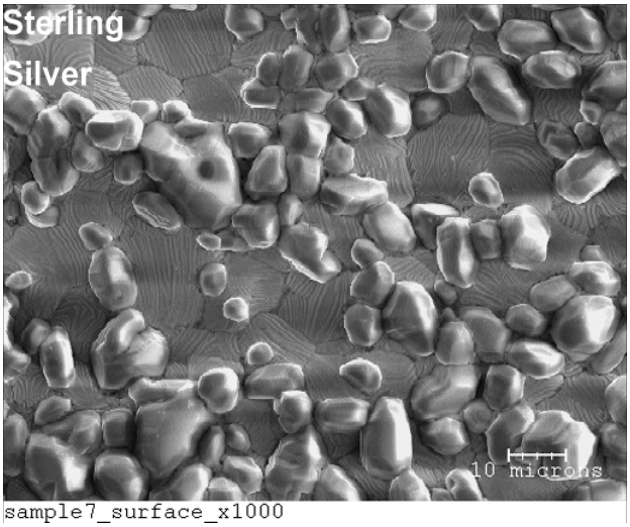

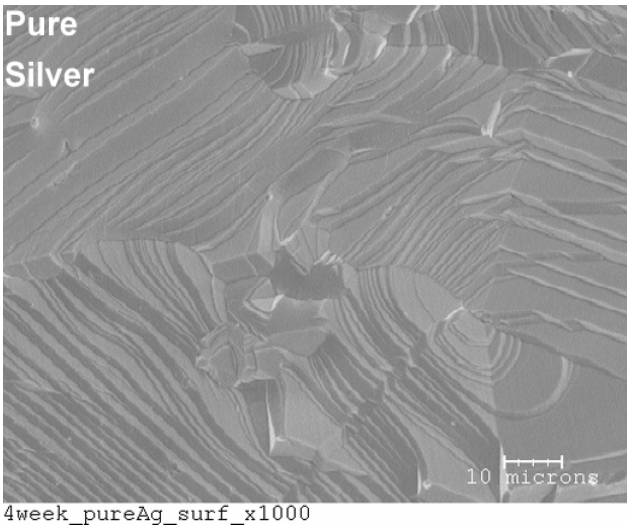

FIGURE 5. SEM Micrograph Comparison of Sterling and Pure Silver Samples after 3-Week High-Temperature Exposure

pressing followed by sintering at high temperature for various periods of time. It was determined that this method did not result in samples that were robust enough for use in the high-temperature evaporation experiments. In order to fabricate samples that were durable enough for testing, it was decided that the method of fabrication be modified. Instead of the ball-milling/pressing/sintering method previously used, it was decided that the oxidation of specific alloys would be a simpler method to produce reliable samples.

Sterling silver has been identified as a candidate for use as a contacting material due to its favorable composition and low cost. Upon oxidation, the copper in the sample becomes copper oxide, which is meant to act as a barrier against evaporation of the silver in the sample, extending the usable life of the cermet. Sterling silver is currently being tested in high-temperature exposure alongside pure silver to gain an understanding of the performance of copper oxide in protecting against silver evaporation. Early results are shown in Figure 4.

It appears that all samples exhibit similar evaporation behavior very early on; however, after several weeks, it appears that the rate of loss for the pure silver samples is lower than that for the sterling silver sample. Samples are also regularly examined for surface changes due to high-temperature exposure. Examples of SEM micrographs for exposed samples are shown in Figure 5.

The sample surfaces exhibit clearly different behavior which may affect the evaporation rates of the samples. Future work will continue to examine the evaporation of sterling silver over long-term high-temperature conditions to evaluate the effect of copper oxide on silver evaporation rate as well as examine surface microstructure changes of the sample.

Another method of fabrication utilizing ball-milling/pressing/hot-pressing is also being developed to fabricate samples composed of Ag/LSM and Ag/cerium. The hot-pressing technique is meant to aid in better dispersion of oxide in the sample as well as make the sample more suitable in terms of robustness for the long-term high-temperature testing.

Conclusions and Future Directions

The project is currently operating under a no-cost extension with an end-date of June 30, 2006. The remaining activities will be completion of a study of methods to seal cracks in $LaCrO_3$ coatings on ferritic alloys and the preparation of the final report.

Special Recognitions & Awards/Patents Issued

1. Provisional patent application: "Iron-chromium-titanium Alloys that Restrict Evaporation of Chromium-containing Vapor Species at Elevated Temperatures"

FY 2006 Publications/Presentations

1. J. E. Hammer, S. J. Laney, R. W. Jackson, F. S. Pettit, and G. H. Meier, "Oxidation Problems Associated with Interconnects in Solid Oxide Fuel Cells", ASM International/TMS, "Materials Solutions", Pittsburgh, PA, September 2005.

2. Q. Ma and J. L. Beuth, Carnegie Mellon University; F. S. Pettit, G. H. Meier, and M. J. Stiger, University of Pittsburgh, "Use of Indentation Fracture Tests to Investigate Toughness Loss Mechanisms in Thermal Barrier Coating Systems", ASM International/TMS, "Materials Solutions", Pittsburgh, PA, September 2005.

3. J. L. Beuth and N. Dhanaraj, Carnegie Mellon University; J. E. Hammer, S. J. Laney, F. S. Pettit, and G. H. Meier, University of Pittsburgh, "Interfacial Fracture Testing to Evaluate the Durability of SOFC Interconnect Alloys", ASM International/TMS, "Materials Solutions", Pittsburgh, PA, September 2005.

4. Professors F. S. Pettit and G. H. Meier presented a two-day course (September 22-23, 2005) on "Science and Technology of Advanced Metallic Systems for Applications in Intermediate Temperature Solid Oxide Fuel Cells (SOFCs)" at the National Energy Technology Laboratory (NETL). The course was attended by approximately thirty scientists and engineers at the NETL site in Morgantown, WV and webcast to universities, national laboratories, and industrial laboratories around the U. S.

5. S. J. Laney, R. W. Jackson, F. S. Pettit, and G. H. Meier, University of Pittsburgh; J. R. Rakowski, ATI-Allegheny Ludlum, "The Effects of Dual Environments and Chromia Evaporation on Metallic Interconnect Behavior", TMS Annual Meeting, San Antonio, TX, March 2006.

6. Q. Ma, J. L. Beuth, F. S. Pettit, G. H. Meier, and M. J. Stiger, "Use of Indentation Fracture Tests to Investigate Toughness Loss Mechanisms in Thermal Barrier Coating Systems", Coatings 2005 (Nitin Padture, Lorraine Francis, Janet Hampikian and Narendra Dahotre, eds.) Proc. Materials Science and Technology 2005, Pittsburgh, September 2005, pp. 3-6.

7. N. Dhanaraj, J. L. Beuth, G. H. Meier, F. S. Pettit, J. Hammer, and S. J. Laney, "Interfacial Fracture Testing to Evaluate the Durability of SOFC Interconnect Alloys", Materials for the Hydrogen Economy (J. J. Petrovic, I. E. Anderson, T. M. Adams, G. Sandrock, C. F. Legzdins, J. W. Stevenson, and Z. G. Yang, eds.), Proc. Materials Science and Technology 2005, Pittsburgh, September 2005, pp. 165-175.

References

1. N. Dhanaraj, J. L. Beuth, G. H. Meier, F. S. Pettit, J. Hammer, and S. J. Laney, "Interfacial Fracture Testing to Evaluate the Durability of SOFC Interconnect Alloys", Materials for the Hydrogen Economy (J. J. Petrovic, I. E. Anderson, T. M. Adams, G. Sandrock, C. F. Legzdins, J. W. Stevenson, and Z. G. Yang, eds.), Proc. Materials Science and Technology 2005, Pittsburgh, September 2005, pp. 165-175.

III.A.31 Electrically Conductive, Corrosion-Resistant Coatings through Defect Chemistry for Metallic Interconnects

Objectives

- To synthesize and characterize coating materials with ultra-low oxygen diffusion coefficient, that are electronically conducive using site-specific doping and through fundamental understanding of defect chemistry, for application on metallic interconnect in intermediate temperature (800°C) solid oxide fuel cells (SOFCs).
- To apply the coatings on low thermal expansion, relatively inexpensive stainless steels and other alloys, and investigate oxidation kinetics in air and fuel atmospheres.
- To conduct a preliminary short stack (4-cell) test, using 5 cm x 5 cm active area cells to validate ex-situ results.
- To initiate work on the development of low-cost processes for the deposition of coatings on metallic interconnects.
- To offer coated interconnect foils to SECA vertical teams under suitable confidentiality agreements.

Approach

- Conduct literature search on the identification of suitable perovskite and nonperovskite materials exhibiting high electronic conductivity but very low oxygen ion conductivity. Non-perovskite materials of interest include spinels and bronzes.
- Synthesize perovskite oxides with transition element on the B-site, with site-specific doping to suppress oxygen vacancy concentration.
- Fabricate sintered bars and discs of the materials. Sintered bars are to be used for the measurement of total conductivity as a function of temperature. Discs are to be used for measuring ionic conductivity using electron blocking electrodes.
- Deposit thin coatings of the materials on stainless steels and nickel-based alloy foils, and investigate oxidation kinetics.
- Conduct theoretical analysis of oxidation kinetics of coated and pristine alloys.
- Develop a method for the measurement of area specific resistance (ASR), and apply it to the foils oxidized under various conditions.

Anil V. Virkar
University of Utah
Department of Materials Science & Engineering
122 S. Central Campus Drive
Salt Lake City, UT 84112
Phone: (801) 581-5396; Fax: (801) 581-4816
Email: anil.virkar@m.cc.utah.edu

DOE Project Manager:
Ayyakkannu Manivannan
Phone: (304) 285-2078
Email: Ayyakkannu.Manivannan@netl.doe.gov

Accomplishments

- Identified a number of materials with low oxygen ion conductivity (possibly lower than 10^{-7} S/cm at 800°C) by taking into account ionic size effect.
- Fabricated $LaMnO_3$ and $LaCrO_3$-based materials with dopant levels as high as 20% on the B-site to suppress oxygen ion conductivity.
- Measured total conductivity over a temperature range from room temperature to 800°C; and measured oxygen ion conductivity at 800°C.
- Sputter-deposited 1 and 3 micron coatings of various materials on Haynes 230, Inconel 718, and SS 430.
- Conducted oxidation studies in air up to 180 days at 800°C for samples having a $LaMnO_3$ based coating.
- Conducted oxidation studies in flowing 10% H_2/90% N_2 gas with 5% humidity up to 90 days for samples having a $LaCrO_3$ coating.
- Examined oxide scale formed and measured its thickness on coated and pristine materials for oxidation times up to 180 days.
- Developed a theoretical model for oxidation kinetics and the experimental oxidation thickness data was verified with this model.
- Measured total ASR of the coated and pristine samples after oxidation for 45 days at 800°C. It was observed that the pristine samples exhibited significant oxidation. However, even samples with as small as 1 micron coating were highly resistant to oxidation.
- Carried out dip coating of $LaMnO_3$ based coatings on SS430 foils.

Future Directions

- Conduct a short stack test with the best coating material, as determined by ex situ oxidation studies.
- Conduct Hebb-Wagner measurements on YSZ/perovskite/YSZ sandwiches made by tape-casting.

Introduction

Planar SOFC stacks are preferred over their tubular counterpart due to compact design, higher power and energy density, and projected lower cost. However, planar SOFC stacks require interconnect or bipolar plates which keep fuel and oxidants separate, and electrically connect adjacent cells. From the standpoint of cost and ruggedness, metallic interconnects are preferred. However, metallic interconnects of choice are stainless steels or nickel-chromium-based alloys, which are prone to oxidation. The oxide scale formed increases the ASR, which adversely affects the SOFC performance and efficiency, and thus in balance also adversely affects the cost. The potential remedy is the development of either baseline alloys that are oxidation-resistant, or suitable coating materials which can suppress oxidation kinetics. From the standpoint of cost and practicality, the preferred approach is the development of suitable coating materials.

To date, several coating materials have been tried, with varying degrees of success. The approach, however, has not been systematic, and has relied on trial and error. As a result, most of the coatings used to date were very thick (several or several tens of microns). This increases the potential for spalling, which is undesirable. The approach selected in this work is based on the fundamental chemistry of materials, which has the potential to develop coatings that are adherent and very thin (typically less than 5 microns, and may be as thin as 1 micron), and yet can suppress oxidation kinetics to greater than 40,000 hours of operating life.

Approach

Possible coating materials are perovskites with a transition metal, capable of exhibiting multiple valence states. An example is $LaMnO_3$. The approach involves doping a material such as $LaMnO_3$ (LM) with suitable elements, which tend to suppress oxygen vacancy concentration, without significantly reducing electronic defect concentration. Powders of various coating materials, doped appropriately, are made. Samples of the materials are made by sintering. Two types of electrical tests are performed: (a) measurement of total electrical conductivity; (b) measurement of oxygen ion conductivity using blocking electrodes. Thin coatings (1 to 5 microns) are then deposited on foils of various alloys. For the initial investigation, Haynes 230, Inconel 718, and SS 430 were the alloys selected. The coated and uncoated foils are subjected to air and fuel, for various periods of time and over a range of temperatures, up to ~800°C. Samples are oxidized for various periods of time, up to a maximum of six months. The oxide scale thickness is measured using scanning electron microscopy (SEM). The observed kinetics of oxidation is compared with the theoretical models developed. The ASR of the samples is also measured as a function of time of oxidation, with measurements conducted over a range of temperatures. Finally, a short stack will be tested using coated interconnects exhibiting the best properties.

Results

1. Identified a number of possible perovskite and non-perovskite materials with potential for good electronic conductivity and low oxygen ion conductivity. This was achieved using crystal chemistry considerations. Criteria based on ionic size were used to identify materials with low oxygen vacancy mobility. Criteria based on defect chemistry were used to identify materials with low oxygen vacancy concentration.
2. Samples of perovskite and non-perovskite structures were fabricated in the form of discs and bars. Total electrical conductivity, which is mainly electronic, was measured over a range of temperatures using the four probe DC method. Figure 1 shows the total conductivity measured as a function of temperature (Arrhenius plot) on several prospective coating

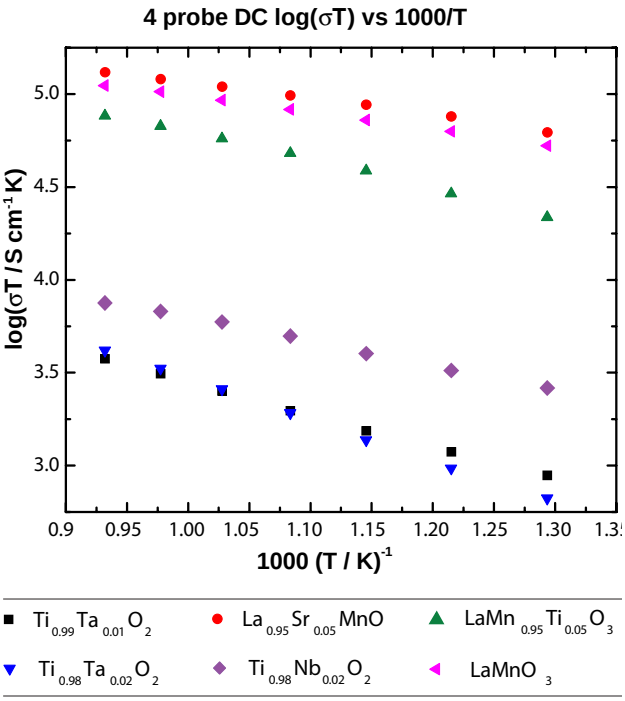

FIGURE 1. Arrhenius plots of conductivity of a number of coating materials. The total conductivity is predominantly electronic, with oxygen ion conductivity orders of magnitude lower.

materials. The lowest measured value was ~4 S/cm, which shows that the ASR is expected to be low using any one of the coatings. Thus, the one with the lowest oxygen ion conductivity is preferred since this will be the most effective in suppressing oxidation kinetics.

3. Experiments were conducted on the measurement of oxygen ion conductivity using blocking electrodes at 800°C. Results showed that the blocking electrodes function successfully. It was decided to use a three electrode configuration (with guard electrode) to eliminate the effects of surface conductivity. Lower values of conductivity were obtained for the sputter coated YSZ/perovskite couple as compared to the co-pressed sandwich structure. This was attributed to better equilibration to steady state in the thinner (sputter deposited) samples. The lowest value of conductivity was 2.0 x 10^{-7} Scm^{-1} and was obtained for titanium-doped $LaMnO_3$ (LMT). Experiments are under way to carry out measurements on tape-cast YSZ/perovskite/YSZ sandwich structures which will have stronger interfaces and thinner YSZ layers.
4. Successfully deposited a number of coating materials on several alloy foils. The thickness of the coating was varied between 1 and 3 microns.
5. Oxidation in flowing air was conducted at 800°C on the coated metal foils (LM, LMT and LSM) for durations up to 4,320 hours (180 days). The oxidized samples were characterized by XRD and SEM. The oxidation products were identified and the oxidation kinetics ascertained by measuring the thickness of the oxide layer as a function of time. The results demonstrated that the LMT coating was the most effective and strontium-doped $LaMnO_3$ (LSM) least effective in suppressing the oxidation kinetics of the alloys (Figures 2 and 3). The results were verified by a theoretical model and demonstrated that the LMT coating was the most protective.
6. Oxidation in flowing 10% H_2/90% N_2 gas with 5% humidity was conducted on the coated metal foils ($LaCrO_3$ and Nb-doped $LaCrO_3$) for durations up to 2,160 hours (90 days). The oxide layer thickness was determined as a function of time. A 1 µm thick $LaCrO_3$ based coating was effective in decreasing the oxidation kinetics by more than an order of magnitude.
7. A spring loaded fixture was used to measure the ASR of the oxidized foils. Conductive paste was not used for these measurements as this could permeate the porous oxide layer and lead to an under-estimation of the ASR value. The ASR of the coated

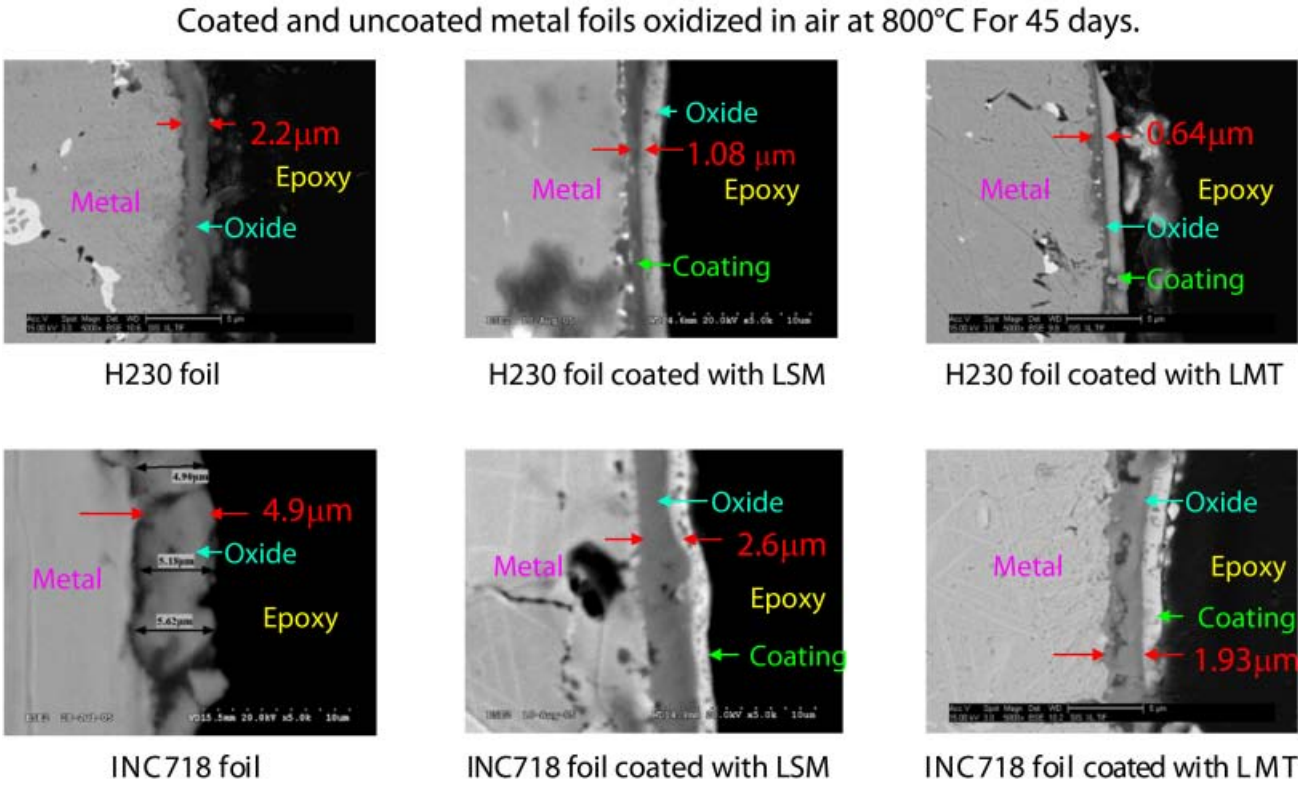

FIGURE 2. Cross sectional SEM micrographs of coated and uncoated metal foils oxidized at 800°C in air for 45 days. The thickness of the oxide layer is smaller for LMT coated foils as compared to LSM coated foils for H230 as well as INC718.

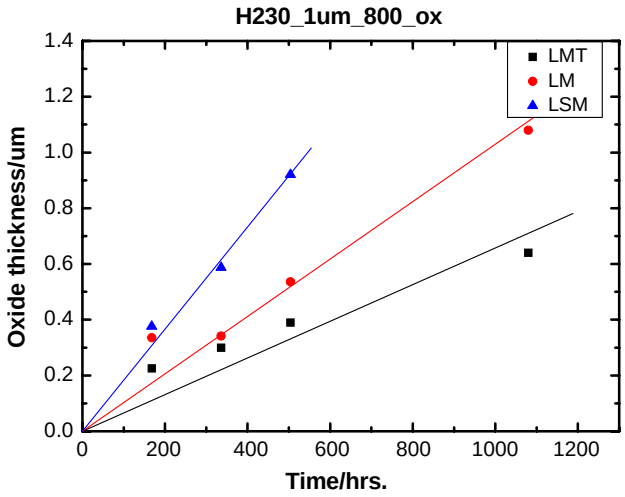

FIGURE 3. Graphical representation of the growth of oxide layer for H230 foil coated with LSM, LM and LMT and oxidized in air for 45 days (1,080 hrs.) at 800°C. The lowest slope for the LMT coated specimen is a validation of the defect chemistry approach.

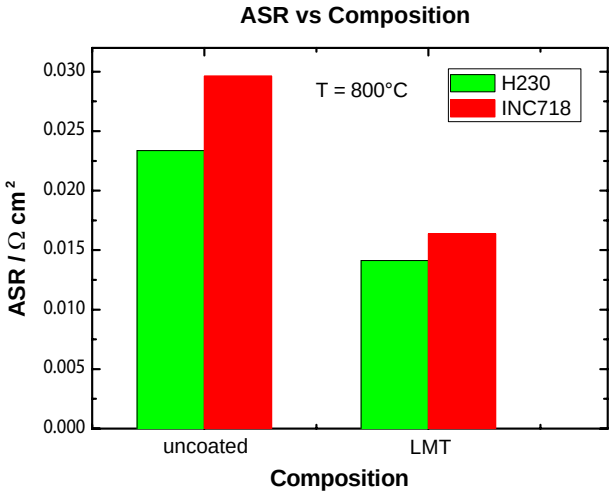

FIGURE 4. Comparison of ASR of uncoated and LMT coated foils of H230 and INC718, oxidized in air for 45 days at 800°C.

foils was compared with that of the uncoated foils. The ASR on the coated (1 micron) and uncoated foils showed that after 1,080 hours (45 days) in air at 800°C, the ASR of the coated foils was typically smaller by about half (Figure 4).

8. LSM and LMT were dip coated on to 2" x 2" SS430 foils. The coatings were cured at 1,000°C for 1 to 5 hours. The samples were characterized by SEM. The coatings were about 5 to 10 µm thick and showed excellent adherence.

Conclusions

1. Defect chemistry plays a major role in oxygen ion transport through oxides, and thus determines the suitability of a given material as a coating. Coating materials based on $LaMnO_3$ (perovskite) and TiO_2 (non-perovskite) were successfully made. It was demonstrated that perovskite coating is an order of magnitude superior to spinel coating.
2. Electronic and ionic conductivities of coating materials are in accord with defect chemistry, and that defect chemistry provides a scientific basis for the design of oxidation-resistant coatings.
3. High quality, strongly adherent coatings can be sputter deposited. The resulting foils exhibit improved oxidation resistance over the baseline foils. Even after several days at 800°C, the coating continues to remain well-bonded.
4. Coated foils also exhibit much lower ASR as compared to pristine foils.

III.A.32 Digital Manufacturing of Gradient Meshed SOFC Sealing Composites with Self-Healing Capabilities

Objectives

- Use three-dimensional printing (3DP) technique to build a shape memory alloy (SMA) skeleton for the seal on the seal-interconnect side.
- Use glass to fill the meshed SMA structure and transition into pure glass seal on the electrolyte side.
- Provide gradient coefficient of thermal expansion (CTE) to greatly reduce the thermal stress.
- Further reduce the thermal stresses in the seal by SMA phase transformation toughening.
- Provide self-healing of cracks by SMA shape recovery during SOFC thermal cycling.

Accomplishments

- Fabricated SMA by arc-melting.
- Homogenized and conducted DSC characterization of SMA.
- Developed multiple AutoCAD drawings of wire structure and 3D printed multiple configurations of the wire structure.
- Refined 3DP technique by modifying the print layer thickness, binder solution, and particles sizes used in the 3DP.
- Fabricated glass by mixing reagent grade oxides, high temperature homogenization, and quenching.

Future Work

- Measure the CTE of SMA and glass.
- Examine the glass microstructure.
- Further refine the SMA microstructure and shape memory effort.
- Integrate SMA and glass.

Dr. Kathy Lu (Primary Contact),
Christopher Story, Dr. W. T. Reynolds, Jr.
Virginia Polytechnic Institute and State University
213 Holden Hall, M/C 0237
Blacksburg, VA 24061
Phone: (540) 231-3225; Fax: (540) 231-8919
E-mail: klu@vt.edu

DOE Project Manager:
Ayyakkannu Manivannan
Phone: (304) 285-2078
E-mail: Ayyakkannu.Manivannan@netl.doe.gov

- Quantify the integrated seal thermal properties and stability.
- Composite seal performance testing.

Introduction

SOFC seals have a demanding set of imposed performance criteria. Of particular importance is the ability to seal between metallic and ceramic components with differing CTEs, and do so while being electrically insulating and exposed to temperature transients from room temperature up to 950ºC. A major roadblock to long-term SOFC operation has been gas leakage through the seal caused by multiple heating and cooling cycles (thermal cycling). The gas seal cracks because the metal and ceramic components that are sealed together shrink and expand differently (CTE mismatch), causing high stresses in the seal.

A host of seal materials has been explored, such as FeCrAlY, DuraFoil, Si-C-N polymers, ceramic and metallic fillers, mica, and glass-ceramic fibers (1-6). However, interdiffusion and durability of some of these materials in the oxidizing environment of SOFC are unknown. Some of these seals require compressive loads or have unknown leakage protection capability. An improved glass matrix should be selected to avoid the above problems. Also, cracking during thermal cycling can be avoided by the integration of a second phase which is a better match to the thermal expansion of the metallic interconnect. A SMA has a CTE close to that of the interconnect and presents the possible benefit of crack healing because of the shape memory behavior when heated.

Approach

The SMA ingot is being fabricated by arc-melting with the desired alloy composition. After the SMA is fabricated, the microstructure and the shape memory effect are characterized. After that, the SMA alloy is broken into small particles and 3D printed into a wire structure. The printed structure is thermally cured and sintered into strengthened wire mesh. Three-dimensional printing allows for the creation of wire diameters between 100-1000 µm and printing layers that are 25-100 µm thick. Sintering densifies the wire mesh and reduces the wire diameter further.

The glass is made by mixing the exact oxide compositions as designed and high temperatures melt

the mixture for composition homogenization. The glass melt can be directly infiltrated into the wire mesh to make the final seal or by filling the wire mesh with glass powder and sintering the glass powder and the wire mesh together.

Seal performance testing will be conducted in a bilayer fixture where the top and bottom layers are commercial cell interconnect and electrolyte. The gas composition that passes through the bilayer structure will be varied and samples will be thermally cycled in the bilayer fixture. Seals will be evaluated by microscopy, adherence testing, and residual stress measurements. At the end of each test, interfacial and bulk characterization of the seal will be performed. From these electrochemical, chemical and thermo-mechanical measurements, the overall stability and electrical performance of the seal will be assessed.

Results

The SMA microstructure and the composition have been analyzed by scanning electron microscopy and energy dispersive spectroscopy. The SMA shows dendritic structures, which indicates small composition variation (Figure 1). Based on this, the SMA is being homogenized at 1075°C for 24 hrs and ramped to 1150°C for 48 hrs with the goal of improving its composition homogeneity and shape memory effect. The ingot is being broken down into powder by cold rolling and milling. Cold-rolling strips off the alloy ingot and coldworks the alloy until cracks form and the alloy breaks into ~0.5 cm size pieces. After the alloy is broken into small pieces, it can be milled by ball milling or spex milling to break the pieces into powder. Characterization of the shape memory effect and the CTE are being conducted through DSC and dilatometry, respectively.

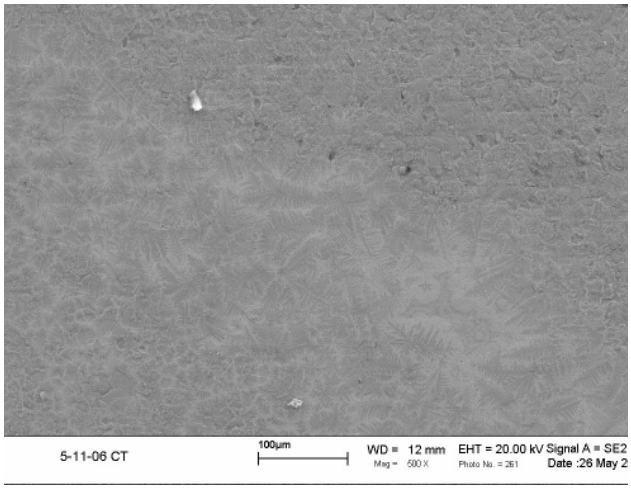

FIGURE 1. SEM Micrograph of the SMA Alloy

Metallic wire meshes have been 3D printed from stainless steel and Ni powders with wire thicknesses of 500 µm and 1 mm, and layer thicknesses of 25 µm – 100 µm. Stainless steel and Ni particles are used to select the optimum printing variables before the SMA is used. Three-dimensional printing with Ni has shown that a binder solution with a higher content of poly-acrylic acid is necessary for Ni based alloys. Figure 2 shows a wire mesh printed from nickel with wire thickness of 500 µm.

Glass material has been fabricated by using >99.9% pure oxides. First, the oxides are milled by a roller mix for homogenization and reducing the size of individual oxide particles. The mixture is then heated in a box furnace for melting and formation of glass. After homogenizing at 1400°C for 2 hrs, the melt is water quenched. A SEM micrograph of the glass material is shown in Figure 3. Currently, the glass microstructure and the CTE are being characterized.

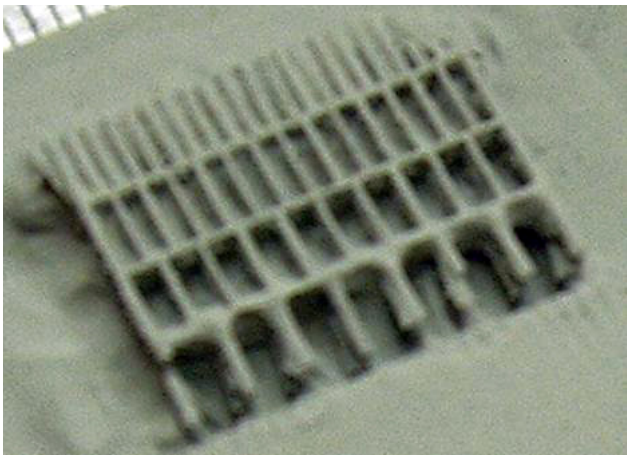

FIGURE 2. 500 μm Wire Diameter Nickel Mesh

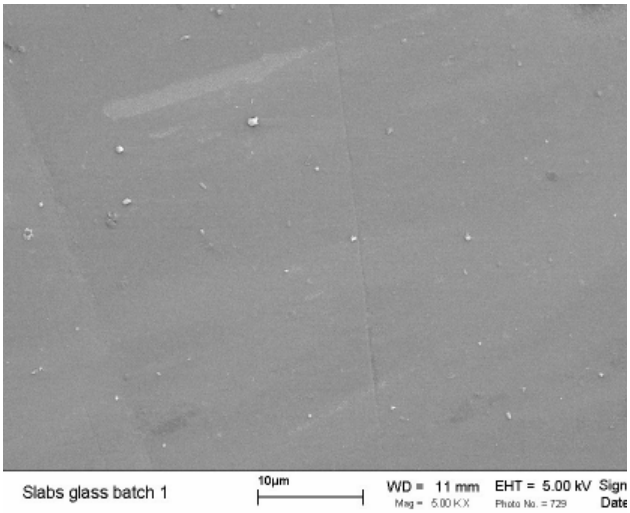

FIGURE 3. SEM Micrograph of the Glass

Conclusions

- SMA has been fabricated by arc-melting.
- SMA has been homogenized by heat treatment. DSC characterization has been conducted.
- AutoCAD drawings of wire structures have been 3D printed.
- Glass has been fabricated by mixing reagent grade oxides, high temperature homogenization, and quenching.

Future Work

- Measure the CTE of SMA and glass.
- Examine the glass microstructure.
- Further refine the SMA microstructure and shape memory effect.
- Integrate SMA and glass.
- Quantify the integrated seal thermal properties and stability.
- Composite seal performance testing.

FY 2006 Publications/Presentations

1. K. Lu, C. Story, and W. T. Reynolds, "Three-Dimensional Printing of Gradient Meshed Solid Oxide Fuel Cell Seal Composites" University Coal Research/Historically Black Colleges and Universities and Other Minority Institutions Contractors Review Conference, June 6-7, 2006. Pittsburgh, PA.

References

1. K. S. Weil, J. Y. Kim and J. S. Hardy, "Reactive Air Brazing: A Novel Method of Sealing SOFCs and Other Solid-State Electrochemical Devices," Electrochemical and Solid-State Letters, 8(2), A133-A136, 2005.

2. K. S. Weil and J. S. Hardy, "Development of a Compliant Seal for Use in Planar Solid Oxide Fuel Cells," *28th International Conference on Advanced Ceramics and Composites*, E. Lara-Curzio and M. J. Readey, eds. 25, pp. 321-326, American Ceramic Society, Cocoa Beach, FL, 2004.

3. Y.-S. Chou and J. W. Stevenson, "Long-Term Thermal Cycling of Phlogopite Mica-Based Compressive Seals for Solid Oxide Fuel Cells," *Journal of Power Sources*, 140, 340–345, 2005.

4. M. Bram, S. Reckers, P. Drinovac, J. Monch, R. W. Steinbrech, H. P. Buchkremer and D. Stover, "Deformation Behavior and Leakage Tests of Alternate Sealing Materials for SOFC Stacks," *Journal of Power Sources*, 138, 111–119, 2004.

5. S. Taniguchi, M. Kadowaki, T. Yasuo, Y. Akiyama, Y. Miyake and K. Nishio, "Improvement of Thermal Cycle Characteristics of a Planar-Type Solid Oxide Fuel Cell by Using Ceramic Fiber as Sealing Material," *Journal of Power Sources*, 90, 163–169, 2000.

6. J. W. Fergus, "Sealants for solid oxide fuel cells," Journal of Power Sources, 147, 46-57, 2005.

III. SECA RESEARCH & DEVELOPMENT

B. Fuel Processing

III.B.1 Technology Development in Support of SECA

Objectives

- Improve the sulfur tolerance of diesel reforming catalysts.
- Determine long-term stability.
- Determine effects of polyaromatics on catalyst activity.

Approach

- Synthesize and characterize perovskites that are stable in hydrogen and oxygen and have redox chemistry on the "B" site.
- Verify that the doped catalysts are chemically and thermally stable and relatively unaffected by sulfur containing fuel.
- Determine reforming efficiency of fuels with sulfur and polyaromatics.

Accomplishments

- The new perovskite catalysts were shown to maintain their activity over 1000 hours in reducing and oxidizing environments.
- Polyaromatics were shown to deactivate the catalyst to some extent and may require alternative treatment.

Future Directions

- Explore materials or engineering improvements to deal with polyaromatics.
- Assist vertical teams to address reformer engineering issues.

Michael Krumpelt (Primary Contact), Di-Jia Liu
Argonne National Laboratory
Argonne, IL 60439
Phone: (630) 252-8520; Fax: (630) 252-4176
E-mail: krumpelt@cmt.anl.gov

DOE Project Manager:
Ayyakkannu Manivannan
Phone: (304) 285-2078
E-mail: Ayyakkannu.Manivannan@netl.doe.gov

Introduction

Auxiliary power units (APUs) for heavy-duty vehicles could reduce emissions and conserve fuel on the North American continent, where engines are kept running while drivers rest. An APU must have enough power to keep the cabin cooled or heated in hot or cold climatic conditions, respectively, and may have to also supply electricity for refrigeration of cargo. The amount of fuel needed will be significant and drivers may resist having to refuel the APU with anything other than the diesel fuel used for the engine.

Converting diesel fuel into a hydrogen-rich gas that is suitable for solid oxide fuel cells is more challenging than converting gasoline because of the multi-cyclic aromatics and the aromatic sulfur compounds in diesel fuel. The sulfur in the fuel adsorbs or reacts with the metal catalyst, deactivating it. Similarly, the poly-aromatics adsorb on the catalyst, and because the kinetics of breaking the H-C and C-C bonds in polyaromatics are slower than in paraffins and olefins, the catalyst becomes less active. Also, the unreacted aromatics tend to form coke. To mitigate these issues, the operating temperature of the reformer must be raised, but this causes the presently used nickel or rhodium catalysts to agglomerate and evaporate.

Approach

At Argonne, we have been actively exploring alternative catalysts that could reduce the material cost yet maintain or improve catalytic activity. In the last two years, we actively engaged the investigation of perovskites as diesel reforming catalyst material due to their propensity to form oxide ion vacancies and electron conductivity. Perovskite is a combination of metal oxides with a typical formulation of ABO_3, where A and B are the elements from alkaline, alkaline earth, and transitional metal groups. The A site ion occupies a dodecahedral interstice coordinated with 12 O, which in turn belongs to eight BO_6 octahedra sharing the corners. The stability is attributed primarily to the Madelung energy of the stacking of rigid BO_6. Both A and B sites in perovskite can be partially exchanged to form $A_{1-x}A'_xB_{1-y}B'_yO_3$, resulting in mixed valance states and enhanced mobility of oxygen in the lattice. In our study, we found that the exchange of the B site can often lead to significant improvement in catalytic reforming activity. For example, we have successfully exchanged

ruthenium in $LaCrO_3$ and found the catalyst provides excellent hydrogen yield, reforming efficiency, and sulfur tolerance during the autothermal reforming study. To further prove that perovskite can be indeed used as the practical catalyst for commercial applications, a series of experiments need to be carried out to test the performance with real commercial diesel and at extended operating duration.

Results

Commercial diesel fuel is a complicated mixture of a variety of hydrocarbons and sulfur containing compounds. The key composition of diesel fuel includes paraffins, napthenes, and mono- and multiple ring aromatics. The catalytic chemistry of each component could be significantly different. More importantly, the cross-interference between different components can significantly complicate the overall reforming chemistry and efficiency. We conducted a systematic study to address the influence on reforming performance from each main group represented by the fuel blend of dodecane (DDN), butylcyclohexane, decalin, butyl-benzene, tetralin and 1-methylnapthlene (1MN). We found that the reforming efficiency and COx selectivity under identical reaction conditions follow the order of paraffins ≈ cycloparaffins > mono-aromatics >> poly-aromatics whereas the formation of residual hydrocarbons mainly in the form of fragmented C2, C3, etc., follows the reversed order. We interpret this trend as the result of rate difference in hydrocarbon decomposition. Aromatics, especially heavy aromatics, have extended π-orbital conjugation and C=C bond is more difficult to be cleaved than alkanes and olefins.

To understand the synergetic effect from different fuel components, we also formulated a simulated diesel containing all aforementioned hydrocarbons, in addition to a representative organic sulfur compound, dibenzothiophene (DBT) with an equivalent sulfur content of 50 ppm by weight. The simulated diesel has a composite molecular formula of $C_{10.7}H_{20.4}$ and heat of combustion is 6453 kJ/mole. For comparison, we also acquired a low-sulfur distillate, JP8, from a commercial source which contains about 60 ppm S by weight. The catalytic reforming study was carried out at 800°C with an oxygen-to-carbon ratio of $O_2/C = 0.5$ and steam-to-carbon ratio of $H_2O/C = 1$. The ATR reaction was performed at a gaseous hourly space velocity of 100,000 hr^{-1} for the better differentiation on the reaction kinetics. Figure 1 shows the total reforming efficiency and the selectivity towards COx for different fuel surrogates, simulated diesel and commercial JP8. We found that, with 5% 1MN in a dodecane mixture, the reforming efficiency is clearly affected by the cross-interference from the polyaromatic compound. The simulated diesel,

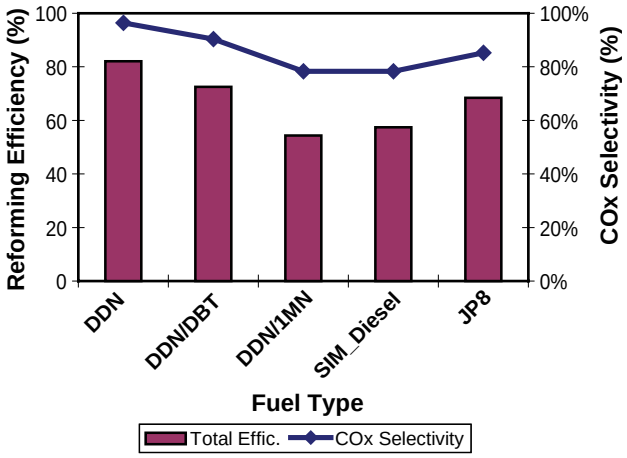

FIGURE 1. Reforming Efficiency and COx Selectivity of $LaCr_{0.95}Ru_{0.05}O_3$ Tested with Different Surrogate Diesel Fuels and JP8

with 3% 1MN but added with 7% monoaromatics, has reached somewhat better efficiency possibly due to the sensitivity towards polyaromatics. A very encouraging observation is that our catalyst performed respectably for the commercial JP8 with reforming efficiency in the 70% range and COx selectivity of near 90%, considered that the study was conducted at the kinetic differential region with low steam content. The performance will obviously improve significantly in an actual catalytic reactor which operates with slower space velocity.

Significant progress was also made to complete the 1000-hour aging study for our benchmark perovskite catalyst. Under ATR reactions, the catalyst is subject to interaction with both a strong reductant such as fuel, and oxidant such as air in the reformate stream. One of the major concerns is the stability of the active center during the repeated swing between reducing and oxidizing environments which could lead to bleaching of atomically dispersed ions such as Ru out of the perovskite lattice. To experimentally address this issue, we conducted two parallel durability tests where $LaCr_{0.95}Ru_{0.05}O_3$ catalyst was subjected to the treatments under either humidified air or simulated reformate containing H_2, CO, CO_2, CH_4, N_2 and 26% H_2O. The aging was carried out at 800°C and a fraction of the sample was taken out in every 200 hours to be tested with various simulated fuel and JP8 at near differential flow conditions. Shown in Figure 2 are the total reforming efficiencies with each fuel at different stages of aging. The general observation suggests that slight degradation occurs although the rate depends on the type of the fuel tested. The reforming efficiency for our chromite catalyst held to about 10% deactivation at the end of test cycle.

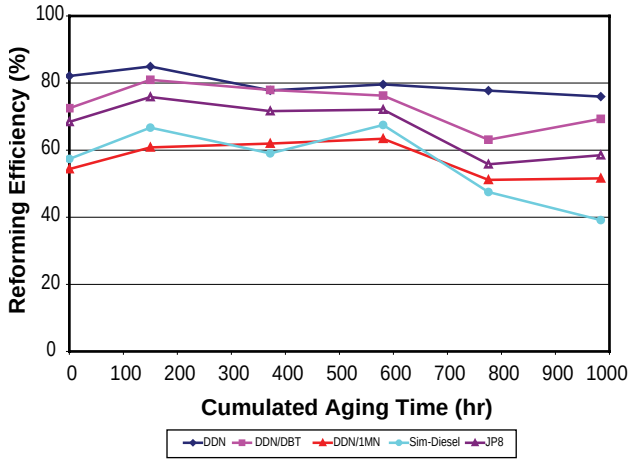

FIGURE 2. Reforming Efficiency of $LaCr_{0.95}Ru_{0.05}O_3$ for Surrogate Diesel Fuels and JP8 Tested at Various Stages of Aging during the 1000-Hour Durability Test in the Simulated Reformate Stream

Conclusion

- The reforming chemistry of the main hydrocarbon representatives in diesel was investigated. The cross-interference from the heavy polyaromatics to the overall reforming efficiency was identified.
- ATR reforming on commercial JP8 was studied and relatively good performance was observed with Argonne's perovskite catalyst.
- Two 1000-hour aging studies in both oxidative and reductive gas flow were carried out and our catalyst showed relatively good durability.

FY 2006 Publication & Presentation

1. Activity and Structure of Perovskites as Diesel Reforming Catalysts for Solid Oxide Fuel Cell, D. J. Liu and M. Krumpelt, *International Journal of Applied Ceramic Technology*, Vol. **2**, No 4, Page 301-307, (2005).

2. Activity and Structure of Perovskites as Diesel Reforming Catalysts for Solid Oxide Fuel Cell, Di-Jia Liu and Michael Krumpelt, *Ceramic Engineering and Science Proceedings (CESP),* Vol. **26**, No. 4, *Advances in Solid Oxide Fuel Cells.*

3. Critical Issues in Catalytic Diesel Reforming for Solid Oxide Fuel Cells, Di-Jia Liu, Mike Krumpelt, Hual-Te Chien and Shuh-Haw Sheen, *to be published at Journal of Material Engineering and Performance.*

III.B.2 Development of Ni-Based Sulfur-Resistant Catalyst for Diesel Reforming

Objectives

- Reform a real diesel fuel containing 50 parts per million sulfur under minimum recycle conditions using a low-cost (hence nickel-based) sulfur resistant catalyst to produce hydrogen and carbon monoxide for use in solid oxide fuel cells.
- Determine conditions that cause catalyst deactivation and ascertain the effectiveness of radio frequency coke suppression in prolonging catalyst activity.
- Measure the effect of frequency and field strength of the applied radio frequency field on suppressing coking of sulfur resistant reforming catalyst.

Accomplishments

- Demonstrated that a low-cost nickel-based catalyst can autothermally reform a 50 ppm S diesel fuel with 20% recycle gas for at least 500 hours without catalyst deactivation, which is a major step towards developing a 5,000 to 10,000 hour stable reforming catalyst.
- Determined that coking is the major form of catalyst deactivation and can be controlled through proper catalyst formulation, introduction of turbulence into the flame front, and by possible application of radio frequency coke suppression.
- Determined that the radio frequency coke suppression effect appears to be linearly dependant upon field strength but is independent of frequency between 50 kHz to 13.56 MHz.

Introduction

For diesel, jet or gasoline to be used in a fuel cell, the liquid hydrocarbon fuel must first be reformed into hydrogen and carbon monoxide. Typically, the hydrocarbon fuel is first mixed with a limited amount of air, and in some systems a small amount of off-gases from the anode of the fuel cell stack to supply steam. The resulting mixture is then passed over a nickel or platinum group metal catalyst to produce hydrogen and carbon monoxide, which are then sent to the fuel cell stack to produce electricity. Reformer catalysts based on low-cost nickel are preferred, because they are cheaper to manufacture and more durable than platinum group metal catalysts. Unfortunately, even sub part per million levels of sulfur in the fuel can poison most reformer catalysts, resulting in a product stream with a high concentration of partially reformed hydrocarbons that will coke or foul the anode catalysts used in solid oxide or other type of fuel cell stack.

Chevron, Argonne National Laboratory, and the National Energy Technology Laboratory at Morgantown are developing Ni-based (low-cost) reforming catalysts that can tolerate the levels of sulfur found in reformulated gasoline or in low sulfur diesel fuel. Developing a sulfur resistant reforming catalyst is a far better approach than trying to adsorb complex sulfur compounds found in the fuel in a separate system prior to reforming, since most adsorbents for branched dibenzothiophenes have low capacities and are often pyrophoric.

Gunther Dieckmann
Chevron Energy Research and Technology Company
100 Chevron Way
Richmond, CA 94802
Phone: (510) 242-2218; Fax: (510) 242-2823
E-mail: ghdi@chevron.com

DOE Project Manager: Magda Rivera
Phone: (304) 285-1359
E-mail: Magda.Rivera@netl.doe.gov

Approach

We have found that the most serious problem with the development of a sulfur resistant reforming catalyst is coking, and that Ni-based catalysts tend to coke more than platinum group metal based catalysts. However, Ni-based catalysts are preferred not only because they are significantly cheaper, but they are also more durable. Both of these issues are critical in ultimately developing a viable low-cost auxiliary power unit for less than $400/kW. Not only does coke block catalytic sites leading to the production of undesirable heavy hydrocarbons that will foul anode catalysts, we have also found that coking leads to aging of the reformer catalyst due to metal stripping. Another problem with both platinum group metal and Ni-based reformer catalyst is that they require periodic regenerations every 8 to 100 hours or so to remove built-up carbon deposits. This can be easily accomplished when the auxiliary power unit is turned off, simply by stopping the flow of hydrocarbon feed over the catalyst before cutting off the flow of air. Normally, the coke on the catalyst is burned off in 1 to 3 minutes. The Chevron catalyst is formulated to remain active following air regenerations.

We tested the Chevron catalyst under autothermal reforming conditions first with a simulated recycle rate of 20% at an oxygen to carbon mole ratio of 1.0 with a steam to carbon mole ratio of 0.2. The purpose of the recycle stream from the SOFC anode is to provide a source of steam to prevent coking. However, late in the project we discovered that it was possible to operate the reformer with just air and diesel fuel alone, particularly if severe turbulence is deliberately introduced into the flame front. This can be achieved by reactor/catalyst geometry and space velocity or by "chopping" or "pulsing" the air supply. The majority of this project was focused on understanding the role radio frequency coke suppression plays in suppressing metal catalyzed coking and thus decrease reformer catalyst deactivation.

Results

We have demonstrated that a 50 ppm S diesel fuel can be autothermally reformed to produce hydrogen and carbon monoxide for use in a solid oxide fuel cell over a low-cost Ni-based catalyst for more than 500 hours with no major sign of catalyst deactivation provided that (1) the catalyst is reformulated to avoid free surface Ni, and/or (2) radio frequency (RF) coke suppression is applied. Figure 1 shows the activity of the catalyst reforming a 50 ppm S diesel fuel as a function of time. In the base case, the activity of the catalyst rapidly decreased after approximately 200 hours due to excessive coking. When a radio frequency field of 50 kHz at 92 V/cm or 350 kHz at 98 V/cm is applied to the catalyst, the coking rates of the catalyst is substantially reduced in these runs. Without RF, the catalyst would require a periodic regeneration or a burn lasting 20 to 30 minutes (under the same flow of air used to reform the fuel); yet under RF coke suppression, the catalyst was regenerated in 5 to 8 minutes for a 10-hour run. Thus, application of a radio frequency electromagnetic field reduced coking by a factor of approximately 4. As a consequence, catalyst activity was stabilized for at least 500 hours. Since the coking rate of diesel drops dramatically with sulfur content and that diesel fuels in Europe and the United States will contain less than 15 ppm sulfur, we anticipate that this catalyst should survive substantially longer than in these "rapid" aging trials.

In Figure 1, we also see in the RF runs that the activity of the catalyst first decreases and then improves before lining out after approximately 125 hours on line. This activation of the catalyst is due to the reaction of "free" Ni or NiO on the surface with the underlying support. The original Ni-based catalyst was formulated to leave "green" free NiO on the surface. It was thought that this "free" nickel on the surface would adsorb sulfur in the front part of the catalyst bed, thereby allowing the back part of the catalyst bed to steam reform the fuel. However, we quickly discovered that the sulfur resistant

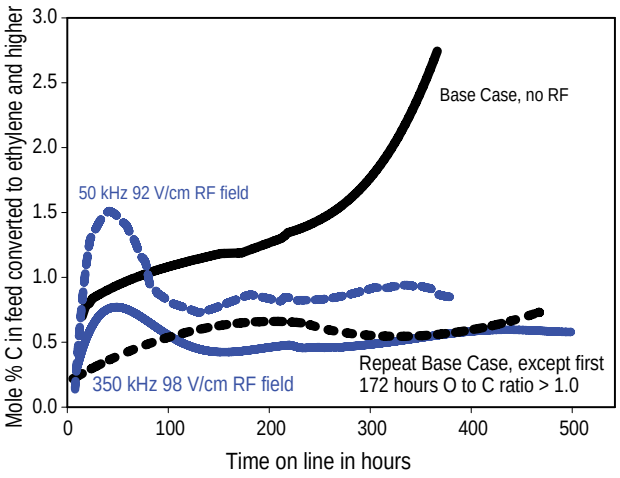

FIGURE 1. Catalytic Activity and Aging of Chevron's Ni-based Catalyst Reforming a 50 ppm S Diesel Fuel with and without Radio Frequency Coke Suppression

reforming activity continued long after the catalyst quit adsorbing sulfur. Thus, we discovered that the sulfur resistance is due to the incorporation of nickel into the support to produce a blue colored catalyst of Ni^{+3} in an octahedral site. In fact, this is the same mechanism of sulfur resistance first proposed by Michael Krumpelt at Argonne National Laboratory in their perovskite based catalysts [1,2], and also imparts the sulfur resistance to the "hexaaluminate" series of catalysts being developed by David Berry and co-workers at the National Energy Technology Laboratory at Morgantown, WV [3]. Thus, in the "RF-on runs", a portion of the Ni on the surface dissolves into the support to develop the sulfur resistance of the catalyst, which is seen as a gradual increase in catalytic activity over time in the first 125 hours.

However, we also discovered that if the catalyst is either calcined at a higher temperature during preparation or as we serendipitously discovered that if the catalyst is run at an O to C ratio higher than 1.0 for even a short period of time, then the coking rate can be reduced to the same level as was seen in the RF coke suppression runs. By operating at a higher O to C ratio (of 1.1), the higher temperature drives the entire free surface Ni into the structure to produce a lower coking catalyst. This first occurred quite by accident during the repeat base case run in Figure 1 (dotted black line). As a result of a crack in the central quartz RF antenna well, extra air was pulled into the reactor for the first 172 hours because the test apparatus was under a slight vacuum. As a result of the higher temperature, the catalyst turned blue. However quite surprisingly, even after the quartz reactor was repaired, this modified catalyst now showed no signs of catalyst deactivation even though no RF was applied, and had the same low coking rate as occurred under RF coke suppression.

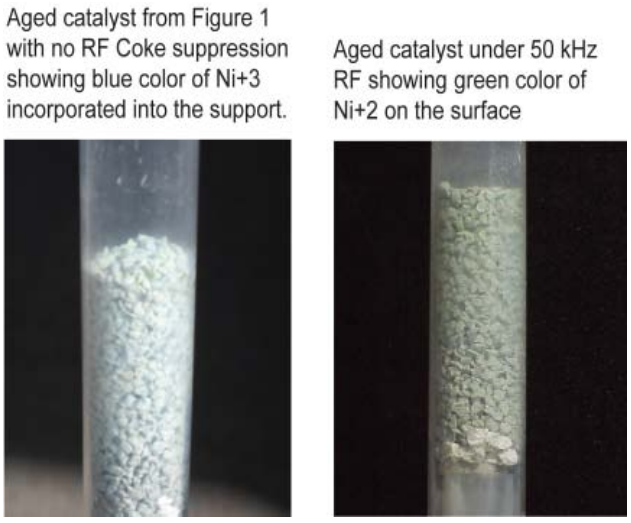

FIGURE 2. Comparison of Chevron's Ni-based Catalysts at the End of Run, Showing that RF Maintains the "Green" Color of Supported NiO (right), While the Base Case Is Blue Due to Incorporation of Ni into the Structure (left)

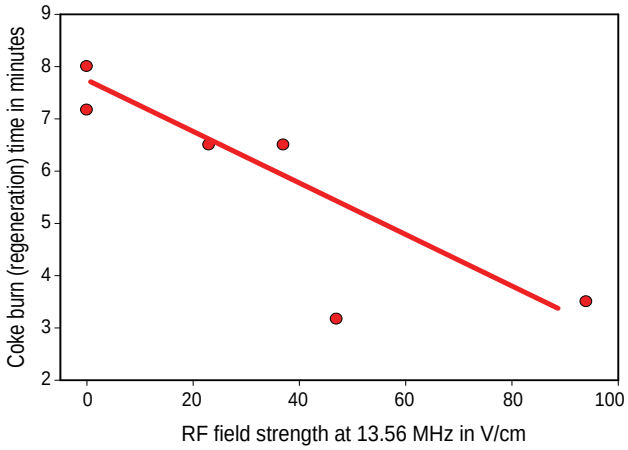

FIGURE 3. Effect of the RF Field Strength on the Coking Rate of the Catalyst

Clearly, if the catalyst is formulated and heat treated so that no free Ni remains on the surface, the coking rate on the catalyst can be reduced by a factor of approximately 4. Figure 2 compares the color of the two catalyst beds showing that RF coke suppression prevents nickel stripping. Thus, after 380 hours on line, the catalyst is still green due to supported NiO, whereas in the repeat RF off case (due to extra air in the beginning) the catalyst is blue.

Figures 3 and 4 show the effect of field strength (at 13.56 MHz) and frequency (at 60 V/cm field strength) on coking rate of the reforming catalyst. Figure 3 shows that the coking rate decreases linearly with increasing field strength, whereas Figure 4 quite surprisingly shows

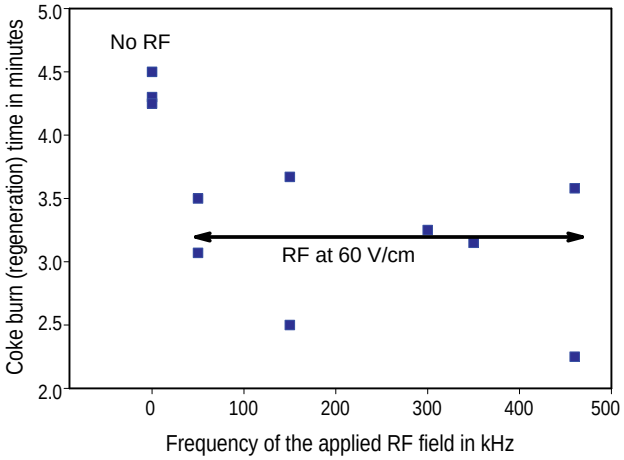

FIGURE 4. Effect of Frequency on the Coking Rate of the Catalyst

that varying frequency over a range of 50 to 460 kHz has no impact on coking rate. In subsequent experiments covered in the final report, the RF coke suppression effect is shown to be independent of frequency over the range of 50 to 13.56 MHz [4].

Finally, we discovered that diesel fuel could be reformed over the catalyst with no additional steam if the oxygen to carbon mole ratio was increased to 1.1. Furthermore, it was subsequentially discovered that the coking rate could be substantially reduced under the higher O to C mole ratio conditions to extremely low levels, if turbulence is introduced into the flame front. This was achieved again, quite serendipitously, by an inadvertent arrangement of reactor geometry and gas space velocity, which caused the flame front to rapidly pulsate. As a result, the coking rate dropped by a factor of 4. In the "real" world, the same effect can be obtained if the air supply would be pulsed to create local environments were the O to C mole ratio would change from about 1.0 to 1.2. When turbulence was used to reduce coking, RF coke suppression reduced coking only an additional 20%. Thus, turbulence is a better tool to suppress coking than is RF coke suppression.

Conclusions and Future Directions

It was demonstrated that a low-cost Ni-based catalyst can reform a 50 ppm S containing diesel fuel with or without recycle gas. In addition, if coking on the catalyst is controlled by proper catalyst formulation, introduction of turbulence into the flame front, and by possible application of a RF electromagnetic field, catalyst deactivation can be avoided for at least 500 hours of operation. This is a good step towards developing a long term stable catalyst capable of reforming ultra low sulfur diesel fuel for at least 5,000 to 10,000 hours.

FY 2006 Publications/Presentations

1. "Development of Ni-based Sulfur Resistant Catalyst for Diesel Reforming" Final Technical Progress Report, Gunther Dieckmann, May 18, 2006.

References

1. "Diesel Reforming with Perovskite Catalysts" Michael Krumpelt, Workshop on Logistic Fuel Desulfurization Technology for Power and Energy Applications, U.S. Army Research Laboratory, Adelphi, MD, September 14, 2005.

2. "Catalysts for Autothermal Reforming" Jennifer Mawdsley, Magali Ferradon, Cecile Rossignol, James Ralph, Laura Miller, John Kopasz, and Theodore Krause, Hydrogen, Fuel Cells & Infrastructure Technologies Program, 2003 Merit Review and Peer Evaluation Meeting, May 19-22, 2003.

3. "Hexaaluminate Catalyst Development", David Berry, 2005 SECA Core Technology Peer Review Workshop, Tampa, FL, January 27, 2005.

4. "Nickel-based Sulfur Resistant Reforming Catalyst with Radio Frequency Coke Suppression", G. H. Dieckmann, Presented at the SECA Diesel Fuel Processing Workshop, Pittsburgh, PA, December 6, 2005.

III.B.3 An Innovative Injection and Mixing System for Diesel Fuel Reforming

Objectives

- Develop reliable, cost-effective diesel fuel injection and mixing concepts for use with auto-thermal reformer (ATR) and catalytic partial oxidation reformer (CPOX) in SOFC auxiliary power generation units (APUs).
- Determine operation and performance limitations of four different injection and mixing concepts for diesel fuel reforming applications.
- Optimize the most promising injector/mixer for diesel fuel reformers to operate with minimal steam/water usage and air supply pressure.

Accomplishments

- Completed the design and fabrication of four different fuel injection concepts for a comparative study, including a multipoint impingement injector, a gas-assisted simplex injector, a piezoelectric injector and a preheating simplex injector.
- Conducted detailed computer analysis and characterization of fuel mixture for all four injector concepts using phase Doppler interferometry, Raman spectroscopy, laser extinction tomography and thermocouple measurements.
- Down-selected the most promising injector/mixer and established operation/performance correlation using the statistical design of experiments technique.
- Submitted two patent applications entitled "Fuel Injection and Mixing Systems and Methods of Using the Same" and "Fuel Injection and Mixing Systems Having Piezoelectric Elements and Methods of Using the Same."

Chien-Pei Mao
Goodrich Turbine Fuel Technologies
811 4th Street
West Des Moines, Iowa 50265
Phone: (515) 271-7291; Fax: (515) 271-7296
E-mail: Chien-Pei.Mao@goodrich.com

DOE Project Manager: Charles Alsup
Phone: (304) 285-5432
E-mail: Charles.Alsup@netl.doe.gov

Subcontractors:
NASA Glenn Research Center, Cleveland, Ohio

Introduction

Fuel reformers are a very important component of SOFC systems, enabling them to compete with conventional auxiliary power units in remote stationary and mobile power generation markets. Current state-of-the-art fuel reformers are limited to using gaseous fuels, such as natural gas, hydrogen and liquefied petroleum gas (LPG). In the near term, however, liquid hydrocarbon fuels and renewable fuels are the preferred choice for SOFC power systems because of their availability and existing distribution networks.

Currently, liquid fuel processing technology is not yet viable for commercial applications in SOFC systems. One of the major technical barriers for liquid fuel processing is reactor durability. The performance of the reforming catalysts in the reactor quickly deteriorates as a result of carbon deposition, sulfur poisoning and loss of precious metals due to sintering or evaporation at high temperatures. To mitigate these problems, research efforts are being conducted to optimize catalyst materials and to improve fuel reactor design/operation.

Approach

One engineering approach that could alleviate problems associated with liquid fuel reactors is improvement of feed stream preparation. Proper feed stream preparation can significantly improve reactor durability and minimize problems of inadequate fuel atomization, wall impingement, mixture recirculation and non-uniform mixing. These problems can easily lead to local conditions that favor carbon deposition, auto-ignition and formation of hot spots in the reactor. Because liquid fuels are extremely difficult to reform, a proper understanding and selection of injection and mixing systems for feed stream preparation plays an essential role in the development of reliable and durable liquid fuel reformers.

Several promising fuel injection and mixing chamber concepts were proposed for a thorough evaluation using both computational and laser diagnostic techniques. The key performance parameters included in the evaluation were fuel atomization, droplet evaporation and mixing, uniformity of mixture temperature, velocity and concentration, wall impingement, flow recirculation, carbon deposits, feed stream supply pressure, power consumption, complexity and reliability of injector design/operation.

Results

Four injector/mixing chamber concepts have been designed and fabricated for a comparative study, including a multipoint impingement injector, a gas-assisted simplex injector, a high-energy piezoelectric injector and a preheating simplex injector. Based on the experimental and analytical results, relative merits were identified for all injector concepts relating to diesel fuel reforming applications.

Computational fluid dynamics (CFD) was utilized to help predict flow rates, pressure drops and flow non-uniformities associated with design modifications in order to reduce development iterations and cost. CFD was also utilized to simulate the overall flow-field structure and potential mixing capabilities, helping to provide a qualitative assessment of the injector/mixer performance under the actual reformer operating conditions. The computation domain contains a flow path from the feed stream inlets through the injector circuits and the mixing chamber, terminating at the 76.2 mm diameter at the entrance of the catalytic reactor. The grid system for the flow path consists of over 1.8 million tetrahedral and prismatic cells, with clustering tailored to regions of expected high gradients. The solutions were obtained using FLUENT 6.1 software to solve the unsteady, Reynolds-averaged Navier-Stokes equations, with the RNG k-ε turbulence model, wall-functions and differential viscosity models. Figure 1 shows a comparison of time-averaged steam mass fraction in a vertical plane between a gas-assisted injector and a preheating injector. CFD predictions indicated that the preheating injector design produces more uniform temperature and species distributions than the other injector concepts.

For fuel atomization evaluation, detailed measurements were made for all four injector sprays at various operating conditions using phase/Doppler interferometry. Two different measurement methods were utilized to obtain droplet size information: a continuous traverse method and a point-to-point method. The continuous traverse method provides mean droplet diameters that represent the entire spray, and the point-to-point method offers detailed local distributions of droplet size, velocity and fuel volume flux. This information is extremely important to help determine the spray dynamic structure and identify differences between injector concepts. Figure 2 presents a comparison of the radial distribution of Sauter mean diameter (SMD) for the impingement injector, gas-assisted injector and piezoelectric injector at a simulated maximum load condition. The SMD values for the preheating injector are very small, in the sub-micron range, and are not included in Figure 2 for a comparison.

For high-temperature evaluation, the injector/mixer systems were delivered to NASA Glenn Research Center for detailed species measurements using the

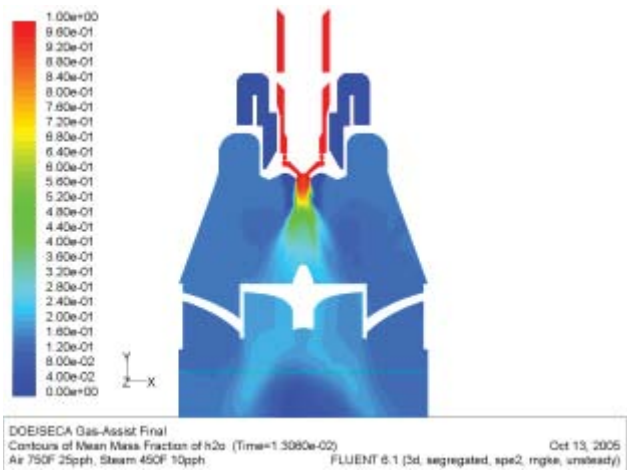

(a) Gas-assisted Injector

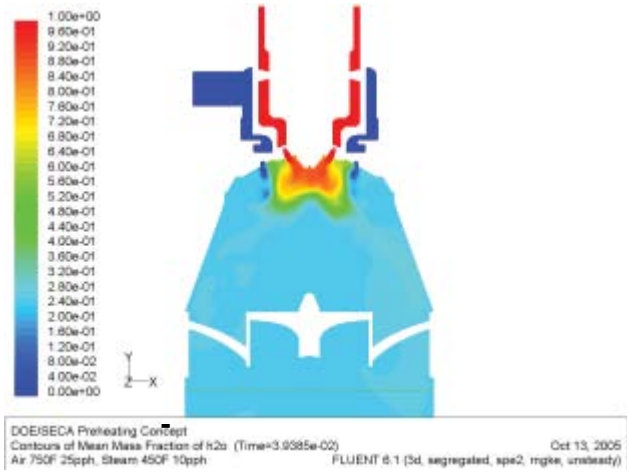

(b) Preheating Injector

FIGURE 1. A Comparison of Time-Averaged Steam Mass Fraction in a Vertical Plane between a Gas-Assisted Injector and a Preheating Injector

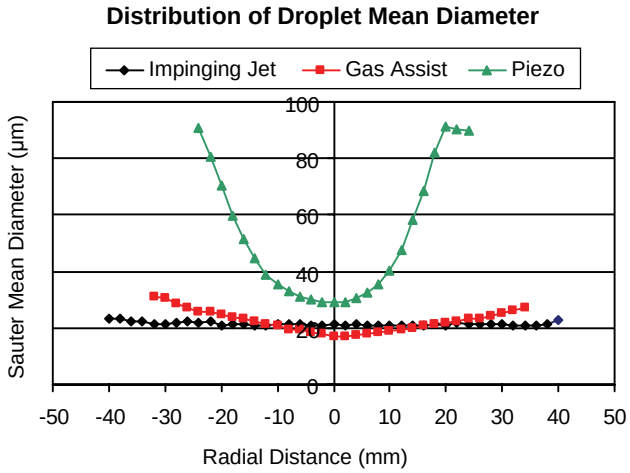

FIGURE 2. A Comparison of the Radial Distribution of SMD for the Impingement Injector, Gas-Assisted Injector and Piezoelectric Injector at a Simulated Maximum Load Condition

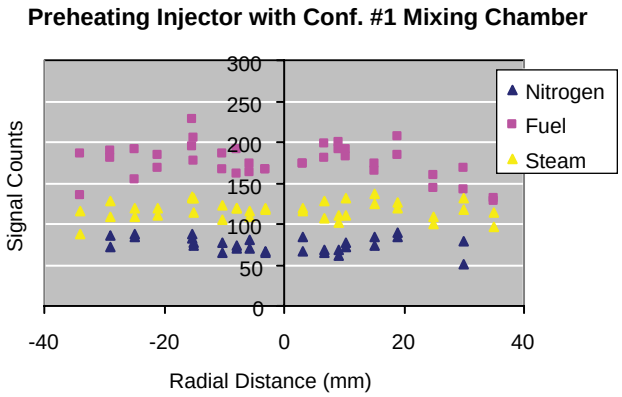

FIGURE 3. Measured Radial Distribution of Species Concentration for a Preheating Simplex Injector Operated with 0.63 g/s Commercial Diesel Fuel, 1.26 g/s Steam at 230°C and 3.15 g/s Airflow at 400°C

Raman spectroscopy instrument. Distributions of fuel, steam and nitrogen were plotted against the radial distances across the flow field to reveal the influence of fuel properties, operating conditions and mixing chamber configurations on feed stream preparation and mixture uniformity. Species measurements were made at an axial distance 65 mm below the mixing chamber exit. The radial distributions of various species were established by making point measurements in 5-mm increments to cover 70 mm of the 75 mm diameter across the flow field. The Raman spectra acquired at various radial locations were processed to determine the area under the Raman peak of each species for signal counts. These signal counts are linearly proportional to the mole fraction of the species detected at the laser probe volume. The higher the signal counts, the higher the species' relative molar fraction is in the flow field. Figure 3 shows the measured species concentration for a preheating simplex injector operating with 0.63 g/s commercial diesel fuel, 1.26 g/s steam at 230°C and 3.15 g/s airflow at 400°C. Compared with the other injector designs, the preheating injector showed the most uniform distribution of species and excellent signal repeatability. During tests, it was observed that the quartz window remained very clean and free of carbon deposits.

Conclusions and Future Directions

- Feed stream preparation and injector selection are extremely important in improving the performance and durability of liquid fuel reformers.
- Extremely fine droplets are required for successful liquid fuel reforming. A SMD value of 15 µm or less may be needed for injector sprays to achieve complete evaporation inside the mixing chamber, in order to mitigate downstream carbon and soot formation.
- The preheating simplex injector appears to be the most promising concept for diesel fuel processing to further the development of SOFC auxiliary power units in commercial diesel truck applications.
- Several operational and technical issues still need to be resolved before incorporating the preheating simplex injector into a practical fuel processing system. These issues include the improvement of injector coking, startup response, fuel fluctuation during load transition and minimizing power consumption.

Special Recognitions & Awards/Patents Issued

1. "Fuel Injection and Mixing Systems and Methods of Using the Same," Patent Pending, April 12, 2006.

2. "Fuel Injection and Mixing Systems Having Piezoelectric Elements and Methods of Using the Same," Patent Pending, December 22, 2005.

FY 2006 Publications/Presentations

1. "Innovative Fuel Injection and Mixing Systems for Diesel Fuel Reforming," SECA 6th Annual Workshop, April 20, 2005, Pacific Grove, CA.

2. "Development of Fuel Injection and Mixing Systems for Diesel Fuel Processing," NETL SECA Fuel Processing Workshop, December 6, 2005, Pittsburgh, PA.

3. "Integrated Injection and Mixing Systems for Diesel Fuel Reforming," U.S. Department of Energy, Office of Fossil Energy Fuel Cell Program, FY 2005 Annual Report.

III.B.4 Reformer for Conversion of Diesel Fuel into CO and Hydrogen

Objectives for Phase I

- Develop low-cost catalysts for use in catalytic membrane reactors for the near complete conversion of commercial diesel fuel into H_2 and CO.
- Demonstrate catalyst tolerance to sulfur contained in commercial diesel fuel at levels of 200 ppm by mass.
- Demonstrate long-term catalytic activity (>1,450 hours) at 1,000°C for reforming commercial diesel fuel.

Approach

- Operate catalysts under conditions which thermodynamically favor formation of H_2 and CO and which completely suppress formation of carbon.
- Choose catalytic materials which do not form thermodynamically stable bulk sulfides under desired reactor operating conditions.
- Develop perovskite-based catalysts for catalytic membrane reactor walls and for catalyst beds which provide highly mobile and reactive oxygen in a dissociated form.

Accomplishments

- Synthesized and tested over 40 catalyst formulations.
- Demonstrated 80-99% conversion of diesel fuel at 1,000°C into H_2, CO, CO_2 and CH_4 for the most active perovskite-based catalysts.
- Demonstrated stable diesel fuel reforming catalytic activity at 1,000°C for two months for one preferred perovskite-based catalyst formulation using commercial diesel fuel containing 200 ppm by mass sulfur.

Jarrod A. Benjamin, Michael V. Mundschau (Primary Contact)
Eltron Research and Development Inc.
4600 Nautilus Court South
Boulder, CO 80301-3241
Phone: (303) 530-0263; Fax: (303) 530-0264
E-mail: eltron@eltronresearch.com

DOE Project Manager: Magda Rivera
Phone: (304) 285-1359
E-mail: Magda.Rivera@netl.doe.gov

Future Directions for Phase II and Beyond

- Will incorporate catalysts onto walls of catalytic membrane reactors to form self-cleaning systems for the elimination of carbon build-up on reactor walls in the cool zones (250 to 950°C) of diesel fuel reformers.
- Will further optimize perovskite-based catalysts for high temperature stability (1,000°C) as well as for use on reactor walls operated in the cooler reactor regions in which the diesel fuel is injected and heated to the preferred reaction temperature.

Introduction

It is desired to convert the hydrocarbons of commercial diesel fuel into a mixture of hydrogen and carbon monoxide which can be used to power solid oxide fuel cells. Thermodynamic calculations summarized in Figure 1 predict that this can be accomplished for stoichiometric mixtures containing one mole of atomic oxygen for each mole of carbon in the diesel fuel if the system is brought to equilibrium at temperatures near 1,000°C. If catalysts are to be used to increase rates of reaction, then the catalysts must be capable of adsorbing and dissociating molecular oxygen into highly active atomic oxygen in order to oxidize the more stable aromatic components of diesel fuel. Catalysts must be stable to at least 1,000°C. Furthermore, catalysts must be tolerant to the sulfur present in commercial diesel fuel.

Thermodynamics also predicts (see Figure 1) that formation of carbon will be highly favored at lower temperatures (300-950°C). A major issue in diesel fuel reformers is the deposition of carbon onto reactor walls as the diesel fuel is heated from ambient temperatures to the desired reforming temperature. The carbon, growing on reactor walls and deposited onto catalyst beds, can rapidly plug fuel reformers. Formation of carbon can be suppressed by addition of steam, CO_2, hydrogen or excess oxygen, but these options lead to reduction of overall fuel cell system efficiencies.

Approach

To eliminate carbon deposition onto the reactor walls in the cool zones of the diesel fuel reformer, without adversely lowering the overall system efficiency by adding excess oxygen, a catalytic membrane reactor is proposed. In such a device (see Figure 2), walls

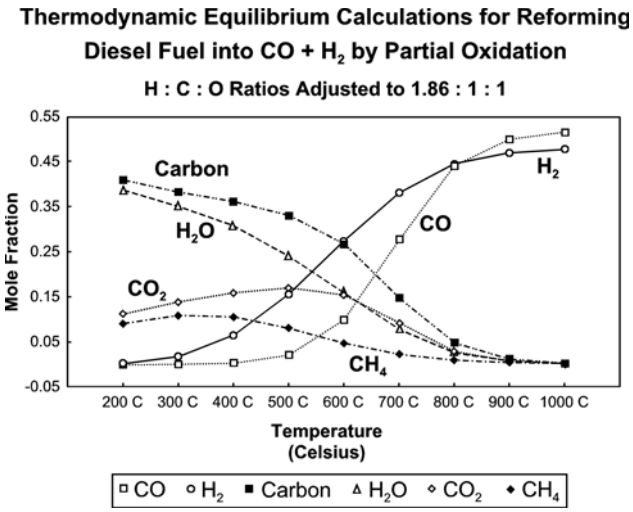

FIGURE 1. Results of thermodynamic calculations predicting that diesel fuel can be converted into the desired hydrogen and carbon monoxide if one mole of oxygen is added for each mole of carbon in the fuel and if the system is brought to equilibrium near 1,000°C. Calculations also predict formation of carbon as diesel fuel is heated to the desired reforming temperature.

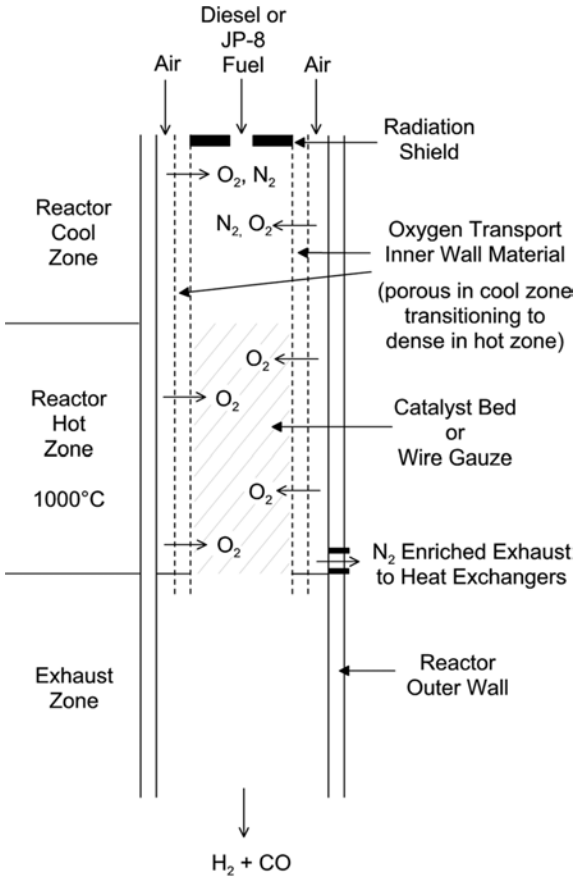

FIGURE 2. Schematic showing the concept of a catalytic membrane reactor in which walls of the reformer are catalytic and provide dissociated oxygen for suppression of deposition of carbon in the reactor cool zones. Reactor walls are self-cleaning.

of the reformer are catalytic and locally provide very high concentrations of atomic oxygen for suppression of the deposition of carbon. The novel feature of the technology is that the reactor walls are essentially self-cleaning, diffusing and effusing oxygen from the outer reactor wall to the inner reactor wall. Oxygen is kept at very high local concentrations near the inner reactor walls, where it is needed to suppress formation of carbon at low temperatures, while the overall concentration of oxygen in the reactor system is kept close to the 1 to 1 ratio of carbon to oxygen required by thermodynamics and for high overall system efficiency.

The catalytic membrane reactor requires very active catalysts for the dissociation of molecular oxygen and for the transport of atomic oxygen into the cool zones of the reactor. Very stable catalysts operating at 1,000°C in the hot zone of the fuel reformer are also required.

Results

Some 40 catalyst formulations were fabricated and tested for activity and stability in reforming commercial diesel fuel containing approximately 200 parts per million by weight sulfur. A number of catalysts with the perovskite crystal structure were designed for high mobility of dissociated oxygen both in the bulk and on the catalyst surface. The perovskite catalysts contained low-cost transition metals which were predicted not to form thermodynamically stable bulk metal sulfides under desired fuel reforming operating conditions. A number of perovskite-based oxidation catalysts showed excellent diesel fuel reforming activity (see Figure 3), exceeding that of Pt-Rh catalysts supported on YSZ.

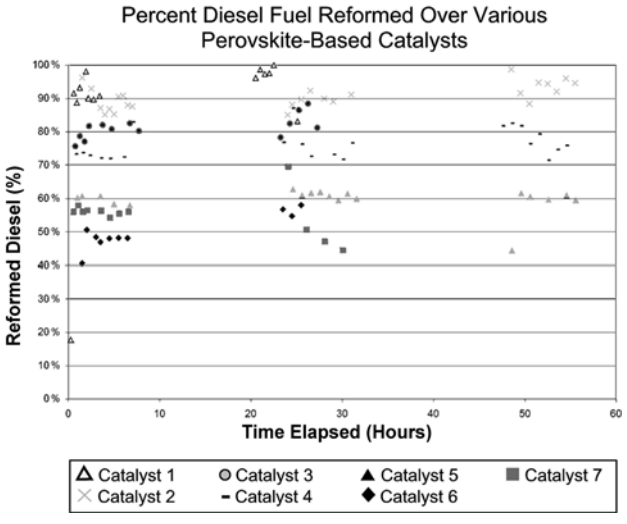

FIGURE 3. Percent of commercial diesel fuel converted into CO, CH_4 and CO_2 for various catalysts operated at 1,000°C. A number of perovskite-based catalysts showed activity superior to Pt-Rh supported on yttria-stabilized zirconia.

Theoretical analysis indicated that a platinum-rhodium gauze would form a near-ideal catalyst in the hot zone. Molecular oxygen is readily adsorbed and dissociated on Pt-Rh surfaces, providing very reactive atomic oxygen. Wire gauzes exposed to diesel fuel and oxygen can operate well above 1,000°C (white-hot) at temperatures for which thermodynamics overwhelmingly favors formation of H_2 and CO and at which sulfides of platinum and rhodium are not stable. However, the cost of platinum-rhodium gauze is prohibitive for most non-military commercial applications. Finely dispersed Pt-Rh supported on yttria-stabilized zirconia (in which the oxides support provides mobile dissociated oxygen as in solid oxide fuel cells) functioned well as a diesel reforming catalyst, but was not stable in long-term tests at 1,000°C due to sintering of the Pt-Rh crystallites (see Figure 4).

The more active perovskite-based catalysts appear to be adequate for use in the cool zones of catalytic membrane reactors (see Figure 3). The preferred perovskite-based catalyst showed stable diesel fuel reforming activity for two months at 1,000°C for commercial diesel fuel containing 200 ppm by mass sulfur (see Figure 4), and should be adequate for use in the catalyst bed of the reformer hot zone.

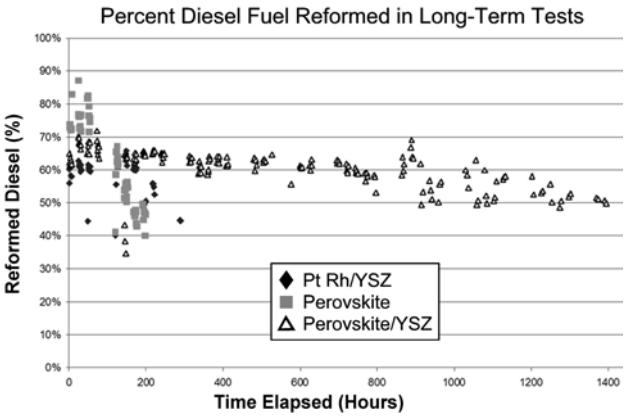

FIGURE 4. Long-term test (>1,450 hours) at 1,000°C, with commercial diesel fuel containing 200 ppm by mass sulfur, showing superior stability of a perovskite-based catalyst relative to Pt-Rh supported on yttria-stabilized zirconia.

Conclusions and Future Directions

Catalysts were developed, based upon oxides with the perovskite crystal structure, which showed high catalytic activity for reforming high-sulfur (200 ppm by mass) commercial diesel fuel into H_2 and CO at 1,000°C. Incorporation of these catalysts into catalytic membrane reactors will allow development of fuel reformers with novel self-cleaning reactor walls sufficient for suppression of deposition of carbon in reactor cool zones while minimizing addition of oxygen and maximizing overall system efficiency desired for solid oxide fuel cells. In future work, the catalysts will be incorporated into the walls of catalytic membrane reactors and used for reforming of commercial diesel fuel and JP-8.

FY 2006 Publications/Presentations

1. "Oxygen Membrane Catalytic Fuel Reforming," NETL SECA Fuel Processing Workshop, December 6, 2005, Pittsburgh, Pennsylvania.

III.B.5 Diesel Plasma Reformer

Objectives

- Perform fundamental research in developing non-thermal plasma technology using model fuels.
- Optimize the plasma reactor's operating parameters for increased synthesis gas (syngas) yield and methane content in the reformate.
- Conduct validation tests for converting the organic sulfur compounds in diesel fuel to hydrogen.

Approach

- Determine the effect of plasma reactor type, residence time, applied power, and carrier gas on diesel conversion.
- Determine the sulfur conversion using optimized reactor conditions.

Accomplishments

- Obtained a three-fold increase in fuel conversion using a plasma reformer.
- Obtained a six-fold increase in hydrogen sulfide (H_2S) concentration in the reformer effluent gas stream.

Future Directions

- Maximize the fuel conversion in the plasma reformer.
- Maximize the sulfur conversion to H_2S in the plasma reformer.

Jennifer Hunt (Primary Contact),
Hossein Ghezel-Ayagh
FuelCell Energy, Inc.
3 Great Pasture Road
Danbury, CT 06813
Phone: (203) 825-6000; Fax: (203) 825-6273
Website: www.fce.com

DOE Project Manager: Magda Rivera
Phone: (304) 285-1359
E-mail: Magda.Rivera@netl.doe.gov

Subcontractor:
Dr. PJ Ricatto, Dr. Kurt Becker
Stevens Institute of Technology, Hoboken, NJ

Introduction

The Solid State Energy Conversion Alliance has targeted Class 8 diesel trucks as a strong early market for 3 to 5 kW solid oxide fuel cell (SOFC) auxiliary power units (APUs). In order to make these units commercially viable by 2010, however, a breakthrough technology is required for processing liquid diesel fuel into a fuel cell grade feed. Our goal in this project is to develop an innovative fuel processing/desulfurization technology, based on the application of silent discharge plasma.

Various catalytic technologies are under consideration for the reforming of diesel fuel. These processes include auto-thermal reforming (ATR), catalytic partial oxidation (CPOx) and steam reforming (SR) [1]. Catalytic steam reforming is the conventional method for converting heavy petroleum-based distillates to a methane-rich gas. However, the reforming and fuel cell catalysts are highly prone to poisoning by the organic sulfurous compounds found in the distillate fuel [2].

Figure 1 shows a schematic of the proposed fuel processing system integrated with a SOFC APU. Diesel fuel and water are vaporized, and sent to the plasma reactor. The plasma reactor converts the diesel fuel to hydrogen, methane and light hydrocarbons. The sulfur compounds in diesel fuel are also converted to hydrogen sulfide in the plasma reactor, and then absorbed in a ZnO bed. The plasma reforming system has a number of key benefits when compared to conventional catalytic fuel processing systems: it is compact and desulfurization

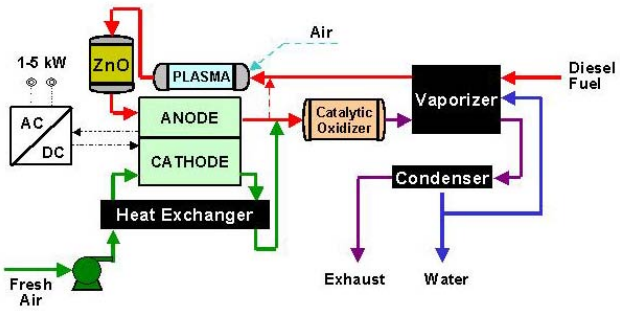

FIGURE 1. SOFC APU Plasma Reformer and ZnO Desulfurization Unit Schematic

and reforming are combined in one reactor. There are no catalysts, therefore reaction rates are not limited by catalyst active surface area. Reliability is increased with no deactivation due to sulfur. There is also the cost consideration; cost is reduced since there are no precious metals. Coking of the diesel fuel is an issue with conventional catalytic technologies but may be unlikely in the plasma reactor due to the presence of steam and the absence of catalytic surfaces.

The term "plasma" is defined as a region in space that has an equal number of positively charged ions and negatively charged electrons. In a non-thermal plasma, energy is channeled into the electrons which may reach temperatures in the range of tens to thousands Kelvin, while the ions and neutrals remain at nearly room temperature. The ions that are created in the plasma region are extremely reactive, and may form intermediate species with diesel fuel in a fashion similar to conventional catalysis. The goal of this project is to optimize the plasma operating conditions to achieve conversion of diesel fuel into a high methane content syngas and to also convert the organic sulfur compounds to H_2S.

Approach

Fundamental research is required to gain an insight into how plasma affects diesel fuel. Parametric tests were conducted to optimize diesel fuel conversion to methane, hydrogen and carbon oxides. The effect of plasma reactor design, residence time, feed composition and power input were quantified in terms of fuel conversion. The fuel conversion was determined via a carbon balance based on the chromatographic analysis of the exit gas stream. The main goal of the parametric study is to increase the concentration of methane in the exhaust stream as polymerizing or cracking the fuel could cause an increase in hydrogen concentration. A "non-reactive" carrier gas with a known flow was used to quantify the results.

Results

The parametric tests of the plasma reformer were conducted using dodecane, a sulfur-free model fuel to simulate diesel fuel. The purpose of using the model fuel was to be able to analyze the data with a greater degree of accuracy. The goal of this study was to investigate how the external system parameters affect the reformation process in the plasma reactor. We investigated the effect of total flow rate, steam to carbon ratio, and power input on the performance of the plasma reactor.

Of all the parameters tested, changing the steam to carbon ratio had the greatest effect on fuel conversion to methane. Fuel conversion and methane production doubled when the steam to carbon ratio also doubled. The power output of the plasma was also investigated and found to have little effect on conversion rate when the power output tripled (from 100 W to 300 W).

The effect of these parameters on dodecane conversion was considered low, and therefore testing continued using JP-5. JP-5 contains aromatics that may provide active sites for the plasma, which the straight chain dodecane lacked. Here we looked at the carrier gas type and reactor design. We investigated three types of carrier gas: argon, nitrogen and air. We saw a three-fold increase in fuel conversion by introducing air as the carrier gas and conducting some partial oxidation in the plasma reformer. This is evidenced by an increase in carbon monoxide concentration using air (4.6%) compared with argon (0.6%). Runs conducted using air but without the plasma produced no carbon monoxide.

We also investigated plasma reactor designs. There were two types of reactors used in the testing: a coaxial dielectric barrier discharge (C-DBD) and a parallel-plate dielectric barrier discharge (PP-DBD). The coaxial dielectric barrier discharge reactor generates plasma in the space between an inner conductor rod (at high voltage) and an outer stainless steel tube (at ground potential). Vaporized fuel, steam and carrier gas flows in space between the inner rod and the tube. The plasma field is generated when high voltage AC power (up to 20 kV at 15–40 kHz) is applied to the inner rod.

The parallel-plate DBD reactor is shown in Figure 2. The stainless steel frame is the grounded electrode and a quartz plate forms the dielectric barrier. A removable copper plate is placed on top of the quartz and acts as the high potential conductor. The vaporized fuel, steam and carrier gas flows in a 1 mm field between the frame and the quartz plate.

Fuel conversion was comparable with either reactor. The parallel plate design easily lends itself to scale-up and is slightly more robust than the coaxial design.

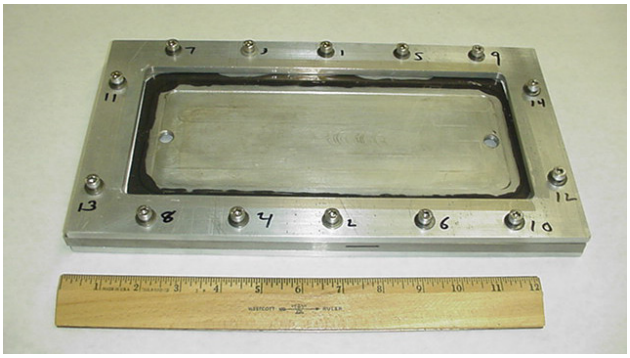

FIGURE 2. Parallel-Plate Dielectric Barrier Discharge Device

The effectiveness of hydrogenating sulfur compounds in JP-5 was determined by measuring the sulfur compounds present in the gas stream. The JP-5 sulfur content was initially 1,100 ppm, much higher than the 50 ppm specification. The higher content was used to insure an appreciable concentration in the effluent. Sulfur content in the gas stream was determined using an Agilent 6890 gas chromatograph equipped with a thermal conductivity detector, a flame ionization detector and a Cevers 355 sulfur chemiluminescence detector. We investigated the effect of carrier gas type and plasma power on the concentrations of sulfur compounds in the reactor exhaust and the results are very encouraging. The total sulfur found in the stream containing the nitrogen purge is roughly equivalent to the sulfur associated with the converted fuel (1.2 ppm in the gas stream). By using air as the carrier gas, however, a 30-fold increase in the sulfur levels was realized (36.6 ppm). Partial oxidation is responsible for some of this increase, but the plasma contributes a 6-fold increase in sulfur levels compared to the no plasma run on air.

We also measured the sulfur content in the condensed liquid after the plasma reformer. The sulfur content dropped ~33% in the liquid, from 1,100 ppm to 740 ppm. This illustrates the possibility of using the plasma reformer as a pretreatment for sulfur containing fuel.

Conclusions and Future Directions

The results achieved under Phase 1 were very encouraging. This project showed a three-fold increase in fuel conversion using a plasma reformer and demonstrated the feasibility of sulfur removal by plasma. More work remains in fully developing the plasma reformer to become a stand alone component in reforming and desulfurizing diesel fuel. This future work is broken into six tasks, the first being overall project management. The second task is to develop a fuel delivery system that produces a steady flow of steam and vaporized diesel fuel to the plasma reactor with accuracy at both 1 kW and 5 kW feed levels. The third task focuses on optimizing a plasma reactor to achieve maximum hydrocarbon conversion efficiency and investigating the use of commercially available plasma systems. The fourth task will investigate plasma-assisted catalytic reforming. The fifth task encompasses both additional parametric testing and computer modeling. Long-term testing is planned for the sixth task.

FY 2006 Publications/Presentations

1. Ghezel-Ayagh, H., Hunt, J., Ricatto, P., and Becker, K., "Diesel Reforming via Plasma", NETL SECA Fuel Processing Workshop, December 6, 2005.

References

1. Borup, R., Parkinson, W. J., Inbody, M., Tafoya, J., and Guidry D.R., "Diesel Reforming for Fuel Cell Auxiliary Power Units," 2004 SECA Review Meeting, Boston, MA, May 11-13, 2004, http://www.netl.doe.gov/publications/proceedings/04/seca-wrkshp/LANL%20-%20Borup.pdf.

2. Krumpelt, M., Liu, D., and Sheen, S., "Diesel Reforming for Solid Oxide Fuel Cell Application," 2004 SECA Review Meeting, Boston, MA, May 11-13, 2004, http://www.netl.doe.gov/publications/proceedings/04/seca-wrkshp/Argonne%20-%20Diesel%20Reforming%20-%20Krumpelt.pdf2.

3. Surdoval, W., "SECA Program Overview," 2004 SECA Review Meeting, Boston, MA, May 11-13, 2004. http://www.netl.doe.gov/publications/proceedings/04/seca-wrkshp/SECA%20Program%20Overview%20-%20Surdoval.pdf.

III.B.6 Fundamental Reforming Studies - Role of Catalytic O_2 Supports on Fuel Reforming

Objectives

- Search for long-duration reforming catalysts in the development of auxiliary power units.
- Investigate the role of oxygen-conducting supports in reforming of diesel fuel compounds and their role in decreasing carbon formation and/or increasing sulfur tolerance.

Approach

- Conduct catalyst characterization and evaluate catalytic hydrocarbon reforming activity for ceria-based catalysts utilizing the partial oxidation of methane (POM).
- Obtain carbon formation trends as a function of oxygen/carbon ratio and find correlation with ionic conductivity.
- Perform mechanistic studies in order to investigate the role of lattice oxygen during the POM. These tests include:
  - Catalyst labeling with $^{18}O_2$.
  - Conducting the POM reaction over $^{18}O_2$ labeled catalysts.
  - Performing prior and post reaction experiments by nuclear reaction analysis (NRA) to complement the isotopic studies and obtain ^{18}O concentration profiles and total oxygen concentration in the catalysts.

Accomplishments

- Demonstrated that catalysts with higher ionic conductivity generated less carbon and catalysts with higher reducibility showed higher conversion.
- Confirmed by isotopic studies and by NRA that lattice oxygen oxidizes methane to generate CO and H_2 during POM.

Future Directions

Compare results obtained for ceria-based catalysts with those of mixed ionic-electronic oxide-based catalysts.

David A. Berry (Primary Contact) and Maria Salazar-Villalpando (Parsons)
U. S. Department of Energy
National Energy Technology Laboratory
P. O. Box 880
3610 Collins Ferry Road
Morgantown, WV 26507-0880
Phone: (304) 285-4430; Fax: (304) 285-4469
E-mail: David.Berry@netl.doe.gov

Subcontractors:
Parsons, Morgantown, WV

Introduction

The U.S. Department of Energy is sponsoring development of high temperature fuel cell power systems based on solid oxide technology through its Solid State Energy Conversion Alliance (SECA) program. The program is geared at mass manufacturing of fuel cells for high volume markets and multiple applications. The fuel processor is a critical component of this system and must be able to provide a clean, tailored synthesis gas to the fuel cell stack for long-term operation. There are several barrier issues that must be overcome to achieve these characteristics. Carbon formation, particularly upon startup, must be minimized to avoid coking of the catalysts in the reformer and downstream fuel cell.

Ceria-based catalysts are being investigated in this work in order to fundamentally understand the role of oxygen-conducting supports in reforming of diesel fuel compounds and their role in decreasing carbon deposition. Ceria-based catalysts have shown ability to decrease carbon formation during partial oxidation of hydrocarbons [1,2]. It has been speculated that this property is due to their high oxygen ion mobility. In this project, this assumption is investigated to elucidate a reaction mechanistic scheme to get a better understanding of carbon formation and mitigation.

Approach

Several metal-deposited catalysts were prepared for this study. Catalyst variables included metal type (Pt, Ni, Rh), support type (Al_2O_3 and CeO_2), dopant type (La, Gd, Zr) and dopant concentration (Gd 10%, Gd 30%). Characterization of ceria-based catalysts included ionic conductivity, temperature programmed reduction profiles, surface areas and catalyst phases. Catalytic activity and stability were determined. Carbon formation trends as a function of ionic conductivity and O/C ratio were obtained. Isotopic studies with ^{18}O

labeled catalysts were performed to study the reaction mechanism of the partial oxidation of methane. Tests by NRA were conducted to investigate the nature of the oxygen species participating in the POM reaction. Methane was utilized to minimize complexity of reforming operations and analysis of results.

Results

Results for the first two years of this project were already included in previous reports. A brief summary is included here. Catalyst characterization was conducted in order to determine the effect of dopant addition to a ceria lattice. Ionic conductivity, catalyst reducibility and crystal phases were determined. Specifically, the addition of gadolinium to the ceria lattice showed a significant ionic conductivity enhancement. For example, at 700°C, pure ceria and gadolinium-doped ceria with 10% gadolinium concentration (GDC10) showed 2.41E-04 and 5.19E-02 S/cm, respectively. Ceria reducibility was also remarkably improved by dopant addition. Particularly, zirconia addition caused an increase in the bulk oxygen reducibility. Relative to CeO_2, the maximum reduction rate appeared at much lower temperature, about 350°C. X-ray diffraction (XRD) characterization showed peaks at 2θ~28° and 33° characteristic of cubic ceria for most of the catayst. In the case of zirconia-doped ceria with 50% zirconia concentration (ZDC50), this material showed broader peaks at 23° and 33.5°, indicating traces of a tetragonal phase. Catalytic activity as a function of temperature from 350 to 850°C illustrated that the light-off temperature for all catalysts was about 550°C. Above 750°C, products showed a H_2/CO ratio of about 2, and methane conversion was about 90%. Carbon deposition of several catalysts with different ionic conductivities was tested as a function of O/C ratio during the partial oxidation of methane at 700°C. Our results indicated that at low O/C ratios, the amount of carbon deposited on the surface catalyst increased. For example, at O/C=0.6, Pt/CeO_2 and Pt/ZDC50 generated 0.5 and 0.3 mg (carbon)/g catalyst, respectively. On the other hand, Pt/GDC30 and Pt/GDC10 generated about the same amount of carbon, 0.1 mg (carbon) /g catalyst. These results led to the conclusion that Pt/GDC10 and Pt/GDC30 are more resistance to carbon deposition due to their high ionic conductivity. Data regarding the effect of O/C feed ratio on the CH_4 conversion (%) during the POM reaction illustrated that for Pt/ZDC50, decreasing O/C ratio from 0.88 to 0.57 caused a decrease in CH_4 conversion of 20%.

This year, isotopic experiments were performed. Only the main results are presented here. For these tests, we preferred to use ^{18}O labeled catalysts to follow the participation of oxide oxygen in the gaseous products rather than using isotopic gaseous reactants. Briefly, catalyst labeling consisted of exposing a pre-reduced

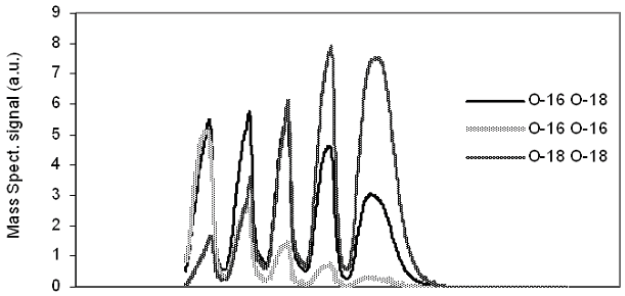

FIGURE 1. Distribution of Oxygen Species During Catalyst "Labeling" with $^{18}O_2$ Doses

catalyst to several doses of $^{18}O_2$ at 700°C. Results in Figure 1 show the mass spectrometer signal for the three oxygen species $^{16}O^{16}O$, $^{18}O^{16}O$ and $^{18}O^{18}O$ at the gas exit of the reactor. Similar results have been reported in the literature for oxygen isotopic exchange experiments with ion-conducting materials [3,4,5,6]. Based on the proposed reaction mechanisms and our results, it is suggested that the formation of $^{16}O^{18}O$ and $^{16}O^{16}O$ at the catalyst surface occurs as written below:

$$[^{18}O_2]_g + [^{16}O]_c \leftrightarrow [^{18}O^{16}O]_g + [^{18}O]_c \quad (1)$$

$$[^{18}O_2]_g + 2[^{16}O]_c \leftrightarrow [^{16}O^{16}O]_g + 2[^{18}O]_c \quad (2)$$

Equation 1 describes the formation of $[^{16}O^{18}O]_g$, where c indicates catalyst and g, gas phase. The formation of $^{16}O^{18}O$ occurs with the participation of one ^{18}O from the gas phase and one ^{16}O atom from the support through the oxygen exchange reaction defined as simple heteroexchange. Regarding $^{16}O^{16}O$, it is generated through the combination of a dioxygen molecule and two oxide oxygen atoms, defined as multiple heteroexchange (2). In similar experiments performed with $Ce_{0.63}Zr_{0.37}O_2$ as a function of temperature, between 30 and 600°C, Madier et al. [7] suggested that not only surface oxygen participates during the isotopic exchange reaction, but bulk oxygen atoms also are exchanged to generate the oxygen products. In a similar publication, Bedrane et al. [8] have reported that conversely to ceria, where oxygen storage capacity is only due to the surface, for zirconia-doped ceria oxides, bulk oxygen has an important role.

Experiments with $^{18}O_2$ were conducted to study the nature of oxygen species participating in the reaction of methane with oxygen to produce H_2 and CO during POM. This reaction was conducted isothermally at 700ºC over ^{18}O labeled Pt/ZDC50 with a mixture of O_2 (2.5 vol%) and methane (5.0 vol%) as a function of time. Figure 2 shows results; it is observed that there are two types of carbon monoxide generated, the isotopic $C^{18}O$ and the "normal" CO. Interestingly, the rate of $C^{18}O$ formation is higher than that of CO formation at the beginning of the reaction. These results led

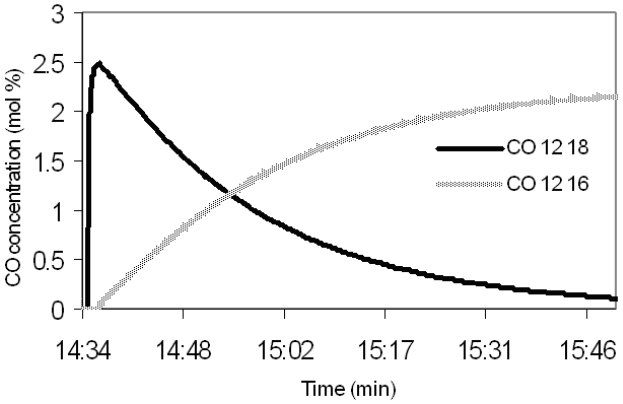

FIGURE 2. Isotopic $C^{18}O$ and "Normal" CO Formation during the POM Reaction over ^{18}O Labeled Pt/ZDC50

to the conclusion that CO formation does not occur in the gas phase, and there is strong evidence of the participation of oxygen originating from the catalyst. It is worth mentioning that the H_2/CO product ratio was 2 during the complete test (the concentration of H_2 is not included in this graph).

Spent catalysts from the POM reaction were analyzed by nuclear reaction to determine ^{18}O oxygen concentration as a function of depth profile. Specifically, ^{18}O labeled Pt/ZDC50 samples prior- and post-POM reaction were tested by using the $^{18}O(p,\alpha)15N$ nuclear reaction. In this experiment, the samples were bombarded with 0.74 MeV H^+ ions. The energy of α particles generated by the nuclear reaction was 3.25 MeV, and the surface barrier detector at 135° scattering angle was used to measure the α particles generated. Results are presented in Figure 3 for catalysts prior- and post-POM reaction. It is immediately obvious that the concentration of ^{18}O in every channel is significantly lower in the post-POM sample than in the fresh (prior-POM) sample. This result is strong evidence that the oxygen specie from the lattice reacts with methane to generate CO^{18} and is replenished from the molecular ^{16}O oxygen initially present with the incoming methane in the gas phase.

Temperature-programmed isotopic exchange reactions with ^{18}O labeled Pt/ZDC50 were performed. Specifically, these reactions were conducted between ^{16}O in the gas phase and the labeled catalyst. Results showed that below 150°C, the oxygen exchange was negligible. At higher temperatures, the exchange rate increased steadily, showing a single maximum peak (530°C) for the formation of the main product, $^{16}O^{18}O$, as illustrated in Figure 4. The formation of $^{16}O^{18}O$ is a function of the dissociation, incorporation, and diffusion steps. Since the $^{16}O^{18}O$ molecule occurs only after the dissociation of the oxygen molecule, we believe that the dissociation step is faster than the incorporation and migration of surface oxygen to the catalyst bulk.

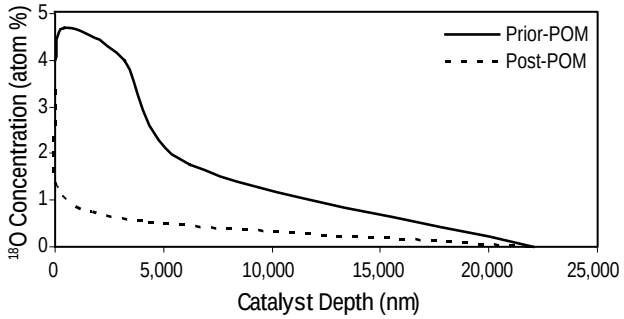

FIGURE 3. ^{18}O Concentration Profiles (atom %) as a Function of Catalyst Depth (nm) for Pt/ZDC50 Prior- and Post-POM at 700°C and O/C=1

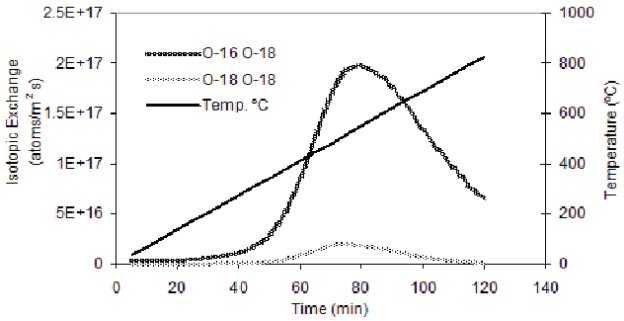

FIGURE 4. Temperature-Programmed Isotopic Exchange over Pt/ZDC50 - Maximum Isotopic Exchange Occurred at 530°C

Conclusions

- Dopant addition significantly enhanced the reducibility and ionic conductivity of pure ceria.
- Catalysts with higher ionic conductivity mitigate carbon deposition.
- Catalysts with higher reducibility showed higher catalytic activity.
- Isotopic studies and post reaction tests by nuclear reaction analysis revealed that CO formation does not occur directly with oxygen in the gas phase during the partial oxidation of methane and that lattice oxygen is the oxygen specie participating in this reaction. Lattice oxygen is replenished from the gas phase.

References

1. Pino L., Recupero V., Beninati S., Shukla A.K., Hegde M.S., Bera P. Applied Catalysis A: General 225 (2002) 63-75.

2. Zhu T.L., Flytzani-Stephanopoulos M. Applied Catalysis A: General 208, 1-2 (2001) 403:417.

3. Boreskov G.K. Faraday Division, Chemical Society (1966) 263-276.

4. Winter E.R.S. J. Chem. Soc. (A) 1968, 2889-2902.

5. Sobyanin V.A., Boreskov G.K., Cholach A.R., Losev A.P. React. Kinet. Catl. Lett., Vol 27, No. 2 (1985) 299-304.

6. Descorme C., Duprez D. Applied Catalysis A: General 202 (2000) 231-241.

7. J. Phys. Chem. B. 1999, 103, 10999-11006.

8. Bedrane S., Descorme C., Duprez D. Catalysis Today 75 (2002) 401-405.

Publications

1. Salazar, Maria; Berry, David A.; Gardner, Todd H.; Shekhawat, Dushyant; Catalytic partial oxidation of methane over Pt/ceria-doped catalysts: effect of ionic conductivity. Applied Catalysis A: General 310 (2006) 54–60.

2. Salazar-Villalpando, Maria D.; Berry, David A.; Gardner, Todd H.; Shekhawat, Dushyant; Celik, Ismail; Synthesis gas by partial oxidation and the role of oxygen-conducting supports: A review. Fuel Cell Science, Engineering and Technology, 2004, June 14-16, 2004, Rochester, New York USA, Fuel Cell. 2004, p. 681-690.

Presentations

1. Salazar, Maria; Berry, David A.; Gardner, Todd H.; Shekhawat, Dushyant; Role of Lattice Oxygen in the Partial Oxidation of Methane over Rh & Pt/Zirconia-Doped Ceria. Mechanistic aspects. Accepted for presentation at the ACS Fall meeting 2006.

2. Salazar-Villalpando, Maria D.; Berry, David A.; Gardner, Todd H.; Shekhawat, Dushyant; Floyd, Donald; Catalytic Partial Oxidation of Methane on Rh-Ceria Based Catalysts. Effect of Reducibility. Presented at AICHE Fall meeting, 2005.

3. Salazar-Villalpando, Maria D.; Berry, David A.; Gardner, Todd H.; Shekhawat, Dushyant; Synthesis Gas by Partial Oxidation and the Role of Oxygen-Conducting Supports: A Review. Presented at the Second International Conference on Fuel Cell Science, Engineering and Technology, June 16, 2004.

III.B.7 Hexaaluminate Reforming Catalyst Development

Objectives

- The development of a durable, low-cost catalyst to reform middle distillate fuels.
- Evaluate the activity and selectivity of transition metal-doped hexaaluminate-type catalysts.
- Evaluate the effect of GDC10 (10 wt% gadolinium-doped cerium oxide) addition to the surface of hexaaluminate-type catalysts as a method of controlling carbon deposition.
- Further elucidate the effect of space velocity on carbon deposition and the presence of olefins.

Approach

- Synthesize and characterize noble metal-doped hexaaluminate-type catalysts.
- Evaluate catalyst activity and selectivity with No. 2 diesel fuel (DF-2).
- Synthesize $BaNi_{0.4}Al_{11.6}O_{19-\delta}$ catalysts with 1, 2 and 3 wt% GDC10 supported on the surface. Test and evaluate the effect of O_2-ion film addition on carbon deposition.

Accomplishments

- Demonstrated 25 hours of stable operation on DF-2 at a gas hourly space velocity (GHSV, at 1 atm and 273.15 K) of 25,000 $cm^3g^{-1}h^{-1}$.
- Synthesized 20 different hexaaluminate-type catalyst formulations.
- Performed catalyst characterization by x-ray diffraction, temperature-programmed reduction and temperature-programmed oxidation (TPO).
- Evaluated the activity and selectivity of synthesized hexaaluminate samples using DF-2.
- Evaluated the effect of adding 1, 2 and 3 wt% GDC10 to the surface of $BaNi_{0.4}Al_{11.6}O_{19-\delta}$ on the formation of carbon.
- Evaluated the effect of GHSV on catalyst selectivity and the formation of olefin compounds and carbon deposition.

Future Directions

- Improved catalyst activity:
  - Evaluate activity and selectivity of platinum group metal-doped hexaaluminate catalysts.
- Improved carbon formation resistance:
  - Continue to evaluate the effect of O_2-ion conducting surface treatments and the use of O_2-ion conducting bed packing materials.
- Improved sulfur resistance:
  - Evaluate the effects of high temperature operation on sulfur resistance.

Todd H. Gardner (Primary Contact), Dushyant Shekhawat and David A. Berry
U. S. Department of Energy
National Energy Technology Laboratory
3610 Collins Ferry Road
P.O. Box 880
Morgantown, WV 26507-0880
Phone: (304) 285-4226; Fax: (304) 285-0943
E-mail: Todd.Gardner@netl.doe.gov

Mark W. Smith
REM Engineering Services, Morgantown, WV

Maria Salazar
Parsons Engineering, Morgantown, WV

Introduction

Reforming middle distillate fuels for distributed fuel cell power is a very attractive source of H_2 and CO. However, these fuels contain heavy hydrocarbons that are prone to coking and contain organ-osulfur compounds which are not easily removed. The simplest reforming technology employs a catalyst to reform the fuel into H_2 and CO and to convert the organo-sulfur compounds into more easily removed H_2S. This approach necessitates the development of a catalyst which does not deactivate under these conditions.

For this application, the National Energy Technology Laboratory (NETL) is developing a new class of catalysts based on transition metal-doped hexaalumina. The use of hexaalumina is of growing importance in catalysis due to its refractory nature [1,2]. The thermal stability of hexaalumina is attributed to its structure, which has proven useful in retaining the large surface area necessary for catalytic reaction [2]. In this project, catalytically active metals are doped directly into the hexaalumina lattice resulting in an atomically dispersed catalyst system that has been shown to possess carbon deposition resistance [3,4].

Approach

At high temperatures, carbon deposition onto the surface of a reforming catalyst occurs predominately through pyrolytic and dehydrogenation reactions. The

selectivity of hydrocarbons toward dehydrogenation into coke occurs when hydrocarbons are adsorbed strongly to the surface of the catalyst [5, 6]. It is, therefore, desirable to design catalyst systems which limit strong hydrocarbon adsorption tendencies and reduce the residence time of the hydrocarbon intermediates on the surface of the catalyst.

The aim of the present study has been to minimize the formation of large ensembles of active sites that are responsible for strongly adsorbing hydrocarbons and sulfur compounds onto the surface of a catalyst. The approach examined here was to substitute catalytically active metals into the framework lattice of a solid oxide. For this application hexaalumina was selected due to its refractory properties. A series of catalysts based on transition metal-doped hexaalumina were prepared by co-precipitation from nitrate salt precursors. The stability of one of the catalysts was assessed over 25 hours of continuous operation on DF-2. Catalyst activity and selectivity were investigated as a function of GHSV. The carbon deposition resistance of $BaNi_{0.4}Al_{11.6}O_{19-\delta}$ treated with 1, 2 and 3 wt% GDC10 was also evaluated.

Results

The effect of adding O_2-ion conducting films to the surface of hexaaluminate catalysts was evaluated as a potential method to mitigate carbon deposition. GDC10 films of 1, 2 and 3 wt% were applied to the surface of a $BaNi_{0.4}Al_{11.6}O_{19-\delta}$ reforming catalyst. The effect of carbon deposition was evaluated by reforming n-tetradecane for 5 hours over the catalysts at a GHSV = 50,000 $cm^3g^{-1}h^{-1}$, an O/C = 1.2, a T = 850°C and a P = 2 atm followed by TPO of the carbon deposits. The TPO results are given in Figure 1. From this figure, a low temperature burn-off peak centered at 350°C was observed for all catalysts. This peak is associated with carbon deposited onto the catalytically active metal site [7]. Higher temperature carbon burn-off was also observed for all four catalysts. Carbon burn-off at higher temperatures is associated with carbon deposited onto the catalyst support. From this figure it is observed that as the GDC10 concentration is increased, the amount of carbon deposited onto the surface of the catalyst was reduced. This indicates that the addition of O_2-ion conducting materials to hexaaluminate catalysts may be an effective approach to reduce carbon deposited onto the catalyst surface.

The partial oxidation performance of a noble metal doped hexaaluminate-type catalyst (HEXM-1) was evaluated by the partial oxidation of DF-2. The catalytic performance of HEXM-1 catalyst is given in Figure 2. The composition of the DF-2 fuel tested is given in Table 1. The reaction conditions investigated were a GHSV = 25,000 $cm^3g^{-1}h^{-1}$, an O/C = 1.2, a total inlet flow rate of 450 sccm (with 50 sccm N_2 diluent) a fuel pre-heat temperature of 350°C, T = 900°C and P = 2 atm.

TABLE 1. DF-2 Composition

Constituent	Concentration (wt%)
Sulfur	9 ppmw
Aromatic	18
Paraffin	38
Naphthenes	44

The first 5 hours of the run were performed on n-tetradecane (TD) to condition the catalyst and baseline catalytic performance. During this time period the catalyst exhibited some changes in selectivity and CO and H_2 yields. The hydrocarbon feed was then switched to DF-2 which resulted in an immediate change in selectivity as well as H_2 and CO yields. This change in catalyst performance is attributed to strongly adsorbing, less reactive feed constituents present in the DF-2.

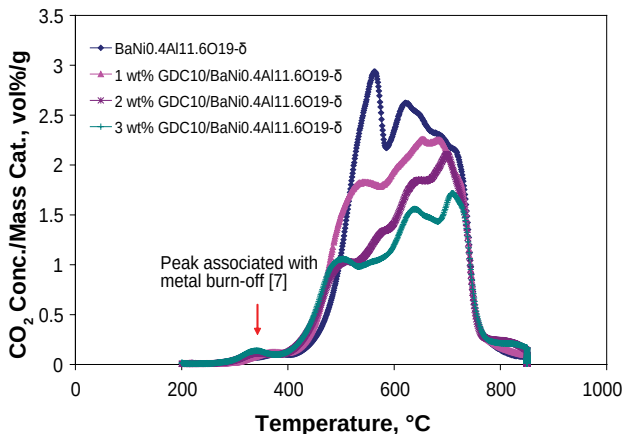

FIGURE 1. The Effect of 1, 2 and 3 wt% GDC10 Addition to $BaNi_{0.4}Al_{11.6}O_{19-\delta}$ on Carbon Deposition

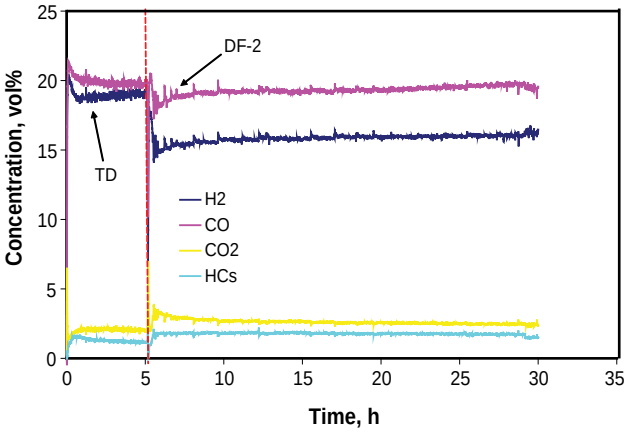

FIGURE 2. The Partial Oxidation of DF-2 over HEXM-1 Catalyst; GHSV = 25,000 $cm^3g^{-1}h^{-1}$, T = 900°C, P = 2 atm, O/C = 1.2

CO_2 and hydrocarbon slip concentrations increased only marginally indicating that catalytic reactions were occurring predominately over gas phase reactions. The catalyst was then run for another 25 hours on DF-2 where it exhibited stable performance.

Also examined was the effect of varying the catalyst space velocity on the partial oxidation performance of HEXM-1 with DF-2. In this study, the O/C = 1.2 was kept constant with a total inlet flow rate of 450 sccm (with 50 sccm N_2 diluent), a fuel pre-heat temperature of 350°C was utilized, the temperature was kept isothermal at T = 900°C and the pressure was kept constant at P = 2 atm. The space velocity of the reactor was varied from 6,250 to 100,000 $cm^3g^{-1}h^{-1}$. The data points were taken after 2 hours into the experimental run. From Figure 3 it is observed that as space velocity is increased, the H_2 and CO concentrations both decreased. With the steepest decrease in H_2 and CO concentration occurring as GHSV was increased from 12,500 and 25,000 $cm^3g^{-1}h^{-1}$. Correspondingly, CO_2 concentration increased with GHSV indicating that gas phase chemistry was also increasing.

From Figure 4, increasing the space velocity also increased the hydrocarbon slip through the catalytic bed. Both methane and ethane concentrations were observed as sharply increasing from 6,250 to 25,000 $cm^3g^{-1}h^{-1}$. Benzene and residual olefins became observable at space velocities in excess of 12,500 $cm^3g^{-1}h^{-1}$.

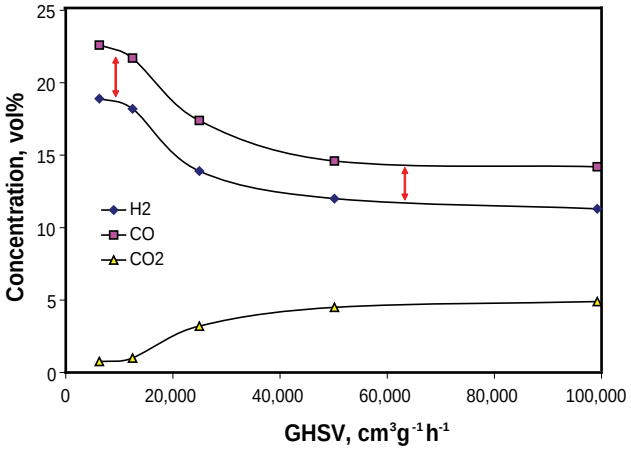

FIGURE 3. The Partial Oxidation of DF-2 over HEXM-1 Catalyst; Effect of Space Velocity on Catalyst Activity; T = 900°C, P = 2 atm, O/C = 1.2

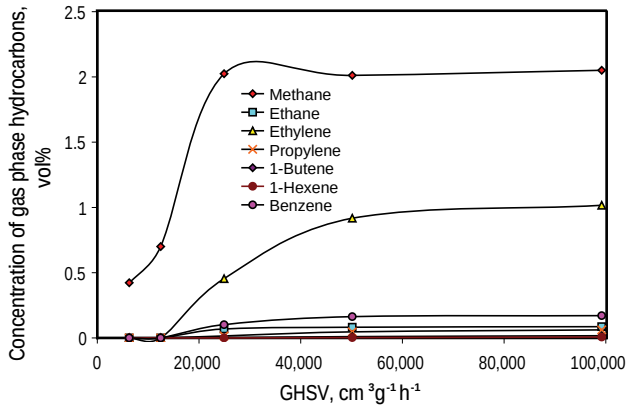

FIGURE 4. The Partial Oxidation of DF-2 over HEXM-1 Catalyst; Effect of Space Velocity on Hydrocarbon Slip; T = 900°C, P = 2 atm, O/C = 1.2

Conclusions

The carbon deposition resistance of a $BaNi_{0.4}Al_{11.6}O_{19-\delta}$ catalyst treated with 1, 2 and 3 wt% GDC10 films was examined. Carbon deposition onto the catalyst surface was shown to decrease with increasing concentration of the GDC10 film. A series of catalysts based on noble metal doped onto hexaalumina were also synthesized. One of the catalysts exhibited excellent stability over 25 hours of continuous operation on DF-2. The activity and selectivity of this catalyst were examined over a range of space velocities. At space velocities exceeding 12,500 $cm^3g^{-1}h^{-1}$ gas phase reaction became more pervasive as well as hydrocarbon slip.

References

1. Machida, M., Shiomitsu, T. and Eguchi, K., *J. Solid State Chem.* 95 (1991) 220-223.

2. Machida, M., Eguchi, K. and Arai, H., *J. Catal.* 103 (1987) 385-393.

3. Xu, Z., Zhen, M., Bi, Y. and Zhen, K., *Catal. Lett.* 64 (2000) 157-161.

4. Gardner, T. H., Shekhawat, D., Berry, D. A., *AIChE Fall Meeting*, Austin, TX (2004).

5. Barbier, J., G. Corro, G., Zhang, Y., Bournonville, J.P., Franck, J. P., *Appl. Catal.* 13 (1985) 245-255.

6. Biswas, J., Bickle, G.M., Gray, P.G., Do, D.D., Barbier, J., *Catal. Rev. Sci. Eng.* 30 (1988) 161.

7. Shamsi, A., Baltrus, J.P. and Spivey, J.J., *Appl. Catal. A* 293 (2005) 145.

FY 2006 Publications/Presentations

1. "Effect of Nickel Hexaaluminate Mirror Cation on Structure Sensitive Reactions during n-Tetradecane Partial Oxidation," Submitted to Applied Catal., Gardner, T. H.

2. "Hexaaluminate Catalysts for the Partial Oxidation of Middle Distillate Fuels," ACS Spring Meeting, Atlanta, GA, 2006, Gardner, T. H., Shekhawat, D., Berry, D. A.

III.B.8 Effects of Sulfur and Polynuclear Aromatics on Catalytic Fuel Reforming

Objectives

- Investigate the effects of sulfur present in diesel fuel on reforming properties.
- Examine the role of support as well as metal catalyst in carbon formation for reforming reactions.
- Study the effects of polynuclear aromatics on reforming properties.

Accomplishments

- Investigated three different catalysts (Rh/$Ce_{0.56}Zr_{0.44}O_2$, Pt/$Ce_{0.56}Zr_{0.44}O_2$) to understand the role of support as well as metal catalyst in carbon formation in the presence of sulfur and aromatics.
- Studied the effects of sulfur on catalytic fuel reforming by introducing a hydrocarbon feed containing 50 ppm or 1,000 ppm sulfur in the form of dibenzothiophene.
- Examined the effects of polynuclear aromatics on reforming properties by feeding a 5 wt% 1-methylnaphthalene containing hydrocarbon feed to the reactor.
- Catalyst recovery after sulfur as well as polynuclear aromatics removal was also assessed for three catalysts studied.

Introduction

The U.S. Department of Energy is sponsoring development of high-temperature fuel cell power systems based on solid oxide technology through its Solid State Energy Conversion Alliance program. The program is geared at mass manufacturing of fuel cells for high volume markets and multiple applications. One of those markets/applications is a diesel-fueled auxiliary power unit for long-haul truck transportation. The fuel processor is a critical component of this system and must be able to provide a clean, tailored synthesis gas to the fuel cell stack for long-term operation. Key characteristics desired for the processor (and the system) include low cost, high efficiency, maximum thermal integration, low maintenance intervals, and acceptable startup and transient response. There are also several barrier issues that must be overcome to achieve these characteristics. Carbon formation, particularly upon startup, must be minimized to avoid coking of the catalysts in the reformer and downstream fuel cell. Fuels containing sulfur can poison both the reforming catalysts and the fuel cell anode. This, coupled with the high aromatic content present in diesel-like fuels, decreases the rate of reforming of other fuel components, such as paraffins, because the aromatics are strongly adsorbed to the active metal active sites. Therefore, it is particularly important to develop a catalyst which is stable and active for the reforming of diesel-like fuels into a hydrogen-rich gas for transportation as well as military applications.

Dushyant Shekhawat (Primary Contact), David A. Berry, Todd H. Gardner
U.S. Department of Energy
National Energy Technology Laboratory
3610 Collins Ferry Rd.
Morgantown, WV 26507-0880
Phone: (304) 285-4634; Fax: (304) 285-0903
E-mail: Dushyant.Shekhawat@netl.doe.gov

Recently, the use of oxygen-conducting catalyst supports have garnered increasing interest due to their higher resistance to carbon formation, particularly for methane reforming [1-3], and resistance to sulfur poisoning as compared to traditional alumina-based supports. A recent review [4] shows that the rate of carbon deposition on nominally similar catalysts (primarily Ni-based) varies by several orders of magnitude, depending on the support. Ceria and zirconia were found to be effective, with a mixed ceria-zirconia support being superior to either in one case [5]. A temperature-dependent mechanism is postulated involving dissociative adsorption of oxygen on the metal and spillover to the support [6]. However, it is not clear if this mechanism would be applicable under conditions present in the reforming of liquid fuels [7].

In this study, the relationship between catalyst support, metal type, and deactivation was studied for three catalysts (Rh/$Ce_{0.56}Zr_{0.44}O_2$, Pt/$Ce_{0.56}Zr_{0.44}O_2$, and Pt/Al_2O_3) in a fixed bed catalytic reactor using a mixture of n-tetradecane (TD) and dibenzothiophene (DBT) or 1-methylnaphthalene (MN) to simulate diesel-like fuels. Reforming tests were conducted with TD to establish a baseline performance, while DBT (50 or 1,000 ppmw) or MN (5 wt% of feed) was added and removed throughout the test to observe their effect on reforming performance. A comparison of these three catalyst configuration is presented.

Approach

TD was used as a model diesel fuel compound to screen catalysts for activity and selectivity. The sulfur

tolerance of the catalysts was assessed through partial oxidation of TD containing 50 or 1,000 ppmw sulfur as DBT. MN (5 wt% of feed) was used as a model compound for polynuclear aromatics present in diesel fuel. These experiments were carried out by first running TD for one hour. Then, TD with 50 or 1,000 ppmw sulfur as DBT or 5 wt% MN was introduced as a step function and run for two hours. The samples were then switched back to the feed containing only TD to examine recovery. Catalyst tests were carried out in a fixed bed continuous-flow reactor. Nitrogen and air feed gases were delivered by mass flow controllers and the liquid feed was delivered by a high accuracy HPLC pump. Experiments were conducted at an O/C = 1.2, a GHSV = 50,000 h^{-1}, and 850°C. The catalyst was diluted with 5/1 quartz sand-to-catalyst ratio (by weight) to avoid preferential gas flow paths and hot spots.

The gases (N_2, O_2, CO, CO_2, and CH_4) were analyzed using a Thermo Onix mass spectrometer. The gaseous hydrocarbon products (C_1-C_6 paraffins, C_2-C_6 olefins, and benzene) were analyzed using a HP5890 gas chromatograph equipped with a flame ionization detector. Yield of product A (H_2, CO, and CO_2) is defined as:

$$\text{Yield of A (\%)} = \frac{\text{Moles of A produced x 100}}{\text{N x moles of hydrocarbon fed to the reactor}}$$

Where, N is the number of moles of hydrogen per mole of hydrocarbon for H_2 yield and is the number of carbons in hydrocarbon fuel for yields of other products. The conversion of hydrocarbons is defined as:

$$\text{Conv (\%)} = \frac{(CO + CO_2 + \sum_{i}^{i=1\text{-}7} iC_iH_f) \text{ x } 100}{\text{N x moles of hydrocarbon fed to the reactor}}$$

Three catalysts used in this study were 1 wt% Pt/γ-Al_2O_3 (SA 198 m^2/g), 1 wt% Pt/ $Ce_{0.56}Zr_{0.44}O_{2-x}$, (SA 70 m^2/g), and Rh/$Ce_{0.56}Zr_{0.44}O_{2-x}$ (SA 69 m^2/g). Zirconia-doped ceria (ZDC), $Ce_{0.56}Zr_{0.44}O_{2-x}$, for the Pt and Rh catalysts were prepared by NexTech Materials (Worthington, OH) using a proprietary hydrothermal method. Oxygen-ion conductivity of ZDC material at 800°C was 4.3 mS/cm. Additional catalytic characterization such as x-ray diffraction (XRD), ion conductivity, and temperature programmed reduction can be found in a different publication [8]. Pt/γ-Al_2O_3 was used as a baseline catalyst and compared with Pt/ $Ce_{0.56}Zr_{0.44}O_{2-x}$ to see the effect of support on the reforming properties in the presence of sulfur. Pt/ZDC and Rh/ZDC were used to study the effect of metal catalyst on the reforming properties in the presence of sulfur.

Temperature programmed oxidation (TPO) of the spent catalyst was used to determine the amount of carbon formed during reforming reactions.

Results

Catalytic partial oxidation (CPOX) of n-tetradecane

Yields of H_2, CO, CO_2, and unsaturates (olefins + benzene); TD conversion; and amount of carbon formed for three catalysts are given in Table 1. All three catalysts studied showed very stable behavior during CPOX of TD for 5 hours. TD conversion to gaseous products was always more than 95%. Pt-based catalysts formed a significant amount of unsaturates and, thus, produced a higher amount of carbon compared to Rh/ZDC (no olefins or benzene formed from Rh/ZDC (see Table 1).

TABLE 1. Yields of H_2, CO, CO_2, and Unsaturates; TD Conversion; and Amount of Carbon Formed from Three Catalysts Studied

	Equilibrium	Pt/Al_2O_3	Pt/ZDC	Rh/ZDC
H_2 yield (%)	87	81	70	81
CO yield (%)	89	81	73	84
CO_2 yield (%)	10	17	20	15
Unsaturates yield (%)	0	0.8	1.5	0.0
Conversion (%)	100	>99	97	>99
Amount of carbon formed (g/g of catalyst)	0	0.85	0.69	0.21

A significant difference observed between these three catalysts was the formation of unsaturates, which are known coke precursors [9]. No unsaturates were observed from CPOX of TD only feed over the Rh/ZDC, whereas a significant amount of unsaturates was formed from Pt-based catalysts. The TPO of carbon deposited on the three catalysts studied is shown in Figure 1. It is obvious from Table 1 and Figure 1 that the amount of carbon deposited on the catalyst during CPOX reforming was directly related to unsaturates formation. The Rh/ZDC catalyst produced the least amount of carbon whereas Pt/alumina produced the highest amount of carbon, as expected from unsaturates formation on these catalysts. The ZDC-supported catalysts yielded a lower amount of carbon compared to the alumina-supported catalyst, most likely due to their oxygen-ion conductivity properties. The high oxygen-ion conductivity of oxygen-ion conducting supports such as ZDC may increase the rate of oxidation of adsorbed carbon species by reactive oxygen species [3]. Consequently, lower carbon deposition on the catalyst surface is observed from reforming reactions over oxygen-ion conducting supported metal catalysts.

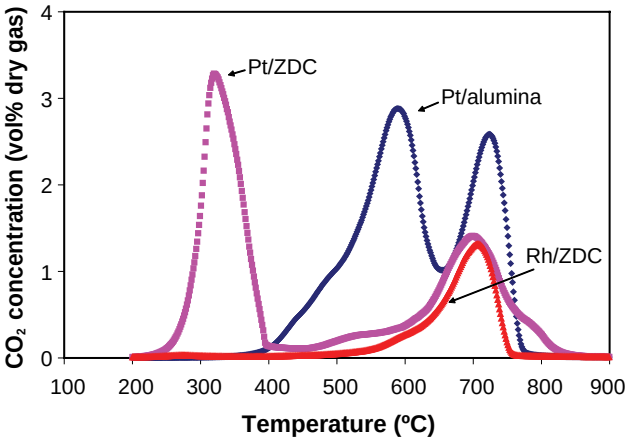

FIGURE 1. TPO of Carbon Deposited Catalysts

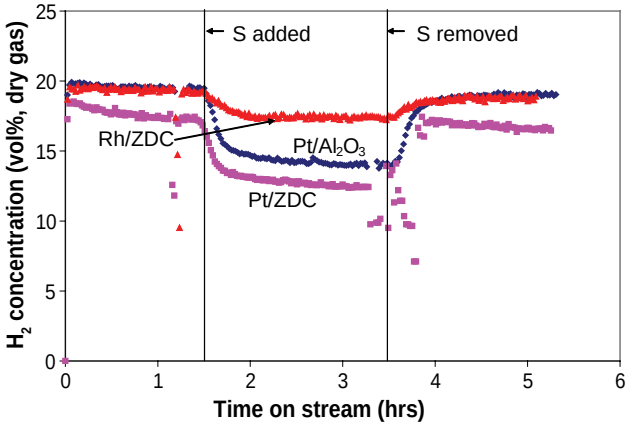

FIGURE 2. Step Response Plot for H_2 Production from TD with 50 ppmw Sulfur

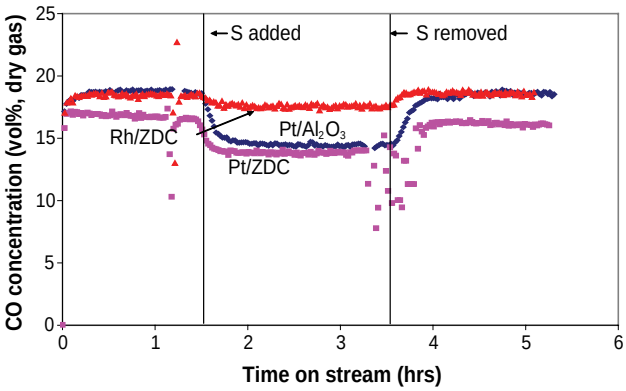

FIGURE 3. Step Response Plot for CO Production from TD with 50 ppmw Sulfur

Two peaks were observed in the TPOs of the Pt-based catalysts as shown in Figure 1. The low temperature peak can be assigned to carbon deposition on metal sites [10] which can be gasified easily at low temperatures because metal catalyzes the carbon gasification. The low temperature peak on Pt/ZDC appeared at a much lower temperature than Pt/alumina – likely due to metal support interactions or different kinds of carbon formation on metal supported on oxide-ion conducting supports. The high temperature peak comes from the carbon deposited on the support. Interestingly, the high temperature peaks of all three catalysts appear at about 700°C, suggesting that this carbon is qualitatively similar for all these catalysts–and is assigned to the carbon deposited on the support. Both ZDC-supported catalysts showed almost similar peaks. However, there is undoubtedly more carbon of this type on the alumina than on the ZDC, which is certainly due to the oxygen-conducting properties of the ZDC. Furthermore, the TPO of used Rh/ZDC catalysts showed only a single peak at 700°C, suggesting that no carbon is formed on the Rh catalyst at the condition studied.

The nature of the metal catalyst also plays an important role in partial oxidation reactions of higher hydrocarbons. Rhodium supported on an oxygen-ion conductive material showed higher activity and lower carbon formation than platinum supported on the same.

CPOX of n-tetradecane in the presence of sulfur

The effects of 50 ppm sulfur as DBT in the feed on H_2 and CO production are shown in Figures 2 and 3, respectively, for all catalysts studied. The concentrations stabilized after 30 minutes online. H_2 and CO concentrations dropped upon introducing 50 ppmw sulfur in the feed for all three catalysts studied. However, the decline in H_2 and CO concentrations was more drastic for the Pt-based catalysts compared to Rh/ZDC. For the Rh catalyst, H_2 and CO concentrations dropped from 20 and 19 vol%, before the step DBT input, to 18 and 18 vol% respectively, after the introduction of DBT. Furthermore, H_2 concentrations continued to decline after introduction of DBT for the Pt-based catalysts while H_2 concentrations dropped to a near-stationary level for the Rh catalysts. Interestingly, CO concentrations dropped to a stationary level after introduction of DBT for all three catalysts studied, suggesting preferential poisoning of the sites responsible for H_2 formation.

However, the higher concentrations (1,000 ppmw) of sulfur significantly affect the performance, particularly of Pt-based catalysts (Figures 4 and 5). By introducing 1,000 ppmw sulfur in the feed, the drop in H_2 concentrations was considerable over time compared to CO or CO_2 concentrations. The H_2/CO ratio before sulfur introduction was >1, while it became <1 (<0.5 for Pt-based catalysts) after sulfur introduction. Also, selectivity to unsaturates increased as selectivity to

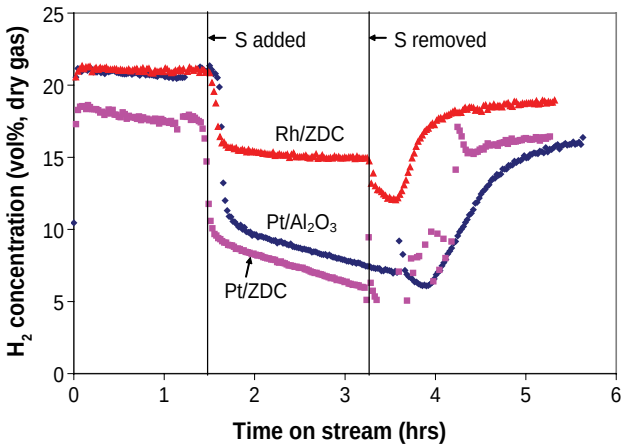

FIGURE 4. Step Response Plot for H_2 Production from TD with 1,000 ppmw Sulfur

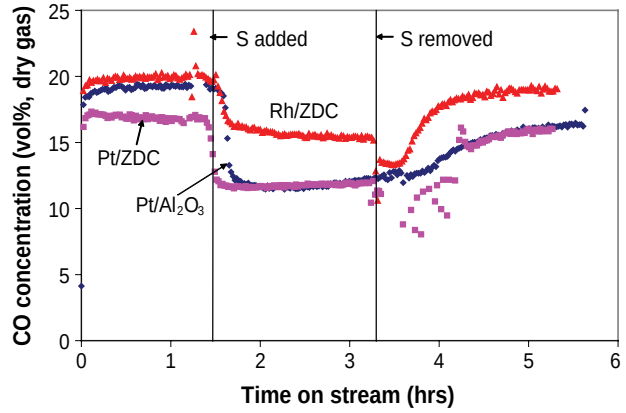

FIGURE 5. Step Response Plot for CO Production from TD with 1,000 ppmw Sulfur

syngas decreased. This was more significant for the Pt-based catalysts, suggesting more gas phase chemistry occurs when the catalyst is deactivated. Consequently, more carbon formation was observed during the reforming of a sulfur-containing feed (Table 2). TD conversion decreased to 70-80% (depending on the catalyst) in the presence of sulfur.

TABLE 2. Amount of Carbon Formed (g/g of catalyst)

	TD	TD + 50 ppm S	TD + 1,000 ppm S	TD + 5% MN
Pt/Al_2O_3	0.85	0.92	2.44	2.88
Pt/ZDC	0.69	-	1.46	1.45
Rh/ZDC	0.21	0.56	0.95	0.89

Catalyst activity was nearly restored for H_2 and CO after removing the sulfur from the feed for the ZDC-based catalysts, but not for the Pt/alumina catalyst, which only partially recovered. Catalyst activity recovery after sulfur removal from the feed for Rh/ZDC and Pt/ZDC suggests that the sulfur is weakly adsorbed on the surface of those catalysts so it can be removed easily afterwards. It was not clear whether sulfur causes deactivation directly by sulfur poisoning or indirectly by excessive carbon formation. However, this kind of catalytic activity drop can be overcome by decreasing the space velocity (to balance the less available surface caused by occupied sulfur) or increasing the temperature to weaken the sulfur-metal interactions.

CPOX of n-tetradecane in the presence of 5 wt% MN

Effects of 5 wt% MN in the feed on reforming activities were similar to 1,000 ppmw sulfur in the feed. H_2 and CO concentrations dropped upon introducing 5 wt% MN in the feed, less significantly for Rh/ZDC compared to Pt-based catalysts. For the Rh catalyst, H_2 and CO concentrations dropped from 21 and 20 vol%, before the step MN input, to 16 and 17 vol% respectively, after the introduction of MN. Similar to sulfur results, H_2 concentrations declined continuously over time after introduction of MN for the Pt-based catalysts while H_2 concentrations dropped to a stationary level for the Rh catalysts. CO concentrations dropped to a stationary level after introduction of MN for all three catalysts studied. Also, by introducing aromatics in the feed, the drop in H_2 concentrations was considerable over time compared to CO or CO_2 concentrations. The H_2/CO ratio before MN introduction was >1, while it became <1 (<0.5 for Pt-based catalysts) after MN introduction. However, catalyst activity was almost completely restored for H_2 and CO after removing the MN from the feed for the Rh/ZDC, but not for the Pt-based catalysts, which only partially recovered. More carbon formation was observed during the reforming of a MN containing feed compared to reforming of TD only feed. Also, hydrocarbon conversion decreased to 70-80% (depending on the catalyst) in the presence of aromatic compound in feed.

Conclusions and Future Directions

- The effects of 1,000 ppmw sulfur and 5 wt% 1-MN in the CPOX of TD include decreased H_2 and CO yields, kinetic inhibition, and reversible deactivation.
- The activity was partially restored after removing the sulfur or aromatics from the feed.
- The Rh/ZDC catalyst showed less kinetic inhibition than either Pt/ZDC or Pt/Al_2O_3.
- The higher oxygen-ion conductivity of the ZDC support appears to improve the resistance to carbon formation in the CPOX of TD.
- Sulfur effects are very catalyst sensitive.

- Rate of carbon formation increased with S in the feed.
- GHSV has to be adjusted to accommodate a decrease in kinetics due to the presence of aromatics or sulfur in the feed.

FY 2006 Publications/Presentations

1. D. Shekhawat, T. H. Gardner, D. A. Berry, J. J. Spivey, Catalytic Reforming of Liquid Hydrocarbon Fuels for Fuel Cell Applications, *Catalysis,* Royal Society of Chemistry, Cambridge, UK, Vol. 19, Chapter 6, 184-253.

2. D. Shekhawat, D. A. Berry, T. H. Gardner, M. Salazar, D. J. Haynes, J. J. Spivey, Support Effects for Pt and Rh-Based Catalysts for Partial Oxidation of n-Tetradecane, *Applied Catalysis A: General*, (in press).

3. D. Shekhawat, T. H. Gardner, D. A. Berry, Fuel Constituent Effects on Fuel Reforming Properties for Fuel Cell Applications, *231st ACS National Meeting*, Mar 26-30, 2006, Atlanta, GA.

4. D. Shekhawat, D. A. Berry, T. H. Gardner, D. J. Haynes, J. J. Spivey, T. Xiao, M. L. H. Green, Partial Oxidation Reforming of n-Tetradecane over Pt and Carbide Catalysts: A Comparative Study, *231st ACS National Meeting*, Mar 26-30, 2006, Atlanta, GA.

5. D. A. Berry, D. Shekhawat, T. H. Gardner, M. Salazar, D. J. Haynes, J. J. Spivey, Support Effects for Pt and Rh-Based Catalysts for Partial Oxidation of n-Tetradecane, *The Fourth International Conference on Fuel Cell Science, Engineering and Technology*, Jun 19-21, 2006, Irvine, CA.

6. D. Shekhawat, D. A. Berry, T. H. Gardner, Diesel Fuel Reforming Studies, 2006 NETL Fuel Reforming Annual Merit Review.

References

1. Huang, T. J., Lin, H. J., and Yu, T. C., 2005, Catal. Lett., **105**(3-4), pp. 239-247.

2. Hamakawa, S., Yoshino, S., Nakamura, J., Liu, Y., Tsyganok, A., Suzuki, K., Murata, K., and Hayakawa, T., 2001, Electrochem. Solid State Lett., **4**(10), pp. D9-D11.

3. Zhu, T. and Flytzani-Stephanopoulos, M., 2001, Appl. Catal. A: Gen., **208**(2), pp. 403-417.

4. Salazar-Villalpando, M., Berry, D. A, Shekhawat, D., Gardner, T. H., and Celik, I., 2004, 2nd ASME Fuel Cell Sci. Eng. and Tech. Conf., pp. 681-690.

5. Descorme, C., Madier, Y., Duprez, D., and Birchem, T., 2000, *Studies in Surface Science and Catalysis (12th International Congress on Catalysis)*, Corma, A., Melo, F. V., Mendioroz, S., and Fierro, J. L. G., eds., Elsevier Science, **vol. 130**, pp. 347-352.

6. Descorme, C. and Duprez, D., 2000, Appl. Catal. A: Gen., **202**(2), pp. 231-241.

7. Shekhawat, D., Gardner, T. H., Berry, D. A. and Spivey, J. J., 2006, *Catalysis*, Spivey, J. J., ed., Royal Society of Chemistry, Cambridge, UK, 2006, **VOL. 19**, Ch. 6, pp. 184-253.

8. Salazar, M., Berry, D. A, Gardner, T. H., Shekhawat, D., and Floyd, D., 2006, *Appl. Catal. A: Gen*, **310**, pp. 54-60.

9. Rostrup-Nielsen, J. R., 1984, "*Catalysis, Science, and Technology*, Anderson, J. R. and Boudart, M., eds., Springer-Verlag, Berlin, **vol. 5**, pp. 1-118.

10. Shamsi, A., Baltrus, J. P., and Spievy, J. J., 2005, Appl. Catal. A: Gen., **293**, pp. 145-152.

III.B.9 Effects of Recycle on Catalytic Fuel Reforming

Objectives

- Study the effects of recycle streams on reforming properties.
- Evaluate anode versus reformer recycle configuration.
- Delineate the effects of individual components present in recycle streams.

Accomplishments

- Evaluated the effects of anode recycle ratios of 0 to 0.5 on reforming properties (yields of H_2, CO, CO_2, and unsaturates, hydrocarbon conversion, and carbon formation). A similar study was also completed for the reformer recycle stream.
- Studied the effects of individual components present in the recycle streams (H_2, CO, CO_2, H_2O, and N_2) on reforming properties.

Introduction

The U.S. Department of Energy is sponsoring development of high-temperature fuel cell power systems based on solid oxide technology through its Solid State Energy Conversion Alliance (SECA) Program. The program is geared at mass manufacturing of fuel cells for high volume markets and multiple applications. One of those markets/applications is a diesel-fueled auxiliary power unit (APU) for long-haul truck transportation. The fuel processor is a critical component of this system and must be able to provide a clean, tailored synthesis gas to the fuel cell stack for long-term operation. Key characteristics desired for the processor (and the system) include low cost, high efficiency, maximum thermal integration, low maintenance intervals, and acceptable startup and transient response. There are also several barrier issues that must be overcome to achieve these characteristics. Carbon formation must be minimized to avoid coking of the catalysts in the reformer and downstream fuel cell. Water can help suppress carbon formation, allow for better thermal integration and system efficiency, and possibly inhibit temperature rise and catalyst sintering. However, the National Energy Technology Laboratory (NETL) is promoting "dry" systems to reduce cost and complexity of overall fuel cell systems. On-board water storage is not an attractive option for many applications including APUs. Therefore, in this study, we explored two possible configurations (see Figure 1) to incorporate higher water concentrations in a "waterless" system: (1) recycle from the reformer exit and (2) recycle from the anode exit back to the reformer inlet. A comparison of these two configurations in terms of reforming properties (yields of H_2, CO, CO_2, paraffins, and unsaturates [C1-C6 olefins and benzene], hydrocarbon conversion, and carbon formation) is presented. The effects of individual recycle components (H_2, CO, CO_2, N_2, and H_2O) on reforming properties are also reported.

Dushyant Shekhawat, David A. Berry (Primary Contact), Todd H. Gardner
U.S. Department of Energy
National Energy Technology Laboratory
3610 Collins Ferry Rd.
Morgantown, WV 26507-0880
Phone: (304) 285-4430; Fax: (304) 285-0903
E-mail: David.Berry@netl.doe.gov

Approach

NETL's SECA Fuel Cell Program requires that the fuel reformer must operate without any onboard water storage to reduce costs as well as overall complexity of the fuel cell system. However, the presence of water in the feed to the reformer is critical in reducing carbon formation on the catalyst surface. Steam facilitates cleaning of the carbon as it forms (Reaction 1) and thus helps in reducing carbon formation on the catalyst.

$$C + H_2O = CO + H_2 \quad (1)$$

Water is a main product along with CO_2 on the fuel cell anode. Therefore, recycling a portion of the anode exhaust stream to the reformer can be a potential onboard source of water. Additionally, CO_2 present in the exhaust stream can be beneficial too. The presence

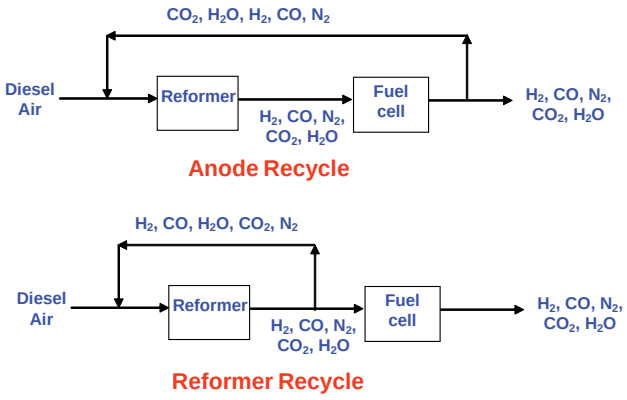

FIGURE 1. Recycle Configurations

of CO_2 in the system can help in reducing carbon formation by the Boudouard reaction:

$$C + CO_2 = 2CO \quad (2)$$

In addition to coke inhibition, CO_2 and H_2O can serve as oxidants for reforming reactions and, thus, increasing hydrocarbon conversion through dry and steam reforming, respectively, of unconverted hydrocarbons in the reformer. Consequently, a lower O/C ratio can also be used. Overall, water can help suppress carbon formation, allow for better thermal integration and system efficiency, and possibly inhibit temperature rise and catalyst sintering.

The reformer recycle stream was also studied as a potential source of water. In this configuration, a part of the reformer exhaust – consisting mainly of CO, H_2, N_2, some water, CO_2, and unconverted lower hydrocarbons – is recycled back to the reformer. It is speculated that H_2 in this stream may check the hydrocarbon dehydrogenation on the catalyst surface, which is believed to be a coke forming reaction.

A mixture of 40 wt% tetradecane, 20 wt% t-butylbenzene, 18 wt% t-butylcyclohexane, and 22 wt% decalin was used as a surrogate diesel fuel for this study. A simulated stream of 24% CO_2, 18% H_2O, 3% H_2, 3% CO, and 52% N_2 was used as anode recycle stream whereas a composition of 24% CO, 22% H_2, 5% H_2O, 1% CO_2, and 48% N_2 was used as a reformer recycle stream. These compositions were estimated using equilibrium calculation based on the surrogate diesel fuel. Also, 80% conversion of syngas in the fuel cell was assumed for the anode recycle stream. However, higher water composition than calculated was used for the reformer recycle stream since it was not possible to pump the water accurately with lower flow rates. Simulated recycle stream and air feed gases were delivered by mass flow controllers and the liquid feeds were delivered by a high accuracy high performance liquid chromatograph (HPLC) dual pump. A recycle ratio range of 0-0.5 was studied for both configurations. These runs were carried out in a fixed bed continuous-flow reactor. Experiments were conducted at an O/C of 1.0, a gas hourly space velocity (GHSV) of 50,000 h^{-1}, and 850°C. γ-Alumina supported rhodium (0.5 wt%) catalyst (surface area 100 m^2/g) was used in this study as a base catalyst. The catalyst was diluted with 5/1 quartz sand-to-catalyst ratio (by weight) to avoid preferential gas flow paths and hot spots. Temperature programmed oxidation (TPO) of the spent catalyst was used to determine the amount of carbon formed during reforming reactions.

The gases (N_2, O_2, CO, CO_2, and CH_4) were analyzed using a Thermo Onix mass spectrometer. The gaseous hydrocarbon products (C_1-C_6 paraffins, C_2-C_6 olefins, and benzene) were analyzed using a HP5890 gas chromatograph equipped with a flame ionization detector. Yield of product A (H_2, CO, and CO_2) is defined as:

$$\text{Yield of A (\%)} = \frac{\text{Moles of A produced x 100}}{\text{N x moles of hydrocarbon fed to the reactor}}$$

Where, N is the number of moles of hydrogen/mole of hydrocarbon for H_2 yields and is the number of carbons in hydrocarbon fuel for yields of other products. The conversion of hydrocarbons is defined as:

$$\text{Conv (\%)} = \frac{(CO + CO_2 + \sum_{i}^{i=1\text{-}7} iC_iH_r) \text{ x } 100}{\text{N x moles of hydrocarbon fed to the reactor}}$$

Results

Effects of Anode Recycle Stream

Yields of H_2, CO, CO_2, lower paraffins and saturates for anode recycle ratios 0 to 0.5 are shown in Figure 2. H_2 and CO yields increased with increasing anode recycle ratio. However, yields of CO_2, paraffins, and unsaturates (C2-C6 olefins + benzene) generally decreased with increasing anode recycle ratio. Negative CO_2 yields (or CO_2 conversion) and >100% CO yields at an anode recycle ratio of 0.2 and above suggest that high concentrations of CO_2 present in the system at higher recycle ratios facilitate the reverse water gas shift reaction ($CO_2 + H_2 = CO + H_2O$). However, H_2 yields increased instead of decreasing as expected from the reverse water gas shift reaction because lower hydrocarbons which were significantly observed at lower recycle ratios were converted in the presence of additional oxidants such as water (steam reforming) and CO_2 (dry reforming) in the feed, thus contributing to increasing H_2 yields as well as to lowering yields of lower hydrocarbons. Liquid hydrocarbon conversion to gaseous products was always close to 100%.

One significant performance difference observed for different recycle ratios was the carbon formation on the catalyst. The amount of carbon deposited on the catalyst

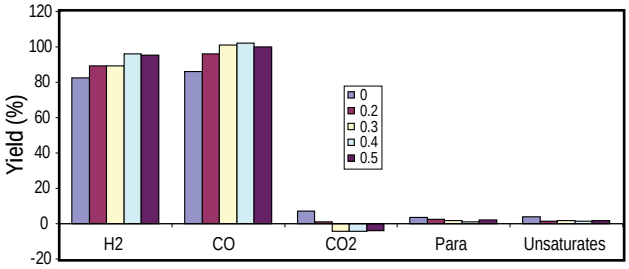

FIGURE 2. Effects of Anode Recycle on Product Distribution

is given in Figure 3 for different recycle ratios used in this study. Interestingly, the carbon formation can be related to unsaturates yield, which generally decreased with increasing anode recycle ratio. The TPOs of carbon deposited on the catalyst at different recycle ratios are shown in Figure 4. Mainly, two peaks were observed in the TPOs of the catalyst used for different recycle ratios. The low temperature peaks (~600°C) can be assigned to carbon deposition on rhodium metal sites, which can be oxidized easily at low temperatures [1]. The high temperature peaks (~800°C) can be attributed to carbon deposited on the support. There was not a certain trend observed for the low temperature peaks with recycle ratio. However, the highest area under the low temperature peak was observed when no recycle stream was used, and the lowest area under the low temperature peak was observed when the recycle ratio was 0.5. On the other hand, the size of the high temperature peaks significantly decreased with increasing anode recycle ratio and only a small hump was observed for anode recycle ratios of 0.4 and 0.5. This suggests that the amount of carbon deposited on the support which is more refractory in nature can be reduced in the presence of a recycle stream.

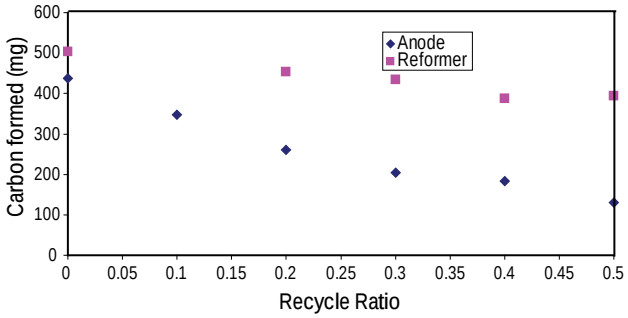

FIGURE 3. Effects of Recycle on Carbon Formation

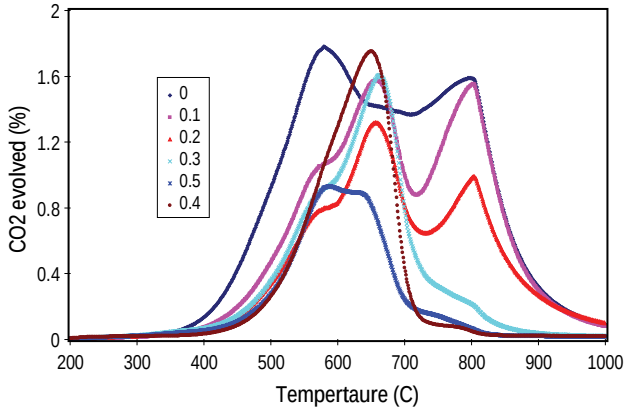

FIGURE 4. Effects of Recycle on Carbon Formation Type: Anode Recycle

Effects of Reformer Recycle Stream

Yields of H_2, CO, CO_2, lower paraffins, unsaturates, and liquid hydrocarbon conversion for reformer recycle ratios 0 to 0.5 are shown in Figure 5. Effects of reformer recycle which was mainly comprised of CO and H_2 were significantly different than the anode recycle. Contrary to anode recycle, H_2 and CO yields and liquid hydrocarbon conversion considerably decreased upon introduction of a reformer recycle while the yields of lower paraffins, unsaturates, and CO_2 increased in the presence of the reformer recycle. Carbon formation was not affected much by introducing a reformer recycle stream (Figure 3).

Effects of Individual Components

Components present in both recycle schemes were the same, but with completely different compositions. Therefore, some of those components may have detrimental effects on the reforming properties while others may have positive effects. To delineate the effects of each recycle component, experiments were conducted to examine the effect of individual components (N_2, H_2, CO, H_2O, CO_2) present in the either of recycle streams on the performance of fuel reforming catalyst. These runs with individual components were conducted using a flow rate equivalent to the recycle ratio of 0.4 and the composition of the simulated recycle stream was 21 vol% of individual components balanced by N_2. In the case of N_2, the whole stream was comprised of only N_2 and this inert stream was used as a baseline for comparison proposes.

The effect of individual components on carbon formation is shown in Figure 6. The presence of CO_2 and H_2O in the recycle stream significantly decreases carbon formation compared to N_2 only in the recycle stream. As mentioned earlier, the presence of CO_2 in the system helps in reducing the catalyst carbon formation by Boudouard reaction ($C + CO_2 = 2CO$), whereas the carbon can be steam-cleaned as it forms in the presence of water in the system ($C + H_2O = H_2 + CO$) and, hence, reducing the amount of carbon formed. The presence

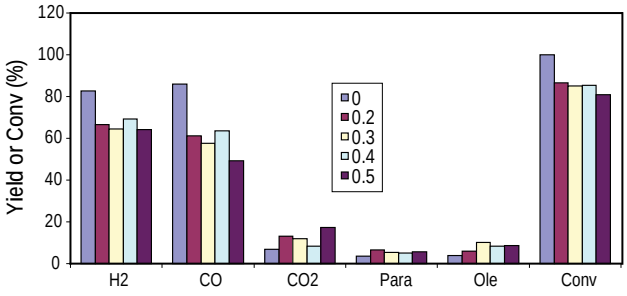

FIGURE 5. Effects of Reformer Recycle on Product Distribution

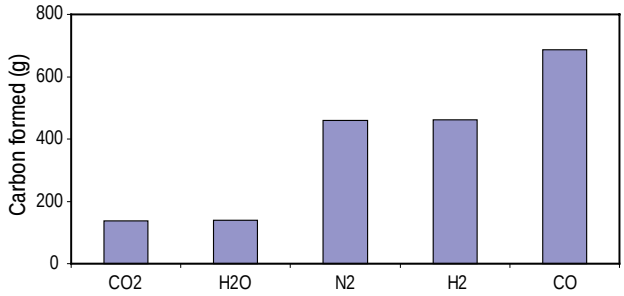

FIGURE 6. Effects of Individual Recycle Components on Carbon Formation

of CO only in the recycle stream considerably increased the amount of carbon formed compared to N_2 only in the recycle stream. Higher CO concentrations facilitate the Boudouard carbon formation and, thus, produce more carbon. Also, the presence of CO may poison the active metal sites and, hence, produce higher amounts of unsaturates due to enhanced gas phase chemistry which results in higher amounts of carbon on the catalyst surface. However, H_2 in the recycle stream has no effects on carbon formation.

Conclusions

- This study was conducted to evaluate the effect of the addition of a recycle stream (from anode and reformer) on the performance (conversion, selectivity, deactivation, etc.) of the fuel reforming catalyst.
- H_2 and CO yields increase while carbon formation decreases with increasing anode recycle ratio.
- H_2 and CO yields, as well as hydrocarbon conversion, decrease with increasing reformer recycle ratio while carbon formation does not change significantly.
- Effect of individual components (CO, CO_2, H_2, and H_2O) present in the recycle stream on the reforming properties compared to N_2 only in the recycle stream: H_2 – no effect, CO – negative effect, CO_2 and water – similar positive effect on carbon formation. CO in the recycle stream enhances carbon formation.

FY 2006 Publications/Presentations

1. D. Shekhawat, T. H. Gardner, D. A. Berry, J. J. Spivey, Catalytic Reforming of Liquid Hydrocarbon Fuels for Fuel Cell Applications, *Catalysis,* Royal Society of Chemistry, Cambridge, UK, Vol. 19, Chapter 6, 184-253.

2. D. Shekhawat, D. A. Berry, T. H. Gardner, Diesel Fuel Reforming Studies, 2006 NETL Fuel Reforming Annual Merit Review, May 4, 2006.

References

1. Shamsi, A., Baltrus, J. P., and Spievy, J. J., 2005, Appl. Catal. A: Gen., 293, pp. 145-152.

III.B.10 Modification of Nickel-YSZ Anodes for Control of Activity and Stability from Carbon Formation during SOFC Operation

Objectives

- Quantify methane steam reforming activity of Ni-yttria-stabilized zirconia (YSZ) anode as a function of processing and operating conditions and pre-treatment.
- Develop methods to adjust and control Ni-YSZ anode activity to provide good thermal management and efficiency for methane on-anode reforming.
- Determine the activity and thermal profile of Ni-YSZ anode wafers under steam methane reforming and compare results with previous powder test results and computational modeling calculations.
- Measure effect of anode formulation on susceptibility toward carbon formation as a function of S/C ratio and concentration of higher hydrocarbons in natural gas.

Accomplishments

- Measured kinetic activity of Ni-YSZ anodes.
- Utilized transmission electron microscopy (TEM) methods to display the formation and sintering of small Ni crystallites present in Ni-YSZ anodes following reduction and steam reforming.
- Designed and constructed new reactor system for anode wafer testing for methane steam reforming.
- Validated thermogravimetric analysis (TGA) method as a viable approach for quantifying and comparing catalysts for carbon formation as function of catalyst composition and reaction conditions.
- Demonstrated the tolerance to carbon formation at low S/C ratios through MgO addition to Ni-YSZ anodes.

David L. King (Primary Contact), James Strohm, Yong Wang, Hyun-Seog Roh, and Xianqin Wang
Pacific Northwest National Laboratory
P.O. Box 999
Richland, WA 99352
Phone: (509) 375-3908; Fax: (509) 375-2186
E-mail: david.king@pnl.gov

DOE Project Manager: Travis Schultz
Phone: (304) 285-1370
E-mail: Travis.Shultz@netl.doe.gov

Technical Advisor: Prabhakar Singh
Phone: (509) 375-5945; Fax: (509) 375-2186
E-mail: prabhakar.singh@pnl.gov

Introduction

During FY 2006, the SECA Core Technology program in Fuel Reforming at Pacific Northwest National Laboratory (PNNL) continued its work on Ni/YSZ anodes and the topic of on-anode reforming of methane and natural gas. A major focus was to quantify anode activity and activity maintenance and to bring this in balance with electrochemical (H_2 and CO oxidation) activity. A second focus was to quantify the potential of MgO addition to Ni-YSZ to reduce the propensity of carbon formation, allowing operation at low S/C ratios. Both efforts are aimed at promoting the thermal efficiency of operation of the fuel cell.

One area of concern is the fact that our Ni-YSZ samples showed significant deactivation during methane steam reforming powder tests at high space velocities. We have substantial evidence that this is a result of Ni sintering under reaction conditions. This sintering behavior must be understood and controlled in order to establish reproducible anode activity. With this in hand, we can proceed to determine if this activity is too high or too low relative to what is required for proper thermal management of the anode, and determine what steps need to be taken to bring this activity in line with requirements. This activity measurement needs to be supplemented with tests of formed anodes, in order to include effects of heat and mass transport on performance and to measure thermal profiles. This work is just initiating, and we describe progress in reactor design and construction. Because of the potential confusion between sintering and carbon-based catalyst deactivation, we have initiated studies using thermogravimetric methods to quantify carbon deposition as a function of operating parameters. Representative results are also reported.

Approach

Our approach has been to study the performance of anode formulations for methane steam reforming in the absence of electrochemical activity, in order to determine the "open circuit" contribution to overall performance as a result of surface structure and

composition. Ni-YSZ formulations have been tested as diluted powders in flow-through tests at high space velocities in order to obtain kinetic information. Because of significant activity declines observed with the freshly reduced Ni-YSZ anodes, we initiated a series of TEM, x-ray diffraction (XRD), and chemisorption studies to look for evidence of nickel metal sintering and/or carbon formation on a series of Ni-YSZ samples, including freshly sintered, following reduction, and following reaction. The next phase, just initiated, will look at testing formed pieces under flow-by operation and much lower space velocities. In the latter case, we will be measuring thermal profile along the flow axis of the Ni-YSZ plate. This will provide critical information on what treatments will be necessary to optimize the reforming activity to match the electrochemical activity and avoid thermal gradients.

To measure resistance to carbon formation, our approach has been a combination of TGA studies coupled with reactor testing. TGA analysis carried out under reaction conditions allows measurement of weight gain, which can be attributed to carbon formation. Reactor testing provides additional information on longer term performance.

Results

Ni-YSZ Activity and TEM Measurements

Our reforming tests with Ni-YSZ as powders have shown an initial decline in activity, lining out at some final value after several hours on-stream. Figure 1 shows a typical activity profile for a Ni-YSZ sample for methane steam reforming. The material was first reduced at 700°C for 1 hour, followed by reaction at 700°C with a feed comprising $H_2O/CH_4/H_2 = 3/1/1$. A decrease in activity by approximately 80% can be observed relative to the fresh catalyst activity. We have consistently seen this type of result over many runs. TEM measurements were carried out on both the fresh (following reduction) and spent (after 65 hours on-stream) samples obtained from the run displayed in Figure 1. The TEM photos are shown in Figures 2 and 3. What we observe with the freshly reduced sample is a large quantity of small Ni crystallites on the surface of the YSZ. The size is typically in the range of 5-20 nm. Following reaction, some crystallites remain, but they have increased in size to typically 20-50 nm. We do not see evidence of carbon on this sample. The change

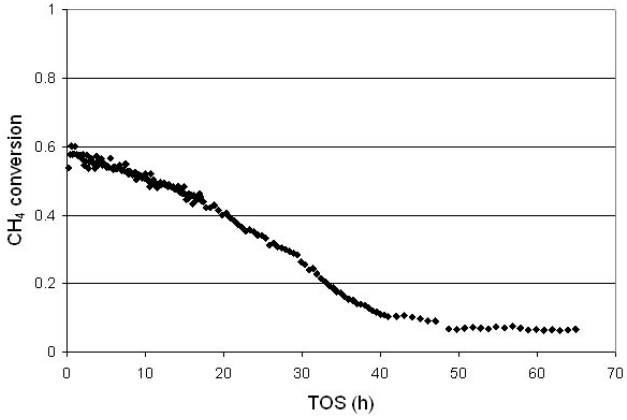

FIGURE 1. Deactivation of Ni-YSZ during Methane Steam Reforming at 700°C, GHSV = 200K, $H_2O/CH_4/H_2$ = 3/1/1

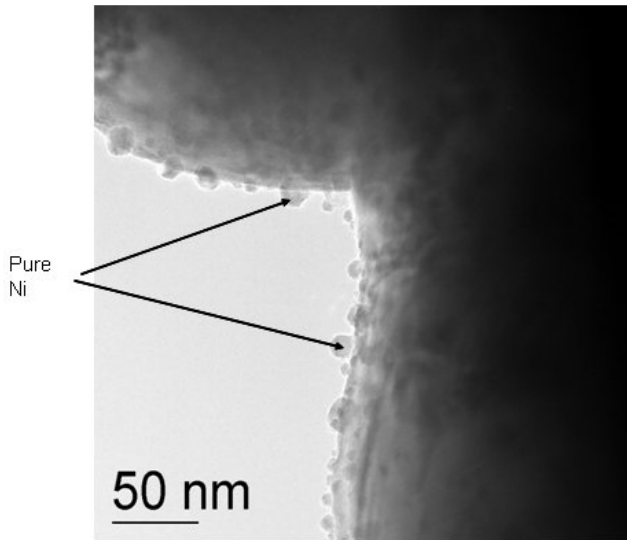

FIGURE 2. TEM of Ni-YSZ after 1 Hour Reduction at 700°C Showing Appearance of Small Ni Crystallites Attached to the Surface of the YSZ Particle

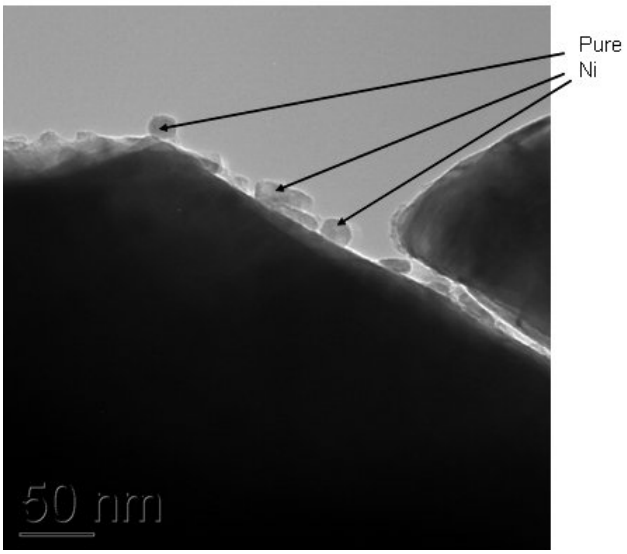

FIGURE 3. TEM of Ni-YSZ after 65 Hours SMR at 700°C, S/C=3, Showing Significant Nickel Particle Sintering

in crystallite size of the Ni particles is due to sintering, facilitated by steam in the presence of hydrogen [1]. The decrease in reforming activity with time is consistent with loss of surface area due to sintering of the Ni crystallites. The lined-out activity reflects that a steady state has been reached, and that further sintering is minimal on the time scale of the experiment. Clearly, if there were no small crystallites present, the activity could be significantly lower, and we have confirmed that by intentionally sintering the sample to the point where no small crystallites are observed. In that case, activity is decreased by at least an additional order of magnitude.

TGA Analysis and Carbon Deposition

We have found that deposition of carbon on Ni-YSZ during steam methane reforming (SMR) is not necessarily reflected in measured catalyst activity with time. Moreover, deactivation due to Ni sintering provides an additional complication, in terms of activity profile, that precludes directly correlating carbon deposition with a decline in activity. Although post-analysis of spent samples by microscopy (TEM) is an effective method to qualitatively measure carbon, this method is not quantitative and does not provide information regarding the rate of carbon formation as a function of conditions. We have implemented TGA analysis to provide a better direct measurement of carbon deposition as the reaction proceeds. Table 1 summarizes the results of TGA measurements of Ni-YSZ exposed to methane steam reforming at three different S/C ratios: 3/1, 2/1, and 1/1. The table also includes results for a Ni-MgO-YSZ sample at 1/1 S/C ratio. MgO- modified Ni-YSZ anode material was synthesized by the glycine nitrate process. In this case, diluted feeds were utilized because of specific laboratory safety precautions and regulations. The results demonstrate a clear effect of S/C ratio on carbon deposition, and it appears that a value of 3 is necessary to maintain carbon to very low levels. On the other hand, very low carbon is deposited with the Ni-MgO-YSZ anode material even at S/C = 1, demonstrating the increased tolerance generated by addition of the MgO. This is consistent with previously reported results by Singh et. al. [2].

TABLE 1. Effect of S/C Ratio on Carbon Deposition with Ni-YSZ and Ni-MgO-YSZ at 700°C

Catalyst	S/C ratio	Weight gain after 20 hours in SR conditions
Ni-YSZ (40% Ni), calcined at 1,375°C	1	~10.6%
Ni-YSZ (40% Ni), calcined at 1,375°C	2	~3.0
Ni-YSZ (40% Ni), calcined at 1,375°C	3	0.2-0.3%
Ni-MgO-YSZ prepared by glycine nitrate, calcined at 800°C	1	0.9
Ni-MgO-YSZ prepared by glycine nitrate, calcined at 1,400°C	1	1.0

Testing of Ni-YSZ Anode Plates

The actual operation of the fuel cell under on-anode reforming conditions will be substantially different from conditions of our Ni-YSZ powder tests. In addition to flow-by rather than flow-through conditions, the porosity of the formed anode will generate diffusion resistances so that the full thickness of the anode might not be utilized. In addition, it is known that the rate of electrochemical oxidation of H_2 and CO is significantly lower than the rate of methane steam reforming with nickel, hence the concern regarding the possibility of generating large endotherms at the front edge of the cell. To move toward more practical operation of the Ni-YSZ anodes for on-cell reforming, we have constructed a reactor that allows testing of the bulk anode for methane steam reforming and allows obtaining thermal profiles both along the flow path and across the anode. The reactor will allow accommodation of different plate thicknesses and lengths in order to determine the depth of penetration of the reacting gases and to determine the extent of reaction along the length of the anode plate. A photograph of the reactor is provided in Figure 4.

FIGURE 4. Ni anode plate reactor designed to operate under realistic flow conditions and to monitor temperatures at several points on the Ni-YSZ plate during reaction. Holes on sides are for cartridge heaters. Tubing extending from the reactor provides access of thermocouples to surface of plate at various locations.

Conclusions and Future Directions

Ni-YSZ under powder testing with flow-through operation shows initial activity decline followed by leveling of activity after tens of hours of operation. As confirmed by TEM results, deactivation is caused by the sintering during reaction of small nickel particles that are sitting on the surface of YSZ particles. These particles likely initially form as nickel evolves from the YSZ matrix (present as NiO) during reduction pretreatment. By controlling this sintering behavior, it appears possible to control the anode activity toward methane steam reforming.

TGA analysis has shown to be effective in measuring the extent of carbon formation during steam reforming reactions over Ni-YSZ. Preliminary results indicate that S/C ratios of 3 may be required to maintain carbon deposition at a low level.

Future directions include:

- Quantify effect of time/temperature/steam concentration on sintering of Ni particles present in reduced Ni-YSZ samples.
- Determine if intentional sintering of Ni-YSZ under controlled conditions provides a viable approach to adjusting catalytic activity for proper thermal management of the cell.
- Obtain activity data, thermal profiles, and activity maintenance data with anode plates in new reactor and quantify amount of thermal gradients formed.
- Evaluate various methods to add Cu to Ni-YSZ to control catalyst activity, and demonstrate the best method using a formed anode in the thermal profile reactor test.
- Compare addition of MgO and CeO_2 to Ni-YSZ for resistance to carbon formation at low S/C ratios, and develop the best synthetic method to implement this material modification.

FY 2006 Publications/Presentations

1. D.L. King, Y. Wang, Y.H. Chin, H.S. Roh, "Development of Modified Nickel-Based Compositions For On-Anode Reforming", SECA Core Technology Program Peer Review presentation, Lakewood, Colorado, October 2005.

2. D.L. King, Y.H. Chin, Y. Wang, H.S. Roh, P. Singh, "Investigation of Supported Bimetallic Ni-Au Steam Reforming Catalysts: Structure and Reactivity", SECA Topical Report, May 2006.

References

1. J. Sehested, Catalysis Today, 111 (2006) 103-110.

2. P. Singh, R. J. Ruka and R.A. George, US Patent 4,894,297, 1990.

III.B.11 Desulfurization of High-Sulfur Jet Fuels by Adsorption and Ultrasound-Assisted Sorbent Regeneration

Objectives

- Develop easily regenerated, stable and high sulfur capacity sorbent for desulfurization of jet fuels containing high sulfur concentrations.
- Develop a solvent regeneration technique assisted by ultrasound in addition to thermal regeneration.

Accomplishments

- Developed a stable and high sulfur capacity sorbent of $PdCl_2$/AC (palladium chloride/activated carbon) that exhibits excellent selective adsorption capability for sulfur-containing compounds from a model jet fuel (400 ppmw-S). More than 20 ml of the model jet fuel was desulfurized to below 1.0 ppmw-S per gram sorbent.
- For the spent $PdCl_2$/AC sorbent, about 65 wt% sulfur can be desorbed in 30 minutes using ultrasound at 50°C. This result indicates that the spent $PdCl_2$/AC sorbent could be effectively regenerated by ultrasound.

Introduction

Liquid-phase sulfur removal from jet fuels is a key area which will help enable the fuel cell program. A new, novel technology of adsorptive desulfurization is explored in this project. In the refineries, desulfurization is accomplished by hydrodesulfurization (HDS), which is a catalytic process using high-pressure hydrogen (40-100 atm) and high temperatures (300-340°C) over a NiMo/alumina catalyst. The adsorptive desulfurization technology being explored involves a simple one-step process under ambient temperature and pressure. If successful, the new technology would replace the conventional technology for desulfurization of petroleum products, and it could also be used for desulfurization as a polishing step for fuel cell applications. At a minimum, new results will be generated from this project that will advance the field of sorbent development for environmental applications.

Ralph T. Yang (Primary Contact), Yuhe Wang
Department of Chemical Engineering
University of Michigan
3074 H.H. Dow, 2300 Hayward Street
Ann Arbor, MI 48109
Phone: (734) 936-0771; Fax: (734) 764-7453
E-mail: yang@umich.edu

DOE Project Manager:
Ayyakkannu Manivannan
Phone: (304) 285-2078
E-mail: Ayyakkannu.Manivannan@netl.doe.gov

Approach

As described below, a number of sorbents were prepared for this work. The sorbents were prepared by standard incipient wetness impregnation and thermal dispersion methods. The selective adsorption experiments using different sorbents were performed in vertical custom-made quartz adsorbers as described elsewhere [1-3]. The fuels collected during the experiments were analyzed using a gas chromatograph equipped with a flame photometric detector. The spent $PdCl_2$/AC sorbent was regenerated by desorption of sulfur compounds in a solvent with heating and ultrasound technique.

Results

After *in situ* activation of the adsorbent, the fuel was allowed to contact the bed, and the sulfur contents in the effluent samples were monitored periodically. Breakthrough adsorption curves were generated by plotting the transient sulfur concentration normalized by the feed versus cumulative fuel volume normalized by total bed weight. The sulfur adsorption amounts (normalized by adsorbent weight) were obtained after integration of the area above the breakthrough curves.

Figure 1 shows the breakthrough adsorption of total sulfur during desulfurization of a model jet fuel with the $PdCl_2/Al_2O_3$, CuCl/AC and $PdCl_2$/AC adsorbents. The model jet fuel was prepared to simulate the commercial jet fuels, and it contained 150 ppmw-S benzothiophene (BT), 250 ppmw-S methyl benzothiophene (MBT) and 700 ppmw naphthalene, in 19.75 wt% benzene + 80 wt% n-octane. It is clear that all of the sorbents are capable of removing benzothiophene and 2-methylbenzothiophene. For the same feed, $PdCl_2$/AC showed the highest capacities among the adsorbents studied. The breakthrough and saturation capacities for total sulfur were 0.126 and 0.187 mmol/g respectively, indicating strong interactions with benzothiophene and 2-methylbenzothiophene molecules. It was found that more than 20 ml of the model jet fuel was desulfurized to below 1.0 ppmw-S per gram sorbent on the fresh $PdCl_2$/AC. From the breakthrough curves, it was also found that the $PdCl_2$/AC sorbent has higher

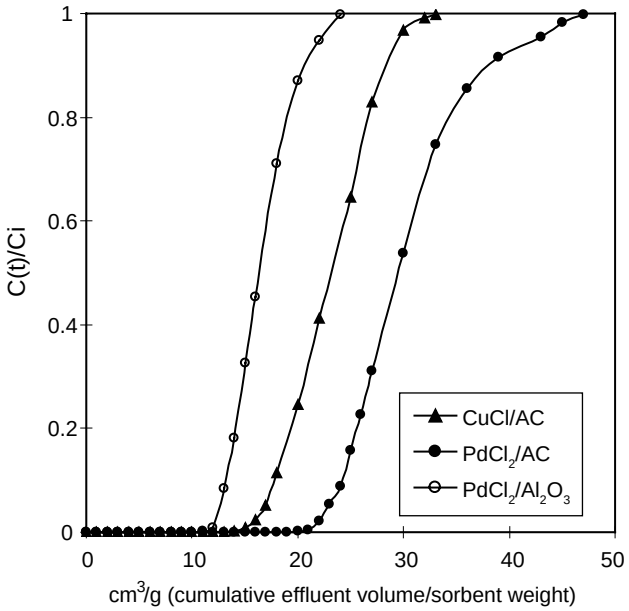

FIGURE 1. Breakthrough of total sulfur in a fixed-bed adsorber with fresh $PdCl_2/Al_2O_3$ (○), CuCl/AC (▲) and $PdCl_2$/AC (●), for model jet fuel (150 ppmw-S BT and 250 ppmw-S MBT in 19.75 wt% benzene + 80 wt% octane containing 700 ppmw naphthalene) at room temperature. Ci is the total sulfur concentration of the feed at flow rate 1 cm^3/10 min (S.V. = 4.6 h^{-1}).

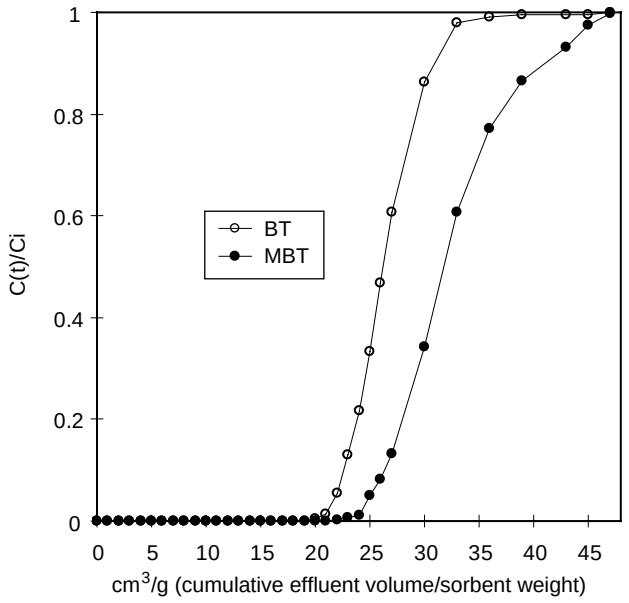

FIGURE 2. Breakthrough of BT and MBT sulfur in a fixed-bed adsorber with fresh $PdCl_2$/AC, for model jet fuel (150 ppmw-S BT and 250 ppmw-S MBT in 19.75 wt% benzene + 80 wt% octane containing 700 ppmw naphthalene) at room temperature. Ci is the total sulfur concentration of the feed at flow rate 1 cm^3/10 min (S.V. = 4.6 h^{-1}).

sulfur capacity than CuCl/AC sorbent has. Since the amount of $PdCl_2$ salt (1.31 mmol·g^{-1}) on activated carbon is similar to the amount of CuCl (1.11 mmol·g^{-1}) on activated carbon, it is reasonable to conclude that the metal salt $PdCl_2$ contributed significantly toward adsorption of the sulfur-containing compounds.

To compare the sulfur capacity of $PdCl_2$ on different supports, desulfurization by $PdCl_2/Al_2O_3$ was tested under the same feed conditions. From the breakthrough curves, the $PdCl_2$/AC sorbent adsorbed almost twice as much sulfur compared with $PdCl_2/Al_2O_3$. This showed that the activated carbon is a more effective support than Al_2O_3 for the $PdCl_2$ supported sorbents for desulfurization of fuel containing benzothiophene and substituted compounds.

From the above results, it is concluded that the metal ion Pd^{2+} is stronger for π-complexation than Cu^+, and the activated carbon is a more effective support than Al_2O_3.

Figure 2 shows the results of desulfurization of model jet fuel over the $PdCl_2$/AC sorbent. The results show that the sorbent can remove 0.069 and 0.091 mmol of benzothiophene sulfur per gram at breakthrough and saturation, respectively, while the sorbent was capable of removing 0.126 and 0.187 mmol of methylbenzothiophene sulfur per gram at breakthrough and saturation for the same model jet fuel, respectively. Figure 2 shows that the $PdCl_2$/AC had a

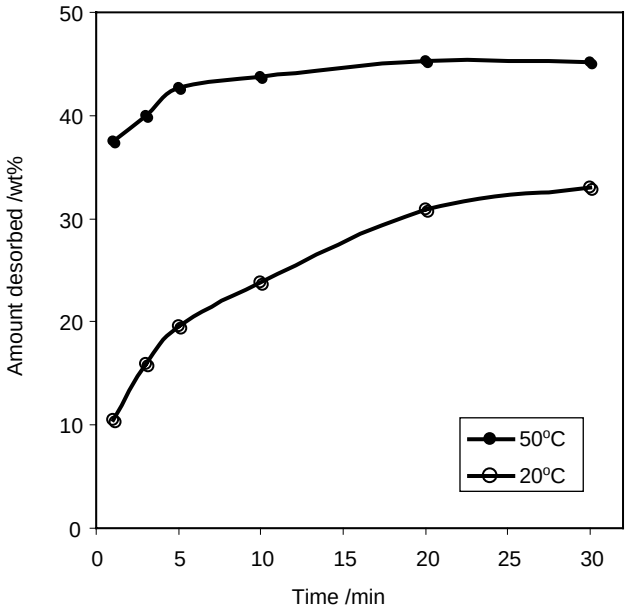

FIGURE 3. Amount of total sulfur desorbed (in percent, g S/g sorbent) from spent $PdCl_2$/AC sorbent regenerated at 20°C (○) and 50°C (●) in a static system with 30 wt% benzene and 70 wt% octane.

selectivity towards heavier, substituted benzothiophene over the nonsubstituted one.

After saturation by the model jet fuel, the spent sorbent was regenerated at 20°C and 50°C in a static bath of solvent. Figure 3 shows the results of desorption

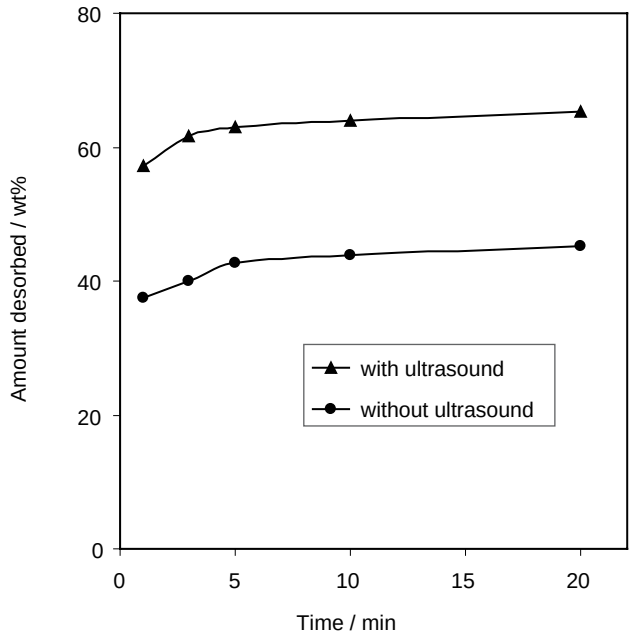

FIGURE 4. Amount of total sulfur desorbed (in percent, g S/g sorbent) from spent $PdCl_2$/AC using ultrasound and no ultrasound at 50°C in a static system with 30 wt% benzene and 70 wt% octane.

in the mixture of 30 wt% benzene and 70 wt% n-octane. The amount of sulfur desorbed depends on the time and temperature. Figure 3 shows that approximately 35 wt% of the total sulfur in the sorbent was desorbed at 20°C and approximately 45 wt% of the total sulfur in the sorbent was desorbed at 50°C after 30 minutes in the solvent.

In our previous study [3], it was found that ultrasound is an effective technique for regenerating spent $CuCl/Al_2O_3$ sorbent. In this work, the ultrasound technique was also applied to regenerate the spent $PdCl_2$/AC sorbent at 50°C. Figure 4 shows the results of desorption with ultrasound and without ultrasound at 50°C. The amount of sulfur desorbed was higher with ultrasound, 65 wt% desorption vs. 45 wt% without ultrasound. This result indicates that the spent $PdCl_2$/AC sorbent could be effectively regenerated by the ultrasound technique.

Conclusions and Future Directions

- $PdCl_2$/AC sorbent showed a high desulfurization capacity for removing sulfur-containing compounds from a model jet fuel. More than 20 ml of the model jet fuel can be desulfurized to below 1.0 ppmw S per gram of sorbent on the fresh $PdCl_2$/AC.
- It was found that the spent $PdCl_2$/AC sorbent could be effectively regenerated by ultrasound. For the spent $PdCl_2$/AC, about 65 wt% of adsorbed sulfur can be desorbed in 30 min using ultrasound at 50°C.

Special Recognitions & Awards/Patents Issued

Two US Patents were issued as a result of previous work that led to this work:

1. U.S. Patent 7,029,574, "Selective adsorbents for purification of hydrocarbons." (April, 2006).

2. U.S. Patent 7,053,256, "Selective adsorbents for purification of hydrocarbons." (May, 2006).

References

1. Yang, R. T.; Hernández-Maldonado, A. J.; Yang, F. H. *Science* 2003, *301*, 79.

2. Hernández-Maldonado, A. J.; Yang, R. T. *J. Am. Chem. Soc.* 2004, *126*, 992.

3. Hernández-Maldonado, A. J.; Qi, G.; Yang, R. T. *Appl. Catal. B.* 2005, *61*, 212.

III.B.12 Hybrid Experimental/Theoretical Approach Aimed at the Development of a Carbon-Tolerant Alloy Catalyst

Objectives

- Utilize hybrid experimental/theoretical framework, combining quantum Density Functional Theory (DFT) calculations and various state-of-the-art experimental tools, to formulate carbon-tolerant hydrocarbon reforming catalysts.
- Employ DFT calculations to develop molecular insights into the elementary chemical transformations that lead to carbon poisoning of Ni catalysts.
- Utilize DFT calculations to identify potential carbon-tolerant alloy catalysts.
- Test the alloy catalysts in steam reforming of methane, propane and isooctane.
- Characterize the tested catalysts.

Accomplishments

- We deduced molecular mechanisms that govern carbon poisoning of Ni catalysts during steam reforming of hydrocarbons.
- We identified, using DFT quantum calculation, a Sn/Ni alloy as a potential carbon-tolerant reforming catalyst.
- We tested a Sn/Ni alloy in steam reforming of methane, propane, and isooctane. We demonstrated that the alloy catalyst is carbon-tolerant under nearly stoichiometric steam-to-carbon ratios. Under these conditions, monometallic Ni catalysts are rapidly poisoned by sp2 carbon deposits.
- We utilized various characterization techniques to characterize the tested catalysts.

Suljo Linic (Primary Contact), Eranda Nikolla, Johannes Schwank
University of Michigan
2300 Hayward
Ann Arbor, MI 48409
Phone: (734) 764-7469; E-mail: linic@umich.edu

DOE Project Manager: Magda Rivera
Phone: (304) 285-1359
E-mail: Magda.Rivera@netl.doe.gov

Introduction

The envisioned shift to a hydrogen economy driven by rapidly evolving fuel cell technology will require an energetically feasible and environmentally friendly conversion of fossil, synthetic, and bio-renewable fuels into hydrogen. To realize this vision, major advances in catalysis are required. Improved hydrocarbon reforming, water gas shift, and preferential CO oxidation catalysts need to be formulated and synthesized. These catalysts need to perform the desired reactions with utmost efficiencies, at reduced costs, and with improved durability. Even though there is a tremendous incentive to develop more efficient catalysts, these materials are currently formulated using inefficient trial-and-error experimental approaches. In this document, we describe a novel hybrid experimental/theoretical effort aimed towards a bottom-up, knowledge-based formulation of carbon-tolerant reforming alloy catalysts.

Our objective is to utilize the hybrid experimental/theoretical framework, combining quantum DFT calculations and various state-of-the-art experimental tools, to formulate and develop carbon-tolerant hydrocarbon reforming catalysts. Unlike current state-of-the-art catalysts, which are often monometallic Ni particles adsorbed on oxide supports, oxide-supported metallic alloy catalysts are the focus of this work. These catalysts could be utilized for hydrogen production from hydrocarbons and as robust solid oxide fuel cell (SOFC) anodes for direct internal reforming.

Approach

We have employed quantum DFT calculations, catalyst synthesis, catalyst testing, and catalyst characterization to identify potential carbon-tolerant reforming alloy catalysts.

DFT calculations allow us to obtain, from first principle and with high accuracy, the ground state geometries and energies of relevant reactants, products, and transition states involved in elementary chemical reactions on catalyst surfaces. [1]

Reactor testing and various characterization techniques are applied to test the predictions of DFT calculations.

Results

One critical issue in hydrocarbon reforming is that current reforming catalysts, such as Ni, facilitate the formation of carbon structures which deactivate the catalyst. [2] The formation of carbon deposits can be partially suppressed by an introduction of steam (steam reforming). Metallic Ni is often used as a catalyst for steam reforming, and generally very high concentrations of steam are required to prevent carbon poisoning of the catalyst. [3] However, a high steam concentration is not desirable because it lowers the energy density of the products. It is imperative to design carbon-tolerant reforming catalysts that can operate with low steam concentrations.

To illustrate the problem of carbon poisoning, Figure 1a shows the results of experimental studies where the deactivation of Ni catalyst supported on YSZ during CH_4 steam reforming was investigated. It is observed that the catalyst activity decreases as a function of the time on stream. The deactivation was a consequence of the formation of large deposits of sp2 carbon networks. Transmission electron microscopy (TEM), energy dispersive x-ray spectroscopy (EDS), and x-ray diffraction (XRD) experiments were utilized to identify the sp2 carbon deposits on the Ni catalyst (Figure 1b shows TEM results). Even more dramatic poisoning of Ni catalysts is observed for other hydrocarbon fuels.

We have utilized DFT calculations to calculate, from first principles, the elementary step reaction energies for methane steam reforming on Ni(111). The DFT results demonstrate that thermodynamically, the most stable state of carbon on Ni(111) is a graphene sheet adsorbed on the surface. DFT calculations also showed that carbon atoms, created in the process of hydrocarbon decomposition on Ni, can be removed from the surface by oxidation, which is accompanied by the formation of CO. The DFT studies suggest that the long-term stability of reforming catalysts is governed by their ability to selectively oxidize carbon (form C-O bonds) and remove it from the surface, while preventing the formation of C-C bonds (see Figure 2).

Motivated by these insights, we have utilized DFT to investigate the elementary steps associated with C-C and C-O bond formation on Ni. In order for C-C bonds to form on a catalyst surface, C atoms need to diffuse on the surface and collide with each other. Similarly, oxidation of carbon atoms requires collisions between C and O atoms on the surface. We have employed DFT to calculate activation barriers for C and O atom diffusion and the activation barriers for C-O and C-C bond formation. Figure 3a depicts the potential energy surface for C-O and C-C bond formation on Ni(111). We find that on Ni(111), the chemical pathways leading to C atom oxidation (C-O bond formation) have comparable overall activation barriers as those for C-C bond formation. Similar activation barriers associated with

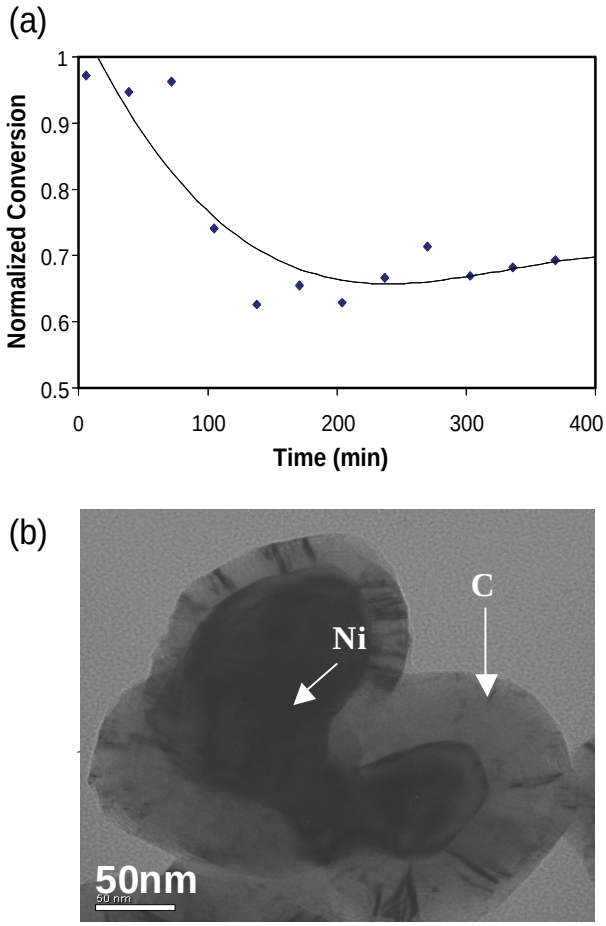

FIGURE 1. (a) Methane conversion over Ni/YSZ (Ni supported on YSZ) catalyst as a function of the time on stream. Steam to carbon ratio was 0.5. (b) TEM studies show that thick graphitic carbon deposits are formed on the Ni catalyst during methane reforming process.

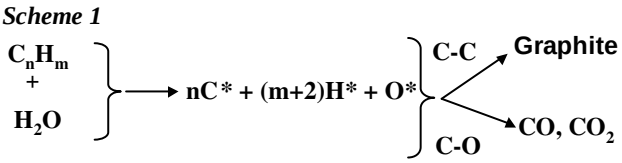

FIGURE 2. Carbon atoms can either react with each other to form sp2 carbon deposits which deactivate the catalyst, or they are oxidized to form CO which desorbs from the surface

C-O and C-C bond formation on Ni suggest that this is not an ideal reforming catalyst. Simply stated, the rate of C-C bond formation is too high to ensure the long lifetime of Ni catalysts.

The DFT calculations presented in Figure 3b show that on a Sn/Ni surface alloy, the relative kinetics of C-O and C-C bond formation is significantly different than on Ni. The dramatic Sn-induced increase in the diffusion barriers suggests that over Sn/Ni, C and O

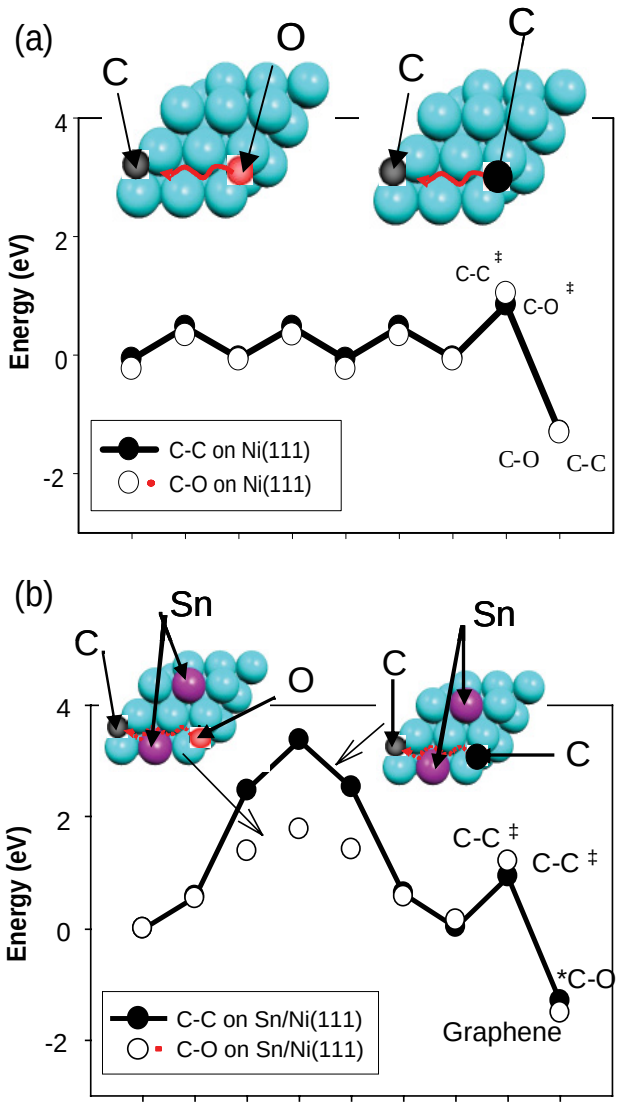

FIGURE 3. DFT calculated energies for C and O atom diffusion and C-O and C-C bond formation on a) Ni(111) and b) Sn/Ni(111). Full dark lines represent the energy landscape associated with the C-C bond formation, while red dotted lines represent the energy for C-O bond formation. Sn is represented by purple balls. C-C‡ represents the DFT calculated energy for the transition state for C-C bond formation, while C-O‡ depicts the transition state for C-O bond formation. Inserts show the lowest energy pathways for C-C (right panel) and C-O (left panel) bond formation. The pathways consists of C (dark atom, right panel) or O (red atom, left panel) atom diffusion over the surfaces and subsequent formation of C-C and C-O bonds, respectively.

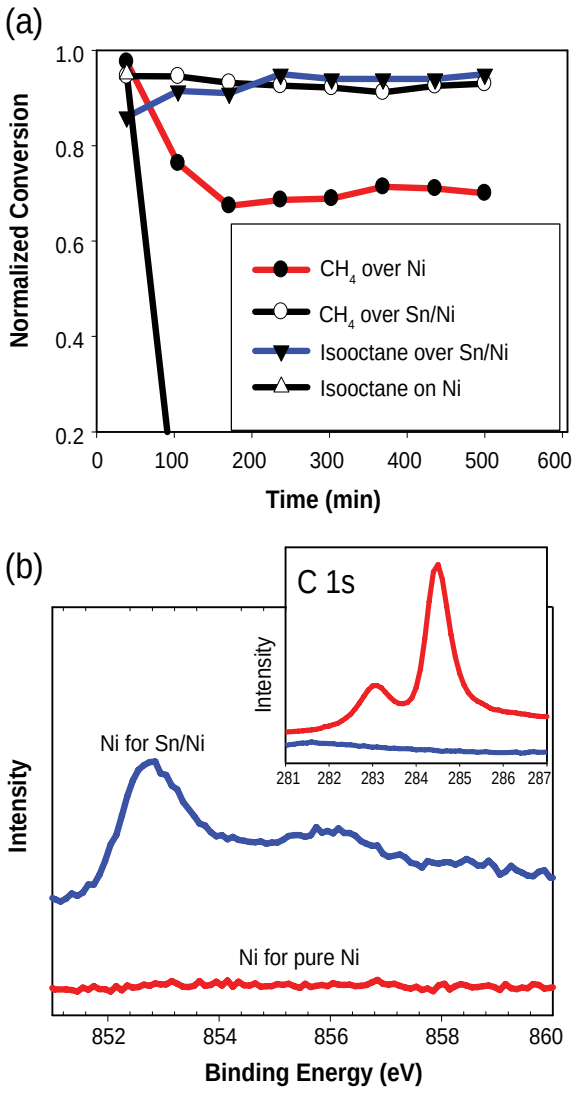

FIGURE 4. (a) Conversion by steam reforming of isooctane over a Sn/Ni alloy catalyst supported on YSZ at the steam-to-carbon ratio of 1.5. Pure Ni supported on YSZ rapidly deactivates under these conditions, while Sn/Ni is very stable. (b) XPS spectra in the energy range corresponding to the Ni signal. The Ni signal is very strong for the used Sn/Ni alloy supported on a YSZ catalyst. Conversely, the Ni signal can not be detected for monometallic Ni supported on a YSZ catalyst. The reason for this is that the Ni catalyst is covered by carbon deposits, as illustrated in the insert, where the XPS spectrum corresponding to carbon peak was collected for a pure Ni catalyst. The carbon XPS spectrum suggests that the Ni catalyst is completely covered with carbon deposits.

atom diffusion becomes kinetically limiting for the respective C-C and C-O bond formation. The DFT calculations suggest that on the alloy surface, the rate of C oxidation is much greater than the rate of C-C bond formation. Furthermore, DFT calculations show that a Sn/Ni surface alloy is the most stable phase thermodynamically, with lower formation energy than Sn bulk alloys or pure Sn and Ni phases.

The predictions of these calculations were examined in experimental studies. Pure Ni and Sn/Ni alloy catalysts were synthesized and tested in steam reforming of methane, propane, and isooctane. The results of steam reforming of methane and isooctane over Ni and Sn/Ni catalysts, obtained in our flow reactor, are shown in Figure 4a. The Sn/Ni alloy catalyst contained 1% Sn by weight with respect to Ni. Methane steam reforming was performed with a steam-to-carbon ratio

of 0.5, while isooctane reforming was performed at a steam-to-carbon ratio of 1.5. Figure 4a illustrates that Sn/Ni is much more stable than monometallic Ni. For example, we observed that in isooctane steam reforming, a monometallic Ni catalyst deactivates within a few minutes. The deactivation is accompanied by a large pressure drop across the reactor, which is a consequence of a rapid buildup of carbon deposits. X-ray photoelectron spectroscopy (XPS), shown in Figure 4b, demonstrates that the Ni catalyst is completely covered by carbon deposits. In post-reaction XPS analysis of Sn/Ni, no carbon electronic fingerprint was measured, indicating that the catalyst is carbon-tolerant. Post SEM, TEM and XRD experiments also showed no signs of carbon formation on Sn/Ni, unlike the Ni catalyst which was completely poisoned by carbon deposits.

Conclusions and Future Directions

We have utilized DFT quantum calculations to develop molecular insights into the mechanism of carbon poisoning.

We have identified C-atom diffusion and C-C bond formation as two critical elementary processes that lead to the formation of extended sp2 carbon networks, which deactivate Ni catalysts. We have also determined that the long-term stability of steam reforming catalysts is governed by their capacity to selectively oxidize carbon atoms while suppressing C-C bond formation.

DFT studies demonstrated that Sn/Ni is more efficient in oxidizing and removing carbon atoms than Ni.

The reactor studies conclusively demonstrated that a Sn/Ni catalyst is much more robust than monometallic Ni for various hydrocarbons.

Post reaction SEM, TEM, EDS, XPS, and XRD characterization studies showed that the main reason for the stability of the alloy catalyst is that small amounts of Sn atomically dispersed in the Ni surface layer prevent the formation of extended sp-2 carbon networks.

Future work will involve exploring alloy catalysts as potential internal reforming anodes for SOFCs.

We also plan to explore the reforming activity of the alloys in the limit of lower loading and smaller particle size. Preliminary DFT studies indicate that the step and edge sites on our alloy catalyst should be more active for C-H bond activation.

Special Recognitions & Awards/Patents Issued

1. Best Paper Presentations, "Experimental/Theoretical Studies Aimed at the Development of Carbon-Tolerant Catalysts", Michigan Catalysis Society Annual Meeting 2006, Dow Chemicals, Midland, MI, May 2006.

2. Best Paper Competition, "Controlling Carbon Chemistry via Alloying: Hybrid Experimental/Theoretical Approach", University of Michigan Engineering Competition 2006, Ann Arbor, MI, March 2006.

FY 2006 Publications/Presentations

1. Nikolla, E., Holowinski, A., Schwank, J., Linic, S., "Controlling Carbon Surface Chemistry by Alloying: Carbon Tolerant Reforming Catalyst", Journal of the American Chemical Society, submitted 2006.

2. Nikolla, E., Schwank, J., Linic, S., "Carbon Tolerant Alloy Catalyst for H_2 Production", Journal of Catalysis, submitted 2006.

3. Nikolla, E., Linic, S., "Hybrid Experimental/Theoretical Approach Aimed at the Development of Carbon Tolerant Alloy Catalyst", ACS Colloids and Surface Science Meeting 2006, Boulder, Colorado, June 2006.

4. Nikolla, E., Linic, S., "Hybrid Experimental/Theoretical Approach Aimed at the Development of Carbon Tolerant Alloy Catalyst", NETL Contactors Meeting 2006, Pittsburgh, Pennsylvania, February 2006.

References

1. B. Hammer, J.K. Nørskov, "Theory of adsorption and surface reactions" in (eds.) R. Lambert and G. Pacchioni, NATO ASI Series E, Kluwer Academic Publishers, Dordrecht 1997.

2. Triantafyllopoulos, N.C. and S.G. Neophytides, *The nature and binding strength of carbon adspecies formed during the equilibrium dissociative adsorption of CH_4 on Ni-YSZ cermet catalysts.* Journal of Catalysis, 2003. 217(2): p. 324-333.

3. H.S. Bengaard, J.K. Nørskov, J. Sehested, B.S. Clausen, L.P. Nielsen , A.M. Molenbroek, and J.R. Rostrup-Nielsen, "Steam Reforming and Graphite Formation on Ni Catalysts", Journal of Catalysis, 2002, 209, 365-384.

III. SECA RESEARCH & DEVELOPMENT

C. Power Electronics

III.C.1 DC-AC Inverter with Reactive-Power-Management Functionality

Objectives

- Determine the operating specifications for the energy converter.
- Determine optimum power designs to meet the system specifications derived during the first task.
- The third objective will be to determine the control components and algorithms needed to optimize the performance of the power hardware, maximizing performance and minimizing power losses and other undesirable byproducts.

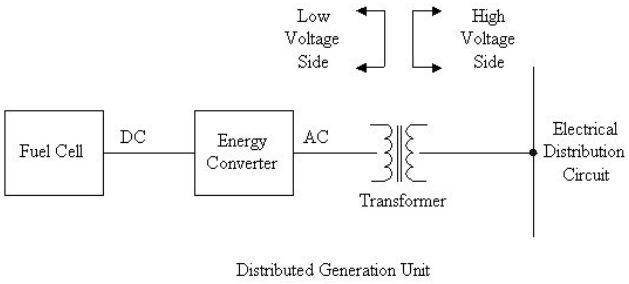

FIGURE 1. Distributed Generation Unit

Introduction

Presently, many electrical power distribution circuits have areas that are supplied with substandard power. This may take the form of voltages being out of tolerance and/or circuits being overloaded. These problems result from the impedance (real or reactive) between the generating plant and the load being higher than what is desired. If the problem is severe enough, failures in the distribution circuit will occur. These problems can be reduced, but not substantially eliminated, by increasing the size of components in the distribution circuit. An alternative to increasing the size of the distribution circuits is to add distributed generation throughout the system. Relatively small generating sources can be located close to significant loads. These generating sources will need to provide reactive power compensation (60 Hz reactive current and harmonic current cancellation) as well as real power injection into the distribution circuit.

A distributed generation unit consists of three major components as shown in the one line diagram of Figure 1. The fuel cell converts fuel to DC power. An energy converter converts the DC power from the fuel cell to 3-phase AC power that is synchronous with the power in the distribution circuit. Besides being able to inject real power generated by the fuel cell into the distribution circuit, the energy converter must also be capable of generating a substantial reactive power component. Finally, the output of the inverter is physically connected to the distribution circuit via a transformer. A single energy converter that is capable of providing real power, 60 Hz reactive power, and harmonic reactive power is less costly and considerably more efficient than providing separate units for these functions.

John N. Mandalakas (Primary Contact),
David J. Shero
Mesta Electronics Inc.
11020 Parker Drive
North Huntingdon, PA 15642
Phone: (412) 754-3000; Fax: (412) 754-3016
Website: www.mesta.com

DOE Project Manager: Don Collins
Phone: (304) 285-4156
E-mail: Donald.Collins@netl.doe.gov

Approach

- Working with a utility consultant, Mesta will develop an accurate set of specifications for the energy converter. From this information, the following items will be defined:
  - Range of real power (MW) and reactive power (MVA) that energy converters should cover to correct existing and potential future problems in distribution circuits. Regarding reactive power, a breakdown of 60 Hz and harmonic current correction needed will be derived.
  - Range of distribution circuit voltages that the energy converter may need to interface with. It is assumed that 12.7 kV will predominate, but planning for other voltages at this early stage may widen the demand for such systems.
  - Range of fuel cell voltage and power capabilities needed. This will define the interface or range of interfaces needed between the fuel cell and the energy converter.
  - Physical size and weight restraints that might enable easier movement and/or installation of equipment.
  - Operating conditions such as temperature, humidity, elevation, etc. that will affect packaging and cooling methods.
  - Environmental concerns that could put limitations on audible noise, electrical noise (RF), etc.

  - Safety concerns that will affect construction (such as preventing accidental exposure of dangerous voltage, etc. to personnel) or control safeguards (such as preventing "islanding" from occurring should there be a loss of power in the distribution circuit).
  - A communications interface and protocol to enable energy converters to be networked to a central control site where their status may be monitored and their control parameters may be altered.
- This set of specifications will be used to guide the design process. The first part of the design will be to identify major components that will make up the energy converter. A block diagram of the energy converter is shown in Figure 2. At the heart of the energy converter is a DC-to-AC converter, commonly referred to as an inverter. The inverter converts DC power originally generated by the fuel cell into 3-phase AC power that is synchronous with the voltage on the electrical distribution circuit. The inverter can pull power from the distribution circuit by producing a voltage slightly lower than the distribution circuit voltage. This power is stored in the capacitance across the DC side of the inverter. If the voltage produced by the inverter is slightly out of phase with the distribution circuit voltage, reactive power is transferred between the energy converter and distribution circuit. The converter can generate either a leading or lagging reactive power, as needed by the system. In a similar manner, the converter can also produce harmonic currents that "cancel" harmonic currents flowing in the distribution circuit.

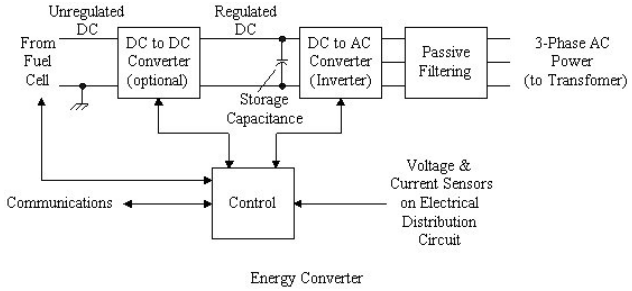

FIGURE 2. Energy Converter

- During Phase I, Mesta will use portions of several Mesta existing product designs to produce a conceptual design for an energy converter.
- The transformer that interfaces the energy converter with the distribution circuit will need to be characterized.
- The control components and algorithms needed to optimize the performance of the power hardware will be studied.
- Mesta will be able to test portions of the new conceptual design in a lab environment using actual hardware during Phase I.
- A final report will then be written summarizing findings during this phase, including system specifications, conceptual designs of the energy converter, budgetary cost estimates to produce the conceptually designed equipment, and test results performed to date.

Results

This is a newly initiated project (awarded 6/28/06). It will proceed for the remainder of the calendar year 2006 and the first quarter of 2007.

III.C.2 Power Electronics for Solid Oxide Fuel Cells

Objectives

- Simulate an existing AC distribution system.
- Convert the existing AC distribution system to a DC distribution system.
- Investigate the merits of using fuel cell direct current as a power source for a DC distribution circuit replacing an already existing AC distribution circuit.

Accomplishments

- Had a kick-off meeting for the DC distribution study.
- Decided on an actual AC distribution system to be modeled.
- Initiated the modeling of the AC distribution system to be used in the study.

Introduction

Deployment of DC fuel cell power assets creates a DC distribution circuit with highly efficient DC-AC inverters installed to provide AC power. The fuel cell power plants may be deployed in a central and/or distributed scheme. The DC-AC inverters can be deployed at each facility, inside the meter, and/or at a regional level such as a neighborhood. Use of inverter technology will enable integration of numerous functions in addition to power management.

Approach

DC distribution concepts devised and studied in this project shall consider the merit of including the following functions and capabilities into the inverter:

Burak Ozpineci (Primary Contact),
Donald J. Adams
Oak Ridge National Laboratory
2360 Cherahala Blvd
Knoxville, TN 37932
Phone: (865) 946-1329; Fax: (865) 946-1262
E-mail: ozpinecib@ornl.gov

DOE Project Manager: Don Collins
Phone: (304) 285-4156
E-mail: Donald.Collins@netl.doe.gov

Subcontractors:
The University of Tennessee, Knoxville, TN

- Remote digital meter reading
- Smart energy management and control
- Demand-side management and load-shedding strategies
- Real-time price signal decision analysis and load control
- Emergency and casualty power management and control
- Dual power (AC and DC) facility circuits
- Reactive power management
- Energy storage power management
- Integration of local/site power generation management
- Other capabilities

Results

Presently, the project is in the modeling and simulation stage. Results will be obtained after the models are complete and the distribution systems have been simulated.

Conclusions and Future Directions

1. Build system simulation models (October 2006) of
   - An AC distribution system (possibly obtained from a utility)
   - A DC distribution system similar to the AC distribution system above
   - A DC distribution system with distributed generation
2. Compare the DC and AC distribution systems using the models (September 2007) with respect to
   - Cost
   - Energy efficiency
   - Reliability
   - Power quality
   - Pollution emissions
   - Losses
   - Net energy consumption
   - Fuel savings
3. Consider the impact of daily, seasonal, weekend, and holiday/special event load variations (September 2007).
4. Consider the availability to maintain the various fuel cell power modules during light load periods as a means to improve availability performance (June 2007).

5. Assess operational and control changes needed to implement a DC distribution system (March 2007).
6. Answer the following questions (January 2007):
   - What value can be derived by using the third phase wire of a legacy AC circuit for high bandwidth data and communication services?
   - Does having this wire available expand the variety and number viable concepts for circuit status/health monitoring and control?

III.C.3 A Low-Cost Soft-Switched DC/DC Converter for Solid Oxide Fuel Cells

Objectives

- Develop a low-cost DC-DC converter for low- to high-voltage power conversion as the standard interface between the SOFC source and the load-side DC-AC inverter.
- Develop a low-cost 5 kW DC-AC inverter with a minimum energy efficiency of 99% operating with >400 VDC input.
- Develop power management control strategies and demonstrate the ability to supply and consume reactive power while simultaneously supplying active power to the utility grid.
- Develop sensory and control logic to enable autonomous/semi-autonomous response to aid supporting grid voltage and frequency needs without nuisance tripping or disconnection of the fuel cell system.

Accomplishments

- Demonstrated a new soft-switching DC-AC inverter with efficiency of 99% at 425 V input voltage and 5 kW output power condition. With inclusion of filter components, the overall efficiency achieves 98% at full load.
- Demonstrated the low input voltage SOFC power conditioning system with a system-level efficiency of 94% at full-load.
- Developed a universal power conditioning system that allows standalone load and grid-tie using digital phase-lock loop technique.

Jason Lai (Primary Contact), Sung Yeul Park, Seungryul Moon, Jian Liang Chen, and Junhong Zhang

Virginia Polytechnic Institute and State University
614 Whittemore Hall
Blacksburg, VA 24061-0111
Phone: (540) 231-4741; Fax: (540) 231-3362
E-mail: laijs@vt.edu

DOE Project Manager: Don Collins
Phone: (304) 285-4156
E-mail: Donald.Collins@netl.doe.gov

Subcontractors:
Southern California Edison, Los Angeles, California

Introduction

The Virginia Tech SECA project has been focusing on high-efficiency low-cost power conversion for the solid oxide fuel cell (SOFC) power conditioning systems. In our Phase I effort, an interleaved soft-switching DC-DC converter has been successfully developed and demonstrated 97% peak efficiency. The focus of this past year was to develop a highly efficient DC-AC inverter as the subsequent stage. Our design target for the DC-AC inverter is to reach near perfect conversion of 99% efficiency. This inverter can be connected through an inductor-capacitor (LC) filter to the standalone household AC loads or a large inductor to the utility grid interconnection.

The DC-DC converter and DC-AC inverter are integrated as the complete power conditioning system (PCS) for SECA SOFC testing to verify the efficiency and to show power flow control capability between fuel cell and utility grid. Through a number of iterations and design optimization, our inverter has successfully demonstrated the 99% efficiency target. Together with the early developed, highly efficient DC-DC converter and an output stage filter, which consumes 1% power, the entire PCS has reached 94% efficiency at the 5 kW full-load condition. For the same input voltage and output power, our SECA Industrial Team partner, Siemens-Westinghouse, reported only 80% efficiency with the PCS purchased from their supplier. A recently developed 48 V input voltage, 1 kW output power state-of-the-art PCS only achieved 88.5% efficiency [1]. With the superior efficiency achieved by the proposed all soft-switching PCS, the significance to the SECA program and SOFC design is a substantial savings on power loss that allows the fuel cell manufacturer to reduce the size of the fuel cell stack and the reduction of fuel consumption.

Approach

Major loss components of the state-of-the-art DC-AC inverter are device conduction and switching losses. The only way to reduce conduction loss is to add as much silicon as possible. However, the device that has been widely used in DC-AC inverters is the insulated gate bipolar transistor (IGBT), which has a fixed junction voltage drop that can never disappear. Our approach is to replace the IGBT with power MOSFET, which is a pure resistive loss device, so its conduction loss can be reduced to less than 1% given sufficient

silicon area. However, the power MOSFET has a body diode, which generates a large reverse recovery loss when it is turned off. Thus, the power MOSFET has never been used in high-voltage high-power DC-AC inverters. To solve the power MOSFET switching loss problem, the proposed approach is to use the advanced soft-switching technique to eliminate the switching loss associated with the MOSFET body diode reverse recovery.

Figure 1 shows the proposed soft-switching inverter circuit. The power MOSFET switches S_1, S_2, S_3, and S_4 are the main switching devices, and the small IGBT switches S_{x1}, S_{x2}, S_{x3}, and S_{x4} are the auxiliary switches. Small resonant inductors L_{ra} and L_{rb} resonate with the capacitors across the main switching devices to produce zero voltage before the switch is turned on, thus avoiding diode reverse recovery loss. The soft-switching principle and control design methodology are described in detail in references [2] and [3].

A circuit diagram of the PCS power stage and control design of the PCS for utility grid-tie are shown in Figure 2. For a standalone PCS, the output only needs to be filtered by inductor L_{o1} and capacitor L_{o2}. For the grid-tie inverter, an additional inductor L_{o2} is needed to reduce the output current ripple content. A circuit breaker (CB) is also needed to connect and disconnect the PCS. A digital signal processor (DSP) based controller has been developed for the power flow control. We designed a phase lock loop (PLL) to obtain the grid synchronization signal and to produce the in-phase or orthogonal sine waves. These sine waves are multiplied with the real power command P_{ref} and reactive power command Q_{ref} to obtain the reference control current i_{ref}. A proportional-integral (PI) controller H_i(s) is designed to obtain the duty cycle signal $d(t)$ and to produce the desired pulse-width-modulation (PWM) signals for the DC-AC inverter switches.

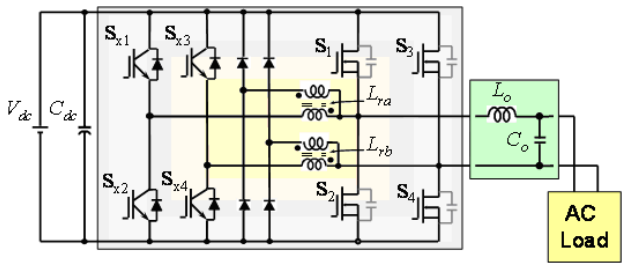

FIGURE 1. Circuit Diagram of the Proposed Soft-Switching Inverter

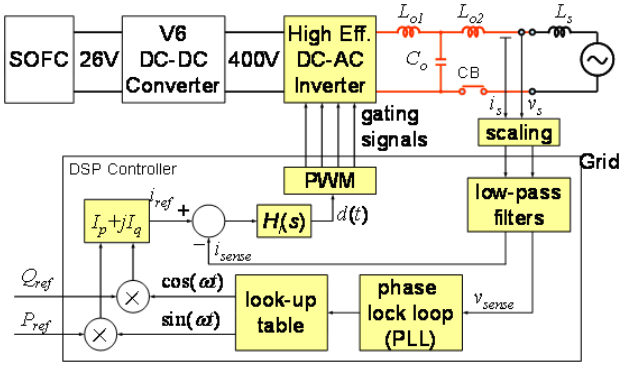

FIGURE 2. Control System of a Grid-Tie SOFC Power Conditioning System

Results

Using the commercially available devices and components, our initial soft-switching inverter design achieved 97.5% efficiency at 5 kW, which was better than most state-of-the-art inverters, but not enough to meet our efficiency goal. We then contacted the power MOSFET manufacturer to solicit a donation of high voltage, high power MOSFET dies for the development of a new soft-switching device module. We received the donation of 100 dies from Infineon and worked with Advance Power Technology to package the phase-leg module to eliminate the parasitic component associated losses. Our second version achieved the design target of 99% efficiency. Under the full-load 5 kW condition, the device steady-state temperature rise is around 20°C with only natural convection heat sinking. Such a "cool" operating condition can ensure long-term reliability of the PCS.

The newly developed soft switching inverter has been integrated with the high-efficiency DC-DC converter for the PCS system-level test. Figure 3 shows the circuit diagram and photograph of the entire PCS efficiency measurement. The fuel cell source voltage V_{fc} is obtained from the SOFC simulator, which consists of a power supply and a source resistance. To ensure accurate reading, a current viewing shunt resistor is connected in between the SOFC simulator and the PCS prototype. The total source resistance including SOFC internal resistance and shunt resistance is

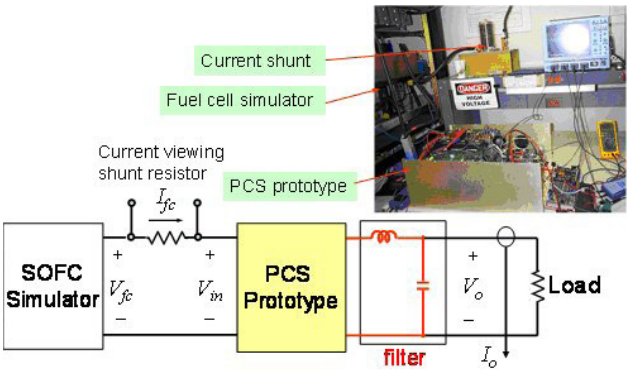

FIGURE 3. The PCS Efficiency Measurement Circuit Diagram and Photograph of Test Setup

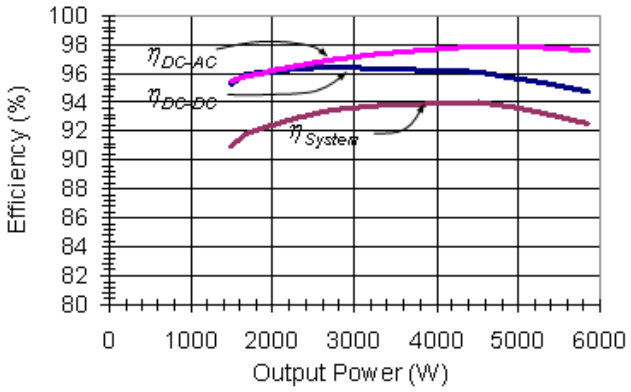

FIGURE 4. The Soft-Switched PCS Efficiency Profiles under the SOFC Simulator Test

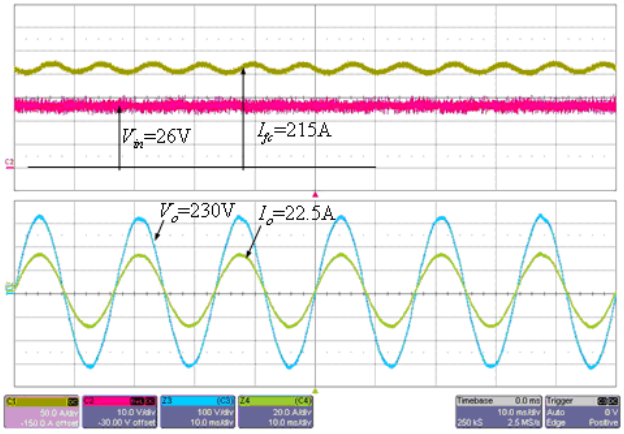

FIGURE 5. The Soft-Switched PCS Input and Output Voltage and Current Waveforms at Full Load

22.423 mΩ. The output of the PCS is connected to a resistive load bank through an LC filter. The load bank sits underneath the bench. The simulator, current shunt, and the PCS hardware prototype along with the measurement instrumentation are shown in the photograph.

The system-level efficiency profiles with SOFC simulator as the source are shown in Figure 4. The no-load simulator output voltage in this case is 32 V. With the total source resistance of 22.423 mΩ, the converter input voltage at 6 kW drops to about 25 V. This new PCS is the only reported all soft switching PCS in the world. The soft switching is not only applied to the DC-DC converter, but also the DC-AC inverter. The DC-AC inverter efficiency η_{DC-AC} including output filter stage peaks at 98% at near full-load condition. This implies that without the output stage LC filter, the power stage DC-AC inverter efficiency peaks at 99%. The DC-DC converter efficiency η_{DC-DC} peaks at 97% at about half load. The overall system efficiency η_{System} peaks at 94% in the load range from 70% to 90%. The test has been extended to 6 kW, or 20% overload without forced-air cooling. The temperature rise of the heat sink is less than 20°C at the full-load condition. It can be foreseen that the unit will be very reliable in long-term operation.

Figure 5 shows measured PCS input and output voltage and current waveforms at the full-load condition. The input voltage V_{in} contains a high-frequency switching ripple, and the input current I_{fc} contains a 120 Hz low-frequency ripple, which can be reduced by the active ripple cancellation technique. The soft-switching inverter was originally designed for better efficiency, but a better waveform quality was also achieved, as indicated in the lower traces of output voltage V_o and current I_o waveform. The major reason for the high-quality sinusoidal waveform is substantial reduction of electromagnetic interference (EMI) emission with the proposed soft-switching technique.

Conclusions and Future Directions

A highly efficient soft-switching DC-AC inverter has been successfully developed. The inverter achieves a near perfect power conversion efficiency of 99%. Together with the previously developed highly efficient DC-DC converter and an output LC filter, the entire power conditioning system has been integrated as the first reported all soft-switching PCS in the world. The unit has been tested using an SOFC simulator as the source. The output stage can be connected to a standalone load as well as the utility grid through an additional inductor and a circuit breaker. Our next step is to test the unit with a Siemens-Westinghouse SOFC under grid-tie condition. The system will include real and reactive power flow control. New sensory and control strategies will incorporate the input from the utility partner – Southern California Edison. Major anticipated accomplishments through future work are listed as follows.

- Develop power management control strategies and demonstrate the ability to supply and consume reactive power while simultaneously supplying active power to the utility grid.
- Develop sensory and control logic to enable autonomous/semi-autonomous response to aid supporting grid voltage and frequency needs without nuisance tripping or disconnection of the fuel cell system.
- Test the entire PCS at EPRI-Solutions to show the performance of EMI and power quality under grid-tie control conditions.

Special Recognitions & Awards/Patents Issued

1. A U.S. patent entitled Multiphase Soft Switched DC/DC Converter and Active Control Technique for Fuel Cell Ripple Current Elimination was filed in November 2005. The patent was originally filed as U.S. Provisional Application Ser. No. 60/654,332 in February 2005.

2. The pending patent has been licensed to PEMDA Corp., Knoxville, Tennessee.

FY 2006 Publications/Presentations

1. S. Moon, S. Park, C. Liu, and J.S. Lai, "Solid Oxide Fuel Cell Current Ripple Impact and Reduction Techniques," *Proceedings of IEEE PESC*, Jeju, Korea, June 2006, pp. 2037–2042.

2. Junhong Zhang and Jih-Sheng Lai, "A Synchronous Rectification Featured Soft-Switching Inverter Using CoolMOS," *Proceedings of IEEE APEC*, March 2006, pp. 810–815.

3. C. Liu, A. Johnson, Jih-Sheng Lai, "A novel three-phase high-power soft-switched DC/DC converter for low-voltage fuel cell applications," *IEEE Transactions on Industry Applications*, December 2005, pp. 1691–1697.

4. Jih-Sheng Lai, Changrong Liu, and Donald Collins, "Active Control Technique for Fuel Cell Ripple Current Elimination," Poster presentation at 2005 Fuel Cell Seminar, Palm Spring, CA, November 2005.

5. Jih-Sheng Lai, "A high-performance V6 converter for fuel cell power conditioning system," *Proc. of IEEE Conference on Vehicle Power and Propulsion*, September 2005, pp. 624-630.

6. Ken Stanton and Jih-Sheng Lai, "A Temperature Dependent Fuel Cell Model for Power Electronics Design," *Proc. of IEEE PESC*, Recife, Brazil, June 2005, pp. 1647-1651.

References

1. D.G. Holmes et. al., "An Innovative, Efficient Current-Fed Push-Pull Grid Connectable Inverter for Distributed Generation Systems," *Proceedings of IEEE PESC*, Jeju, Korea, June 2006, pp. 1054–1060.

2. J.-S. Lai and J. Zhang, "Efficiency Design Considerations for a Wide-Range Operated High-Power Soft-Switching Inverter," *Proceedings of IEEE Industrial Electronics Conference*, Raleigh, NC, Nov. 2005, pp. 604-609.

3. Junhong Zhang and Jih-Sheng Lai, "A Synchronous Rectification Featured Soft-Switching Inverter Using CoolMOS," *Proceedings of IEEE APEC*, Dallas, TX, March 2006, pp. 810–815.

III. SECA RESEARCH & DEVELOPMENT
D. Modeling and Simulation

III.D.1 An Integrated Approach to Modeling and Mitigating SOFC Failure

Objectives

- Generate new scientific and engineering knowledge to better enable SECA industry teams to develop low-cost solid-oxide fuel cell power generation systems.
- Create technology breakthroughs to address technical risks and barriers that currently limit achievement of the SECA performance and cost goals for solid-oxide fuel cell systems.
- Transfer new science and technology developed in the Core Technology Program to the SECA industry teams.

Accomplishments

- Developed and implement a suitable failure effects analysis (FEA) tool for analysis of fracture failure in the context of various pre-existing flaws within SOFC cells under various operating conditions. The program Fracture Mechanical Analyzer (FMA) was developed and transferred to SECA.
- Developed higher order (second and third) analytical model of the SOFC heating/cooling during start-up/shut-down in the limit of optically thin anode-electrolyte-cathode (PEN) layers assembly and local thermal equilibrium between the layers.

Introduction

It is well known that thermal transients and gradients impose states of stress within SOFC cell materials that may result in crack initiation, propagation and subsequent structural failure or performance degradation in short-term operation; furthermore, due to a variety of mechanisms, performance may significantly decrease over time. The commercial viability of SOFC power generation systems is dependent upon making significant progress in the durability and reliability of cell and stack structures. However, no systematic study of the causes or physical drivers of cell failure and degradation have been conducted; as a result, no coherent degradation or useful life prediction modeling methodology is currently available. A new modeling methodology could significantly contribute to efficient development of SECA SOFC system performance requirements.

Additionally, previous modeling attempts to characterize SOFC failure modes have been limited because of simplified transport models. One dimensional, "bulk" electrochemical and thermal models have been applied, and these models have been decoupled (i.e., interdependency between electrochemistry and thermal transport neglected). In order to create greater fidelity within thermomechanical failure analysis models, interdependency between structural issues and electrochemical/thermal transport phenomena must be characterized. This requires a multi-physics modeling approach as demonstrated in this research.

Jianmin Qu (Primary Contact), Andrei Fedorov, Samuel Graham and Comas Haynes
Georgia Institute of Technology
801 Ferst Drive, N.W.
Atlanta, GA 30332-0405
Phone: (404) 894-5687; Fax: (404) 894-0186
E-mail: jianmin.qu@me.gatech.edu

DOE Project Manager: Travis Shultz
Phone: (304) 285-1370
E-mail: Travis.Shultz@netl.doe.gov

Approach

The recent shift of SOFCs to anode-supported structures, in which a thin film electrolyte is sintered onto the anode support, has further hampered structural modeling due to the large aspect ratio between the anode/electrolyte layers and cell length. Yet due to thermal mismatch between these layers and the cell operating conditions, significant thermal stresses are created within the cell structure, which may eventually lead to failure, making fracture analysis a critical part of thermomechanical modeling of SOFCs. Specifically, simulation tools are needed to obtain fracture mechanics parameters, such as the stress intensity factors (SIFs), and to understand the influence of thermal gradients on crack behavior.

To meet this need, a computer program called Fracture Mechanical Analyzer (FMA) was developed to calculate the SIFs of 3-D cracks, including interfacial cracks in the PEN structure subjected to combined mechanical and thermal loadings [1-3]. The FMA program, written in MatLab language, is essentially an "add-on" to any commercial finite element software. It computes the energy release rate and the individual SIFs based on the crack-tip displacement fields computed from any commercial finite element software.

Additionally new models were developed to analyze the thermal behavior in SOFCs and transient modeling of the SOFC unit cell is a prerequisite to mitigating

thermo-mechanical failure caused by thermal gradients and cycling at start-up/shut-down. At start-up, it is desirable to heat the cell as quickly as possible under the constraint of some maximum allowable temperature gradient. Thermal modeling focused on correlating the heating rate and the observed temperature gradients, and was presented in a manner that easily yields this information for the cell designed.

Three models of increasing complexity and accuracy were developed. The first two models assume that the cell is thermally thin, that is, the cell materials have high thermal diffusivity so thermal field development in the solid intimately follows that in the heating air. The third model relaxes this assumption and gives consideration to the thermal resistance and latency (thermal energy storage) of the cell materials. Results from these models were compared to the transient solution obtained by the fully 3-D transient Fluent model to identify the "best" model featuring the least degree of complexity and computational expense yet resulting in sufficient accuracy of simulation results.

Results

The 3-D structural analysis was separated into two steps: a global cell model and a local fracture model. The global–local modeling technique extrapolated the boundary displacements and temperature fields from a location in the full-scale model to the smaller local fracture model. This fracture model would be able to incorporate a higher density of nodes at the crack edge over that of a full-scale model featuring a crack. Fracture parameters were then determined by using the FMA program.

Figure 1 is a diagram of the global model used for analysis, Figure 2 is an example of the normalized stress curve seen in the model for a given set of boundary conditions, and Figure 3 is a plot of the SIF of a vertical penny crack in the anode versus differing electrolyte heights. The stress intensity factor plotted is KI which means a tensile stress is seen in the anode during cool down from operation such that if the temperature change was high enough the crack would grow upwards to the electrolyte. This model assumed a temperature drop of 200°C which was not sufficient for crack growth.

In the thermal analysis after reviewing the results and analysis of the simplified analytical transient heating models and the numerical, 2-equation, non-equilibrium model, guidance was provided concerning model selection and limits of applicability. Thermal

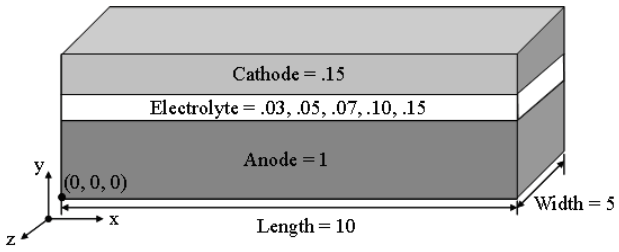

FIGURE 1. Model Configuration for PEN Layer

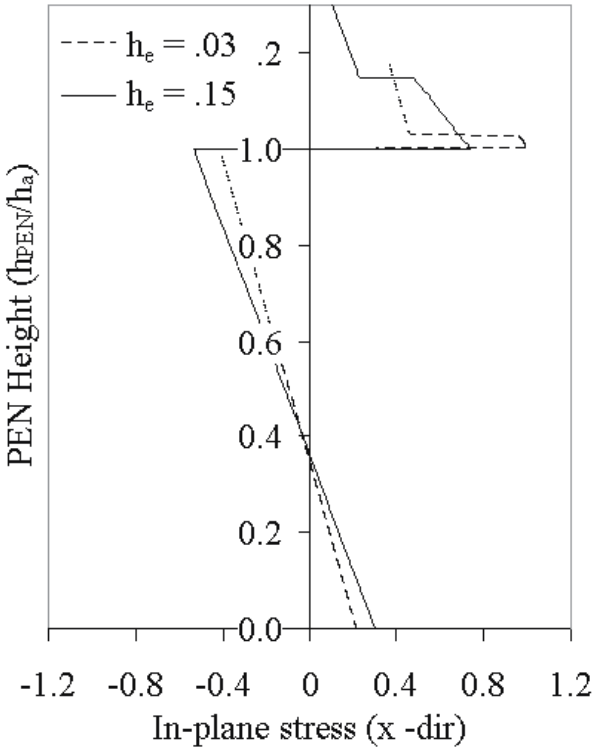

FIGURE 2. In-Plane Stress for Positive Temperatures versus PEN Height

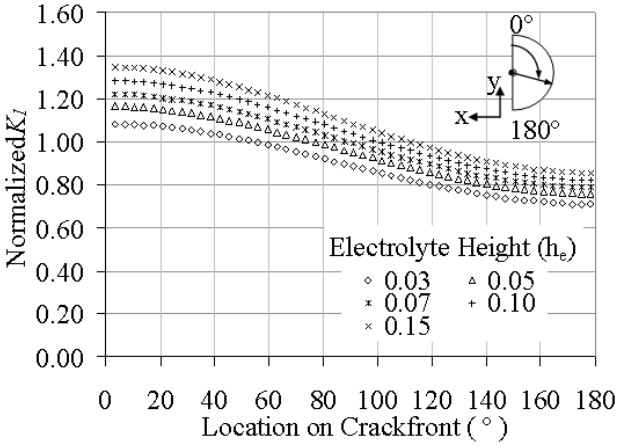

FIGURE 3. Mode I SIF for Crack in Anode for Different Electrolyte Heights with Crack Center at (2.5, 0.6, 0)

modeling efforts thus far have focused on correlating the heating rate and the observed temperature gradients in a unit cell heated by flowing hot air into the oxidizer channel. The linear rate of temperature rise, *K*, and mean velocity, *U*, of the heating air are design variables that can be controlled in maintaining temperature gradients below a given threshold while minimizing heating time requirements. In the analysis of each simplified model, the predictions of heating time and maximum temperature gradient developed in the cell were compared to results from 3-D, computational fluid dynamics (CFD) Fluent model simulations. Thus, we assessed the capability of these models to predict these *global* quantities while making no judgment concerning the ability of the models to accurately predict *detailed* time-varying temperature fields.

The model predicts heating time and temporal temperature gradient to a high degree of accuracy (~2% error) compared to CFD results. Model predictions of maximum spatial temperature gradient (along the flow direction) are less precise (< 20% error). For the values of *K* and *U* given, the 1st and 2nd order models yield almost identical results and outside this range the 2nd order model does not improve accuracy except in the case of predicting temperature gradients at very low velocity (< 1 m/s) and K < 0.1 °C/s . The 3rd order, 2-equation model is also not an improvement over the 1st model, and, in fact, has limited ability to predict temperature gradients due to its strong dependence on the solid-gas heat transfer coefficient in the air channel.

Figure 4 is a design map, based on this research, for the specific unit cell geometry and materials described in the March 2004 report. One way to use the map is to draw a horizontal line corresponding to the maximum allowable temperature gradient. Values of *K* and *U* below this line can be selected such that the heating time (horizontal axis) is minimized. This gives some flexibility in choosing *K* and *U* but these parameters may be limited by other system considerations such as pumping power, or heater size. Alternatively, the heating time requirement could be imposed, and then *K* and *U* selected such that temperature gradient is minimized. Use of the map in this way gives approximate values of *K* and *U*, which are an excellent starting point for performing CFD simulations of the heating/cooling process if detailed results are required.

Conclusions and Future Directions

- The FMA program was used in conjunction with the ANSYS commercial software to demonstrate a method to study structural failure in the PEN despite issues with the aspect ratios of the material layers and difficulties in performing a complex fracture analysis.

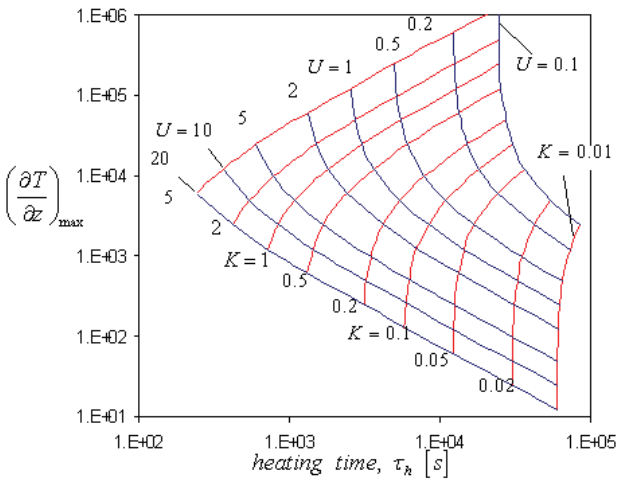

FIGURE 4. Design map showing maximum temperature gradient vs. heating time for various values of *K* and *U*. Given the maximum allowable temperature gradient, *K* and *U* can be selected such that heating time is minimized. This map is specific to the unit cell geometry and materials under consideration, and a temperature rise of 600ºC from ambient to operating temperature.

- For the global model studied, failure would most likely occur in the anode as crack growth towards the electrolyte during cooling.
- If details of the 3-D time-varying temperature fields are desired, then transient CFD modeling is required (at significant computational expense), but 2nd and 3rd order analytical models were not significantly improved over the 1st order model.
- The 1st order model may safely be used within the range of validity that was established and for the purpose of predicting total heating time, and maximum temperature gradients developed during a heating/cooling process.
- Several future possibilities for structural analysis include the study of thermal fatigue as the anode cycles between tension and compression and incorporating the impact of mechanical constraints into the failure analysis.

FY 2006 Publications/Presentations

1. Johnson, Janine and Jianmin Qu. Three-Dimensional Numerical Simulation Tools for Fracture Analysis in Planar Solid Oxide Fuel Cells (SOFCs). 2006. Cocoa Beach, FL, United States: American Ceramic Society, Westerville, OH 43086-6136, United States.

2. Johnson, Janine and Jianmin Qu, An interaction integral method for computing the stress intensity factors of planar cracks in non-uniform temperature fields. Engineering Fracture Mechanics, *submitted May 2006*.

References

1. Gosz, M., M. Dolbow, and B. Moran, Domain integral formulation for stress intensity factor computation along curved three-dimensional interface cracks. International Journal of Solids and Structures, 1998. 35(15): p. 1763-1783.

2. Nahta, R. and B. Moran, Domain integrals for axisymmetric interface crack problems. International Journal of Solids and Structures, 1993. 30(15): p. 2027-40.

3. Johnson, Janine, Fracture failure of solid oxide fuel cells, in Mechanical Engineering. 2004, Georgia Institute of Technology: Atlanta. p. 114.

III.D.2 Analysis of Percent On-Cell Reformation of Methane in Solid Oxide Fuel Cell Stacks: Thermal, Electrical, and Stress Analysis

Objectives

- Quantify the effect of varying the percentage of the steam-methane reformation reaction occurring on-cell on the thermal, electrical, and mechanical performance of a generic SOFC stack design.
- Determine the optimal on-cell reformation percentage.
- Demonstrate - with simulations of stack operation - how the optimal methane fuel mixture can be used to improve stack performance.

Accomplishments

- Discovered that at least 40% of the steam-methane reformation reaction could be performed on-cell for cross-flow and counter-flow stacks of 10x10 cm and 20x20 cm cell sizes.
- Identified that at least 80% of the steam-methane reformation reaction could be performed on-cell for co-flow configuration stacks because the stack performance improved continuously with increasing percent on-cell reformation.
- Demonstrated that the thermal and mechanical performance could be manipulated with on-cell reformation without adverse effects to the electrical performance of the stack.

Introduction

The solid oxide fuel cell (SOFC) industry continues to develop larger, more powerful cell stacks for stationary power applications, and thermal management remains a critical issue for the reliable operation of these stacks. On-cell steam-methane reformation is an effective means of removing excess heat generated within large SOFC stacks. The endothermic reformation reaction, when employed directly on the anode, immediately removes excess heat generated by the electrochemical oxidation reactions. Thus on-cell reformation (OCR) is attractive because of the decreased thermal load it can provide as well as the cost benefits of decreased reformer and heat exchanger size. The challenge presented by OCR is related to the rapid kinetics of the reformation reaction on a standard Ni-YSZ anode. With increasing percent OCR, the resultant endotherm can cause a significant local temperature depression near the fuel inlet on the anode. Cooling near the fuel inlet and subsequently increased heating downstream due to increased hydrogen concentration and electrical current density can create a large difference between the minimum and maximum temperatures on the cell (ΔT). Along with the cell ΔT there can be an increase in the thermal stresses on the anode creating an unreliable condition for cell operation. This study was performed to analyze the effect of various percent OCR on the thermal, electrical, and mechanical performance of typical planar SOFC designs with 10x10- and 20x20-cm active cell areas.

Mohammad A. Khaleel (Primary Contact), Kurt Recknagle, Brian Koeppel, Xin Sun, John Vetrano, and Sato Yokuda
Pacific Northwest National Laboratory (PNNL)
902 Battelle Blvd.
Richland, WA 99352
Phone: (509) 375-2438; Fax: (509) 375-4392
E-mail: moe.khaleel@pnl.gov

DOE Project Manager: Travis Shultz
Phone: (304) 285-1370
E-mail: Travis.Shultz@netl.doe.gov

Approach

A computational modeling tool for simulating the multi-physics of SOFC operation was used in this study. The PNNL-developed SOFC-MP code solves the equations for mass transport, energy, and electrochemistry required to predict the fluid flow, temperature, species, and current density distributions in a three-dimensional SOFC geometry [1,2,3]. The 3-dimensional model geometries and boundary conditions were similar to those of earlier work by this group [4]. The electrochemistry model used was described by Chick et al. [5], calibrated for application to planar stack simulations [6,7], and updated to provide an improved anode concentration polarization model [8]. The steam-methane reformation model was described by Recknagle et al. [9] and revised to include a 1st order Arrhenius rate expression derived experimentally at PNNL [10].

In the study it was assumed the unreformed fuel mixture containing methane, steam, and nitrogen passed through a fuel stream pre-heater to an external reformer where various percentages of the methane were reacted using excess steam in a steam-to-carbon ratio of 2. The anode input gas mixture was then determined based on the water-gas-shift reaction equilibrium at 750°C. This study examined fuels with compositions representing 0 to 80% OCR as summarized in Table 1.

TABLE 1. Molar Compositions of Fuel Mixtures Supplied from External Reformer to the Stack

% OCR	H_2	CO	H_2O	CO_2	CH_4	N_2
0	0.538	0.127	0.181	0.052	0.000	0.101
20	0.465	0.096	0.232	0.059	0.039	0.109
40	0.376	0.064	0.295	0.062	0.084	0.118
60	0.264	0.033	0.377	0.058	0.137	0.129
80	0.118	0.008	0.488	0.042	0.202	0.142

In the simulations, the iterative solutions for all cases were well converged with respect to mass, momentum, energy, chemistry, and electrochemistry. For these analyses, the electrochemical performance of a cell operating on the fully pre-reformed fuel was taken to be 0.60 A/cm^2 at 0.68 volts and 75% fuel utilization, at an average cell temperature of 750°C. All solutions used adjustable inflow temperature and cell voltage to achieve an average cell temperature of 750°C and current density of 0.6 A/cm^2, respectively. Because all cases simulated stack operation at the same average temperature and current density except for variations in the output power, the differences in net heat load were attributable to the heat removed by OCR. Subsequently, the thermal performance of each stack could be compared directly. Two air flow rates were used to examine the air cooling effect at 30% and 15% air utilization.

After the electrochemical-thermal solution was obtained, the resulting temperature profile was used as the thermal load in the subsequent structural analysis to calculate stresses in the cell. The maximum principal stress of the anode was then obtained for each of the cases. For the structural evaluation, minimal displacement support boundary conditions were used at the bottom of the cell. These simplified boundary conditions do not constrain the unit cell model as completely as if it was within a full stack, and are suitable for direct case-to-case comparisons of the stress in a trend analysis as is presented here.

Results

Figure 1 shows the cell ΔT (triangular icons), and the maximum principal stress (S1) in the anode (red square or green "x" icons) for the 10x10-cm counter-flow stack as a function of percent OCR. The scale for the cell ΔT is on the left of the figure and the scale for the stress on the right. With 30% air utilization, cell ΔT for this stack varied between 45° and 85°C with a minimum at 40% OCR. The anode stress followed the trend of ΔT closely also reaching a minimum value at 40% OCR for 30% air use. As shown by the green curve in Figure 1, when more air was supplied to the stack (15% air use) the variation of stress was decreased,

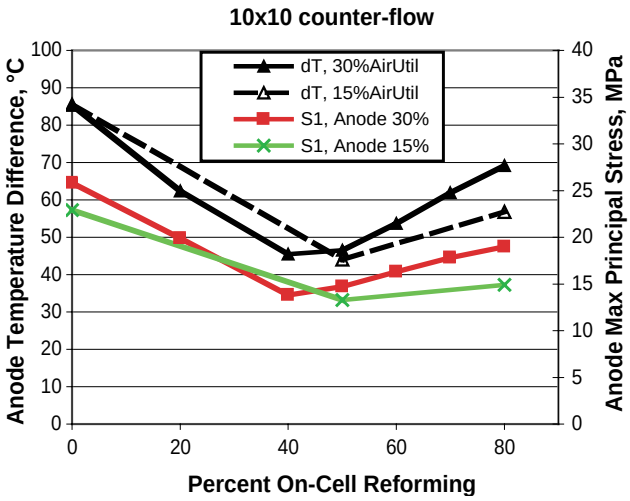

FIGURE 1. Cell Temperature Difference (ΔT) and Maximum Principal Stress (S1) versus % OCR for 10x10-cm Counter-Flow Cases

but the magnitude of the stress was not decreased substantially. For both air utilizations, the anode stress was at least 14 MPa.

Table 2 summarizes cases for each stack configuration and cell size with 30% and 15% air use, and the percent OCR in which the anode stress was minimum, including the data point representing the 10x10 cm counter-flow stack described in Figure 1. The 10x10-cm cross-flow stack results were similar to the counter-flow results featuring a minimum anode stress and ΔT at intermediate OCR (50%) with 30% air use. With more cathode air (15% air use) neither the maximum temperature nor the anode stresses were significantly reduced. The 10x10-cm co-flow stack results, with 30% air use, showed little change to the magnitude of ΔT and a slight decrease of anode stress for increasing percent OCR. The co-flow stack also showed a benefit from increased cathode air (15% air use) in the form of decreased ΔT and stress over the full range of percent OCR. Stresses in the anode were similar in magnitude to those predicted for the counter- and cross-flow stacks with a minimum value of approximately 15 MPa. Gross electrical power density of 0.4 W/cm^2 was virtually unaffected for each of the 10x10-cm stacks.

Cell ΔT and anode stresses were substantially larger in the 20x20-cm stack simulation results than those of the 10x10-cm cases. Similar to the 10x10-cm cases, the anode stresses were minimum values at intermediate percent OCR for 30% air use in cross- and counter-flow configurations. With 15% air use the cross and counter-flow stacks benefited most from 0% OCR while the co-flow stack had decreased stress, ΔT, and maximum temperature at 80% OCR. In each 20x20-cm case the electrical power density deviated little from the nominal value of 0.4 W/cm^2.

TABLE 2. Summary of Results and Related %OCR with Minimum Anode Stress

Cell Size / Air Use, %	Flow Configuration	% OCR	Temperature, °C		Anode Stress S1max, MPa	Power, W/cm^2
			Maximum	ΔT		
10x10 / 30%	Cross	50	775	74	14.2	0.403
	Co-flow	80	779	74	17.2	0.403
	Counter	40	768	45	13.8	0.405
10x10 / 15%	Cross	50	774	66	14.0	0.405
	Co-flow	80	777	66	14.8	0.403
	Counter	50	768	44	13.3	0.406
20x20 / 30%	Cross	50	866	241	60.2	0.399
	Co-flow	80	844	178	40.0	0.403
	Counter	60	832	196	71.7	0.409
20x20 / 15%	Cross	0	851	191	45.2	0.397
	Co-flow	80	817	124	25.5	0.404
	Counter	0	851	188	45.4	0.415

Conclusions

- The analyses showed that the anode stress achieved local minima along with the temperature difference on the cell with 40 to 50% OCR in counter-flow and cross-flow stacks of 10x10-cm size.
- Unlike the cross-flow and counter-flow stacks, the co-flow stack showed substantial thermal benefit due to increased air flow (15% air utilization) as the anode stress and cell temperature difference was decreased over the full range of OCR.
- Within the 20x20-cm cases the co-flow configuration stack had the smallest anode stresses and cell temperature difference, both of which were continuously decreased with increasing OCR.
- Gross electrical power density of 0.4 W/cm^2 was virtually unaffected for each 10x10-cm case; little power density variation was predicted in the 20x20-cm cases as well.
- For the conditions and particular generic stacks of this study, the results suggest 40 to 50% reformation on-cell should be considered for cross-flow and counter-flow stacks, and OCR as high as 80% with at most 15% air utilization should be desirable in co-flow stacks.

Future Directions

- Modeling will be performed in support of experiments to modify anode material providing optimal anode activity for thermal performance.
- Optimize the thermal, mechanical, and electrical performance of stacks of larger size and varying design.

FY 2006 Publications/Presentations

1. Recknagle KP, ST Yokuda, DT Jarboe, and MA Khaleel. 2006. *Analysis of Percent On-Cell Reformation in SOFC Stacks: Thermal, Electrical, and Stress Analysis*. SECA Topical Report.

2. Recknagle KP, DT Jarboe, DL King, MA Khaleel, and P Singh. 2005. *Modeling of On-Cell Reformation in SOFC Stacks: The Effect of Methane Conversion Activity Manipulations on Stack Performance*. SECA Topical Report.

3. Recknagle KP, DT Jarboe, KI Johnson, VN Korolev, MA Khaleel, and P Singh. 2005. *Electrochemistry And On-Cell Reformation Modeling For Solid Oxide Fuel Cell Stacks*. 30th International Conference & Exposition on Advanced Ceramics and Composites, Cocoa Beach FL, January 24, 2006.

4. Khaleel MA, KP Recknagle, JS Vetrano, X Sun, BJ Koeppel, KI Johnson, VN Korolev, BN Nguyen, AM Tartakovsky, and P Singh. Recent Development of Modeling Activities at PNNL. SECA Core Technology Program Peer Review, Lakewood, CO, October 25-26, 2005.

References

1. Khaleel MA. 2005. "Finite Element SOFC Analysis with SOFC-MP and MSC.Marc/Mentat-FC." Proceedings of the Sixth Annual SECA Workshop. National Engineering Technology Laboratory, Morgantown, West Virginia.

2. Khaleel MA, Z Lin, P Singh, W Surdoval, and D Collins. 2004. "A Finite Element Analysis Modeling Tool for Solid Oxide Fuel Cell Development: Coupled Electrochemistry, Thermal, and Flow Analysis in Marc." J. Power Sources, 130(1-2):136-148.

3. Recknagle KP, RE Williford, LA Chick, DR Rector, and MA Khaleel. 2003. "Three-dimensional thermo-fluid electrochemical modeling of planar SOFC stacks." J. Power Sources, 113:109-114.

4. Recknagle KP, DT Jarboe, DL King, MA Khaleel, and P Singh. 2005. Modeling of On-Cell Reformation in SOFC Stacks: The Effect of Methane Conversion Activity Manipulations on Stack Performance. PNNL-15311, Pacific Northwest National Laboratory, Richland, Washington.

5. Chick LA, JW Stevenson, KD Meinhardt, SP Simner, JE Jaffe, and RE Williford. 2000. "Modeling and Performance of Anode-Supported SOFC." 2000 Fuel Cell Seminar – Abstracts, pp. 619-622.

6. Chick LA, RE Williford, JW Stevenson, CF Windisch Jr, and SP Simner. 2002. "Experimentally-Calibrated, Spreadsheet-Based SOFC Unit-Cell Performance Model." 2002 Fuel Cell Seminar - Abstracts.

7. Keegan K, M Khaleel, L Chick, K Recknagle, S Simner, and J Deibler. 2002. "Analysis of a Planar Solid Oxide Fuel Cell-Based Automotive Auxiliary Power Unit." Society of Automotive Engineers, Congress 2002 Proceedings, 2002-01-0413.

8. Williford RE, LA Chick, GD Maupin, SP Simner, and JW Stevenson. 2003. "Diffusion Limitations in the Porous Anodes of SOFCs." J. Electrochemical Soc. 150(8): A1067-A1072.

9. Recknagle KP, P Singh, LA Chick, and MA Khaleel. 2004. "Modeling of SOFC Stacks with On-Cell Steam-Methane Reformation at PNNL." PNNL-SA-43248, Proceedings of the Fuel Cell 2004 Seminar, San Antonio, Texas.

10. King DL, Y Wang, Y Chin, Y Lin, H Roh, and R Romiarek. 2005. "Controlling Activity and Stability of Ni-YSZ Catalysts for On-Anode Reforming." Presented at SECA Core Technology Program Review Meeting, Tampa, Florida.

III.D.3 SOFC Modeling at PNNL

Objectives

- Develop and validate the multi-physics solid oxide fuel cell (SOFC) modeling tool to simulate the coupled SOFC stack performance.
- Utilize computational techniques for the mitigation of performance degradation and optimization of modular SOFC stack and systems design.
- Obtain necessary materials properties to support the development and optimization of SOFC designs through modeling.
- Disseminate/transfer modeling tool to all SECA industry teams and appropriate Core Technology Program (CTP) participants.

Accomplishments

- Implemented finite element SOFC electrochemistry module (SOFC-Multi Physics, SOFC-MP) fully compatible with the MARC finite element mesh and modeling capabilities to solve the coupled flow, electrochemistry, and heat transfer solution in the fuel cell under steady state conditions.
- Demonstrated a stack design tool for structural analysis from MSC Software called Mentat-FC, based on the SOFC-MP modeling capability for electrochemical, flow, and thermal analyses of SOFCs.
- Established a methodology to assess glass-ceramic seal failure and developed a continuum damage mechanics model based on the experimental stress/strain response for G18 sealing glass. The damage model was implemented in MSC MARC and was used for SOFC stack stress analysis to predict accumulated damage and failure of the seals under thermal-mechanical loading.

Mohammad A. Khaleel (Primary Contact), Xin Sun, Kurt Recknagle, Brian Koeppel, John Vetrano, Nghiep Nguyen and Wenning Liu
Pacific Northwest National Laboratory
P.O. Box 999
Richland, WA 99352
Phone: (509) 375-2438; Fax: (509) 375-4392
E-mail: moe.khaleel@pnl.gov

DOE Project Manager: Travis Shultz
Phone: (304) 285-4577
E-mail: Travis.Shultz@netl.doe.gov

- Conducted a comprehensive training program covering the full suite of SOFC modeling tools at the SECA Modeling Workshop.
- Developed a probabilistic-based component design methodology for SOFC stacks. This method takes into account the randomness in SOFC material properties as well as stresses arising from different manufacturing and operating conditions.
- Developed an integrated modeling/experimental framework to predict the life of SOFC interconnect materials. The effects of interconnect oxide growth on its structural integrity upon isothermal cooling have been studied using finite element analyses.

Introduction

In order to efficiently develop and optimize planar SOFC stacks, it is desirable to experiment numerically with the effects of stack component mass, geometry, flow rates of the gaseous reactants, electrical loading, and simulated aging. The computation of representative baseline cases, validated by experimental data, has been used to develop better understanding of the stack behavior while avoiding costly and time-consuming experiments. In order to model the multi-physics associated with an SOFC stack, a simulation tool, SOFC-MP was developed. This modeling tool combines the versatility of a commercial multi-physics code and a validated electrochemistry calculation routine. Its function is to predict the flow and distribution of anode and cathode gases, temperature and current distributions, and fuel utilization. The fundamental building blocks of modeling and simulation tools are electrochemical models, fluid flow simulations, computational mechanics and experimental data.

The multi-physics modeling tools developed were then used in studying the full range of design criteria as well as in material development and degradation modeling. On the stack level, a probabilistic-based component design methodology was developed. This method takes into account the randomness in SOFC material properties as well as stresses arising from different manufacturing and operating conditions. For SOFC materials development and degradation study, different degradation mechanisms for different SOFC components, i.e., seal and interconnect, have been considered in order to predict the useful operating time for the stack. Detailed seal and interconnect degradation mechanisms have been modeled and their influences on stack performance have been quantified.

Approach

- Maintain and enhance the integrated modeling tools developed under the SECA core program for evaluating fuel cell stack design concepts by the industrial teams.
- Investigate the effects of materials degradation on cell performance and cell life.
- Investigate the effects of cell geometric design, material property distributions and operating condition on SOFC reliability.

Results

Coarse Methodology – Finite Element Approach

An evaluation of the Mentat-FC and SOFC-MP modeling procedure was performed by studying temperature and stress predictions for a realistic planar design. The objective was to compare the predicted results from the highly efficient finite element model (generated with the Mentat-FC parametric graphical user interface (GUI) and solved by the SOFC-MP solver) with pre-existing results from a highly detailed but computationally expensive computational fluid dynamics (CFD) model. Results from the CFD model were available for an anode-supported planar cross-flow model with six fuel and air inlets/outlets. These results consisted of three cases that modeled i) pre-reformed fuel, ii) fuel with methane content for on-cell reformation, and iii) on-cell reformation using a lower activation energy to simulate a reduced reaction rate. The cell design and the operating conditions were replicated using the parametric build option in the Mentat-FC GUI to construct a highly similar geometry. There were minor features that differed between the two models (e.g. rounded outer corners, bolt holes), but all the essential geometric features of sizes, thicknesses, heights, and flow areas and all the operating conditions for fuel composition, inlet temperatures, velocities, and electrochemistry options were identical. The resulting temperature and stress distributions were presented and compared (Figure 1). In general, the temperature predictions were well matched for the geometry both qualitatively and quantitatively. Differences in the peak temperatures were noted and thermal distributions on the stack exterior were slightly different.

Coarse Methodology – Design Sensitivity Study

A probabilistic-based component design methodology has been developed for SOFC stacks. This method takes into account the randomness in SOFC material properties as well as stresses arising from different manufacturing and operating conditions. The purpose of this work is to provide the SOFC designers a 'coarse' design methodology such that the desired

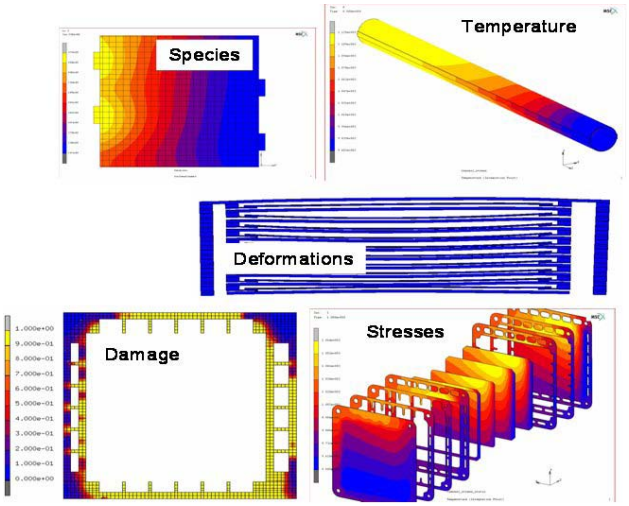

FIGURE 1. Typical SOFC-MP Modeling Results

level of component reliability can be achieved with deterministic design functions using an equivalent safety factor to account for the uncertainties in material properties and structural stresses. Component failure probabilities for the current design were then calculated under different operating conditions.

Seal Property Measurement, Prediction and Degradation Modeling

The glass-ceramic sealant G18 was expected to exhibit stress relaxation at elevated temperatures due to the viscoelastic response of the residual glass content. This would be important to include in SOFC stress analyses to better capture the stress state of the stack components. The continuum damage mechanics model for the glass-ceramic material developed previously was extended to include a viscoelastic response at high temperatures. A Maxwell-type model was used to capture the stress relaxation and used viscosities for the G18 material experimentally obtained at temperatures of 700-800°C (Figure 2). The response of the material model was demonstrated to capture the effect of viscosity and loading strain rate. The model was demonstrated in a single cell stack and compared to results using the previous elastic damage model (Figure 3). The stress relaxation made the cell more compliant and showed beneficial relaxation of the anode stresses through two thermal cycles.

Interconnect Degradation and Spallation Study

The effects of various oxide scale thickness on bulk and interface stresses are predicted for the ferritic stainless steel interconnect material, Crofer 22 APU, under isothermal cooling condition and micro-indentation. The goal of the study is to utilize the

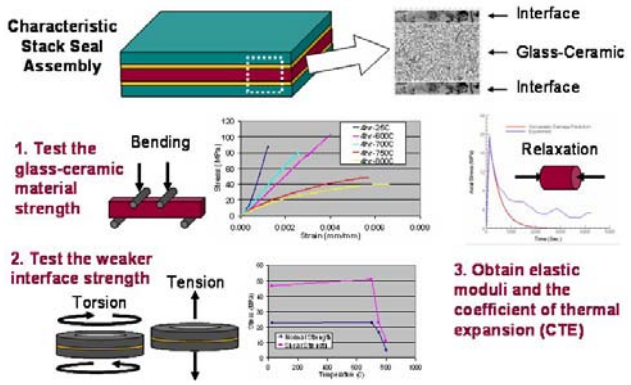

FIGURE 2. Seal Property Characterization

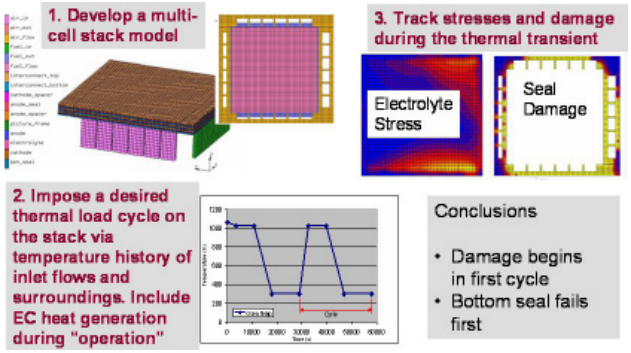

FIGURE 3. Seal Damage Modeling

measurement methodology and the associated quantified interfacial strength developed by other SECA team members in predicting possible scale spallation for different scale thickness, therefore indicating the possible interconnect life under isothermal cooling conditions (Figure 4).

Conclusions and Future Directions

- Continue to validate the model and to transfer the modeling tools technology to the SECA industry teams and work with them to increase utilization of the tools.
- Continue to add improved material models and numerical procedures to the modeling tools.
- Quantify bond strength of oxide/substrate for ferritic stainless steel to predict interconnect life under normal operating temperatures.
- Evaluate creep of glass-ceramic seals during thermal cycling operations.
- Develop seal property predictions via homogenization methods to identify desirable composite seal structures for stacks.

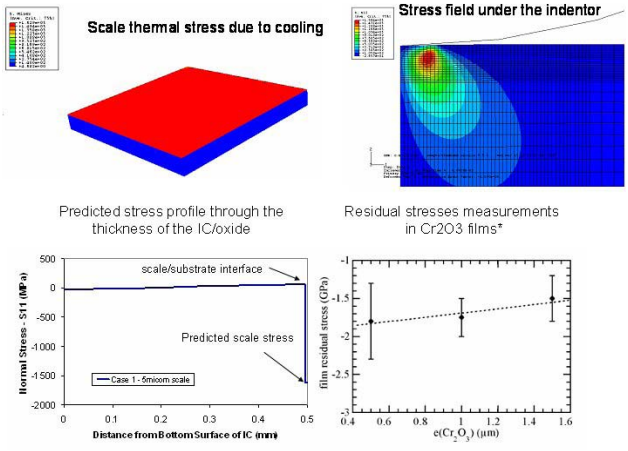

FIGURE 4. Interconnect Degradation and Life Modeling

- Develop analytical methods to evaluate the time-dependent mechanical behavior (creep, thermal fatigue, loss of interconnect contact) of fuel cell stacks/components and influence on electrochemical performance.

FY 2006 Publications/Presentations

1. "Effects of Oxide Thickness on Scale and Interface Stresses under Isothermal Cooling and Micro-Indentation", X. Sun, W.N. Liu, P. Singh and M.A. Khaleel, SECA Topical Report.

2. "Analysis of Seal Damage During Thermal Cycling of a Multi-Cell SOFC Stack", B.J. Koeppel, B.N. Nguyen, and M.A. Khaleel, SECA Topical Report.

3. "Experimental Characterization, Model Development, and Numerical Analysis of Glass-Ceramic Sealant Relaxation Under Thermal-Mechanical Loading", B.J. Koeppel, B.N. Nguyen, J.S. Vetrano, and M.A. Khaleel, SECA Topical Report.

4. "Mechanical Testing of Glass Seals for Solid Oxide Fuel Cells", J.S. Vetrano, Y.-S. Chou, G.J. Grant, B.J. Koeppel, B.N. Nguyen, and M.A. Khaleel, SECA Topical Report.

5. "Crack Growth in Solid Oxide Fuel Cell Materials: From Discrete to Continuum Damage Modeling", B.N. Nguyen, B.J. Koeppel, S. Ahzi, M.A. Khaleel and P. Singh, J. Am. Ceram. Soc. 89 [4] 1358–1368 (2006).

6. "On the Nonlinear Behavior of Glass-Ceramic Seal and Its Application in Planar SOFC Systems", B.N. Nguyen, B.J. Koeppel, J.S. Vetrano and M.A. Khaleel, Proceedings of FUELCELL2006 The 4th International Conference on Fuel Cell Science, Engineering and Technology June 19-21, 2006, Irvine, CA, FUELCELL2006-97057.

7. "Mechanical Property Characterizations and Performance Modeling of SOFC Seals", B.J. Koeppel, J.S. Vetrano, B.N. Nguyen, X. Sun, and M.A. Khaleel, 30th International Conference on Advanced Ceramics, Cocoa Beach, FL, January 23-27, 2006.

8. "Modeling and Measurement of Materials Behavior in Solid Oxide Fuel Cells", J. S. Vetrano, Y-S. Chou, B. Koeppel, B. Nguyen, M. Khaleel, Fuel Cell Seminar 2005, Palm Springs, CA.

9. "Multi-Component-Based Reliability Design for SOFC – A Coarse Design Methodology", X. Sun, A. Tartakovsky and M.A. Khaleel, Fuel Cell Seminar 2005, Palm Springs, CA.

10. Recent Development of Modeling Activities at PNNL, M.A. Khaleel, K.P. Recknagle, J.S. Vetrano, X. Sun, B.J. Koeppel, K.I. Johnson, V.N. Korolev, B.N. Nguyen, A.M. Tartakovsky, and P. Singh, SECA Core Technology Program Peer Review, Lakewood, CO, October 25-26, 2005.

III.D.4 Determination of Electrochemical Performance and Thermo-Mechanical-Chemical Stability of SOFCs from Defect Modeling

Objectives

- Advance the fundamental understanding of the continuum-level electrochemistry of oxide mixed ionic-electronic conductors (MIECs) in relation to their performance in SOFCs.
- Obtain fundamental constants required for implementing the continuum-level electrochemical model from experiment.
- Extend the models to multilayer structures and incorporate microstructural effects.
- Verify the models through experiment.
- Develop a transient version of the continuum-level electrochemical model.
- Obtain time constants for various transport processes from electrical impedance spectroscopy to examine the effects of transients on SOFC performance.
- Develop and deliver software modules for incorporation of the continuum-level electrochemical model into SOFC failure analysis software used by National Energy Technology Laboratory, Pacific Northwest National Laboratory, Oak Ridge National Laboratory, and the SECA industrial teams.

Accomplishments

- Completed a continuum-level electrochemical model (CLEM) for *steady state* conditions, using potential dependent boundary conditions and non-linear Galvani potential.
- Completed a CLEM for *transient* conditions, using potential dependent boundary conditions and a linear Galvani potential.
- Compiled software modules for vacancy concentration and electron concentration in *n*-type and *p*-type MIECs.
- Extended the CLEM to thermo-mechanical and thermo-chemical properties of MIECs.
- Extended the CLEM to YSZ/LSM (YSZ/lanthanum strontium manganate) and YSZ/LSCF (YSZ/lanthanum strontium cobalt ferrite) bilayers.
- Measured the thermal expansion of ceria and acceptor-doped ceria in air and reducing atmospheres. Results concur with model predictions.
- Obtained time constant for equilibration of material after a change in P_{O_2} during chemical expansion.
- Measured the elastic moduli of ceria, gadolinia-doped ceria (GDC) and YSZ in reducing (H_2) and oxidizing atmospheres (air) using nondestructive and (nanoscale) destructive techniques; both showed that reducing conditions cause a ~30% decrease in the elastic modulus relative to air. Results concur with model predictions.
- Evaluated polycrystalline elastic modulus of ceria after heat treatment in air and in hydrogen using 4-point bending test–results are consistent with nanoindendation results and model.
- Measured the fracture toughness of ceria and GDC in reducing (H_2) and oxidizing atmospheres (air); results show that reducing conditions cause a ~37% increase in the fracture toughness relative to air.
- Deconvoluted transport processes for optimally sintered LSM and LSCF, with time constants ranging from 10^{-10} (charge transfer) to 10^{5} seconds (gas diffusion).
- Established a relationship between electrochemical and microstructural properties: dissociative adsorption polarization resistance increases as pore surface area decreases and charge transfer polarization resistance increases as triple phase boundary length increases.

Eric D. Wachsman (Primary Contact), Keith L. Duncan, Fereshteh Ebrahimi
Department of Materials Science and Engineering, University of Florida
Gainesville, FL 32611-6400
Phone: (352) 846-2991; Fax: (352) 846-0326
E-mail: ewach@mse.ufl.edu

DOE Project Manager: Travis Shultz
Phone: (304) 285-1370
E-mail: Travis.Shultz@netl.doe.gov

Introduction

For extensive deployment of SOFCs into industrial and consumer markets to become a reality, some key hurdles need to be cleared. Three of these hurdles are (i) mechanical, (ii) chemical and (iii) transient stability of SOFCs. In our research we are tackling these hurdles by developing models to relate point defect population distribution and microstructure to the electrochemical and mechanical properties of SOFC components, which are then the actual determinants of the thermo-mechanical, thermo-chemical and transient stability of

SOFCs. These fundamental-level models can then be incorporated into system-level models to predict and analyze SOFC performance and response to various inputs.

Approach

To develop models for the relationship between point defect population distribution and microstructure to the electrochemical and mechanical properties of SOFC components, first we modeled the generation of point defects in oxide MIECs as a function of atmosphere (P_{O_2}) and temperature. Next we modeled the transport and distribution of defects in an MIEC in a P_{O_2} gradient, by solving the Nernst-Planck, mass conservation and charge conservation equations for Laplacian and non-Laplacian potential distributions. These two steps produced a CLEM that relates point defect concentration to operating conditions and material properties. Hence, by modeling or applying relationships between point defects and indices for thermo-mechanical, thermo-chemical and transient stability, secondary relationships between these indices and the SOFC operating conditions and material properties can be derived. Finally, experiments have been conducted to confirm the predictions of the models as well as to give more insight into the factors and mechanisms that play a role in the performance of the SOFC components and the overall stability of the SOFC.

Results

CLEM–Defect Thermodynamics. To obtain defect concentration dependence on P_{O_2}, equations that are continuous across at least two regimes were derived [1]. Excellent results were obtained when these equations were fitted to experimental data [1]. The ability to predict defect concentration as a function of P_{O_2} then allows us to model various MIEC properties that depend on P_{O_2} such as conductivity, chemical expansion ad elastic modulus.

CLEM–Defect Transport. To model defect transport in MIECs we solved the Nernst-Planck, material balance, and current density equations with *potential-dependent* boundary conditions and without assuming a linear, i.e., Laplacian, potential distribution [2]. Our results predict the transport properties of the MIEC components and SOFC performance. Assuming a linear potential ignores the efficiency sapping effects of mixed conduction and using *fixed* boundary conditions lessens the effects of concentration gradients; together they lead to overestimation of cell performance.

Figure 1 shows a comparison of our results compared with that of Kim *et al* [3] for modeling the current-voltage (I-V) characteristics of a Ni-YSZ/YSZ/LSM cell. We modeled cell performance with similar

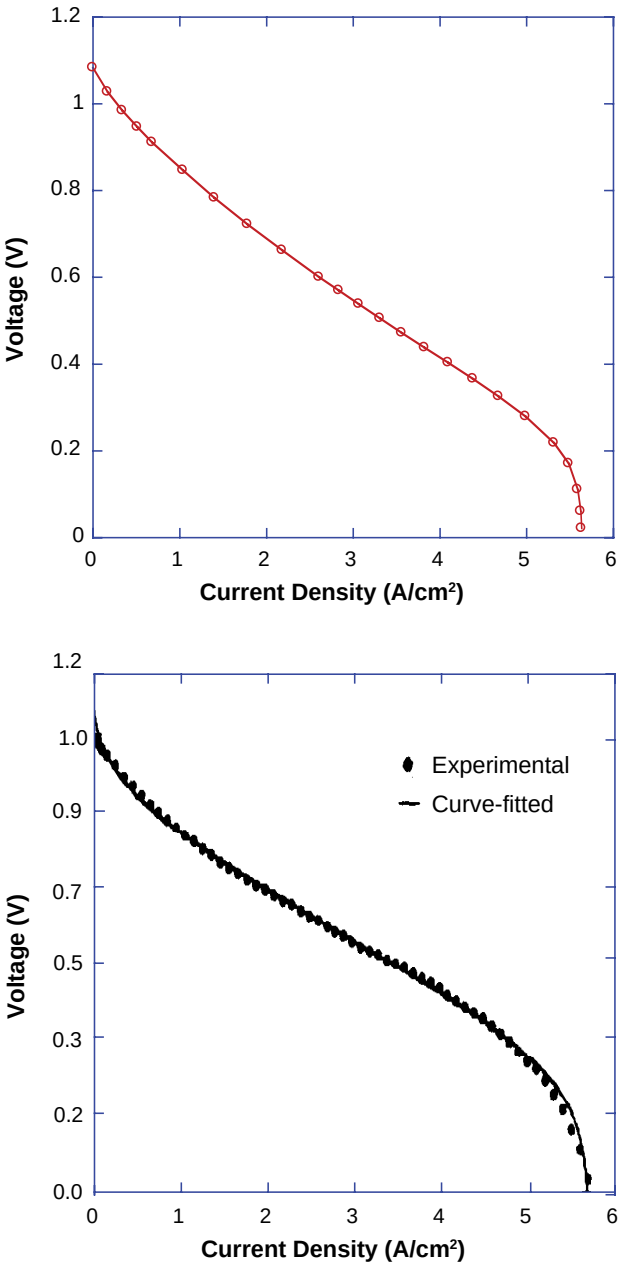

FIGURE 1. Comparison of Theoretical Models Fit to Experimental Data (top); Present Work (bottom) Kim *et al* [3]

accuracy to Kim *et al*. However, less fitting parameters (3 vs. 10) were used in our model. Moreover, because our model does not assume a uniform vacancy concentration, it is amenable for modeling cells with alternative electrolytes, e.g., GDC.

CLEM–Chemical Expansion. To extend the CLEM to chemical expansion of MIECs, a relationship for chemical expansion was derived, as follows

$$\frac{\Delta l}{l_0} = \alpha \Delta T + \frac{\beta}{a_0} c_V \qquad (1)$$

where T is temperature, $\Delta l/l_0$ is expansion and β is a material constant related to lattice structure. This allows us to predict the chemical expansion of various SOFC components and associated stresses caused by mismatches between components or P_{O_2} gradients. Figure 2a shows an excellent fit between model and experimental data and that there is significant chemical expansion in ceria and GDC, which correlates to the onset of mixed conduction [1].

CLEM–Mechanical Properties. To extend the CLEM to mechanical properties of MIECs, a relationship between defect population and elastic modulus, E, was derived by considering that the bond energy, *U*, between atoms in a crystal, may be approximated by $U = A/r^n - B/r^m$; where *r* is the interatomic distance, and *A*, *B*, *n* and *m* are empirically determined constants [4]. Thus, the elastic modulus for a perfect crystal, $E \approx 1/r_0(d^2U/dr^2)_{r=r_0}$ [4]; or

$$E(x) \approx E^*\left(\theta c_V(x)+1\right)^{-(n+3)} \qquad (2)$$

where c_V is vacancy concentration, θ is an empirically determined constant, and E^* is the stoichiometric elastic modulus.

Using a triboindenter, we measured the elastic modulus of individual grains of ceria, GDC and YSZ samples annealed in a range of P_{O_2}'s between air and H_2. The results, Figure 2b, show good fits of the model to experiment. Therefore, we can predict how the mechanical properties of SOFC components will change as a function of P_{O_2}.

Comparisons of the elastic modulus for polycrystalline samples with nanoindentation results (intrinsic elastic modulus) for both ceria and YSZ are shown in Figure 3. Although the samples experienced the same thermo-chemical treatment, a lower modulus

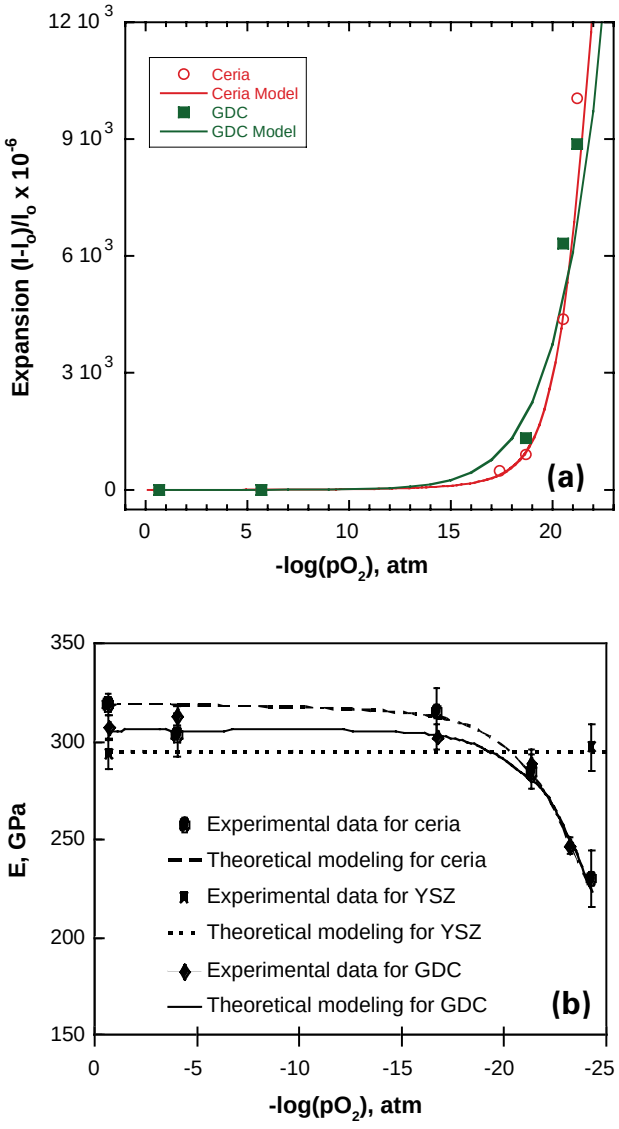

FIGURE 2. Data and model fit for (a) Chemical expansion of ceria and GDC at 1073 K (b) Elastic moduli of ceria, GDC and YSZ as a function of P_{O_2}.

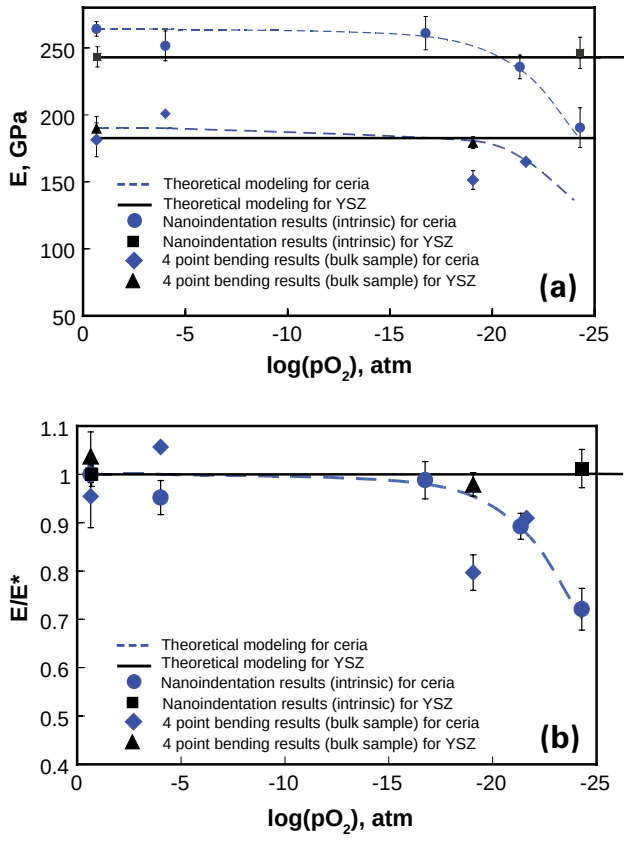

FIGURE 3. Comparison of the intrinsic elastic modulus (from nanoindentation) and polycrystalline elastic modulus (from 4-point bending) of ceria and YSZ (a) elastic modulus as a function of P_{O_2} (b) the relative change of elastic modulus as a function of P_{O_2}.

was obtained from the 4-point bend test compared to the intrinsic modulus. The reasons for this observed difference stem from the different nature of the experiments as well as the effects of pores/microcracks in the polycrystalline sample, which were caused by processing and heat treatment.

More importantly, however, Figure 3b shows that the relative change in elastic modulus as a function of P_{O2}, obtained from either test is the same and is exactly predicted by the model. This is an emphatic validation of the model's correctness and indicates that oxygen vacancies play an important role in the thermo-mechanical properties of polycrystalline ceramics.

The effects of lattice vacancy concentration on fracture toughness (K_{IC}) of ceria were measured using Brazilian disc samples loaded under mode I conditions [5]. Fracture toughness test results are shown in Table 1. The sample heat treated in air has a room temperature K_{IC} value of 0.96 MPa.m$^{1/2}$. Surprisingly, K_{IC} increased as much as 30-40% for the samples heat treated under reducing conditions.

TABLE 1. Fracture Toughness (K_{IC}) of Ceria

Heat Treatment	# of Samples Tested	P_{O2}, atm.	K_{IC}, MPa.m$^{1/2}$
H_2	2	4.5 x 10^{-22}	1.32±0.04
H_2/H_2O	2	1.5 x 10^{-20}	1.40±0.01
N_2	1	4.5 x 10^{-6}	0.92
Air	3	0.21	0.96±0.05
As-sintered	1	------	0.91

Fracture toughness can also be expressed in terms of the critical elastic energy release rate, G_C, as: $K_{IC} = \sqrt{(G_C E)}$. In brittle materials, G_C is proportional to the energy released in creating new surfaces. Since elastic modulus, E, decreases with decreasing P_{O2}, this indicates that exposure to low P_{O_2} increases G_C and that there is some relationship between G_C and oxygen vacancy concentration.

To understand the higher toughness values for the samples heat treated in P_{O_2}'s, the fracture surface was studied using scanning electron microscopy (SEM), which revealed that the sample heat treated in air has a relatively smooth fracture surface, but the sample has a notably rougher fracture surface when heat treated in H_2, which is consistent with the higher K_{IC} value. Possible factors for the rough fracture surface are, pore-crack interactions, microcrack formation, internal stresses and phase transformation.

We have identified the primary contributions to the impedance of LSM cathodes on YSZ electrolyte substrates for conventional SOFCs. The processes and their related time constants are shown in Figure 4 and Table 2. This now enables cathode developers to correctly assess how changes in cathode parameters [e.g., triple-phase boundary (TPB), porosity, etc.] affect each transport process. Moreover, knowing the time constant for each process helps in predicting SOFC response in transient conditions.

Chemical-Stability. The CLEM was applied to the chemical stability of LSM/YSZ and LSCF/YSZ interfaces, including electrode microstructure. The results provide the P_{O_2} at the interface, and thereby the

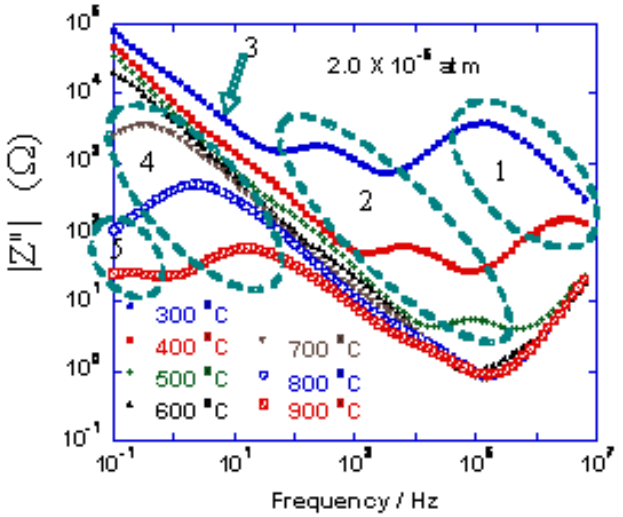

FIGURE 4. Deconvolution of LSM/YSZ/LSM symmetric cell impedance from AC-Impedance Spectroscopy. The transport process corresponding to each number is given in Table 2.

TABLE 2. Deconvolution of AC-Impedance Spectra for LSM/YSZ/LSM Symmetrical Cells

Process	"*m*" in log R ∝ *m*log P_{O_2}	Activation energy, E_a (eV)	Time constant, τ (s) @ 800°C
1. Ionic diffusion through electrolyte bulk	0.0084	1.10	
2. Ionic diffusion across electrolyte grain boundary	-0.022	1.04	
3. Charge transfer of O^{2-} from TPB into YSZ	-0.046	0.97	8.5 x 10-5
4. O_2 dissociation and surface diffusion on LSM	-0.15	1.2	0.18
5. Gas diffusion through porous electrode	-1.1	~0.04	5.9

interfacial stability, as a function of operating conditions (more detail may be obtained from previous reports).

Transient Response. The CLEM has been extended to transient conditions (more detail may be obtained from previous reports). To obtain solutions, we assumed a linear potential distribution. This assumption is best applied to predominantly ionic conductors, e.g., YSZ or predominantly electronic conductors, e.g., LSM.

Software Development. The development of software modules for the CLEM is in progress. At this point, the program for the *steady-state* CLEM for defect generation and transport has been completed. Two languages were used, C++, because it is the industry standard, and PHP, because of its web oriented features.

Conclusions and Future Directions

- A continuum-level electrochemical model has been developed that improves on preceding efforts by including a non-linear potential distribution and by including potential dependent boundary conditions.
- The continuum-level electrochemical model has been extended to describe thermo-mechanical, thermo-chemical and transient stability in MIECs.
- Experimental results concur with the predictions of the continuum-level electrochemical model for electrical conductivity.
- Nanoindentation (intrinsic) tests on ceria, GDC and YSZ with different level of oxygen concentration revealed that the elastic modulus of ceria and GDC decreases considerably as the oxygen lattice vacancy concentration increases. The elastic modulus of YSZ within the studied P_{O_2} and temperature range was insignificantly changed due to the small number of lattice vacancy produced. GDC and ceria showed very similar trends.
- Four-point bend (polycrystalline) tests on ceria, GDC and YSZ with different levels of oxygen concentration revealed that the elastic modulus of ceria and GDC decreases considerably as the oxygen lattice vacancy concentration increases and the elastic modulus of YSZ within the studied P_{O_2} and temperature range was insignificantly changed due to the small number of lattice vacancy produced.
- The P_{O_2} dependence obtained from nanoindentation (intrinsic) and 4-point bend (polycrystalline) tests are both consistent with each other and the model. This indicates that oxygen vacancies play an important role in the thermo-mechanical properties of polycrystalline ceramics.
- In order to separate the effects of oxygen vacancies on K_{1C}, future work on high temperature microstructure/fracture surface analysis and molecular dynamic simulations is needed.
- The continuum-level electrochemical model has been validated through experiment for thermo-mechanical properties (elastic modulus and thermo-chemical expansion).
- The *steady-state* version of the continuum-level electrochemical model has been written in C++ and PHP.

FY 2006 Publications/Presentations

1. Y. Wang, K. Duncan, E. Wachsman, F. Ebrahimi, *Solid State Ionics,* submitted.

2. K. L. Duncan, Y. Wang, S. R. Bishop, F. Ebrahimi and E. D. Wachsman, *J. Amer. Ceramics Soc.,* (2006) accepted.

3. E. D. Wachsman, "Fundamental Studies of SOFC Materials,", *DOE - SECA Core Technology Program Peer Review Meeting*, Denver, CO, October 25-26, 2005.

4. Y. Wang, K. Duncan, E. Wachsman and F. Ebrahimi, "Effects of Oxygen Vacancy Concentration on Mechanical Properties of Cerium Oxide", *ECS Transactions Solid State Ionic Devices IV*, (2005).

5. S. R. Bishop, K. L. Duncan, E. D. Wachsman, "Chemical Expansion of SOFC Materials" *The 208th ECS meeting, The Electrochemical Society*, Los Angeles, CA, October 2005.

6. S. R. Bishop, K. L. Duncan, E. D. Wachsman, "Chemical Expansion of SOFC Materials" *The 30th International Conference on Advanced Ceramics and Composites. The American Ceramics Society*, Cocoa Beach, FL, January 2006.

7. J. R. Smith, A. Chen, D. Gostovic, D. Hickey, D. P. Kudinger, K. L. Duncan, K. Jones, and E. D. Wachsman, "The Relationship Between Cathode Microstructure and Electrochemical Behavior for SOFCs", *30th International Conference & Exhibition on Advanced Ceramics & Composites*, Cocoa Beach, FL, January 2006.

8. J. R. Smith, K. L. Duncan, M. E. Orazem, and E. D. Wachsman, "Evaluation of Time Constants Governing the Cathodic Reaction in SOFCs", *208th Meeting of the Electrochemical Society*, Los Angeles, CA, October 2005.

References

1. K. L. Duncan, Y. Wang, S. R. Bishop, F. Ebrahimi and E. D. Wachsman, *J. Amer. Ceramics Soc.,* (2006) accepted.

2. K. Duncan, *Ph. D. Thesis*, University of Florida (2001).

3. J.-W. Kim, A. V. Virkar, K.-Z. Fung, K. Mehta, and S. C. Singhal, *J. Electrochem. Soc.*, **146** (1999) 69-78.

4. M. Barsoum, *Fundamentals of Ceramics* (McGraw-Hill, 1977).

5. D.K. Shetty, A.R. Rosenfield and W.H. Duckworth, *Engineering Fracture Mechanics*, **26** (1987) 825.

III.D.5 An Investigation to Resolve the Interaction between Fuel Cell, Power Conditioning System and Application Load

Objectives

- Comprehensive experimental validation and parametric study of the effects of electrical feedbacks on PSOFC and PSOFC stack.
- Design of optimal and reliable power-management control system for mitigation of electrical-feedback effects on PSOFC and to maximize the efficiency.
- Balance-of-plant subsystem (BOPS) parametric optimization for optimal start-up, steady-state, and transient performance.
- Investigation of the impacts of the electrical feedback on the long-term degradation of the SOFC stack.

Accomplishments

- Completed experimental validation of several electrical feedback effects, such as, the load transients, multiple load transients, low-frequency ripple, etc.
- Conducted comprehensive parametric analysis of the effects of the load transient, low-frequency (LF) ripple, power factor, and harmonic distortion on the performance and efficiency of the stack.
- Developed a ripple-mitigating highly efficient PES, which can be used for experimental validation of modeling data by integrating with an experimental PSOFC stack.
- Development of power-management control strategies for PES and BOPS to enhance the performance and life of the PSOFC.

Sudip K. Mazumder[1] (Primary Contact), Sanjaya Pradhan[1], Joseph Hartvigsen[2], S. Elangovan[2], Hollist Michelle[2], Michael von Spakovsky[3], Douglas Nelson[3], Diego Rancruel[3], Miladin Radovic[4], Edgar Lara-Curzio[4] (collaborator), Mohammed Khaleel[5] (collaborator)

[1] University of Illinois at Chicago
[2] Ceramatec Inc.
[3] Virginia Tech
[4] Oak Ridge National Laboratory (ORNL)
[5] Pacific Northwest National Laboratory (PNNL)

University of Illinois at Chicago
851 South Morgan Street
1020 Science and Engineering Offices, M/C 15
Chicago, IL 60607
Phone: (312) 355-1315; Fax: (312) 996-6465
E-mail: mazumder@ece.uic.edu

DOE Project Manager: Magda Rivera
Phone: (304) 285-1359
E-mail: Magda.Rivera@netl.doe.gov

Introduction

Planar solid oxide fuel cell stacks (PSOFCSs), in PSOFC based power-conditioning systems (PCSs), are subjected to electrical feedbacks due to the switching power electronics and the application of loads. These feedbacks (including load transient, current ripple due to load power factor and inverter operation, and load harmonic distortion) affect the electrochemistry [1-5] and the thermal properties [6] of the planar cells thereby potentially deteriorating the performance and reliability of the cells. Therefore, a comprehensive spatio-temporal simulation model of the SOFC PCS is essential to investigate the potentially degrading impacts of such electrical feedbacks on the PSOFC. To ascertain the efficacy of any such model, and for accurate prediction of the impacts of the electrical feedbacks, experimental validation of the models both in steady state and transience is required.

The parametric study of these electrical feedbacks can only predict the short-term degrading impacts on the PSOFCS. However, for the PSOFC PCS to meet the lifetime specifications, a long-term study needs to be conducted which can predict the deteriorating impact of some of the effects in the long term. Since it is impossible to conduct long-term (order of 1,000 hours) study of the large-scale simulation model of the PSOFC PCS, this study needs be conducted experimentally.

The slow response time of the BOPS mechanical system as compared to the fuel-cell electrochemistry and the PES has been a major concern for fuel cell system designers [7-8]. To avoid the low reactant condition, energy buffering devices like a battery, which would provide the additional energy immediately to the load during the load transient, is needed in conjunction with the fuel cell stack [7]. To optimize the size and response of the battery while eliminating the degrading impacts of the load transient on the stack, a control strategy needs to be developed which would control the energy flow between the energy generator (fuel cell stack) and the energy buffering device (battery).

Approach

A detailed study is conducted on the electrical-feedback effects (including load transients, current ripple variations due to load power factor and inverter operation, and load harmonic distortions) that have an impact on the electrochemistry and the thermal properties of the SOFC, thereby affecting the performance and reliability of the cells. Subsequently, detailed experimentation is carried out to validate the simulation data on interaction analyses.

The test bed consists of a stack prototype with the power electronics system, as shown in Figure 1. The stack consists of 25 planar cells in series. In the stack, all the planar cells are mounted in a single manifold. Each cell has an electro-active area of 64 cm^2.

Using this validated model, parametric analyses on the impacts of transience, power factor, and distortion of the application load as well as LF current ripple is conducted. The study clearly establishes that sizing of the SOFC stack needs to take into account ripple magnitude and input-filter design simultaneously.

To study the effect of two of the important electrical feedbacks in the long term, two sets of experimental test beds are built using the similar cells used for the transient experiment. The degradation study of ripple is conducted on a 5-cell stack connected to a boost converter, and a 5-cell stack connected to the constant load. The duty ratio of the switch of the boost converter is modulated sinusoidally at 60 Hz. The average current drawn from both the stacks are kept at approximately 13 A. The open circuit voltage of the 5-cell stack is 5.087 V. Similarly, for the study the long-term degradation effect due to the load transient, a 25-cell planar stack is connected to a programmable DC-DC converter followed by a load resistance. The DC-DC converter is programmed to draw 13 A current for first 20 minutes and 2.2 A for the next 10 minutes in every half an hour. Therefore, the average current drawn from the stack is 9.4 A. The open circuit voltage (V_{oc}) of the stack is 24.75 V. For the 5-cell stacks, the flow rates of H_2, N_2 and air are 1.9 slpm, 0.33 slpm and 7.65 slpm, respectively. The air inlet temperature is kept at 800°C and the core temperature is 850°C.

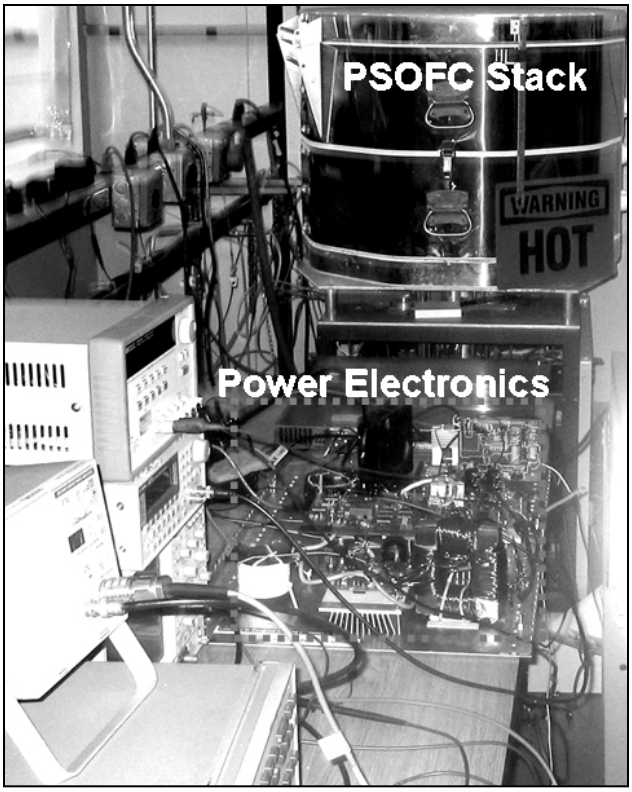

FIGURE 1. Experimental Setup of the 25 Cell PSOFC Stack with the PES

Based on the electrical-feedback analyses, a novel patent-pending topological power-management controlling strategy and architecture for a SOFC PCS has been designed. This improves steady-state energy efficiency of the PES (almost flat efficiency across the power range as compared to progressively drooping efficiencies as in conventional case) and hence the PCS by optimizing the fuel utilization in the stack in the steady-state. Further, using a multi-loop feedback, the control also integrates to a battery-buffer control to mitigate the effect of the load transient on the SOFCS (e.g., fuel utilization). A new methodology has also been developed to systematically relinquish the control of the battery (after transience phases out) at a rate governed by the control bandwidth of the BOPS.

To determine the optimal synthesis/design and dynamic operation of the SOFC system, a parametric system optimization is conducted. This requires the optimal synthesis/design and dynamic operation of each of the BOPS subsystems to be carried out in an integrated fashion, leading to the establishment of a feasible system super-configuration which provides high efficiency and reliability. The results of the parametric studies based on the super-configuration were used to determine the most promising subset of this super-configuration based on system response, fuel consumption, capital cost, operational constraints, etc. The resulting reduced super-configuration was subjected to a large-scale synthesis/design optimization while taking into account its effects on system operation, i.e., on the dynamic response of the system. The parametric studies showed this configuration to provide adequate fuel efficiency.

Results

Figures 2a and 2b show the drop in the output voltage of the stack model and the experimental stack prototype, respectively, due to the subjected load

transient of 2 A to 12 A. This also leads to an increase in the mean temperature of the stack.

The effect of the ripple is validated using a sinusoidally modulated bidirectional DC-DC converter connected across the stack. The current drawn from the stack contains LF ripple with frequency (120 Hz) twice that of the sinusoidal AC (60 Hz) output. Figures 3a and 3b show the effect of a LF (120 Hz) ripple on the 1-D stack model and the experimental prototype, respectively.

To achieve very high efficiency, the stack must be operated at a particular current level (this corresponds to the maximum operable fuel utilization) as shown in Figure 4. However, due to the presence of LF ripple in the stack current, the operating mean stack current has to be decreased, to avoid zero-reactant condition, as illustrated in Figure 4.

Due to non-unity power factor of the load, the ripple in the stack current increases. This ripple further depends on the output capacitance connected across

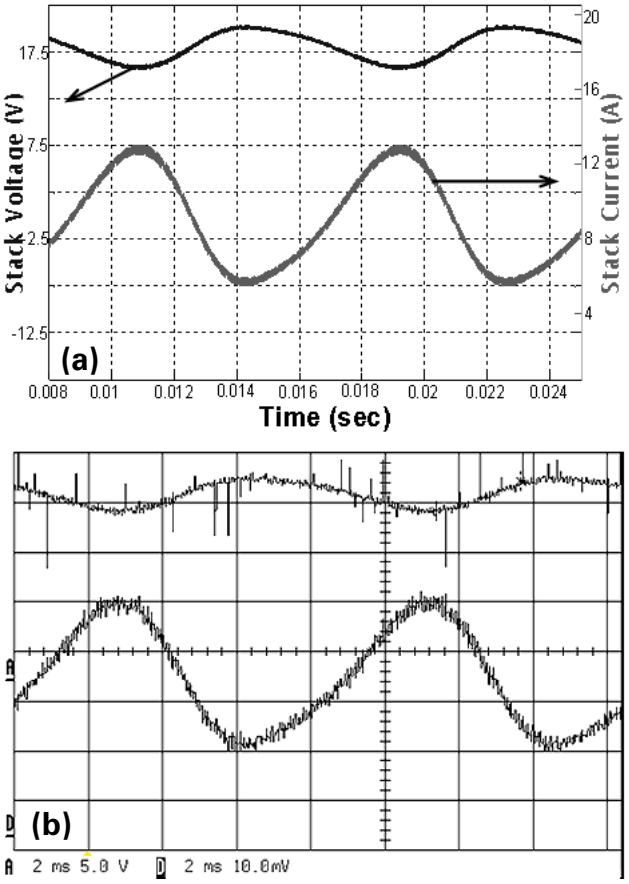

FIGURE 3. (a) Effect of 40 Percent Current Ripple on the Stack Voltage of 1-D Model; (b) Experimental Validation of the Ripple Effect on Planar SOFC Stack; Scope Channels A and D Show the Stack Voltage and Current, Respectively

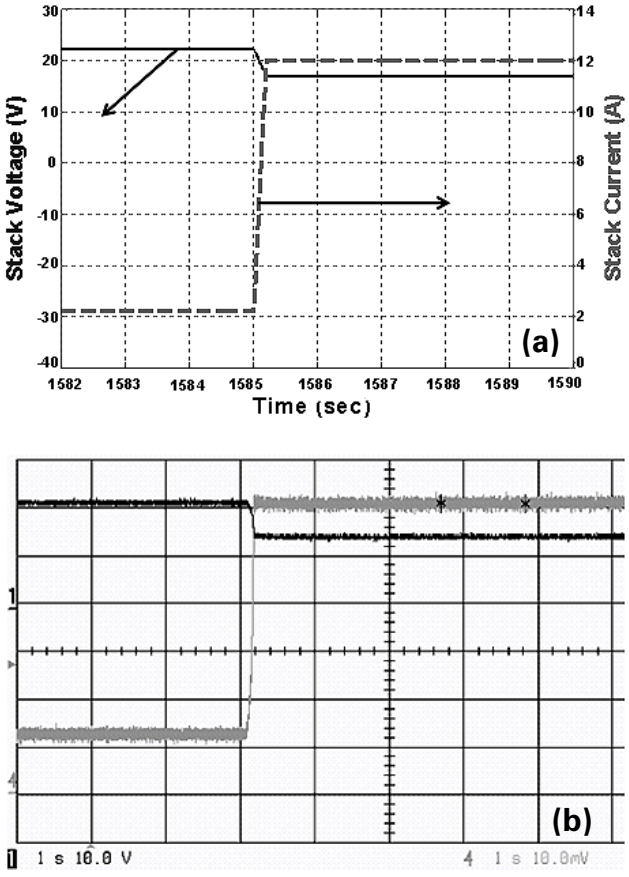

FIGURE 2. (a) Effect of Load Current Transient (2.2 A to 12 A) on the Voltage of the Stack Model; (b) The Experimental Validation of Its Effect on the Planar Stack; Scope Channel 1 (10 V /div) and Channel 4 (2 A/div) Measure the Stack Voltage and Current, Respectively

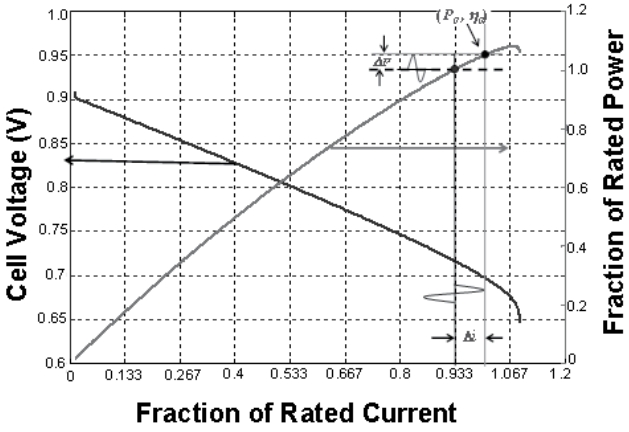

FIGURE 4. Effect of LF Ripple on the Performance and Efficiency of the Stack

the DC bus. Figure 5 shows the effect of load power factor variations on the stack current ripple at various capacitances and at a constant active power drawn by the load. Therefore, a decrease in the load power factor decreases the efficiency of the stack. However, the increase in the mean temperature is minimal.

An increase in the harmonic distortion of the AC load increases the distortion in the output ac current due to increase in the magnitude of the harmonic components as well their phase. This distortion in the AC current also introduces distortion in the current drawn from the planar stack. At a fixed power factor of the fundamental current, the ripple in the stack current decreases with an increase in the total harmonic distortion (THD) of the load.

Figure 6 shows the percentage degradation of the ASR (area specific resistance) in the stacks after approximately 900 hours of study due to the load transient and the LF ripple. This shows that, the degradation of the ASR due to the load transient is very high as compared to the stack carrying constant current. Similarly, increase in the ASR of the stack with LF ripple current is higher as compared to the stack feeding constant current.

Finally, the response of the designed power management system is investigated. The PCS is subjected to a load transient at time t = 0.02 second. As a result, the stack output current increases to meet the new load demand. However, the increase in the battery current prevents the surge in the stack current, and stabilizes the stack voltage close to its nominal value. Figure 7a shows the response of the battery current after the load transient with BOPS flow adjustments. Since the current drawn from the stack is independent of the load current, the fuel utilization of the stack remains unaltered as shown in Figure 7b. Hence, this completely alleviates the effect of the load transient on the fuel cell stack.

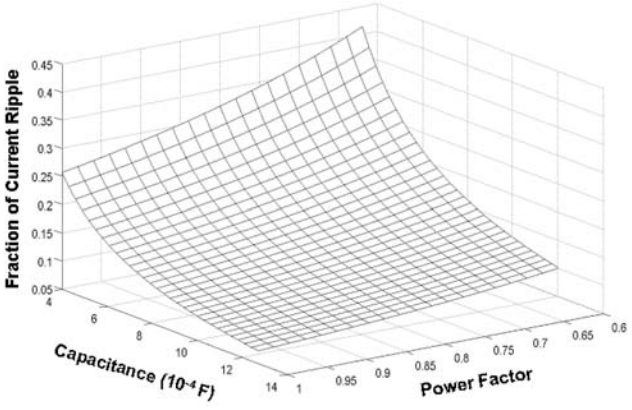

FIGURE 5. Effect of Power Factor of the Load on the Magnitude of Stack Current Ripple

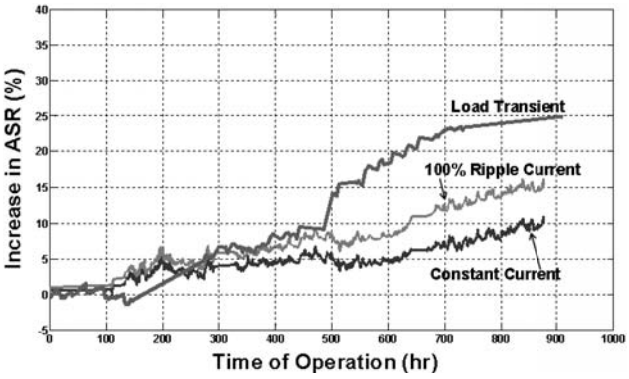

FIGURE 6. Comparison of Long-term ASR Degradation Due to LF Ripple, Constant Current and Load Transient

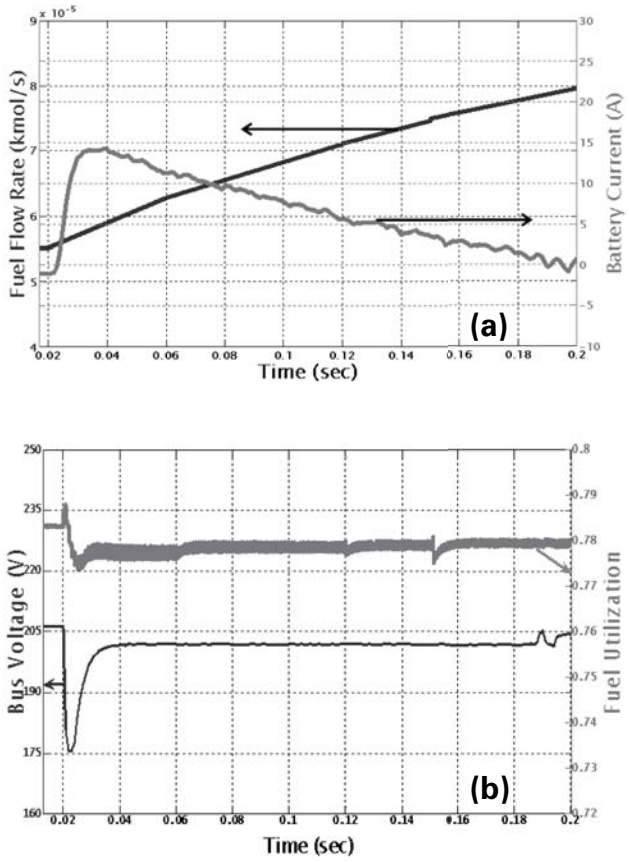

FIGURE 7. (a) Response of the Battery Current to a Sudden Load Transient Which Is Followed by the Flow Adjustment of BOPS; (b) Response of the Bus Voltage and Fuel Utilization to a Sudden Load Transient Which Is Followed by the Flow Adjustment of BOPS

Conclusions

A comprehensive investigation of several different electrical feedbacks induced due to the power electronics subsystem (PES) and the application load (AL), which may potentially affect the performance and durability of planar solid-oxide fuel cell stack (PSOFCS), was conducted. The accuracy of the model and their ability in determining the effects of several electrical feedbacks on PSOFC during the transient and in the steady state were experimentally validated. Using the validated model, accurate estimations of the impacts of several electrical feedback effects on the performance and durability of the PSOFC PCS were conducted using parametric study. An experimental degradation study was done to estimate the long-term effects of the load transient and the ripple on the performance of the stack. Specifically, the following conclusions were drawn:

- The no-load to full-load transient increases the current density in the planar fuel cell abruptly and immediately. The higher level of current density increases the fuel utilization and the polarization voltage leading to a drop in the cell voltage. This change in the fuel utilization is detrimental to the cell performance and efficiency.
- The load transient not only increases the mean temperature but also changes the spatial distribution of stack temperature. This variation depends on the magnitude of the current transient and is independent of the slew rate of the transient. The load transients accelerate the degradation of the ASR of the planar cell. Therefore, they deteriorate the efficiency of the stack. To prevent this, suitable energy buffering techniques should be available to eliminate the effect of the load transient from the stack.
- The higher ripple current magnitude in the stack current forces a decrease of the operating fuel utilization of the stack, and hence, lowers the stack efficiency. However, this has negligible impact on the stack temperature. In the long-term, the ripple current accelerates the degradation of the ASR, deteriorating the efficiency of the stack.
- Lower power factor of the load increases the magnitude of current ripple drawn from the stack, and this reduces the efficiency of the stack. The effect of the load power factor on the stack temperature is minimal.
- Higher THD of the AC load decreases the magnitude of current ripple drawn from the stack. However, it has negligible impact on the stack temperature.

The parametric study provided a detailed insight into the effects of several electrical-feedback effects on the planar solid-oxide fuel cell (PSOFC) stack and the PSOFC power conditioning system (PCS) as a whole. This facilitates the design of control and optimization of PSOFC PCS parameters towards the achievement of a highly-efficient and reliable power system.

Determination of the optimal synthesis/design of the BOPS was done using optimal synthesis/design and dynamic operation of each of the auxiliary power unit subsystems in an integrated fashion. For the individual subsystems, the proposed dynamic iterative local-global optimization approach provides optimal configurations even in the strictest of the transients, optimizing the system cost and performance.

The efficiency of the power converter system was maximized using efficient power sharing. The control strategy completely eliminates the effect of the load transient on the fuel cell stack by providing the additional load current from the battery. Secondly, in the steady-state it maximizes the efficiency of the system by optimizing the fuel utilization in the stack. Based on the strategy designed here, a planar solid-oxide fuel cell based power conditioning system shows a remarkable increase in efficiency.

References

1. Hsiao, Y. C., and Selman, J. R., 1997, "The Degradation of SOFC Electrodes," *Proceedings of Solid State Ionics*, vol. 98, pp. 33-38.

2. Huang, X., and Reifsnider, K., 2001, "Modeling Long-Term Performance of Solid Oxide Fuel Cells: A Phenomenological Approach," *15th Annual Conference of Fossil Energy Material*s, Knoxville, TN.

3. Achenbach, E., "Response of a Solid Oxide Fuel Cell to Load Change," *Journal of Power Sources*, vol. 57, pp. 105–109, 1995.

4. Gemmen, R. S., 2003, "Analysis for the Effect of Inverter Ripple Current on Fuel Cell Operating Condition," *Journal of Fluids Engineering*, vol. 125, issue 3, pp. 576-585.

5. Hartvigsen, J., Elangovan, S., and Khandkar, A., 1993, *Science and Technology of Zirconia V*, Edited by Badwal, S., Bannister, M., and Hannink, R., Technomic Publishing Company, Inc., Lancaster, Pennsylvania.

6. Yakabe, H., Ogiwara, T., Hishinuma, M., and Yasuda, I., 2001, "3D Model Calculation for Planar SOFC," *Journal of Power Sources*, 102, pp. 144-154.

7. S.K. Mazumder, S. Pradhan, J. Hartvigsen, M. von Spakovsky, and D. Rancruel, "Effects of battery buffering and inverter modulation on the post load-transient performance of planar solid-oxide fuel cell", *IEEE Transactions on Energy Conversion*, in press for publication, 2006.

8. Mazumder, S.K., Acharya, K., Haynes, C.L., Williams, R., von Spakovsky, M. R., Nelson, D. J., Rancruel, D. F., Hartvigsen, J., and Gemmen, R. S., 2004, "Solid-Oxide-Fuel-Cell Performance and Durability: Resolution of the Effects of Power-Conditioning Systems and Application Load," Special Issue on Distributed

Generation, *IEEE Transactions of Power Electronics*, vol. 19, pp. 1263-1278.

FY 2006 Publications/Presentations

1. S. K. Pradhan, S.K. Mazumder, J. Hartvigsen, M. Hollist, "Effects of electrical feedbacks on planar solid-oxide fuel cell", *ASME Journal of Fuel Cell Science and Technology,* accepted for publication, 2006.

2. R.K. Burra, S.K. Mazumder, "A ripple-mitigating and energy-efficient fuel cell power-conditioning system", *IEEE Transaction of Power Electronics*, accepted for publication, 2006.

3. S.K. Mazumder, S. K. Pradhan, J. Hartvigsen, M. von Spakovsky, and D. Rancruel, "Effects of battery buffering and inverter modulation on the post load-transient performance of planar solid-oxide fuel cell", IEEE Transactions on Energy Conversion, in press for publication, 2006.

Special Recognitions & Awards/Patents Issued

1. S.K. Mazumder, S. K. Pradhan, and R. K. Burra, A novel power-management control for fuel cell power conditioning system, USPTO Provisional Patent Filing #CZ029, November 2005.

2. S. K. Mazumder, R. K. Burra, and K. Acharya, A novel efficient and reliable dc-ac converter for fuel cell power conditioning, USPTO Patent Application# 20050141248, September 2004.

3. Dr. Mazumder presented the Keynote Lecture on fuel cell power electronics at the ASME Third International Conference on Fuel Cell Science, Engineering and Technology, held at Yipsilanti, Michigan between May 23–25, 2005.

III.D.6 Advanced Measurement and Modeling Techniques for Improved SOFC Cathodes

Objectives

- Develop microelectrodes for improved isolation and measurement of the SOFC cathode overpotential (resistance) on cells having a thin electrolyte membrane.
- Develop nonlinear electrochemical impedance spectroscopy (NLEIS) for use in identifying what steps limit SOFC cathode performance.
- Generate a more detailed understanding of the electrochemistry governing SOFC cathodes, facilitating discovery and design of improved cathode materials and microstructures.

Accomplishments

- Developed microelectrode techniques to better isolate the electrochemical response of SOFC cathodes under realistic fabrication and operating conditions.
- Measured the *i-V* characteristics, impedance, and NLEIS of porous and thin-film $La_{1-x}Sr_xCoO_{3-\delta}$ (LSC) electrodes on rare-earth-doped ceria, including 1st, 2nd, and 3rd harmonics.
- Developed *1-D* models for the harmonic response of porous and thin-film LSC electrodes, allowing interpretation of harmonic data.
- Identified *dissociative adsorption* as a critical step in O_2 reduction on electron-rich materials such as LSC, with consequences for new catalyst development.

Introduction

Many promising new cathode materials for solid oxide fuel cells incorporate *mixed conducting ceramics* (materials which carry both oxygen ions and electrons) in order to substantially enhance oxygen reduction at reduced temperature [1]. For example, $La_{1-x}Sr_xCo_{1-y}Fe_yO_{3-\delta}$ (LSCF) cathodes utilize a significant portion of the electrode material surface, extending the reaction up to 10 microns from the electrode/electrolyte interface [2]. While these electrodes have proven promising in early exploratory research, they are only empirically understood [3], far from optimized [4,5], and can react unfavorably with the electrolyte [6,7]. Significant modification of these materials, or development of new materials, is required to bring this type of electrode to commercial fruition.

In order to address these issues, we believe a new generation of diagnostic tools is required to accelerate screening, fabrication, optimization, and long-term performance evaluation of cathode materials. The role of this project has been twofold. First, we have developed a technique involving microelectrodes (made using standard materials and fabrication techniques) that offers improved accuracy, faster throughput, and broader screening capabilities. Secondly, we have developed an extension of electrochemical impedance spectroscopy (EIS) that involves perturbation and detection of nonlinear electrode response. This technique, called *nonlinear electrochemical impedance spectroscopy* (NLEIS) [8,9], provides much higher resolution in terms of identifying rate-determining steps, separating anode and cathode response, and potentially improved prediction cell performance based on half-cell measurements.

Stuart B. Adler (Primary Contact), Jamie R. Wilson, Shawn L. Huff, and Yunxiang Lu

University of Washington
Department of Chemical Engineering, Box 351750
Seattle WA 98195-1750
Phone: (206) 543-2131; Fax: (206) 685-3451
E-mail: stuadler@u.washington.edu

DOE Project Manager: Lane Wilson
Phone: (304) 285-1336
E-mail: Lane.Wilson@netl.doe.gov

Approach

Figure 1 shows a schematic of the microelectrode cell design we are currently pursuing. The light area on the electrolyte surface is a mask layer that regulates where the working and reference electrodes make contact to the electrolyte. In this way, the ohmic losses are well defined, and confined to a region close to the working electrode (cathode) of experimental interest. Numerical simulations of this arrangement suggest that it provides a high degree of accuracy and frequency isolation. The mask layer is currently fabricated by screenprinting and firing a MgO/spinel mixed powder ink onto a dense (fired) tape of Sm-doped ceria (SDC) electrolyte. The electrodes are subsequently processed onto the cell under the same conditions as any ordinary cell. Electrochemical measurements are then made, and performance normalized to the actual area of the working electrode.

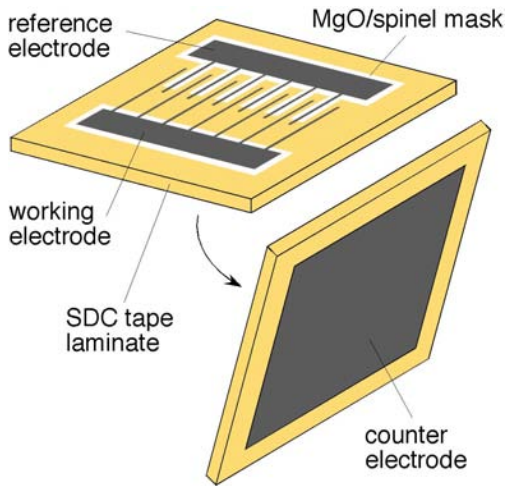

FIGURE 1. Cell Configuration of a Microelectrode Half-Cell

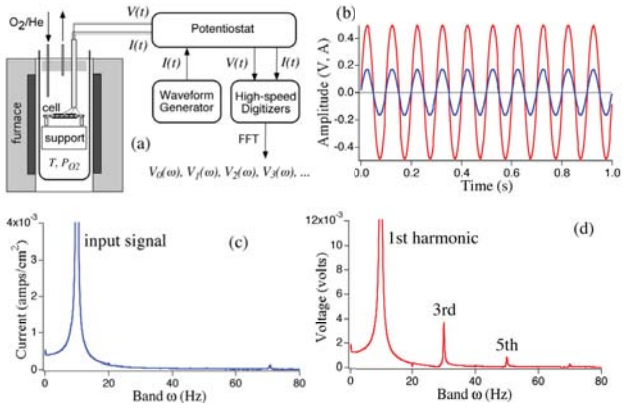

FIGURE 2. Schematic of NLEIS, as applied to SOFC cathodes. (a) Experimental set-up. (b) Current input and voltage response at 10 Hz for a symmetric cell of $La_{0.6}Sr_{0.4}FeO_{3-d}$ on SDC at 750°C in air. (c) Fourier transform of current signal. (d) Voltage signal.

Figure 2 outlines how we conduct a typical NLEIS experiment. The cell is placed in a controlled atmosphere chamber within a furnace, and interfaced to a potentiostat using spring-loaded gold (Au) current collectors. A sinusoidal current perturbation of variable amplitude is applied to the cell. Voltage and current data are synchronously digitized, and Fourier transformed to obtain frequency domain signals, from which the 1st harmonic (impedance) and higher order harmonics can be readily quantified. This technique has the ability to identify very small nonlinearities (~10^{-3} of the main signal), and naturally filters out non-periodic or asynchronous signals, including small performance drifts or noise. More details regarding the acquisition and processing of NLEIS data are given elsewhere [8].

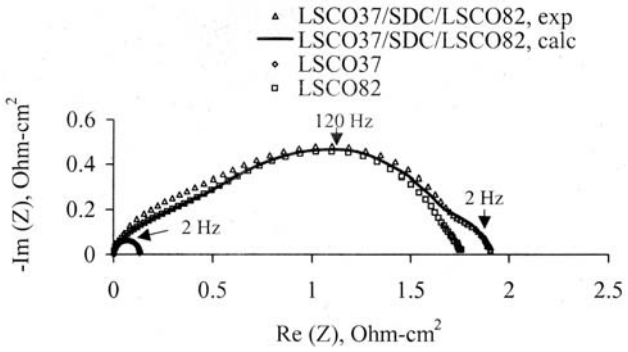

FIGURE 3. Impedance of LSC/SDC Cells in Air at 750°C

Results

Microelectrodes. Figure 3 shows the measured impedance of three cells. The first cell consists of a Sm-doped ceria (SDC) electrolyte, coated on one side with a full-sized (1 cm^2) porous $La_{0.3}Sr_{0.7}CoO_{3-\delta}$ (LSC-37) electrode, and on the other with a full-sized porous $La_{0.8}Sr_{0.2}CoO_{3-\delta}$ (LSC-82) electrode. The other two cells are microelectrode half-cells, consisting of LSC-37 and LSC-82 working electrodes, respectively, on SDC. Both half-cells have a 1 cm^2 LSC-82 counterelectrode. With the exception of the mask layer, the microelectrode half-cells were processed identically to the cell with full sized electrodes. Due to differences in composition and processing temperature, the LSC-37 and LSC-82 electrodes have very different characteristics; the impedance magnitude of the LSC-82 electrode is about 10 times larger than the LSC-37 electrode, and it has a characteristic frequency approximately 100 times higher.

As shown in Figure 3, the impedance of the LSC-37/SDC/LSC-82 cell consists of two arcs, which presumably represent contributions of the two electrodes, respectively. In contrast, the microelectrode half-cells show only one arc, which differ from each other in resistance and frequency response. After area normalization, the impedance of the two half-cells were added, yielding a "calculated" impedance spectrum for a LSC-37/SDC/LSC-82 cell, assuming the same ohmic membrane resistance as the actual cell. The data lie nearly on top of each other, which is a testament to both the accuracy and frequency isolation of the microelectrodes, as well as the reproducibility of fabrication in this case.

NLEIS. As shown by Kawada [10], the traditional impedance (EIS) response of a dense thin film LSC electrode can be used to isolate and quantify the oxygen exchange reaction at the surface.

However, other than telling us the P_{O2} dependence of the oxygen exchange rate, there is nothing distinguishing about the EIS signal that reveals anything about the mechanism itself. The EIS response of

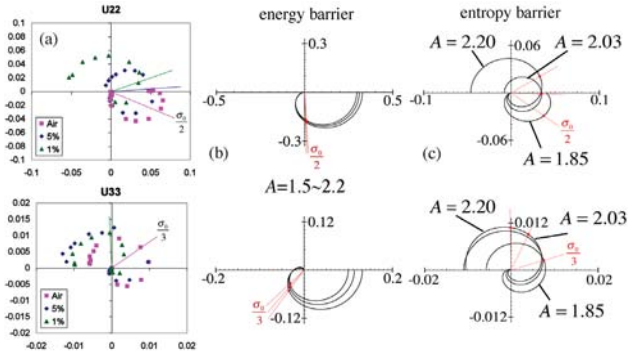

FIGURE 4. (a) 2nd and 3rd harmonic responses U_{22} and U_{33} of a dense thin-film $La_{0.6}Sr_{0.4}CoO_{3-\delta}$ electrode on samaria-doped ceria as a function of P_{O2} at 725°C. The data have been scaled relative to the 1st harmonic. The marked lines are phasors indicating the phase of the data where the frequency is an indicated fraction of the measured characteristic frequency σ_0. (b) and (c) Predicted response based on models discussed in the text.

this type of electrode is almost perfectly semicircular, exhibiting no changes in shape with T or P_{O2}.

In contrast, Figure 4(a) shows Nyquist plots of the 2nd and 3rd harmonic responses, U_{22} and U_{33}, of a dense LSC thin film made by Kawada's group. The size, shape, and phase of the higher harmonics vary strongly over the small range of P_{O2} conditions. The shape changes are specific, including a nullification (change in sign) in the second harmonic at low frequency. The phase of the higher harmonics rotate in a distinct pattern as the P_{O2} is decreased. Figures 4(b) and 4(c) show simulations of the higher harmonics based on two different models for the O_2 exchange reaction. In Figure 4(b), we consider the reaction to be limited by an *energetic* barrier to O_2 dissociation, as is often assumed in the literature. In Figure 4(c), the reaction is limited by the low probability of dissociative adsorption (*entropy barrier*). While both models predict exactly the same EIS response (a semicircle), the first model (energy barrier) is completely inconsistent with the higher harmonic data. Numerous other models that assume various rate-limiting steps (including molecular adsorption, or ion incorporation into the bulk) also fail. Only the model that assumes dissociative adsorption as limiting appears to explain our data. The model is consistent in magnitude, sign, and phase rotation with P_{O2}, and this P_{O2} dependency can be explained quantitatively in terms of the thermodynamic properties of the film.

If our interpretation is correct, it suggests that the strong Arrhenius dependence seen by workers in the exchange rate vs. temperature is not a true activation barrier. Rather, the strong temperature dependence arises from a large negative enthalpy of dissociative adsorption. At higher temperatures more sites on the surface become available, causing an increase in the dissociative adsorption rate. This result raises the question about whether researchers in this area are barking up the wrong tree. If oxygen reduction is governed by dissociative adsorption, and the adsorption sites are already maximized in terms of concentration, efforts to more easily break the O_2 bond will not help. Useful alternative strategies might include a) increasing the stability of reduced diatomic intermediates at high temperature, thereby increasing their lifetime on the surface, or b) enhancing surface diffusion of oxygen vacancies, thereby decreasing the time between collisions with unstable short-lived diatomic intermediates. In contrast, strategies attempting to decrease the energetic barrier to O_2 dissociation could actually backfire, since any thermodynamic stabilization of monatomic oxygen might lower surface site concentrations.

Conclusions and Future Directions

- Microelectrodes potentially offer an easy, low-cost way to isolate the performance of a particular electrode, while maintaining the composition, microstructure, and processing of that electrode as closely as possible to the real thing.
- NLEIS appears to be a very useful and powerful new technique, which provides higher resolution than traditional linear impedance for distinguishing specific mechanisms governing electrode response.
- Oxygen reduction on mixed conducting perovskite surfaces appears to be limited by site availability for dissociative adsorption rather than scission of the O_2 bond. Developers of new catalysts may wish to consider this in developing new materials strategies.

Special Recognitions & Awards/Patents Issued

1. *Charles W. Tobias Young Investigator Award* of the Electrochemical Society (SBA, 2004).

2. S. B. Adler, S. L. Huff, D. T. Schwartz, and J. R. Wilson, "Method for conducting nonlinear impedance Spectroscopy", U.S. and Foreign Patent applications (2006).

FY 2006 Publications/Presentations

1. Wilson, J.R., Schwartz, D.T., and Adler, S.B., *Electrochimica Acta.* **51** (8-9), 1389 (2006).

References

1. Adler, S.B.; Factors governing oxygen reduction in solid oxide fuel cell cathodes, Chemical Reviews 104 (10): 4791-4843, October 2004.

2. Wilson, J.R., Schwartz, D.T., and Adler, S.B., *Electrochimica Acta*. **51**(8-9), 1389 (2006).

3. Wilson, J.R., Schwartz, D.T., Adler, S.B., Sase, M., and Kawada, T., *to be published*.

4. Kawada, T.; Suzuki, J.; Sase, M.; Kaimai, A.; Yashiro, K.; Nigara, Y.; Mizusaki, J.; Kawamura, K.; Yugami, H. Journal of the Electrochemical Society 149, E252-E259 (2002).

III. SECA RESEARCH & DEVELOPMENT

E. Balance of Plant

III.E.1 Hybrid Ceramic/Metallic Recuperator for SOFC Generator

Objectives

- Design and fabricate a three-pass, cross flow heat exchanger utilizing metallic materials for the first and second pass and ceramic material for the high temperature third pass.
- Further develop molds and casting techniques to produce a ceramic monolith with the necessary heat transfer surface.
- Characterize the performance of the hybrid recuperator and evaluate its ability to withstand thermal shock.

Accomplishments

- Contractual details were completed and work on this project was initiated on June 28, 2006.
- Acumentrics' recuperator test stand was upgraded to allow for separate control of the air side and exhaust side gas streams. A new furnace plenum will also permit higher exhaust side recuperator pressure drops to be tested.

Introduction

Solid oxide fuel cells (SOFCs) are one of the most efficient and cleanest power generating systems being developed. SOFCs can operate on presently available fossil fuels and do not require precious metal catalysts which can be prohibitively expensive. SOFCs achieve this, in part, by operating at relatively high temperatures in the range of 800 to 1,000 degrees Celsius. Although these operating temperatures are well within the range of standard ceramic and refractory materials, where metals are required, expensive high alloy materials must be utilized.

A key component in the SOFC generator is the cathode air heat exchanger or recuperator. The function of the recuperator is to ensure that the cathode air, and thereby the cells, are at sufficient temperature to permit ion mobility, and to improve overall SOFC system efficiency by reducing stack losses. Since the heat capacities of the gases on each side of the recuperator are essentially the same and high heat exchange is essential, the recuperator requires a large heat transfer area. To date metallic recuperators have been utilized and the state-of-the-art metallic recuperator is estimated to cost around $200/kW assuming volume production. This is a significant portion of the overall generator cost which must be between $400 and $1,000/kW to achieve commercial viability. This work is aimed at developing a low-cost recuperator through the use of a combination of low-cost ceramic and metallic materials along with low-cost manufacturing techniques.

Anthony F. Litka (Primary Contact), Norman Bessette
Acumentrics Corporation
20 Southwest Park
Westwood, MA 02090
Phone: (781) 461-8251; Fax: (781) 461-1261
E-mail: tlitka@acumentrics.com

DOE Project Manager: Charles Alsup
Phone: (304) 285-5432
E-mail: Charles.Alsup@netl.doe.gov

Subcontractors:
Blasch Precision Ceramics, Albany, NY

Approach

The work to be conducted will focus on the development and demonstration of a "hybrid" recuperator which combines a high temperature ceramic section with a low temperature metallic section to reduce the overall cost of the unit while achieving the high effectivenss and long life required by an SOFC generator. This arrangement will take advantage of the high temperature, low fouling capability of a ceramic heat exchanger core while allowing lower grade metallic materials, with high extended surface area, to be used in medium to low temperature regions. By incorporating the ceramic and metallic sections into a single unit, costly interconnect ducting and fittings along with associated support structure and insulation will not be required, significantly reducing the cost over non-integrated solutions. Figure 1 shows an exploded view of the concept.

Results

Previous to the award of this SBIR grant, Acumentrics (as part of its Solid State Energy Conversion Alliance grant) and Blasch Precision Ceramics, (co-funded by New York State Energy Research and Development Authority) designed, manufactured and tested a three pass, cross flow ceramic monolith recuperator. Although significant strides were made in manufacturing the monolith and establishing simple methods of attaching inlet and outlet plenums, the heat exchange effectiveness of the unit (approximately 67%) was below that required for

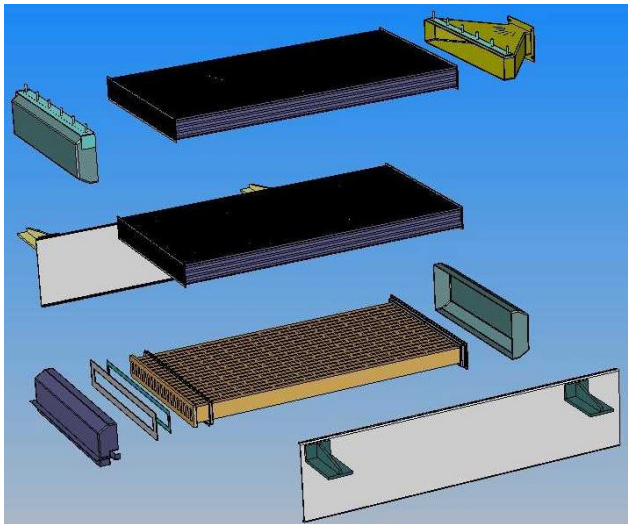

FIGURE 1. Exploded View of the Hybrid Heat Exchanger Concept

FIGURE 2. Three-Pass, Cross Flow Ceramic Monolith

efficient operation of the SOFC generator (>80%). The low effectiveness is in part a result of utilizing a low-cost, "net" shape casting technique which does not require costly machining. The casting technique requires relatively large wall thickness to achieve a structurally sound, leak-free monolith and limits the incorporation of extended surface area (fins). Figure 2 shows an example of the three-pass, cross flow ceramic monolith.

Additionally, Acumentrics has worked with a third party heat exchanger manufacturer in the design and testing of three-pass, cross flow and counter flow metallic recuperators which can meet the SOFC goals but require the use of high alloy materials to withstand the relatively high inlet exhaust temperatures (950°C) and corresponding high air preheat temperature (800°C) of the SOFC application. As shown in Figure 3, the metallic recuperator utilizes a fin core technology. The fin core consists of rectangular tubes with corrugated, fin material within the tubes and sandwiched between tubes.

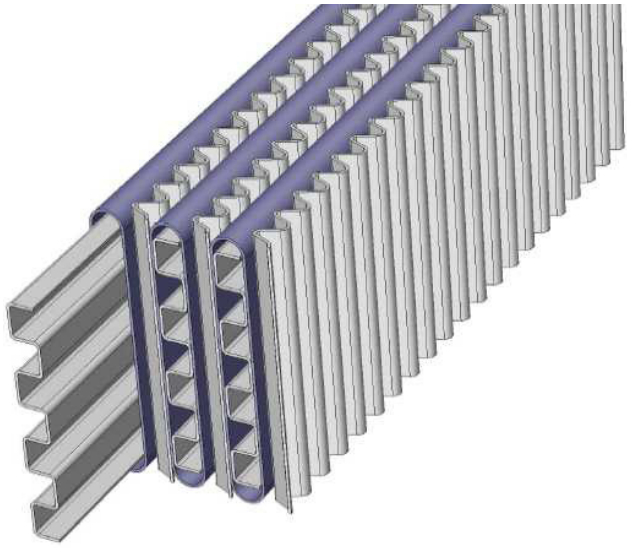

FIGURE 3. Metallic, Fin Core Geometry

Testing of recuperators has been performed in a dedicated recuperator test stand which simulates Acumentrics' SOFC generator geometry as far as the cathode air flow and temperature conditions are concerned. This facility was upgraded to permit separate control of the air side and exhaust side gas streams. A new furnace plenum was also designed and built which will permit testing of recuperators with higher exhaust side pressure drops.

Conclusions and Future Directions

The work to be conducted under this Phase I SBIR grant will prove the technical viability of the "hybrid" cross flow recuperator. The specific Phase I technical objectives are:

1. Perform thermal modeling to determine the required geometries of the individual passes to achieve the desired final and intermediate gas and material temperatures.
2. Define acceptable operating temperatures for candidate tube, fin and plenum materials.
3. Design and test a suitable attachment method to seal and support the ceramic monolith within the recuperator framework.
4. Design and fabricate a mold capable of forming the prototype single pass ceramic monolith.
5. Fabricate ceramic monoliths of oxide bonded silicon carbide and alumina oxide.
6. Determine the heat exchange characteristics of the individual ceramic and metallic sections.
7. Determine the performance of the integrated, "hybrid" recuperator. Conduct both long-term steady state and cyclic testing.

The successful accomplishment of these objectives will answer the following questions:

1. Can a ceramic monolith be successfully integrated into a multi-pass, cross flow recuperator?
2. Can adequate gas sealing be maintained at the metallic/ceramic interface?
3. Can the differential thermal expansions of the materials be dealt with to avoid stress build up on the components?
4. Can greater than 80% effectiveness be obtained in this “hybrid” approach?

III.E.2 Advanced Net-Shape Insulation for Solid Oxide Fuel Cells

Objectives

- Develop a new product line of low-cost, alumina-based, silica-free, net-shape insulation materials for SOFC systems.
- Optimize materials processing to achieve low thermal conductivity in CERamic CAstable NAnoMaterial (CERCANAM) materials.
- Demonstrate long-term stability (>2,000 hours) of gallate SOFC button cells with selected CERCANAM compositions in the fuel and air sides.

Accomplishments

- CERCANAM was successfully tested for over 5,000 hours in a gallate SOFC button cell test apparatus.
- Developed a scaled-up process to increase the slip batch size from 200 gm (in Phase I and early Phase II) to 5 kg.
- Demonstrated examples of making thick and thin sections of net-shape insulation using CERCANAM (scaled up the thickness of cast specimens from <1/8" [<12.5 mm] to 2" [50 mm]).
- Developed several complementary production-friendly processes to successfully fabricate insulation parts: (i) dry powder pressing, (ii) tape casting, and (iii) slip casting process.
- Presented a business plan at the DOE Commercialization Assistance Program (CAP) Forum based on CERACANAM technology for SOFC insulation and high temperature applications.

Akash Akash (Primary Contact), Gordon Roberts, Taylor Sparks, Mark Henry, and Balakrishnan Nair

Ceramatec, Inc.
2425 South 900 West
Salt Lake City, UT 84119
Phone: (801) 956-1032; Fax: (801) 972-1925
E-mail: akash@ceramatec.com

DOE Project Manager: Travis Shultz
Phone: (304) 285-1370
E-mail: Travis.Shultz@netl.doe.gov

Introduction

The goal of this project is to develop a low-cost insulation material for SOFCs. Most commercially available insulation materials contain silica (5-100%). The presence of silica in the SOFC insulation is detrimental to the performance of the SOFC. Further, most insulations are available in the form of sheets, blocks, or panels which then have to be machined to get the desired fit around the fuel cell stack. Often, the machining cost can be a significant portion of the overall SOFC insulation installation cost. Thus, manufacturing techniques that produce appropriately shaped silica-free insulation parts without extensive machining and post-processing are very attractive for SOFC insulation.

Approach

A new castable alumina (silica-free) insulation has been developed that utilizes the benefits of having fine porosity and high total porosity (low density) in order to obtain low thermal conductivity. The proposed technology is based on reaction bonding between alumina and a phosphate containing compound. This idea has led to the development of a new family of materials called CERCANAM. The reaction bonding approach eliminates the need for high temperature sintering and allows one to obtain net-shape components by casting or pressing the slip into the desired mold, followed by a low temperature (~900°C) firing.

Results

Two different versions of CERCANAM-based insulation material have been developed for different applications within the SOFC system. These versions are called low density (<1.0 g/cc) and high density (>1.5 g/cc), respectively. The low density insulation would be the primary insulative (front face) component for the active fuel cell. The high density version will be suitable for applications where high temperature, structural load-bearing capability is required (like rails, guide posts, or bottom support panels). The properties of these two types of insulation are listed in Table 1 below.

An array of ceramic processes has been developed to enable low-cost manufacturing of this insulation: (i) dry powder pressing (isostatic or uniaxial - for making complex shapes like tubes, etc.); (ii) tape casting (for thin, wrap-around insulation sheets); and (iii) slip casting (for making thick panels or complex parts).

TABLE 1. Properties of CERCANAM-based SOFC Insulation

	Low Density CERCANAM*	High Density CERCANAM*
Density Range (g/cc)	0.6 – 1.0 g/cc	1. 5 – 3.0 g/cc
4-pt Flexural Strength (MPa)	< 1 MPa	10 – 70 MPa
Thermal Conductivity at 800°C (W/mK)	0.2-1.0 W/mK	1-5 W/mK
Thermo-Chemical Stability	Stable at high temperature in air, CO, CO_2, H_2, H_2O, JP-8, Diesel vapor, Methanol vapor - No wt. loss	Stable at high temperature in air, CO, CO_2, H_2, H_2O, JP-8, Diesel vapor, Methanol vapor - No wt. loss
Coefficient of Thermal Expansion	~8 ppm	~8 ppm

* Depending on the end requirements, the starting raw ingredients and slip composition can be appropriately chosen to achieve a specific density, flexural strength, and thermal conductivity value. Hence, a range of values is provided instead of absolute values. For example, a 0.7 g/cc low density CERCANAM may have a flexural strength of <1 MPa and thermal conductivity of 0.2 W/mK. For the high density CERCANAM (after 900°C firing), a wide range of density-flexural strength combinations can be designed into the material: 1.7 g/cc – 10 MPa; 2.0 MPa – 20 MPa; 2.4 g/cc – 40 MPa; and 2.7 g/cc – 70 MPa. When compared to commercially available insulation for structural applications, these are the highest reported strengths (for comparative density values) seen in product literature, as published by competitive insulation providers. The pore sizes range from nano to sub-micron to micron (<100 μm) sizes.

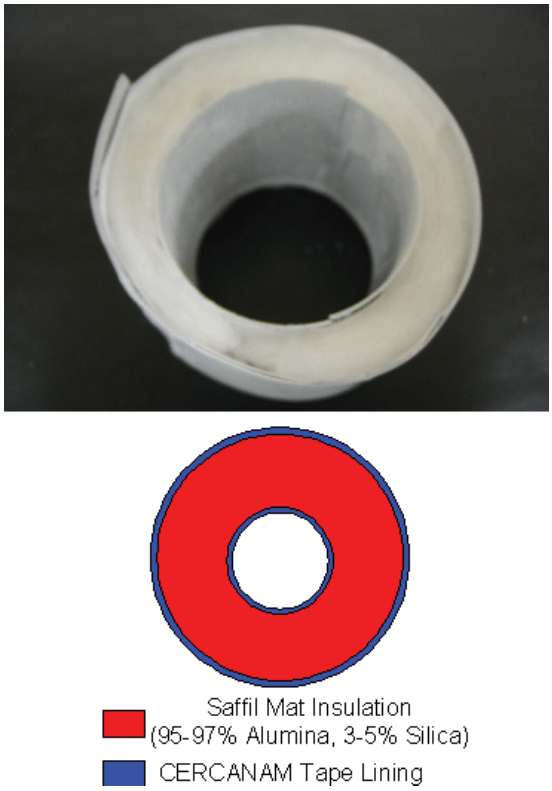

FIGURE 1. CERCANAM Tape Used to Encapsulate Saffil Fiber-Based Insulation for Added Mechanical and Thermal Protection

Figures 1 and 2 give examples of various products made using these different manufacturing techniques. In Figure 1, CERCANAM tape was used to encapsulate Saffil fiber-based mat insulation (95-97% alumina, 3-5% silica). Saffil mat insulation has a density of 0.35 g/cc and a thermal conductivity of 0.18-0.28 W/mK between 600°C – 800°C. The inner and outer CERCANAM lining (100 mil thick) provides added mechanical, thermal, and chemical protection to the Saffil insulation. The Saffil fiber-based insulation, by itself, does not have any structural integrity. However, the final fired composite structure shown in Figure 1 is easy to handle, is workable, and can take very small loads. In this way, the Saffil insulation can be fully enclosed within CERCANAM layers (including the top and bottom areas – not shown in Figure 1). Since the cost of Saffil mat and blanket insulation is $100 and $280 per cu. ft., respectively, this could be a very cost effective alternative approach for insulating SOFC systems. In Figure 2, an example of a 1.5" thick CERCANAM insulation is shown along with a second example of a net-shaped (rectangular picture frame) insulation made via a casting route. In the past, casting > 1/8" thick samples had been a significant challenge which has now been overcome by using a proprietary mixing process that allows for making high solids loading slips.

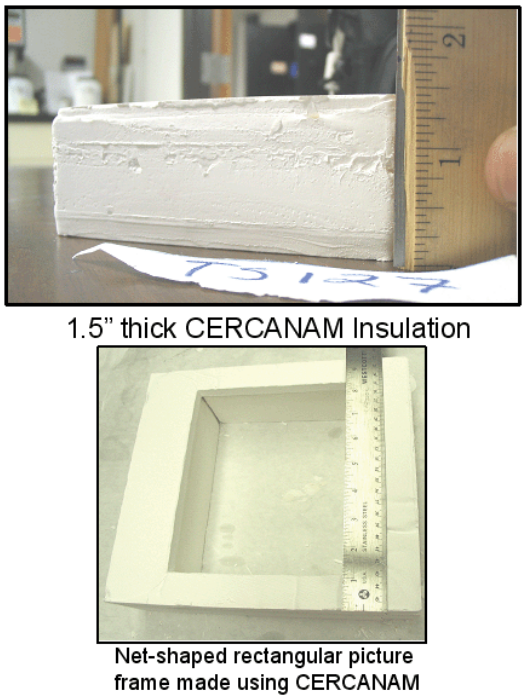

FIGURE 2. Examples of Thick, Net-Shape Insulation Samples Made Using CERCANAM

To test the CERCANAM insulation for its affect on SOFC performance over a long-term period, CERCANAM samples were introduced into the air and

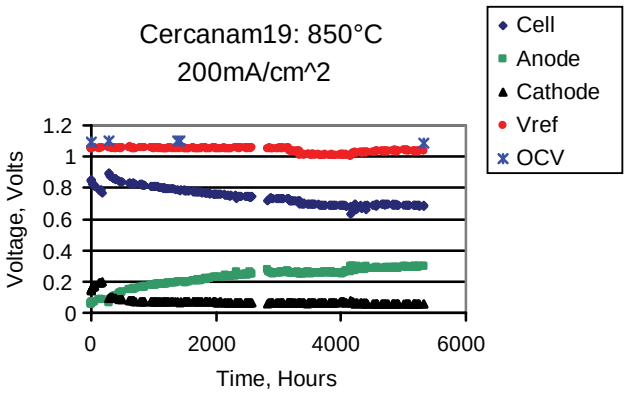

FIGURE 3. Gallate button cell performance test (up to 5300 hours) with CERCANAM samples on cathode and anode sides (CERCANAM samples were inserted into the anode and cathode sides at the 380th and 668th hour, respectively).

fuel (H_2) streams on the cathode and anode sides of the gallate button cell, and the fuel cell performance was monitored for over 5000 hours at 850°C. No cell degradation was seen, suggesting excellent thermo-chemical stability of this material (Figure 3).

A complete business plan for CERCANAM-based insulation was developed under the DOE project with feedback from Dawnbreaker Inc. This helped us to understand what kinds of issues (technology or business oriented) we need to solve, what kinds of risks we should expect, and what kinds of strategies we ought to develop in order to commercialize CERCANAM materials. The business plan was presented at the DOE CAP Forum in Falls Church, Virginia, in October 2005.

Future work will involve (i) developing a detailed cost analysis for producing products in a (future) manufacturing-type set-up and (ii) completing a SOFC system cost-benefit analysis to understand the complete system impact (material and installation cost) and compare the results with conventional approaches currently used for SOFC insulation.

Conclusions

- Successfully demonstrated long-term compatibility of CERCANAM insulation in SOFC systems.
- Developed several complementary fabrication processes for low-cost manufacturing.
- Scaled up the sample thickness of cast specimens from 1/8" to 2" (16x improvement).
- Developed and presented a business plan at the DOE CAP Forum.

Special Recognitions & Awards/Patents Issued

1. A provisional patent was filed in Oct 2005 on this technology. A full utility patent is due to be filed in July 2006.

FY 2006 Publications/Presentations

1. A. Akash, B. Nair, M. Wilson, Q. Zhao, and J. Persson, "Net-Shaped Nanoceramics," Amer. Ceram. Soc. Bull., Vol. 84 [6], 16-18, 2005.

2. A. Akash, B. Nair, J. Hartvigsen, M. Wilson, Q. Zhao, and J. Persson, "Ceramics Shape up for Fuel Cell Systems," The Fuel Cell Review, p. 33, Oct/Nov 2005.

3. Business Plan Presentation at the DOE CAP Forum, Oct 24-25, 2005.

III.E.3 Advanced Control Modules for Hybrid Fuel Cell/Gas Turbine Power Plants

Objectives

The overall project goal is to develop advanced and intelligent control algorithms for hybrid fuel cell/gas turbine (FC/T) power plants. The specific objectives are:

- Establish a dynamic modeling environment to facilitate simulation studies, as well as development and testing of control algorithms.
- Increase reliability and availability to extend service life of the components in the hybrid FC/T power plant.
- Develop robust controllers that maintain stable operation and high performance in the presence of disturbances.
- Develop optimal control strategies to improve performance and to accommodate fast response during rapid transients.
- Accommodate measurement errors, as well as sensor and actuator faults to reduce the number of unplanned shutdowns.
- Integrate robust and optimal controllers into an overall supervisory framework.

Accomplishments

- Completed development of modular dynamic models for internally reforming carbonate fuel cell (Direct FuelCell®, DFC®) and solid oxide fuel cell (SOFC) as well as balance-of-plant equipment including a micro-turbine generator. The models were based on the MATLAB®/ Simulink® programming environment.
- Completed integration of sub-MW hybrid DFC/T® and SOFC/T simulation programs.
- Developed control strategies for fuel cell stack temperature, gas turbine operation, and fuel feed rate during start-up and power ramps.
- Completed input/output pairing ensuring stable plant operation and minimal interactions among control loops.
- Designed and validated decentralized multi-loop feedforward/feedback control structure.
- Completed off-line optimization studies for eighteen ramp and step load profiles while maximizing efficiency.
- Developed an inferential control strategy for adjusting fuel flow rate via estimation of disturbances in fuel composition.

Hossein Ghezel-Ayagh (Primary Contact), S. Tobias Junker
FuelCell Energy, Inc.
3 Great Pasture Road
Danbury, CT 06813
Phone: (203) 825-6048; Fax: (203) 825-6273
E-mail: hghezel@fce.com

DOE Project Manager: Magda Rivera
Phone: (304) 285-1359
E-Mail: Magda.Rivera@netl.doe.gov

Subcontractors:
National Fuel Cell Research Center (NFCRC), Irvine, CA
Carnegie Mellon University (CMU), Pittsburgh, PA
Pennsylvania State University (PSU), State College, PA

Introduction

The control system for Fuel Cell/Turbine hybrid power plants plays an important role in achieving synergistic operation of subsystems, improving reliability of operation, and reducing frequency of maintenance and downtime. The control strategy plays a significant role in system stability and performance as well as ensuring the protection of equipment for maximum plant life. Figure 1 shows a simplified process diagram of an internally reforming SOFC/T system, which is being studied for development of advanced control algorithms. The system is based on an indirectly heated Brayton cycle. The anode exhaust, which contains unreacted fuel, is mixed with the cathode exhaust in a catalytic oxidizer, where oxidation of fuel is completed. The oxidizer exhaust passes through a heat recovery unit in which it preheats the compressed air before entering the turbine. The hot compressed air is expanded through the turbine section, driving an electric generator.

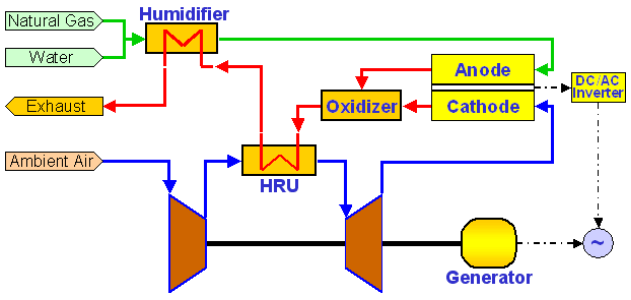

FIGURE 1. Conceptual Process Flow Diagram for the SOFC/T System

Dynamic simulation has proven to be a powerful design tool to study the transient behavior of fuel cell/gas turbine hybrid systems. Development of an advanced control strategy is facilitated by using a dynamic model both as a simulation test bed and as part of the controller itself. Components of the advanced control module include a neural network supervisor, robust feedback controllers, and predictive system models. These advanced control components are used in the development and demonstration of an innovative algorithm that optimally and robustly controls hybrid power systems. The algorithm can easily be adapted to the type of fuel used, whether natural gas, coal gas, or digester gas.

Approach

The advanced control module shown in Figure 2 is based on a feedforward/feedback structure. It consists of a combined robust controller and a neural network supervisor that together manipulate the actuators to optimally control the hybrid system during load ramps. The feedforward controller will provide optimal dynamic scheduling based on the prescribed load profile and trends. Because the optimization routines are computationally too intensive for real-time application, they are carried out off-line. The resulting data is then used to train a neural network supervisor. The feedforward controller performance depends strongly on the accuracy of the model employed to tune it. A feedback control strategy is utilized to compensate for setpoint deviations caused by imperfect feedforward control moves and to counteract process disturbances such as variations in fuel composition and ambient temperature. The feedback controller will be designed to be robust to modeling errors and process disturbances.

Results

Integrated system dynamic models were developed for both SOFC/T and DFC/T systems based on the principles of conservation of mass and energy. The architecture of the computer models in MATLAB/ Simulink allows for flexibility in development of integrated system models via interconnection of component models. The dynamic model of the integrated SOFC/T system was utilized to investigate improvements in control strategies related to the operation of the power plant. The study resulted in simple and cost effective approaches for operation of the SOFC/T system over a wide range of power output. The addition of supplementary fuel to the oxidizer and deployment of micro-turbines with variable speed capabilities were shown to be among the preferred thermal management strategies.

Analyses of the relative gain array of the system at several operating points have given insight into input/output pairing for decentralized control [1]. To control the stack temperature during transient load changes, a cascade control structure was developed to accommodate the large time constant of the fuel cell stack in rapid load following applications. Inferential sensing of the fuel composition was implemented using voltage as an indicator of varying fuel concentrations. This algorithm was implemented to manipulate the fuel flow, which resulted in making SOFC/T systems robust to varying fuel compositions.

The resulting system control approach is shown to have transient load-following capability over a wide range of power, ambient temperature, and fuel concentration variations. The results in Figure 3 demonstrate the robustness to ambient temperature variation by maintaining both fuel cell temperature and system power close to their setpoints.

A nonlinear programming framework has been developed to determine optimal operating policies for hybrid FC/T power systems. The approach consists

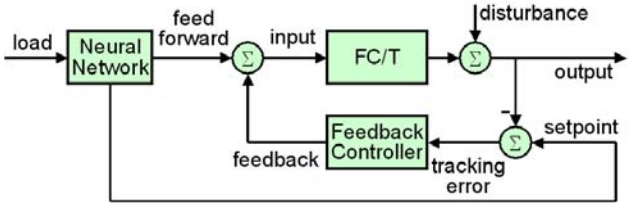

FIGURE 2. Advanced Control Module Comprising the Neural Network Supervisor and Robust Feedback Controller

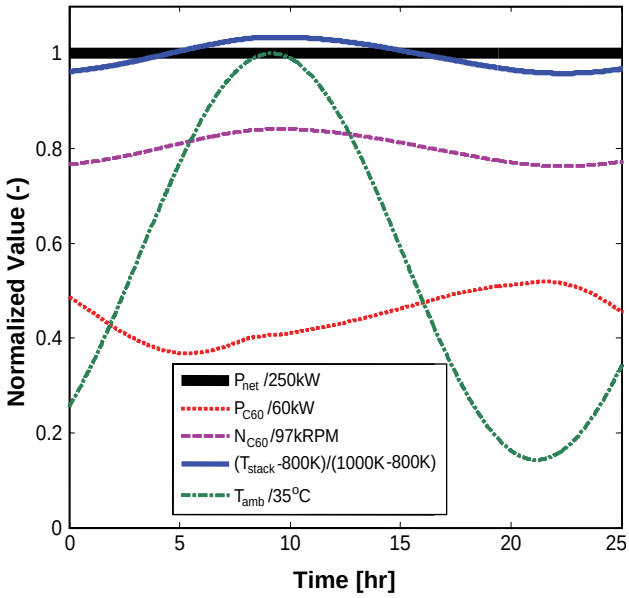

FIGURE 3. Controlled System Response to a Diurnal Ambient Temperature Variation from 5°C to 35°C

of a dynamic model of the system, reformulated as a set of index 1 differential algebraic equations [2]. The system model was discretized with an implicit Runge-Kutta method and formulated in the AMPL modeling environment. This allowed for the straightforward solution of a dynamic optimization problem using large-scale nonlinear programming solvers; the IPOPT solver was used for this project [3]. The computer model was utilized in the optimization of operating trajectories, including ramping the entire power range at various speeds as well as local stepping studies at various power levels. Optimization studies were performed and feedforward control moves and setpoints were provided to Matlab/Simulink to visualize and interpret the results. Eighteen case studies showed that the dynamic optimization could be performed quickly with excellent results.

The optimization problem was augmented by an efficiency measure. Because of its built-in flexibility, the program was easily adapted to maximize efficiency. The ramping and stepping studies were repeated, with higher efficiencies achieved while tracking the desired profiles. Results show that it is possible to operate the power plant as desired while simultaneously enhancing efficiency. Figure 4 shows the achieved efficiency improvement for a load stepping study by comparing the results with and without the inclusion of the efficiency measures in the optimization's objective function.

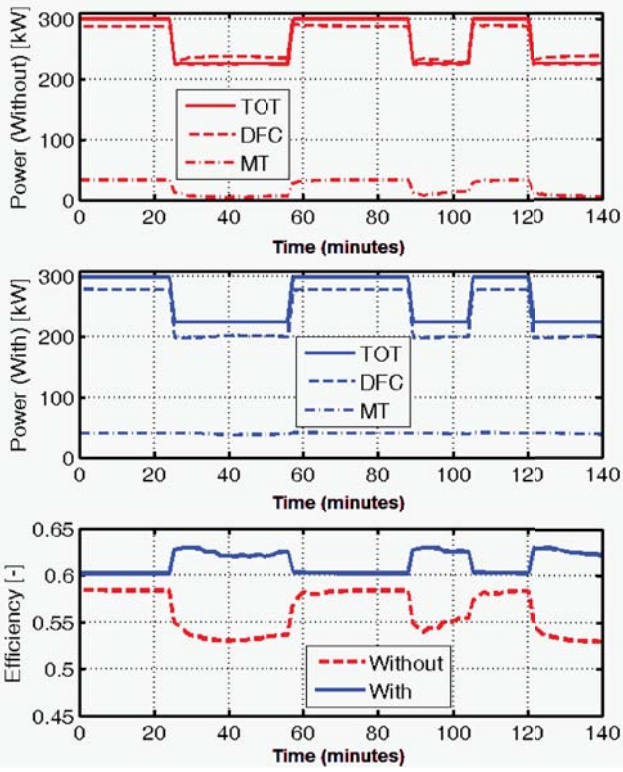

FIGURE 4. Trajectory Planning for Step Profile with and without the Inclusion of Efficiency in the Objective Function

Conclusions and Future Directions

Summary and conclusions of results obtained this year include:

- A thorough control design study resulted in a system design suited for control over a wide range of operating powers.
- Optimal input/output pairings for minimal interactions in a multi-loop feedback structure were identified via a relative gain array analysis.
- The feedback control structure was augmented by advanced control elements including feedforward look-up tables to ensure robust control in light of process uncertainty.
- The developed control system is capable of responding to rapid changes in load demand while simultaneously being able to reject disturbances in ambient temperature and fuel composition.
- The dynamic optimization framework facilitated studies of both power ramps at varying rates and stepping studies at various power levels while maximizing plant efficiency. This data will be utilized for neural network training.
- The optimization framework's applicability to parameter estimation and inferential control was demonstrated. Case studies, using the developed algorithms, verified that accurate estimation of variations in fuel composition is feasible, allowing for compensation of fuel flow and resulting in increased reliability of operation.

Overview of future work includes:

- Develop a centralized linear quadratic regulator including state estimation via Kalman filtering and determine whether it can improve robustness of the decentralized multi-loop controller.
- Develop a neural network framework suitable for online control supervision. Train the neural network with results from the control optimization studies.
- Develop fuzzy logic fault detection and fault accommodation techniques.
- Integrate the individual control strategies into the simulation environment for extensive testing of the algorithms for their stability and robustness.

FY 2006 Publications/Presentations

1. S. Kameswaran, D. Ko, L.T. Biegler, S.T. Junker, and H. Ghezel-Ayagh, *Optimal Off-Line Trajectory Planning for Load Ramping of Hybrid Fuel Cell/Gas Turbine Power Generating Plants*, AIChE Annual Meeting, Cincinnati, OH, November 2005.

2. *Advanced Control Modules For Hybrid Fuel Cell/Gas Turbine Power Plants,* DE-FG02-02ER86140, Semi-annual

Technical Progress Report No. 5, Reporting Period: 06-27-05 to 12-26-05, January 2006.

3. R.A. Roberts, J. Brouwer, F. Jabbari, S.T. Junker, and H. Ghezel-Ayagh, *Control Design of an Atmospheric Solid Oxide Fuel Cell/Gas Turbine Hybrid System: Variable versus Fixed Speed Gas Turbine Operation*, Accepted for Publication in the Journal of Power Sources, March 2006.

4. F. Mueller, F. Jabbari, J. Brouwer, R.A. Roberts, S.T. Junker, and H. Ghezel-Ayagh, *Control Design for a Bottoming Solid Oxide Fuel Cell Gas Turbine Hybrid System*, 4th ASME International Conference on Fuel Cell Science, Engineering and Technology, Irvine, CA, June 2006.

References

1. S. Skogestad and I. Postlethwaite, *Multivariable Feedback Control – Analysis and Design*, John Wiley & Sons, New York, 1996.

2. S. E. Mattsson and G. Söderlind, *Index Reduction in Differential-Algebraic Equations Using Dummy Derivatives*, SIAM J. Sci. Comp. 14:677–692, 1993.

3. A. Wächter and L. T. Biegler, *On the Implementation of a Primal-Dual Interior Point Filter Line Search Algorithm for Large-Scale Nonlinear Programming*, Math. Program., 106: 25-57, 2006.

III.E.4 Hot Anode Recirculation Blower (HARB) for SOFC Systems

Objectives

- Develop configuration that can pump anode gas at 850°C.
- Develop thermal choke design and component test at full temperature (850°C).
- Verify bearing/seal selection and design.
- Integrate and evaluate controller/motor.
- Develop low-cost integrated assembly to provide required performance and offer low cost in high volume.

Accomplishments

- Completed bearing selection and design process; selected grease-for-life bearing with greater than 40,000 hours of life.
- Identified candidate pump head materials to ensure 40,000 hours of reliable high-temperature blower operation.
- Performed detailed thermal/structural analysis of the HARB prototype blower to optimize design configuration for proper thermal response and structural robustness.
- Completed detailed cost analysis of the prototype blower for DOE and SECA review.
- Manufactured test rig hardware to verify thermal choke effectiveness.
- Demonstrated the successful performance of the thermal choke through laboratory experimentation. Tests were completed to nearly 600°C.

Dr. Mark C. Johnson (Primary Contact),
Dr. Dan S. McGuinness
Phoenix Analysis and Design Technologies (PADT)
ASU Research Park
7755 S. Research Dr., Suite 110
Tempe AZ 85284-1803
Phone: (480) 813-4884; Fax: (480) 813-4807
E-mail: mark.johnson@padtinc.com

DOE Project Manager: Magda Rivera
Phone: (304) 285-1359
E-mail: Magda.Rivera@netl.doe.gov

Introduction

This effort involves the development of a robust, low-cost, high-temperature anode recirculation blower (HARB) for use with solid oxide fuel cell (SOFC) systems (see Figure 1). SOFC system designers believe considerable improvements are achievable in water management, fuel utilization, stack operating efficiency, or system controllability if an anode recirculation pump is employed. The opportunity here is to develop a low-cost pump that can provide this function.

The challenge is to develop a pump that is durable and can survive in a very harsh environment. Unlike proton exchange membrane fuel cell (PEMFC) systems, SOFC systems operate at very high temperatures (~850°C). Depending on system architecture, the proposed pump may very well be exposed to these extreme conditions. Yet, the electric motor, controller, and bearings in the system must be kept at much cooler temperatures than the process flow. Therefore, the focus of this project is to develop an innovative approach to pump this hot process flow while providing cool temperatures for the sensitive pump components. Additionally, innovation is required to provide this capability and maintain low costs in high-volume production.

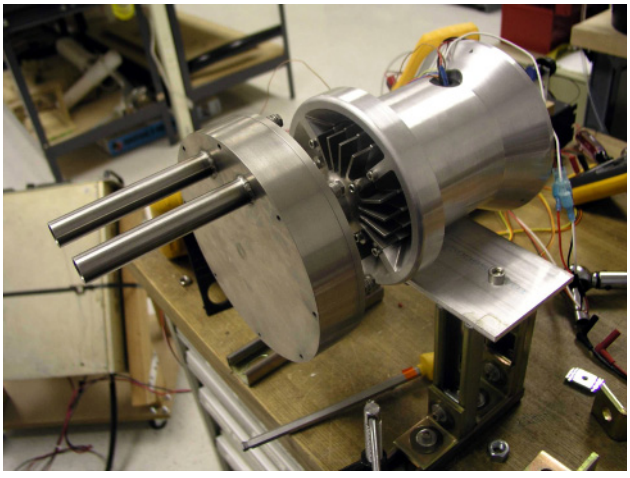

FIGURE 1. Phase I HARB Prototype Blower

Approach

The approach used to develop this pump emphasizes design iterations with a reduction to working prototypes in rapid succession. In Phase I, the major pump configuration and material selection were achieved with the aid of finite element modeling (FEM). FEM was done for all critical components to understand their temperature and stress situation. Many computer iterations were done. In particular, the thermal choke approach was confirmed and refined analytically.

After material selection and pump configuration were completed, CAD modeling and detailed drawings were done. The resulting design was procured and tested to verify performance and temperature levels. The testing confirmed the analysis and showed excellent correlation with prediction (see results section).

Results

The most important result from recent effort is the temperature data that was obtained from testing the prototype blower. The temperature data is shown in Figure 2 and is compared to an analytical prediction. This test shows surface temperatures on the outside of the thermal choke when the unit was run with ~600°C inlet temperature gas flow temperatures. The test rig that was used to create this data is shown in Figure 3.

A full view of the temperatures inside the machine, while operating at 850°C, is shown in the cross-sectional view of Figure 4.

Additionally, a cost study was completed for high-volume production of the blower shown in Figure 1. We found that the costs were too high, even in high volume, because of the size and materials used in the prototype. Therefore, based on the Phase I test results, a Phase II blower has been designed which meets long-term cost objectives. This is the most important result of our efforts to date, and the proposed design is shown in Figure 5.

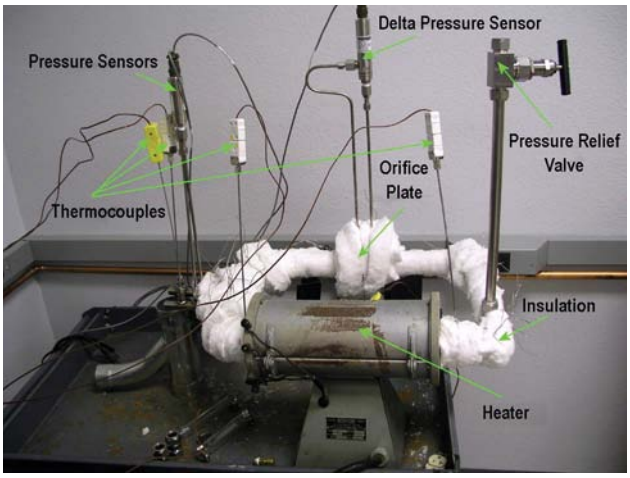

FIGURE 3. Phase I Laboratory Test Rig

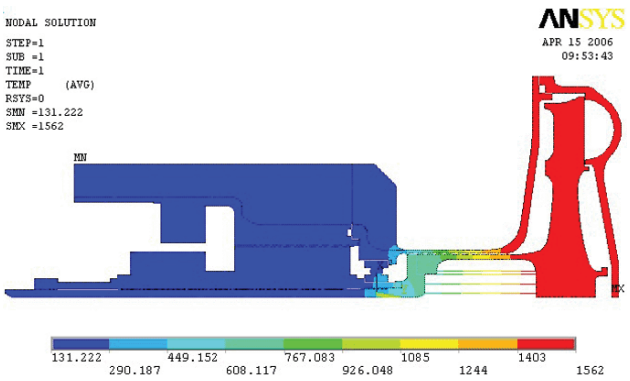

FIGURE 4. Analytical Temperature (F) Predictions for the HARB Blower

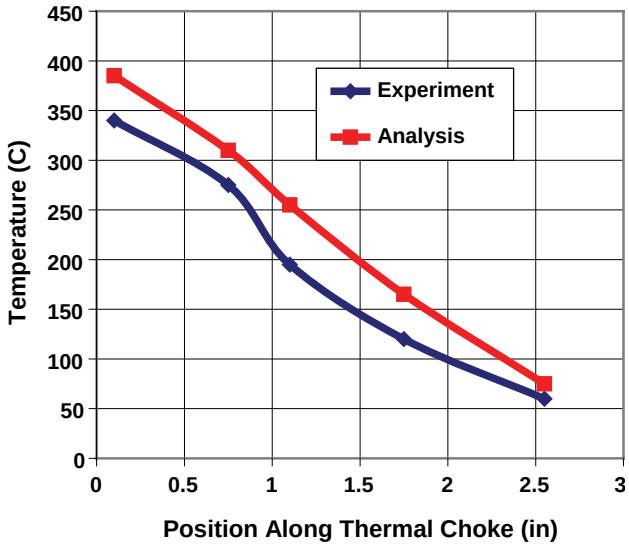

FIGURE 2. Thermal Choke Temperature Distribution (comparison between measured and analytical)

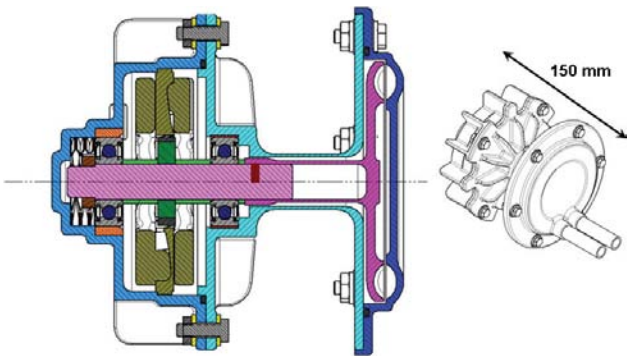

FIGURE 5. Cross-Section and Isometric View of Reduced-Cost Phase II Blower

Conclusions and Future Directions

Based on the work completed to date, a low-cost blower has been designed which will be undergoing development during Phase II. The major objectives for this effort are shown in Table 1.

TABLE 1. Phase II Primary Technical Objectives

OBJECTIVE		DISCUSSION
1	Complete details of reduced-cost design	Figure 5 presents a look at the cost-reduced configuration. However, it's necessary to finish this work by completing analyses and detailed drawings.
2	Characterize 850°C operation	The Phase I effort verified the thermal management design at part temperature (~600°C). In Phase II, hardware will be procured and a new blower constructed based on the Phase II reduced-cost concept. It will be tested at full temperature under a wide variety of conditions.
3	Demonstrate forward bearing life	In Phase I the forward bearing configuration was designed to survive at high temperatures (150°C). In Phase II several bearing tests will be conducted to verify this life and adjust the bearing approach accordingly.
4	Develop low-cost motor and controller	PADT has designed motors and controllers in the past. This application de-emphasizes performance in exchange for cost. Controller may be available off-the-shelf, or a prior PADT design will be modified.
5	Develop and integrate novel pump head aerodynamics	PADT is proposing a modified regenerative pump head which allows for a *much reduced impeller cost*. This is accomplished by using a technology that develops high pressure with a small wheel with relatively low tip speed.
6	Integrate improvements	Now we can integrate the low-cost motor design, improved pump head, best bearings tested to date, the sensorless controller, cast components, and any other lessons learned from the characterization and early endurance testing of objective 2, into the HARB design.
7	Validate design	Procure hardware and build three (3) HARB Phase II blowers. Conduct a bank of validation tests. A final low-cost version of the pump will be tested on a 5,000 hour endurance test at full power and high temperature. This will flush out any design flaws or issues and prepare us for low-volume production for SOFC demonstration projects.

III.E.5 Foil-Bearing Supported High-Speed Centrifugal Cathode Air Blower

Objective

Design a foil-bearing supported high-speed centrifugal cathode air blower (CAB) meeting all the technical requirements of SECA members and develop a process to reduce the manufacturing cost of CABs to $100 per unit based upon a production volume of 50,000 units/year.

Accomplishments

- The project is in the early stages of CAB design.
- Initial CAB design point performance calculations were made.

Introduction

The goal of the Solid State Energy Conversion Alliance (SECA) is to develop commercially-viable ($400/kW) 3 to 10 kW solid oxide fuel cell (SOFC) systems by year 2010. SOFC power generation systems are attractive alternatives to current technologies in diverse stationary, mobile, and military applications. SOFC systems are very efficient, from 40 to 60 percent in small systems and up to 85 percent in larger cogeneration applications. The electrochemical conversion in a SOFC takes place at a lower temperature (650 to 850ºC) than combustion-based technologies, resulting in decreased emissions – particularly nitrogen oxides, sulfur oxides, and particulate matter. These systems all offer fuel flexibility, as they are compatible with conventional fuels such as hydrogen, coal, natural gas, gasoline, or diesel. Despite these advantages, advances in balance of plant (BOP) component design must be developed before the SECA program goal can be realized.

Giri Agrawal (Primary Contact), Bill Buckley, Dennis Burr, Sam Rajendran
R&D Dynamics Corporation
15 Barber Pond Road
Bloomfield, CT 06002
Phone: (860) 726-1204; Fax: (860) 726-1206
E-mail: agragiri@rddynamics.com
Website: www.rddynamics.com

DOE Project Manager: Charles Alsup
Phone: (304) 285-5432
E-mail: Charles.Alsup@netl.doe.gov

SOFC systems require blowers to provide motive force to incoming atmospheric air, in order to overcome the pressure drop in the various valves and heat exchangers, and in the fuel cell stack. The energy required to drive this component is typically one of the largest parasitic loads for the SOFC system; consequently, high blower efficiency is paramount to high system efficiency. Furthermore, blower reliability is critical to ensure safe long-term system operation.

Approach

- In Phase I, a CAB will be concepted and designed based on a previously developed fuel processor blower. A process will be developed for reducing the manufactured cost of CABs to $100 per unit, based upon a production volume of 50,000 units per year.
- In Phase II, a detailed design of the CAB will be completed and a prototype manufactured and tested using cost reduction techniques identified in Phase I.
- Phase III will start the commercialization phase of the project. CAB field demonstrations will be initiated with SECA members and other potential original equipment manufacturers. Distributors will be identified and contacted.

Results

A preliminary design has been performed. The CAB has been designed as a centrifugal compressor running at 80,500 rpm. In order to meet high reliability, the rotating assembly will be supported on foil air bearings.

The proposed CAB will be driven by a brushless permanent magnet DC motor or switched reluctance motor. Such motors have shown high efficiency and high reliability for the power range required for the CAB.

The cathode air blower will be similar to a previously designed, manufactured and successfully tested proton exchange membrane fuel processor system (FPS) air blower, which was built by R&D Dynamics for UTC Fuel Cells under a DOE-funded project. The FPS blower is shown in Figures 1 and 2. It is foil-bearing supported and is of a high-speed centrifugal type design. The CAB will be affordable, efficient, reliable, small, lightweight, and meet turndown requirements.

The FPS rotating assembly, shown in Figure 3, is made up of the impeller, journal bearing shaft, motor rotor, thrust bearing shaft and hall magnet assembly. The shaft components are held together in compressive preload by a tie rod that runs through the center of the shaft. The resulting rotating assembly is extremely lightweight and rigid.

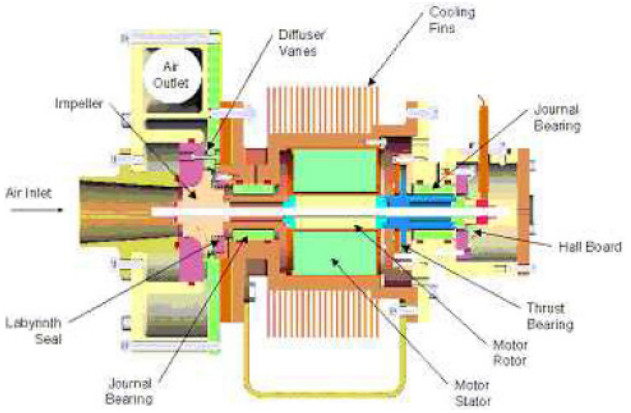

FIGURE 1. Cut Away View of FPS Blower

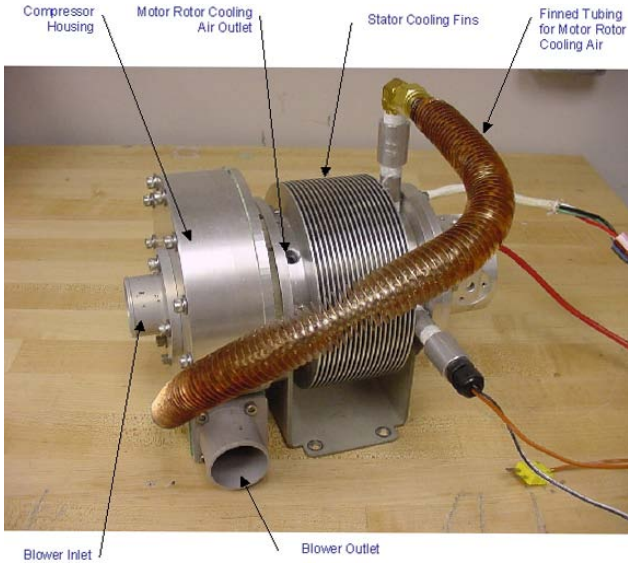

FIGURE 2. Actual FPS Blower

FIGURE 3. FPS Blower Rotating Assembly

CAB Technical Requirements

Specific blower performance requirements are dependent upon the design of the SOFC system with which it is associated; nevertheless, the following representative nominal requirements, in lieu of design-specific data, will be addressed:

Fluid Type	Atmospheric Air
Pressure Ratio	1.1 to 1.2
Peak Airflow	1,500 SLPM
Speed Control	Variable Speed
Turn-Down Ratio	5:1
Overall Efficiency	≥60%
Design Life	>40,000 hours @ 100% Duty Cycle
Maintenance	Interval >10,000 hours
Target Cost	<$100 per unit based on 50,000 units/year
Noise	<70 dBA
Contamination of Process Air	None desired

Preliminary Performance of CAB Blower (Design Point)

Type	Centrifugal
Impeller Diameter	1.67 inches
Inlet Pressure	14.7 psia
Inlet Temperature	68°F
Outlet Pressure	17.64 psia
Outlet Temperature	103.7°F
Pressure Ratio	1.2
Mass Flow Rate	3.98 lbm/min
Adiabatic Efficiency	79%
Speed	80,500 rpm

Conclusions and Future Directions

The project has encountered no technical or manufacturing cost barriers to date which would prevent the objectives from being met.

III.E.6 Foil Gas Bearing Supported High Speed Centrifugal Anode Gas Recycle Blower

Objective

Demonstrate the feasibility of using a foil gas bearing supported high-speed centrifugal anode gas recycle blower (FBS-AGRB) to help SECA members meet their SOFC goal of higher efficiency and lower overall system cost.

Accomplishments

- Designed a prototype FBS-AGRB having the following features:
  - Low-cost design which met "design for manufacturing and assembly" (DFMA) concepts
  - High-temperature capability >850°C
  - Oil-free gas bearings
  - No gas leakage out of the blower
  - No sulfur leakage into the fuel stream from blower components
  - No free silica exposure into the fuel stream
  - No heavy metal leakage into the fuel stream
  - No parasitic cooling required
  - >40,000 hour lifetime
  - Maintenance free
  - High-efficiency high-speed motor and centrifugal rotor
  - High-temperature and hostile environment capability
  - Scalability to larger sizes
- Demonstrated the conical foil gas bearing key technology with breadboard testing

Giri Agrawal (Primary Contact), Bill Buckley, Dennis Burr, Sam Rajendran
R&D Dynamics Corporation
15 Barber Pond Road
Bloomfield, CT 06002
Phone: (860) 726-1204; Fax: (860) 726-1206
E-mail: agragiri@rddynamics.com
Website: www.rddynamics.com

DOE Project Manager: Magda Rivera
Phone: (304) 285-1359
E-mail: Magda.Rivera@netl.doe.gov

Introduction

The goal of the Solid State Energy Conversion Alliance (SECA) is to develop commercially-viable ($400/kW) 3 to 10 kW solid oxide fuel cell (SOFC) systems by year 2010. SOFC power generation systems are attractive alternatives to current technologies in diverse stationary, mobile, and military applications. SOFC systems are very efficient, from 40 to 60 percent in small systems and up to 85 percent in larger co-generation applications. The electrochemical conversion in a SOFC takes place at a lower temperature (650ºC to 850ºC) than combustion-based technologies, resulting in decreased emissions – particularly nitrogen oxides, sulfur oxides, and particulate matter. These systems offer fuel flexibility, as they are compatible with conventional fuels such as hydrogen, coal, natural gas, gasoline or diesel fuel. Despite these advantages, advances in balance-of-plant components must be developed before the SECA program goal can be realized.

SOFC systems that incorporate some recycling of the anode exhaust gas, which is mixed with incoming fresh fuel prior to entering the pre-reformer, have a higher efficiency and offer the potential for lower overall system cost. An anode gas recycling blower (AGRB) is an attractive solution to perform this task.

Approach

A foil bearing supported high-speed centrifugal anode gas recycle blower was selected to meet the requirements of SOFC systems because of its potential for:

- Low-cost using simple design and less material
- Highest blower efficiency via high speed centrifugal impeller
- High-temperature capability using foil gas bearings, switched reluctance (SR) motor and sensor-less controller
- Contamination-free using oil-free foil gas bearings and hermetically sealed blower
- High reliability from foil gas bearings and SR motor

Results

The blower was designed for an inlet gas temperature of 600 to 850ºC, atmospheric pressure, pressure rise of 4 to 10 inches of water, and a flow of 100 standard liters per minute (slpm), which is nominally

composed of 46 slpm H_2O, 27 slpm CO_2, 20 slpm H_2, and 7 slpm CO. Overall efficiency meets or exceeds 40% under the aforementioned operating conditions. The unit has a variable speed control with a flow turndown ratio of 5 to 2. The blower unit will have a design life of >40,000 hours, with a 100% duty cycle and 10,000 hour maintenance interval. The unit will be able to tolerate at least 30 thermal cycles, between operating and room temperatures, over its design life. The unit cost of the blower for production rates of >50,000 units was estimated to be less than $100. Additional design requirements listed below were also addressed:

- Design for scalability
- No gas leakage
- No sulfur leak into the fuel stream
- No free silica exposure into the fuel stream
- No heavy metal leakage into the fuel stream
- No cooling required from the system other than from the process fluid
- No purge gas required
- Blower shaft temperature was estimated to be below water dew point
- Mechanical type seals were not required
- Design explosion-proof
- No corrosion/carbon deposition

Design points for the FBS-AGRB were as follows:

Shaft Speed	>90,000 rpm
Pressure Ratio	1.025
Pressure Rise	25.4 cm of water (10” of water)
Inlet Pressure	1.01 bar (14.69 psia)
Outlet Pressure	1.08 bar (15.06 psia)
Inlet Temperature	850ºC (1,562ºF)
Outlet Temperature	857.3ºC (1,575.2ºF)
Gas Constant	0.369 J/kg ºC (68.64 ft-lbf/lbm R)
Specific Heat Ratio	1.274
Mass Flow	1.54 g/s (0.204 lbm/min)
Volume Flow	100 slpm
Impeller Isentropic Power	15.6 Watt

A cut-section view of the blower is shown in Figure 1.

Key technologies were incorporated into the blower design, including state-of-the-art aerodynamics, conical gas bearings, SR motor, and sensor-less controller. Design analysis included, critical speed analysis, thermal analysis and stress analysis. The conical bearings were a ground breaking technology best suited for this application and testing was done to confirm their feasibility and applicability to support both radial and thrust loads. An exploded view of a conical bearing is shown in Figure 2.

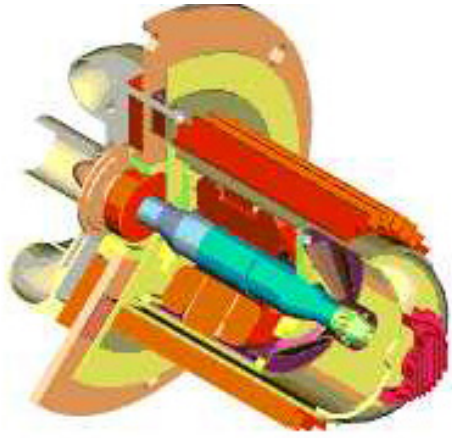

FIGURE 1. Cut-Section View of FBS-AGRB

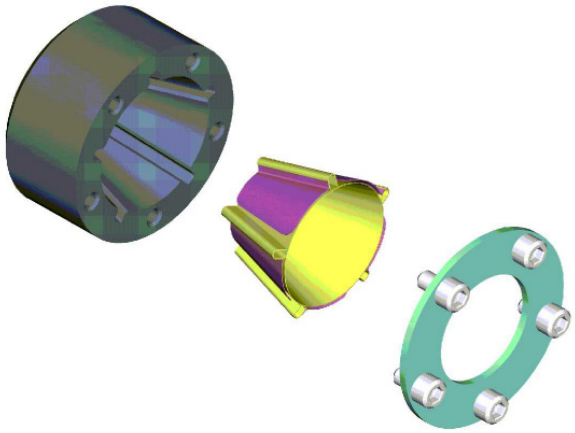

FIGURE 2. Exploded View of Conical Bearing

A breadboard conical bearing test rig was built and is shown with conical test bearing hardware in Figures 3 and 4, respectively. The test rig is capable of testing many combinations of conical bearings at loads and speeds while measuring bearing friction. The rig is comprised of three major sections: the upper section is the housing of the turbine, the mid section is the housing of the journal and thrust bearings, and the lower section is the housing of the conical test bearing and a piston. A fixture was also designed and manufactured for separately measuring breakaway torque and load on the conical bearing. The conical bearing lifted off steadily at different loads and the torque was low, which means power loss is very low. The bearing showed no signs of being stressed. The testing proved the technical feasibility of using conical bearings.

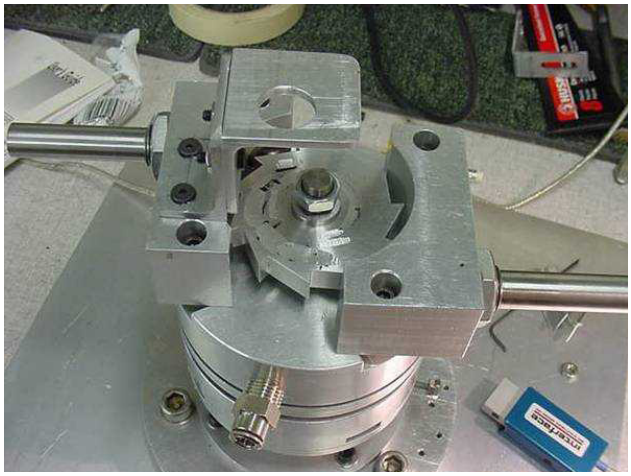

FIGURE 3. Breadboard Conical Bearing Test Rig

FIGURE 4. Conical Test Bearing Hardware

A cost analysis of the blower was performed by two methods. The first method was based on historical data, past experience at R&D Dynamics and discussions with vendors. The second method was based on automobile standards where cost of existing equipment was scaled to new equipment by varying weight and quantity. Both methods assumed a 50,000 unit production rate per year. Production blower cost varied from $95 to $114 per unit. This represents a cost target that is very favorable to meeting overall SOFC system cost goals.

Conclusions and Future Directions

- Key blower technologies were proven by extensive design and analysis.
- The high-temperature blower design evolved to be a successful design which can achieve the SECA goal.
- Conical bearing breadboard testing proved the technical feasibility of conical bearings.
- The blower cost was estimated to be less than $100 at a production volume of 50,000 units/year.

Phase I is complete. Work needs to be continued in Phase II as follows:

- Develop a prototype blower
- Test at high-temperature condition
- Incorporate rigorous “design for manufacturing and assembly” techniques to reduce cost
- Demonstrate blower to SECA members
- Test blowers at SECA member’s fuel cell systems

FY 2006 Publications/Presentations

1. “Foil Bearing Supported High-Speed Centrifugal Blower,” SECA Core Technology Program Peer Review, October 25-26, 2005, Lakewood, CO.

III.E.7 Low-Cost/High-Temperature Heat Exchanger for SOFCs Using Near-Net-Shape Ceramic Powder Forming Process

Objectives

- Design a counter flow heat exchanger for cathode preheat of solid oxide fuel cells.
- Develop a computational model to accurately predict the effectiveness of heat exchangers.
- Demonstrate a process of forming ceramic composite heat exchangers using rapid prototype tooling and a proprietary near-net-shape powder forming process.
- Optimize the heat exchangers for high effectiveness and low pressure drop using computational fluid dynamic (CFD) simulation.
- Validate the CFD simulations with experimental data collected from the heat exchangers under actual operating conditions.

Accomplishments

- Designed, fabricated, and validated experimentally to within 3% a 62% effective, computationally modeled heat exchanger operating at 900°C and a 5 kW flow rating.
- Designed an 83% effective computational heat exchanger model.
- Manufactured a 15 cm x 35 cm one-piece complex Si-SiC prototype using rapid prototype tooling and a near net shape forming process (see Figure 1).
- Tested a 73% effective 15 cm x 55 cm one-piece prototype at 980°C and a 5 kW flow rating.
- Developed a methodology for accurately modeling and simulating the effects of geometry changes computationally to achieve an effectiveness between 70% and 90% while maintaining a pressure drop of less than 10" w.c.

Tom Briselden (Primary Contact), Christopher Wyant, Nathan Lang
Spinworks, LLC.
5451 Merwin Lane
Suite 207
Erie, PA 16510
Phone: (814) 899-4871; Fax: (814) 314-0288
Website: www.spin-works.com

DOE Project Manager: Magda Rivera
Phone: (304) 285-1359
E-mail: Magda.Rivera@netl.doe.gov

Subcontractors:
Penn State Erie, School of Engineering and Engineering Technology, Erie, Pennsylvania

Introduction

Without a low-cost high-temperature heat exchanger, the solid oxide fuel cell system (SOFC) may not meet the electric conversion efficiency goal of 60% and installation cost of $400/kW. Because it operates at temperatures near 750°C, exhaust gases exceeding this temperature may remove a substantial amount of the energy supplied to the fuel cell. Capturing this high quality energy and preheating the fuel cell's cathode air is a promising method to improve SOFC efficiency.

One method of capturing high quality energy is through the use of heat exchangers. Traditional alloy-

FIGURE 1. Prototype Heat Exchanger

based and ceramic heat exchangers have a prohibitive life cycle cost impact on the SOFC due to high initial costs and material limitations such as creep, thermal shock, and sulfidation attack. An opportunity exists for a low-cost, high-temperature cathode air SOFC heat exchanger that can operate under the following challenging conditions:

- 750°C to 1,000°C
- 11.7 kg air/kW hr
- 32°C/cm temperature gradient
- 50 ppm sulfur
- 70% to 90% effectiveness
- < 5" w.c. pressure drop on the hot side
- < 10" w.c. pressure drop on the cold side
- Withstand over 2,000 thermal cycles from ambient temperature to maximum operating temperature
- 40,000 hours life
- 10,000-hour maintenance interval
- Minimal Si or Cr carryover to eliminate membrane contamination
- < 10% impact on the overall installation cost of the SOFC

Approach

The approach taken was to develop a system in which a heat exchanger can be optimized for any SECA member's specifications, the necessary tooling rapid prototyped from that optimized shape, and finally the heat exchanger formed and tested under actual operating conditions. This system allows full mass customization of the heat exchangers while keeping the forming and firing process essentially the same for manufacturing.

A commercially available, low-cost Si-SiC material was used to manufacture a highly effective (between 70% to 90%) heat exhanger. The material has a proven life history greater than 100,000 hours in high temperature natural gas and air environments with severe thermal shock. Minimal Si carryover into the fuel cell membrane is estimated. Complex helical shaped heat exchangers were designed in three dimensions and computationally modeled. A rapid prototype tool was used to facilitate a near-net-shape, patented, ceramic powder formed, one-piece component. It is estimated that the one-piece method will result in a low-cost (< 10% of SOFC system cost), high-temperature heat exchanger with a life expectancy that meets the goals of SECA members.

Results

The first step of this process was to validate the computational analysis. To accomplish this, simulations of four simple counter-flow heat exchangers were analyzed computationally. At the same time, the four heat exchangers were manufactured and tested experimentally. The initial flow and wall surface characteristics were set as a result of these four simple heat exchanger tests. These flow and wall characteristics were then used as the inputs into all successive simulations.

A computational study was then conducted to determine the change in effectiveness that varying the inlet conditions and the geometry of the heat exchangers (including the number of flow channels, the twist rate, and differing mass flow rates) would have (see Figure 2). The end result of this study was a 50% effective heat exchanger that fits the SECA inlet and pressure drop requirements.

A theoretical analysis was then performed to optimize each flow channel in the heat exchanger. The optimization was done in regards to a heat transfer "Figure of Merit" (maximizing the surface heat transfer coefficient for a given pressure drop). This resulted in a 12% increase in effectiveness with no additional pressure drop in the same size heat exchanger.

The tooling required to manufacture this 62% effective heat exchanger was then rapid prototyped and the heat exchanger was manufactured. The testing on the heat exchanger was performed on a 5 kW heat exchanger test rig developed in house. This test rig simulates the effluents coming off of a 2.5 to 6.25 kW fuel cell in operation. The mass flow rate and temperature of the effluents, as well as the incoming preheat air, are monitored and controlled. The pressure drop and outlet temperature of each channel can also be monitored. The computational results, using the flow and wall characteristics developed in the validation

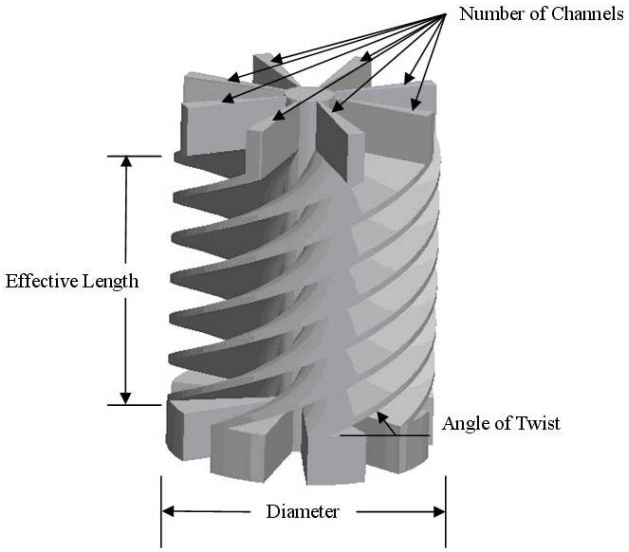

FIGURE 2. Heat Exchanger Geometry

stage of the project, were validated to within 3% in effectiveness (59% effective in experiment). Further simulations and tests were performed using mass flow rates simulating effluents from 2.5 to 6.25 kW fuel cells at 800°C and one special case which was a 3.0 kW equivalent operating at 725°C. This data was then used to validate the CFD simulations (see Figure 3).

Upon proving that the computational analysis accurately predicts the effectiveness of the heat exchangers with varying geometries and inlet conditions, heat exchangers have been computationally designed with an effectiveness range as high as 83%; however, these heat exchangers were outside the current manufacturing capabilities. Concurrently, heat exchangers were formed, fired, and tested for 5 kW fuel cells with as high as 73% effectiveness and at inlet temperatures as high as 980°C.

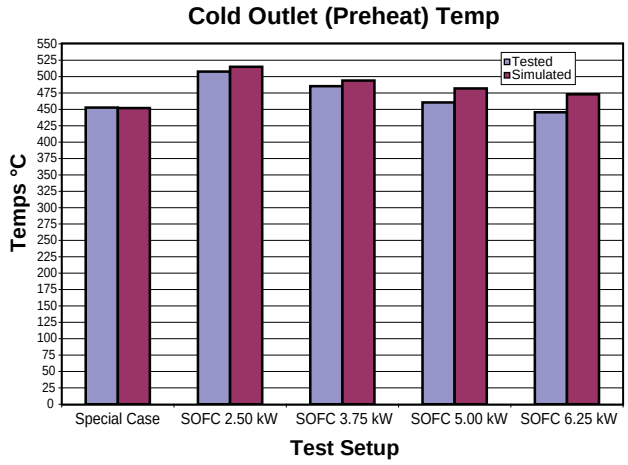

FIGURE 3. Preheat Temperature Comparison

Conclusions and Future Directions

By using a patented near-net-shape ceramic powder forming process and supplementing it with the ability to fully optimize the design for any inlet conditions and any operating constraints (size, pressure drop, manifolding, etc.) and easily prototype the tooling required for forming, fully functional and optimized heat exchangers can be produced for costs within the SECA requirements.

The future plans for this project are to:

- Using computational analysis, identify the key variables that maximize effectiveness and minimize component volume for a 3 kW to 10 kW SOFC helical fluent channel heat exchanger.
- Using advanced 3-D modeling, rapid prototyping, and near-net-shape powder forming, design and manufacture one-piece helical fluent channel prototypes with an effectiveness between 70% and 90%.
- Test the prototypes under simulated SOFC conditions between 650°C to 1,000°C to validate performance and manufacturing integrity.
- Utilizing input from SECA members, market data, and the performance map, design custom ThermCor™ prototypes and ceramic and ceramic/metallic manifolds to interface with SOFC systems.
- Using the HeatCor™-Industrial pilot manufacturing plant (11,000 units/year at $400/unit-5 kW) as a benchmark, implement design for manufacturing build to order, mass customization, and other key technical upgrades to design a 50,000 unit/year plant to produce a $250/unit, 5 kW heat exchanger.
- Produce and test “commercial ThermCor™ prototypes” for SOFC systems.

III.E.8 Feasibility of a SOFC Stack Integrated Optical Chemical Sensor

Objectives

- Design of thermally stable nano-cermets using radio frequency magnetron sputtering techniques
- Synthesis of nano-cermets with a narrow particle diameter distribution
- Probe Au nanoparticle surface plasmon resonance (SPR) properties and Pd-YSZ (yttria-stabilized zirconia) optical properties as a function of temperature and chemical exposure

Approach

- Synthesis of Au-YSZ nano-cermets using physical vapor deposition techniques
- Characterize Au nanoparticles using optical and microstructural analytical techniques
- Testing of thermal stability (500-1000°C) of nano-cermets and their corresponding optical properties
- Determine the thermal and chemical stability (CO, NO_2, hydrogen) of nano-cermets and the corresponding optical properties

Accomplishments

- The detection of CO using all-optical techniques was demonstrated at an operating temperature of 500°C in the presence of an air carrier gas

Future Directions

- Evaluate the long term stability of the Au-YSZ films towards both temperature and CO exposures
- Characterize the CO sensing capabilities of the Au-YSZ films as a function of oxygen background pressure, temperature and Au content
- Evaluate the sensing properties of the Au-YSZ tailored nanocomposite films for the detection of sulfur compounds, H_2 and NO_2

Michael A. Carpenter
College of Nanoscale Science and Engineering
University at Albany – SUNY
Albany, NY 12203
Phone: (518) 437-8667; Fax: (518) 437-8603
E-mail: mcarpenter@uamail.albany.edu

DOE Project Manager: Magda Rivera
Phone: (304) 285-1359
E-mail: Magda.Rivera@netl.doe.gov

Introduction

The DOE-NETL Innovative Concepts Phase II Program is investigating the feasibility of harsh environment compatible chemical sensors based on monitoring the surface plasmon resonance (SPR) bands of metal nanoparticle doped YSZ nano-cermets, as a function of fuel concentrations, impurities e.g. CO and temperature (500-900°C). In particular, Au nanoparticles exhibit a strong SPR band whose shape and spectral position is not only highly dependent on the refractive index of the host medium but also on chemical reactions at the interface between the metal and the surrounding environment.[1]

In this report, the operational range of Au nanoparticle based sensing of CO was extended up to 500°C through the use of a materials system comprised of Au nanoparticles embedded in an yttria-stabilized zirconia (YSZ) matrix. A reversible change in the optical properties of this nanocomposite is observed upon exposure to gas cycles of air and an air/CO mixture. The sensing mechanism has been attributed to high temperature interfacial charge transfer chemical reactions, occurring at the perimeter of the Au nanoparticles, which inject charge into the Au nanoparticle causing changes in both the position and shape of the SPR band. These reactions are presumed to be associated with the reduction of the YSZ matrix and the oxidation of CO, via a charge transfer reaction between YSZ bound oxygen anions, formed through the dissociative adsorption of oxygen molecules on YSZ at high temperatures, and the Au nanoparticles.

Approach

The Au-YSZ nanocomposite films are deposited using dual target confocal physical vapor deposition, with the metal and metal oxide sputtering gun deposition rates tuned to achieve the desired metal-to-metal oxide composition. Thermal annealing in argon at temperatures above their respective operating temperatures is used both to thermally stabilize the films and also to grow nanoparticles of a given size. Materials characterization of the films using scanning electron microscopy (SEM), Auger spectroscopy, Rutherford backscattering spectroscopy (RBS) and x-ray diffraction (XRD) analyses is used to determine the microstructural and composition properties. Ex situ optical characterization using ultraviolet to

[1] Kreibig, U.; Vollmer, M.; *Optical Properties of Metal Clusters*; Springer, New York, 1995.

visivle (Uv-Vis) absorption spectroscopy and spectro-ellipsometric analysis is used to correlate the material properties with the resulting optical properties. In situ Uv-Vis spectroscopy utilizing a charge-coupled device (CCD)-based detection system as a function of both temperature and chemical exposure is used to determine the gas sensing properties with a time resolution on the seconds scale. Test gases include, CO, NO_2 and hydrogen which will provide a range of reducing and oxidizing environments whose absorption spectra effects combined with theoretical calculations will help deconvolute changes in both the dielectric and the chemical environment surrounding the bimetallic and metallic nanoparticles.

Results

Figure 1a displays the absorption spectrum along with a corresponding Lorentzian fit to the data for a representative Au-YSZ film in the spectral region between 470 and 920 nm at 500°C in an air background. Noise levels at the longer wavelength limit of the spectrum become rather pronounced due to the incomplete removal of the Xe lines from the absorption spectrum. The SPR band peaks at approximately 600 nm and was fitted to a Lorentzian curve, with an R^2 value of 0.998, in the region between 560 and 800 nm, to extract the changes in the spectrum upon exposure to the air/CO mixture. This fitting range was dictated at the shorter wavelengths by the Au interband transitions which have an onset at approximately 520 nm, while wavelengths longer than 800 nm were ignored due to the pronounced noise levels. Figure 1b displays the absorption spectra of the Au-YSZ nanocomposite for both the air and an air/CO (1 vol.%) gas mixture. In both cases, a SPR absorption band at approximately 600 nm was observed. However, upon exposure to CO, the SPR band slightly blue shifts and becomes narrower, with no measurable change in the baseline of the spectrum at the short and long wavelength limits. The inset of Figure 1b displays the difference spectrum obtained by subtracting the fitted air and air/CO absorption spectra. The CO sensing signal is defined as the peak to peak difference between points A and B on the difference spectrum.

Figure 2 displays the resulting CO sensing signal as a function of time for the Au-YSZ film upon exposure to 1, 0.75, 0.5, 0.25 and 0.1 vol.% CO concentrations in air at 500°C. The change in the absorption spectra upon exposure to CO was reversible, and the sensing signal increased with increasing CO concentration. A background signal of approximately 0.04 is observed during each of the air cycles and is attributed to the incomplete subtraction of the fitted spectra due to the noise levels observed in the raw data. The response time, i.e., the time required for the sensing signal to

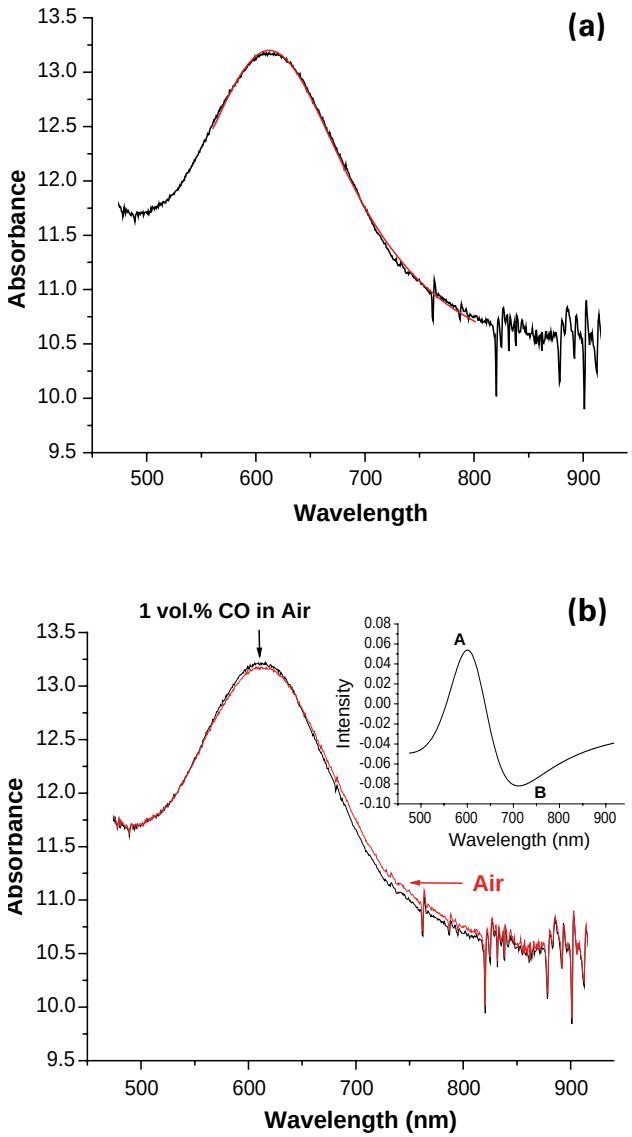

FIGURE 1. a) Absorbance spectra of the Au-YSZ nanocomposite film in air at 500°C with a corresponding Lorentzian curve fit (red line). b) Absorption spectra for air and 1 vol.% CO in air exposures at 500°C. The inset displays the difference spectrum obtained by subtracting the fitted data resulting from the air and the air/CO exposures.

obtain its maximum value upon exposure to CO, was approximately 40 s at all CO concentrations, with recovery in the subsequent air pulse displaying a two-stage mechanism comprised of a fast, approximately 60 s, initial stage, followed by a slower, approximately 1000 s, stage.

Figure 3 reports the change in sensing signal, normalized to that observed for the 1 vol.% CO exposures, plotted versus CO concentration at 500°C. The data in Figure 3 were obtained from three individual runs and indicate a reproducible response towards CO at this temperature. The increase in signal was nearly

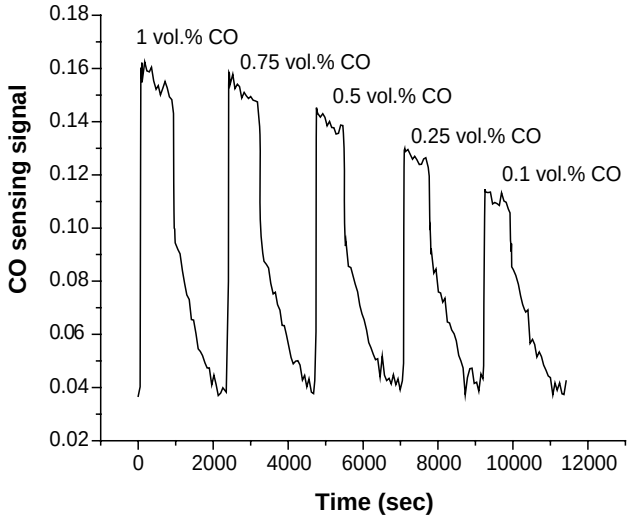

FIGURE 2. Sensing Signal Response Curve of the Au-YSZ Nanocomposite Film upon Exposure to 1, 0.75, 0.5, 0.25 and 0.1 vol.% CO in Air at 500°C

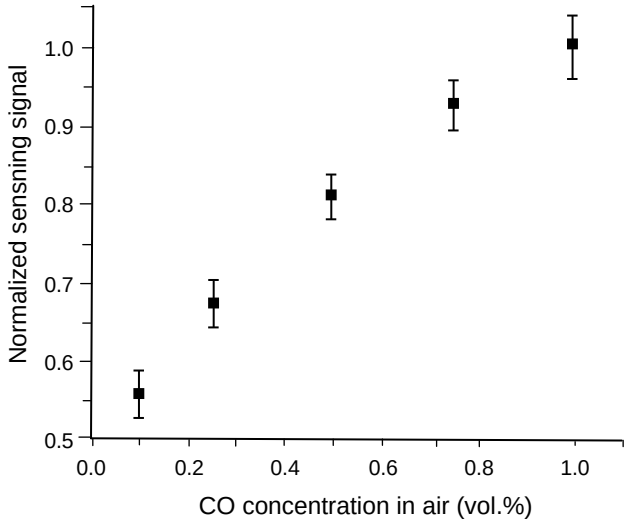

FIGURE 3. Normalized sensing signal change versus CO concentration at 500°C averaged over three separate exposure experiments. The signal at 1 vol.% CO in air was normalized to be unity.

linear over a CO concentration range between 0.1 and 1 vol.%. While this initial data set is promising for the potential development of an optical-based method for the detection of CO under harsh operating conditions, a complete set of reliability tests will be required and are underway to determine the long term operating characteristics of this nanocomposite material.

This behavior of the SPR band, upon exposure to CO, was not observed when using nitrogen as the carrier gas, indicating an oxygen dependent reaction mechanism. Additionally, the SPR band showed no measurable signal change upon exposure to CO at temperatures below approximately 400°C. The oxygen and temperature dependent characteristics, coupled with the oxygen ion conduction properties of the YSZ matrix are indicative of charge transfer reactions occurring at the 3-phase boundary region between oxygen, Au and YSZ, which result in charge transfer into the Au nanoparticles. These reactions are associated with the oxidation of CO, and a corresponding reduction of the YSZ matrix. The chemical reaction induced charge injection into the Au nanoparticles results in the observed blue shift and narrowing of the SPR band.

Conclusions

- The nanocomposite films exhibited an SPR absorption band around 600 nm, which upon exposure to CO in an air ambient at 500°C underwent a reversible blue shift and a narrowing of the full width half maximum.
- The change in the SPR band increased linearly with increasing CO concentration in the range between 0.1 to 1 vol.%.
- The presence of O_2 and sufficiently high temperatures for oxygen ion transport in YSZ were confirmed to be essential elements for the sensing mechanism.
- The behavior of the SPR band upon exposure to CO in the presence of air, was attributed to changes both in the free electron density of the Au nanoparticles and in the interfacial chemistry due to reactions associated with the reduction of the YSZ matrix and oxidation of CO.

FY 2006 Publications/Presentations

1. "Development and Characterization of Au-YSZ Surface Plasmon Resonance Based Sensing Materials: High Temperature Detection of CO", George Sirinakis, Rezina Siddique, Ian Manning, Philip H. Rogers, Michael A. Carpenter, accepted to *J. Phys. Chem. B.*

2. "All-optical Detection of CO and NO_2 at High Temperatures by Au-YSZ Nanocomposites", G. Sirinakis, R. Siddique, P. H. Rogers, I. Manning, M. A. Carpenter, Materials Research Society Meeting, Spring 2006.

III.E.9 Low-Cost, High-Temperature Recuperators for SOFC Fabricated from Machinable Ceramic (Ti_3AlC_2)

Objectives

- Verify corrosion resistance of machinable ceramic for SOFC recuperator application.
- Design and fabricate a proof-of-concept recuperator core.
- Demonstrate proof-of-concept recuperator core performance and durability when exposed to SOFC recuperator operating conditions.

Accomplishments

This project has been selected for award of a Phase I SBIR grant.

Introduction

Achieving low system cost for SOFC technology requires novel approaches to the materials used for the air preheat recuperator. The recuperator is needed to heat up large quantities of air (~6 to 7 times in excess of stoichiometric requirements). The cost of existing recuperator designs is high primarily because of the high cost of the materials used. Heat resistant metal alloys tolerant of gas temperatures up to 1,000°C such as the Inconel-series metal alloys are typically used. These alloys are expensive, difficult to machine, and cannot be cast into near-net shape, leading to bulky heat exchanger designs. Further, the recuperator surfaces exposed to air need to be aluminized to prevent chromia poisoning of the cathode. The aluminizing further increases cost.

A new class of machinable, easily fabricated ceramic materials with good high temperature properties has been discovered (see Figure 1). Examples of this material class that are particularly well suited for the recuperator application are Ti_3SiC_2 and Ti_3AlC_2. The high temperature mechanical and thermal properties, the high temperature stability, and the manufacturability make this class of ceramics an ideal material for high temperature recuperators, specifically for air preheaters for SOFC.

Detlef Westphalen (Primary Contact), John Dieckmann, Anant Singh
TIAX LLC
Acorn Park
Cambridge, MA 02140
Phone: (617) 498-5821; Fax: (617) 498-7206
E-mail: westphalen.d@tiaxllc.com

DOE Project Manager: Charles Alsup
Phone: (304) 285-5432
E-mail: Charles.Alsup@netl.doe.gov

Subcontractors:
3-ONE-2 LLC, Voorhees, NJ

Approach

TIAX will develop an approach for fabrication of SOFC recuperators with machinable ceramic using crossflow and counterflow plate-fin heat exchanger configurations. During the Phase I work, we will first verify the machinable ceramic's corrosion resistance when exposed to SOFC exhaust products at 1,000°C operating temperature. In addition, a small proof-of-concept recuperator core will be designed, fabricated, and tested. Testing will include heat transfer performance testing, maximum-temperature endurance testing, and thermal cycling. This work will establish the feasibility of the material for the intended use in a SOFC recuperator.

FIGURE 1. Examples of Fabricated and Machined Ti_3SiC_2 and Ti_3AlC_2

IV. SECA FUEL CELL COAL BASED SYSTEMS

IV.1 Coal-Based Solid Oxide Fuel Cell Power Plant Development

Objectives

The objective of the Coal-Based Solid Oxide Fuel Cell (SOFC) Power Plant Development program is to develop a cost-competitive, highly efficient, multi-MW SOFC power plant system to operate using coal-derived syngas with near-zero emissions. This project is being merged into an existing FuelCell Energy (FCE) SECA Phase I project with similar SOFC cell and stack development objectives. Specific program technical objectives are as follows:

- Scale up existing SOFC cell area and stack size (number of cells) for large-scale, multi-MW power plant systems.
- Increase SOFC cell and stack performance to maximize power and efficiency operating on coal-derived fuels. Achieve a minimum 50% overall system efficiency (based on higher heating values) from coal-derived fuels.
- Design, build and test proof-of-concept multi-MW SOFC power plant system including gas turbine (>1 MW) for high efficiency with 90% CO_2 separation for carbon sequestration. The testing will be conducted at FutureGen.
- Achieve system cost of <$400/kW for a multi-MW power plant, exclusive of coal gasification and CO_2 separation subsystem costs.

Approach

The project is organized in three phases according to schedule and technical objectives:

- Phase I of the project will focus on cell and stack development activities. This will include scale-up of existing SOFC cell area and stack size (number of cells) and performance improvements. Preliminary design engineering and analysis for multi-MW power plant systems will also be conducted. The Phase I deliverable will be a test demonstration of a representative SOFC stack building block unit on simulated coal syngas.
- Phase II of the project will focus on modularization of the Phase I stack building block units into MW-size modules. Detailed design engineering and analysis for multi-MW power plant systems will also be conducted. The Phase II deliverable will be a test demonstration of a MW-size representative SOFC stack module on simulated coal syngas.
- Phase III of the project will focus on design and fabrication of a proof-of-concept multi-MW power plant including an indirectly heated turbine for high efficiency and CO_2 separation for low emissions. The Phase III deliverable will be long-term testing of a multi-MW size power plant at FutureGen.

Jody Doyon
Vice President, Government Programs Administration
FuelCell Energy, Inc.
3 Great Pasture Road
Danbury, CT 06813
Phone: (203) 825-6125; Website: www.fce.com
E-mail: jdoyon@fce.com

DOE Project Manager: Travis Shultz
Phone: (304) 285-1370
E-mail: Travis.Shultz@netl.doe.gov

Subcontractor:
Versa Power Systems Inc.
900 18th Street, Suite 130
Golden, CO 80401-1887
Website: www.versa-power.com

Accomplishments

- Increased SOFC cell area and number of cells per stack building block unit resulting in ~5-fold increase in stack volumetric power output (SECA Phase I accomplishment).
- Completed SECA Phase I 3 kW SOFC stack test demonstration. The 121-cm^2 area, 112-cell tall stack and system was operated for over 2,000 hours, including seven load transients, two thermal cycles and peak power demonstration.
- Developed preliminary factory cost bill-of-materials for stack and 3 kW system for DOE third party audit validation.

Introduction

FuelCell Energy has been selected by the Department of Energy (DOE) to participate in a multi-phase project for development of very efficient coal to electricity power plants with near-zero emissions. This project is being merged into an existing FCE SECA Phase I project with similar SOFC cell and stack development objectives. As illustrated in Figure 1, FCE is ideally suited for this project based on their experience in various DOE-managed projects to develop commercial large-scale, MW size fuel cell power plants; high-efficiency hybrid fuel cell–turbine systems; and SOFC cells and stacks with their SOFC technology partner, Versa Power Systems (VPS).

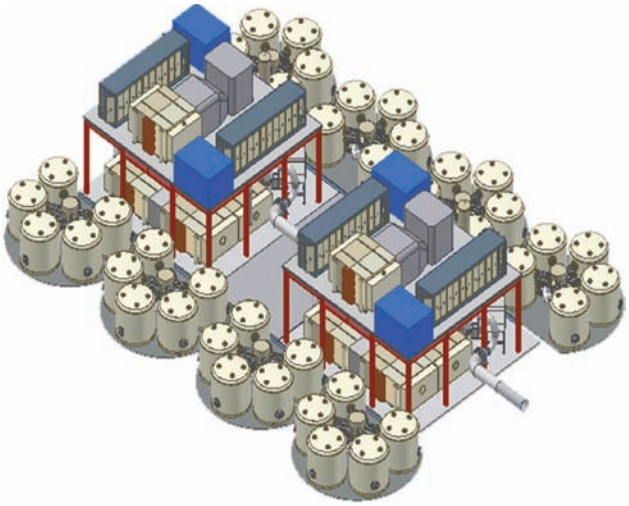

FIGURE 1. Coal-Based, Multi-MW SOFC Power Plant Development

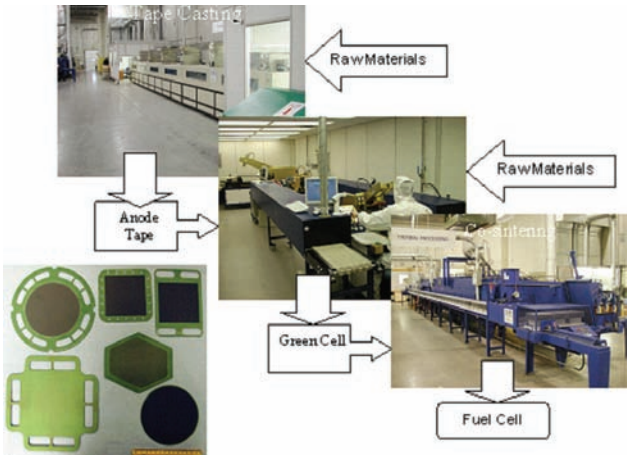

FIGURE 2. Versa Power Systems SOFC Manufacturing

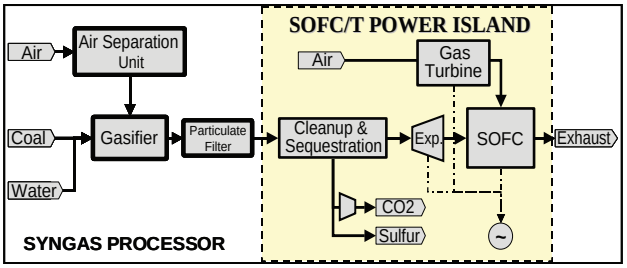

FIGURE 3. Coal-Based, Hybrid SOFC-Turbine Simplified System PFD

The primary objective of the project is to develop an affordable, multi-MW size SOFC based power plant system for utilization of synthesis gas (syngas) from a coal gasifier. One of the key objectives is the development of fuel cell technologies, fabrication processes, manufacturing infrastructure and capabilities for scale-up of SOFC stacks for large multi-megawatt, base-load power generation plants. FCE will use the VPS SOFC cell and stack design currently being developed in an FCE SECA Phase I project as the basis for this project. VPS has well-established processes, quality procedures and equipment for the manufacture of small to intermediate size cells and stacks as depicted in Figure 2. This serves as a solid basis for cell area and stack size scale-up to be conducted in this project. The other key objective is implementation of an innovative system concept in design of a multi-MW power plant with anticipated efficiency approaching 60% of the higher heating value of coal. Figure 3 shows a simplified process flow diagram (PFD) for the proposed power plant system. Combined with existing carbon dioxide separation technologies, the power plant is expected to achieve greater than 50% overall efficiency while emitting near-zero levels of emissions of SOx, NOx, and greenhouse gases to the environment.

Approach

The path forward for development of coal-based multi-MW power plants includes a multi-faceted approach for both SOFC stack module design as well as development of a hybrid fuel cell/gas turbine system. The technical approach consists of an innovative fuel cell stack configuration, fabrication of scaled-up cells, newly developed fuel cell seals, novel implementation of a fuel cell clustering concept and integration of SOFC clusters with a gas turbine. The future development plans include investigation of both fabrication and operational issues related to scale-up of the fuel cell active area. An innovative and patented power cycle will be utilized to achieve very high efficiencies by integration of the fuel cell with an indirectly heated gas turbine. The power plant design is projected to have a factory cost of $400/kW, based on a production capacity of about 1.4 GW/year or twelve 120 MW power plants per year. This cost is very competitive with today's cost of combined cycle technologies.

The project is organized in three phases according to schedule and technical objectives. Details for the three phases are as follows:

Phase I (2-3 years)

- Scale up SOFC cell area and stack height (number of cells) and improve performance for a multi-kW stack building block unit.
- Design a baseline system that meets the program technical objectives.
- Ensure power plant design is consistent with a projected cost of $600/kW for a multi-MW system (exclusive of coal gasification and CO_2 separation subsystem costs).

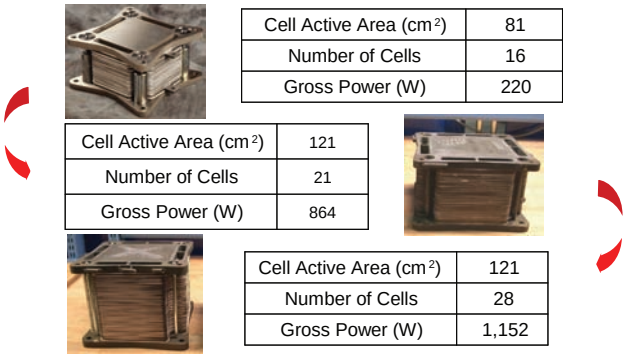

FIGURE 4. SOFC Scale-up in SECA Phase I Project

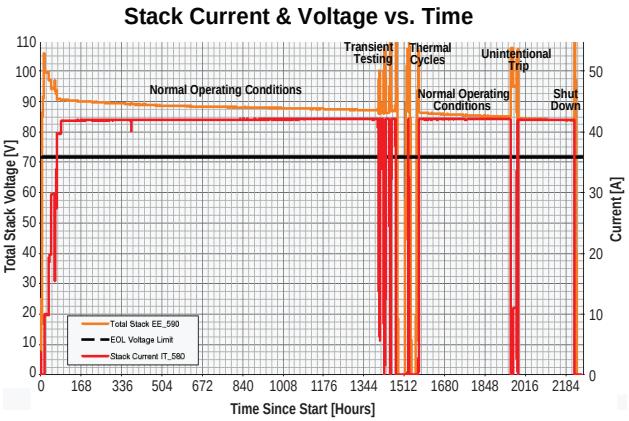

FIGURE 5. SECA 3 kW SOFC System Performance

- Fabricate and validation test a representative stack building block unit on simulated coal syngas.

Phase II (2 years)

- Develop a detailed design and cost analysis for the proposed power plant system that meets program objectives.
- Ensure power plant design is consistent with a projected cost of $400/kW for a multi-MW system (exclusive of coal gasification and CO_2 separation subsystem costs).
- Fabricate and validation test a representative fuel cell module building block unit for the multi-MW power plant on simulated coal syngas.

Phase II (5 years)

- Complete detailed design for multi-MW power plant system that meets program objectives.
- Procure and fabricate SOFC stack and system components and assemble proof-of-concept multi-MW power plant system including gas turbine (>1 MW).
- Locate coal gasifier site and integrate multi-MW power plant.
- Conduct long-term (~25,000 hours) test demonstration of multi-MW power plant system on coal-based syngas meeting program technical objectives for performance (power, efficiency), durability (load transients and thermal cycles), degradation and cost.

Results

FCE has been engaged in a DOE-managed SECA Phase I project to develop a 3-10 kW SOFC power plant system since April, 2003. FCE has been asked to re-scope this project's technical objectives to merge with the Coal-Based SOFC Power Plant Development program objectives. This request is based on similarities of the technical objectives for cell and stack development in both programs, as well as FCE's experience with commercial MW size fuel cell power plant development, high-efficiency hybrid fuel cell–turbine systems and SOFC cell and stack development with VPS (see Figure 1). Much progress has been made in the SECA Phase I project on cell and stack scale-up and increased performance. As shown in Figure 4, increased SOFC cell area and number of cells per stack building block unit has provided an approximate 5-fold increase in stack volumetric power output. The FCE team recently completed a 3 kW test demonstration as part of the SECA program requirement with a stack tower configuration containing five of these scaled-up SOFC stack building block units. Figure 5 shows results of this milestone performance test that included seven load transients, two full thermal cycles and peak power demonstration. Initial data analysis indicates the test exceeded all SECA program performance requirements. Results are being compiled for DOE review and audit by a third party expert. A stack factory cost estimate has been developed for DOE auditors to review. The stack cost estimate is better than that required by the SECA program metric.

Summary

- FuelCell Energy (FCE) has been selected by the Department of Energy (DOE) to participate in a multi-phase project for development of very efficient coal to electricity power plants with near-zero emissions. This project is being merged into an existing FCE SECA Phase I project with similar SOFC cell and stack development objectives.
- The primary objective of the project is to develop an affordable, highly efficient, multi-MW size SOFC based power plant system for utilization of syngas from a coal gasifier.
- FCE is ideally suited for this project based on their experience with commercial MW size fuel cell power plant development, high-efficiency hybrid

fuel cell–turbine systems and SOFC cell and stack development with their technology partner, Versa Power Systems.

- Accomplishments in FCE's SECA Phase I project synergistic with this project include expanded manufacturing process capabilities and scale-up of SOFC cell area and stack height, resulting in ~5-fold increase in volumetric power density.
- A SECA Phase I 3 kW SOFC stack test demonstration of a system containing scaled-up stack units was completed as final validation of the scale-up process and components.
- The FCE team developed a preliminary factory cost bill-of-materials for the stack and 3 kW system to be audited by a DOE third party expert. Initial assessment indicates stack and 3 kW system costs meet or exceed SECA Phase I program requirements.

FY 2006 Publications/Presentations

1. "Coal Based Large SOFC/T Systems", H. Ghezel-Ayagh, J. Doyon, Fuel Cell Energy Inc; Paper presentation at the 2006 Fuel Cell Seminar on November 13-17, Honolulu, Hawaii.

2. "Development of Solid Oxide Fuel Cells at Versa Power Systems", B. Borglum, E. Tang, M. Pastula, R. Petri, Versa Power Systems; Paper and presentation at the 2006 Fuel Cell Seminar on November 13-17, Honolulu, Hawaii.

IV.2 Solid Oxide Fuel Cell Coal-Based Power Systems

Objectives

- Develop and optimize a design of an integrated gasification fuel cell (IGFC) power plant incorporating a solid oxide fuel cell (SOFC)/gas turbine (GT) hybrid system that will produce highly efficient, environmentally benign and cost-effective electrical power from coal.
- Define and design a proof-of-concept system (POC) derived from the IGFC design and demonstrate operation with required performance characteristics.
- Resolve identified barrier issues concerning the SOFC and develop and demonstrate a SOFC building block for multi-MW system applications.

The project consists of three phases. Phase I of the project focuses on designing and estimating the cost of the IGFC system as well as the proof-of-concept system and resolving barrier issues relating to the SOFC, culminating in the demonstration of a fuel cell stack having the features suitable for use in a building block stack for multi-MW applications. Phase II involves optimizing and finalizing the IGFC and proof-of-concept designs and costs and testing a fuel cell module under hybrid conditions as a demonstration of the building block stack for the IGFC. Phase III aims at field-testing of a proof-of-concept system for extended periods to validate integration and demonstrate required performance characteristics.

Approach

Phase I

- Establish a baseline design of an IGFC system.
- Define a POC system.
- Identify the requirements of the systems, develop suitable system design, model and analyze the systems to evaluate performance and compare system performance with requirements for gap closure and system optimization.
- Conduct a cost estimate study to assess system costs.
- Evaluate a suitable stack design for operation under hybridized coal gas conditions using the Solid State Energy Conversion Alliance (SECA) technology as the baseline.
- Address critical technological issues concerning SOFC fabrication/manufacturing, scaleup, hybridized coal gas operation, and life/degradation.
- Build and test a stack having the features suitable for incorporation into a SOFC/GT system for IGFC applications.

Nguyen Minh (Primary Contact), Jim Powers
GE Energy, Hybrid Power Generation Systems
19310 Pacific Gateway Drive
Torrance, CA 90502-1031
Phone: (310) 538-7250; Fax: (310) 538-7204
E-mail: nguyen.minh@ge.com

DOE Project Manager: Travis Shultz
Phone: (304) 285-1370
E-mail: Travis.Shultz@netl.doe.gov

Accomplishments

Phase I of the project was initiated in October 2005, and the key accomplishments achieved to date are summarized below.

- Sixteen system design options for an IGFC plant were identified and evaluated. Two concepts were selected as the main go-forward options, with two other identified as viable risk-mitigation approaches.
- Initial IGFC analyses indicate that 50% higher heating value (HHV) efficiency with 90% CO_2 isolation is achievable.
- Product requirements for an IGFC plant were defined based on market data and DOE requirements.
- Key parameters that determine sintering behavior of large cells were identified.

Future Directions

Continue activities defined in the Phase I project plan, including:

- Develop and evaluate IGFC and POC system design concepts.
- Develop methodologies and models and conduct cost estimate of baseline IGFC system.
- Fabricate large-area cells. Modify and optimize fabrication process parameters for producing large-area cells.
- Measure SOFC performance maps over pressure and fuel composition ranges of interest.
- Establish baseline SOFC degradation rate in coal-based hybrid conditions and develop mitigation plan.
- Build and operate stacks incorporating large-area cells with simulated coal gas.

Introduction

This project aims at developing a highly efficient, environmentally benign, and cost-effective multi-MW solid oxide fuel cell (SOFC) based power system operating on coal. The project will be a critical step towards the overall goal of realizing large (>100 MW) fuel cell power systems that will produce electrical power at greater than 50% overall efficiency (HHV) from coal to AC power, including CO_2 separation preparatory to sequestration. The overall approach for this project is to integrate the SOFC with a gas turbine (GT) in a SOFC/GT hybrid power island. This power island is the primary power generation section of an overall IGFC coal-based power plant. This hybridization approach will provide a step-change improvement in performance over today's technology and a system efficiency greater than that achievable by either a simple cycle SOFC IGFC or an integrated gasification combined cycle (IGCC). The project consists of three phases and the key features of each of the phase are summarized in Figure 1.

Approach

The project is structured around three phases to address the system design of a cost-effective >100 MW IGFC system; advancement of SOFC fuel cell technology needed to meet the system requirements; validation of the technology through early component tests; and a proof-of-concept (POC) demonstration testing.

The focus of Phase I of the project is to develop the design of an IGFC power plant based on SOFC/GT hybrids and a proof-of-concept of that system, to resolve critical technological issues of the SOFC, and to demonstrate a fuel cell stack having the features required for multi-MW IGFC applications. To support this objective, the Phase I work concentrates on two main areas: system/product development and stack technology development.

- **System design development.** This work aims to establish a baseline design of an IGFC system and to define a proof-of-concept system. The effort will focus on identifying the requirements for the systems, developing suitable system designs, modeling and analyzing the systems to evaluate performance, and comparing system performance with requirements for gap closure and system optimization. A cost estimate study will be conducted to assess system costs.
- **Stack technology development.** This work aims to develop a high-performance, low-cost SOFC stack suitable for hybridization with a GT for multi-MW IGFC systems. The effort will involve evaluating a suitable design for the stack under hybridized coal gas conditions and addressing critical technological issues concerning fabrication/manufacturing scale-up, hybridized coal gas operation, and life/degradation. A stack having the features suitable for incorporation into a SOFC/GT system for IGFC applications will be fabricated and tested.

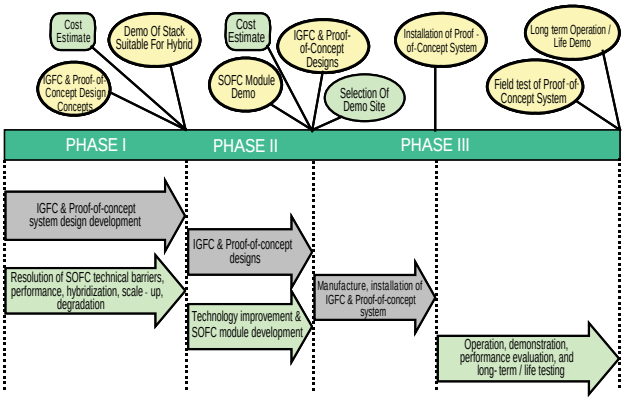

FIGURE 1. Overall Project Summary

Results

System Design Development

A survey of IGFC systems reported in the literature was conducted to establish the background for developing potential conceptual designs in this project. From the survey and brainstorming sessions, sixteen system design options for an IGFC plant were identified. In order to evaluate the system efficiency and CO_2 isolation performance potential of the concepts, simplified ASPEN models were created for several concepts. These models did not encompass the gasification system but used it as an interface (i.e., syngas and steam flows); therefore, certain assumptions had to be made. The results of the models indicate that 50% HHV efficiency with 90% CO_2 isolation is achievable for several IGFC designs. Based on these preliminary results, two concepts were selected as the main go-forward options, with two others identified as viable risk-mitigation approaches. The requirements for the IGFC conceptual system design have been established:

- 600 MW net power
- 50% HHV efficiency
- 90% CO_2 isolation
- < $400/kW for power producing blocks
- Bituminous coal, 10% moisture

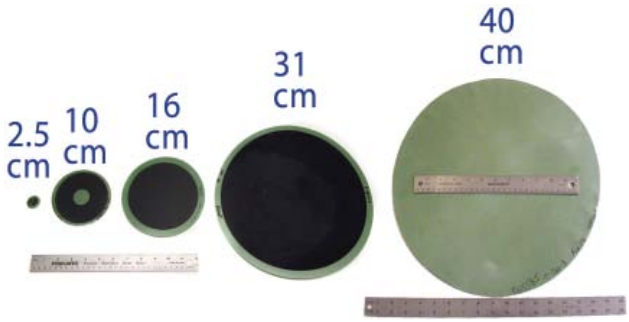

FIGURE 2. Large-Area SOFCs

Stack Technology Development

The tape calendering process has been used to fabricate SOFC cells. Using this process, cells sizes up to 40 cm have been successfully demonstrated (Figure 2). In terms of scale-up, a critical issue in manufacturing large-area cells by tape calendering is controlling the failure rate (yield) during the critical firing step. During the firing step, as the tape changes from the plastic to the brittle state, the probability of failure increases with increase in cell size. During firing, major causes for cell cracking include thermal gradients and stresses in the sintering tape; frictional forces between the sintering tape and non-sintering setter plate; and changes in the strength of the tape as a function of temperature. An improved understanding of the influence of these parameters is very important for process design and optimization for successful large-area cell fabrication. A list of key factors affecting the firing behavior of tapes has been compiled. Several parameters were subsequently identified based on ease of experimentation, and a screening design of experiments to understand the influence of these factors on firing yield was developed.

Conclusions and Future Directions

In the system development area, IGFC system concepts have been identified that are capable of meeting the DOE requirements of 50% HHV efficiency and 90% CO_2 isolation. These concepts are similar in nature to previously evaluated IGFC designs. Near-term system work focuses on developing detailed conceptual designs of the IGFC system and conducting preliminary system cost estimates.

In the stack development area, key factors affecting cell manufacturing scale-up by tape calendaring were identified, and a screening design of experiments was initiated. Near-term SOFC stack work focuses on developing a suitable stack design for IGFC system applications, optimizing the tape calendering process for manufacturing large-area cells, making cells and stacks and testing performance and degradation in pressurized coal-gas conditions.

IV.3 Coal Gas Fueled SOFC Hybrid Power Systems with CO_2 Separation

Objectives

- Optimization of the Siemens DELTA-N solid oxide fuel cell (SOFC) and scale-up of its dimensions for pressurized operation.
- Verification by test of cell, stack, and module on coal-derived syngas.
- Corroboration of the technical and economic feasibility of a >50% efficient SOFC-based large capacity (>100 MWe) coal-fueled baseline power plant.
- Test on coal syngas of a fully functional 50% efficient proof-of-concept (POC) unit of lesser multi-MWe capacity.

Approach

- Analytical modeling to optimize the DELTA-N cell for pressurized operation.
- Develop a viable cell manufacturing processes and fabricate cells.
- Verify by parametric testing cell performance and durability.
- Analyze, design, and develop a fuel cell stack.
- Prepare the preliminary design of a module aggregating fuel cell stacks.
- Test a thermally self-sustaining fuel cell stack on simulated coal syngas at the power system operating pressure.
- Identify and analyze cycle concepts.
- Select a baseline system cycle.
- Prepare the conceptual design for the baseline system.
- Corroborate via independent audit the technical and economic feasibility of the baseline system.
- Develop the conceptual design, performance analysis, and cost analysis for the POC system.

Joseph F. Pierre
Manager, Government Programs
Siemens Power Generation
Stationary Fuel Cells
1310 Beulah Road
Pittsburgh, PA 15235
Phone: (412) 256-5313; Fax: (412) 256-2012
E-mail: joseph.pierre@siemens.com

DOE Project Manager: Don Collins
Phone: (304) 285-4156
E-mail: Donald.Collins@netl.doe.gov

Accomplishments

- Evaluated eight baseline system candidate cycle concepts.
- Developed a figure-of-merit system with which the candidate systems are to be compared.
- Identified a preferred cycle configuration and a back-up cycle configuration.
- Modeled nine cell cross section designs and solved for temperature and thermal stress fields.
- Identified and initiated the evaluation of multiple stack designs and configurations.

Future Directions

- Define baseline cycle.
- Execute cell and stack performance test.
- Select cell configuration.
- Complete the conceptual design for the module.

Introduction

Siemens Power Generation Stationary Fuel Cells (SFC) will develop a MWe-class pressurized solid oxide fuel cell/gas turbine (PSOFC/GT) hybrid power system to operate on coal-derived synthesis gas and demonstrate operation at greater than 50% electrical efficiency (basis: higher heating value [HHV] of coal) with greater that 90% CO_2 capture. The system will be scalable to sizes greater than 100 MWe output and, when offered in commercial quantities, will have a target cost of $400/kWe including any extraordinary costs of integration to the balance-of-plant. Corroboration of the technical and economic feasibility of the PSOFC/GT hybrid power system will be achieved through the conceptual design of a large (>100 MWe) baseline power plant and the subsequent design, development, fabrication, and test of a proof-of-concept (POC) system. The POC will have an identical cycle, be of multi-MWe capacity, and demonstrate an electrical efficiency >50% (coal HHV).

The proposed cycle concept couples an oxygen-blown coal gasification system with an ion transfer membrane (ITM). Chosen for performance and simplicity, the candidate cycle uses a high-pressure ratio gas turbine to supply air to multiple SOFC modules. The ITM processes remove oxygen from the SOFC cathodes to supply it for power plant needs. The SOFC modules will be based upon SFC's DELTA-N cell design, developed under its SECA program. The cell geometry will be optimized for operation at elevated pressure.

Cell and stack performance and durability will be verified via performance testing at elevated pressure.

Approach

Several candidate cycle configurations will be developed that could be implemented at the >100 MWe PSOFC/GT power system level. Each configuration will be modeled to estimate electrical efficiency of the system and values of key operating parameters (e.g. mass flow rate, temperature, and pressure) for major components. Also to be considered in addition to system efficiency are cost as reflected by system complexity and the potential for POC testing at lesser multi-MWe capacity.

SFC is developing under the SECA program a new cell and stack design that combines the seal-less stack feature and a cell with a flattened multi-connected tubular cathode with integral ribs. This new design has a closed end similar to the Siemens circular tubular design. Analytical modeling will be utilized to optimize the number and dimensions of ribs for maximum power, the distribution of fuel flow and air flow, and structural stability against thermal stresses during operation from atmospheric to elevated pressure. Additionally, active length and width will be optimized based on practical limitations for cell fabrication and generator utility. The pressure optimized DELTA-N cells will be bundled into an array or bundle (stack) of electrically connected fuel cells forming a monolithic structure. A typical stack will consist of bundles connected in series arranged in parallel rows. The proposed SOFC stack concept is based on technology that has been developed and proven as part of previous generator design and testing programs, a series of atmospheric and pressurized bundle tests, and the 220 kWe pressurized SOFC generator designed, built and operated in the pressurized PSOFC/GT hybrid power system. Further innovation will be required, particularly in the development of low-cost ceramic materials, net shape component fabrication, and a high power density stack configuration to reduce the overall cost of the system. Cell and stack performance at elevated performance will be characterized via a series of single and multi-cell tests.

Results

Eight candidate cycles for the baseline system have been identified and evaluated. A figure-of-merit system for selecting the preferred candidate was developed and employed in a rigorous down-selection process. A preferred baseline system configuration along with a backup cycle configuration was identified. The preferred baseline system, shown in Figure 1, meets the efficiency objective, employs the seal-less SOFC cell and module configuration, and has the potential to use a low temperature, low complexity polymer membrane CO_2 separation system.

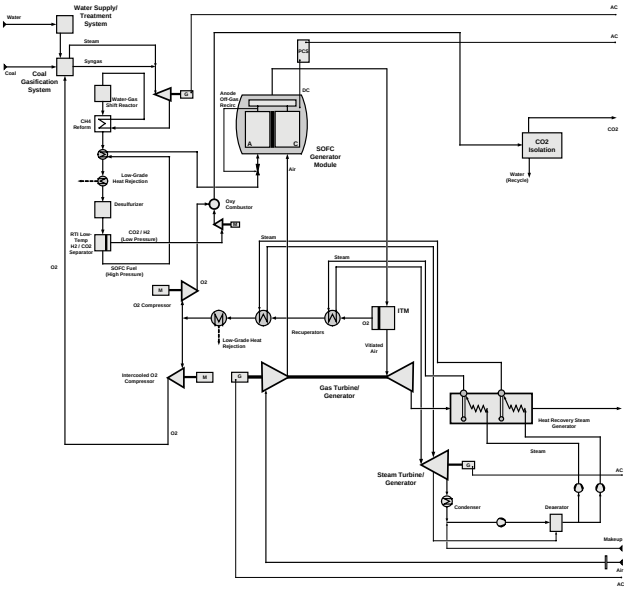

FIGURE 1. Baseline System Configuration

Nine cell cross-sections were modeled and solved for temperature and thermal stress fields. Potential causes for stress concentration were identified for the internal up-down air flow configuration.

A number of different SOFC stack configurations were developed and are under evaluation. These concepts include once-through, up-down, and DELTA-N cells with air feed tubes, respectively. These respective concepts, in the early stages of development, include a number of innovative features aimed at reducing the manufacturing and assembly costs and providing increased power density.

Conclusions

Systems analysis indicates the performance objectives (>50% electrical efficiency, net ac/coal HHV) can be achieved by a system employing the separated anode-cathode streams or the seal-less configuration. The traditional seal-less stack configuration will utilize a less complex balance-of-plant, which is expected to translate into lower system cost.

V. FUEL CELL SYSTEMS

V.1 Direct Fuel Cell/Turbine Power Plant

Objectives

The overall project goal is to develop ultra-high efficiency power plants based on Direct FuelCell/Turbine® (DFC/T®) technology. The specific objectives are:

- Develop the conceptual design of multi-megawatt (MW) hybrid DFC/T systems with efficiencies approaching 75% (natural gas fuel), and with sulfur and nitrogen oxide emissions < 0.01 lb/million BTU.
- Verify commercial viability of the DFC/T systems for near-term deployment.
- Design a packaged sub-MW DFC/T system for distributed power generation.
- Verify the potential benefits of hybrid technology and show its readiness for commercialization by the grid-connected field demonstration of a sub-MW DFC/T power plant at a customer site.

Accomplishments

- Completed preliminary design of a 40-MW DFC/T hybrid system, including site plan and fuel cell module layouts. Estimated plant capital cost and performance characteristics of the 40-MW power plant.
- Completed detailed design of the sub-MW class DFC/T (Alpha) unit, including equipment and piping layouts (isometric drawings), structural supports, process instrumentation, DC-to-AC power conditioning, and power distribution drawings.
- Developed the process control system design and software, including details of microturbine operation, power plant start-up/shutdown strategies, safety alarms, human machine interface (HMI) display screens, programmable logic controller (PLC) program codes, and the control philosophy for operation of the Alpha DFC/T unit.
- Completed fabrication of the Alpha DFC/T unit by integration of a full-size 250 kW DFC stack with a Capstone C60 microturbine. Performed conditioning and checkout tests of the fuel cell stack module, and the acceptance tests of the key balance-of-plant (BOP) equipment. Integrated the fuel cell stack module with the balance-of-plant equipment.
- Completed factory acceptance testing (in grid-connect mode) of the Alpha DFC/T packaged power plant in FuelCell Energy, Inc. (FCE) facilities in Danbury, CT, achieving 323 kW net AC output at 56% electrical efficiency (lower heating value, LHV-based). Conducted emission tests showing that the Alpha unit met California Air Resources Board's (CARB) 2007 standards/requirements.
- Completed installation and commissioning of the Alpha unit at the Montana demonstration site. Initiated the operation of the unit at Billings Clinic, which is a large regional hospital in Billings, MT.

Hossein Ghezel-Ayagh (Primary Contact), Dilip Patel, Jim Walzak, Fred Michelson, S. Tobias Junker
FuelCell Energy, Inc.
3 Great Pasture Road
Danbury, CT 06813
Phone: (203) 825-6048; Fax: (203) 825-6273
E-mail: hghezel@fce.com

DOE Project Manager: Travis Shultz
Phone: (304) 285-1370
E-mail: Travis.Shultz@netl.doe.gov

Subcontractors:
Capstone Turbine Corporation, Chatsworth, CA
Montana State University, Bozeman, Montana
CTA Architects Engineers, Billings, Montana

Introduction

FCE's DFC/T hybrid system concept is based on integration of the company's Direct FuelCell® with a gas turbine. A simplified process flow diagram of the DFC/T system is shown in Figure 1. The power plant design utilizes a heat recovery approach for extraction of heat from the BOP. The fuel cell plays the key role by producing the larger share of the power (>80%). The gas turbine is utilized for generation of additional power by recovering the fuel cell byproduct heat in a Brayton cycle, as well as for providing the air for the fuel cell operation.

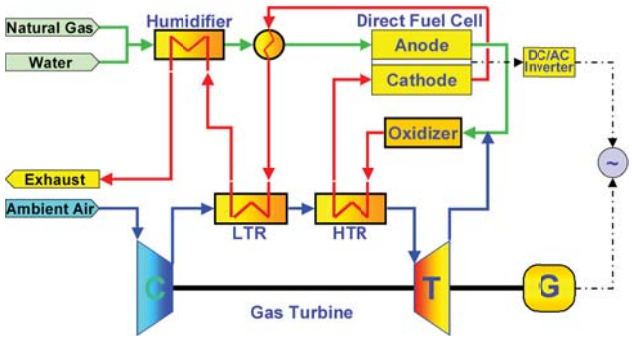

FIGURE 1. DFC/T® Ultra High Efficiency System Concept

Features of the DFC/T system include electrical efficiencies approaching 75% on natural gas (60% on coal gas), direct reforming internal to the fuel cell, minimal emissions, reduced carbon dioxide release to the environment, simple design, and cost competitiveness with existing combined cycle power plants.

Approach

The DFC/T system concept was initially implemented in a power plant test facility (pre-Alpha power plant) by integration of a 250 kW DFC stack and a Capstone microturbine. The focus of the pre-Alpha testing was the verification of the DFC/T concept, development of critical system components, and acquisition of design information for development of power plant products. The results from the proof-of-concept tests established the foundation for the design of the packaged sub-MW units.

The hybrid technology development plan includes the design, construction, and testing of two sub-MW DFC/T units. The tests will demonstrate grid-connected operations and help assess the efficiency potential of the sub-MW plants, while providing valuable data on integration and operation of DFC/T power plants. The first unit, "Alpha", was factory tested at FCE headquarters in Danbury, CT and later shipped to a demonstration site in Montana. The test results and experience from the Alpha unit are being used to refine the design for the "Beta" unit, which will undergo six months of demonstration testing at a demonstration site to be selected.

Results

Multi-MW Power Plant Design:

The preliminary design of a 40 MW power plant hybrid system concept was completed. An overall layout/plot plan of the 40 MW plant is shown in Figure 2. The site is approximately 273 ft x 325 ft in size. The design is based on a scalable approach using FCE's existing M-10 (MW-scale) fuel cell modules in a cluster arrangement. The fuel cell cluster design has five M-10 modules in a cluster with common distribution piping for the fuel and oxidant gases. Based on the scalable overall plant design concept, the plant is arranged in three sections (power blocks) in addition to the centralized equipment. Each power block consists of two clusters of fuel cell modules together with supporting equipment. The centralized equipment, which supports all three sections, includes a gas turbine, an anode gas oxidizer and other common site equipment such as a fuel clean-up subsystem and a water treatment subsystem. The gas turbine incorporated in the 40 MW plant design is a Man Turbo Model 1304-11 (MAN Turbomachinery, Inc.). Key characteristics of the gas turbine include: pressure ratio of 8 and turbine inlet temperature of about 1800°F.

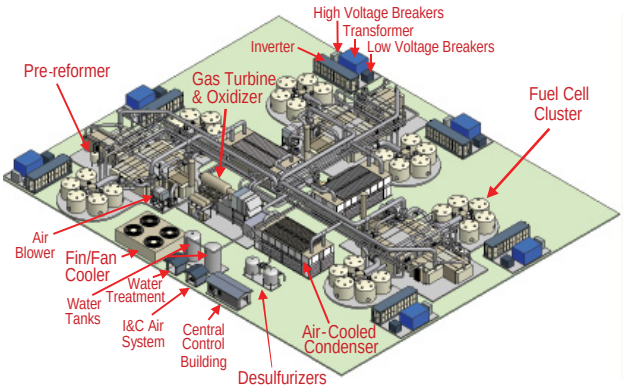

FIGURE 2. 40-MW DFC/T® Power Plant Layout and Site Plan for Near-Term High Efficiency Power Generation

Sub-MW Power Plant Design And Demonstrations:

Fabrication of the Alpha sub-MW DFC/T hybrid power plant, based on the detailed design developed, was completed. The Alpha unit consists of three main sections: 1) mechanical BOP, 2) DFC stack module, and 3) electrical BOP; all three sections are transportable as separate units. The modular design of the power plant sections allows for ease of installation and service. The power-conditioning module of the Alpha unit includes a DC-to-AC inverter and a tie-in connection for the microturbine. Fabrication of a 250 kW stack module for integration in the Alpha DFC/T was completed at FCE's Torrington (CT) manufacturing plant. The conditioning and checkout tests of the fuel cell stack module were performed prior to its integration with the BOP equipment, including a 60 kW Capstone microturbine.

Factory testing of the Alpha unit was conducted in FCE's Danbury (CT) facility. The factory testing included grid-connected operation, validation of plant performance, and emission tests. The Alpha DFC/T hybrid power plant achieved a power generation level of over 320 kW at 56% fuel efficiency based on the lower heating value (LHV) of natural gas. Figure 3 shows a computer screen shot taken during the power plant operation and documenting the plant performance. Preliminary tests indicated that the Alpha unit successfully met CARB 2007 emission standards for NO_x, carbon monoxide, and volatile organic compounds (VOC) at rated power. Table 1 presents a summary of the emission test results. Upon successful completion of the factory testing, the Alpha power plant was shipped to the Montana demonstration site.

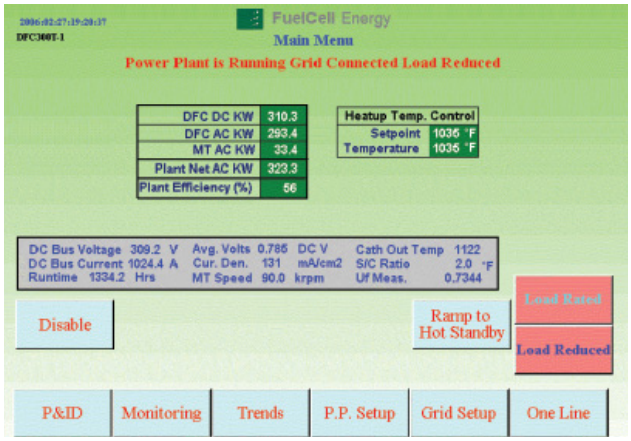

FIGURE 3. Alpha Sub-MW DFC/T® Power Plant Performance Achieved during Factory Tests in FCE's Danbury (CT) Facility

TABLE 1. Alpha DFC/T Packaged Power Plant Met California Air Resources Board's 2007 Emission Standards

	lb/MW-hr		
	NOx	VOC	CO
DFC/T *	0.004	0.002	0.075
CARB-'07 weighted emission limit	0.07	0.02	0.1

* Tests on 02/21/06, Average 307 kW

The Alpha unit was then installed at Billings Clinic in Montana for field demonstration tests (Figure 4). The unit continues to generate power at high efficiency for the Billings Clinic. Design of the second sub-MW DFC/T unit, "Beta", has been initiated. Design input based on operational data, and lessons learned during Alpha unit factory tests and operations at Montana demonstration site are being incorporated into the design of the Beta power plant.

Conclusions and Future Directions

The fabrication of the Alpha hybrid power plant based on the detailed design developed, and factory testing at FCE's Danbury facilities were completed. The factory tests were performed for more than six months, including the initial performance and control checkout tests. During the grid-connected operation, the Alpha unit achieved 323 kW net AC output at 56% electrical efficiency (based on natural gas LHV) – a record-setting performance in a sub-MW class power plant. The Alpha unit also met CARB 2007 emission standards in preliminary emission tests. The Alpha power plant was shipped to the Montana demonstration site. It was installed at Billings Clinic, restarted and successfully placed in operation.

FIGURE 4. Alpha DFC/T® Unit after Installation at Billings Clinic, the Montana Demonstration Site

A scalable approach for the multi-MW plant design based on fuel cell clusters of the existing 1-MW (M-10) modules has been developed. Preliminary design of a 40-MW hybrid system for near term deployment was completed.

The following future activities are planned under the project:

- Analyze Alpha unit data and implement design improvements based on the Alpha unit operational data and performance, in the second sub-MW DFC/T (Beta) unit.
- Complete demonstration site selection, review and site preparation for the Beta unit.
- Fabricate the Beta DFC/T unit (including fabrication, conditioning and acceptance tests of the fuel cell module), perform factory tests of the integrated Beta unit, and conduct six-month field demonstration test of the unit at the selected site.

FY 2006 Publications/Presentations

1. Hossein Ghezel-Ayagh, S. Tobias Junker, Dilip Patel, Fred Michelson, Jim Walzak, and Hansraj Maru, "Development of SubMW Hybrid Direct FuelCell/Turbine Power Plant", Presented at Fuel Cell Seminar 2005, Palm Springs, CA, November 14-18, 2005.

2. Direct Fuel Cell/Turbine Power Plant, Semi-Annual Technical Progress Report (November 1, 2005 through April 30, 2006), submitted to DOE by FCE, Contract No. DE-FC26-00NT40798.

3. H. C. Maru and H. Ghezel-Ayagh, "Direct Carbonate Fuel Cell – Gas Turbine Combined Cycle Power Plant", Presented in European Fuel Cell Forum, Lucerne, Switzerland, July 5-8, 2005.

V.2 High Temperature Solid Oxide Fuel Cell Development

Objective

- To complete the development of tubular SOFC technology to the point of acceptable risk for private sector commercialization.

Approach

- Verification of cell performance and durability.
- Development, qualification, and implementation of cell manufacturing processes at rates commensurate with commercial production.
- Development, qualification, and implementation of lower cost bundling techniques.
- Development of a reduced-cost module.
- Design of cost effective balance-of-plant systems and components.
- Design, fabrication, and operation of pre-commercial SOFC power systems.

Accomplishments

- Established the SFC200 as the market entry product.
- Achieved more than 10,000 hrs of operation with minimal degradation for an atmospheric plasma spray (APS)-manufactured SOFC.
- Completed more than 10 thermal cycles with negligible voltage loss for an APS-manufactured cell.
- Optimized the design and reduced the cost of certain module components including air feed tubes, stack reformer boards, and high purity insulation.
- Developed, optimized, and designed advanced, cost-effective balance-of-plant concepts.
- Completed cell and bundle production for the first two SFC200 SOFC power systems.
- Completed fabrication of the first SFC200 SOFC power system.
- Initiated the factory acceptance test for the first SFC200 SOFC power system.
- Successfully restarted the SFC100.

Future Directions

- Develop a lower-cost air electrode tube making process.
- Identify and qualify low-cost cell materials.
- Qualify the plasma spray cell manufacturing processes and equipment.
- Demonstrate control and reproducibility of the bundling process.
- Qualify lower-cost bundling processes.
- Define and evaluate advanced module design concepts.
- Complete the first SFC200 factory acceptance test.
- Deliver, install, and operate at the customer site the first SFC200.

Joseph F. Pierre
Manager, Government Programs
Siemens Power Generation
Stationary Fuel Cells
1310 Beulah Road
Pittsburgh, PA 15235
Phone: (412) 256-5313; Fax: (412) 256-2012
E-mail: joseph.pierre@siemens.com

DOE Project Manager: Don Collins
Phone: (304) 285-4156
E-mail: Donald.Collins@netl.doe.gov

Introduction

The objective of the Cooperative Agreement between the U.S. Department of Energy (DOE) and Siemens Power Generation Stationary Fuel Cells (SFC) is to complete the development of SFC's tubular solid oxide fuel cell (SOFC) to the point of acceptable risk for commercialization. Our efforts are focused primarily on cost-reduction activities in order to drive down the cost of the SFC200 to commercially acceptable levels. In support of this commercial focus our technology development and cost-reduction efforts are categorized into five main areas; cells, bundles, the SOFC module, balance-of-plant (BOP), and systems. Within each of the main areas, we have prioritized our development efforts to focus on those activities that have the greatest impact on product cost and have a high potential for success without compromising system performance, reliability, or safety.

The Cooperative Agreement will culminate in the field test at the customer site of a SOFC combined heat and power system (identified as the SFC200).

Approach

The goal of achieving commercially competitive SOFC power systems requires low-cost cell manufacturing, and cost effective fabrication and assembly of SOFC bundles, modules, and BOP systems. Activities under the cell manufacturing and

development task are directed to improve and optimize the raw materials, simplify cell processing conditions, and develop and qualify lower cost manufacturing techniques. New materials and the latest manufacturing techniques and processes are qualified via a series of electrical performance and mechanical stability tests.

In the bundling area, our efforts are focused on the development of commercially viable cell-to-cell and bundle-to-bundle connections, respectively, that are amenable to automation. Qualification and verification of the latest cell and bundle connections, improved bundling processes and process conditions, and enhanced bundling techniques are accomplished via multi-cell and bundle tests, respectively.

Our SOFC module design process ensures that all objectives related to the functionality and performance, cost, ease of assembly, and serviceability are incorporated early in the design process. Extensive use of computational fluid dynamics is employed to validate the designs, and where appropriate, the latest module design concepts are incorporated into and validated via bundle tests.

Many of the components in the SFC200 power system BOP have unique functional requirements that often require a one-of-a-kind component or subsystem. These items are considered to be strategic because an SOFC power system cannot be viably configured without them. When strategic equipment items are identified and/or developed, we verify by test their functionality and cost implications on the SFC200.

Lastly, the implementation of the latest cell and module technology and the most recent cost reduction features are incorporated into fully integrated SOFC power system field tests for verification and validation.

Results

Our market entry was defined to be a 125 kWe combined heat and power system (SFC200). At its nominal rating, the SFC200 will deliver a net 125 kWe AC to the grid at an electrical efficiency of ~45% (lower heating value). Thermal output in the form of hot water is anticipated to be ~100 kWt, thus achieving an overall efficiency of ~80%. In support of this, our development and cost reduction efforts are categorized into five areas: cells, bundles, the SOFC module, balance-of-plant, and systems.

Significant progress in the cell manufacturing and development area was made in the past year as evidenced by the following:

- The air electrode tube extrusion process was simplified resulting in a reduced rejection rate and thus an improved tube-making yield rate.
- Specifications and preparation techniques for lower cost plasma spray electrolyte and plasma spray fuel electrode powders, respectively, were developed, tested, verified, documented, and implemented into the cell manufacturing process.

Cells manufactured using these latest specifications and techniques demonstrated electrical performance equal or superior to cells manufactured via the electrochemical vapor deposition (EVD) process. The cell manufacturing campaign for the first two SFC200s was successfully completed.

In the bundling area, efforts were directed to the development of cell-to-cell and bundle-to-bundle connections, respectively, that are amenable to automated production. These efforts resulted in:

- The development of a second generation cell-to-cell connection.
- The successful demonstration, via multi-cell and bundle tests, of the mechanical and structural integrity of the new cell-to-cell connection.
- The development of an advanced bundle-to-bundle welding technique that shows great promise for future automation.

The bundles for the first two SFC200s were successfully fabricated using the latest manufacturing and production techniques.

The design of the SOFC module for the SFC200 was successfully competed. The module for the first SFC200 was assembled and assembly of the module for the second SFC200 is underway.

Numerous innovative concepts that will result in a lower cost, more reliable module were tested in a series of 5 kWe bundle tests. They include reduced-cost air feed tubes; lower cost, high purity insulation; optimized stack reformer boards; enhanced designs of the fuel, air, and exhaust plena, respectively; stack support structures; and the fuel feed system. In particular, a 5 kWe bundle test, incorporating the latest cell manufacturing processes and bundling techniques successfully operated for more than 8,000 hours with no evidence of cell degradation. Included in this period of operation are more than 5,000 hours of operation at an independent facility where the system's performance was verified. A second 5 kWe generator test, operated solely at a customer facility has accumulated more than 1,700 hours of operation. A third 5 kWe generator test, using cells manufactured with a composite interlayer operated for more than 1,100 hours and produced the highest power density achieved to date for a tubular SOFC.

Many of the components in the SFC200 power system BOP have unique functional requirements that often require a one-of-a-kind component or subsystem. These items are considered to be strategic because an SOFC power system cannot be viably configured without them. The integration of these components and subsystems within the balance-of-plant and with the SOFC module requires optimization of the interfaces between the two systems. The functional specifications of the BOP subsystems and components were revised based on the design of the SOFC module. Other accomplishments with the BOP area include:

- Definition of a safe, cost-effective, and functional BOP.
- Optimization of the orientation of the BOP relative to the SOFC module.
- Conceptual and detailed designs of the respective systems, subsystems, and components comprising the BOP.
- Development of advanced system and subsystem concepts that enable elimination of previously required components.
- Identification of low-cost, high-performance desulfurizing reagents.
- Validated by bench testing new components and BOP subsystems.

The fabrication of the first SFC200 SOFC power system was completed and is being readied for its factory acceptance test (FAT). Upon successful completion of the FAT, the SFC200 will be shipped to the customer site for continued operation. A second SFC200 is currently being fabricated. Lessons learned from the fabrication of the first SFC200 have resulted in cost reductions in module assembly labor.

The stability and reliability of Siemens' tubular SOFC technology continues to be demonstrated with the successful re-start and operation of the SFC100. This system was installed at the customer site and has operated at the site for more than 8,800 hours with an availability exceeding 99.5%. Total operating time for the 100 kWe system at all three sites now exceeds 29,000 hours, with no evidence of voltage degradation.

Conclusions

Our continued and increased efforts to reduce the cell, module, and BOP costs are well defined and progressing according to schedule. The implementation of the latest cell, module, and BOP technology and the most recent cost-reduction features were incorporated into the first SFC200.

VI. ADVANCED RESEARCH

VI.1 Proton Conducting Solid Oxide Fuel Cell

Objectives

- Identification of dopant type and concentration in a perovskite host to achieve high proton conductivity and high protonic transference number under SOFC operating conditions.
- Selection of dopant type and concentration in a perovskite host to provide resistance to reactivity towards CO_2 and H_2O.
- Evaluation of electrode materials using symmetric cells and full cells in button cell configuration.
- Test button cells using syngas as fuel for cell performance and endurance.

Approach

- Select an appropriate B-site dopant in a perovskite matrix by evaluating protonic conductivity and transference number in SOFC relevant atmospheres.
- Investigate stability of compositions in syngas.
- Select a composition and evaluate in button cell tests.

Accomplishments

- The project is in the initial stages of compositional evaluation.

Future Directions

- Selection and verification of compositions for high protonic conductivity, transference number, and stability in syngas.
- Evaluation of performance in button cell tests.

S. (Elango) Elangovan (Primary Contact), J. Hartvigsen, B. Heck
Ceramatec, Inc.
2425 South 900 West
Salt Lake City, UT 84119-1517
Phone: (801) 978-2162; Fax: (801) 972-1925
E-mail: Elango@ceramatec.com

DOE Project Manager: Lane Wilson
Phone: (304) 285-1336
E-mail: Lane.Wilson@netl.doe.gov

Introduction

One of the prime attractions of fuel cells is the possibility of realizing energy conversion efficiencies much higher than possible with the thermal cycle systems. The basis of this difference is that thermal cycle system efficiencies are bounded by Carnot cycle thermodynamics, whereas fuel cell efficiencies are determined by chemical equilibrium thermodynamics and non-equilibrium force-flux relationships that govern charge, mass, momentum and energy transport. Materials have been developed which function as high temperature solid electrolytes in fuel cell applications. Two of the most widely considered materials are yttria stabilized ZrO_2 (YSZ) which transports oxygen ions and gadolinium doped $BaCeO_3$ which transports protons [1].

The thermodynamic difference between proton and oxygen ion cells is manifest in reversible potential variation with reactant utilization as a function of product water location. Excess air flow, used to remove the heat generated by cell operation, results in a lower water concentration in the cathode stream of a proton cell than in the anode stream of an O^{2-} cell.

Reversible potential variation with fuel utilization is shown for both proton and oxygen ion cells in Figure 1. The proton cell has a substantially higher reversible potential across the full range of fuel utilization. An interesting observation is that steam ratios greater than stoichiometric (S/C=2) increase the high utilization potential of a proton cell while oxygen ion cell potentials are uniformly higher with sub-stoichiometric steam ratios. This is due to the use of carbon monoxide via

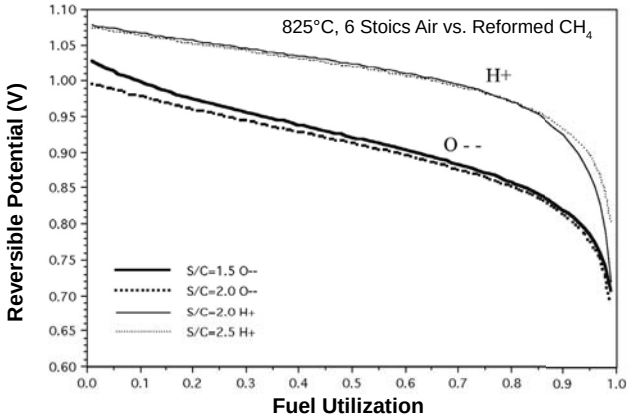

FIGURE 1. Comparison of Reversible Cell Potential

the shift reaction. The oxygen ion cell generates water in the anode stream so inlet compositions can be water deficit (high potential) and still have sufficient water to drive the shift reaction as utilization increases. The proton cell, on the other hand, must have sufficient or even excess water at the inlet to drive the shift reaction at high utilizations. However, water in the anode stream does not directly enter in the calculation of proton cell potentials and thus has little effect on the potential until higher utilizations where shift produced hydrogen is important. Thus, high temperature proton conductors have a thermodynamic advantage over oxygen ion conductors.

Comparable electrolyte ionic conductivities are required to take practical advantage of the thermodynamic benefit. Applications driven by maximizing efficiency at the expense of power density would favor proton cells. Thus, the opportunity for very high efficiency operation is one of the primary motivating factors for investigating proton conducting solid oxide fuel cells (P-SOFC). However, to date the research work on P-SOFC has lagged far behind the well-known YSZ-based oxygen conducting solid oxide fuel cells (O-SOFC). The challenges that have been encountered in P-SOFC systems are discussed below.

Proton Conductivity

As mentioned earlier, the differences in electrolyte ionic conductivity may be greater than differences in driving force and must be included in any comparison of an operating cell at a fixed current density. In general, the protonic conductivity of commonly known perovskite materials such as doped $SrCeO_3$ and $BaCeO_3$ are considerably lower than the oxygen ion conductivity of YSZ. The proton conductivity ranges from 5×10^{-3} to 2×10^{-2} S/cm at 800°C [2,3,4,5,6]. While the high end of this range is comparable to the oxygen conductivity of 8-YSZ, the perovskite materials also possess some level of oxygen ion conductivity and electronic conductivity at various temperatures. Thus, the protonic transference number varies as a function of temperature. While the doped $BaCeO_3$ composition functions as an effective electrolyte, an increase in hydrogen conductivity is preferable to fully exploit the benefit of high efficiency with high power density.

Stability

One of the biggest technical challenges lies in maintaining the chemical stability of the perovskite in the presence of CO_2 and moisture; both are present in a typical hydrocarbon fuel. Numerous studies have confirmed the instability of the perovskite compositions.

It has been shown [7] that partial replacement of the B-site dopant with Zr completely eliminates this reaction. A similar improvement in stability in moist conditions was also reported with Zr substitution [8]. However, the stability improvement is at the expense of protonic conductivity. The proton conductivity was found to decrease monotonically with increasing Zr content [9,10,11].

Thus, what is required for successful development of a P-SOFC is an electrolyte material that has high proton conductivity to achieve a low area specific resistance, high protonic transference number relative to oxygen transference number to realize high efficiency, and stability in CO_2 and H_2O without compromising protonic conductivity for cell operation using practical hydrocarbon fuels.

Approach

Perovskite compositions that are known to exhibit protonic conductivity will be evaluated for dopant study. The B-site dopants, typcially rare earth metals, have been shown to increase the proton conductivity of perovskites such as $BaCeO_3$. Several dopants and dopant levels will be screened to identify compositions that have high conducivity and stability. The best composition will be evaluated in button cell tests using hydrogen and syngas fuels.

Results

Materials synthesis is in progress.

References

1. Iwahara, H., Hibino, T., and Yamada, M., Proc. 3rd International Symosium on Solid Oxide Fuel Cells, p 137, Singhal and Iwahara eds., Honolulu, Hawaii, 1993.

2. H. Iwahara, T. Esaka, H. Uchida, N. Maeda, Solid State Ionics 3/4, 359 (1981).

3. H. Iwahara, H. Uchida, N. Maeda, J. Power Sources 7, 193 (1982).

4. H. Iwahara, H. Uchida, I. Yamasaki, Int. J. Hydrogen Energy 12, 73 (1987).

5. H. Iwahara, Solid State Ionics 28–30, 573 (1988).

6. N. Bonanos, K.S. Knight, B. Ellis, Solid State Ionics 79 (1995) 61.

7. T.R. Armstrong et al., "Stability of Perovskite Hydrogen Separation Membranes," AR Materials Conference, Baltimore, MD, April 2003.

8. N. Taniguchi et al., "Endurance Against Moisture for Protonic Conductors of Perovskite-Type Ceramics and Preparation of Practical Conductors," Solid State Ionics 145, 349–355 (2001).

9. K.H. Ryu and S.M. Haile "Chemical Stability and Proton Conductivity of Doped Perovskite Oxides in the $BaCeO_3$-$BaZrO_3$ System," Solid State Ionics 125 (1999) 355-367.

10. K Katahira, Y. Kohchi, T. Shimura, H. Iwahara, "Protonic Conduction in Zr-substituted $BaCeO_3$", Solid State Ionics, 138, 91-98 (2000).

11. S. Wienströer and H.-D. Wiemhöfer, "Investigation of the Influence of Zirconium Substitution on the Properties of Neodymium-Doped Barium Cerates," Solid State Ionics 101-103, 1113-1117 (1997).

VI.2 Photo-Activated Low Temperature, Fuel Cell Power Source

Objectives

- Investigate photoactivation as a means of deconvoluting the role of charge transfer from other rate limiting steps controlling electrode kinetics in SOFC structures.
- Evaluate the potential for reduced temperature operation with improved conversion efficiencies, extended life, simplified fabrication and reduced cost.

Accomplishments

- Demonstrated reduction in electrode impedance of a $SrTi_{1-x}Fe_xO_3$ ($x = 0.35$) model electrode by 73% under low intensity illumination.
- Completed design and construction of high temperature Kelvin probe for in situ work-function and surface photovoltage spectroscopy.

Introduction

Fuel cells convert the chemical energy stored in hydrogen or hydrocarbon fuels to electrical energy via electrochemical reactions at the anode and cathode. They offer higher efficiency and reduced emissions of greenhouse gases, such as CO_2, compared to conventional combustion processes. SOFCs, in particular, offer unrivaled energy conversion efficiency and fuel flexibility and therefore are expected to play a key role in the forthcoming hydrogen economy era. At present, however, SOFCs are too expensive for commercial applications. The high cost of this technology is largely due to the use of expensive refractory materials that need to operate at temperatures as high as 1,000°C in conventional SOFC designs. These high temperatures are required to reduce the ohmic resistance of the oxygen-ion electrolyte (typically yittria-stabilized zirconia, YSZ) in large-scale SOFCs. The use of thinner electrolytes (~10 µm) in intermediate temperature (IT)-SOFCs and thin film electrolytes ($<<$ 1 µm) in micro-SOFCs, currently being examined as alternative power sources for portable electronic devices, however, ensure short diffusion paths and correspondingly low ohmic resistances, thereby putting the burden of performance largely on the electrodes. Finding methods to increase the electrochemical performance of the electrodes is thus a key enabling technology for high performance micro-SOFCs designed to operate at moderate temperatures. Achieving improvements in electrode kinetics is important, as well, for increasing the power output of IT-SOFCs of traditional size scales. Unfortunately, despite many years of research, much remains unclear regarding the dominant loss mechanisms and limiting reaction steps at the electrodes. Therefore, it has been difficult to develop new electrodes that meet the demands for high electrochemical performance at reduced operation temperatures.

Harry Tuller (Primary Contact),
Avner Rothschild
Massachusetts Institute of Technology
Department of Materials Science & Engineering
77 Massachusetts Ave., Room 13-3126
Cambridge, MA 02139
Phone: (617) 253-6890; Fax: (617) 258-5749
E-mail: tuller@mit.edu

DOE Project Manager: Lane Wilson
Phone: (304) 285-1336
E-mail: Lane.Wilson@netl.doe.gov

Approach

This research aims at exploring the use of light as a means of deconvoluting the role of charge transfer from other steps involved in the electrode kinetics. In addition, thin film electrodes with well defined patterns, obtained by lithography and etching techniques, are used to overcome limitations related to the complex microstructures achieved at the electrode/electrolyte interface following powder processing and sintering routes typically used in conventional SOFC designs. Success along these lines is expected to lead to improved understanding of the electrode reaction mechanism and the rate limiting step(s) in SOFC and provide guidelines to design new electrodes with enhanced electrochemical performance.

In this study, illumination is utilized in several important ways. First, illumination is a means for generating excess electron-hole pairs and thereby investigating the role that minority electronic charge carriers play in the charge transfer reaction. The changes induced by illumination in the magnitude of the electrode impedance, and the activation energy which characterizes it, will provide direct evidence for the role of specific electronic charge carriers in controlling electrode kinetics. Second, the wavelength dependence of illumination serves as a powerful tool in investigating the role of localized versus delocalized states in the electronic band structure of the model electrode system, $SrTi_{1-x}Fe_xO_3$ (STF), in which the band structure as well as the level of mixed ionic-electronic

conduction can be manipulated by controlling the fraction of Fe substitution for Ti [1]. Further insight is obtained by carrying out spectroscopic measurements using monochromatic light to probe surface states (e.g., ionized oxygen adions) and correlating the surface exchange kinetics with their energy levels with respect to the band structure of the cathode material. This is achieved with the use of surface photovoltage spectroscopy (SPS) measurements [2].

Results

$SrTi_{1-x}Fe_xO_3$ targets with x = 0.05 (STF05) and 0.35 (STF35) were prepared by a conventional solid-state reaction method using commercial $SrCO_3$, TiO_2, and Fe_2O_3 powders. The powders were mixed in appropriate amounts to obtain the desired compositions, ball milled for 2 h, and subsequently calcined in air at 1,200°C for 15 h. Phase and chemical compositions were examined by x-ray diffraction (XRD) and x-ray energy dispersion spectroscopy (EDS). Subsequently, the STF powders were pressed into 1-inch pellets and sintered in a tube furnace at 1,400°C in air for 10 h. The pellets' density was about 93% of the theoretical density.

Thin film (film thickness between 65 and 230 nm) electrodes of STF35 were deposited by pulsed laser deposition (PLD) on YSZ solid electrolyte (SE) substrates (double-side polished, 100 direction, oriented crystals, 15×15×0.5 mm^3) as shown in Figure 1a. STF35 electrodes of different area and triple phase boundary (TPB) length were prepared in order to examine the reaction path of the oxygen reduction reaction (ORR) in the dark and under illumination. The small area micro-electrodes ensure that their resistance dominates the overall resistance of the electrochemical test structures depicted in Figure 1b wherein the resistance of the counter electrode at the bottom of the SE substrate is negligible due to the respective size ratio. The STF35 films were shown via XRD to be polycrystalline and of the expected perovskite structure. Some degree of preferential orientation along the (100) direction was observed. The chemical composition of the films was examined using Rutherford Backscattering Spectrometry (RBS) and it was found to be commensurate with the composition of the target material (STF35).

The electrode resistance of the STF35 shown in Figure 1a was measured by electrochemical impedance spectroscopy (EIS) using electrochemical test structures as depicted in Figure 1b. These measurements were carried out in a unique microprobe system equipped with gas, temperature, and illumination controls that was recently constructed in our laboratory. The system comprises a stainless steel vacuum chamber with a temperature controlled stage capable of reaching up to 1,200°C in air or other gas atmospheres. The chamber is equipped with four micro-manipulators for

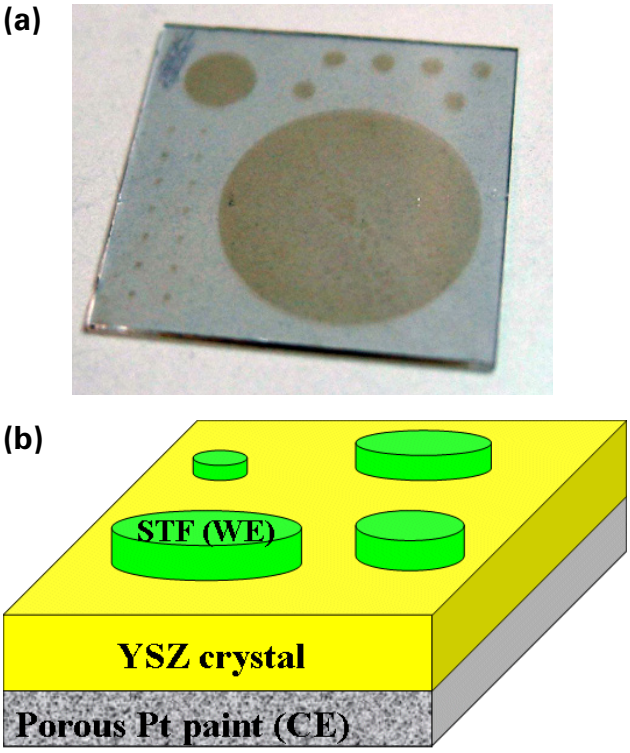

FIGURE 1. (a) STF35 Thin Film (65 nm) Electrodes on YSZ Substrate (15×15 mm^2); (b) Schematic Diagram of the Electrochemical Test Structure

making contact to micro-patterned electrodes, with ~1 µm spatial resolution. State-of-the-art equipment is available to carry out a wide variety of electrical and electrochemical measurements in the DC and AC domains. An illumination system consisting of a 100 W quartz-tungsten-halogen (QTH) light source, monochromator, and fiber optics (Oriel) enables sample illumination for investigating the effect of photons on the electrode resistance and other electrochemical properties of the sample. The wavelength and intensity of the incident light can be varied in a controlled manner. A picture of the system is shown in Figure 2.

An exemplary impedance spectrum with the large STF35 (65 nm thick) electrode as the working electrode (WE) and porous Pt electrode as counter electrode (CE) is shown in Figure 3. This measurement was carried out in the dark, at 400°C, under flow of 400 sccm of dry air. No DC polarization was applied between the WE and the CE. The different contributions to the overall impedance response of the samples were analyzed using the equivalent circuit model shown in the inset of Figure 3. This model circuit includes contributions from the series resistance of the electrodes and electrical leads (R1), the SE impedance (R2 and CPE2), the constriction impedance of the SE (R3 and CPE3), and the CE and WE electrodes impedances (R4 and CPE4 and R5 and CPE5).

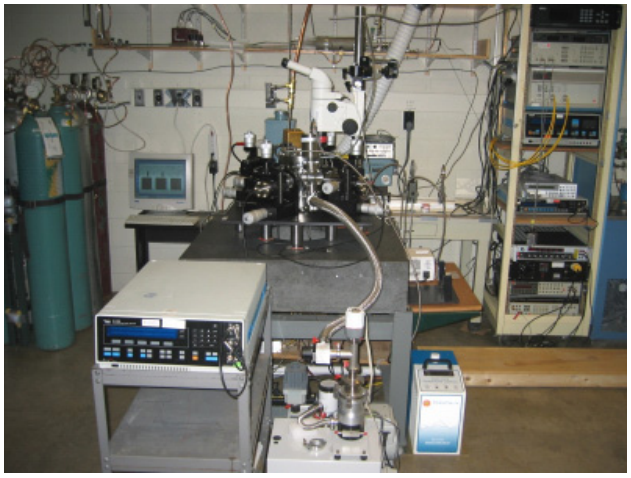

FIGURE 2. Photograph of the Microprobe Characterization System

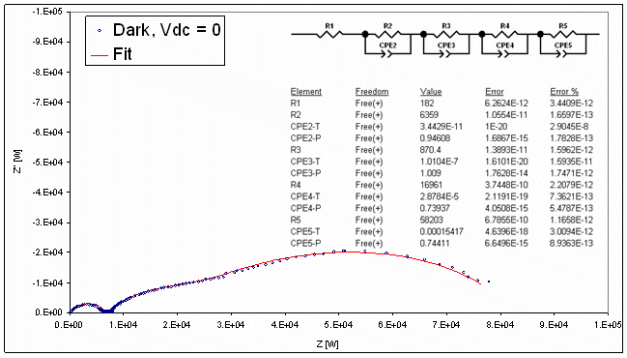

FIGURE 3. Impedance spectrum with the large STF35 electrode (cf. Figure 1a) serving as the WE, at T = 400°C, in air (flow rate = 400 sccm), under dark condition, with no DC polarization applied between the WE and CE. The inset shows the equivalent circuit and the resultant values of the circuit elements.

Figure 4 compares the impedance response, under anodic bias of 100 mV applied to the STF electrode (the WE), in the dark and under full (broadband) illumination of the light source (no filters or grids were used in this measurement). Note that the illumination power is considerably reduced from the source (100 W) to sample. We expect the reduction in power intensity to be at least 90-95%. On top of that, the illuminated area is ~1,000 mm^2, whereas the STF electrode area is only ~60 mm^2. Thus, the effective illumination power is estimated to be approximately 300-600 mW, which includes the entire spectral bandwidth (between 200 and 2,000 nm). We expect that only a small fraction of this bandwidth in the UV range (~200-400 nm) is effectively absorbed by the STF electrode, further reducing the effective illumination power to ~30-60 mW or less. Yet, the electrode impedance was reduced by 73% under illumination, as shown in Figure 4.

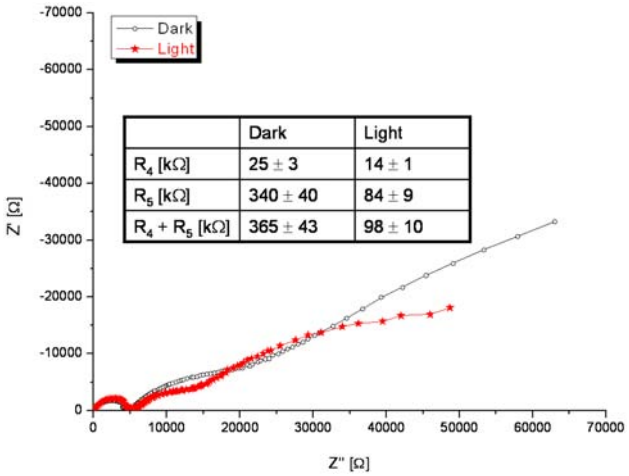

	Dark	Light
R_4 [kΩ]	25 ± 3	14 ± 1
R_5 [kΩ]	340 ± 40	84 ± 9
$R_4 + R_5$ [kΩ]	365 ± 43	98 ± 10

FIGURE 4. Impedance spectra with the large STF35 electrode (cf. Figure 1a) serving as the WE, at T = 400°C, in air (flow rate = 400 sccm), under anodic polarization of 100 mV applied between the WE (+) and CE (-). The response under dark is shown in black, the response in low-power broadband light conditions shown in red. The inset table shows the respective electrode resistances R4 and R5.

Conclusions and Future Directions

- Illumination of a model electrode-electrolyte interface demonstrated the ability to modulate electrode impedance; future work to further characterize this phenomenon includes:
  - Examining compositions (x) of the model electrode $SrTi_{1-x}Fe_xO_3$ in which the band structure as well as the level of mixed ionic-electronic conduction can be manipulated by controlling fraction of Fe substitution for Ti.
  - Carrying out spectroscopic measurements using monochromatic light to probe surface states and correlating surface exchange kinetics with their energy levels achieved with use of surface photovoltage spectroscopy (SPS) measurements.
  - Modeling the role of photogenerated carriers in controlling charge transfer limited processes.

References

1. A. Rothschild, W. Menesklou, H. L. Tuller, and E. Ivers-Tiffée, "Electronic Structure, Defect Chemistry, and Transport Properties of $SrTi_{1-x}Fe_xO_{3-y}$ Solid Solution," *Chem. Mater.* (in print).

2. A. Rothschild, A. Levakov, Y. Shapira, N. Ashkenasy and Y. Komem, "Surface Photovoltage Spectroscopy Study of Reduced and Oxidized Nanocrystalline TiO_2 Films," *Surf. Sci.* 532-535 (2003) 456-460.

FY 2006 Publications/Presentations

1. A. Rothschild, W. Menesklou, H. L. Tuller, and E. Ivers-Tiffée, "Electronic Structure, Defect Chemistry, and Transport Properties of $SrTi_{1-x}Fe_xO_{3-y}$ Solid Solution," Chem. Mater. (in print).

2. H.L. Tuller, "Some Insights Derived from the Study of Lithographically Defined Electrodes," U.S. Department of Energy- University of Florida High Temperature Electrochemistry Center Workshop: Fundamental Mechanisms of SOFC Cathode Reactions, Cocoa Beach, FL, January, 2006.

3. H.L. Tuller, "Micro-ionics: Prospects for Micro-Fuel Cells, Micro-Sensor Arrays and New Science," Pacific Northwest National Laboratory, Richland, WA, May, 2006.

4. H.L. Tuller, "Prospects for Micro-ionic Devices," National Microelectronics Centre Barcelona, Spain, June 23, 2006.

VI.3 A High Temperature (400 to 650°C) Secondary Storage Battery Based on Liquid Sodium and Potassium Anodes

Objectives

- Develop an energy storage device based on an alkali metal ion conducting beta" alumina solid electrolyte (BASE) (high temperature battery).
- Investigate materials for suitable electrochemical couples.
- Fabricate both tubular and planar BASE possessing high strength, high conductivity, and high moisture-resistance.
- Design and construct an optimized planar battery.
- Evaluate the charge-discharge capability of batteries at elevated temperatures.

Accomplishments

- Fabricated Na-BASE tubes by MSRI's patented vapor phase process.
- Constructing a battery tester with controlled temperature and atmosphere.
- Identification of suitable materials for electrochemical couples.

Introduction

A solid oxide fuel cell (SOFC) is an energy conversion device, which efficiently converts the chemical energy in hydrocarbon fuels directly into electricity at a high efficiency without the need for moving parts, except those for auxiliary pumps and blowers. As an electricity generator, its most efficient, practical and realistic use is in combination with an efficient energy storage device for electric-power generation and distribution application, particularly for utility load leveling and peak shaving. However, the associated energy storage devices of the integrated energy conversion-storage system must be capable of a very high roundtrip efficiency. Suitable batteries and reversible SOFC (solid oxide electrolysis cell – SOEC) could be the candidates serving as the energy storage devices in different energy forms, which are electrical energy and chemical energy carried by hydrogen. Due to the inherent limitations, such as hydrogen gas storage and parasitical losses, the SOEC doesn't have enough high roundtrip efficiency. Instead, load leveling batteries, which have been under development widely outside of the U.S., are capable of achieving a high roundtrip efficiency. An advanced high-temperature energy storage battery, based on an alkali metal ion conducting beta" alumina solid electrolyte (BASE) and a non-corrosive metal salt, is proposed and will be developed to demonstrate a roundtrip efficiency in excess of 90%.

A liquid alkali metal-BASE battery (ALL-BASE) is comprised of an alkali metal ion conducting BASE sandwiched between a liquid alkali metal as the anode and a metal salt as the cathode. At elevated temperatures during discharge, the alkali metal is oxidized at the anode forming metal ions, which migrate through the BASE and react with metal salt at the cathode. During charge, the above processes are reversed. In addition to the inherent advantage of the high roundtrip efficiency, the high-temperature ALL-BASE battery proposed can be thermally integrated with intermediate temperature SOFC (IT-SOFC) stacks, forming an economical, compact, lightweight hybrid system with very high system efficiency.

Greg Tao (Primary Contact), Neill Weber, and Anil Virkar
Materials and Systems Research, Inc.
5395 West 700 South
Salt Lake City, Utah 84104
Phone: (801) 530-4987; Fax: (801) 530-4820
E-mail: gtao@msrihome.com

DOE Project Manager: Heather Quedenfeld
Phone: (412) 386-5781
E-mail: Heather.Quedenfeld@netl.doe.gov

Subcontractors:
University of Utah, Salt Lake City, Utah

Approach

This project is directed toward the development of a high temperature (400~650°C) secondary storage battery based on ALL-BASE technology. Two types of high temperature batteries, sodium-based and potassium-based, will be developed.

The first type of battery, a sodium-based ALL-BASE, is based along similar lines to the one used in the ZEBRA batteries [1], but differs in three important aspects. They are: (a) The cathode uses salts which are not corrosive. Thus, inexpensive metallic materials can be used for the container, also facilitating the design and fabrication of compact, planar batteries. (b) Allows operation over a wider temperature range, making it possible to thermally integrate with a SOFC in a single thermal enclosure. (c) The batteries will be based on

ultra-high strength, non-water sensitive, BASE [2-5]. This also allows for the fabrication of compact, planar cells, which can be readily integrated with a planar SOFC stack in a single thermal enclosure, as shown schematically in Figure 1.

The second type, which is a potassium-based ALL-BASE battery, is analogous to the sodium BASE battery, wherein the sodium ion is replaced by the potassium ion. Although the potassium BASE (K-BASE) has a lower ionic conductivity at 300°C than Na-BASE, the conductivity is still orders of magnitude higher than a typical oxygen ion conductor, such as yttria-stabilized zirconia (YSZ) used in a SOFC. At temperatures above 400°C, K-BASE is still an excellent K-ion conductor. In addition to possessing the three important aspects listed for the first type of battery, the K-BASE has three other unique prospectives: (1) With typical chlorides as cathodes, a potassium anode exhibits higher open circuit voltage (OCV) than sodium. For example, with a Na anode and Na-BASE, and $CuCl_2$ as the cathode, the OCV at 800 K (527°C) is 2.857 V, while with a K anode and K-BASE, the OCV is 3.19 V. (2) The density of potassium is 0.86 g/ml vs. 0.98 g/ml for sodium. Thus, it offers an advantage from the standpoint of weight and specific energy. (3) MSRI's patented process allows for easy fabrication of K-BASE, which is not feasible using the conventional process [2-5].

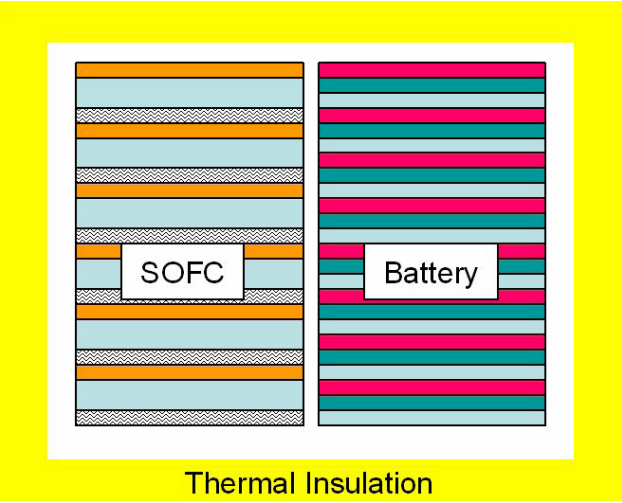

FIGURE 1. Proposed Thermally Integrated SOFC and Secondary Storage Battery System

Results

This project has barely started, and the accomplishments up-to-date are briefly described in what follows.

Identification of Suitable Electrochemical Couples

Identification of suitable electrochemical couples for the ALL-BASE battery is being performed. The prospective electrochemical couples should be sufficiently energetic, lightweight, not corrosive, not too volatile, and capable of forming a stable, porous metal structure in the cathode upon discharge. Since the anode is either liquid sodium or liquid potassium, the possible candidates for the cathode can be several metal salts. The metals, whose salts are used in the cathode, should be considerably more noble than sodium or potassium. This ensures a large enough free energy change upon discharge. The maximum amount of electrical energy that can be derived is $|\Delta G^o|$ (with $\Delta G^o < 0$), where the ΔG^o is the free energy of the reaction between sodium (or potassium) and the salt to form sodium (or potassium) salt and metal. The corresponding OCV is thus given by $E = -\Delta G^o/(nF)$, where n is the number of electrons participating the overall reaction and F is the Faraday constant (96,487 C/mol.). Table 1 lists the preliminary OCV calculations for a few potential candidate salts for the cathode.

As shown in Table 1, from the several possibilities for the electrochemical couples, the preferred ones (from the standpoint of specific energy) are the $CuCl_2$/Na and $CuCl_2$/K couples, with OCVs of 2.857 V for Na and 3.19 V for K, respectively. The AgF/Na and AgF/K

TABLE 1. A Material List of Possible High Temperature Electrochemical Couples

Electrochemical couple Na/Salt or K/Salt	ΔG^o for the reaction in kJ/mol. at 800 K	Open circuit voltage (OCV) (V)	Specific energy for the couple at 90% discharge efficiency in Wh/mol.	Specific energy for the couple in Wh/kg at 90% efficiency	Molar mass of the couple in kg
Na/$CuCl_2$	-551.357	2.857	137.8	763	0.1804
K/$CuCl_2$	-615.665	3.19	153.9	724	0.2126
Na/AgCl	-250.897	2.508	62.72	377.1	0.1663
K/AgCl	-274.237	2.842	68.56	377.9	0.1814
Na/AgF	-332.682	3.447	83.17	554.8	0.1499
K/AgF	-327.639	3.396	81.91	493	0.1660

couples are attractive from the standpoint of high open circuit voltage (about 3.4 V). Another attractive possibility is the use of AgF_2 as the cathode. At this point, no data regarding free energy are available. However, it is known that AgF_2 is quite stable and melts at 690°C [6]. The use of AgF_2 affords the possibility of increasing the specific energy since two atoms of fluorine are tied up with one atom of silver. Thus, upon discharge, two molecules of NaF (or KF) are formed. In addition, there are other possibilities. However, relevant thermodynamic data are not readily available. A detailed survey of the available thermodynamic data of other prospective electrochemical couples is continually being conducted in this project. If electrochemical couples superior to those given in Table 1 are identified, preliminary experiments will be conducted using the identified couples.

Fabrication of Tubular Na-BASE by MSRI's Patented Vapor Phase Process

The conventional process for the fabrication of Na-BASE involves sintering compacts of calcined powder containing BASE (and other sodium aluminates including $NaAlO_2$) at elevated temperatures (~1,600°C) in enclosed MgO containers to suppress vapor phase loss of Na_2O [7]. The necessity of using containers increases cost. Also, as some $NaAlO_2$ always remains along the grain boundaries, BASE made by the conventional process is susceptible to moisture and CO_2 attack from the atmosphere. In addition, the fracture strength of BASE made by the conventional process is generally low – on the order of 200 MPa or less. Also, the conventional approach cannot be used to make K-BASE since it does not form by a high temperature reaction.

MSRI has developed a novel process based on the concept of coupled transport, which has many advantages over the state-of-the-art [2-5]. The novel process for the fabrication of BASE by the vapor phase method developed at MSRI is described in what follows, and is used to fabricate both Na-BASE and K-BASE samples.

BASE Fabrication Process

(1) A slurry of a powder mixture of α-Al_2O_3 and tetragonal zirconia (3 mol.% Y_2O_3 + ZrO_2) is made. (2) The slurry is cast to form a tape of the desired thickness (~200 to 300 microns). (3) The tape is cut into square pieces of the desired dimensions (7 cm x 7 cm), or circular in shape for circular cells. (4) The cut pieces are sintered in air at ~1,400°C. The actual temperature will depend on the quality of powders. It can be as low as ~1,350°C. This leads to the formation of a fully dense (>99% of theoretical density) two phase material containing α-Al_2O_3 + tetragonal zirconia polycrystal. (5) The sintered pieces are then placed in a ceramic crucible surrounded by BASE powder as the source of Na_2O (or K_2O). This packing powder is made by conventional calcination, but is reused numerous times, each time simply replenishing the Na_2O (or K_2O) content by adding Na_2CO_3 (or K_2CO_3). The crucible is then heated to ~1,400°C and maintained at 1,400°C for about 15 to 20 minutes. Thereafter, the furnace is turned off. Upon cooling, highly conductive, strong and moisture/CO_2-resistant BASE results, ready for use in battery applications.

FIGURE 2. Photograph of Several Na-BASE Tubes Made (about 15 cm in length) by MSRI's Patented Vapor Phase Process

Figure 2 shows a photograph of several BASE tubes made by the MSRI patented vapor phase process, which also readily allows for the fabrication of thin, flat BASE plates, not feasible by the conventional process due to the warpage associated with liquid phase sintering in the conventional process. Typical BASE tubes fabricated by the conventional process for use in Na-S batteries are well in excess of 1 to 1.5 mm in thickness leading to a high ohmic area specific resistance (ASR). In contrast, the BASE made by this novel, patented process exhibits excellent properties, unmatched by BASE made using conventional processes.

Conclusions and Future Directions

- Several Na-BASE tubes with thin wall thickness have been fabricated using MSRI's patented vapor phase process. The tubes made are moisture resistant.
- Several suitable materials for high temperature electrochemical couples have been identified. Those couples will be further evaluated by measuring the OCVs.
- K-BASE tubes and square samples will be fabricated applying the same process as for making Na-BASE.

- ALL-BASE batteries will be constructed and tested in a controlled environment at elevated temperatures from 400°C to 650°C. The discharge depth and voltage vs. current characteristics will be evaluated.

References

1. C.-H. Dustmann, "ZEBRA Batteries Set to Take on the World", Batteries International, July (1994).

2. A. V. Virkar, J-F. Jue, and K-Z. Fung, "Alkali Metal Beta and Beta" Alumina and Gallate Polycrystalline Ceramics and Fabrication by a Vapor Phase Process", U. S. Patent No. 6,117,807.

3. A. V. Virkar, J-F. Jue and K-Z. Fung, "Alkali-Metal Beta and Beta" Alumina and Gallate Polycrystalline Ceramics and Fabrication by a Vapor Phase Method", U. S. Patent No. 6,537,940, Date of Issue: March 25, 2003.

4. A. V. Virkar, T. J. Armstrong, N. Weber, K-Z. Fung and J-F. Jue, in "High Temperature Materials", edited by S. C. Singhal, PV 2002-5, The Electrochemical Society, Inc., Pennington, NJ (2002).

5. G-Y. Lin and A. V. Virkar, J. Am. Ceram. Soc., 84 [6] 1321-26 (2001).

6. "CRC Handbook of Chemistry and Physics", 58th Edition, CRC Press, Cleveland, OH (1977).

7. J. L. Sudworth and A.R. Tilley, "The Sodium Sulfur Battery", Chapman and Hall, London, England, (1985).

VI.4 A Thin Film, Anode-Supported Solid Oxide Fuel Cell based on High Temperature Proton Conducting Membrane for Operation at 400 to 700°C

Objectives

- Measure conductivity of K-doped and Y-doped $BaZrO_3$ (KBYZ) in H_2-H_2O and air-H_2O containing atmospheres over a range of temperatures from 400 to 700°C.
- Fabricate KBYZ thin film, Ni + KBYZ anode-supported button cells (at least 2 cm² active area) with a two phase, composite mixed ionic electronic conducting (MIEC) perovskite cathode, comprising a proton conductor (KBYZ) and an electronic conductor.
- Conduct electrochemical tests on button cells with humidified H_2 as fuel and air as oxidant over a range of temperatures from 400 to 700°C.

Accomplishments

- The chemical stability of $BaZrO_3$ over $BaCeO_3$ was confirmed from thermodynamic calculation.
- The procedure for powder preparation using planetary milling was established.
- Experimental test and analysis systems were set up.

Introduction

The key attribute of an oxygen ion-conducting electrolyte for the solid oxide fuel cell (SOFC) has one significant and unavoidable shortcoming, namely fuel dilution. Since water vapor (and CO_2 if CO is in the fuel) are formed at the anode, the fuel continually becomes depleted, which is undesirable. Fuel dilution can be avoided provided a proton conducting solid electrolyte is used, since in such a case the water vapor is produced at the cathode where it mixes with excess air and does not significantly lower the cell voltage. Since fuel dilution can be avoided, at all times during cell operation, the pressure of hydrogen can be maintained at a value near the feed composition, which leads to little anode concentration polarization and relatively low anode activation polarization due to high hydrogen partial pressure. These advantages are expected to facilitate more efficient operation of the SOFC based on proton conducting membranes. A fuel cell based on high temperature proton conductor (HTPC) has other important attributes such as thermal integration capabilities and no CO poisoning which allows the use of non-precious metal catalysts.

High temperature proton conductors are based on perovskite type materials (ABO_3) containing oxygen vacancies. Such materials can absorb water vapor and become proton conductors. Of the materials investigated to date, doped $BaCeO_3$ exhibits the highest proton conductivity. Thus, much work has been conducted on this material and another ceria-based material, $SrCeO_3$ which also exhibits high proton conductivity. The very low stability of these cerates, however, has been a problem [1]. It was experimentally shown that $BaCeO_3$ decomposes in the presence of liquid water [2]. Studies have also shown that $BaCeO_3$ and $SrCeO_3$ are not stable in CO_2-containing atmospheres below 800°C [3,4]. Even though fuel cells made using these materials may not present a significant problem for limited periods of time at higher temperatures, their long term stability is problematic on repeated thermal cycling and especially when used in a thin film form as required for an SOFC. Other materials of interest from the standpoint of conductivity are rare earth oxide doped $BaZrO_3$ and $Ba_3Ca_{1+x}Nb_{2-x}O_{9-\delta}$ (BCN), although these materials exhibit lower conductivity than $BaCeO_3$ and $SrCeO_3$.

Joon-Ho Koh (Primary Contact), Mick Barton
Materials & Systems Research, Inc.
5395 West 700 South
Salt Lake City, UT 84104
Phone: (801) 530-4987; Fax: (801) 530-4820
E-mail: jkoh@msrihome.com

DOE Project Manager: Lane Wilson
Phone: (304) 285-1336
E-mail: Lane.Wilson@netl.doe.gov

Subcontractor: Dr. Anil V. Virkar
The University of Utah, Salt Lake City, UT

Approach

In addition to the ability to dissolve water vapor into the lattice and transport protons, the stability of the material in water vapor must be demonstrated. Work done to date has demonstrated that unlike $BaCeO_3$ and $SrCeO_3$, materials such as $BaZrO_3$ or BCN are stable in water. Their stability has been demonstrated by heat-treating them in an autoclave at temperatures as high as 500°C and water vapor pressures as high as 180 bars [5]. Somewhat lower proton conductivity of $BaZrO_3$-based HTPC compared to $BaCeO_3$ and $SrCeO_3$ is related in part to the lower overall basicity. For proton conduction, it is necessary that a sufficient

amount of H_2O dissolve into the perovskite lattice. The affinity towards water vapor can be described in terms of basicity of the material. It is known that for the A-site of perovskite materials (ABO_3), basicity increases in the order Sr → Ba, and for the B-site it increases in the order Zr → Ce. The lower proton conductivity of $BaZrO_3$ thus in part is attributed to its lower basicity.

The suggested approach is to start with a material of proven stability, such as $BaZrO_3$, but then add other elements (dopants) to enhance its basicity. The most basic ions are the alkali ions such as sodium and potassium. At 1,000 K, the partial pressure of H_2O for the formation of $Ba(OH)_2$ is ~0.45 atm, while that for the formation of KOH (alkali earth metal hydroxide) is only ~3×10^{-7} atm. Thus, the incorporation of potassium into the perovskite lattice should significantly increase affinity for H_2O, and thus should enhance protonic conductivity. Doping on the B-site with an alkali ion, however, will not be feasible due to the large difference in electrical charge (+1 vs. +4) and also due to the larger size of alkali ions, with the exception of lithium, compared to the typical B-site ion. However, the ionic sizes of divalent alkaline earth ions (Ba, Sr, etc.) are comparable to monovalent alkali ions (Na, K, etc.). Thus, the suggested approach is to dope on the A-site with an alkali ion instead of the usual B-site to create oxygen vacancies. In addition, a small amount of yttrium is doped on the B-site for the purpose of preventing possible microcracking associated with tetragonal to monoclinic phase transformation if a small amount of ZrO_2 precipitates form. The resultant material ($K_xBa_{1-x}Y_yZr_{1-y}O_{3-\delta}$) should have higher affinity towards water uptake (due to the presence of potassium in the lattice), but at the same time, the material should be stable by virtue of the presence of $BaZrO_3$ as the major constituent.

Results

From a chemical equilibrium point of view, the stability of $BaCeO_3$ and $BaZrO_3$ under typical SOFC conditions can be compared by calculation of the free energy changes for the following reactions with *(M)* = Ce or Zr. Thermodynamic data were obtained from the literature [6,7].

$$Ba(M)O_3 \rightarrow BaO + (M)O_2$$

$$Ba(M)O_3 + H_2O \rightarrow Ba(OH)_2 + (M)O_2$$

$$Ba(M)O_3 + CO_2 \rightarrow BaCO_3 + (M)O_2$$

The calculation of the standard free energy changes for these reactions shows that in all cases the reactions of $BaZrO_3$ require larger values of ΔG^o than $BaCeO_3$ (Figure 1). Therefore $BaZrO_3$ is less likely to react under the SOFC conditions than $BaCeO_3$.

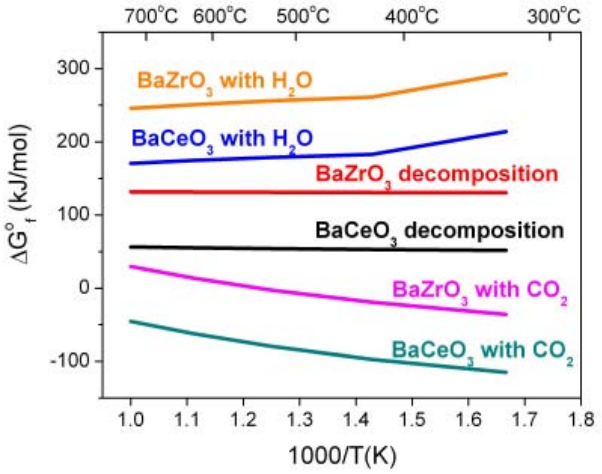

FIGURE 1. Comparison of the Standard Free Energy Changes of $BaCeO_3$ and $BaZrO_3$ for Several Reactions: Decomposition, Hydrolysis, and Reaction with CO_2 [Thermodynamic data from Reference (6) for $BaCeO_3$ and Reference (7) for other compounds]

Powders and samples are currently being processed for experimental tests. Powders of K_2CO_3, $BaCO_3$, Y_2O_3, and ZrO_2 are mixed in the requisite ratio, and ball-milled. The target K-contents are 10% ($K_{0.1}Ba_{0.9}Y_{0.04}Zr_{0.96}O_{3-\delta}$) and 20% ($K_{0.2}Ba_{0.8}Y_{0.04}Zr_{0.96}O_{3-\delta}$). The powder mixture is calcined at 1,250°C for 2 hours in a covered zirconia crucible. The calcined powder (which forms doped-$BaZrO_3$) is ground to nano-size by planetary milling. The planetary mill equipment (Retsch PM-100) has been set up and ready for use (Figure 2).

The past preliminary test did not produce nano-size powders, and the reasons were identified: (a) too much solvent, (b) single-step milling process, and (c) inappropriate size of milling media. The conditions will be improved by adjusting and optimizing media sizes, a ratio of solvent/powder/media, milling time, and rotation speed. A multi-step processing with different media (from large to small) will be employed.

Anode-supported fuel cells will be fabricated by sintering thin KBYZ film on a porous structure of Ni and KBYZ. In order to lower the sintering temperature and minimize the loss of volatile potassium compounds, an average powder size of 250 nm is required. The target sintering temperature is 1,450°C. A porous structure of an electronic conductor and KBYZ as cathode will be printed. The fabricated cell will be tested at 400-700°C for current-voltage characteristics. The test system was prepared and set up as shown in Figure 3. Current interruption tests and measurement of complex impedance spectra will be carried out to evaluate the ohmic resistance and the various polarization contributions. The system for these analyses was set up using an oscilloscope (Agilent 54622A), an

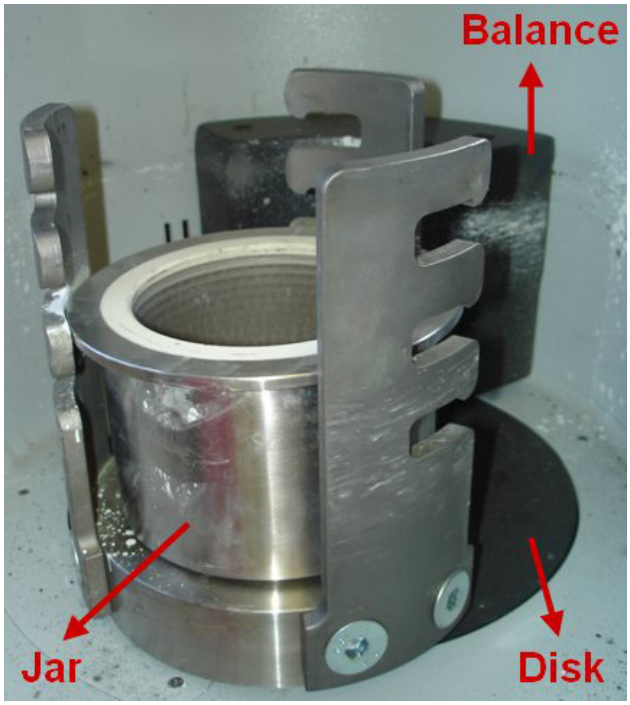

FIGURE 2. A Photo of the Planetary Milling System

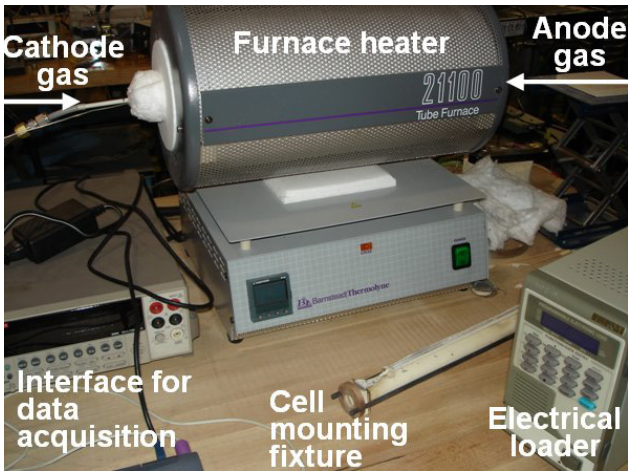

FIGURE 3. A Photo of the Cell Test System

electrochemical interface (Solatron SI 1287), and an impedance analyzer (Solatron SI 1260), as shown in Figure 4.

Conclusions and Future Directions

One of the challenges is to prepare nano-size KBYZ powders that can keep the sintering temperature at or below 1,450°C. The current primary approach is to use the planetary mill. Alternative approaches based on chemical methods such as combustion synthesis or sol-gel processing will also be considered in the future if necessary.

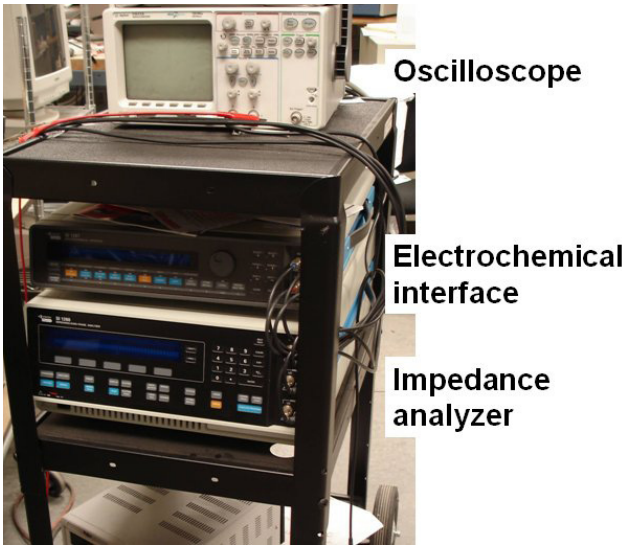

FIGURE 4. A Photo of the Electrochemical Analysis System

References

1. "Proton-Conducting Oxides," Kreuer K.D. *Annual Review of Materials Research*. 33 (2003) 333-359.

2. "Stability of $BaCeO_3$-Based Proton Conductors in Water-Containing Atmospheres," Bhide S.V., Virkar A.V. *Journal of The Electrochemical Society*. 146(6) (1999) 2038-2044.

3. "Synthesis of strontium and barium cerate and their reactions with carbon dioxide," Scholten M.J., Schoonman J., Miltenburg J.C., Oonk H.A.J. *Solid State Ionics*. 61 (1993) 83-91.

4. "Perovskite solid electrolytes: Structure, transport properties and fuel cell applications," Bonanos N., Knight K.S., Ellis B. *Solid State Ionics*. 79 (1995) 161-170.

5. "Transport Properties of Potassium-Doped $BaZrO_3$ in Oxygen- and Water-Vapor-Containing Atmospheres," Patnaik A.S., Virkar A.V., *Journal of The Electrochemical Society*. 153(7) (2006) A1397-A1405.

6. "The Thermodynamic Properties of $BaCeO_3$ at Temperatures from 5 to 940 K," Scholten M.J., Schoonman J., Miltenburg J.C.V., Cordfunke E.H.P. *Thermochimica Acta*. 268 (1995) 161-168.

7. "Thermochemical Data of Pure Substances: Parts I and II," (3rd Edition) Barin I. VCH Publication, Weinheim (1995).

VI.5 High Temperature Electrochemistry - Montana State University

Objectives

- Develop thin corrosion resistant coatings on steel interconnect plates that are (1) good electron conductors, (2) thermally stable, (3) good barriers to outward diffusion of Fe and Cr from the interconnect plate, and (4) good barriers to inward oxygen diffusion and growth of oxide scale.
- Characterize the behavior of SOFC interconnect material systems under relevant exposures to develop understanding of essential interfacial chemistry and transport mechanisms.
- Investigate Cr poisoning processes in SOFCs through quantitative measurements of (1) Cr volatility rates from coated/uncoated steel surfaces, and (2) oxygen diffusion and surface exchange rates for electrolyte and cathode materials with surface impurities.
- Investigate the possibility of engineering pore structures and determine their impact on SOFC performance.
- Determine the effects of interfacial strain from lattice mismatch at interfaces of technologically relevant SOFC materials.
- Investigate potential for brazed seals for SOFCs.
- Create an x-ray-compatible electrochemical cell to study the SOFC structural and electronic properties under operational conditions.
- Fabricate and characterize proton conducting ceramics for use in hydrogen separation membranes, intermediate-temperature solid oxide fuel cells, hydrogen pumps, water electrolyzers, and hydrogen sensors.
- Measure and analyze anode gas flow and tortuosity for various anode structures.
- Develop a physically-based dynamic model for a solid oxide fuel cell stack.
- Develop a fuel cell model reference simulator.
- Demonstrate modular power electronics that can be used with transient recognition control (TRC) and develop and demonstrate TRC for fuel cell systems in a field programmable gate array (FPGA) system.
- Develop a DC/DC converter of $40/kW cost and 97% efficiency for the fuel cell powered residential power system.
- Develop a load sharing control method for paralleled DC/AC converters in fuel cell power plants that can ensure the load sharing error is less than 10% in both steady-state and transient conditions.

Lee H. Spangler (Primary Contact),
Richard Smith, Yves Idzerda, Hugo Schmidt,
Hashem Nehrir, Steven Shaw, Stephen Sofie,
Max Deibert, Hongwei Gao
Montana State University
207 Montana Hall
Bozeman, MT 59717
Phone: (406) 994-2891; Fax: (406) 994-2893
E-mail: spangler@montana.edu

DOE Project Managers:
Heather Quedenfeld
Phone: (412) 386-5781
E-mail: Heather.Quedenfeld@netl.doe.gov

Lane Wilson
Phone: (304) 285-1336
E-mail: Lane.Wilson@netl.doe.gov

Subcontractors:
Arcomac Surface Engineering, Bozeman, MT

Accomplishments

- Demonstrated a rapid, quantitative process using ion beam analysis (Rutherford backscattering spectroscopy, RBS) to measure the evolution in time of Cr volatility for steel surfaces with and without protective coatings.
- Measured oxygen diffusion and surface exchange coefficients for CoMnO coatings deposited on 430 SS, and for surfaces of crystalline YSZ, using nuclear reaction analysis.
- Demonstrated the superior oxidation resistance for short times (<100 hrs) for homogeneous, sputtered CrAlN coatings as compared to multilayered CrN/AlN coatings.
- Developed protective coatings on ferritic steels which demonstrate excellent SOFC interconnect performance, i.e., long-term surface stability, high electronic conductivity and low Cr volatility.
- A vacuum brazing system was designed and constructed and a custom synthesized braze was fabricated at Montana State University (MSU) to improve characteristics of the commercial vehicle in which the successful removal of undesirable silicon components was achieved.
- The Freeze-Tape Casting system is now set up and operational in addition to the freeze drying system for fabrication of graded porous electrode tapes.
- Identified a novel mechanism that may be a serious bottleneck to SOFC performance whereby the strain energy at an SOFC interface is accommodated and distributed over a larger volume (thickness) by modifying the chemical construction of the SOFC

material to improve the lattice mismatch. This new interfacial region has reduced oxygen vacancy mobility.

- Created an x-ray-compatible electrochemical cell and initiated measurements of temperature-dependent structural changes for SOFC materials.
- Optimized fabrication and sintering processes to obtain dense Y-doped Ba(Ce, Zr)O_3 proton-conducting ceramics and dense Ni/ceramic cermets with homogenous Ni distribution.
- Achieved good proton conductivities of $Ba_{0.98}(Ce_{0.65}Zr_{0.15}Y_{0.2})O_3$ ceramics at intermediate temperatures (500º-700ºC), such as 4.37×10^{-3} $W^{-1}cm^{-1}$ at 500ºC, 7.23×10^{-3} $W^{-1}cm^{-1}$ at 600ºC, and 1.01×10^{-2} $W^{-1}cm^{-1}$ at 700ºC.
- Analyzed anode gas flow results in literature and showed that they indicate tortuosity in the 2 to 4 range.
- Developed a physically-based dynamic model for a 5-kW SOFC stack in the widely used MATLAB/SIMULINK simulation environment.
- Developed and tested circuits for driving fuel cells and/or short stacks with scaled load currents with bandwidths in excess of 100 kHz.
- Demonstrated fixed-point TRC control methods, including transient overlap.
- Implemented TRC at the register transfer level in a Xilinx FPGA.
- Developed a modular power electronics printed circuit board setup using off-the-shelf converters.
- Developed a new DC/DC converter for the fuel cell residential power system. Built both the power circuit and the control circuit of the DC/DC converter. Tested the energy conversion capability of the power circuit and the interleave control functionality of the control circuit.
- Developed and simulated a new load sharing control method for paralleled DC/AC inverters in fuel cell power plants. The simulation results showed that the method could achieve accurate d-q current sharing among all inverters and high-performance zero sequence current control for each of the inverters.

Introduction

MSU-HiTEC is pursuing multiple sub-projects related to the performance, degradation, basic science, and power system engineering relevant to solid oxide fuel cells and electroceramics. These can broadly be categorized into two major groups: 1) materials studies and 2) power electronics and control studies.

Materials Studies

The requirements of low cost and high-temperature corrosion resistance for bipolar interconnect plates in SOFC stacks have directed attention to the use of steel plates with more oxidation resistant compositions. However, volatile Cr species from the chromia-based oxide scales on these steels find their way to the triple-phase boundary, leading to rapid degradation of fuel cell performance. Coatings can serve not only to slow oxidation rates on steel surfaces, but also as diffusion barriers for the Cr-derived species from the steel, slowing the SOFC stack degradation process. We have characterized the oxidation resistance and diffusion behavior of steel plates with coatings of CrAlON and CoMnO, deposited using rf magnetron sputtering and filtered arc deposition techniques. We have also developed a relatively quick, quantitative procedure using Rutherford backscattering spectroscopy (RBS) to measure the time evolution of Cr vaporization rates.

SOFCs are layered devices. The interfacial stress can lead to changes in the electronic, chemical, and structural properties of the materials in the interfacial region that can impact ion transport and other mechanisms that affect fuel cell performance. We have developed a suite of element and site-specific x-ray spectroscopy and x-ray scattering techniques that probe these buried interfacial region properties.

The development of dense and chemically stable proton conducting ceramics with high proton conductivity is critically important for applications of hydrogen separation membranes, proton-conducting-based solid oxide fuel cells, hydrogen pumps, water electrolyzers, and hydrogen sensors. The present work optimized fabrication and sintering processes to obtain dense and stable Y-doped Ba(Ce, Zr)O_3 ceramics with high proton conductivities.

Anode-supported solid oxide fuel cells require careful design of the relatively thick anode so fuel gas flow through the anode to the solid electrolyte is not excessively impeded. Experimental work on freeze-tape casting methods to develop graded pore structures is now underway. Detailed analysis of the flow of the fuel gas, and the exhaust gas generated at the anode-electrolyte interface, has been initiated.

Power Electronics and Control Studies

Solid oxide fuel cells are advanced electrochemical energy conversion devices operating at a high temperature, converting the chemical energy of fuel into electric energy at high efficiency. They perform in a fundamentally different fashion than most power systems in wide-scale deployment today. As a result, there is need to develop power electronics, control systems, and system tools that will allow the electrical

engineering community to begin development of systems before SOFC stacks are commercially available.

SOFC dynamic modeling is of interest for predicting SOFC performance and controller design for different applications, e.g., for SOFC load transient mitigation and distributed power generation applications.

We are developing a fuel cell reference simulator that will mimic the electrical terminal characteristics of a single cell or short stack but at relevant (kilowatt) power levels. This instrumentation will accelerate development of control systems and power electronics by allowing electrical engineers to work with small, laboratory prototype fuel cells to develop full-scale balance of plant and systems.

Fuel cells are highly efficient but respond slowly to load transients. Additionally, large transients may result in localized heating within the fuel cell and result in degradation of the stack. We are developing novel transient recognition control schemes that will allow intelligent control of fuel cells in multi-source systems. We are also investigating methods of making control systems modular to match the SECA goal of modular fuel cells. Without this, power electronics would require redesign when different numbers of SECA modules are ganged together.

Approaches

Coatings were deposited on 430 and Crofer steel coupons using rf magnetron sputtering at MSU and filtered arc deposition at Arcomac Surface Engineering, Inc. Nitrogen and oxygen gasses were added to the Ar sputtering gas during the growth processes. For sputtered coatings, the Cr/Al composition ratio in the coatings was varied in a combinatorial approach. The coatings were subsequently annealed in air for up to 100 hours at 800°C. The composition of the coated plates, elemental diffusion, and oxidation were characterized using RBS and non-Rutherford backscattering analysis for lighter elements.

In collaboration with coating providers, our group investigates a wide variety of coating techniques, compositions and architectures on different ferritic steels of interest for SOFC interconnects. We subject coated and uncoated materials to SOFC relevant environments and characterize material behavior using an array of analytical techniques and tools, including area specific resistance measurements, indentation testing, surface and cross-section optical and scanning electron microscopy, energy dispersive x-ray spectroscopy, electron backscattered diffraction, x-ray diffraction, Cr volatility measurements using transpiration, and induction-coupled plasma mass spectrometry.

For the Cr volatility measurements, Cr-containing vapors from the steel coupons in a tube furnace at 800ºC were transported with various flow rates of humid air to a Si wafer at ~110ºC near the end of the quartz tube in the furnace, where the vapors adsorbed on the Si surface. The Si wafers were subsequently analyzed for Cr surface concentrations using Rutherford backscattering. Separate experiments with Cr_2O_3 powder as the Cr vapor source established the quantitative reliability of this approach.

The SOFC interfacial stress is controlled by either depositing SOFC films ($La_{0.5}Sr_{0.5}CoO_3$, or LSCO, and $La_{2/3}Ca_{1/3}MnO_3$, or LCMO) grown by pulsed laser deposition on appropriate substrates of known lattice mismatch or by capping thick SOFC structures with wedges of overlayers of known lattice mismatch. This latter method allows for control of the total stress energy with wedge thickness. We have used element and site-specific x-ray spectroscopy and x-ray scattering to study the electronic, chemical, and structural properties of the as-grown systems. Furthermore, films will be similarly studied at operational conditions by using an x-ray compatible electrochemical cell.

By using an optimized Glycine-Nitrate process and investigating the sintering at a series of temperatures and various atmospheres, dense Y-doped Ba(Ce, Zr)O_3 ceramics can be obtained. By using the impedance spectroscopy technique, the proton conductivities of grains and grain boundaries were investigated at different temperatures and atmospheres.

The Stefan-Maxwell equation provides a set of differential equations for analyzing flows of each of several gas constituents. Under the condition of fuel gas starvation at the anode-electrolyte interface, these equations can be solved for the anode pore average tortuosity if other experimental parameters are known.

A dynamic model for a 5-kW tubular SOFC stack has been developed based on the SOFC thermodynamic and electrochemical properties and on the mass and energy conservation laws with emphasis on the fuel cell electrical (terminal) characteristics. The SOFC model mainly consists of an electrochemical sub-model, a thermodynamic sub-model, and an electrical circuit model representing the double-layer charging effect. The effect of internal temperature and pressure inside the SOFC on the steady-state V-I (output voltage vs. current) and P-I (output power vs. current) characteristics, and on SOFC response to sudden load changes, were evaluated.

The approach for the fuel cell reference simulator is to develop instrumentation that will mimic the electrical terminal characteristics of a short stack or single cell at power levels. This instrumentation will accelerate development of control systems and power electronics by allowing electrical engineers to work with prototype fuel cells and stacks in full-scale systems.

The approach for transient recognition control is to build a model that recognizes the long-term demand of incoming load transients and controls the fuel cell portion of a multi-source system to meet the long-term demand.

The idea for modular fuel cell power electronics is to investigate a power electronics design paradigm that complements the scalability advantages of fuel cells.

In the DC/DC converter project, we use active switches to control the voltage and therefore the current of the leakage inductance of the transformer and use interleave control to reduce the cost and improve the efficiency of the converter. In the load sharing control project, we drop the d-q voltage with the d-q current in each of the paralleled inverters and control the zero sequence current of each inverter with a newly proposed synchronized pulse-width modulation method.

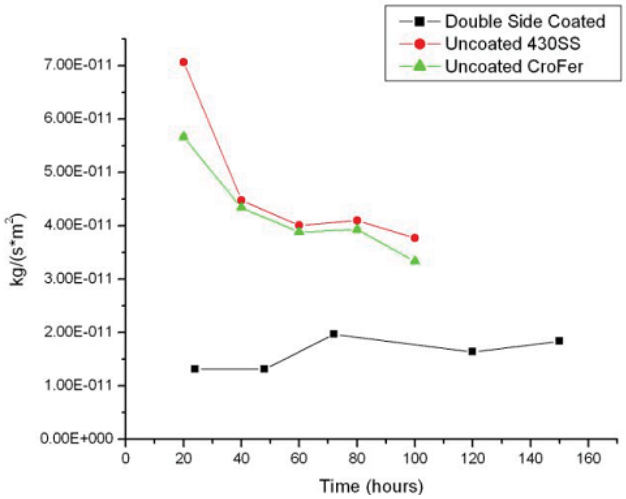

FIGURE 1. Cr Vaporization Rates of Coated and Uncoated Steels as a Function of Time at 800°C in Humid Air

Results

Significantly improved SOFC interconnect performance has been realized using protective coatings developed by our group. This includes a dramatic improvement in long-term surface stability, increased electronic conductivity, and substantial Cr volatility reduction. Quantified results include the essential absence of physical or chemical changes within the coating for over 1,000 hours at 800°C in air through several thermal cycles; stable area specific resistance values of <10 mΩ·cm^2 for over 1,000 hours in air at 800°C; and a 32-fold reduction in Cr volatility versus uncoated 430 stainless steel. For sputtered CrAlON coatings, we observed that Al-rich coatings are more susceptible to oxidation than Cr-rich coatings and that a Cr/Al ratio of 0.9 provides good oxidation resistance.

We contrasted the early time evolution of Cr volatility for 430 SS and for CroferAPU22, the latter with and without a CoMnO spinel coating deposited using a combination of filtered arc and rf magnetron sputtering processes. The coated materials showed a significant reduction in Cr volatility indicating that such coatings may be a viable strategy for prevention of Cr poisoning of SOFCs (Figure 1).

By using polarization dependent x-ray absorption spectroscopy (XAS), we have examined the chemical state of different elements of $La_{2/3}Ca_{1/3}MnO_3$ (LCMO) and $La_{0.5}Sr_{0.5}CoO_3$ (LSCO) at room temperature as a function of the stress within the films created by the substrate or overlayer lattice mismatch on which the film is grown. We have found that as the stress is changed from compressive to tensile stress, the chemical state of the Co in the interfacial region changes dramatically, although the structure of the film remains essentially unchanged. The SOFC films were grown in a series of thicknesses (up to 2500 Å) on various single crystal substrates [strontium titanate - $SrTiO_3$ (STO), neodymium gallium oxide - $NdGaO_3$ (NGO), strontium ruthenate - $SrRuO_3$ (SRO), and lanthanum aluminum oxide - $LaAlO_3$ (LAO)]. Representative of the results are the XAS spectral shifts of LSCO as the thickness of an LAO overlayer is increased (Figure 2). The stress response is for the SOFC to create a compositional gradient to distribute the stress energy over a larger volume (film thickness). The compositional gradient region represents a region where the transition metal ion valence is changing and the oxygen vacancy diffusion is far from optimum. In some extreme cases, the oxygen vacancy diffusion may become negligible, compromising SOFC performance.

We optimized the fabrication processes of Y-doped Ba(Ce, Zr)O_3 ceramics and Ni/ceramic cermets. Proton conductivities of the grains and grain boundaries in the ceramic samples were investigated by impedance spectroscopy in different atmospheres (3% H_2/97% He with saturated water vapor, air, and air with saturated water vapor). Figure 3 shows the conductivity Arrhenius plot of $Ba_{0.98}(Ce_{0.65}Zr_{0.15}Y_{0.2})O_3$ ceramics at temperatures 100°-800°C. The activation energy changes near 600°C, which may indicate a conduction mechanism change. Coors and Readey [1] first observed a marked change of proton conductivity activation energy in $Ba(Ce_{0.9}Y_{0.1})O_3$ ceramics at ~250°C. Accordingly, our substitution of Ce with Zr significantly increased this transition temperature. The activation energies in our samples (0.29 and 0.58 eV) are very close to those (0.26 and 0.56 eV) of Coors and Readey. Good proton conductivities of $Ba_{0.98}(Ce_{0.65}Zr_{0.15}Y_{0.2})O_3$ ceramics at intermediate temperatures (500°-700°C) were obtained, such as 1.01×10^{-2} $\Omega^{-1}cm^{-1}$ at 700°C.

Literature results for anode saturation current density for various combinations of fuel and diluent input gases were analyzed to calculate the average anode

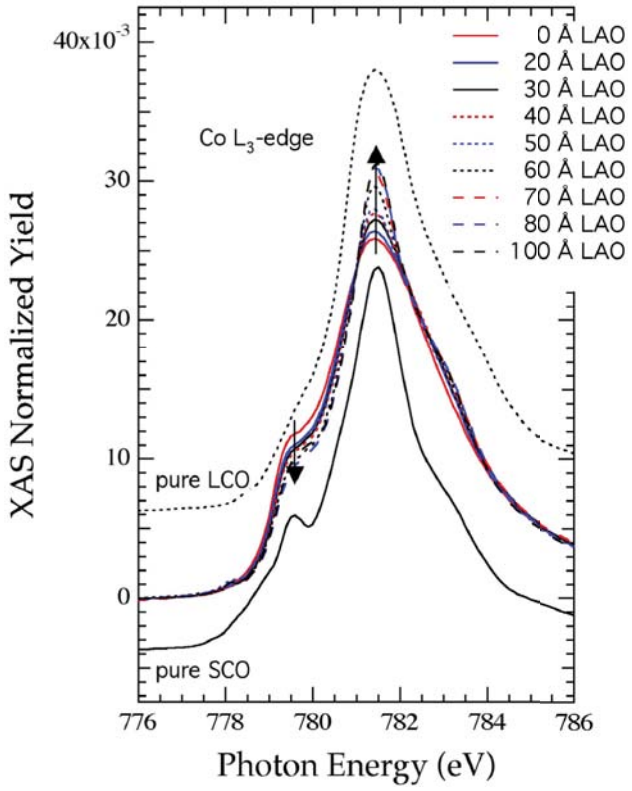

FIGURE 2. Co $L_{2,3}$ edge XAS spectra for LSCO thin films capped with LAO shown as a function of overlayer thickness (increased induced stress in the LSCO films). Also shown are spectra for pure SCO and pure LCO.

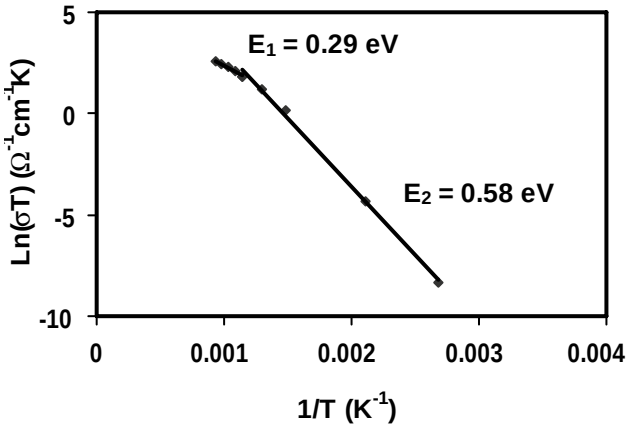

FIGURE 3. Arrhenius plot of proton conductivities (grain plus grain-boundary conductivities) of $Ba_{0.98}(Ce_{0.65}Zr_{0.15}Y_{0.2})O_{3-\delta}$ ceramics, with activation energies $E_1 = 0.29$ eV at 600-800°C and $E_2 = 0.58$ eV at 100-600°C.

pore tortuosity. Physically reasonable tortuosity values of 2 to 4 were calculated, much lower than some values in the literature. Detailed understanding of anode gas flow as influenced by tortuosity and other factors is required to optimize anode design in anode-supported SOFCs.

The voltage and power output of the SOFC stack model depend on conditions including fuel composition, fuel flow, oxidant flow, anode and cathode pressures, cell temperature, load current and the electrical and thermal properties of the cell materials. There is a time constant associated with the SOFC stack output voltage due to the double-layer charging effect (in the millisecond range), one due to the internal pressure (in the second range), and one due to temperature (in the minute range). Figure 4 (top) shows the V-I characteristics of the SOFC stack model (developed at MSU) at different temperatures, and Figure 4 (bottom) shows the same characteristics from the SECA model for a single cell provided to us.

Challenges for the fuel cell reference simulator addressed in this last year's work included developing high-performance analog electronics to drive current on the fuel cell side of the system, and high power voltage output amplifiers to drive the load side of the system. We assembled the voltage amplifier by paralleling three off-the-shelf amplifiers. The fuel cell side current source required custom design, and a printed circuit board was fabricated and modified to achieve acceptable performance. A working prototype design has been finalized and tested in the loop using a dry cell as a substitute for the fuel cell. Preliminary results show that this system mimics the dynamic response of the small power source (such as a button-cell SOFC) with high fidelity, but amplifies power levels to the several kilowatt range.

For the modular power electronics demonstration, we were able to use six Synqor power electronics modulars to create a multisource converter that could be used in conjunction with TRC. Unfortunately, the proposed scheme for controlling current on the fuel cell of this converter did not work due to the design of Synqor's current sharing. We were able to develop an alternative strategy but have not yet tested it.

An implementation of TRC in a Xlinix FPGA was accomplished. Although this implementation lacks some of the refinements needed for production use, it does demonstrate the feasibility of using transient recognition control for real-time mitigation of fuel cell/transient interactions.

The power circuit of the DC/DC converter can successfully boost a 25 V DC voltage to a 350 V one. The control circuit of the DC/DC converter can successfully produce proper control signals to implement the interleave control.

Simulation results showed that the proposed load sharing control method could achieve even load sharing among all inverters and control the zero sequence current of each inverter.

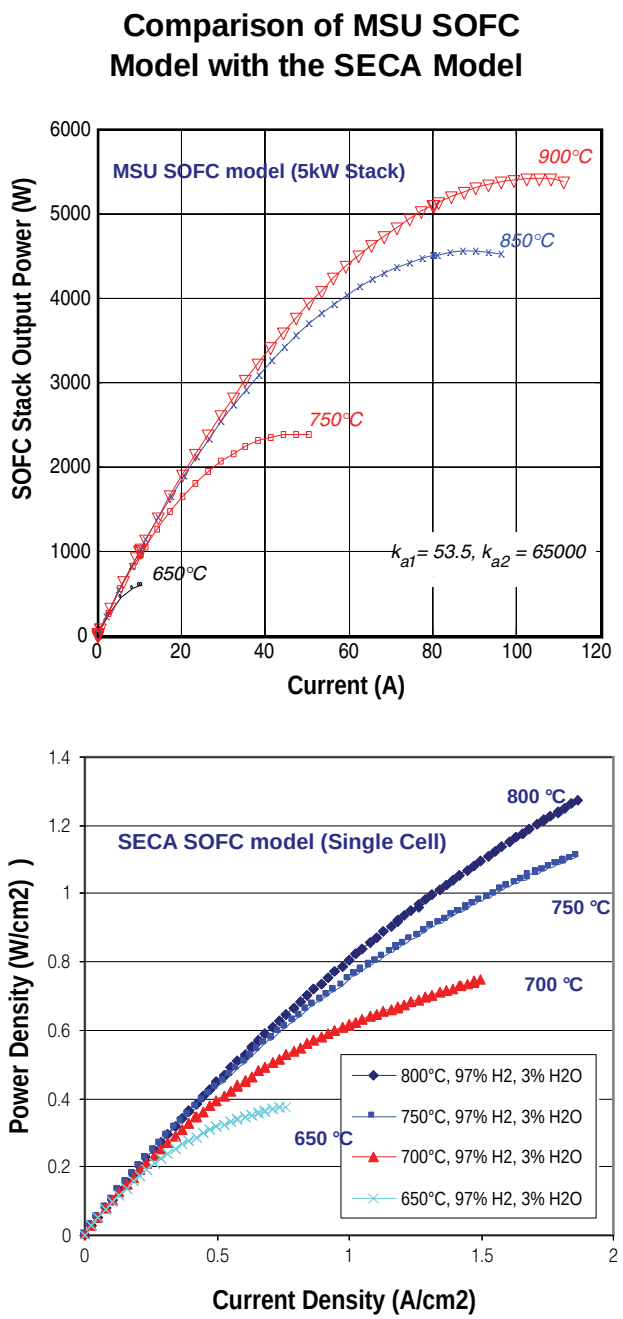

FIGURE 4. V-I Characteristics of the SOFC Model at Different Temperatures

Conclusions and Future Directions

We have explored a wide variety of coating techniques, compositions and architectures to enable the use of inexpensive ferritic steels as interconnects in SOFCs operating at 800°C. A combination of a filtered arc deposited adhesion-promoting, electronically conductive diffusion barrier CrAlYO bottom segment coating, followed by a filtered arc-assisted electron beam evaporated Cr-retentive and cathode compatible CoMnO top segment coating demonstrates excellent SOFC interconnect operating characteristics on commercially available 430 stainless steel. Future work will focus on optimizing coating composition and architecture and evaluating material systems under more prototypical SOFC exposures. Measurements of corrosion resistance with structured coatings, e.g., substrate/bondcoat/topcoat, to achieve good coating adhesion are planned. Measurements of oxygen transport in coatings and the effects of Cr surface contamination on oxygen exchange at cathode/electrolyte surfaces are underway. Growth of thin, dense YSZ films on porous YSZ anode material is currently under investigation for fabrication of thin SOFCs with reduced operating temperatures.

We will conduct similar X-ray experiments for other candidate SOFC materials such as $La_{0.5}Sr_{0.5}FeO_3$ and under operating fuel cell conditions.

Simulation results from the dynamic SOFC model developed compare well with the data provided to us from the SECA Excel model and in the SOFC research literature. The model is implemented in MATLAB/SIMULINK, a common modeling package used by the electrical engineering community and should help that community develop familiarity with SOFCs.

The fuel cell reference simulator development is making good progress. It is an important tool for allowing development of power electronics and control for SOFCs in parallel with the SOFC development. We need to complete whole system testing of the simulator.

We need to revise our proposed method for testing the interleaved modular power electronics and integrate this with TRC.

Special Recognitions & Awards/Patents Issued

1. TRC patent is pending.

2. S.R. Shaw received a National Science Foundation Career award.

FY 2006 Publications/Presentations

1. A. Kayani, R.J. Smith, S. Teintze, M. Kopczyk, P.E. Gannon, M.C. Deibert, V.I. Gorokhovsky, V. Shutthanandan, "Oxidation Studies of CrAlON Nanolayered Coatings on Steel Plates," *Surface Coatings and Technology*, accepted 2006.

2. A. Kayani, T.L. Buchanan, M. Kopczyk, C. Collins, J. Lucas, K. Lund, R. Hutchison, P.E. Gannon, M.C. Deibert and R.J. Smith, "Oxidation Resistance at 800°C for Magnetron-Sputtered CrAlN Coatings on 430 Steel," presented at International Conference on Metallurgical Coatings and Thin Films, San Diego, CA, May, 2006; submitted for publication to *Surface and Coatings Technology*, February 2006.

3. C. Collins, J. Lucas, T.L. Buchanan, M. Kopczyk, A. Kayani, P.E. Gannon, M.C. Deibert, R.J. Smith, D.S. Choi, V.I. Gorokhovsky, "Chromium Volatility of Coated and Uncoated Steel Interconnects for SOFCs," presented at International Conference on Metallurgical Coatings and Thin Films, San Diego, CA, May, 2006; submitted for publication to *Surface and Coatings Technology*, February 2006.

4. C. Wang and M.H. Nehrir, "A Dynamic SOFC Model for Distributed Power Generation Applications," Proceedings, 2005 Fuel Cell Seminar, Palm Springs, CA, November 2005.

5. C. Wang and M.H. Nehrir, "Distributed Generation Applications of Fuel Cells," Proceedings, 2006 Power Systems Conference, Clemson, SC, March 2006.

6. C. Wang and M.H. Nehrir, "Load Transient Mitigation for Solid Oxide Fuel Cells," Proceedings, 2006 ASME Fuel Cell Science, Engineering and Technology Conference, Irvine, CA, June 21, 2006.

7. C. Wang, M.H. Nehrir, and H. Gao, "Control of PEM Fuel-Cell Distributed Generation Systems," paper to be presented at the 2006 IEEE Power Engineering General Meeting, Montreal, Canada, June 2006; published in *IEEE Transactions on Energy Conversion*, Vol. 21, No. 2, June 2006.

8. E. Negusse and Y.U. Idzerda, "Extraction of Roughness Parameters from Specular X-Ray Resonant Scattering," *J. Appl. Phys.*, 2005. 97: p. 10C901.

9. J. Dvorak, Y.U. Idzerda, D.A. Arena, Y.G. Zhao, S.B. Ogale, T. Wu, T. Venkatesan, R. Godfrey and R. Ramesh, "Are Strain-Induced Effects Truly Strain Induced? A Comprehensive Study of Strained Lcmo Thin Films." *J. Appl. Phys.*, 2005. 97: p. 10C102.

10. M.H. Nehrir, "Modeling and Control of SOFC for Distributed Generation Applications," presentation of SOFC Dynamic model development at NETL, Morgantown, WV, March 2006.

11. M.H. Nehrir, C. Wang, and S.R. Shaw, "Fuel Cells: Promising Devices for Distributed Generation, Understanding their Modeling and Need for Control," *IEEE Power and Energy Magazine*, Vol. 4, No. 1, January/ February 2006.

12. P.E. Gannon, V.I. Gorokhovsky, M.C. Deibert, R.J. Smith, A. Kayani, P.T. White, Z. Gary Yang, J.W. Stevenson, S. Visco, C. Jacobson, H. Kurokawa, S.W. Sofie, "Enabling Inexpensive Metallic Alloys as SOFC Interconnects: an Investigation into Hybrid Coating Technologies to Deposit Nanocomposite Functional Coatings on Ferritic Stainless Steels," presented at 135th annual TMS meeting, San Antonio, TX, March 2006, accepted for publication in *International Journal of Hydrogen Energy*.

13. P.E. Gannon, V.I. Gorokhovsky, M.C. Deibert, R.J. Smith, A. Kayani, S. Sofie, Z. Gary Yang, J.W. Stevenson, S. Visco, C. Jacobson, H. Kurokawa, "Investigating Hybrid Filtered Arc Plasma Source Ion Deposition Technologies to Deposit Nanostructured Functional Coatings on Ferritic Stainless Steels. Part II: Simulated Solid Oxide Fuel Cell Interconnect Performance," presented at 2006 International Conference on Metallurgical Coatings and Thin Films; manuscript in preparation.

14. R. Sharma and H. Gao, "A New DC-DC Converter for Fuel Cell Powered Distributed Residential Power Generation Systems," presented in IEEE Applied Power Electronics Conference and Exposition, Dallas, TX, March 2006.

15. R. Sharma and H. Gao, "Low Cost High Efficiency DC-DC Converter for Fuel Cell Powered Auxiliary Power Unit of a Heavy Vehicle," accepted for publication in *IEEE Transactions on Power Electronic*s, November 2005.

16. S.R. Shaw, "Transient Recognition Control for Fuel Cell Systems," SECA CTP Peer Review Meeting (Invited), October 25, 2005.

17. T. Zhu, "Extended Cluster Weighted Modeling Methods for Transient Recognition Control," Ph.D. Thesis, June 2006.

18. V.I. Gorokhovsky, P.E. Gannon, M.C. Deibert, R.J. Smith, A. Kayani, M. Kopczyk, D. VanVorous, Z. Gary Yang, J.W. Stevenson, S. Visco, C. Jacobson, H. Kurokawa, S.W. Sofie, "High Temperature Oxidation, Cr Volatility and Surface Electrical Conductivity of Ferritic Steel with Filtered Arc and Hybrid Filtered Arc-Assisted EBPVD Coatings," accepted for publication in *Journal of the Electrochemical Society*.

19. V.I. Gorokhovsky, P.E. Gannon, M.C. Deibert, R.J. Smith, A. Kayani, S. Sofie, Z. Gary Yang, J.W. Stevenson, "Investigating Hybrid Filtered Arc Plasma Source Ion Deposition Technologies to Deposit Nanostructured Functional Coatings on Ferritic Stainless Steels. Part I: Deposition Process Parameters and Basic Coating Characteristics," presented at 2006 International Conference on Metallurgical Coatings and Thin Films; manuscript in preparation.

20. C. Wang, M.H. Nehrir, "A Physically-Based Dynamic Model for Solid Oxide Fuel Cells," paper conditionally accepted for publication in the *IEEE Transactions on Energy Conversion* (April 2006).

References

1. W.G. Coors, D.W. Readey, "Proton Conductivity Measurements in Yttrium Barium Cerate by Impedance Spectroscopy," *Journal of the American Ceramic Society*, 85 (2002) 2637-40.

VI.6 Advanced Fuel Cell Development

Objectives

- Evaluate DOE-sponsored SOFC systems.
- Measure response of SOFCs to coal contaminates and develop analysis tools to understand SOFC performance on coal syngas.
- Assess the dynamic performance of SOFC components and systems (e.g., hybrid and simple cycles), and determine control requirements for these advanced systems.
- Develop new coating methods for low-cost fuel cell metallic components.

Accomplishments

- Installed and operated the SECA Phase I prototype unit made by Delphi into the DOE Fuel Cell Test Facility to verify performance vs. SECA Phase I requirements.
- Measured the effect of hydrogen chloride, potentially one of the greatest (by volume) trace contaminate species after hydrogen sulfide, on SOFC performance, and developed detailed transport models to predict SOFC performance on coal syngas.
- Experimentally quantified the control response of hot and cold by-pass flows on hybrid operation, and obtained experimental validation of thermal gradient induced current recirculation within an SOFC cell following load loss.
- Advanced electrophoritic coating methods to allow application of manganese-cobalt and iron-nickel thin film coatings on SOFC metallic components.

Introduction

The U.S. DOE is supporting the development of solid oxide fuel cells through the Solid State Energy Conversion Alliance (SECA) program so that future coal-based power plants will achieve the highest possible fuel efficiency while protecting our environment. The goal of the SECA program is to provide low-cost fuel cell systems for multiple markets (e.g., stationary and automotive) as a stepping stone to low-cost coal-based plants. While several industry teams are currently developing SOFC systems for near-term markets, to achieve future coal-based operation will require new and innovative SOFC design and analysis tools, materials, and test and evaluation capability. The work performed here accomplishes all these by: 1) developing test capability for the evaluation of SOFC systems and components; 2) measuring the effects of coal syngas on cell performance; 3) applying advanced analysis tools for the purpose of understanding solid oxide fuel cell operation on coal syngas; and 4) developing low-cost manufacturing options for metal materials used in SOFCs.

Randall Gemmen
National Energy Technology Laboratory
3610 Collins Ferry Rd.
Morgantown, WV 26507
Phone: (304) 285-4536
E-mail: Randall.Gemmen@netl.doe.gov

Subcontractors:
The Georgia Institute of Technology, Atlanta, GA
University of West Virginia, WV

Approach

Systems Test and Evaluation Capability–Last year, the U.S. Department of Energy National Energy Technology Laboratory completed construction of a fuel cell test facility for evaluating the performance of prototype fuel cell systems developed by government sponsored fuel cell developers, Figure 1. The facility is configured to handle fuel cell systems running on natural gas or methane with a nominal power rating of 3 to 10 kW. As reported below, in FY 2007 this facility was used to evaluate two SECA prototype units.

Dynamic System and Component Studies–Both model and experimental studies are used to investigate the performance of fuel cell components and systems under real-world dynamic conditions. For systems studies, the focus is on hybrid systems, which is a key technology anticipated for future coal-based power plants. Here we employ a 'hardware-in-the-loop' approach whereby an experimental gas turbine is coupled to necessary hardware components (i.e., pipe volumes) that simulate the presence of a fuel cell via a real-time dynamic model. For component studies, the focus has been on fuel cell dynamics, and our approach is applying models to resolve conditions that exist when large load changes occur (events not commonly covered in the literature). Such conditions are of particular interest for SOFC operation given their relative sensitivity to increased thermal gradients that might arise, and it is important that models accurately predict the fuel cell response. In prior work, it was shown that these large transients induce conditions within the cell that result in current reversal, Gemmen and Johnson, (2005). To validate these results, this

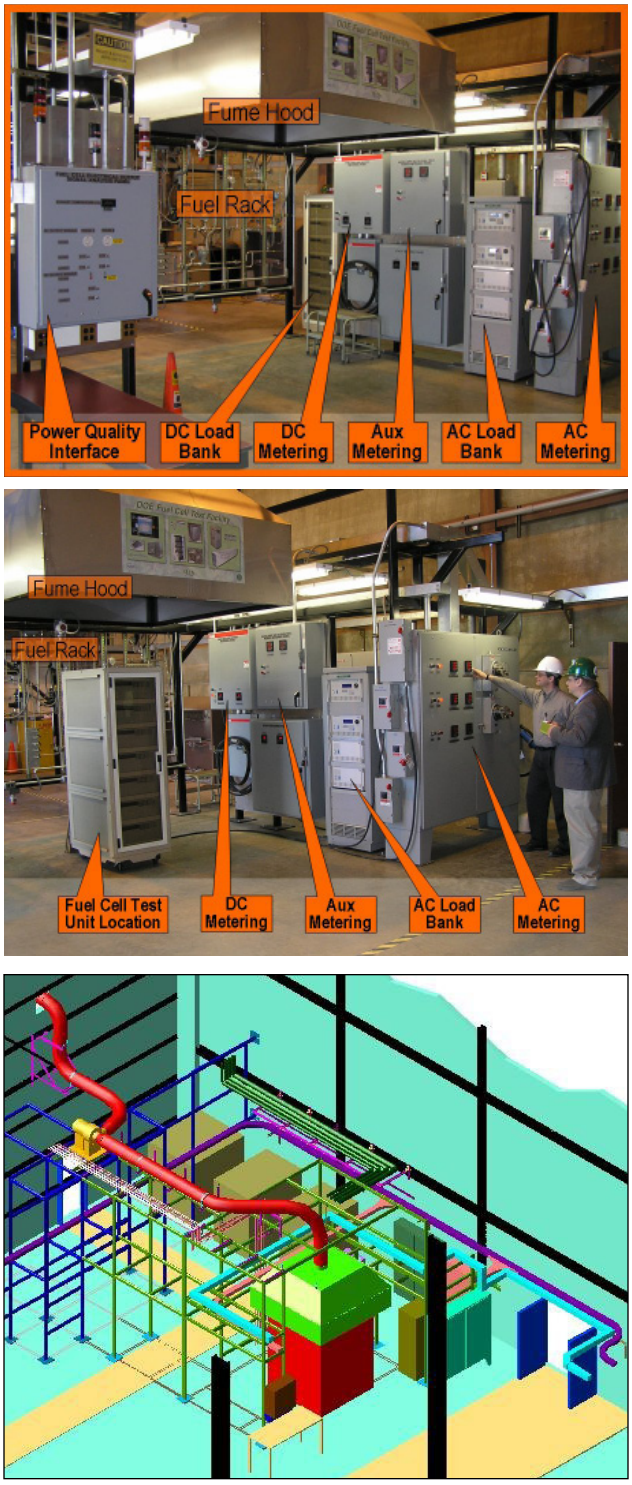

FIGURE 1. Photos and Layout of the DOE Fuel Cell Test Facility

project experimentally studied reverse current conditions induced by temperature variations.

Coal Syngas Operation–This year, we have begun investigating the effect of trace syngas elements (e.g., Cl, As, Cd, Hg, P) on SOFC operation. Our approach is to individually inject such elements in the forms that they exist under post syngas clean-up conditions into the fuel gas passing over an SOFC button cell. Because future cleanup systems have not been fully identified, these tests are performed over a range of temperatures and specie concentrations. Finally, plans are now under way to support a short term test at a U.S. gasification facility to directly assess SOFC operation on today's gasifier and cleanup technology.

Coatings for Metallic SOFC Components–There is a need to identify low-cost coating methods for the low-cost iron alloy steels used in SOFCs. The approach taken in this portion of our work is to investigate electrophoritic deposition methods. Such methods have an advantage in regards to their ability to deposit coatings on potentially intricate metallic components (components that have machined or stamped features to allow improved operation of the fuel cell). The goal of the tests performed this past year is to determine the proper liquid electrolyte compositions that provide the desired phase formations in the deposited coating. Systems studied thus far are Mn-Co and Fe-Ni coating systems.

Results

Systems Test and Evaluation Capability–This year, two SECA prototype units are to be independently tested by NETL. The first, by Delphi Corporation, has already completed testing, and analysis of the data is underway. Preliminary results show an average DC output efficiency of 31% over a 1-hour test. No measurable degradation (to within experimental resolution) was determined over the first 10-day portion of testing analyzed as of this writing. The second unit, by FuelCell Energy and Versa Power Systems Corporations, is currently being installed and testing should be completed by the end of the fiscal year.

Dynamic System and Component Studies–The hybrid simulation facility experimentally investigated the effect of cathode air bypass control on plant response. Two cases were investigated: (1) constant inlet temperature control via a combustor; (2) constant fuel input to the cathode inlet combustor. The work was published in the proceedings of the 2006 ASME Fuel Cell Conference, Tucker et al. (2006). Results showed that the initial plant response was due to fuel cell thermal energy output response which was lowered following a drop in cathode flow, Figure 2. As Figure 2 also shows, there is an immediate associated drop in turbine speed as well. This result was the same for both cases studied (albeit less for the case where fuel input was held fixed). The conclusion is that control of inlet combustor temperature cannot be used to manage short term changes in gas turbine response due to cathode air flow changes.

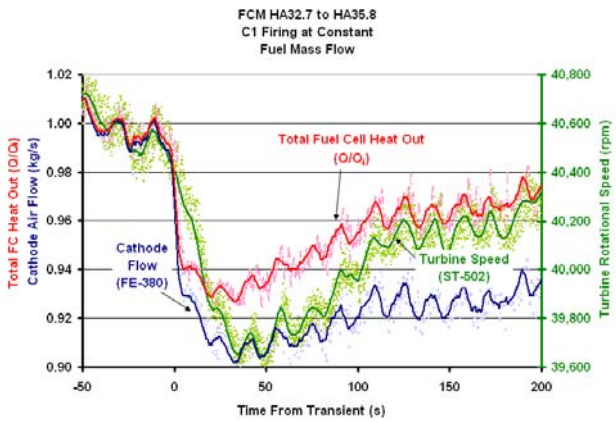

FIGURE 2. Cathode Air Inlet Flow, Turbine Rotational Speed and Total Fuel Cell Thermal Output Energy as a Function of Time Following Hot Air By-Pass Change

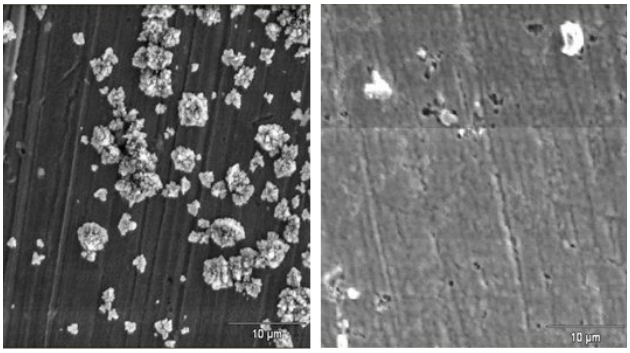

FIGURE 3. SEM images of deposits of Co on metallic substrates. The image on the left is of a deposit of Co from a simple solution of $CoSO_4$, and the image on the right shows the same deposition product, except that 0.0025M saccharin has been added to the solution.

Finally, regarding fuel cell component dynamic load studies, experimental results confirmed model predictions that show how thermal gradients result in internal current circulation upon loss of load, Gemmen et al. (2006). It is concluded that applications of models to study large load loss conditions, such as may be done to predict failure and degradation responses of fuel cells, will need to include electrolysis capability to achieve accurate predictions of the cell response.

Coal Syngas Operation–Both theoretical and experimental work has been performed to identify trace components that are reactive to nickel-based anodes. Because there is very little information regarding gas and solid phase components emitted from the gasifier and cleanup systems, detailed thermodynamic studies, using the FactSage software, were performed to guide the experimental work. Findings from the study showed that many of the trace species in the coal syngas will not likely interact with the SOFC anode. The elements Be, Cr, K, Na, V, and Z were all found to form condensed phase species under warm gas cleanup system conditions. Hence, it is likely that these species will not pose any great threat to SOFC anode operation except for potential gasifier/cleanup upset conditions. Finally, the thermodynamic evaluations showed that Sb, As, Cd, Hg, Pb, P, and Se vapor phase forms were found in the coal syngas at warm gas cleanup conditions which would allow the species to travel to the SOFC module and potentially interact with the SOFC anode. Hence, these components will be the focus of further thermodynamic and experimental work.

Coatings for Metallic SOFC Components–The electrophoritic research, Johnson et al. (2006) determined that saccharin addition to the deposition solution acts as a leveling agent, leading to much smoother films, Figure 3. It is also necessary to adjust the deposition potentials of the Mn/Co solution by complexation of the Co^{2+} ion with ethylenediamine tetraacetic acid (EDTA) and control of the Mn deposition species by adjusting the pH of the solution. In the case of the Ni/Fe solution, the relatively close standard reduction potentials for Ni and Fe means that chelation of the Ni^{2+} cation by EDTA suffices to adjust the deposition potential for the alloy solution. For the Mn/Co alloy deposition, it is important to take care not to drive the water splitting reaction so fast that localized pH levels cause hydroxide formation on the work piece. We have begun studying the oxidation process for the deposited alloys, and thus far spinel phases have been detected by x-ray diffraction after the alloy coated samples. It is not clear at this time what specific spinel has formed, and further analysis by scanning electron microscopy (SEM) and energy dispersive x-ray spectroscopy will be accomplished.

Conclusions and Future Directions

The DOE Fuel Cell Test Facility has begun independently evaluating SECA prototype units, and will be providing results to the SECA Program Management for their evaluation and assessments regarding progress being made in meeting SECA goals. Two Phase I units were tested in FY 2006, and the remaining four units will be tested in FY 2007. Beginning in FY 2007, the major level of future work will be in investigating coal-based fuel cell systems, and in particular the effects of trace species on fuel cell operation. Tests for the effects of Sb, As, Cd, Hg, Pb, P, and Se based compounds on fuel cell performance remains to be completed. While these studies will be the main focus, we also anticipate the need to improve our understanding of these future coal-based systems via steady and dynamic modeling investigations in order to be assured that proposed hybrid systems will operate safely. Finally, progress is still needed to achieve low-cost metallic components

suitable for SOFC conditions. Hence, continued work at developing low-cost coating methods will continue so that sufficiently dense and uniform thin film protective coatings, for both coal-based and non-coal-based SOFC systems, can be achieved.

Special Recognitions & Awards/Patents Issued

1. Best Paper Award–Cycle Innovation Committee of the ASME Turbo Expo. Shelton, M., I. Celik, I., E. Liese, D. Tucker, "A Study in the Process Modeling of the Startup of Fuel Cell/Gas Turbine Hybrid Systems," Paper No. GT2005-68466, ASME Turbo Expo 2005, Power for Land, Sea, and Air, June 6-9, 2005, Reno, NV.

FY 2006 Publications/Presentations

1. Gemmen, R., C. Johnson, "Effect of Load Transients on SOFC Operation–Current Reversal on Loss of Load," J. Power Sources, 144 (2005), pp. 152-164.

2. Gemmen, R., C. Johnson, "Thermal Gradient Induced Current Recirculation on Load Change in Solid Oxide Fuel Cells" Paper No. FUELCELL2006-97187, Proceedings of the Fourth International Conference on Fuel Cell Science, Engineering and Technology, June 19-21, 2006, Irvine, CA.

3. Gemmen, R., J. Trembly, "On the Mechanisms and Behavior of Coal Syngas Transport and Reaction within the Anode of a Solid Oxide Fuel Cell," submitted to J. Power Sources, 2006.

4. Johnson, C., R. Gemmen, C. Cross, "Alloy Films Deposited by Electroplating as Precursors for Protective Oxide Coatings on Solid Oxide Fuel Cells Metallic Interconnect Materials," to be presented at the Material Science and Technology Conference and Exposition, October 15-19, Cinergy Center, Cincinnati, OH.

5. Trembly, J.P., R.S. Gemmen, and D.J. Bayless, "The Effect of Coal Syngas with Hydrogen Chloride on the Performance of a Planar Solid Oxide Fuel Cell," 31st International Technical Conference on Coal Utilization & Fuel Systems, Clearwater, FL, May 21-25, 2006.

6. Trembly, J.P., R.S. Gemmen, and D.J. Bayless, "A Study of the Transport of Coal Syngas Species through a Solid Oxide Fuel Cell Anode," The 23rd International Pittsburgh Coal Conference, Pittsburgh, PA, September 25-28, 2006.

7. Tucker, D., L. Lawson, T. Smith, C. Haynes, "Evaluation of Cathodic Air Flow Transients in a Hybrid System Using Hardware Simulation," Paper No. FUELCELL2006-97107, Proceedings of the Fourth International Conference on Fuel Cell Science, Engineering and Technology, June 19-21, 2006, Irvine, CA.

8. Tucker, D., L. Lawson, J. VanOsdol, J. Kislear, A. Akinbobuyi, "Examination of Ambient Pressure Effects on Hybrid Solid Oxide Fuel Cell Turbine System Operation Using Hardware Simulation" Paper No. GT2006-91291, Proceedings of the ASME Turbo Expo 2006, May 8-11, 2006, Barcelona, Spain.

References

1. Gemmen, R., C. Johnson, "Effect of Load Transients on SOFC Operation–Current Reversal on Loss of Load," J. Power Sources, 144 (2005), pp. 152-164.

2. Gemmen, R., C. Johnson, "Thermal Gradient Induced Current Recirculation on Load Change in Solid Oxide Fuel Cells" Paper No. FUELCELL2006-97187, Proceedings of the Fourth International Conference on Fuel Cell Science, Engineering and Technology, June 19-21, 2006, Irvine, CA.

3. Tucker, D., L. Lawson, T. Smith, C. Haynes, "Evaluation of Cathodic Air Flow Transients in a Hybrid System Using Hardware Simulation," Paper No. FUELCELL2006-97107, Proceedings of the Fourth International Conference on Fuel Cell Science, Engineering and Technology, June 19-21, 2006, Irvine, CA.

4. Johnson, C., R. Gemmen, C. Cross, "Alloy Films Deposited by Electroplating as Precursors for Protective Oxide Coatings on Solid Oxide Fuel Cells Metallic Interconnect Materials," to be presented at the Material Science and Technology Conference and Exposition, October 15-19, Cinergy Center, Cincinnati, OH.

VI.7 Component Manufacturing and Optimization of Protonic SOFCs

Objectives

- Demonstrate p-SOFC performance of ≥125 mW/cm^2 at 600°C, using scalable manufacturing approaches and improved cell electrodes.
- Demonstrate enhanced cell electrode performance through compositional and microstructural tailoring. Demonstrate (cathode + anode) contributions of <0.5 Ω-cm^2 to cell area specific resistance (ASR) at 600°C.
- Establish tape casting and sintering routes to produce conventional electrolyte components at the button cell and 10 x 10 cm cell size. Minimize cell membrane thickness, with a target of ASR of <1.0 Ω-cm^2.
- Produce of Zn-modified BYZ $Ba(Zr_{1-X}Y_X)O_{3-\delta}$ electrolyte powders at the 600 g batch size, using scalable preparation routes, and demonstrate that these powders in tape cast forms can be sintered to densities of more than 95% ρ_{th} at temperatures of less than 1,400°C.

Accomplishments

- Demonstrated solid state synthesis route as a promising route for production of the proton conducting electrolyte material.
- Densified $BaZr_{0.85}Y_{0.15}O_3$ with ZnO doping (BYZ-Zn) material to 94% theoretical density at 1,550°C.

Matthew M. Seabaugh (Primary Contact), Kathy Sabolsky, Sergio Ibanez, Edward M. Sabolsky, and Michael J. Day
NexTech Materials, Ltd.
404 Enterprise Drive
Lewis Center, OH 43035
Phone: (614) 842-6606; Fax: (614) 842-6607
Website: www.nextechmaterials.com

DOE Project Manager: Lane Wilson
Phone: (304) 285-1336
E-mail: Lane.Wilson@netl.doe.gov

Subcontractor: Dr. Sossina Haile
Professor of Materials Science and of Chemical Engineering
Steele Laboratories, Room 307
Materials Science, 309-81
California Institute of Technology
1200 E. California Boulevard
Pasadena, CA 91125
Phone: (626) 395-2958; Fax: (626) 395-8868
Website: http://addis.caltech.edu/

Introduction

Protonic solid oxide fuel cells (p-SOFCs) offer unique characteristics compared to competing technologies. In a p-SOFC, protons diffuse from the anode to the cathode through a thin membrane layer, generating power from the electrochemical reaction. P-SOFCs are characterized by their potential for high fuel utilization without steam diffusion limitation, and their intermediate operating temperatures (450-600°C). P-SOFCs avoid steam formation at the anode (experienced by SOFCs), maintaining high fuel concentration over the anode, allowing high fuel utilization and high-efficiency operation. The cells operate at temperatures that increase the reaction kinetics compared to PEM fuel cells, but are low enough to offer the potential for metal interconnects without corrosion. If operating temperatures can be kept at the lower end of this range (using thin membranes and efficient electrodes) conventional high temperature seals may become practicable, avoiding a design issue of SOFC systems.

To date, p-SOFC development has been hampered by processing difficulties associated with ceramic proton-conductors. In this project, NexTech and Caltech will collaboratively advance the materials science and manufacturing technology for ceramic p-SOFCs. Using materials processing strategies for $Ba(Zr_{0.8}Y_{0.2})O_3$ identified by Caltech, NexTech will fabricate its thin-membrane electrolyte-supported cells using proprietary designs well suited to the BYZ material set. This demonstration will require the transition of demonstrated laboratory processes to commercially viable approaches. Caltech will assist this transition and use the resultant cell platform to optimize p-SOFC electrodes. The successful completion of this project will shift p-SOFC development from electrolyte development to electrode optimization and the large cell demonstration.

Approach

Researchers at Caltech have developed a chemical approach in which a sintering aid is used to enhance grain growth and enable densification at reduced temperatures [1]. From a comprehensive screening of transition metal oxides, it was determined that ZnO enhances sintering without generating deleterious intermediate phases or introducing excessive electronic conductivity.

NexTech has developed cost-effective manufacturing processes for a range of state-of-the-art SOFC cell designs. These efforts have revealed the manufacturing and performance strengths and weaknesses of various cell manufacturing approaches. Based on this experience, NexTech developed target specifications for an optimized solid oxide fuel cell, a planar cell component with a thin (≤50 µm) electrolyte, a 30-50 µm thick anode (to improve fuel oxidation kinetics) and a 30-50 µm thick cathode (to minimize oxygen diffusion limitations). The cell should be mechanically robust and have a dense periphery to simplify sealing.

The cell developed by NexTech offers an excellent demonstration platform for protonic electrolyte and fuel cell research. The principal manufacturing steps for the cell platform are tape casting and co-sintering. The processing routes developed at Caltech have been demonstrated with glycine-nitrate produced powders having surface area values (5-8 m^2/g), ideal for tape casting approaches. In this project, NexTech will tailor this process for scaled-up powder production and validate its utility in tape casting and cell fabrication experiments.

Results

ZnO-doped $BaZr_{0.85}Y_{0.15}O_3$ (BYZ-Zn) material was synthesized by the solid state route, producing powder with 11.4 m^2/gm surface area, reasonable for the tape casting approach. The solid state synthesis route was selected due to its scalability and high throughput.

Figures 1 and 2 show the results of the dilatometry and the sintering study for BYZ-Zn synthesized by the solid state route. The dilatometry data shows that the material starts to sinter around 1,100°C and completes its shrinkage by 1,500°C. The sintering study shows that BYZ-Zn sinters to 94% theoretical density at 1,550°C, confirming that the solid state synthesis is a promising route for production of the BYZ-Zn material.

Conclusions and Future Directions

The solid state synthesis route is a promising route for production of the BYZ-Zn material and fabrication of dense electrolyte components at reasonable sintering temperatures. The ongoing work focuses on development of tape casting formulations using the synthesized powder for production of thin electrolyte substrates for fuel cell evaluations.

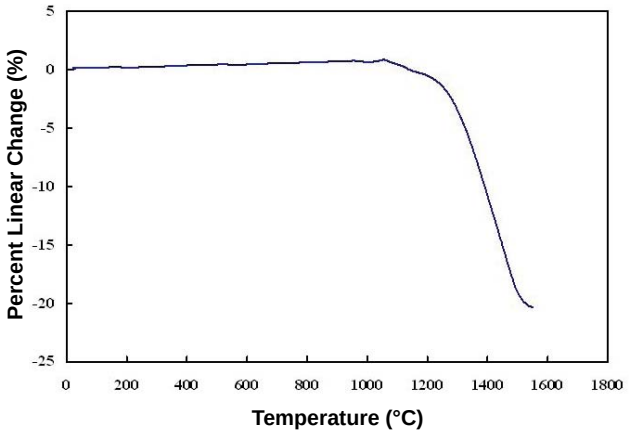

FIGURE 1. Dilatometry Data for BYZ-Zn Synthesized by Solid State Route

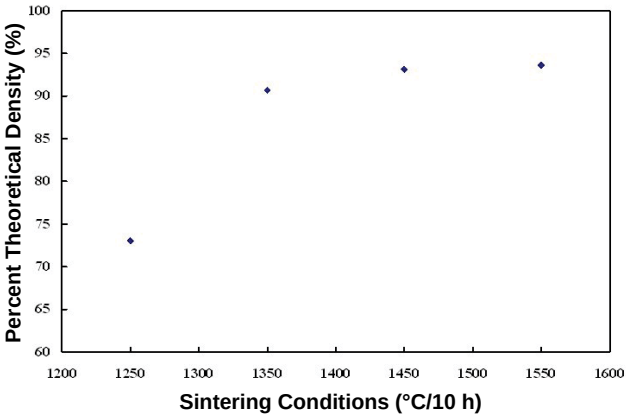

FIGURE 2. Sintering Study for BYZ-Zn Synthesized by Solid State Route

References

1. Babilo, P., and Haile, S.M., *J. Am. Ceram. Soc.*, 88 (9), 2362-2368 (2005).

VI.8 High Temperature Fuel Cells for Cogeneration of Chemicals and Electricity

Objectives

- Determine the thermal self-sustainability, temperature gradients, electrical output, product composition, efficiency, and syngas productivity of a methane electrochemical partial oxidation (EPOx) reactor.
- Develop methods to avoid coking, and prove that excellent stability against coking can be achieved during long-term operation.
- Explore the use of alternative anode materials in order to eliminate coking with methane and other hydrocarbons and also allow redox cycling.
- Evaluate the technical and economic viability of the proposed technology based on the above information.

Accomplishments

- We have shown that a change in the gas flow geometry of the SOFC tests yields an improvement in methane conversion to syngas from approximately 70% to over 90%. This is significant because it proves the EPOx SOFC reactors can provide very high conversion to syngas.
- Modeling results (in collaboration with Professor Robert Kee at Colorado School of Mines) have shown that adding an anode barrier layer can keep the Ni-YSZ anode completely outside of the thermodynamic coking range. This is important because it demonstrates that this geometry can be expected to provide stable operation over long time periods.
- Substantial increase in the cell stability parameter range (critical current decrease by a factor of approximately 2 times) was demonstrated by adding small amounts (approximately 20%) of air or CO_2 to the methane fuel feed.

Scott A. Barnett (Primary Contact), Manoj Pillai, Yuanbo Lin

Northwestern University
Department of Materials Science and Engineering
Evanston, IL 60208
Phone: (847) 491-2447; Fax: (847) 491-7820
E-mail: s-barnett@northwestern.edu

DOE Project Manager: Heather Quedenfeld

Phone: (412) 386-5781
E-mail: Heather.Quedenfeld@netl.doe.gov

Introduction

In the first year of this Phase I project, we have demonstrated the feasibility of combined chemical and electricity cogeneration using solid oxide fuel cells (SOFCs). Suitable operating conditions were established for doing electrochemical partial oxidation of natural gas that produced maximum electrical power output while providing maximum conversion of the fuel to synthesis gas (H_2+CO). The problem of coke formation on the SOFC anodes was addressed, with a new barrier layer approach and changes in fuel composition shown to increase the parameter range for stable coke-free operation.

This approach has significant potential economic advantages. That is, when SOFCs become cost effective for electricity generation, the syngas becomes a low-cost by-product. This could provide an important new route to low-cost hydrogen and gas-to-liquid fuels. From another perspective, the ability to sell both electricity and chemicals increases the value of the SOFCs, improving their prospects for commercialization.

Approach

Extensive electrical testing of anode-supported SOFCs with methane fuel was done in combination with gas chromatograph and mass spectrometer measurements of reaction products for a range of conditions. While these were single-cell tests, the cell area and current were large enough to achieve partial oxidation stoichiometry ($O^{2-}/CH_4 \approx 1$) for reasonable fuel flow rates. Cell stability was tested versus operating conditions, additions of H_2O/CO_2 to the methane, and catalyst/barrier layers. Successful testing for over 300 hours was also carried out. These experiments provided the experimental proof that SOFCs can act as effective devices for cogenerating electricity and syngas.

Detailed modeling was carried out in collaboration with Colorado School of Mines, providing detailed predictions of gas composition gradients within the anode and anode flow field. The work focused on the effect of anode barrier layers on overall cell/stack performance and changes in the gas composition within the Ni-YSZ anode that influence anode coking. Most model input parameters were quantitatively established by structural evaluation of the SOFCs and barriers

combined with calibration experiments on the SOFCs prior to methane testing. These experiments provided a compelling explanation for how direct-methane SOFCs can work without coking, and also a means for predicting conditions for stable SOFC operation.

Results

Extensive cell electrical testing showed results as expected for anode-supported SOFCs operated with methane fuel [1]. For example, at 750°C and 0.7 V, the current density was 0.8 A/cm^2 and the power density was 0.57 W/cm^2. Differentially pumped mass spectra from the SOFC anode gas stream (Figure 1) showed a decrease in methane-related (mass 16) peaks and an increase in hydrogen (mass 2) and CO (mass 28) with increasing SOFC current density. (Note that the methane flow rate was fixed such that the ratio O^{2-}/CH_4 was proportional to the current density.) H_2 and CO reached maximum values at $O^{2-}/CH_4 \approx 0.7$ before decreasing with further increases in O^{2-}/CH_4. The CO_2 content (mass 44) remained low at low O^{2-}/CH_4 but then increased more rapidly when O^{2-}/CH_4 increased above 0.7.

These trends agree with the equilibrium thermodynamic prediction, except that CH_4 did not decrease to zero at large O^{2-}/CH_4, and the peak H_2 and CO content appears well below the predicted value $O^{2-}/CH_4 = 1$. Both these differences can be explained if a fraction of inlet CH_4 flow does not react, possibly due to the flow geometry of our SOFC test. In order to test the above idea, we did additional experiments with an altered geometry where all the CH_4 flowed over the full radius (approximately 1 cm) of the anode. Figure 2 shows schematically the original and new geometries and plots the methane utilization versus O^{2-}/CH_4 for both cases. The methane utilization saturates at approximately 70% for the original geometry, but for the altered geometry increases continuously to approximately 90% with increasing O^{2-}/CH_4 to 1. In the new geometry, the H_2 and CO mass spectrometer peaks increase continuously with increasing O^{2-}/CH_4 in this range, in better agreement with the thermodynamic prediction. The maximum measured syngas production rate estimated based on mass spectrometer sensitivities was approximately 20 sccm cm^{-2}.

Taken together, the above results demonstrate that a direct-methane SOFC can work very effectively for both producing electricity and converting methane to syngas.

In order to maintain thermal balance in an EPOx SOFC, it may be useful to operate at voltage (*V*) values as low as 0.4 V. Electrical test results show the low voltage actually provides higher power density than $V = 0.7$ V. Another advantage of lower *V* is that decreasing from a typical SOFC $V = 0.7$ V to 0.4 V approximately doubles *J*. That is, the oxygen ion current density and the syngas production rate are approximately doubled. However, this way of operating a SOFC, with pure methane fuel, low *V*, and high current density, is unusual, so it is important to demonstrate that the cells can operate stably. Endurance tests carried out on a number of cells showed stable operation. Figure 3 shows an example of a SOFC life test conducted for over 300 hours. The test was carried out with an anode catalyst layer using dry methane at 30 sccm, $O^{2-}/CH_4 = 0.82$, $V \approx 0.4$ V, and 750°C. The SOFC showed a slight performance decrease during the first 150 hours (which is not unusual for SOFCs), followed by stable operation for the final 200 hours. Subsequent scanning electron microscopy-energy dispersive x-ray spectroscopy observations showed that no carbon was present on the anode.

We have been fortunate to develop a collaboration with Professor Robert Kee at Colorado School of Mines, who has well-developed models that account for the

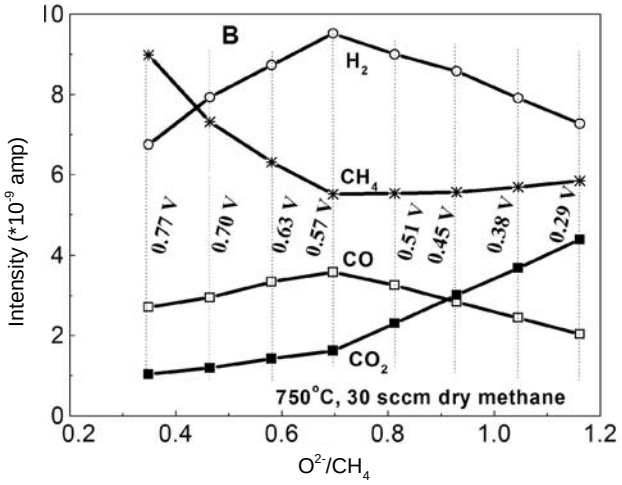

FIGURE 1. Product Gas Composition versus Oxygen to Methane Ratio

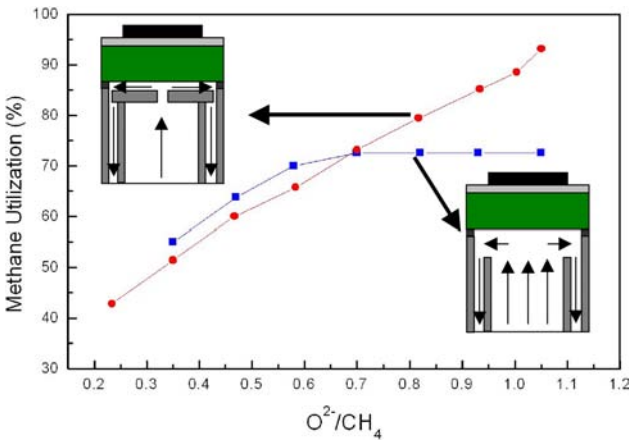

FIGURE 2. Comparison of Methane Utilization versus Oxygen to Methane Ratio for Two Gas Flow Geometries

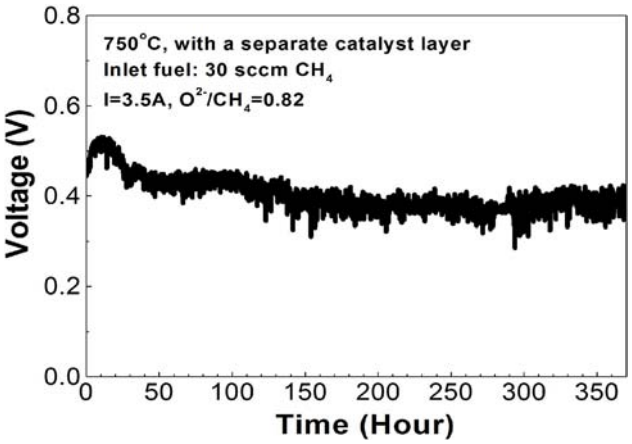

FIGURE 3. SOFC Stability Test during Methane EPOx Operation

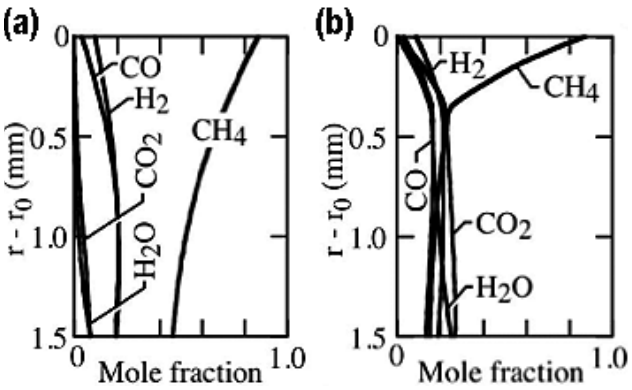

FIGURE 4. Calculated Gas Composition versus Position during Direct-Methane SOFC Operation within the Ni-YSZ Anode (a) and a Ni-YSZ Anode with a 0.3 mm Thick Barrier Layer (b)

details of flow, reactions, and electrochemistry within the anode compartment of a SOFC. Detailed structural information (e.g., layer thicknesses, porosities) measured from the specific SOFCs, along with known reaction rates on Ni-YSZ anodes, are input in order to make the results more quantitative. Further model calibration of gas transport within the anode microstructure was achieved by matching the calculations to experimental cell calibration measurements in different hydrogen-steam mixtures.

The simulation was then applied to methane operation, using the above anode information as well as prior data on reforming reaction rates within Ni-YSZ anodes. Some of the results are shown in Figure 4, which compares a case of a conventional Ni-YSZ anode (Figure 4a) with a Ni-YSZ anode with a 0.3 mm thick zirconia barrier layer (Figure 4b) [2]. The figures show the gas composition profile from the gas flow side (top) to the electrolyte (bottom). In Figure 4a, the decrease in CH_4 content approaching the electrolyte side is seen, along with an increase in the products H_2O and CO_2. With the barrier layer, the methane content within the Ni-YSZ portion is substantially decreased, whereas the products H_2O and CO_2 tend to be trapped in the anode. The overall result is that the fuel composition in the Ni-YSZ anode is kept outside of the equilibrium coking range. This is an important result helping to explain how direct-methane SOFCs can maintain stable operation.

Experiments have been done to determine the effects of adding small amounts (approximately 20%) of air or CO_2 to the methane fuel. Initial results suggest that the additions increase the parameter range for stable coke-free operation.

Conclusions and Future Directions

The above cell test and mass spectrometer results demonstrate that direct-methane SOFCs can effectively produce electricity and convert methane to syngas. Cell stability testing has continued to help delineate the stable operation range for SOFCs with methane fuel. Model calculations of the anode compartment in SOFCs have also been important for understanding how anode barrier layers allow stable operation by keeping the Ni-YSZ anode outside of the equilibrium coking range.

In future work, we will continue ongoing work on cell stability, including effects of barrier layers and modifications of the fuel composition (i.e., adding small amounts of air, steam, or CO_2). Note that the work with air will also serve to show the effects of contamination in natural gas. We will also conduct tests with simulated natural gas containing realistic amounts of ethane and propane. Other experiments will include testing of ceramic anode SOFCs, more long-term testing, and testing of larger-area devices.

Simulation work will continue in order to obtain more accurate predictions of gas composition and temperature gradients within the anode, as well as overall stack performance. The simulations will also be carried out with air addition to methane, suitable for improving thermal balance in stand-alone reactors, and with steam/CO_2 addition, suitable for use in tandem with a source of heat and steam/CO_2 such as a coal gasifier. Decisions will be made as to the best operating conditions for free-standing devices versus devices operated with an external source, and the best catalyst/barrier layer combination will be selected.

FY 2006 Publications/Presentations

1. Zhongliang Zhan, Yuanbo Lin, Manoj Pillai, Ilwon Kim, Scott A Barnett, "High-Rate Electrochemical Partial Oxidation of Methane in Solid Oxide Fuel Cells," J. Power Sources, in press.

2. Huayang Zhu, Andrew M. Colclasure, Robert J. Kee, Yuanbo Lin, Scott A. Barnett. "Anode Barrier Layers for Tubular Solid-Oxide Fuel Cells with Hydrocarbon Fuel Streams," J. Power Sources, in press, 2006.

3. Robert J. Kee, Huayang Zhu, Andrew M. Colclasure, Yuanbo Lin, and Scott A. Barnett, "Tubular Solid-Oxide Fuel Cells Using Either Anode Recycle or Barrier Layers," Proceedings of the 7th European Fuel Cell Forum, Ulf Bossel, Editor, Paper Number B074, 2006.

4. Robert J. Kee, Huayang Zhu, Andrew M. Colclasure, Yuanbo Lin, and Scott A. Barnett, "Tubular Solid-Oxide Fuel Cells Using Either Anode Recycle or Barrier Layers," Presented at 7th European Fuel Cell Forum, Lucerne, Switzerland, July 3-7, 2006.

5. Scott A. Barnett, "Energy Applications of Solid Oxide Fuel Cells," 2006 Taiwan – Midwest-USA Symposium on Science and Engineering, Evanston, IL, June, 2006.

6. Scott A. Barnett, "Solid Oxide Fuel Cells: New Materials and New Applications," Montana State University, Bozeman, MT, March, 2006.

7. Yuanbo Lin, Zhongliang Zhan, Ilwon Kim, Scott A. Barnett, "Co-Production of Hydrogen/Syngas and Electricity by Direct-Methane Solid Oxide Fuel Cells," American Ceramic Society Meeting, Cocoa Beach, January, 2005.

8. Scott A. Barnett, "Solid Oxide Fuel Cells: New Materials and New Energy Alternatives," Carnegie-Mellon University, Dept. of Materials Science colloquium, December, 2005.

9. Scott A. Barnett, "Solid Oxide Fuel Cells and the Hydrogen Economy," Colorado School of Mines, Chemical Engineering Department, December, 2005.

References

1. Y. Lin, Z. Zhan, J. Liu, and S.A. Barnett, "Direct Operation of Solid Oxide Fuel Cells with Methane Fuel," Solid State Ionics, 176, 1827-1835 (2005).

2. Y. Lin, Z. Zhan, and S.A. Barnett, "Improving the Stability of Direct-Methane Solid Oxide Fuel Cells Using Anode Barrier Layers," Journal of Power Sources, In Press.

VI.9 High Temperature Electrochemistry Center - PNNL

Objectives

The High Temperature Electrochemistry Center provides crosscutting, multidisciplinary research that supports the Office of Fossil Energy's mission to improve the efficiency and minimize the environmental consequences of electrical power generation from fossil fuels.

- Develop reversible solid oxide fuel cell technology capable of efficiently producing hydrogen in an electrolysis mode as well as producing electrical power from stored hydrogen in the fuel cell mode.
- Develop energy storage concepts that utilize electrochemical processes at high temperatures.
- Develop oxide-based thermoelectric materials and forms that can be used to produce electricity from waste heat available from fuel cell systems.
- Investigate how the performance of solid oxide fuel cells may be affected by contaminants present in coal gas.

Accomplishments

- Electrode inefficiencies in reversible fuel cells have been established as a function of temperature, steam, and hydrogen partial pressure. Nickel-based hydrogen electrodes show higher activity in the fuel cell than electrolysis direction, while the opposite was found for titanate/ceria hydrogen electrodes. Interfacial depletion of oxygen vacancies for mixed conducting oxygen electrodes resulted in limiting currents in the electrolysis direction. Full reversible fuel cell stacks showed higher resistances in the electrolysis versus fuel cell direction, consistent with electrode studies.
- An *n*-type oxide material has been developed that exhibits a thermoelectric figure of merit more than three times higher than that of any other known *n*-type bulk oxide and is stable to high temperatures. When coupled with high-yield *p*-type oxides, these new *n*-type materials will enable the development of efficient thermoelectric generators capable of generating electricity from waste heat available from fuel cell systems.
- Densification of lanthanum strontium manganite oxygen electrode materials at substantially lowered temperatures was achieved by both thermal and oxygen partial pressure cycling. Enhanced sintering occurred in the 700-1000°C range, hundreds of degrees cooler than the usual processing temperature for lanthanum manganites. This behavior is the result of a super-stoichiometric oxygen content, which leads to high metal vacancy concentrations in the perovskite lattice.

L.R. Pederson (Primary Contact), O.A. Marina, S.C. Singhal, X.-D. Zhou, G.W. Coffey, J.S. Hardy, B.P. McCarthy, D. Nguyen, Z. Nie, and E.C. Thomsen

Pacific Northwest National Laboratory
902 Battelle Blvd., PO Box 999
Richland, WA 99352
Phone: (509) 375-2731; Fax: (509) 375-2167
E-mail: larry.pederson@pnl.gov

DOE Project Managers: Heather Quedenfeld and Lane Wilson

Phone: (412) 386-5781
E-mail: Heather.Quedenfeld@netl.doe.gov
Phone: (304) 285-1336
E-mail: Lane.Wilson@netl.doe.gov

Subcontractors:

Montana State University, Bozeman, Montana
University of Florida, Gainesville, Florida

Introduction

The High Temperature Electrochemistry Center (HiTEC) brings together researchers from national laboratories and universities to address topics of relevance to solid oxide fuel cells (SOFCs) operating on fuels derived from coal, in support of DOE's Solid State Energy Conversion Alliance (SECA) program. Research performed under HiTEC is intended to be generally of longer term and more fundamental in nature than that conducted by the SECA core technology or industry teams. The National Energy Technology Laboratory, Montana State University, The University of Florida, and the Pacific Northwest National Laboratory (PNNL) currently are contributors to HiTEC.

Specific research topics in energy conversion and storage being addressed by the overall program include high temperature steam electrolysis/reversible fuel cell development, interaction of fuel cell anodes with coal-based contaminants, fundamental studies of reactions at the cathode/electrolyte interface, advanced x-ray studies of buried interfaces, the development of corrosion-inhibiting multilayer film technology, modeling and simulation of ion transport processes, waste heat recovery with oxide-based thermoelectrics, and fuel cell diagnostics and controls. Research conducted by HiTEC will help guide the development of advanced fuel cell materials with superior performance, thereby leading to improved SOFC performance when operated on coal-derived fuels.

Approach

Research activities being conducted at PNNL include topics relevant to reversible fuel cells, high temperature thermoelectric generators to convert waste heat to electricity, energy storage concepts, and investigations of hydrogen electrode interactions with coal-based contaminants. Reversible fuel cells offer the capability of producing hydrogen fuel from steam during periods of excess grid capacity, and converting that hydrogen to electricity during later periods of high demand. Research has been focused on understanding electrode activity and stability issues in high steam partial pressures and other conditions unique to this approach. Limits of stored charge and energy in electrochemical cells with composite electrodes are being investigated as a possible means of improving fuel cell load management. New oxide compositions exhibiting high thermoelectric figures of merit are being developed for possible use in thermoelectric generators capable of operating at high temperatures typical of fossil energy conversion devices. Layered structures are being emphasized as a means of limiting the thermal conductivity while maintaining high thermoelectric yields and high electrical conductivity. Also being investigated are interactions of the hydrogen electrode with contaminants known to be present in coal gas. This research will help establish criteria for cleanup of coal gas intended as fuel for SOFCs.

Research at PNNL is conducted in collaboration with Montana State University and the University of Florida. Joint research activities emphasize the development of a fundamental understanding of reactions and processes that occur at the electrode-electrolyte-gas interface, critical to the operation of a wide range of electrochemical technologies including fuel cells, electrolyzers, sensors, and gas separation membranes. Joint research includes the development of simulation methods, which provide insight on ion and electron transport mechanisms; the structure and thermodynamic properties of vacancy clusters; and oxygen reactions at surfaces and interfaces.

Results

Reversible Fuel Cell Studies. Reversible fuel cells offer a potentially attractive means of energy storage, allowing hydrogen fuel production during periods of excess grid capacity and enabling that chemical energy to be converted to electricity during periods of greater need. Reversible fuel cell stacks were produced from anode-supported cells with a Ni/YSZ anode, a cathode composed of $La_{0.60}Sr_{0.40}Co_{0.20}Fe_{0.80}O_x$, and 7 micron-thick YSZ electrolyte, and tested in both fuel cell and electrolysis modes at various steam partial pressures. Losses were consistently higher in the electrolysis than fuel cell mode, as shown in Figure 1, but were largely independent of the steam partial pressure until greater than 90% conversion.

Half-cell measurements performed for several hydrogen and oxygen electrodes showed inherent differences in performance in the fuel cell and electrolysis directions. The activity of the Ni/YSZ hydrogen electrode was clearly higher in the fuel cell mode, as shown in Figure 2. Current-voltage characteristics are consistent with charge transfer as the rate-limiting step in the fuel cell direction, whereas mass transfer contributions were significant

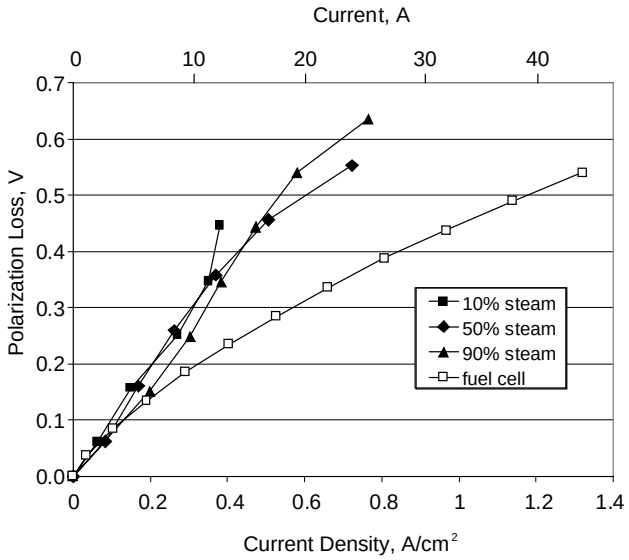

FIGURE 1. Polarization losses versus current density for an anode-supported stack, corrected for initial steam/hydrogen concentrations and reaction at 750°C. The anode was composed of Ni/YSZ, while the cathode was $La_{0.60}Sr_{0.40}Co_{0.20}Fe_{0.80}O_x$. Losses were higher in the electrolysis than fuel cell mode, consistent with the results of half-cell tests.

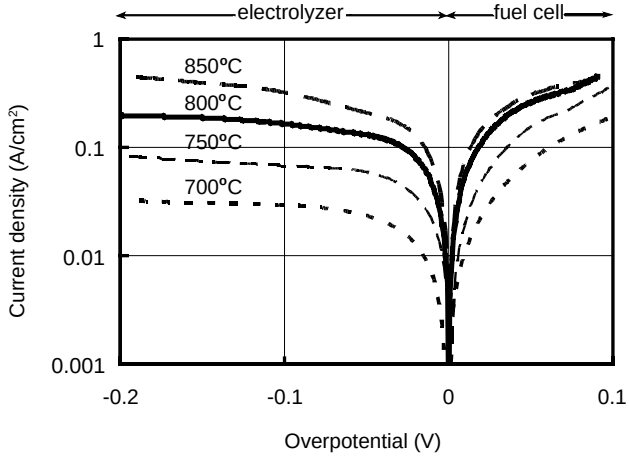

FIGURE 2. Current-overpotential dependencies obtained on Ni-YSZ electrode at $H_2/H_2O/N_2 = 10/70/20$ in the temperature range 700-850°C, showing higher activity in the fuel cell than electrolyzer direction.

in the electrolysis direction. Titanate-ceria composite hydrogen electrodes were also evaluated and were found to be more active than standard Ni/YSZ compositions for steam electrolysis, whereas the two electrodes show similar activity as the anode in a solid oxide fuel cell. Oxygen electrodes consistently gave higher activity in the fuel cell direction, especially for compositions that exhibit substantial mixed electron and ion conductivity. An example of this behavior is given in Figure 3 for a substituted lanthanum copper ferrite composition. Under cathodic polarization, currents rose more rapidly than expected for charge transfer control, while limiting currents were attained under anodic polarization. This behavior is attributed to the production of oxygen vacancies under cathodic polarization and to the depletion of oxygen vacancies at the interface under anodic polarization. Oxygen electrodes such as lanthanum manganite are not mixed conductors and give much more symmetric anodic and cathodic polarization losses. Though somewhat more resistive in the electrolysis than fuel cell direction, reversible fuel cells appear to be an attractive option for energy storage. If operated above the thermal neutral potential of approximately 1.3 volts per cell, the overall electrolysis reaction is exothermic and the stack can be operated without supplemental heat.

Oxide-Based Thermoelectric Material Development. The thermoelectric properties of layered perovskite materials are being investigated, focusing on *p*-type alkaline earth cobalt oxides and on *n*-type substituted indium oxides. Research on thermoelectric materials involves developing novel synthetic routes to anisotropic materials; determining oxygen nonstoichiometry, particularly associated with transition metal-oxygen planes; and understanding fundamental physics related to anisotropic properties of thermoelectrical power, electrical resistivity, and thermal conductivity. Unlike traditional thermoelectric materials, these oxides are compatible with high temperatures produced in fossil energy conversion systems.

A new *n*-type material consisting of substituted indium oxide has been developed that exhibits a thermoelectric yield more than three times higher than that of any other known bulk oxide. Figure 4 provides figure of merit results for the new material as well as literature results for substituted manganese oxides, which are the best performing *n*-type oxides reported previously. The substituted indium oxide composition shows exceptionally high, metal-like electrical conductivity, greater than 1200 S/cm at 1000°C, and a Seebeck coefficient greater than 110 V/K at that temperature. A small thermoelectric generator consisting of 10 *p*-*n* junctions was constructed by coupling this new *n*-type material with *p*-type layered cobaltites. Such devices would allow waste heat from fuel cells and other fossil energy conversion systems to be converted to electricity.

Enhanced Sintering of Lanthanum Manganite Oxygen Electrodes. In collaboration with the University of Missouri-Rolla, anomalous shrinkage behavior of porous Sr-doped lanthanum manganite ($La_{1-x}Sr_xMnO_{3+\delta}$ or LSM, where x = 0.0 to 0.4) has been studied as a function of thermal cycling, oxygen partial pressure, and Sr dopant concentration. Densification has been observed at temperatures hundreds of degrees lower than the sintering temperature. LSM is an unusual material in that there exists excess oxygen in the lattice in air, actually expressed as an increased number of

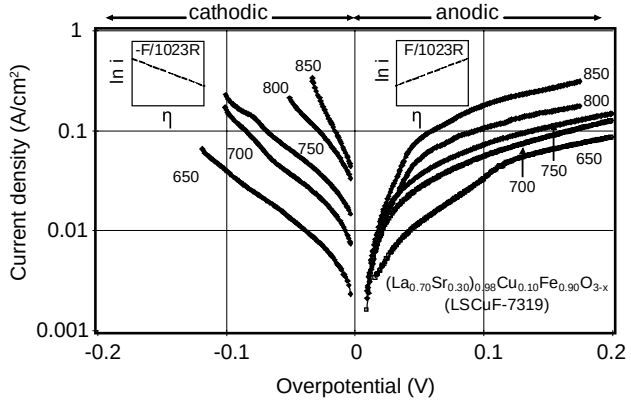

FIGURE 3. Cathodic and anodic overpotentials versus current density for LSCuF-7319 on YSZ with a 3 micron-thick samaria-doped ceria interlayer. Cathodic current densities increased faster than expected for Tafel behavior, while anodic current densities appeared to be reaching a limiting value due to interfacial depletion of oxygen vacancies.

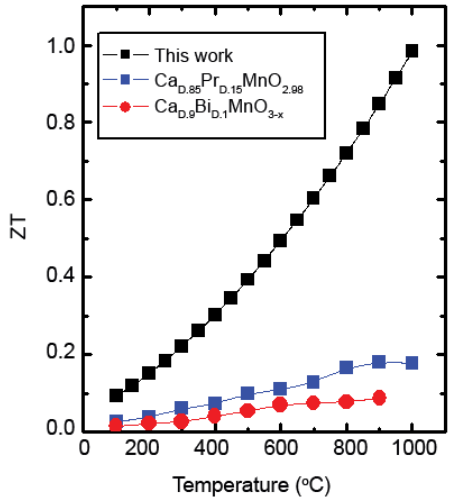

FIGURE 4. Thermoelectric figure of merit versus temperature for n-type bulk oxides. Results for substituted manganese oxides are from Cong et al., Physica B – Cond. Matt. 353, 18 (2004). A new n-type material has been developed with a figure of merit more than three times higher than that of any other known bulk oxide.

metal vacancies. That excess oxygen disappears under conditions possible with cathodic polarization, at about 10^{-3} atm oxygen partial pressure. When cycled between high and low oxygen partial pressures, defects are either created or annihilated to maintain a Schottky equilibrium, resulting in the formation of microscopic voids. These voids can coalesce, eventually leading to densification. This research is pertinent to both the electrochemical and thermal cycling of fuel cells that utilize manganite-based oxygen electrodes.

Conclusions and Future Directions

- Area specific resistances of a reversible fuel cell operating in the electrolysis direction are higher than those in the fuel cell direction, largely due to the performance of the oxygen electrode. Especially for mixed conducting oxygen electrode compositions, depletion of interfacial oxygen vacancies under anodic polarization resulted in lower electrode activity. Nickel-based hydrogen electrodes also showed higher activity in the fuel cell than electrolysis direction, though the opposite was found for titanate/ceria hydrogen electrodes. Future research will focus on electrode and interfacial stability, including those changes induced by repeated changes in the operational mode of a reversible fuel cell.
- A new *n*-type oxide has been identified that exhibits a thermoelectric figure of merit more than three times higher than that of any other known *n*-type bulk oxide and is stable to high temperatures. Previously, only *p*-type oxides with comparable properties had been known. Such materials would enable waste heat available in fossil energy conversion systems to be efficiently converted to electricity. Future research will focus on modifying both the composition and microstructure of this *n*-type material to further enhance its thermoelectric properties.
- Thermal and oxygen partial pressure cycling has been shown to lead to low temperature densification of lanthanum strontium manganite oxygen electrode. This behavior is the result of a super-stoichiometric oxygen content and thus high metal vacancy concentrations unique to the manganite perovskites. Thermal and oxygen partial pressure cycling created temporal gradients in the metal vacancy concentrations, leading to enhanced mobility. Future research on oxygen electrodes will be directed towards the rare earth nickelates, which are unusual in that they contain interstitial oxygen not possible in the perovskite structure.
- Gasified coal contains minor and trace constituents that could impact the stability and performance of a fuel cell system. Investigations will be performed to determine the sensitivity of nickel-based hydrogen electrodes to various coal gas constituents, which will aid in establishing cleanup standards for coal gas intended to supply fuel cells.
- Fundamental studies of the limits of stored charge in high temperature electrochemical cells with composite electrodes will be conducted. Initial studies have achieved capacitances greater than 20 farads per gram and greater than 15 joules per gram active material. Such phenomena may prove useful as a means of electrical energy storage in fuel cell systems. Future studies will include how electrode composition and structure affect stored charge, charge and discharge kinetics, and mechanisms of self-discharge.

Special Recognitions & Awards/Patents Issued

1. PC Rieke, GW Coffey, LR Pederson, OA Marina, JS Hardy, P Singh, and EC Thomsen. Patent Application: US03036800, "Copper-Substituted Perovskite Compositions for Solid Oxide Fuel Cell Cathodes and Oxygen Reduction Electrochemical Devices."

2. OA Marina and LR Pederson. Patent Application US20050250000, "Novel Composite Solid Oxide Fuel Cell Anode Based on Ceria and Strontium Titanate."

FY 2006 Publications/Presentations

1. Radhakrishnan R, Virkar AV, and Singhal SC. "Estimation of charge-transfer resistivity of Pt cathode on YSZ electrolyte using patterned electrodes." J. Electrochem. Soc. 152 (5): A927-A936, 2005.

2. Radhakrishnan R, Virkar AV, and Singhal SC. "Estimation of charge-transfer resistivity of $La_{0.8}Sr_{0.2}MnO_3$ cathode on $Y_{0.16}Zr_{0.84}O_2$ electrolyte using patterned electrodes." J. Electrochem. Soc. 152 (1): A210-A218, 2005.

3. Simner SP, Anderson MD, Xia GG, Yang Z, Pederson LR, and Stevenson JW. "SOFC performance with Fe-Cr-Mn alloy interconnect." J. Electrochem Soc. 152 (4): A740-A745, 2005 (partial support).

4. Simner SP, Anderson MD, Pederson LR, Stevenson JW. "Performance variability of La(Sr)FeO_3 SOFC cathode with Pt, Ag, and Au current collectors." J. Electrochem Soc. 152 (9): A1851-A1859 2005 (partial support).

5. Zhou XD, Pederson LR, Cai Q, Yang J, Scarfino BJ, Kim M, Yelon WB, James WJ, Anderson HU, Wang C. "Structural and magnetic properties of $LaMn_{1-x}Fe_xO_3$ ($0 < x < 1.0$)." J. Appl. Phys 99 (8): Art. No. 08M918 2006.

6. Pederson, LR, Singh R, and Zhou X-D. "Application of vacuum deposition methods to solid oxide fuel cells – a review." Vacuum 2006 (in press).

7. Marina OA, Williams MC, Coffey GW, Meinhardt KD, Nguyen CD, Pederson LR, and Thomsen EC. "Electrode performance in reversible solid oxide fuel cells." Revised manuscript submitted to J. Electrochem. Soc. 2006.

8. Marina OA, Pederson LR, Thomsen EC, and Meinhardt KD. "Fuel Electrodes for Reversible Solid Oxide Fuel Cells: Reactivity, Kinetics, and Stability." 30th International Conference on Advanced Ceramics & Composites, Cocoa Beach, Florida, January 2006.

9. Marina OA, Pederson LR, Coffey GW, Thomsen EC, and Meinhardt KD. "Generation of Hydrogen in Reversible Solid Oxide Fuel Cells." 209th Meeting of the Electrochemical Society, Denver, Colorado, May 2006.

10. Zhou X-D, Windisch Jr. CF, Thomsen EC, Cai Q, Hardy JS, Coffey GW, Yang J, Yelon WB, and Pederson LR. "Electrochemical and Structural Properties of Ceramic Protonic Conductors." 209th Electrochemical Society Meeting, Denver, Colorado, May 2006.

11. Hardy JS, Canfield NL, Crum JV, Bandyopadhyay A, Weil KS, and Pederson LR. "Co-Synthesis of Mixed-Conducting Composites for Hydrogen Separation: Compositional Considerations." TMS Annual Meeting and Exposition, San Antonio, Texas, March 2006 (invited).

VI.10 Effect of Coal Contaminants on Solid Oxide Fuel Cell System Performance and Service Life

Objectives

- Determine the sensitivity of solid oxide fuel cell performance to trace level contaminants present in coal-derived gas streams.
- Assess the catastrophic damage risk and long-term cumulative effect of trace level contaminants.
- Assess the life expectancy of solid oxide fuel cell systems fed with coal-derived gas streams.

Accomplishments

- Conducted a critical review of literature which indicated that Ni-cermet-based solid oxide fuel cells (SOFC) are vulnerable to degradation in the presence of contaminants that are expected to be present in a coal-derived fuel gas stream.
- Performed thermodynamic calculations to determine the speciation of various contaminants at SOFC operating temperatures.
- Assembled and tested several Ni-cermet SOFCs under varying conditions with select contaminants in a simulated coal-derived gas stream.

Introduction

SOFCs have high fuel-to-electricity conversion efficiency, environmental compatibility (low NO_x production), and modularity. They operate in the temperature range 600°C-1,000°C and can use fuel streams containing both H_2 and CO. Thus, they are ideal candidates to be integrated with a gas stream from an advanced coal gasifier. However, impurities containing virtually every element in the periodic table are present in coal (Clarke and Sloss, 1992) and many become constituents of coal-derived gas. The distribution of trace level contaminants between gaseous and solid phases depends on the individual gasification processes. The contaminants associated with the gaseous phase have deleterious effects on the performance and lifetime of coal-derived gas fed SOFCs.

The well-known impurities in the coal-derived gas stream include H_2S, NH_3, and HCl vapors; metal impurity species of alkali metals such as Na and K; volatile metals such as Zn, Cd, and Hg; metalloids such as As, Se, and Sb; and transition metals such as Ni, Cr, Mn, and V (Pigeaud and Helble, 1994). The concentrations of the trace elements in coals vary widely from sub-ppm levels to 0.1% depending on the coal rank and location of the deposit. Some of these contaminants such as H_2S are removed by several methods. This program addresses effect of the key impurities such as HCl, methyl chloride, zinc, mercury, arsenic, phosphorous on the efficiency and lifetime of SOFCs.

Gopala N. Krishnan (Primary Contact) and Palitha Jayaweera
SRI International
333 Ravenswood Ave.
Menlo Park, CA 94025
Phone: (650) 859-2627; Fax: (650) 859-2111
E-mail: gopala.krishnan@sri.com

DOE Project Manager:
Ayyakkannu Manivannan
Phone: (304) 285-2078
E-mail: Ayyakkannu.Manivannan@netl.doe.gov

Subcontractors:
RTI International

Approach

The research program includes a literature review, thermodynamic calculations, and a comprehensive experimental and analytical study to assess the impact of trace contaminants on SOFC performance.

1. A review of the scientific literature provided a preliminary assessment of the effect of trace level contaminants on the performance of the SOFC.
2. Thermodynamic equilibrium calculations allow the identification of the chemical nature of the trace contaminants as they pass through the gas cleanup system from the coal gasifier and enter the SOFC anode.
3. A well-defined experimental program is designed to substantiate the preliminary assessment based on thermodynamic calculations and literature data.

In this program, the SOFC anodes (Ni-cermet) are exposed to a simulated coal gas containing individual contaminants at the operating temperature range of the SOFC (800°C to 1,000°C) for an extended period of time. During such exposure, the electrical performance of the SOFC is monitored and compared with another cell that is exposed to a clean simulated coal gas stream to determine the performance degradation. After the exposure period, the anodes are analyzed for the accumulation of the contaminants by the well-known

methods including inductively coupled plasma-atomic emission, and graphite furnace-atomic absorption spectroscopies.

Results

We reviewed the information available in the literature relating to the effect of trace element contaminants on the SOFC performance and nickel reforming catalysts and performed thermodynamic equilibrium calculations to determine the chemical nature and abundance of relevant trace element species as a function of temperature in the range expected in a coal gasification system and SOFC operating conditions.

Of the limited number of investigations that have been conducted to determine the effect of contaminants in the coal-derived gas on the performance of SOFC, H_2S has received most attention followed by NH_3 and HCl vapor (EG & G Technical Services, 2002). At 1,000°C, NH_3, at about 5,000 ppm levels, did not have a measurable effect. HCl at 1 ppm level did not affect the performance of the SOFC either, although higher levels may have a long-term effect. H_2S at 1 ppm level showed an immediate degradation, but then it stabilized with no long-term effect. Higher levels of H_2S and HCl and lower operating temperatures can lead to a significant degradation of SOFC performance (Singhal and Kendall, 2003). Studies of nickel reforming catalysts have also shown that the presence of 1 ppm of As_2O_3 in the feed steam will impair the performance of the reformer in a matter of few days and the effect is irreversible (Twigg, 1996).

We performed thermodynamic equilibrium calculations using gas streams representative of an oxygen-blown slagging gasifier. Based on their abundance in coal, volatility during gasification, and their potential effect on the SOFC performance, the components likely to contribute to degradation when the SOFC anode is operated with coal gas stream are metalloids such as As, Sb, and Se; vaporizable metals such as Zn, Cd, Hg, and Pb; transition metals such as Fe, Cr, and V; and chlorine compounds such as HCl and CH_3Cl. For these calculations, we assumed that the system pressure will be 10 atm and the components will be initially present at 10 ppm level. We calculated the most likely species that will be present at SOFC operating temperatures.

Figure 1 shows a representative thermodynamic calculation performed for arsenic. During coal gasification, arsenic is converted into a hydride, most likely in the form of AsH_3(g). We calculated the fate of AsH_3(g) in the gas stream as it is being heated to the SOFC operating temperature and the results are shown in Figure 1. At these temperatures, the predominant species is As_2(g). Similar to As, Sb is predominantly to be present as Sb_2(g).

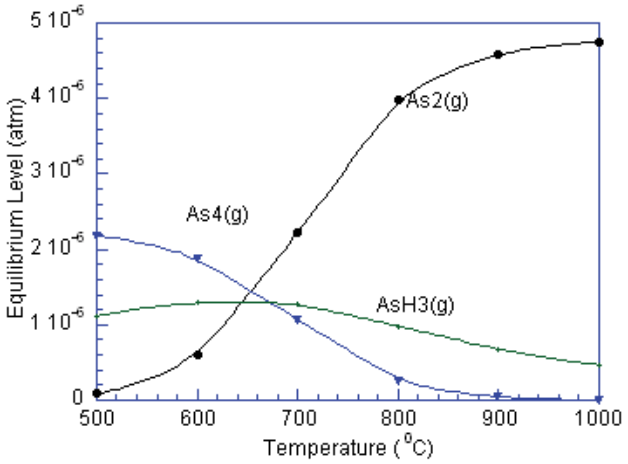

FIGURE 1. The Equilibrium Level of Arsenic Species (Inlet Level 10 ppm) as a Function of Temperature at 10 atm in a Gas Stream Representative of an Oxygen-Blown Slagging Gasifier

The promising sorbent for reducing H_2S level in the coal gas stream at elevated temperatures contains zinc compounds (e.g., zinc titanate or zinc aluminate). In the coal gas streams and HCl levels, zinc can be present as Zn or $ZnCl_2$ vapors. Similarly, cadmium is likely to be present as Cd(g) or $CdCl_2$(g). Under gasification conditions, Hg is present mainly as Hg(g). The most likely form of Pb species are Pb(g), PbCl(g) and $PbCl_2$(g). The actual concentrations of these species will depend on the type of coal used.

HCl(g) is a known contaminant in the coal derived gas stream and it is thought to be present in the range 10 to 300 ppm. Although the preliminary results indicate that HCl may not be a serious poison at levels of about 1 ppm, HCl(g) can transport other impurities such as Fe, Cr, Zn, and Pb as volatile chloride species. In desulfurization systems using organic solvents such as monoethyl amine (MEA), HCl can react with the solvent to form CH_3Cl species at low temperatures. Our calculations indicate the trace levels of CH_3Cl will be converted to CH_4 and HCl gases.

In parallel to literature review and thermodynamic calculations, we initiated an experimental program using solid oxide Ni-cermet fuel cell samples from InDec B. V., Netherlands (4.5 cm^2 active area). They have electrolyte layer of dense YSZ of 4 to 6 µm in thickness, porous anode layer of 5 to 10 µm, porous anode support layer of 520 to 600 µm, and a porous LSM-YSZ cathode layer of 30 to 40 µm thick. The cells were operated at 750°C to 850°C with syngas (30% CO, 30.6% H_2, 11.8% CO and 27.6% H_2O) under 1 A load. The select contaminants (10-50 ppmv) were added to the feed gas stream.

After stabilization in the simulated coal-derived gas mixture without known contaminants, the cell was exposed to a low level of select contaminants

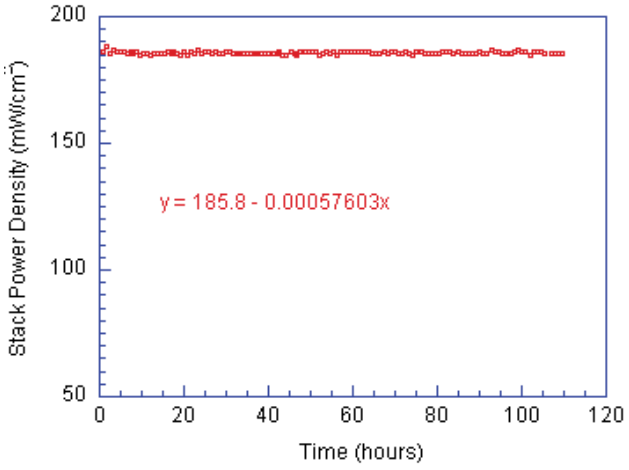

FIGURE 2. The Performance of Cell #6 at 800°C at 1A Load with Simulated Coal-Derived Gas (100 cc/min) Containing Approximately 40 ppm of HCl Vapor

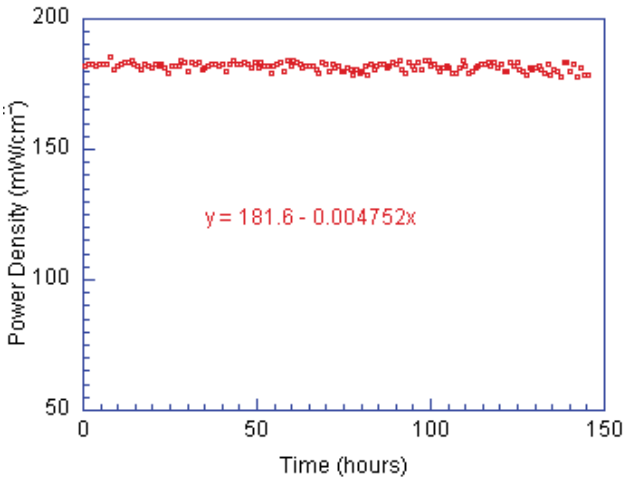

FIGURE 3. The Performance of Cell #7 at 800°C at 1A Load with Simulated Coal-Derived Gas (100 cc/min) Containing Approximately 40 ppm of CH_3Cl vapor.

(10-50 ppmv) by adding them into the simulated gas mixture. Figure 2 shows the performance of this cell (#6) in the gas mixture containing approximately 40 ppm HCl for 100 hours. An examination of the data shows that a gradual performance degradation in the presence of the HCl vapor. In a similar test, we exposed another cell (#7) to approximately 40 ppm CH_3Cl (another potential contaminant in coal-derived fuel gas streams) in the simulated coal-derived gas mixture. Figure 3 shows the exposure testing data of this cell to CH_3Cl during a period of 100 hours.

In the 100-hour test period at 800ºC, cell performance was degrading at 0.0006 mW/cm^2 per hour for HCl, and 0.05 mW/cm^2 per hour for CH_3Cl. If the degradation continues, it may be a significant loss over the 30,000-hour expected operating life of the SOFC.

Conclusions and Future Directions

- A review of the available literature indicates that Ni-cermet-based SOFCs are vulnerable to degradation in the presence of contaminants that are expected to be present in a coal derived fuel gas stream. Whereas the effect of some contaminants such as H_2S, NH_3 and HCl has been studied, the effect of other contaminants has not been ascertained.
- The literature relating to the catalytic activity of Ni-based catalysts indicated that many of the potential contaminants could have a deleterious activity of Ni-based SOFCs. S, Cl, P, As, and Bi-containing compounds reduced the chemisorption of H atoms or CO on nickel surfaces leading to a reduction in the catalytic activity that involves H_2 or CO, as would be the case in a SOFC anode.
- A slow degradation of in the power density of the SOFC cell was observed with HCl and CH_3Cl contaminants during the test period of 100 hours at 800ºC (0.0006 mW/cm^2 per hour for HCl, and 0.05 mW/cm^2 per hour for CH_3Cl). Experiments are in progress for other test conditions.
- We will expose the SOFC cells to additional contaminants such as PH_3, AsH_3, Hg, and Zn in the range of 1 to 10 ppm levels for a minimum of 100 hours at 700°C to 900°C and characterize the changes in the performance of fuel cells by monitoring current-voltage characteristics.

FY 2006 Publications/Presentations

1. Effect of Coal Contaminants on Solid Oxide Fuel System Performance and Service Life, Quarterly Technical Progress Report 1 covering the period October 1, 2005 through December 31, 2005.

2. Effect of Coal Contaminants on Solid Oxide Fuel System Performance and Service Life, Quarterly Technical Progress Report 2 covering the period January 1, 2006 through March 31, 2006.

References

1. Clarke, L. B. and L. L. Sloss (1992). Trace Elements – Emissions from Coal Combustion and Gasification, IEA Coal Research, London.

2. EG & G Technical Services (2002). Fuel Cell Handbook, 6th edition, DOR/NETL 2002-1179.

3. Pigeaud, A. E., and J. J. Helble (1994). "Trace Species Emissions for IGFC," Proceedings of the Coal-Fired Power Systems 94 – Advances in IGCC and PFBC Review

Meeting, Eds. H. M. McDaniel, R. H. Staubly, and V. K. Venkataraman, DOE/METC-94/1008.

4. Singhal, S. C. and K. Kendall (2003). High Temperature Solid Oxide Fuel Cells: Fundamentals, Design, and Applications, Elsevier, Oxford, England.

5. Twigg, M. (1996), Catalyst Handbook, 2nd edition, Manson Publishing Ltd, London, England.

VI.11 Techno-Economic Feasibility of Highly-Efficient Cost-Effective Thermoelectric-SOFC Hybrid Power Generation Systems

Objectives

Phase I

- Create innovative integrated SOFC-Thermoelectric (TE) technical concepts meeting the requirements of 65% electric efficiency and $400/kWe.
- Develop techno-economic models to assess the feasibility of the created concepts using trade studies.

Phase II

- Propose development and risk-mitigation tasks for inserting the proposed technology into a coal-based power plant.

Accomplishments

- Generated 10 component and system technical concepts.
- Benchmarked the TE-material technologies, emphasizing power generation using SOFC exhaust heat.
- Developed system level performance and cost modeling tool.
- Identified a pressurized SOFC with TE power generation as the optimal system configuration.

Future Directions

- Complete the optimization in design and operating envelopes.

Jifeng Zhang (Primary Contact), Jean Yamanis, Benoit Olsommer
United Technologies Research Center
411 Silver Lane MS 65
East Hartford, CT 06108
Phone: (860) 610-7461; Fax: (860) 660-8442
E-mail: ZhangJ@utrc.utc.com

DOE Project Manager: Magda Rivera
Phone: (304) 285-1359
E-mail: Magda.Rivera@netl.doe.gov

Subcontractor:
Lon Bell, BSST LLC, Irwindale, CA

- Evaluate the barriers and enablers in terms of technology and cost.
- Create Phase II development plan.

Introduction

A thermoelectric (TE) material can generate power directly when it is conducting heat from a hot fluid to a cold one, known as Seebeck Effect. In a solid oxide fuel cell (SOFC), the exhaust fluid leaving the stack and its afterburner typically has a high temperature of around 800°C. In today's SOFC designs, the exhaust heat is usually recovered in a heat exchanger, or preheater, to preheat the fuel or air entering the stack. A TE generator can be used for the same heat recovery purpose and also for converting part of the heat to electricity directly. The additional electricity increases the system power generation efficiency, and has the potential to meet the SECA power efficiency goal of 65%.

The major issue in a SOFC-TE hybrid power generation system is the trade-off between the gain in efficiency and the associated cost. Major factors affecting system performance and cost include SOFC pressurization, exhaust heat temperature and flow rate, TE size, material cost, and TE power efficiency under exhaust heat conditions, among others such as blower efficiency. This study is concerned with the trade-off between the performance and cost in reaching the overall system performance and cost target.

Approach

The proposed approach is tailored to 10 kWe SOFC-TE modules with the prospect of studying the impact of capacity ranging from 5 kWe to 200 kWe power plants. In-depth system/component techno-economic models will be developed and verified for the proposed SOFC-TE integrated system. The models will be exercised to explore the design and operating techno-economic envelopes (trade-offs). Several existing TE-material technologies will be evaluated and benchmarked in support of the selection of strategic partner(s) for Phase II. Product requirements and specifications (system/components) will result from the techno-economic analysis. An evaluation of the critical barriers/enablers will lead to the creation of a development plan for Phase II.

Results

TE Material Benchmarking

A list of close to 30 TE materials studied or commercialized in America, Asia and Europe was reviewed varying from manufacturing processes to material structure. TE materials at high and medium temperature range were the focus for power generation from SOFC exhaust. TE materials with a thermoelectric figure of merit (ZT) around 1 at medium temperature levels have achieved fair commercialization with high technology readiness levels [1]. Higher ZTs of 3.2 have been achieved at Lincoln Lab [2] but, to our best knowledge, all reported TE materials with high ZTs today have technology readiness level below or equal to 4.

Concept Generation

Ten concepts were generated to integrate the two subsystems, SOFC and TE, considering the system efficiency and cost targets. Among these concepts, three are in terms of system configuration, for which the number of TE generators and the TE relative positions with respect to the SOFC components are proposed. Another three concepts are related to the design of new components or the performance and cost tradeoffs for certain components. The rest of the concepts are for power conditioning system integration.

The pros and cons of the above concepts were analyzed qualitatively from configuration and practicality standpoints. Trade studies using physics-based models were used for the analysis of the other remaining concepts.

System Modeling Analysis

Cost and physics-based models are used to compare the systems and to support the concept selection process.

One of the system concepts mentioned above has been identified as the best system to meet the 65% system electrical efficiency at a cost of $432/kWe assuming a ZT of 2 for the TE generator. It consists of one TE generator integrated in a pressurized SOFC system that has a stack pressure of approximately 4 atm and uses a separate air blower for the TE generator, as shown in Figure 1. The baseline (used for comparison) ambient pressure SOFC system in this study has an efficiency of 43% (based on lower heating value). Using two TE generators, the system efficiency can increase up to approximately 55%. To reach 65% system efficiency, a pressurized SOFC integrated with a Brayton cycle is necessary. In such a configuration, however, the TE module tends to generate less power than in an ambient pressure SOFC. The reasons for this are summarized hereafter. The exhaust gas from the SOFC afterburner first passes through a turbine and its temperature is lowered after the expansion process. In addition, the cooling air for the high-stage TE generator has a higher temperature due to compression than in an ambient SOFC. These combined effects reduce the amount of energy available for the TE generator and also reduce the temperature difference between the hot and cold fluids across the TE generator.

An alternative to increase the TE generator performance is to feed the ambient "cold" air first to the TE and then to the air compressor. However, the gain on the TE power generation is outweighed by the additional compression work to compress the "hot" air and results in lower system efficiency.

The system efficiency as a function of the system pressurization ratio is shown in Figure 2. System efficiency shows a peak around a pressure ratio of 4. At pressure ratio ~4, the TE generator contributes approximately 2 percentage points to the system efficiency of 63%. At higher pressure ratios, the drop in system efficiency is dominated by the turbine-compressor module. Additional investigation and system optimization is underway to reach 65% system efficiency.

The air preheater in Figure 1 can be used as another TE generator to produce additional power. However, as shown in Figure 3, as this TE generator size becomes larger, i.e., the number of parallel elements increases from 0 to 18,000, the system cost increases from $510/kW to $560/kW but the efficiency increases only ~1%. This TE generator therefore does not seem to be cost-effective. In addition, the heat transfer capability using TE materials is reduced compared to a metal heat recovery device. This means that a higher heat transfer area is required to achieve the same performance than a

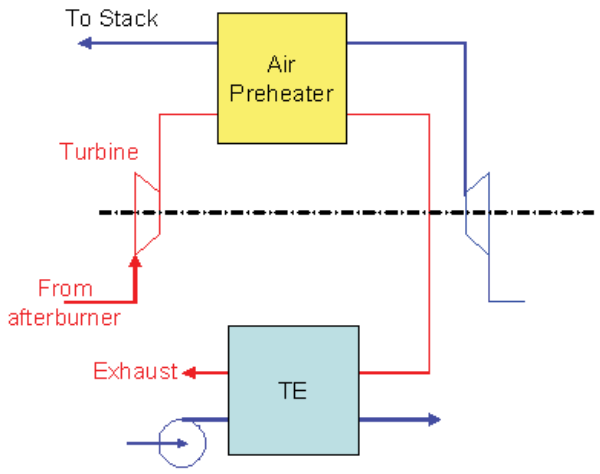

FIGURE 1. TE Generator and SOFC Integration Scheme

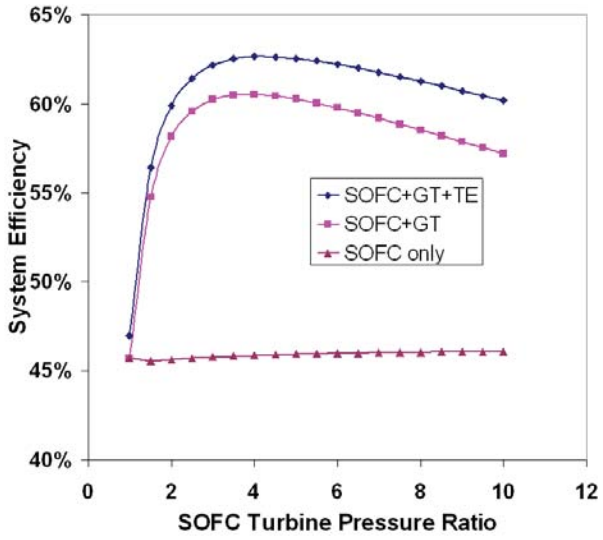

FIGURE 2. System Efficiency at Different SOFC Pressure Ratios

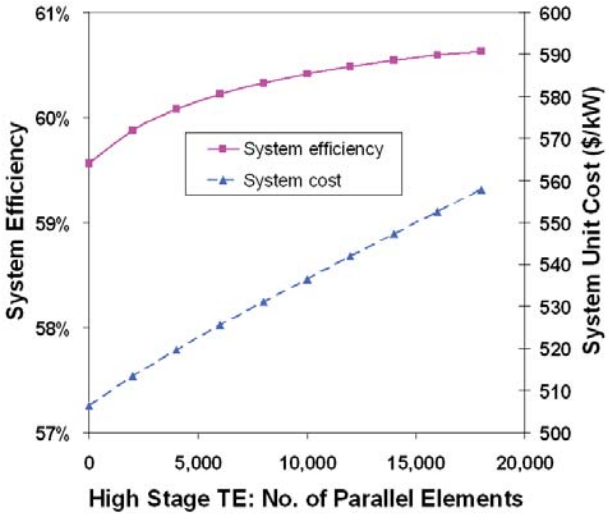

FIGURE 3. Power Cost When Using Air Preheater as a TE Generator

pressurized SOFC-TE with only one TE power generator module as depicted in Figure 1.

As the TE efficiency is a function of ZT, the system efficiency with different ZTs is modeled with a SOFC pressure ratio of 4, as shown in Figure 4. When the ZT changes from 1 to 3.5 [3], the TE generator efficiency increases from 0.06 to 0.14. Because TE power generation is only a small portion of the system power, the system efficiency increases by only less than 2 percentage points.

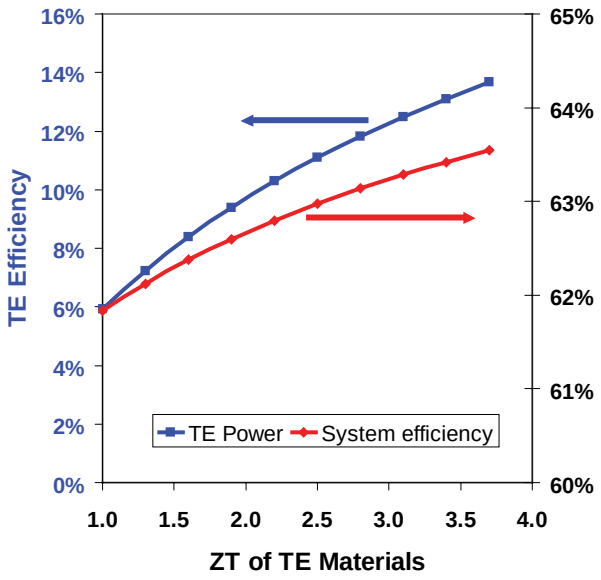

FIGURE 4. System Efficiency with TE Materials Having Different ZTs

Conclusions

- The TE contribution to the system is small due to system thermodynamic constraints.
- The best system configuration is a pressurized SOFC with a bottoming TE power generation module.
- In the pressurized SOFC-TE systems, the TE power generator module contributes approximately 2% (absolute) of the system efficiency.
- The maximum system efficiency obtained to date is 63% and further system optimization is underway to meet the performance and cost targets.

References

1. Bottner, "Micropelt Miniaturized Thermoelectric Devices: Small Size, High Cooling Power Densities, Short Response Time", ICT 2005, Clemson, S.C.

2. Temperature Rises for Devices That Turn Heat Into Electricity, Robert F. Service, Science 29 October 2004 306: 806-807.

3. Bell, L. E., "Use of Thermal Isolation to Improve Thermoelectric System Operating Efficiency," Proceedings 21st International Conference on Thermoelectrics, Long Beach, CA, August 2002.

VI.12 High Temperature Electrochemistry - University of Florida

Objectives

- Apply computational approach to develop fundamental understanding of ionic transport and heterogeneous electrocatalysis in SOFCs.
- Develop high resolution characterization techniques to quantify electrode microstructures.
- Combine heterogeneous catalysis, electrochemistry, and microstructure characterization techniques to de-convolute contributions to electrode polarization.

Accomplishments

- Utilized *ab initio* and molecular dynamic simulations to calculate defect and defect cluster formation energies and effect on ionic transport.
- Computationally and experimentally determining thermo-mechanical properties based on fundamental thermodynamic/bond-energy constants.
- Used atomic-level simulation methods to elucidate the effects of non-stoichiometry and temperature on the elastic properties of CeO_{2-x}.
- Determined adsorption and absorption energies for O on and in $LaFeO_3$ (110) using first principles, and electronic structure calculations.
- Developed high resolution focused ion beam (FIB) - scanning electron microscopy (SEM) characterization technique and applied to SOFC cathodes to quantify 3-D microstructure.
- Developing unique electrocatalytic techniques to determine fundamental oxygen exchange kinetics (k/D) on cathode surfaces based on O-isotope exchange as a function of applied voltage/current.

Eric D. Wachsman
University of Florida
Gainesville, FL 32611-6400
Phone: (352) 846-2991; Fax: (352) 846-0326
E-mail: ewach@mse.ufl.edu

DOE Project Managers: Heather Quedenfeld and Lane Wilson
Phone: (412) 386-5781
E-mail: Heather.Quedenfeld@netl.doe.gov
Phone: (304) 285-1336
E-mail: Lane.Wilson@netl.doe.gov

Introduction

To fully achieve the tremendous socio-economic benefits of electrochemical energy conversion and power generation, fundamental scientific breakthroughs in the transport of ionic species through electrolyte/membranes and reaction rates at electrode surfaces are necessary. Therefore, the mission of the University of Florida High Temperature Electrochemistry Center (HiTEC) is to develop a fundamental understanding of ionic transport in, and electrocatalytic (electrochemical catalysis) phenomena on the surface of, ion-conducting materials. The research spans the range from first-principles calculations and molecular dynamic simulations of ionic transport and gas-solid interactions of novel ion-conducting materials and electrocatalysts to development of advanced technology devices for efficient energy utilization:

SOFCs – Increasing the ionic conductivity and electrode reaction rates results in higher power density cells at lower operating temperature. These higher power density cells will dramatically reduce the cost of fuel cell technology, thus, overcoming the final hurdle (cost) to widespread commercial deployment.

Membranes – Membrane reactors are a major component of the FutureGen Initiative. Improving the transport of ions through the membrane and reaction rates at the membrane surface will help achieve dramatic breakthroughs in industrial energy efficiency and cost of hydrogen production.

Sensors – By developing a fundamental understanding of the gas-solid reactions that occur on sensor electrodes we will be able to develop sensors that are highly sensitive and selective to specific gaseous pollutants. These sensors will allow more accurate control of combustion resulting in greater fuel economy and reduced air pollution.

Approach

Our computational research focuses first on gaining insight into mechanisms of ion transport and heterogeneous electrocatalysis, and then on applying this fundamental knowledge to the design of new materials. Using electronic structure calculations and large-scale atomic-level simulation on cluster parallel computers we are elucidating the fundamental processes of ion transport in various electrolyte and electrode materials. Among the effects being explored are defect clustering on ionic transport and the use of doping to increase ionic transport. The effect of grain boundary interfaces

is being determined from simulations of ionic transport in polycrystalline materials. The insights gained from these simulations will help guide the development of higher conductivity electrolyte and electrode materials.

In addition, we are using similar calculations to develop a fundamental understanding of heterogeneous electrocatalytic phenomena at the surface of ion-conducting ceramics. Because cathode polarization limits the performance of SOFCs at low temperature, the insights gained from this study will lead to the development of lower polarization SOFC cathodes at lower temperatures. In addition, these computational methods will be used to determine the mechanisms responsible for the cathode performance degradation.

We are developing high-resolution, quantitative, microstructural characterization techniques based on a FIB-SEM. This includes development of mathematical techniques to create a 3-D reconstruction of the entire porous electrode structure as well as to quantify electrode microstructural features (e.g., triple phase boundary length, porosity and tortuosity). In addition, we are using the FIB-SEM to prepare samples for high resolution transmission electron microscope (HRTEM) analysis of specific interfaces for analysis of issues such as tertiary phase formation, cathode degradation, etc.

Finally, using heterogeneous catalysis techniques: temperature programmed desorption (TPD), temperature programmed reaction (TPR), and oxygen-isotope exchange; combined with electrochemistry techniques: impedance spectroscopy, current-voltage (I-V), and conductivity relaxation; and the microstructural characterization and computational approach (above); we are de-convoluting the various contributions to electrode polarization to obtain a more fundamental understanding, and develop a methodology to design improved performance electrodes in the future.

Results

Computational - The thermal and mechanical properties of CeO_{2-x} were simulated by molecular dynamics (MD), with interatomic interactions described by a conventional Buckingham potential plus Coulombic interactions. The lattice parameter expanded with both increasing temperature and oxygen vacancy concentration (non-stoichiometry, x), consistent with experimental observations as shown in Figure 1a. The coefficient of thermal expansion for different compositions was also calculated. A detailed study of the mechanical properties was performed with the MD simulation. The elastic constants C_{11}, C_{12}, and C_{44} were calculated as a function of composition ($0 \le x \le 0.3$) and temperature (0 - 1500 K). These values were used to obtain the bulk modulus, Young's modulus, and shear modulus for the corresponding compositions and were found to be in agreement with experimental values.

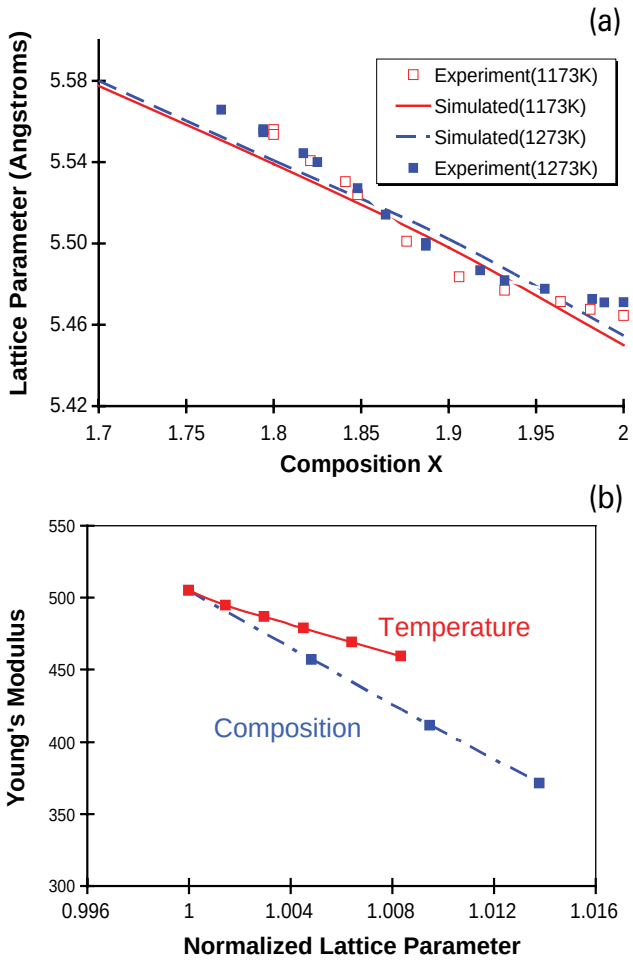

FIGURE 1. (a) Comparison of Lattice Parameter Between Calculated and Published Data; (b) Comparison of Young's Modulus Dependence on Temperature and Composition

The comparison between temperature and composition effects on Young's modulus (Figure 1b) indicates a greater effect due to oxygen vacancy concentration than temperature. Simulations on the oxygen vacancy diffusion mechanism are underway.

In addition, we optimized the conditions under which first principles, electronic structure calculations of $LaFeO_3$ should be carried out - *density functional theory (DFT) calculations within the generalized gradient approximation (GGA) as implemented by Perdew, Burke, and Ernzerhof (PBE), including the projector augmented wave (PAW) approximation with the Vienna Ab-initio Simulation Package (VASP)*. In our optimizations, the supercell shape and volume was free to change and all the ions were free to move to lower their total energy and decrease the forces on the atoms. The calculated values are in good agreement with experimental values and predict that $LaFeO_3$ undergoes a rhombohedral, Jahn-Teller-induced distortion in agreement with experimental data.

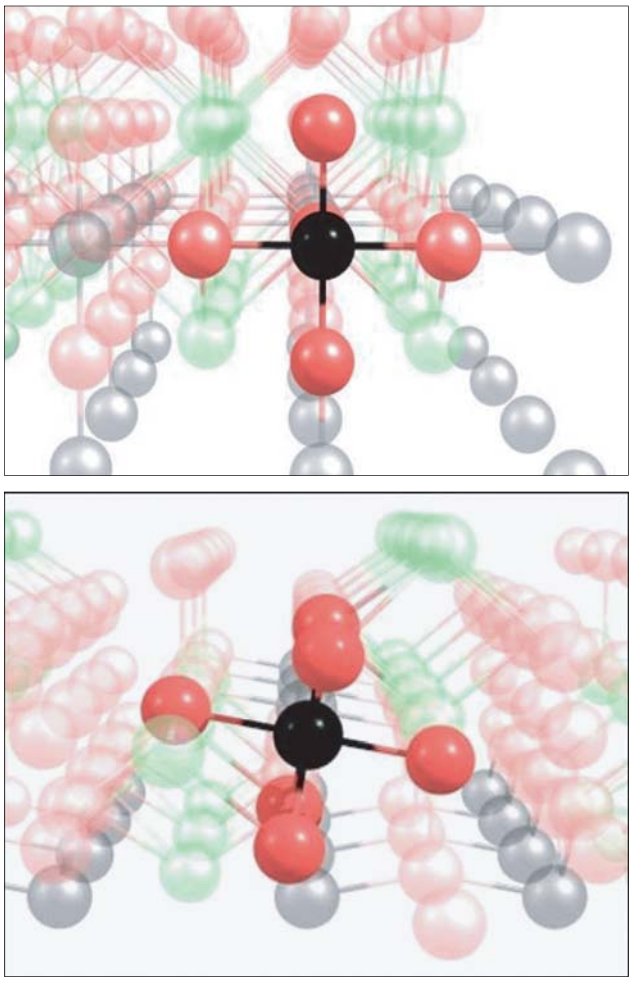

FIGURE 2. Calculated $LaFeO_3$ Bulk and Surface Configurations

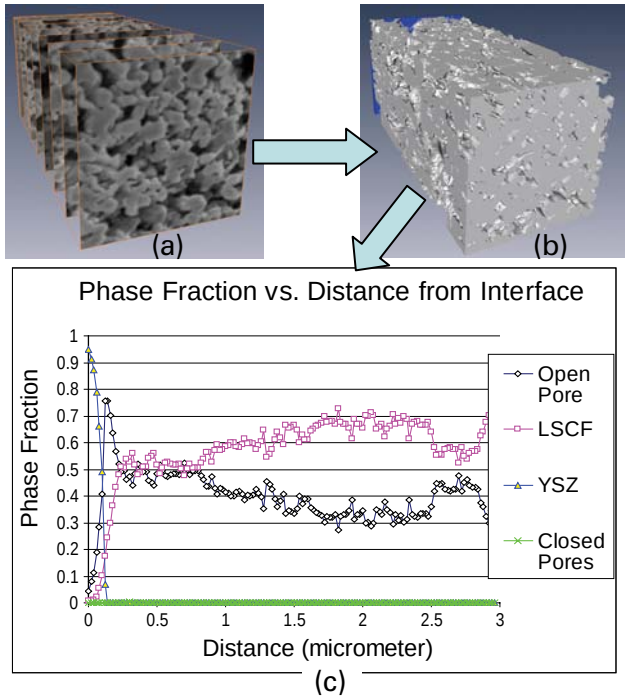

FIGURE 3. FIB-SEM serial sectioning and imaging of LSCF, conducted at ~20 nm intervals. (a) The resulting two-dimensional (2-D) images are stacked and aligned with the aid of fiducial marks.
(b) 3-D reconstruction of the serially sectioned region of interest.
(c) The reconstruction is then manipulated to quantify microstructural properties of the porous cathode such as average particle size, average pore size, closed porosity, open porosity, tortuosity, surface area, interface area, and porosity grading.

The energy of oxygen adsorption on the LaO-terminated $LaFeO_3$ (110) surface and absorption in bulk $LaFeO_3$ were calculated (Figure 2). In the case of absorption, the defect formation energy of the oxygen interstitial is determined to be 2.26 eV. The energy of adsorption is predicted to be -3.65 eV for a La-La bridge site and -3.13 eV for a La-O bridge site. Therefore, for the (110) surface the preferential mechanism is for oxygen to adsorb on a La-La bridge site. These calculations are continuing for the FeO-terminated surfaces.

Microstructural Characterization – The FIB-SEM was used to evaluate LSM and LSCF cathodes on YSZ. The ion beam is rastered across the region of interest (ROI) to remove material while the SEM field emission gun is utilized to image the freshly milled surface with a secondary electron detector down to a 3 nm lateral resolution (Figure 3a). After the SEM image has been acquired a subsequent section of material is ablated with the FIB and the serial process continues to the desired depth. This serial process allows us to create a fully interactive 3-D reconstruction of the electrode microstructure (Figure 3b).

The resultant 3-D microstructure is then qualitatively and quantitatively analyzed. For example, Figure 3c shows the pore, LSCF and YSZ volume fractions as a function of distance from the electrode/electrolyte interface (x=0). Moreover, using this technique on LSM/YSZ samples sintered at various temperatures we can quantify the decrease in TPB length (Figure 4a) and increase in pore size (Figure 4b) as a function of sintering temperature.

The dual beam FIB-SEM also expedites TEM sample preparation. This is done by utilizing the FIB to micromachine and micropolish sectional HRTEM samples, allowing for pinpointing ROIs such as the cathode/electrolyte interface. This was done across the LSM/YSZ interface using an HRTEM with EDS to determine nano-scale compositional changes (Figure 5) and with electron diffraction (Figure 6) to differentiate the crystal structures as a function of sintering.

Deconvolution of Electrode Polarization - Finally, we are using heterogeneous catalysis techniques (TPD/

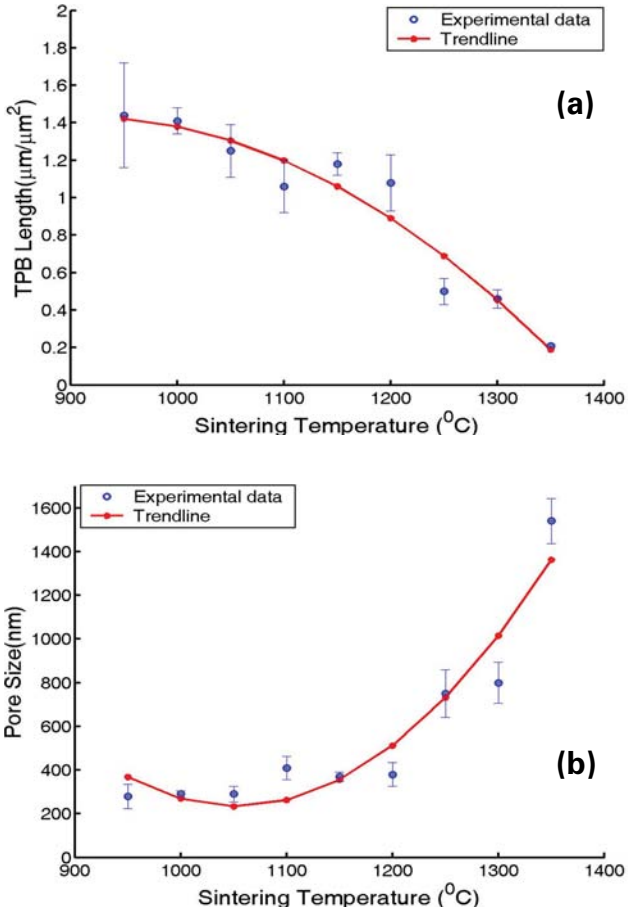

FIGURE 4. TPB Length (a) and Pore Size (b) of LSM Cathode as a Function of Sintering Temperature

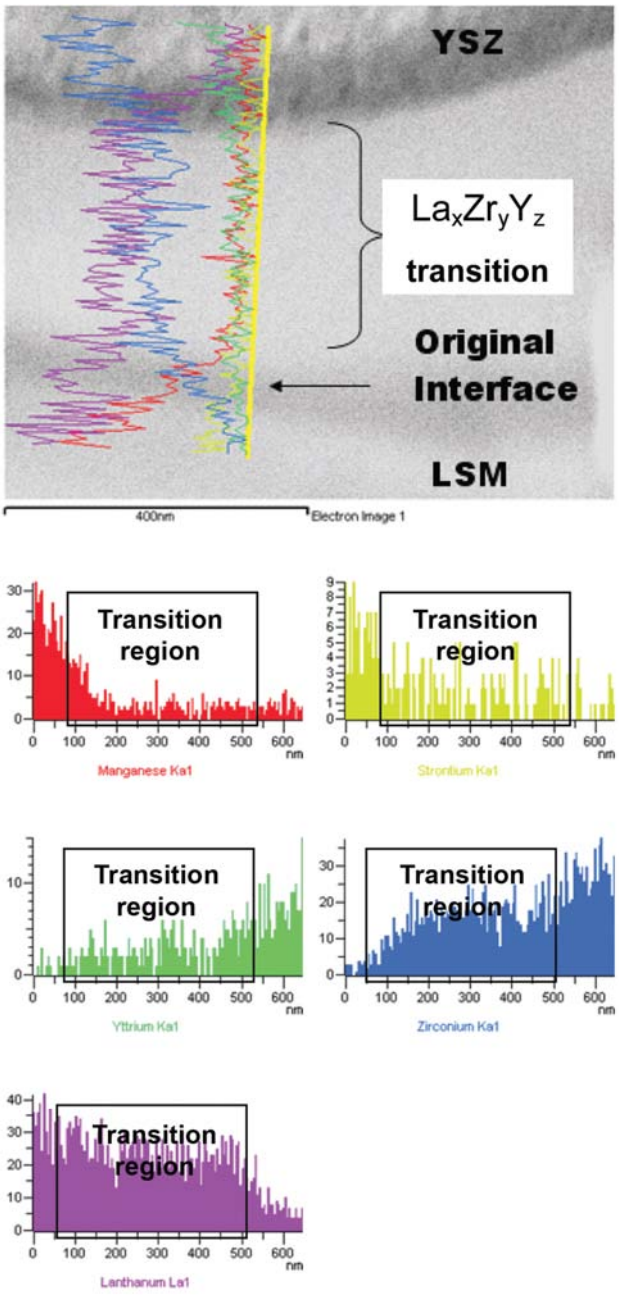

FIGURE 5. LSM/YSZ interface by high resolution STEM. Interface region (~350 Å wide) is distinguishable by intensity contrast. EDS analysis relates the contrast differences to changes in composition showing La diffuses into the YSZ region forming a $La_xZr_yY_z$ type interface phase.

TPR and oxygen-isotope exchange) combined with electrochemistry techniques (impedance spectroscopy, I-V, and conductivity relaxation) and the microstructural characterization and computational approaches to obtain a more fundamental understanding of the various contributions to electrode polarization.

We have set up a high sensitivity (ppb) mass spectrometer and have performed TPD and TPR experiments on LSF-based cathode materials. This has been modified to incorporate O^{18} exchange experiments. We have fabricated a sample holder that allows us to do these experiments *in situ* under applied potentials and currents. In addition, we have set up and validated a conductivity relaxation apparatus and are modifying it to allow *in situ* sampling with the mass spec. The resulting apparatuses are unique in their ability to separate out surface exchange (k) and diffusion (D) coefficients and the effects of potential/current on the electrocatalytic phenomena of activation polarization.

Using impedance spectroscopy we have separated out the various contributions to polarization of LSM, LSF, and LSCF cathodes. The same samples were then analyzed with the FIB-SEM to quantitatively relate microstructure to polarization (e.g., Figure 7). As can be seen, there is a direct correlation between the impedance we attribute to dissociative adsorption and pore surface area (normalized to the cathode volume). Similar trends have been observed for charge transfer resistance and TPB length.

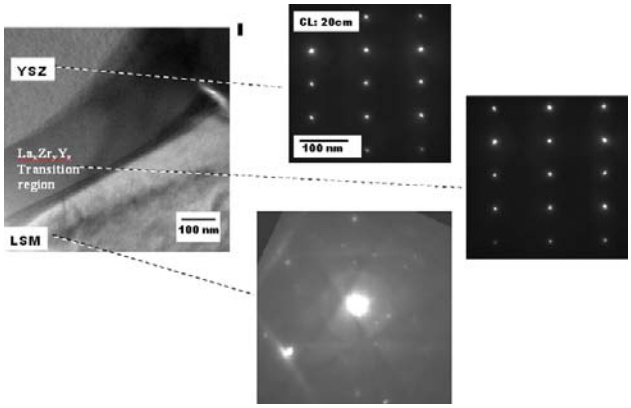

FIGURE 6. TEM diffraction patterns of YSZ and LSM are distinctly different. The diffraction pattern of the transition region is the same as that of the YSZ region. Similarity in the crystal structure between YSZ and the interface region suggests that the interface is formed by the diffusion of La from the LSM region into YSZ forming the transition region.

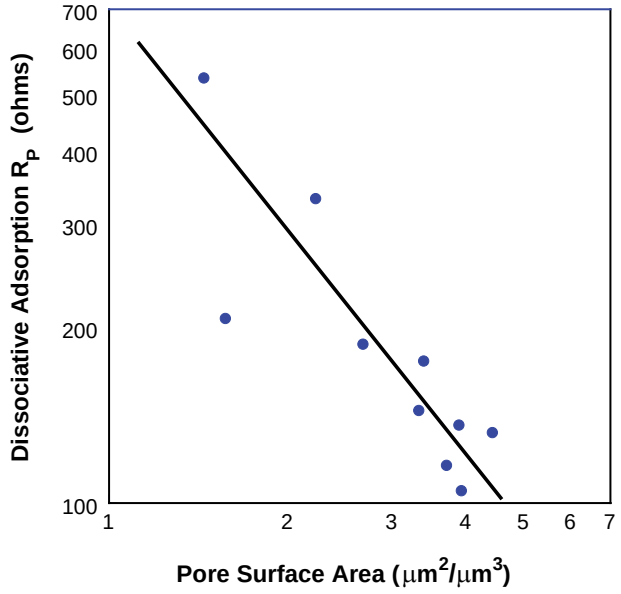

FIGURE 7. Relation Between Impedance (Dissociative Adsorption) and Microstructure (Normalized Pore Surface Area) for an LSM Cathode

Conclusions and Future Directions

- Demonstrated that computational simulations of thermo-mechanical properties are consistent with experimental results, and show the importance of oxygen vacancy concentration on lattice expansion.
- Computationally determined adsorption and absorption energies for O on/in $LaFeO_3$ (110) cathodes. Results indicate preference for La-La surface sites. Calculations to continue on Fe terminated surfaces.
- Developed high resolution FIB-SEM characterization technique and applied it to SOFC cathodes. Demonstrated that results can be used to produce 3-D reconstructions. Quantification of LSM, LSF, and LSCF cathode microstructures is underway.
- Developing unique electrocatalytic techniques to determine fundamental oxygen exchange kinetics (k/D) on cathode surfaces. The resultant experimental data combined with computational results will be used to design improved cathode materials.
- Combined microstructural characterization of LSM cathodes with impedance spectroscopy results to de-convolute polarization mechanisms and quantify the effect of microstructure on electrode polarization. These experiments will continue and we will apply to LSF and LSCF cathodes.

FY 2006 Publications/Presentations

1. "High Temperature Materials," K. E Spear, S. Visco, E. J. Wuchina and E. D. Wachsman, *Interface*, The Electrochemical Society, **15-1**, 40-44 (2006).

2. "Ionic Conduction in Zirconia Films of Nanometer Thickness," X. Guo, E. Vasco, S. Mi, K. Szot, E. D. Wachsman, and R. Waser, *Acta Materialia*, **53**, 5161-5166 (2005).

3. "Schottky Barrier Formed by Network of Screw Dislocations in $SrTiO_3$," X. Guo, Z Zhang, W. Sigle, E. D. Wachsman, and R. Waser, *Applied Physics Letters*, **87**, 162105 (2005).

4. "The Search for a Low Temperature SOFC; How Low Can We Go?" E. D. Wachsman, Stanford University Seminar, March 24, 2006, Stanford, CA.

5. "Investigations Into Cathode Mechanisms and Novel Materials Development," E. D. Wachsman, UF-DOE High Temperature Electrochemistry Center Workshop on Fundamental Mechanisms of SOFC Cathode Reactions, January 27, 2006, Cocoa Beach, FL.

6. "Application of Computational Methods to Understanding SOFC Cathode Mechanisms", J. He, C.-W. Lee, E. Wachsman, S.B. Sinnott, M.W. Finnis, E.C. Dickey, UF-DOE High Temperature Electrochemistry Center Workshop on Fundamental Mechanisms of SOFC Cathode Reactions, January 27, 2006, Cocoa Beach, FL.

7. "Physical Origin of the Low Grain Boundary Conductivity of Oxygen Ion Conductors: Zirconia and Ceria," X. Guo and E. D. Wachsman, American Ceramic Society, January 22-27, 2006, Cocoa Beach, FL.

8. "Fundamental Studies of SOFC Materials," E. D. Wachsman, DOE - SECA Core Technology Program Peer Review Meeting, October 25-26, 2005, Denver, CO.

9. "Schottky Barrier Formed by Network of Screw Dislocations in $SrTiO_3$", X. Guo, E. D. Wachsman, Z. Zhang, W. Sigle and R. Waser, The Electrochemical Society, October 16-21, 2005, Los Angeles, CA.

10. "Ionic Conduction in Zirconia Films of Nanometer Thickness", X. Guo, E. D. Wachsman, E. Vasco, S. Mi, K. Szot and R. Waser, The Electrochemical Society, October 16-21, 2005, Los Angeles, CA.

11. "The Search for a Low Temperature SOFC; How Low Can We Go?" E. D. Wachsman, Montana State University HiTEC Seminar, October 6, 2005, Bozeman, MT.

12. "Effect of Oxygen Sublattice Ordering on Conductivity in Highly Defective Fluorite Oxides," E. D. Wachsman, American Ceramic Society, September 11-16, 2005, Maui, HI.

VI.13 A High Temperature Electrochemical Energy Storage System Based on Sodium Beta Alumina Solid Electrolyte (BASE)

Objectives

Phase I

- To synthesize planar, thin, strong BASE using a patented vapor phase process.
- To fabricate metal end caps and the associated hardware for the construction of planar BASE-based electrochemical energy storage systems.
- To construct electrochemical cells comprising of a sodium anode, BASE, and selected cathodes.
- To electrochemically test cells (discharge-charge) over a range of temperatures and up to the highest possible depths of discharge.
- To conduct theoretical analysis of the electrochemical energy storage system from the standpoint of maximum possible capacity, efficiency, and integrability with power generation systems.

Phase II

- To construct a planar stack of ten Na/BASE/optimized cathode cells.
- To operate a stack for a minimum of 100 charge-discharge cycles.
- To thermally cycle the stack between the operating temperature and room temperature.
- To disassemble the stack and conduct post mortem analysis.

Approach

- Fabricate BASE discs by the method of die pressing or tape casting and BASE tubes by the method of slip casting using a vapor phase process.

Anil V. Virkar
University of Utah
Department of Materials Science & Engineering
122 S. Central Campus Drive
Salt Lake City, UT 84112
Phone: (801) 581-5396; Fax: (801) 581-4816
E-mail: anil.virkar@m.cc.utah.edu

DOE Project Manager: Lane Wilson
Phone: (304) 285-1336
E-mail: Lane.Wilson@netl.doe.gov

- Measure the conductivity of BASE tubes by assembling a symmetric cell with zinc chloride – sodium chloride eutectic mixture.
- Construct tubular electrochemical cells that could be assembled in three different states: discharged state, charged state, and partially charged at eutectic composition.
- Conduct experiments to test the electrochemical working of tubular cells and to analyze the voltage response of the charge-discharge cycles.
- Construct planar cells and to test the electrochemical working of the same by analyzing the voltage response of the charge-discharge cycles.
- Conduct several freeze-thaw cycles on the planar cells and test the performance of the same after undergoing thermal cycles.
- Test the stability of BASE as electrolyte with zinc chloride as the cathode.

Accomplishments

- BASE discs were successfully fabricated by tape casting, sintering and vapor phase treatment.
- BASE tubes were successfully fabricated by slip casting, sintering and vapor phase treatment.
- BASE was shown to be stable in aqueous media (no $NaAlO_2$ at grain boundaries).
- Electrochemical cells were designed, constructed, and tested.
- No incorporation of zinc within the BASE structure was observed, suggesting that BASE is stable in the battery environment.
- A tubular electrochemical cell with a zinc chloride cathode was successfully discharged at 2 V.
- Planar cells were designed and assembled.
- Freeze-thawing of planar cells was done a couple of times followed by several charge-discharge cycles without failure of the electrolyte. These tests were conducted at an operating temperature of 350°C.

Future Directions

- Assemble a planar stack of five Na/BASE/$ZnCl_2$ cells and test the electrochemical working of the cell stack.
- Construct and test electrochemical cells comprising of a sodium anode, BASE, and alternative cathodes.
- Integration of the high temperature energy storage system based on BASE with a power generation system.

Introduction

The demand for electricity varies depending upon the time of the day: low demand during night and high demand during day. All power plants are designed for peak power which leads to the underutilization of excess capacity during off peak periods. One of the main reasons for the emergence of electrochemical energy storage devices, such as batteries, is that power plants can be designed for average demand. This will augment the capacity of power plants as the excess energy during off peak periods will be stored for use later during high peak demands. This strategy is expected to lower capital costs.

Sodium beta" alumina solid electrolyte, commonly referred to as BASE, is an excellent conductor of sodium ions at 300°C. This cell has liquid sodium as the anode, BASE as the electrolyte and liquid $ZnCl_2$ as the cathode. During charging and discharging, sodium ions pass through the BASE electrolyte from cathode to anode and anode to cathode, respectively. The current applications of this solid electrolyte include the Na-S battery, the Zebra battery and the sodium heat engine. The Na-S battery has a demonstrated life of greater than 7 years in a 500 kW size. This shows that BASE has outstanding stability in rather corrosive environments – far superior than any other solid electrolyte being considered for active electrochemical devices. Work to date shows that BASE is the only known solid electrolyte with such a wide range of applicability (from as low as ~ 100°C to over 1,000°C), and excellent stability in strongly reducing and oxidizing environments.

Approach

BASE discs were fabricated using the method of tape casting of alumina + zirconia followed by vapor phase conversion (Figure 1). The dispersant used was KD1. BASE tubes were fabricated by the method of slip casting with Darvan C as the deflocculent. The conductivity of BASE tubes was measured by assembling symmetric cells. A eutectic mixture of NaCl-$ZnCl_2$ was used as both the electrodes in the symmetrical cell. The cell was then cycled at constant current mode supplying 500 mA for 50 hours. The operating temperature was 350°C. A few BASE samples were put in an aqueous solution of NaOH (40(w/v) %) and boiled for 5 hours. This test was conducted to make sure that the samples would survive in a basic aqueous environment. The x-ray diffraction patterns and microstructures of the samples after treating with NaOH were taken and analyzed. Experiments were conducted to test the electrochemical working of the tubular cells assembled in the discharged state, charged state and partially charged state at eutectic composition. Planar cells were designed and assembled using the tape cast BASE discs. The working of planar cells was tested at the constant current mode and the cells were thermally cycled between the operating temperature and room temperature. The performance of the planar cells was monitored after several freeze-thaw cycles. An experiment was conducted to test the stability of BASE in a zinc chloride environment. BASE tubes were soaked in molten zinc chloride at a temperature of 430°C for 22 hours. The samples were weighed before and after the treatment with $ZnCl_2$. Then, the samples were analyzed using scanning electron microscopy (SEM). Chemical line scan was done on the samples using SEM for analyzing the composition of the samples. The next step is to design and assemble a planar stack of five cells.

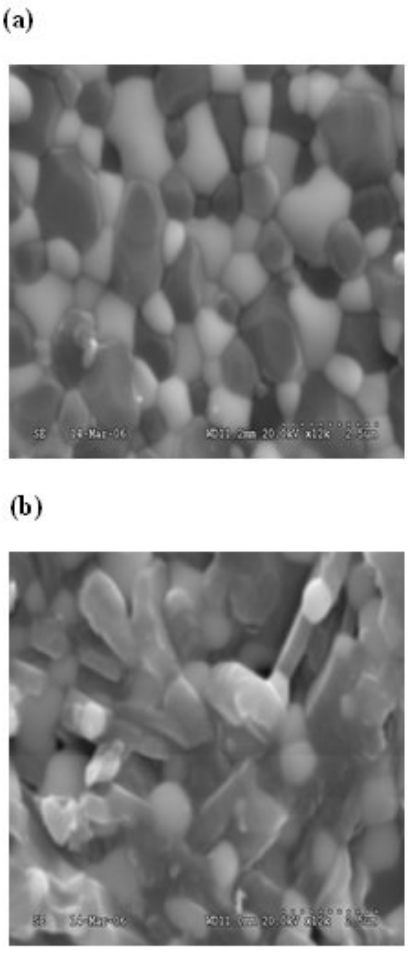

FIGURE 1. Microstructures of (a) As-Sintered Tape Cast Sample and (b) BASE Tape after Vapor Phase Conversion

Results

1. The voltage response of the symmetrical cell was analyzed. There was no evidence of an increase in resistance with time. From the values of voltage and current obtained from the experiment, the resistance of the overall cell was calculated to be 0.15 Ω. This includes the resistance of the BASE tube, molten salts and the polarization resistance.
2. The x-ray diffraction pattern of the sample which was treated with NaOH solution was analyzed. The analysis of peaks showed no difference from the BASE before treating with NaOH solution. There was no significant difference in the surface of the samples other than the sample was slightly etched.
3. A number of tubular cells were assembled and tested to study the electrochemical working at an operating temperature of 350°C. The analyses of the voltage response of the cells showed a fairly constant discharge voltage of about 2.0 V when operated under the constant current mode (Figure 2). The last cell assembled in the fully charged state was discharged for about 20 hours with a constant discharge voltage of 1.9 V.
4. A planar cell was assembled in the partially discharged state at eutectic composition (Figure 3). Voltage responses of the charge-discharge cycles of the planar cells were analyzed (Figure 4). The cell was operated for about 2 hours after each freeze-thaw cycle (Figure 5). The open circuit voltage obtained was about 2.35 V. The cell was operated at a constant current of 100 mA and at a temperature of 350°C.
5. Stability of BASE in a $ZnCl_2$ environment was tested by soaking BASE samples in molten zinc chloride. The samples were weighed before and after the experiment and no change in weight was observed.

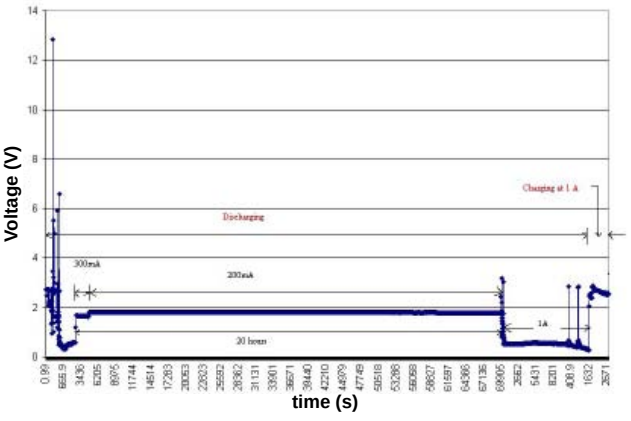

FIGURE 2. Voltage response of the discharging and charging of tubular cell assembled in the fully charged state. This shows that a tubular cell can be successfully discharged and charged.

FIGURE 3. Assembled View of the Planar Cell

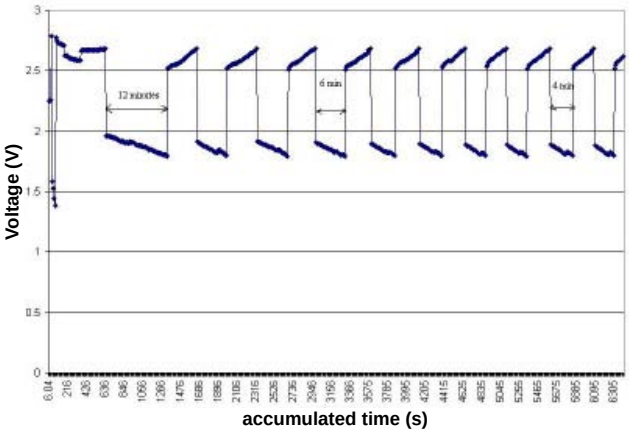

FIGURE 4. Voltage response of the charging and discharging of the planar cell assembled in the partially charged state. This shows that a planar cell could be subjected to repeated charge-discharge cycles.

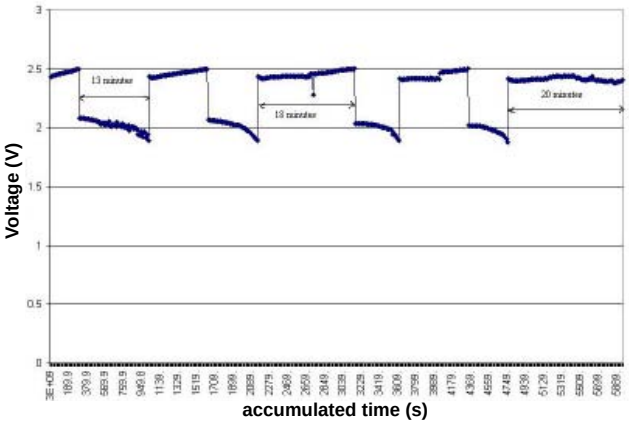

FIGURE 5. Voltage Response of the Charging and Discharging of the Planar Cell after Two Freeze-Thaw Cycles

Conclusions

1. Thin BASE discs were fabricated by tape casting and BASE tubes were successfully made by slip casting.
2. An electrochemical cell using $ZnCl_2$ electrodes showed that there is no increase in resistance, even after repeated cycling, suggesting that the BASE is stable in the atmosphere, and the proposed concept is viable.
3. Preliminary work shows that a complete cell could be assembled in the discharged state, and could be charged with a sodium anode.
4. Stability of BASE in an aqueous medium was demonstrated. This BASE has little affinity for water unlike the state-of-the-art BASE.
5. Electrochemical cells were successfully discharged.
6. Planar cells were assembled and tested to study the working of the same. From the voltage response it could be inferred that the planar cells can withstand several freeze-thaw cycles without any electrolyte failure.
7. The displacement reaction does not take place between $ZnCl_2$ and the BASE as there was no change in weight of the samples when treated with molten zinc chloride.

VI.14 Direct Utilization of Coal Syngas in High Temperature Fuel Cells

Objectives

- Identify the fundamental mechanisms of carbon deposition and sulfur poisoning on anodes.
- Develop novel materials to minimize the impact of contaminants on fuel cell performance.
- Characterize the effects of major trace contaminants found in coal syngas.
- Propose remedies for adverse effects of contaminants on fuel cell performance.

Accomplishments

This project has been selected for funding under the DOE EPSCoR (Experimental Program to Stimulate Competitive Research) State Implementation Grant Award Program and will begin conducting research in the fall, 2006. There are no accomplishments to report at this time.

Introduction

This project is supported under the DOE EPSCoR, a program designed to enhance the capabilities of EPSCoR states in energy research and economic development through the support of advanced research at academic institutions. Our vision is to establish an internationally recognized, sustainable fuel cell research center for coal-based clean power generation which serves as a technology resource for the emerging fuel cell industry in West Virginia. Our strengths are in applying nano-technology to develop and fabricate materials for advanced coal-based fuel cells; establishing a state-of-the-art material characterization and fuel cell testing laboratory; and modeling fuel cells from atomistic to continuum scales using high performance computing. We have formed a multidisciplinary team of eleven research professionals who have worked together for several years and have strong credentials in their respective areas of expertise. Under the present proposal, we will develop a laboratory infrastructure, solidify interactive working relationships, and attain national recognition for the work conducted by the center in the area of coal-based clean power generation via fuel cells. Our project will be conducted in collaboration with the National Energy Technology Laboratory (NETL). This project is to be funded for a 3-year effort.

Richard Bajura, WV DOE EPSCoR Principal Investigator, Ismail Celik, Technical Principal Investigator

National Research Center for Coal and Energy
West Virginia University
385 Evansdale Drive
Morgantown, WV 26506-6064
Phone: (304) 293-2867 Ext. 5401; Fax: (304) 293-3749
E-mail: bajura@wvu.edu

DOE Project Manager: Kristin Bennett
Phone: (301) 903-4269
E-mail: Kristin.Bennett@science.doe.gov

DOE Technical Manager: Lane Wilson
Phone: (304) 285-1336
E-mail: Lane.Wilson@netl.doe.gov

Approach

The focus areas for the proposed research project are the modeling, manufacture, and testing of anode materials for solid oxide fuel cells (SOFCs) operating on coal syngas (CSG). The objectives are to identify the fundamental mechanisms of carbon deposition and sulfur poisoning on the anode, and to develop novel materials to minimize the impact of these contaminants on fuel cell performance. We shall also characterize the effects of major trace contaminants found in CSG and propose remedies for adverse effects.

DOE EPSCoR requires that research funded under the State Implementation Grant Program be conducted as a coordinated effort involving clusters of investigators focusing on specific projects. An overview of the cluster program is shown in Figure 1. The research cluster is based on a multi-scale, multi-disciplinary approach conducted by nine faculty members in four departments at West Virginia University (WVU). The work is organized under four integrated projects: (1) anode material development and experimental characterization of fuel cell anodes, (2) sub-micro-scale modeling, (3) multi-scale continuum modeling, and (4) laboratory testing of individual fuel cells and fuel cell systems.

The strength of the research cluster is in the integration of knowledge obtained from experiments (Projects 1 and 4) with multi-scale computational models (Projects 2 and 3). At all stages, information, predictions, and data will be exchanged between researchers in the projects.

At the end of three years, we anticipate four outcomes. First, we will have identified the fundamental processes characterizing the operation of

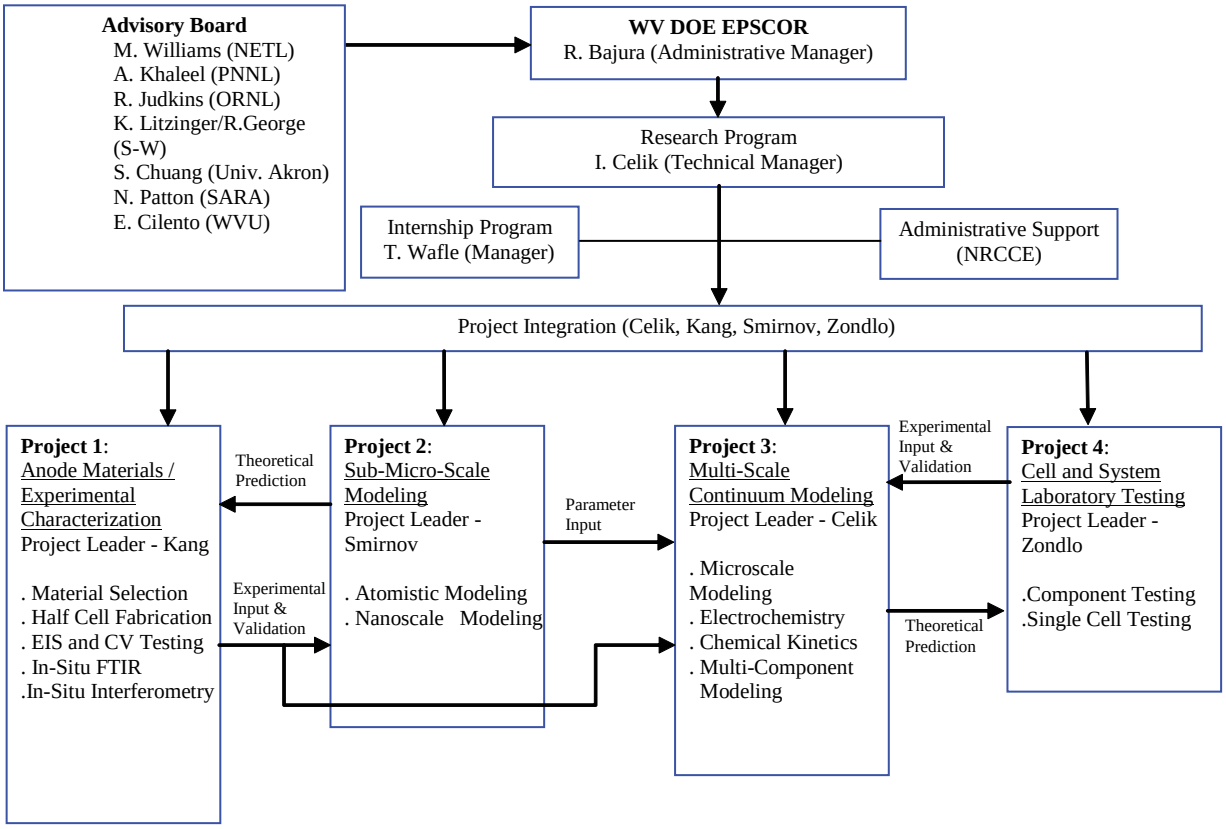

FIGURE 1. Flow Chart of the Research Program and Organizational Structure.

SOFC anodes from the atomic level to the level of the operating fuel cell. Second, strategies will be developed for constructing SOFCs that exhibit stable operation with coal syngas. Third, the research infrastructure (equipment for analysis and for fabrication, computers for modeling) and collaborations across disciplines and departments at WVU will be well developed for future research on fuel cells. Fourth, a program of educating and training future energy researchers will be established.

VII. Acronyms & Abbreviations

°C	Degree(s) Celsius
°C/min	Degree(s) Celsius per minute
°F	Degree(s) Fahrenheit
2PB	Two-phase boundary
1-D	One-dimensional
3-D	Three-dimensional
3DP	Three-dimensional printing
A	Ampere(s)
Å	Angstrom(s)
ABO_3	Perovskite type materials
A/cm^2	Amp(s) per square centimeter
AC	Alternating current
AC	Activated carbon
AcerSoc	American Ceramic Society
ACS	American Chemical Society
AFM	Atomic force microscope
Ag	Silver
AgF_2	Silver difluoride
AGRB	Anode gas recycle blower
Al	Aluminum
AL	Application load
ALL-BASE	A liquid alkali metal beta alumina solid electrolyte battery
Al_2O_3	Alumina, aluminum oxide
AMPL	A Mathematical Programming Language
ALC	Allegheny Ludlum Technical and Commercial Center
ANL	Argonne National Laboratory
APS	Atmospheric plasma spray
APU	Auxiliary power unit
Ar	Argon
As	Arsenic
As_2	Diatomic arsenic
AsH_3	Arsenic hydride
As_2O_3	Arsenic oxide
ASE	Arcomac Surface Engineering, LLC
ASM	ASM International, formerly American Society for Metals
ASME	American Society of Mechanical Engineers
ASR	Area specific resistance
ASTM	American Society for Testing and Materials
ASU	Arizona State University
ATI	Allegheny Technologies, Inc.
atm	Atmosphere(s)
ATR	Auto thermal reformer
Au	Gold
A.U.	Arbitrary units
AZ	Arizona
B	Boron
B_2O_3	Boron (III) oxide
Ba	Barium
BaO	Barium oxide
$BaCeO_3$	Barium cerate
BASE	Beta alumina solid electrolyte
$BaZrO_3$	Barium zirconate
Be	Beryllium
BCAS	Barium-calcium-aluminosilicate
BCN	$Ba_3Ca_{1+x}Nb_{2-x}O_{9-\delta}$
BOP, BoP	Balance of plant
BOPS	Balance of plant subsystem
BSE	Back scattered electron
BT	Benzothiophene
BTU	British thermal unit
BYZ	Barium zirconium yttrium oxide
BYZ-Zn	Zinc oxide doped barium zirconium yttrium oxide
C	Carbon
C++	A computer program language
Ca	Calcium
CaO	Calcium oxide
CA	California
CAB	Cathode air blower
CAD	Computer aided design
CANBUS	Controller area network bus
CAP	Commercialization Assistance Program
CARB	California Air Resources Board
CB	Circuit breaker
CCVD	Combustion chemical vapor deposition
Cd	Cadmium
$CdCl_2$	Cadmium chloride
C-DBD	Coaxial dielectric barrier discharge
Ce	Cerium
CE	Counter electrode
CeO_2	Ceric oxide
CERCANAM	Ceramatec Castable Nano Material
CFD	Computational fluid dynamics
CH_4	Methane

CHP	Combined heat and electrical power
Cl	Chlorine
CLEM	Continuum-level electrochemical model
cm	Centimeter(s)
cm^2/s	Square centimeter(s) per second
cm^2	Square centimeter(s)
cm^3	Cubic centimeter(s)
CMU	Carnegie Mellon University
CO	Carbon monoxide
CO	Colorado
Co	Cobalt
CO_2	Carbon dioxide
COE	Cost of electricity
CoO	Cobalt oxide
COx	Oxides of carbon (e.g., CO, CO_2)
CPG	Cummins Power Generation
CPOX	Catalytic partial oxidation
Cr	Chromium
Cr_2O_3	Chromic oxide
CrO_3	Chromium trioxide (chromic acid)
CT	Connecticut
CTE	Coefficient of thermal expansion
CTP	Core Technology Program
Cu	Copper
CuCl	Copper (I) chloride
$CuCl_2$	Copper (II) chloride
CVD	Combustion chemical vapor deposition
dBA	Decibels
DBD	Dielectric barrier discharge
DBT	Dibenzothiophene
DC	Direct current
DC	District of Columbia
DC/AC	Direct current to alternating current
DDN	Dodecane
DF-2	Number 2 diesel fuel
DFC	Direct Fuel Cell
DFC/T®	Direct Fuel Cell/Turbine®
DFMA	Design for manufacturing and assembly
DFT	Density functional theory
DOE	U.S. Department of Energy
DSC	Differential scanning calorimetry
DSP	Digital signal processor
dT	Temperature difference
DTA	Differential thermal analysis
EBPVD	Electron beam physical vapor deposition
E-BRITE	Fe-26Cr-1Mo alloy
EDS	Energy dispersive x-ray spectroscopy
EDTA	Ethylenediamine tetraacetic acid
EDX	Energy dispersive x-ray
EDXS	Energy dispersive x-ray spectroscopy
EIS	Electrochemical impedance spectroscopy
EMI	Electromagnetic interference
EPOx	Electrochemical partial oxidation
EPRI	Electric Power Research Institute
eV	Electron volts
EVD	Electrochemical vapor deposition
EXAFS	Extended x-ray absorption fine structure spectroscopy
F	Farad (capacitance unit)
F	Fluorine
FAD	Filtered arc deposition
FAPSID	Filtered arc plasma source ion deposition
FAT	Factory acceptance test
FB-ARGB	Foil gas bearing anode gas recycle blower
FBS-AGRB	Foil gas bearing supported anode gas recycle blower
FC	Fuel cell
FCE	FuelCell Energy, Inc.
FC/GT	Fuel cell gas turbine
FC/T	Hybrid fuel cell/gas turbine
Fe	Iron
FE	Failure effects analysis
FEM	Finite element modeling
FIB	Focused ion beam
FL, Fl.	Florida
FMA	Fracture mechanical analyzer
FPGA	Field programmable gate array
FPS	Fuel processor system
FSS	Ferritic stainless steel
ft	Foot (feet)
Ft-lbf/lbm	Foot-pound force per pound mass
FY	Fiscal year
(g)	Gas
g	Gram(s)
ΔG	Enthalpy; free energy
Ga	Gallium
GA	Georgia
g/cc, g/cm^3	Gram(s) per cubic centimeter
Gd	Gadolinium
GDC	Gadolinia-doped ceria
GDC10	Ten weight % gadolinium doped cerium oxide
GE	General Electric

GGA	Generalized gradient approximation
GHSV	Gas hourly space velocity
gm	Gram(s)
GPa	Gigapascal(s)
g/s	Gram(s) per second
GT	Gas turbine
GUI	Graphical user interface
GW	Gigawatt(s)
h	Hour(s)
H_2	Diatomic hydrogen
HARB	High-temperature anode recirculation blower
HC	Hydrocarbon
HCl	Hydrogen chloride
HDS	Hydrodesulfurization
He	Helium
HEXM-1	Hexaaluminate-type catalyst
Hg	Mercury
HHV	Higher heating value
HI	Hawaii
HiTEC	High Temperature Electrochemistry Center
HMI	Human machine interface
H_2O	Water
H_2S	Hydrogen sulfide
HPD	High power density
HPGS	Hybrid Power Generation Systems (General Electric)
HPLC	High performance liquid chromatograph
HRTEM	High resolution transmission electron microscope
hr	Hour(s)
hrs	Hours
HTPC	High temperature proton conductor
HTR	High temperature reduction
Hz	Hertz
I	Current
IC	Interconnection, interconnect
ICP	Inductively coupled plasma
IEA	International Energy Agency
IEEE	Institute of Electrical and Electronics Engineering
IGBT	Insulated gate bipolar transistor
IGCC	Integrated gasification combined cycle
IGFC	Integrated gasification fuel cell
IL	Illinois
in	Inch(es)
IPOPT	Interior Point OPTimization
IT-SOFC	Intermediate-temperature solid oxide fuel cell
ITM	Ion transport membrane
i-V, I-V	Current-voltage
J	Joule(s)
J/kg	Joule(s) per kilogram
JP-5	A kerosene-based jet fuel
JP-8, JP8	A kerosene-based jet fuel
K	Kelvin
K	Potassium
K-BASE	Potassium-based beta alumina solid electrode
KBYZ	Potassium-doped and yttrium-doped barium zirconate
kcal/mole	Kilocalories per mole
K_2CO_3	Potassium carbonate
KD1	A polyester/polyamine condensation polymer, used as a dispersant
KF	Potassium fluoride
kg	Kilogram(s)
kg/s	Kilogram(s) per second
kg/kW	Kilogram(s) per kilowatt
kHz	Kilohertz
kJ	Kilojoule(s)
KOH	Alkali earth metal hydroxide
kPa	Kilopascal(s)
kV	Kilovolt(s)
kW	Kilowatt(s)
kΩ	1000 ohms
kW/l	Kilowatt(s) per liter
kWe	Kilowatt(s) electric
kWh	Kilowatt-hour(s)
l	Liter(s)
La	Lanthanum
LA	Louisiana
$LaAlO_3$	Lanthanum aluminum oxide
$LaCoO_3$	Lanthanum cobalt oxide
$LaCrO_3$	Lanthanum chromite
LAFAD	Large area filtered arc deposition
$LaFeO_3$	Lanthanum iron oxide
$LaMnO_3$	Lanthanum manganite
LAO	Lanthanum aluminum oxide
lb	Pound(s)
lbm	Pound mass
lbm/min	Pound mass per minute
LC	Inductor-capacitor

LCMO	Lanthanum calcium manganese oxide ($La_{2/3}Ca_{1/3}MnO_3$)
LF	Low-frequency
LHV	Lower heating value
LLC	Limited Liability Company
LM, $LaMnO_3$	Lanthanum manganite
LMT	Titanium doped lanthanum manganite
LPG	Liquefied petroleum gas
LSC	Lanthanum strontium cobaltite (lanthanum strontium cobalt oxide)
LSC-37	$La_{0.3}Sr_{0.7}CoO_{(3-\delta)}$
LSC-82	$La_{0.8}Sr_{0.2}CoO_{(3-\delta)}$
LSC50	$La_{0.5}Sr_{0.5}CoO_{(3-\delta)}$
LSCF	Lanthanum strontium cobalt ferrite
LSCO	$La_{0.5}Sr_{0.5}CoO_3$
LSCo	Strontium doped lanthanum cobalt oxide
LSF	Lanthanum strontium ferrite
LSGM	Lanthanum strontium magnesium gallate (lanthanum strontium gallium magnesium oxide)
LSM	Lanthanum strontium manganite (lanthanum strontium manganese oxide)
LTR	Low temperature reduction
m	Meter(s)
m^2	Square(s) meter
m^2/g	Square meter(s) per gram
MA	Massachusetts
mA	Milliampere(s)
mA/cm^2	Milliampere(s) per square centimeter
MACOR	Machinable ceramic
MBT	Methylbenzothiophene
MD	Molecular dynamics
ME	Microelectrode
MEA	Monoethyl amine
METC	Morgantown Energy Technology Center
MeV	Mega-electron volt(s)
mg	Milligram(s)
mg/cm^2	Milligram(s) per square centimeter
Mg	Magnesium
MgO	Magnesium oxide
μg	Microgram(s)
MgO	Magnesium oxide
MHz	Megahertz
MIEC	Mixed ionic electronic conductors, mixed ionic electronic conducting
MIM	Metal injection molding
min	Minute(s)
ml	Milliliter(s)
μm	Micrometer(s), micron(s)
mm	Millimeter(s)
mm/min	Millimeter(s) per minute
mm/sec	Millimeter(s) per second
mmol	Millimole(s)
1MN, MN	1-methylnapthlene
Mn	Manganese
MN	Minnesota
$MnCr_2O_4$	Manganese chromium spinel
MnO	Manganese oxide
Mn_2O_3	Manganese oxide
Mo	Molybdenum
MΩ	Milli-ohm(s)
$mOhm.cm^2$, $m\Omega{\cdot}cm^2$	Milli-ohm square centimeter
mol%	Molar percent
MOSFET	A pure resistive loss device
MPa	Megapascal
ms	Millisecond
MSRI	Materials and Systems Research, Inc.
MT	Montana
mV	Millivolt(s)
MW	Megawatt(s)
mW	Milliwatt(s)
mW/cm^2	Milliwatt(s) per square centimeter
N_2	Diatomic nitrogen
Na	Sodium
$NaAlO_2$	Sodium aluminate
NaF	Sodium fluoride
Na-BASE, Na/BASE	Sodium-based beta alumina solid electrolyte
NaOH	Sodium hydroxide
NASA	National Aeronautics and Space Administration
Nd	Neodymium
$NdGaO_3$	Neodymium gallium oxide
NETL	National Energy Technology Laboratory
NGO	Neodymium gallium oxide
NH_3	Hydrogen nitride (ammonia)
Ni	Nickel
NiMo	Nickel molybdenum
NiO	Nickel monoxide, nickel oxide
Ni-YSZ	Nickel-yttria-stabilized zirconia
NLEIS	Nonlinear electrochemical impedance spectroscopy
nm	Nanometer(s)

NM	New Mexico
NO_2	Nitrogen dioxide
NOx	Oxides of nitrogen
NRA	Nuclear reaction analysis
NV	Nevada
O_2	Diatomic oxygen
O/C	Oxygen to carbon ratio
OCR	On-cell reformation
OH	Ohio
ORNL	Oak Ridge National Laboratory
ORR	Oxygen reduction reaction
P	Phosphorous
P	Pressure
P_{O2}	Partial pressure of oxygen
P-SOFC	Proton conducting solid oxide fuel cells
Pa	Pascal(s)
PA	Pennsylvania
PADT	Phoenix Analysis and Design Technologies
PAW	Projector-augmented wave
Pb	Lead
$PbCl_2$	Lead chloride
$PbCl_4$	Lead chloride
PBE	Perdew, Burke and Ernzerhof
PCS	Power conditioning system
Pd	Palladium
$PdCl_2$	Palladium chloride
PEN	Positive-electrolyte-negative (cathode-electrolyte-anode)
PES	Potential energy surface
PEM	Proton exchange membrane
PEMFC	Proton exchange membrane fuel cell
PFBC	Pressurized fluidized-bed combustion
PFD	Process flow diagram
PHP	A computer programming language
P-I	Power versus current
PI	Proportional-integral
PI	Principal investigator
Pitt	University of Pittsburgh
PLC	Programmable logic controller
PLD	Pulsed laser deposition
PLL	Phase lock loop
PNNL	Pacific Northwest National Laboratory
POC	Proof-of-concept
POM	Partial oxidation of methane
PP-DBD	Parallel-plate dielectric barrier discharge
ppm	Part(s) per million
ppmv	Part(s) per million by volume
ppmw	Part(s) per million by weight
psi	Pound(s) per square inch
psia	Pound(s) per square inch absolute
psig	Pound(s) per square inch gauge
p-SOFC	Protonic solid oxide fuel cell
PSOFC	Planar solid oxide fuel cell
PSOFC/GT	Planar solid oxide fuel cell gas turbine
PSOFCS	Planar solid oxide fuel cell stack
Pt	Platinum
Pt/Al_2O_3	Platinum alumina
PT/ZDC	Platinum zirconia doped ceria
PVB	Polyvinyl butyral
PWM	Pulse-width-modulation
QC	Quantum chemistry
QTH	Quartz-tungsten-halogen
R	Rankine
R&D	Research and development
RBS	Rutherford backscattering spectroscopy
RDF	Radial distribution function
RF	Radio frequency
Rh	Rhodium
Rh/ZDC	Rhodium zirconia doped ceria
ROI	Region of interest
Ru	Ruthenium
s	Second(s)
S	Sulfur
S1	Maximum principal stress
SAG	Simulated anode gas
SAM	Scanning Auger mapping or scanning Auger microprobe analysis
Sb	Antimony
Sb_2	Diatomic antimony
SBIR	Small Business Innovation Research
S/cm	Siemen(s) per centimeter
SC	South Carolina
ScSZ	Scandium-stabilized zirconia
ScSZ-10	Fully stabilized ScSZ: 90 mol% ZrO_2, 10 mol% Sc_2O_3
ScSZ-6	Partially stabilized ScSZ: 94 mol% ZrO_2, 6 mol% Sc_2O_3
sccm	Standard cubic centimeter(s) per minute
sccm/cm	Standard cubic centimeter(s) per minute per centimeter
SCG	Simulated cathode gas
SDC	Samaria-doped ceria
Se	Selenium

sec	Second(s)
SE	Solid electrolyte
SECA	Solid State Energy Conversion Alliance
SEM	Scanning electron microscopy
SERS	Surface-enhanced Raman signal
SFC	Stationary Fuel Cells (Siemens Power Generation)
SF100	A solid oxide fuel cell system
SF200	A solid oxide fuel cell combined heat and power system
Si	Silicon
SiC	Silicon carbide
SIF	Stress intensity factor
SLPM, slpm	Standard liters per minute
SMA	Shape memory alloy
SMD	Sauter mean diameter
Sn	Tin
SO_2	Sulfur dioxide
SOFC	Solid oxide fuel cell
SOFC-MP	Solid oxide fuel cell multi physics
SOFC/T	Solid oxide fuel cell/turbine
SOFC-TE	Solid oxide fuel cell thermoelectric
SOx	Oxides of sulfur (e.g., SO_2)
SPR	Surface plasmon resonance
SPU	Stationary power unit
SR	Steam reforming
SR	Switched reluctance
Sr	Strontium
$SrCeO_3$	Strontium cerate
SrO	Strontium oxide (strontia)
SRO	Strontium ruthenate
$SrRuO_3$	Strontium ruthenate
$SrTiO_3$	Strontium titanate
SS	Stainless steel
SSC	Strontium samarium cobalt
STF	$SrTi_{1-x}Fe_xO_3$
STF05	$SrTi_{1-x}Fe_xO_3$with x=0.05
STF35	$SrTi_{1-x}Fe_xO_3$with x=0.35
STO	Strontium titanate
S.V.	Space velocity
T	Temperature
ΔT	Temperature difference
TD	n-Tetradecane
TE	Thermoelectric
TEM	Transmission electron microscopy or tunneling electron microscopy
TERS	Tip-enhanced Raman scattering
Tg	Glass transition temperature
THD	Total harmonic distortion
Ti	Titanium
TiO_2	Titanium dioxide
TMS	The Metallurgical Society
TN	Tennessee
TOMMI	Temperature optical-mechanical measuring instrument
TPB	Triple-phase boundary, three-phase boundary
TPD	Temperature-programmed desorption
TPO	Temperature-programmed oxidation
TPR	Temperature-programmed reaction
TRC	Transient recognition control
TX	Texas
UHV	Ultra high vacuum
UK	United Kingdom
ULSD	Ultra-low sulfur diesel
UMR	University of Missouri - Rolla
UBM	Unbalanced magnetron
US, U.S.	United States
USPTO	United States Patent and Trademark Office
UT	Utah
UTC	United Technologies Corporation
UV	Ultraviolet
UV-VIS	Ultraviolet to visible
V	Vanadium
V	Volt(s)
VA	Virginia
VASP	Vienna Ab initio Simulation Package
V-I	Voltage-current
V/cm	Volt(s) per centimeter
VDC	Volt(s) direct current
VOC	Volatile organic compound(s)
vol	Volume
vol%	Volume percent
VPS	Versa Power Systems
W	Watt(s)
W/cm^2	Watt(s) per square centimeter
Wh	Watt hour(s)
W	Tungsten
WA	Washington
WE	Working electron
Ω	Ohm(s)
WC	Tungsten carbide
W/cm^2	Watt(s) per square centimeter

We	Watt(s) electric
W/m-K	Watt(s) per meter-Kelvin
wt	Weight
wt%, wt.%	Weight percent
W/tube	Watt(s) per tube
WV	West Virginia
WVU	West Virginia University
XANES	X-ray absorption near edge spectroscopy
XAS	X-ray absorption spectroscopy
Xe	Xenon
XPS	X-ray photoelectron spectroscopy
XRD	X-ray diffraction
Y	Yttrium
Y_2O_3	Yttrium oxide (yttria)
YSZ	Yttria-stabilized zirconia
Zn	Zinc
$ZnCl_2$	Zinc chloride
ZnO	Zinc Oxide
ZDC	Zirconia-doped ceria
ZDC50	Zirconia doped ceria with 50% zirconia concentration
Zr	Zirconium
ZrO_2	Zirconium dioxide (zirconia)
ZT	Thermoelectric figure of merit
Ω	Ohm(s)
Ωcm_2	Ohm(s) centimeter squared

VIII. Primary Contact Index

IX. Organization Index

X. Contract Number Index

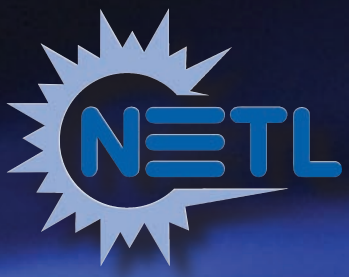

National Energy Technology Laboratory

1450 Queen Avenue SW
Albany, OR 97321-2198
541-967-5892

2175 University Avenue South
Suite 201
Fairbanks, AK 99709
907-452-2559

3610 Collins Ferry Road
P.O. Box 880
Morgantown, WV 26507-0880
304-285-4764

626 Cochrans Mill Road
P.O. Box 10940
Pittsburgh, PA 15236-0940
412-386-4687

One West Third Street, Suite 1400
Tulsa, OK 74103-3519
918-699-2000

Wayne A. Surdoval
SECA Coordinator
412-386-6002
wayne.surdoval@netl.doe.gov

Visit the NETL website at:
www.netl.doe.gov

Customer Service:
1-800-553-7681

U.S. Department of Energy
Office of Fossil Energy

Printed in the United States on recycled paper

September 2006